A STUDY OF TITANIUM-BEARING OXIDES IN HEAVY MINERAL DEPOSITS ALONG THE EAST COAST OF SOUTH AFRICA

BY

VICTOR EMMANUEL HUGO

Submitted in partial fulfilment of the
requirement for the degree of
Doctor of Philosophy,
in the
Department of Geology and Applied Geology
University of Natal

1993

Durban
1993

ABSTRACT

Heavy mineral deposits along the east coast of South Africa represent the world's largest demonstrated resource of beach placer ilmenite. This mineral occurs as homogeneous, subrounded grains, with chemical compositions close to pure $FeTiO_3$. Concentrates contain between 48 and 52 per cent TiO_2, with minor impurities of MnO, MgO, and Cr_2O_3.

Most coastal ilmenites are unaltered or display only incipient alteration, but the entire spectrum of alteration products from ilmenite to rutile or anatase, is observed. Transmission electron microscopy of weathered ilmenites reveals that ilmenite commonly alters to pseudorutile and then to rutile or anatase, as described by Teufer and Temple (1966) and Grey and Reid (1975). Ilmenite may also alter directly to rutile (or anatase) in a single-stage process. In addition, ilmenite altered by high temperature oxidation and hydrothermal processes is found in the deposits. There is good mineralogical evidence that the alteration of ilmenites found in the coastal sediments is best described by a multistage model, in which some ilmenite grains were altered prior to final deposition.

Other common iron-titanium oxides in the deposits include magnetite, rutile and hematite, which may occur as discrete grains or as composite grains of two or more oxides. Ilmenite and magnetite in the coastal sediments are derived from rocks of both the Karoo Igneous Province and the Natal Basement, while rutile is derived solely from the latter. Ilmenites from certain rock groups may be distinguished on the basis of their chemical composition. However, magnetite chemistry is a better indicator of provenance, and

magnetites from the above two sources can be clearly distinguished. The petrography of the iron-titanium oxides may be used as a provenance indicator, but may be misleading, as the proportions of the oxide intergrowths change with transport and weathering.

Variations in the proportions and chemical compositions of iron-titanium oxides and other heavy minerals within the coastal sediments are caused by provenance, selective sorting during deposition, age of the deposit, weathering, and the recent geological history of the area. A model is proposed in this study which describes the formation of the heavy mineral deposits in relationship to the above influences.

PREFACE

The experimental work described in this thesis was carried out in the Department of Geology and Applied Geology, University of Natal, Durban from March 1989 to December 1991, under the supervision of Professor David H. Cornell.

The experimental work related to the transmission electron microscopy study described in this thesis was carried out in the Department of Earth Sciences, University of Cambridge, England from October 1990 to March 1991, under the supervision of Dr Andrew Putnis.

These studies represent original work by the author and have not been submitted in any form to another University. Where use was made of the work of others it has been duly acknowledged in the text.

ACKNOWLEDGEMENTS

This study was made possible by funding from Richards Bay Minerals (RBM) and the Foundation for Research and Development, and I am most grateful for their support. I would also like to thank RBM for the use of their analytical equipment, and numerous other facilities for the preparation of the final manuscript.

I would like to thank:

My supervisor, Professor David Cornell, for his guidance during my research and for meticulously editing several versions of this thesis. I would also like to thank him for arranging my visit to Cambridge University.

Mr John Selby who arranged the funding from Richards Bay Minerals and who maintained a keen interest in the progress of my research.

Dr Andrew Putnis and the many other staff members of the Department of Earth Sciences, University of Cambridge, who helped me during my study visit to this University. Dr Putnis also kindly helped to edit the sections related the transmission electron microscopy study.

Mrs A. Pietersen (née Turner) for drafting the map of the study area.

The Department of Geology, Rhodes University, for the use of their electron microprobe and Mr Rob Skae who assisted with the analytical procedure.

Mr P. Evers and Ms F. McDonald who assisted in the operation of the JEOL JSM-35 and Hitachi 520 scanning electron microscopes.

Dr Ian Grey, CSIRO, Australia, for kindly providing samples of altered ilmenite concentrate from the Capel and Eneabba orebodies.

Ms D. Meth, Ms A. Pietersen (née Turner), Mrs L. Turner and Mr G. Milne of the University of Natal, Durban for providing various samples.

Mr J. Barnes of RBM who supplied a number of borehole samples and proof-read parts of the final manuscript.

All the staff members at RBM who helped with sample preparation and analyses.

Messrs G. Chetty and V. Pakkirri, of the Department of Geology, University of Natal, for preparing numerous polished thin-sections.

Dr Peter Heaney and Dr Gordon Nord for teaching me the "art" of transmission electron microscopy and for enlightening discussions about mineralogy, geology in general, world politics, and the quality of English beer.

I am also in debt to my parents who selflessly supported me through much of my university studies and who have waited patiently for me to finish my doctorate. Finally, I reserve my deepest gratitude for my wife, Janet-Louise Sutherland, for her love and support during this long and arduous undertaking, and for proof-reading numerous versions of this thesis.

TABLE OF CONTENTS

Ms D. Meth, Ms A. Pietersen (née Turner), Mrs L. Turner and Mr G. Milne of the University of Natal, Durban for providing various samples.

Mr J. Barnes of RBM who supplied a number of borehole samples and proof-read parts of the final manuscript.

All the staff members at RBM who helped with sample preparation and analyses.

Messrs G. Chetty and V. Pakkirri, of the Department of Geology, University of Natal, for preparing numerous polished thin-sections.

Dr Peter Heaney and Dr Gordon Nord for teaching me the "art" of transmission electron microscopy and for enlightening discussions about mineralogy, geology in general, world politics, and the quality of English beer.

I am also in debt to my parents who selflessly supported me through much of my university studies and who have waited patiently for me to finish my doctorate. Finally, I reserve my deepest gratitude for my wife, Janet-Louise Sutherland, for her love and support during this long and arduous undertaking, and for proof-reading numerous versions of this thesis.

TABLE OF CONTENTS

CHAPTER ONE

INTRODUCTION

1.1 SOUTH AFRICAN HEAVY MINERAL DEPOSITS

The presence of heavy minerals in beaches and dunes along the coastline of South Africa was discovered in the 1920's (MacPherson, 1982). Heavy mineral deposits are found along the east coast between East London and the Mocambique border, and from Strandfontein to the Orange River mouth along the west coast (Figure 1.1). Demonstrated resources of heavy mineral sands containing ilmenite, rutile, and zircon along the east coast are estimated at 2476 million tons (Wipplinger, 1985). Along the west coast demonstrated resources containing the above minerals are estimated at well over 100 million tons of heavy mineral sands (Wipplinger, 1985).

Heavy mineral deposits have been mined at Umgababa (1960's) and Morgan's Bay (1950's and 1960's) in the past, although these operations were short-lived. The Late Pleistocene-Holocene dunes north of Richards Bay are the only deposit presently being mined. However, a number of companies are either exploring for deposits, or engaged in feasibility studies of lease areas in southern Africa. The production of ilmenite, rutile and zircon has grown steadily since mining operations began at Richards Bay, so that in 1990 South Africa produced 700 000 tonnes of titanium-slag (a beneficiated product of ilmenite), 70 000 tonnes of rutile (Heap, 1991) and 150 000 tonnes of zircon (Skidmore, 1991). After Australia, the country is presently the second largest producer of titanium feedstocks and zircon in the western world. Despite this, very little research has been done on the heavy mineral deposits of South Africa and no specific study of the mineralogy of the titanium-bearing heavy minerals has been undertaken.

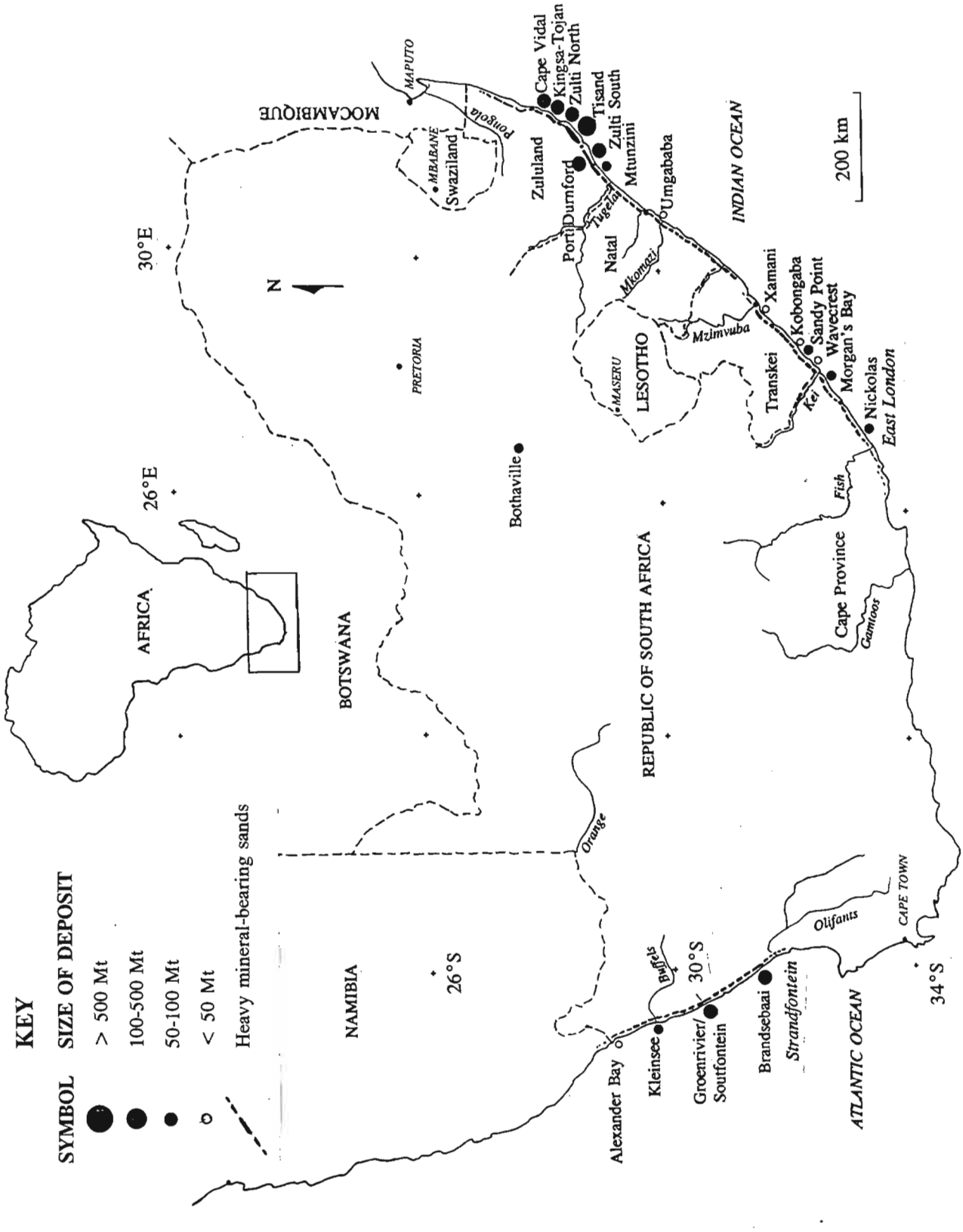

Figure 1.1 Locality map of the heavy mineral provinces in South Africa. Summary descriptions of the heavy mineral deposits are given in Table 3.1 (page 46).

1.2 THE IRON-TITANIUM OXIDES

Titanium-bearing minerals of the system FeO-Fe_2O_3-TiO_2 are ubiquitous to the heavy mineral deposits of South Africa. Ilmenite ($Fe^{2+}Ti^{4+}O_3$) and rutile (TiO_2) are the most important minerals. The first is the most abundant economic mineral in the deposits, and is the largest global resource of titanium. Rutile, although less abundant, is still the major feed used in the production of titanium sponge metal and TiO_2 pigment by the chloride process.

Ilmenite has a wide range of chemical compositions because Mg^{2+}, Mn^{2+} and Fe^{3+} can substitute for Fe^{2+} in the ilmenite structure. The mineral may also contain small quantities of Cr, Zn, Cu, Al, Si and Ca. High levels of these elements lower the quality of an ilmenite concentrate because they decrease the grade of TiO_2 and represent unwanted impurities in titanium feedstocks. The mineral also forms a large variety of intergrowths with other iron-titanium oxides as a result of exsolution, oxidation or hydrothermal processes. Ilmenite "locked" with these phases have different chemical compositions and physical properties to homogeneous ilmenite. Furthermore, ilmenite undergoes alteration in the weathering environment by a process which results in iron being removed from the ilmenite structure and the consequent enrichment of titanium in altered grains, while the physical properties of the mineral are changed. It is well established that the magnetic susceptibility and density of ilmenite decreases as the degree of alteration increases (Temple, 1966; Wort and Jones, 1981; Frost *et al.*, 1986; Larrett and Spencer, 1971). A knowledge and understanding of these variations in ilmenite mineralogy is therefore vital to the exploitation of heavy mineral deposits. It influences not only the grade of deposit, but also the quality and recoverability of ilmenite, which is largely dependent on the chemistry and magnetic susceptibility of the ilmenite grains. In addition, source rocks may be characterised by ilmenite composition and petrography (as well as those of other iron-titanium oxides such as magnetite). These minerals can therefore be used for provenance studies as demonstrated by Darby (1984), Basu and Molinaroli (1989) and Grigsby (1990).

1.3 SCOPE AND OBJECTIVES

This work represents a comprehensive study of titanium-bearing oxides in deposits along the east coast of South Africa. This study area was chosen for a number of reasons. The geological and geographical variations, in source rocks, shoreline morphology and climatic conditions along this coastline, were expected to lead to variations in the titanium-bearing minerals and the heavy mineral suites. The deposits are accessible and easy to sample whereas access to many of the west coast deposits is restricted as they are within the lease areas of diamond mines. Furthermore, the mining operation at Richards Bay provides a "type deposit" with which other east coast deposits can be compared in terms of mineral quality and recoverability. Although this work focuses on titanium-bearing oxides in the east coast deposits, some comparisons are made with minerals from the west coast, and from other countries, such as Australia and North America.

The overall objective of this work is to gain a greater knowledge and understanding of the chemical and physical properties of the titanium-bearing oxides in heavy mineral deposits. This will aid the exploration for, and recovery of, the strategic metal titanium. The study is largely qualitative and no attempt is made to provide quantitative data concerning the grade and size of deposits. The following aspects of the titanium-bearing oxides are covered:

1. A mineralogical description of these minerals in terms of petrography, chemistry and physical properties.
2. A description of ilmenite alteration, a study of the degree of alteration in different environments, and a discussion of alteration mechanisms, compared with those of previous authors.
3. The determination of the source rocks of the iron-titanium oxides.
4. The determination of variations in the proportions, chemical and physical properties of titanium-bearing minerals along the coastline and in different types of deposits (eg. beach and dune).
5. The reasons for the variations mentioned in 4 and the implications these hold for exploration and exploitation.

1.4 OUTLINE OF THESIS

Chapter 2 provides an introduction to the geology, mineralogy, production and uses of titanium. The major rock and sedimentary titanium deposits of the world are outlined and the South Africa deposits are placed in a global context.

The geological and geomorphological setting of the heavy mineral occurrences of the study area is outlined in Chapter 3. The coastline is divided into 4 regions, according to shoreline morphology, geographical setting and provenance, and the heavy mineral deposits within each of these regions is described. The regional geology of the study area is described, as this influences the provenance and formation of the deposits. Chapter 4 describes the sampling and analytical techniques used in the study.

The mineralogy of the iron-titanium oxides is described in detail in Chapter 5. Emphasis is placed on the chemical and petrological variations originating in the source rocks, as these are preserved during erosion and transportation and provide important clues to the provenance of the oxide grains.

Chapter 6 describes a study of the alteration of ilmenite in the weathering environment. This includes a transmission electron microscope study of altered ilmenites from Australia and South Africa, together with detailed petrographic examination of ilmenite alteration in the study area. Three types of ilmenite alteration are found in the South African deposits, and a model is proposed for the paragenesis of altered ilmenite in the coastal deposits.

The provenance of the iron-titanium oxides is investigated in Chapter 7. Source rocks are identified and the chemistry and petrography of ilmenite and magnetite is used to distinguish these minerals from different rock types.

Chapter 8 describes the variations in heavy minerals and iron-titanium oxides found in the coastal sediments. The influences of the energy of the depositional environment, age, geographical location, and provenance are investigated. Finally, a model for the formation of the heavy mineral deposits is proposed. The findings of the study are summarised in Chapter 9.

CHAPTER TWO

THE GEOLOGY, MINING AND USES OF TITANIUM

This chapter serves as a brief introduction to the metal titanium, its mineralogical and geological occurrence, mining, production and uses. The South African deposits are placed in a global perspective.

2.1 TITANIUM - THE METAL

Titanium (Z = 22, A = 47.88) is the ninth most abundant of all elements and comprises 0.6 per cent of the earth's crust by weight. It was discovered by William Gregor in 1791 (Williams, 1974). The metal has a melting point of 1667°C, is less dense than iron (4.25 $g.cm^{-3}$ compared to 7.87 $g.cm^{-3}$ at 20°C), yet is almost as strong as steel and nearly as resistant to corrosion as platinum (Hammerbeck, 1976). The metal's very high strength/density ratio makes it ideally suited to the manufacture of strong, light-weight alloys. This ratio is up to two times that of stainless steels, while some titanium alloys with characteristics similar to high-strength steel are only 60 per cent as dense (Knittel, 1983).

Titanium dioxide (TiO_2) is a white pigment without equal as it has a high opacity, is chemically inert and non-toxic, and is relatively inexpensive. The pigment is produced by two methods - the sulphate method, which uses ilmenite as a feedstock and the chloride method which uses rutile and beneficiated ilmenite products as feedstock. At present the greatest demand for the metal is as titanium dioxide and only about 5 per cent of titanium minerals produced is consumed in the production of titanium metal (Towner, 1988).

2.2 MINERALOGICAL AND GEOLOGICAL OCCURRENCE

2.2.1 Mineralogy

Titanium occurs in the crust in two predominant minerals: ilmenite and rutile. Ilmenite is a common accessory mineral in many igneous and metamorphic rocks. The mineral can contain up to 6 per cent Fe_2O_3 (Ramdohr, 1950) and forms an extensive solid solution with hematite at temperatures above 600°C. Magnesium and manganese may substitute for ferrous iron in ilmenite, giving rise to the rare end-members geikeilite ($MgTiO_3$) and pyrophanite ($MnTiO_3$).

Ilmenite is a common detrital mineral in sediments. In near-surface environments it often undergoes alteration by a process in which the iron is oxidised and leached from the ilmenite grain, resulting in the enrichment of titanium until it consists of TiO_2, either in the form of rutile or anatase. Rutile is stable over a wide range of geological conditions and consequently is a widespread accessory mineral in metamorphic gneisses and schists and in some igneous rocks such as pegmatites. Its stability and hardness result in rutile being a common detrital mineral. Other major titanium-bearing minerals include anatase and brookite (the low temperature polymorphs of rutile), perovskite ($CaTiO_3$), sphene ($CaTiSiO_5$), titanomagnetite and titanohematite. Anatase is usually formed by the alteration of other titanium minerals, is a minor constituent of some igneous and metamorphic rocks and is commonly found in granite pegmatites and hydrothermal veins, or as an authigenic mineral in sediments. Titanium is also found in a number of other minerals and a summary of the major and minor titanium-bearing minerals is given in Table 2.1. More detailed descriptions of the common titanium-bearing minerals are given in Chapter 5.

Titanium mineral deposits have been classified by Force (1991). His classification scheme is reproduced in Table 2.2 which clearly shows that the most important economic deposits are those found in igneous rocks and unconsolidated sediments. The world's demonstrated resources of rutile and ilmenite in these deposits are estimated to be 29 million tonnes and

Table 2.1 More common, naturally occurring titanium minerals and their geological occurrence. The silicate minerals - biotite, augite, melanitic garnet, calcic amphiboles - which contain small quantities of titanium are not included in the table.

Mineral/Term	Formula	TiO_2 (%)	Geological Occurrence
Ilmenite	$FeTiO_3$	45-53	Common accessory mineral in most igneous and metamorphic rocks. May reach economic proportions in anorthosite and gabbro. Common detrital mineral.
Rutile	TiO_2	95-100	Common accessory in medium to high grade metamorphic rocks, also found in granite pegmatite and as accessory in some ore deposits. Common detrital mineral and alteration product of ilmenite and other titanium minerals.
Anatase	TiO_2	95-100	Low-temperature polymorph of rutile. Usually secondary or authigenic, formed by the alteration of other titanium minerals. Also found in hydrothermal veins and granite pegmatite.
Brookite	TiO_2	95-100	Metastable polymorph of rutile and anatase. Found in cavities, fissures and veins. Weathering product of other titanium minerals.
Pseudorutile	$Fe_2Ti_3O_9$	60-65	Alteration product of ilmenite in sediments. Common phase in altered ilmenite concentrate.
Altered ilmenite	$FeTiO_3$ - $Fe_2Ti_3O_9$	53-70	Term for the alteration products of ilmenite consisting of mixtures of ilmenite, pseudorutile and leucoxene. Common in heavy mineral sand.
Leucoxene	high TiO_2	70-100	Term for high TiO_2 alteration products of ilmenite, usually consisting of microcrystalline rutile, or anatase, with minor pseudorutile, ilmenite, hematite or goethite.
Titanite (sphene)	$CaTiSiO_5$	40	Widely distributed accessory mineral in intrusive igneous, low grade metamorphic rocks and as a detrital mineral.
Perovskite	$CaTiO_3$	58	Accessory mineral in subsilicic igneous rocks, chondrite meteorites, contact metamorphic aureoles in carbonate rocks or marble.
Pseudobrookite	Fe_2TiO_5	33	Accessory in rhyolite, quenched dikes, lava flows, and basic igneous rocks. Forms as an oxidation product of ilmenite and titanomagnetite.
Ulvöspinel	Fe_2TiO_4	36	Accessory mineral in basic igneous rocks, usually found as exsolution lamellae in magnetite.
Kennedyite	$Fe_2MgTi_3O_{10}$	62	Isostructural with pseudobrookite, occuring as laths in olivine rich rocks.
Titanomagnetite	$(Fe,Ti)_3O_4$	0-34	Term for optically homogeneous Fe-Ti spinel containing magnetite and ulvöspinel in solid solution. Common accessory in basic igneous rocks
Titanohematite	$(Fe,Ti)_2O_3$	0-30	Term for optically homogeneous hematite-ilmenite$_{ss}$. Common accessory in acid intrusive and anorthosite suites.
Geikielite	$MgTiO_3$	66	Forms solid-solution series with ilmenite. Ilmenites with high geikielite contents are common in kimberlite.
Pyrophanite	$MnTiO_3$	53	Forms solid-solution series with ilmenite. Ilmenite with high pyrophanite contents is found in intrusive acid suites.
Brannerite	$(U,Y,Ca,Fe,Th)_3Ti_5O_{16}$		Found in sedimentary uranium deposits.

Table 2.2 Classification of titanium-mineral deposits and their economic significance (After Force, 1991).

Class	Type	Typical Mineralogy	Importance[1]	Example
1. Metamorphic	a. Eclogite	Rutile	B	Piampaludo, Italy
	b. Aluminosilicate	Rutile	E	Evergreen, Colorado
	c. Ultramafic contact	Rutile	E	Dinning, Maryland
2. Igneous	a. Magmatic ilmenite	Ilmenite	A	Allard Lake, Canada
	b. Anorthosite margin	Rutile, Ilmenite	C	Roseland, Virginia
	c. Albitite	Rutile	E	Kragero, Norway
	d. Alkalic	Perovskite, rutile, brookite	C	Powerhorn, Colorado
3. Hydrothermal	a. Porphyry	Rutile	C	Bingham, Utah
4. Sedimentary	a. Fluvial	Ilmenite, rutile	A	Sierra Leone
	b. Glaciolacustrine	Ilmenite	C	Port Leydon, New York
	d. beach (strandline)	Ilmenite, altered ilmenite, rutile, leucoxene	A	Eneabba, Australia
	e. coastal aeolian	Ilmenite, altered ilmenite, rutile, leucoxene	A	Richards Bay, South Africa
	f. lithified palaeo-beach	Ilmenite, altered ilmenite, rutile, anatase	C	Bothaville, South Africa
5. Weathered	a. Alkali parent rock	Anatase	B	Tapira, Brazil
	b. Mafic parent rock	Ilmenite	D	Roseland, Virginia
	c. Placer parent	Altered ilmenite, leucoxene	A	Trail Ridge, Florida (in part)

[1] A, of great importance; B, of probable great importance in the near future; C, of possible importance; D, of moderate importance; E, of minor importance.

about one billion tonnes, respectively (Table 2.3). Over 70 per cent of the world's ilmenite resources is found within igneous and metamorphic deposits, but these only account for about 40 per cent of the world's annual ilmenite production (Towner, 1986). Nearly all the rutile resources are found in unconsolidated placer deposits. Large resources of anatase (over 60 million tonnes) are found within an alkaline pipe near Tapira, Brazil, however, these deposits have never been fully exploited. South Africa contains the highest demonstrated resources of sedimentary ilmenite in the world (85 million tons) and large resources of rutile (5 million tons).

2.2.2 *Igneous rock deposits*

Ilmenite may be abundant in basic magmatic rocks where it is commonly intergrown with magnetite, hematite, or rarely with rutile. Although enormous resources of ilmenite and titaniferous magnetite may be present in cumulate layers within these rocks, the minerals are often so intimately intergrown that the titanium cannot be recovered. A good example is the titaniferous magnetite layers of the Bushveld Complex, South Africa which are mined for their vanadium contents. Molyneux (1970) reported the presence of 21 magnetite layers, containing between 10-25 per cent TiO_2 (Reynolds 1978a). Von Gruenewalt (1977) estimated the titanium, iron and V_2O_5 resources in the main layers, to a depth of 30 m, to be in the order of 1000 million tonnes of magnetite. However, only minor amounts of ilmenite occur as homogeneous grains and the bulk of the titanium is present as microscopic ilmenite and ulvöspinel intergrowths within magnetite grains that cannot be separated (Reynolds, 1978a). South Africa also has large titanium reserves found within several other igneous complexes, namely the Mambula, Rooiwater, Usushwana complexes and the Kaffirskaal intrusion. The iron-titanium mineralogy of these deposits has been extensively described by Reynolds (1978a, 1978b, 1986a, 1986b, 1986c and 1986d). As with the Bushveld iron-titanium ores, the low grades, beneficiation problems and the high cost of mining prevent the exploitation of these deposits for titanium.

Table 2.3 World demonstrated resources (millions of tons) of rutile, ilmenite and anatase in placer and igneous deposits (1983-1985), estimated by the Bureau of Mineral Resources, Australia (cited by Towner, 1986), and Lynd and Lefond (1983).

Mineral	Country	Placer (Mt)	Hard Rock (Mt)
Rutile	Australia	8	-
	Sierra Leone	3	-
	South Africa	5	-
	India/Sri Lanka	6	-
	USA	2	-
	CIS (e)	3[2]	-
	China	unknown	-
	Italy	-	5[1]
Total		27	5
Ilmenite	Australia	41	-
	South Africa	85	-
	U.S.A. (e)[2]	22	32
	Canada (e)	-	75
	Norway	-	128
	CIS (e)	'large'	212
	India/Sri lanka	60	-
	Finland	-	5
	China (e)	24	192
	Malaysia (e)	3-5	-
	Brazil	4[3]	-
Total		240	644
Anatase	Brazil	-	67[4]

[1] metamorphic rock; [2] e = estimated; [3] from Lynd and Lefond (1983); [4] from Lynd and Lefond (1983), citing Anon. (1980).

Nearly all the economic titanium rock deposits mined at present are found within Precambrian andesine anorthosite massifs (Herz, 1976a). Titanium oxides in these rocks include ilmenite, ilmeno-hematite, ilmeno-magnetite, titanomagnetite, rutile and ulvöspinel (Buddington *et al.*, 1963). Where ilmenite is associated with magnetite these minerals form granular intergrowths, which produce concentrates consisting of homogeneous grains. In deposits where ilmenite is associated with hematite these minerals are intimately intergrown due to exsolution and yield ilmeno-hematite or hemo-ilmenite concentrates (Lynd and Lefond, 1983). A brief description of the more important igneous titanium deposits is given in Table 2.4.

Titanium rock deposits consisting of minerals other than ilmenite are also found, but are far less common and few have been mined. Large resources of anatase and ilmenite are found in a carbonatite pipe, some 6 km in diameter, situated at Tapira, 50 km southeast of Araxá, Brazil (Herz, 1976b). A deposit in southwestern Colorado is estimated to contain about 50 million tonnes of TiO_2 in the form of perovskite (Thompson 1977). More detailed descriptions of titanium minerals found in other rock deposits are given by Force (1976) and Force (1991).

2.2.3 Sedimentary deposits (mineral sands)

Through the processes of weathering and erosion, titanium-bearing minerals are released from the crystalline rocks in which they formed and introduced into fluvial systems which transport the minerals to coastlines. Deposition of these minerals may occur in a number of sedimentary environments, but economic concentrations are most common in beach and dune deposits, formed by wave and wind action respectively. The mechanisms of concentration are described in greater detail in Chapter 3. The sedimentary deposits may be classified into the following types according to sedimentary environment and state of lithification, after Macpherson and Masters (1983):

1. Marine shoreline placers - the heavy minerals are usually concentrated in flat-lying beds or ribbons in beach, near-shore and, less frequently, estuarine environments, which often cannot be distinguished from each other (Baxter, 1977).

Table 2.4 Description of major igneous titanium deposits. Large deposits are also found in China (Brady, 1981) and in the Ural Mountains, Ukraine, but no published data of these deposits is available.

Deposit	Host Rock Type	Ore Genesis	Mineral Assemblage	Grades/Resources	References
Allard Lake District, Quebec, Canada Lac Tio = major deposit	Precambian anorthosite and gabbroic anorthosite in the Morin series	late magmatic segregation and injection into fractures within cooling anorthosite. disseminated ore bodies represent magmas, in which incomplete segregation occurred	massive, coarse-grained ilmenite-hematite lodes in anorthosite; disseminated Ti-magnetite, ilmenite-$hematite_{ss}$ in gabbroic rock	100 Mt of ilmenite containing 32 per cent TiO_2 and 36 % Fe	Rose (1969), Hammond (1952), Gillson (1932)
Storgangen, Tellnes and Rodsand deposits, southwestern Norway	Precambrian Egersund-Ogna anorthosite massif	magmatic differentation from same leuconorite magma as surrounding anorthosite, and intrusion into earlier-formed anorthosites	ilmenite with minor exsolved hematite and granular magnetite	Tellnes deposit - about 200 Mt of ilmenite containing about 45 % TiO_2, 34 % FeO and 12.5 % Fe_2O_3.	Geis (1971), Dybdahl(1960), Bugge (1978), Anon (1978)
Sanford Lake District, Adirondack Mountains, USA	orebodies located within anorthosite and gabbro in large anorthositic massif	magmatic segregation as a result of gravitation segregation and filter-pressing of the residual melt by injection into the wall-rock	ilmenite associated with titaniferous magnetite and minor ulvospinel	Grades range from 9.5 to 30 % TiO_2. 0.5 % V_2O_5 occurs within magnetite	Buddington *et al.* (1955), Evrand (1949)
Otanmaki deposit, Finland	orebodies occur in hundreds of lenses located along the contacts between amphibolite and anorthosite of the Otanmaki complex	intrusive bodies of ilmenite and magnetite	ilmenite associated with granular magnetite, minor $ilmenite\text{-}hematite_{ss}$	25 Mt containing about 30 % ilmenite and 40% magnetite, 0.26 % V_2O_5	Harki (1956), Isokangas (1978)

2. Aeolian - the heavy minerals occur disseminated throughout dunes or concentrated in stringers along dune foresets.
3. Alluvial placers - these are less common than the previous two types of deposit, but economic occurrences are known to occur, for example, the rutile deposits mined in Sierra Leone and the tin deposits in Malaysia, which produce ilmenite as a by-product.
4. Lacustrine - such deposits are uncommon, but an example is the Lake Huron deposits, Canada (Martini, 1975).
5. Palaeo-placers - these may consist of either the lithified or unlithified equivalents of the above deposits, which have been preserved for a sufficient period to allow for lithological changes to occur, such as lithification, or mineral alteration which results in iron staining of grains and the increase in clay content in deposits. Such deposits are usually found some distance from present day coastlines. The fossil beach deposits in the Vryheid Formation (Karoo Sequence) are an example of lithified palaeo-placer deposits (Behr, 1965; Behr, 1986)

Some features of important sedimentary deposits are summarised in Table 2.5. Although the TiO_2 composition of unaltered ilmenite is between 45 to 52 per cent, the TiO_2 contents of ilmenite concentrates from different deposits may be much higher (up to 70 %) depending on the degree of alteration of ilmenite in the deposit. Further information concerning these deposits may be found in Lynd and Lefond (1983) and Force (1991), who describe the major world occurrences in detail.

Table 2.5 Description of the important sedimentary titanium deposits.

Province	Deposit & Company	Type	Age	HMS[1]	Resources	References
Western Australia, Bunbury-Busselton area	South Capel, Capel (AMC)	palaeo-beach placer	Early Pleistocene	ilmenite - 75 % rutile - 1 zircon - 9 monazite - 0.5 leucoxene -	7.9 Mt heavy minerals	Welch, *et al.* (1975)
	North Capel, Capel (Westralian Sands Ltd.)	palaeo-beach placer	Bassendean age, 70 - 100 thousand years B.P.	ilmenite - 84 % zircon - 4 rutile - 1 monazite - 0.2 leucoxene -		Welch, *et al.* (1975)
	Yoganup and Boyanup, Bunbury (Westralian Sands Ltd.)	palaeo-beach placer	Late Pliocene	ilmenite - 75 to 86 zircon - 5 to 18 rutile - 0.4 to 1.5 monazite - 0.2 to 1.1 leucoxene		Welch, *et al.* (1975) Baxter (1977) Masters (1989)
	Minninup, Capel (Cable Sands Ltd.)	beach and dune, associated with a prograding beach	Holocene, 4000 B.P. to present	ilmenite: 77 % zircon: 2-6 % rutile: 0.8-2 %		Baxter (1977)
Western Australia, Waroona line	Waroona, Hamel (Cable Sands Ltd.)	palaeo-lacustrine, fluviatile, aeolian and beach placer	Early Pleistocene	ilmenite - 80-82 zircon 4-5 leucoxene 1-3		Baxter (1977)
Western Australia, Eneabba area	Eneabba (Allied Eneabba, subsidiary of AMC Ltd.)	palaeo-beach placer palaeo-dune	Early Pleistocene to Late Tertiary	ilmenite - 60 rutile - 12 zircon - 24 monazite - 2 leucoxene - 2	20 Mt heavy minerals	Baxter (1977) Lissiman and Oxenford (1975, 1973)
Western Australia, Jurien	Cooljarloo, Jurien (Minproc Chemicals and KMCC W.A Ltd.)	environment of deposits not known		ilmenite 60 % zircon 12 % rutile 5 % monazite and leucox.	569 Mt reserves, containing 19 Mt heavy minerals: 11.8 Mt ilmenite 0.8 Mt rutile 2.1 Mt zircon	Anon (1989) Baxter (1977) Anon (1991a) Moore (1990)

[1] HMS = Heavy mineral suite

continued overleaf

Table 2.5 Description of important sedimentary titanium deposits (cont.)

Province	Deposit & Company	Type	Age	HMS[1]	Resources	References
Eastern Australia, Queensland[3]	North Stradbroke Island, Brisbane (CRL[2])	beach strandlines, coastal dunes, transgressive dune systems	Pleistocene	ilmenite 50 % rutile 16 % zircon 12 %	1.5 Mt rutile 1.4 Mt zircon (1985)	McKellar (1975) Towner (1986) Blaskett and Hudson (1967)
Eastern Australia, New South Wales[4]	Tomago, Newcastle (R.Z. Mines Ltd.)	beach barrier, aeolian deposits	Pleistocene to Holocene, 140 000 to 6000 years B.P.	ilmenite rutile zircon monazite	0.35 Mt rutile 0.4 Mt zircon 0.15 Mt ilmenite	
	Stockton and Viney Creek (Mineral Deposits Ltd.)	aeolian		ilmenite rutile zircon monazite	43 000 t rutile 17 000 t zircon	Suttill (1987)
South Africa	Richards Bay, Natal (RBM)	aeolian	Late Pleistocene to Holocene	ilmenite: 50 % zircon: 3 % rutile: 7 % monazite: < 0.5 %	37 Mt ilmenite 4.8 Mt zircon 2.1 Mt rutile	Fockema (1986) MacPherson (1982) Hugo (1988)
	Brandsebaai, Vanrhynsdorp (AAC - project in development)	placer, aeolian cover sands	Late Miocene to Holocene	zircon: 9 % ilmenite: 26 % rutile: 1-2 % (garnet:43 %)	400 Mt heavy mineral sands	Anon (1991b) Coetzee (1957) Smyth (1992) Anon (1992b)
Sierra Leone	Mogbwemo, Sherbo River (Sierra Rutile Ltd.)	alluvial	Tertiary and Pleistocene	rutile (ilmenite)	Up to 30 Mt sand, containing 2-3 % rutile	Spencer and Williams (1964) Anon. (1981)
India	Manavalakurichi	beach placer		ilmenite		Lynd and Lefond (1983)
	Quilon, Kerala (Kerala Minerals and Metals Ltd.)	barrier beach, aeolian			Up to 80 % heavy minerals in beach sands	Lynd *et al.*, (1954).
	Chatrapur, Orissa State (Indian Rare Earths)			ilmenite		

[1] HMS = Heavy mineral suite

continued overleaf

Table 2.5 Description of important sedimentary titanium deposits (cont.)

Province	Deposit & Company	Type	Age	HMS[1]	Resources	References
United States of America	Trail Ridge, Florida (DuPont)	palaeo-shoreline forming broad sand ridge by the reworking of deltaic sediments	Pliocene to Pleistocene	ilmenite (altered) + leucoxene: 45 % zircon (rutile)	4 % heavy minerals	Pirkle and Yoho (1970) Lynd *et al.* (1954)
	Green Cove Springs, Florida (AMC Ltd.)	palaeo-beach ridge		ilmenite (altered) leucoxene, monazite	3 to 4 % heavy minerals	Pirkle *et al.* (1974)
Sri Lanka	Pulmoddai (Ceylon Mineral Sands Corp.)	beach placer along present shoreline	Holocene	ilmenite: 70-75 % rutile: 10-12 % zircon: 8-10 % monazite: ≈ 0.4 %	5 Mt of titanium minerals	Anon (1974) Bailey *et al.* (1956)
Malaysia	Perak and Ipoh	alluvial tin deposits (ilmenite recovered as by product)				
Brazil	Espirito Santo	beach placers along present shoreline	Holocene	ilmenite: 35-75 % monazite: 1-20 % zircon: 5-35 % rutile: 0.5-5 %		Gillson (1950) Lynd *et al.* (1954)
Madagascar	Fort Dauphin (QIT)	beach placer	Pleistocene	alt ilm (rutile, zircon, monazite)	60 million tonnes of sand	Bartle (1988)
Mocambique	Congolone	coastal aeolian	Pleistocene to Holocene	ilmenite: 77 % zircon: 7 % rutile: 2 % monazite: 0.2 %	ilmenite: 4 Mt zircon: 0.4 Mt rutile: 0.1 Mt	Brown and Nossal (1990) Bailey *et al.* (1956)
New Zealand	Barrytown, west coast of South Island (Fletcher Challenge Ltd.)	beach placer	Pleistocene	ilmenite: as high as 44 % of sands (gold)	average ilmenite grade: 12-13 % ilmenite	Mann and James (1986)
CIS (formerly the USSR)	Dnepr River, Ukraine	alluvial placer		ilmenite (rutile and zircon)		Towner (1984)
China, Peoples' Republic of	Guandong-Guangxi coast and Hainan Island	coastal deposits		ilmenite		Towner (1984)

[1] HMS = Heavy mineral suite

2.3 MINING AND RECOVERY OF TITANIUM

2.3.1 General methods

Ilmenite in hard rock deposits is mined by conventional open-cast or underground methods depending on the depth of the deposit and the amount of overburden material. Ore dressing involves comminution followed by concentration using gravity and magnetic separators. As the ilmenite concentrates from these deposits tend to have low TiO_2 values (see Table 2.4) certain mines upgrade the TiO_2 content of their product by smelting the ilmenite to produce pig iron and titanium slag, which commands a far higher price and has greater market uses.

Unconsolidated sedimentary heavy mineral deposits are most commonly mined by suction dredge methods. Artificial ponds are created which contain suction-cutting dredges and floating gravity concentrators. The dredges advance by undercutting and collapsing the exposed face of the ore-body. The released sand is then pumped as a slurry to the concentrator, where it is passed through screens to remove oversize material, such as gravel, boulders and roots. The heavy minerals are separated from the lighter gangue minerals, such as quartz and feldspar, using sluices, spirals or Reichart-cone gravity separators to produce a heavy mineral concentrate. In some instances it is not possible to mine the deposit by dredging because the sediment is too consolidated. Such deposits are excavated by draglines or front-end loaders and the ore is concentrated in gravity concentrators situated close to the mine. The tailings are used as backfill and to reconstruct the original topography. The mined areas are re-vegetated in programs designed to restore the ecology to its former state.

Further processing of the ore is dependent on the heavy mineral suite of the ore body, the grain-size of the minerals (both ore and gangue phases) and the presence of coatings or stainings. Mineral separation circuits are designed specifically for each deposit. Most mineral concentrates are produced using a combination of density, magnetic and electrostatic separators.

2.3.2 Mineral processing at RBM

As an example, the mineral separation at Richards Bay Minerals (RBM) is described briefly and illustrated in Figure 2.1. The dunes are mined by suction dredges which feed the sand to a floating concentrator. Here, gravity circuits are used to separate the heavy minerals from the lighter quartz gangue, which is redeposited in the dunes by tailings stackers. Magnetite is removed by low intensity wet magnets and combined with tailings. The heavy mineral concentrate is transported to the mineral separation plant.

Ilmenite is separated from other phases using wet, high-intensity magnets and is concentrated further by oxidative roasting of the ilmenite concentrate, followed by further magnetic treatment. The roasting process increases the Fe^{3+}/Fe^{2+} ratio within the ilmenite, thus increasing its magnetic susceptibility and allowing the ilmenite to be separated from minerals such as chromite (Lee and Poggi, 1978). This separation is necessary as titanium products with high chromium levels are unsuitable for use as feedstock in the sulphate process of TiO_2 pigment production. The final ilmenite concentrate is upgraded by smelting in arc furnaces to produce titanium slag, containing 85 per cent TiO_2 and molten iron. The iron is tapped off and chemically treated to produce various grades of pig iron, whilst the slag is cooled and then crushed and milled. An alternative method of beneficiating ilmenite is to produce synthetic rutile by a process which reduces and then leaches the ilmenite to produce a product with greater than 90 per cent TiO_2. Lee and Sohn (1989) note that the methods of producing synthetic rutile include: sulfation (Barksdale, 1966; Judd and Palmer, 1973); selective chlorination (Doraiswany *et al.*, 1959; Neurgaonkar *et al.*, 1986); reduction (Yamada, 1976; Kahn, 1984); slagging (Elger and Stickney, 1971; Elger *et al.*, 1986) and sulfidization (Heister *et al.*, 1974).

Material not reporting to ilmenite streams undergoes further density and magnetic separation to produce a monazite stream and a non-magnetic stream which contains rutile and zircon. Small tonnages of monazite are concentrated further by density and magnetic methods to form a monazite product containing approximately 63 per cent total rare earths.

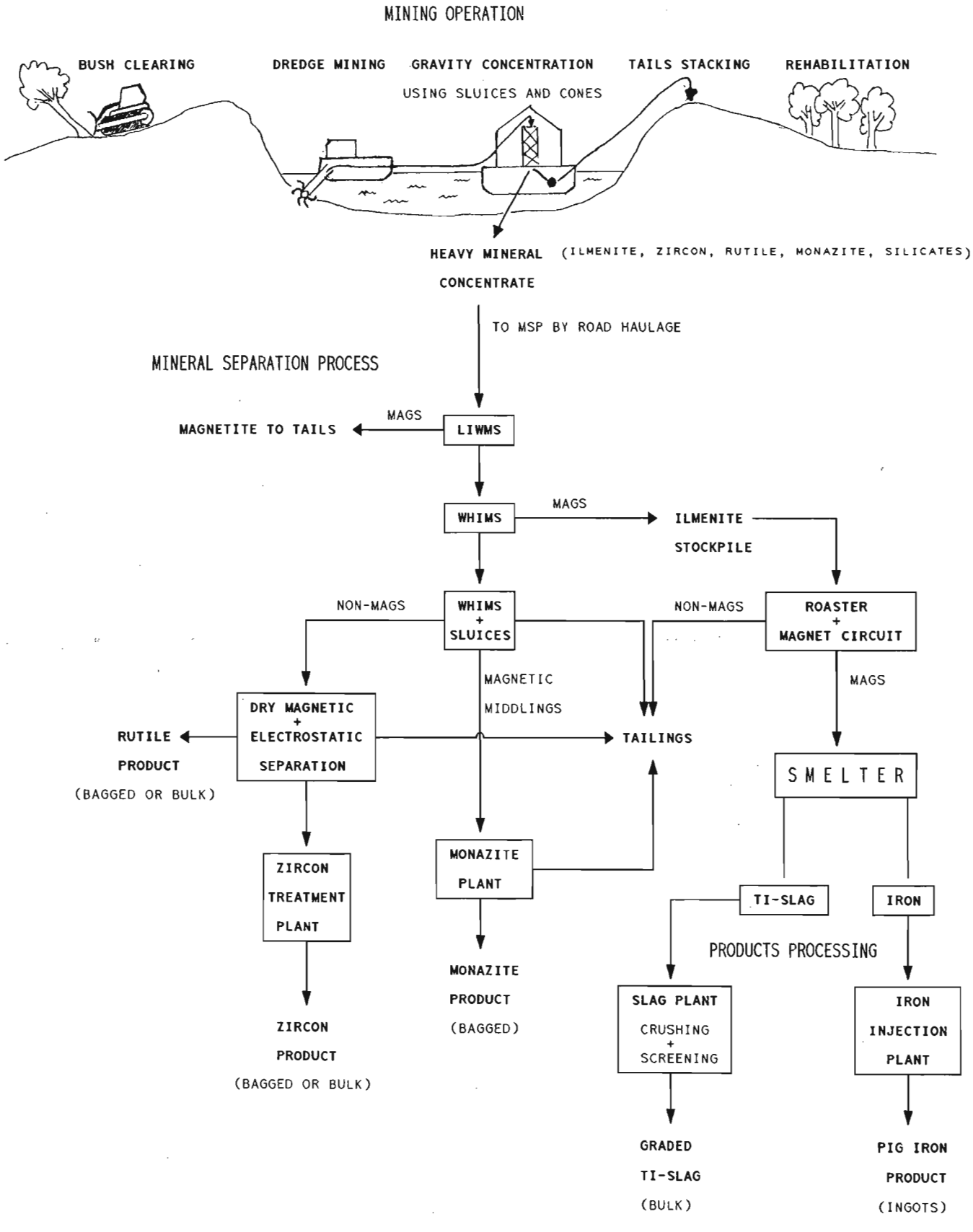

Figure 2.1 Schematic diagram illustrating the mineral processing at Richards Bay Minerals. (LIWMS = low intensity wet magnets; WHIMS = wet high intensity magnets).

Zircon and rutile are separated into two circuits using high-tension electrostatic separators. Impurities are removed from the circuits by further electrostatic and magnetic separations and large silicate grains are removed by screening. The final rutile product consists of about 85 per cent rutile and 15 per cent leucoxene, with minor impurities and contains about 94 per cent TiO_2. The zircon concentrate undergoes leaching in H_2SO_4 to remove iron staining and is then calcined to improve its appearance before being sold. More detailed information about the mining and recovery methods at Richards Bay are given by Lee and Poggi (1978), MacPherson (1982) and Hugo (1988).

2.4 USES OF TITANIUM

2.4.1 Pigment production

Over 90 per cent of titanium ore mined is used in the production of TiO_2 pigment (Anon, 1988). Refraction and reflection of white light occurs at the interface of a pigment and the medium in which it is dispersed and the opacity increases with the number of interfaces. Titanium dioxide has a high refractive index and can be produced with a fine particle size, which makes it an excellent opacifier. TiO_2 pigment is produced by two methods - the sulphate and chloride processes. In the sulphate method, ilmenite or titanium slag are dissolved in concentrated sulphuric acid at high temperatures to form water soluble sulphates:

$$\underset{\text{ilmenite}}{FeTiO_3} + 3H_2SO_4 \rightarrow \underset{\text{solution}}{Ti(SO_4)_2} + \underset{\text{precipitate}}{FeSO_4} + 3H_2O \qquad \text{---- (2.1)}$$

After purification and cooling to remove the iron as $FeSO_4.7H_2O$, the titanium is precipitated in a fine colloidal form by hydrolysis:

$$\underset{\text{solution}}{Ti(SO_4)_2} + 3H_2O \rightarrow \underset{\text{colloid}}{TiO_2.H_2O} + 2H_2SO_4 \qquad \text{---- (2.2)}$$

The addition of small rutile nuclei crystals prior to hydrolysis results in the TiO_2 pigment taking the form of rutile during calcining; without such seed the pigment would have the structure of anatase (Anon, 1988). After calcining the product may be milled to form the optimum particle size of 0.2 to 0.3 μm and is then subjected to surface treatments to produce the desired pigment properties. Rutile pigments are used exclusively in the paint industry as they have a higher refractive index than anatase pigments and are less susceptible to degeneration by ultra violet light.

The chloride process, developed in the 1950's by Du Pont Ltd., originally used only rutile as feedstock. In recent years chloride process producers have devised the technology which allows them to use lower grade feed materials and to blend different types of titanium products for their feed (Gadsden, 1982). In the process, rutile, synthetic rutile or blended high-grade TiO_2 products (greater than 60 % TiO_2) are reacted with chlorine, using coke as a reductant:

$$TiO_2 + 2C + 2Cl_2 \rightarrow TiCl_4 + 2CO \qquad \text{---- (2.3)}$$

The titanium tetrachloride is then superheated in oxygen in a reaction chamber at over 1000°C to form TiO_2 pigment, with the optimum crystal size by the reaction:

$$TiCl_4 + O_2 \rightarrow TiO_2 + 2Cl_2 \qquad \text{---- (2.4)}$$

The chloride process has the following advantages over the sulphate process:

1. The process is simpler than the sulphate method.
2. The $TiCl_4$ made in the intermediate stage can be readily purified by distillation.
3. The chlorine used in the reaction can be recycled, producing small quantities of waste such as iron chloride. In contrast the sulphate process creates large quantities of ferrous sulphate and dilute sulphuric acid pollutants.

Despite the much cheaper price and greater availability of ilmenite feedstock for the sulphate process, the proportion of TiO_2 produced by chloride processes has grown from

nil in the early 1950's to 50 percent in 1990 (Ellis, 1989). This is due to the increasing pressure of environmental legislation in many countries and the preference of pigment consumers for chloride-grade pigment (Heap, 1991). A number of sulphate plants have attempted to overcome their effluent problems by producing gypsum ($CaSO_4$) from their waste H_2SO_4 and by using higher-TiO_2 feedstock to reduce the amount of ferrous sulphate waste (Gadsden, 1982). The sulphate and chloride processes of pigment production are described in greater detail by Lynd and Lefond (1983), Hamor (1986), MacKey (1972a) and Anon (1988).

The bulk of titanium pigments produced is consumed by the paint industry, which uses an estimated 60 per cent of world production. TiO_2 pigments are also used in the paper industry to improve opacity, brightness and printability of paper products, and in the plastics industry to impart whiteness, chemical inertness and ultra violet resistance.

2.4.2 Other uses of titanium

Titanium metal for the aerospace and chemical industries is the second largest use of titanium. The metal is produced in two forms from rutile and other high-grade TiO_2 products: titanium sponge and ingots. Prior to 1970 titanium alloys were almost exclusively used in the aerospace industry, where their high strength/density ratio and high melting point were utilised in the manufacture of jet engine parts and structural parts in aircraft (Knittel, 1983). By the mid-1980's only 63 per cent of titanium metals were consumed by the aerospace industry. The metal is now also used by power stations for heat exchanger tubing and in desalination, chemical and petroleum plants where the strength, heat and corrosive resistant properties of the metal are used to protect processing equipment (Knittel, 1983; Lynd and Lefond, 1983).

Rutile is also used in electronic components where it has good semiconductor properties; as both the active agent and inactive support in catalysts; as coatings for welding rods and as an opacifier in ceramics (Knittel, 1983; Whitehead, 1983).

2.5 PRODUCTION OF TITANIUM MINERALS AND PRODUCTS

The majority of the world's titanium mineral production comes from seven countries - Australia, Canada, South Africa, United States of America, India, Sierra Leone and Malaysia. Australia is the world's dominant producer of both rutile and ilmenite, producing about 50 per cent of the world's annual supply for both minerals (Heap, 1991). In contrast, the production and consumption of TiO_2 pigment, sponge metal and products manufactured from these, is dominated by industrialised countries such as the U.S.A., Japan and European countries. Salient western world production capacity figures and prices for titanium products from 1960 to 1990 are given in Table 2.6. Production statistics for countries with centralised economies (ie. The Peoples' Republic of China and the Commonwealth of Independent States) are erratic and incomplete and are not included in Table 2.6. These figures are drawn primarily from data published in *Australian Mineral Industry Annual Review* and *Metals and Minerals Annual Review* (formerly the *Mining Annual Review*).

The western world production of titanium feedstock has increased steadily over the last 30 years (Figure 2.2). These increases are the result of continued expansion of production capacity of the TiO_2 pigment industry and to a lesser extent, titanium sponge manufacture (see Table 2.6). The growth in production has been encouraged by steadily increasing prices (Figure 2.3), which are the result of strong demand, and often short supply of both feedstock and manufactured goods, coupled with inflation. Since mining operations commenced at Richards Bay, South Africa's share of world rutile and ilmenite (as titanium slag) production has increased continuously (Figure 2.4). A recently completed expansion project at RBM and the development of Anglo American's deposit at Brandsebaai will result in South Africa occupying a leading position as a producer of titanium minerals.

A comparison of the proportions of titanium feedstock produced from 1960 to 1990 reveals a marked increase in the amount of upgraded TiO_2 products produced at the expense of rutile and ilmenite (see Figure 2.2) This is the result of strong demand for high grade TiO_2 feedstock, caused by a shift away from the sulphate process, coupled with the need

to find cheaper and more abundant substitutes for rutile, which is both expensive (about 1½ times the price of any other feedstock) and far less abundant than ilmenite (see Table 2.3, page 12). A further advantage of upgraded ilmenite products, over ilmenite concentrate, is their higher market value; titanium slag and synthetic rutile currently command 3 and 5 times higher prices than ilmenite, respectively (see Figure 2.3). In addition, products such as titanium slag may be used in both pigment processes, increasing marketability. As a result, the demand for ilmenite as a feedstock declined since 1970. In contrast the amount of ilmenite used in the production of titanium slag and synthetic rutile has risen in the same period (Figure 2.5) and since 1987 has exceeded the amount sold as concentrate.

Table 2.6 Summary of Western World titanium production

2.6 A Titanium feedstock production capacity (Mt)

Year	Rutile	Ilmenite Mined	Ilmenite Prod.	Ti Slag	Syn. Rutile	Leucoxene
1960	0.10	1.60	1.16	0.27		
1961	0.10	1.80	1.27	0.33		
1962	0.14	2.08	1.81	0.27		
1963	0.18	2.13	1.80	0.33		
1964	0.19	2.18	1.74	0.43		
1965	0.21	2.74	1.67	0.39		
1966	0.23	2.16	1.78	0.37		
1967	0.26	3.00	1.85	0.42		
1968	0.28	3.17	2.14	0.60		
1969	0.35	3.22	2.33	0.68	0.01	
1970	0.37	4.55	2.69	0.65		
1971	0.41	4.37	2.48	0.77		0.01
1972	0.37	4.50	2.64	0.84		0.02
1973	0.34	4.80	2.71	0.86	0.07	0.02
1974	0.33	4.91	2.90	0.85	0.07	0.01
1975	0.37	4.07	2.53	0.75	0.11	0.01
1976	0.40	4.47	2.77	0.81	0.18	0.01
1977	0.40	4.38	2.94	0.69		0.01
1978	0.33	4.86	3.06	0.85	0.20	0.02
1979	0.37	4.09	3.09	0.91	0.16	0.01
1980	0.44	3.81	2.81	1.30		0.03
1981	0.38	5.66	3.02	1.16		0.04
1982	0.36	4.52	2.39	1.09		0.03
1983	0.34	4.34	2.05	1.05		0.03
1984	0.37	5.02	2.93	1.20	0.22	0.04
1985	0.41	5.11	2.88	1.19	0.22	0.04
1986	0.47	5.99	2.39	1.75	0.36	0.05
1987	0.47	5.78	2.21	1.90	0.36	0.04
1988	0.49	6.08	2.23	1.83	0.43	
1989	0.50	6.52	2.98	1.89	0.44	0.02
1990	0.55	6.97	3.48	1.90	0.45	0.02

2.6B Western world production of ilmenite (Mt/y)

Country	1960	1965	1970	1975	1980	1985	1990
Australia	0.07	0.40	0.73	0.95	1.41	1.43	2.00
Canada	0.40	1.07	0.64	0.75	1.85	1.88	1.76
United States	0.59	0.80	0.79	0.70	0.50	0.29	0.26
South Africa		0.90	0.02		0.33	0.77	1.19
Norway	0.21	0.25	0.55	0.75	0.83	0.74	0.85
Finland		0.93	0.14	0.15	0.16	0.05	
Malaysia	0.11	1.08	0.13	0.15	0.19	0.16	0.50
India	0.22	0.03	0.05	0.10	0.16	0.15	0.30
Spain		0.05	0.03	0.03			
Sri Lanka					0.07	n.a.	0.10
Others		0.10	0.21	0.08	0.30		

2.6C Western World Production of rutile (kilo ton/y)

Country	1960	1965	1970	1975	1980	1985	1990
Australia	79.0	190.0	364.0	342.0	294.0	211.6	280.0
United States	6.9	4.8	0.0	9.1	10.0	30.0	30.0
South Africa	2.8	n.a.	0.0	0.0	48.0	60.0	70.0
Sierra Leone	0.0	n.a.	0.0	0.0	10.0	80.6	150.0
Others	2.0	1.4	4.6	6.0	27.0	30.0	20.0

2.6D Western world production of Ti-Slag (kilo ton/y)

Country	1960	1965	1970	1975	1980	1985	1990
Canada	268	385	650	750	850	800	1100
South Africa					350	450	700
Norway							100

2.6E World Production capacity of synthetic rutile (kilo ton/y)

Country	1986	1987	1988	1989	1990
Australia	60.00	272.00	272.00	270.00	270.00
India	50.00	50.00	50.00	30.00	40.00
Japan	48.00	48.00	48.00	50.00	50.00
United States	100.00	100.00	85.00	90.00	90.00

2.6F Western World production of sponge metal (t/y)

Country	1984	1985	1986	1987	1988	1989	1990
United States	22136	21100	15600	18000	22000	25200	25900
Japan	15413	22260	12500	10000	16400	21300	25100
United Kingdom	2275	2000	200	2000	4800	4900	4200

2.6G Western world production of TiO2 pigment (Mt/y)

Country	1985	1986	1987	1988	1989	1990
United States	0.81	0.98	1.05	1.09	1.23	1.36
W Europe	0.79	1.05	1.05	1.13	1.18	1.17
E Europe	0.08	0.19	0.19	0.20	0.20	0.20
Japan	0.23	0.24	0.24	0.26	0.27	0.27
Australia		0.07	0.07	0.07	0.14	0.10
Others	0.54	0.10	0.10	0.09	0.12	0.15

2.6H Titanium Feedstock prices 1969 - 1991

Year	Rutile A$/t	Ilmenite A$/t	Cand. Slag US$/t	SA Slag US$/t	Syn. Rut. A$/t	Leucoxene A$/t
1969	119	10	45			
1970	140	11	45			
1971	130	12	48			93
1972	115	12	50			76
1973	163	12	61			76.7
1974	330	17	60			76.7
1975	250	17	75			119
1976	235	18	90			154
1977	205	17.5	102	150		147
1978	205	17.5	110	135		134
1979	240	18	115	135	187	147
1980	330	23	135	175	250	208
1981	285	27	150	190	235	206
1982	260	33	150	190	200	207
1983	290	28	162	185		220
1984	425	35	185	198		270
1985	520	55	196	212		269
1986	550	47	213	228		382
1987	620	75	220	230		410
1988	600	73	230	255	376	409
1989	675	85	260	275	442	459
1990	880	87	260	270	484	552
1991	650	90	280	310		520

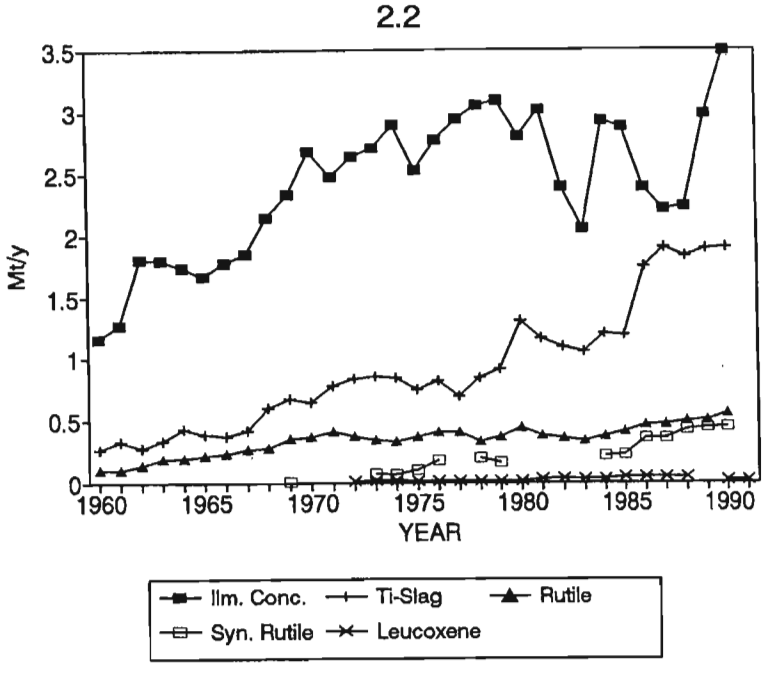

Figure 2.2 Western world production capacity of titanium feedstocks (1960 to 1990). Data from Table 2.6A.

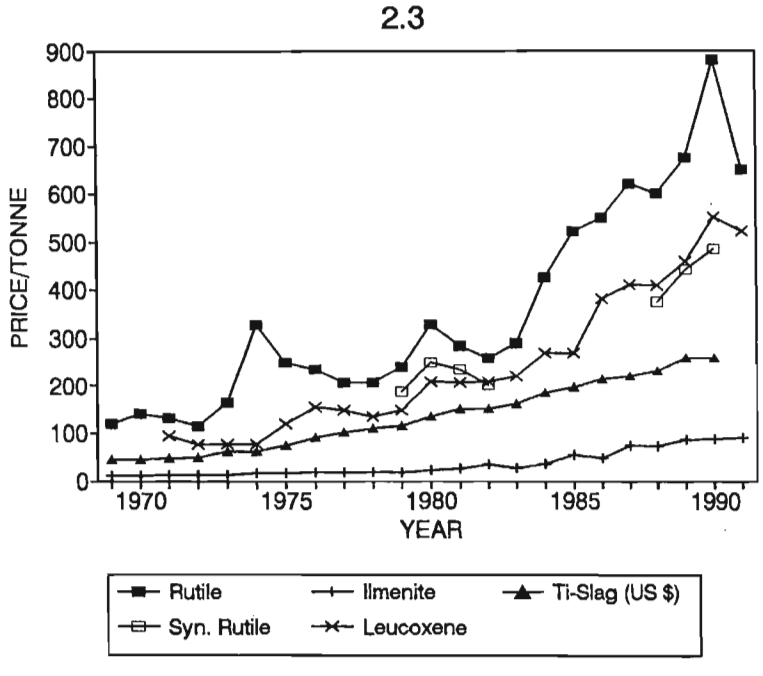

Figure 2.3 Average prices of titanium feedstocks (1969 to 1991) in A $. Data from Table 2.6H. Note that the price of South African Ti-slag is given in US $ (1 US $ is equal to approximately 2.5 A $, at 1993 exchange rates) .

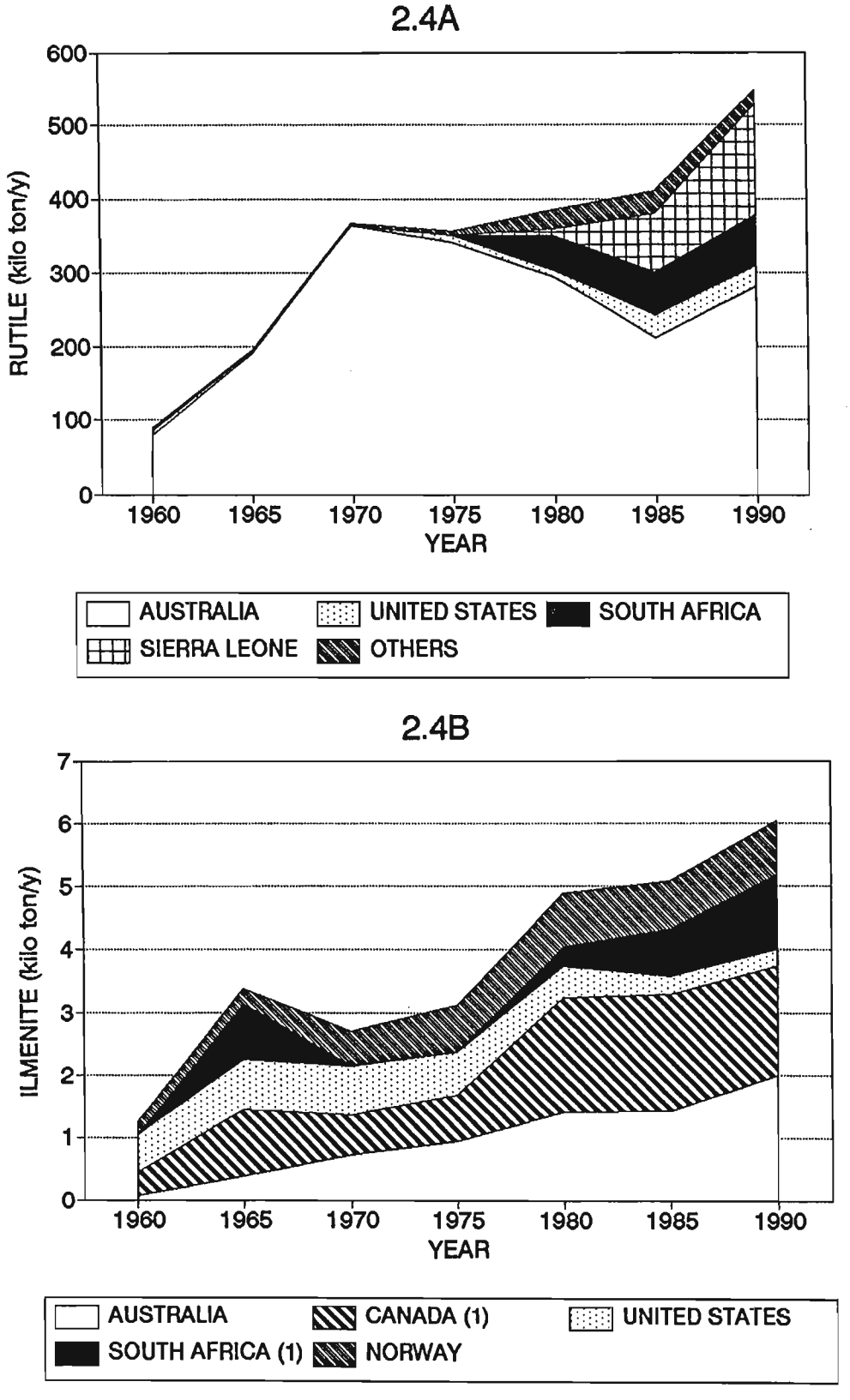

Figure 2.4 **A.** World production capacity of rutile by country (1960 to 1990). **B.** World production capacity of ilmenite by country (1960 to 1990). [1] South African and Canandian ilmenite is used solely for the production of Ti-slag.

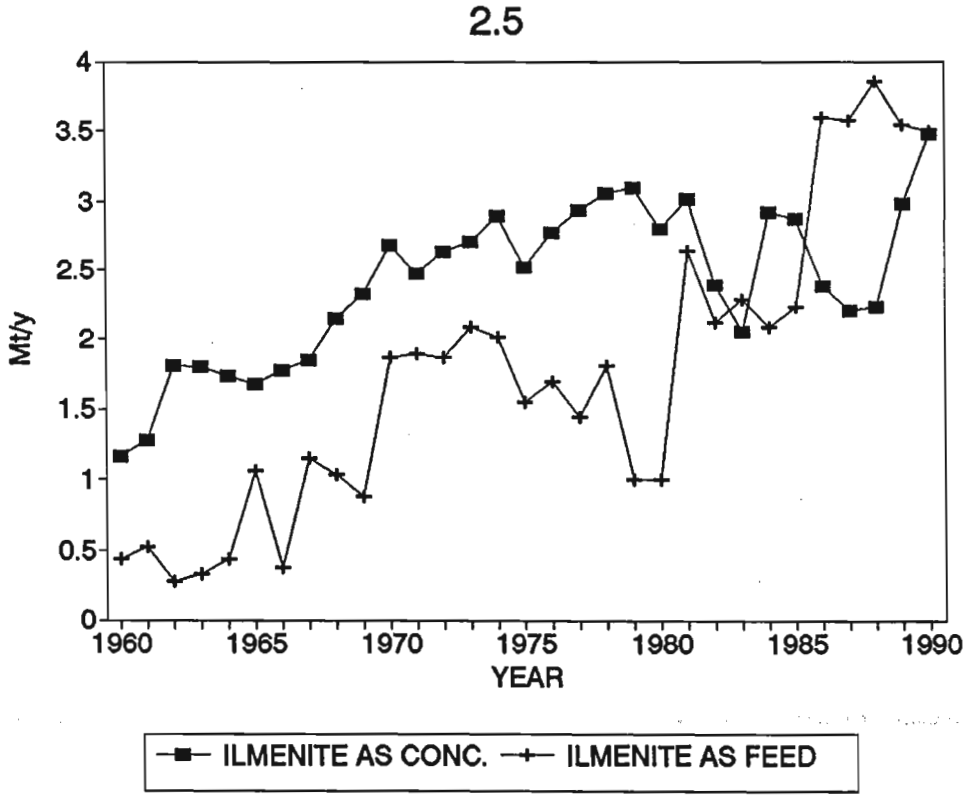

Figure 2.5 Comparison of tonnes ilmenite sold as concentrate and tonnes ilmenite used to produced Ti-slag or synthetic rutile (1960 to 1990).

CHAPTER THREE

GEOLOGICAL AND GEOMORPHOLOGICAL SETTING

3.1 INTRODUCTION

The heavy mineral deposits in the area of study occur within several ages of Cainozoic aeolian sediments. These may form either individual dune cordons, as noted along the Zululand coastal plain, or as complexes containing dunes of different ages stacked against one another. The most economically viable deposits occur in modern dunes, forming high coastal dune ridges or cordons along the Zululand coastline.

A knowledge of the geological and geomorphological setting of these deposits is important if variations in the petrography, distribution and alteration state of titanium-bearing minerals is to be understood. The regional geology within the catchment areas of present-day river systems is outlined to give an indication of provenance and to place the geological history of the study area in context. The coastline may be divided into regions according to shoreline morphology, geographical setting and provenance. The heavy mineral deposits within each of these regions are described in terms of location, sedimentary environment and age.

3.2 REGIONAL GEOLOGY

The outcrop distribution of the major stratigraphic units within the eastern seaboard of South Africa is shown in Map 1 (see enclosed folder). The geology of the area, which ranges from Archean to Holocene, is briefly described in the following sections. The major source rocks of the sedimentary iron-titanium oxides are described in greater detail in Chapter 7.

3.2.1 Kaapvaal Province

Rocks of this Archean province consist mainly of granitoids and gneisses with deformed greenstone relicts, which are overlain by the supracrustal Pongola Sequence.

3.2.2 Natal Metamorphic Province

The Proterozoic Natal Metamorphic Province (*circa* 1250 - 900 Ma) crops out in a series of basement inliers, which cover some 1000 km^2 (Thomas *et al.*, 1990). The province has been subdivided into 3 stratigraphic units by Thomas (1989). The rocks of the northern Tugela Terrane comprise amphibolite, biotite-, hornblende-plagioclase- and quartz-feldspar gneiss, and magnetite quartzite. The central Mzumbe Terrane consists of a sequence of amphibolite-grade gneisses and schists (Mapumulo Group), together with pre- to syn-tectonic granitoid-gneisses. The southern Margate Terrane consists of granulite grade supracrustal gneisses, which have been intruded by various granitoid plutons, which may reach batholithic proportions (Thomas, 1988, 1989).

3.2.3 Natal Group

The sedimentary sequence of the Ordovician-Silurian Natal Group consists predominantly of quartz sandstone, with a basal conglomerate and minor arkosic sandstone, siltstone and shale. The group forms a clastic wedge of varying thickness (from a few metres to over 600 m) and unconformably overlies the basement rocks (Linström, 1987).

3.2.4 Karoo Sequence

The Karoo Sequence ranges in age from Carboniferous to Jurassic and underlies most of the provenance area. The Dwyka Formation diamictite forms the base and unconformably overlies older rocks. It is conformably overlain by continental sandstone and shale of the Ecca and Beaufort Groups and the Molteno and Elliot Formations. These sedimentary rocks formed in fluvio-deltaic and braided river environments at the margins of shallow

inland basins under increasingly arid conditions (Ryan and Whitfield, 1979). The fine-grained, cross-bedded sandstone of the overlying Clarens Formation is generally considered to be aeolian in origin.

The central Karoo Sequence is capped by a thick succession of tholeiitic basalt lava (Drakensberg Formation) of Late Triassic to Jurassic age. To the east, early Jurassic and younger basalt and rhyolite build a thick succession, monoclinally warped to the east, forming the Lebombo-Nuanetsi-Sabi lineament stretching from Natal to Mocambique. Associated with the volcanic rocks are dykes and sills of dolerite and gabbro, which are commonly found within the sediments of the Karoo Sequence, but rarely occur within the Natal Group and basement rocks (Eales *et al.*, 1984). The intrusions, together with less abundant granites, granophyres and undersaturated alkaline rocks, occur over a vast area and demonstrate that the lavas are small erosional remnants of a much thicker and more extensive volcanic sequence (Eales *et al.*, 1984).

3.2.5 Cretaceous Period

The diastrophism of the late Jurassic markedly affected the coastal outline and continental margin of the east coast (Maud, 1961). Early terrigenous conglomerates of the lower Cretaceous Makatini Formation were deposited as alluvial fans on the downwarped margins produced by the breakup of Gondwanaland (Hobday, 1979). These grade upwards and eastwards into cross-bedded sandstone, marine marl and siltstone of the Mzinene and St Lucia Formations, which underlie most of the Zululand coastal plain and are found underlying off-shore sediments (Maud, 1968; Kennedy and Klinger, 1975). The Cretaceous beds show only depositional dips and have not been affected by tectonic movement since their deposition (Maud, 1968). This implies that the major features of the South African landscape were formed before the Cretaceous.

3.2.6 Cainozoic sediments

Owing to the poor fossil record and lack of suitable rocks, no clear dividing line has been established between the Tertiary and Quaternary successions (SACS, 1980) and these periods are described together.

A thin layer (less than 50 m) of early Tertiary (Palaeocene) siltstone disconformably overlies the Upper Cretaceous sediments near the present coastline (Maud and Orr, 1975). Localised developments of a fossil-rich coquinoid limestone and overlying calcarenite, of Late Tertiary age are found at Uloa and a few other localities in Zululand. Southward extensions of these sediments are found overlying Palaeocene sediments in drill-core recovered from Richards Bay (Maud and Orr, 1975).

Quaternary sediments were deposited during a period of fluctuating sea-level as a consequence of continental uplift during the Pliocene to Mid-Pleistocene and glacio-eustatic changes in the Late Pleistocene (Hays and Pitman, 1973; Truswell, 1977). During this period sea levels have stood below the present level (Figure 3.1), except for brief interglacial periods (Williams *et al.*, 1981). Mid to Late Pleistocene sea-levels are characterised by extended periods of glaciation (Riss and Würm periods), separated by the brief Eemian interglacial period (*circa* 130 000 to 115 000 B.P.). The Holocene is characterised by the Flandrian transgression, during which time sea levels have risen from a nadir of more than - 130 m to about 2 m above present level at *circa* 5000 B.P. (Yates *et al.*, 1986; Reddering, 1987). Since this time sea level has dropped to its present level, but is presently rising.

The Quaternary deposits consist of unconsolidated wind-blown sand, aeolianite and beach rock occurring along the modern coastline and the continental shelf and cover the older sediments of the Zululand coastal plain.

3.2.7 Outline of source rocks of heavy minerals

The primary sources of ilmenite and magnetite are a number of rock types from the Natal Metamorphic Province, the Karoo Igneous Province and the Kaapvaal Craton. The primary sources of rutile, zircon and garnet are the Archean and Proterozoic basement rocks (Hammerbeck, 1976; Fockema, 1986). The heavy minerals are also reworked from the sedimentary rocks of Ordovician to Pleistocene age.

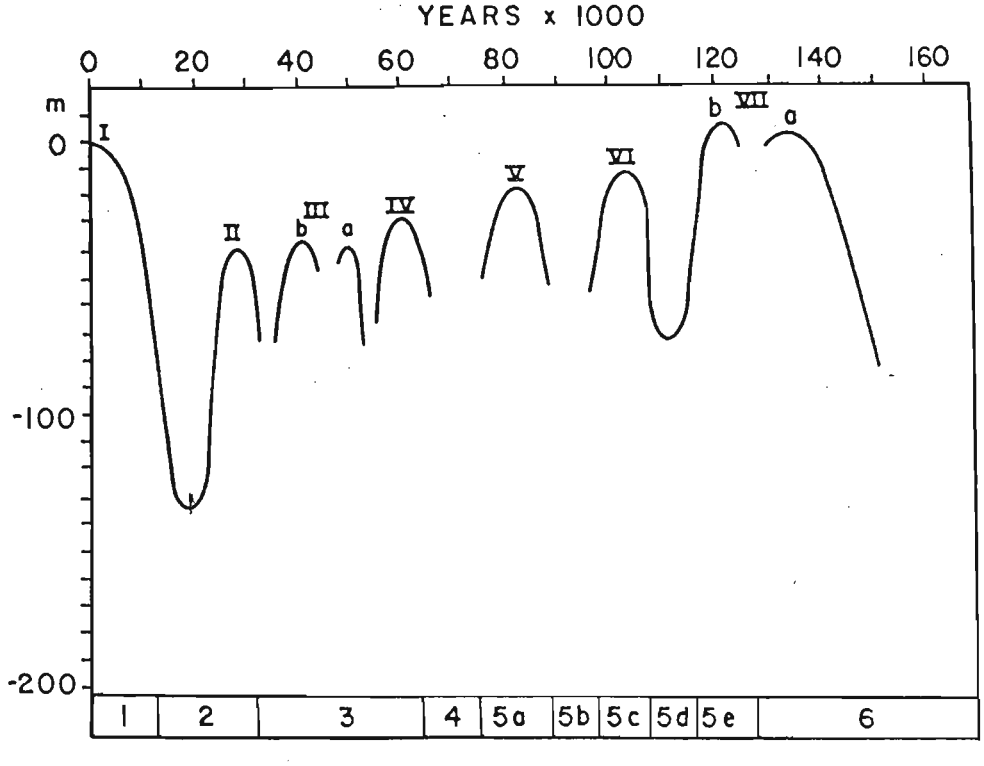

Figure 3.1 Sea-level curve from the Mid-Pleistocene to present relative to present sea-level. After Williams *et al.* (1981).

3.3 GEOMORPHOLOGY OF THE STUDY AREA

3.3.1 General characteristics

Two distinct features of the south-eastern African coast, formed by the breakup of Gondwanaland are the linear coastline, which stretches from south of East London to the Tugela River and the very narrow and steep continental margin. The continental margin (Figure 3.2) may be as narrow as 3 km along parts of the coast, but widens gradually south of Port St. Johns to more than 50 km near Port Elizabeth. The shelf also widens considerably between Durban and Richards Bay where the Tugela Cone is situated. The adjacent continental slope is steep, with values of 12° off the Transkei coast (Flemming, 1981). The shelf break is intermittently dissected by submarine canyons and interrupted by a number of south-facing structural offsets, which may be linked to structural displacements affecting the entire continental margin (Flemming, 1981).

The climate varies from warm temperate in the eastern Cape to sub-tropical north of the Transkei. Rainfall in Natal and Zululand occurs in the summer months, but the Eastern Cape and parts of the Transkei experiences bimodal rainfalls in spring and early autumn. The major winds are bidirectional, alternating between north-easterly and south-westerly winds striking the coastline at an oblique, or semi-parallel direction (Tinley, 1985).

The near-shore zone of the continental shelf is dominated by high-energy, south-westerly swells (Flemming, 1981) and a micro- to macrotidal environment. These swells are refracted to form waves approaching the shore from the south-east. These generate longshore drift of near-shore sediment to the north and the formation of zetaform (half-heart) bays (Tinley, 1985). At present much of the coastline is undergoing erosion due to a global rise in sea level and only isolated areas, such as north of Tugela River, are prograding (McCarthy, 1988a).

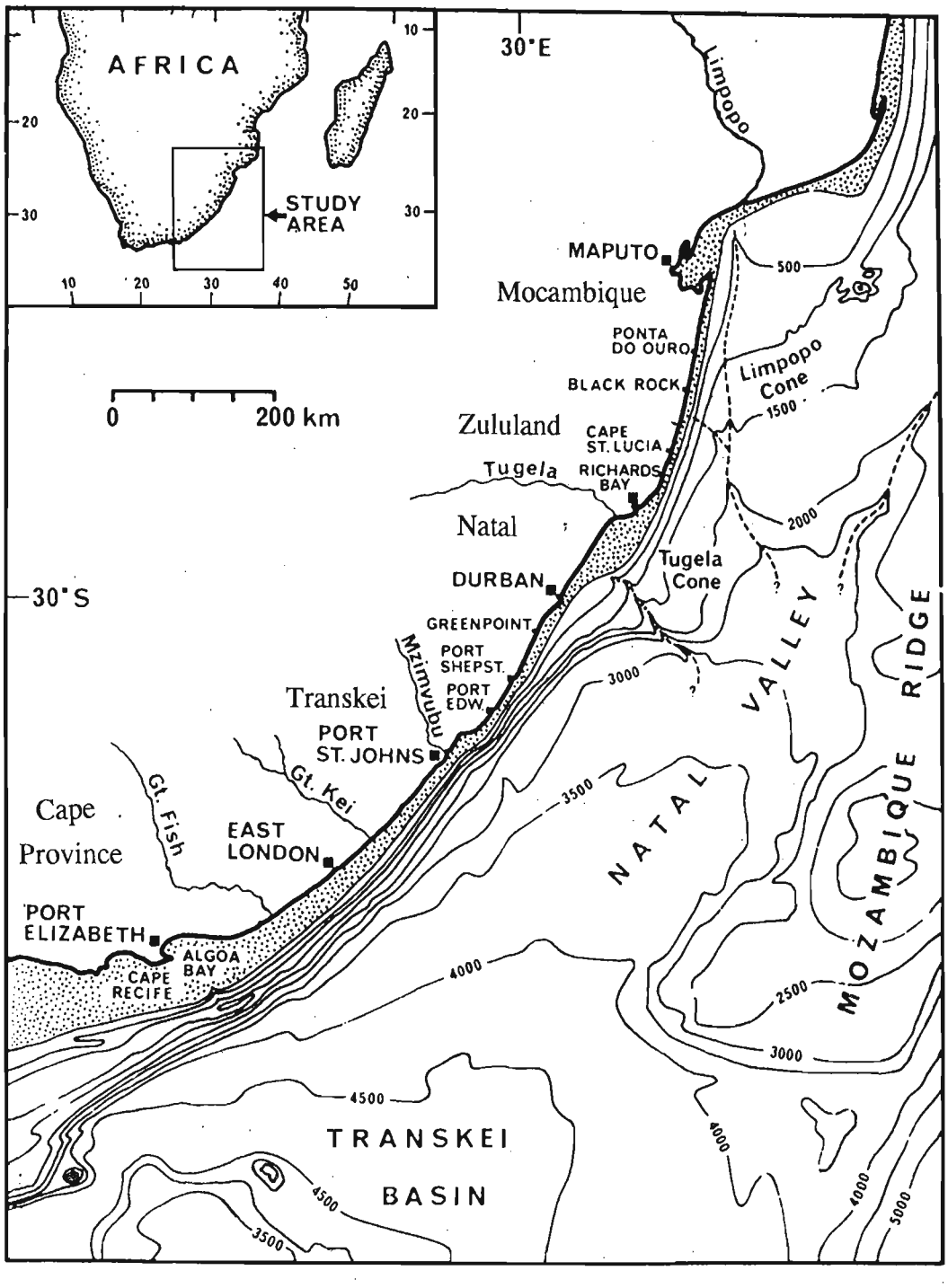

Figure 3.2 Map illustrating the linear coastline, the narrow continental margin and steep continental margin along the east coast of southern Africa. All depth contours are in metres. After Flemming (1981).

The coastline is also characterised by the formation of estuaries and lagoons at river mouths. In many cases the estuaries are isolated from the sea by beach or dune barriers, which are only breached during periods of flood. The estuaries have been formed by the Flandrian marine transgression, flooding river valleys which had incised deeply into coastal rocks during the Late Pleistocene glaciation (Sydow, 1988; Ramsey, 1991). Geomorphologically the study area may be divided into 3 broad regions which are described in the subsequent sections.

3.3.2 Zululand

Parallel dune ridges, typical of a prograding shoreline, are found from Tugela River to Mtunzini (see Map 1). The ridges extend several kilometres inland where they encroach on older fixed dunes. The coarse-grained sandy beaches are extensive and continuous.

A coastal plain of flat-lying sediments and a low elevation extends from Mtunzini northwards into Mocambique (Maud, 1968). The plain widens towards the north and reaches a width of 45 km at the Mocambique border. The coastline consists of a zigzag pattern of linear, coarse-grained sandy beaches cut into unconsolidated aeolian sands (Plate 3.1A). Widely spaced headlands are formed by beach rock and aeolianites (Tinley, 1985). An almost continuous cordon of Late Pleistocene - Holocene dunes occurs adjacent to the modern beaches along the Zululand coast from Port Durnford northwards. The dune cordon is high and narrow and is stabilised by vegetation and forestation (Plate 3.1B).

The major rivers in the area include the Umhlatuze, Umfolozi, Mkuze and Pongola Rivers (Map 1). Access of rivers to the sea has been blocked by the coastal dune cordon and the rivers flow into large, shallow, lakes, such as Lake St Lucia. The mouth of Pongola River is currently situated in Mocambique, but it probably drained into the Indian Ocean near Lake Sibaya during Pleistocene times (Ramsey, 1991). The catchment area of these rivers includes Archean and Proterozoic basement rocks, Karoo sedimentary rocks and the igneous rocks of the Lebombo lineament (Map 1).

Plate 3.1A Coastal dune cordon and partly eroded sandy beach 2 km north of Richards Bay after a heavy storm in July 1992. The shoreline is very dynamic and within 6 months the eroded beach material had been replaced. Note how cobbles and heavy minerals are concentrated on the beach surface by the storm conditions.

Plate 3.1B: Aerial view looking south over Lake Nbablane from the Zulti North orebody (1993), Richards Bay (see Map 1). Note how the densely vegetated dune cordon forms a barrier between the sea and the flat, coastal plain. The dredge mining seen in the foreground is currently taking place both north and south of the Nbablane estuary mouth.

Plate 3.1 A

Plate 3.1 B

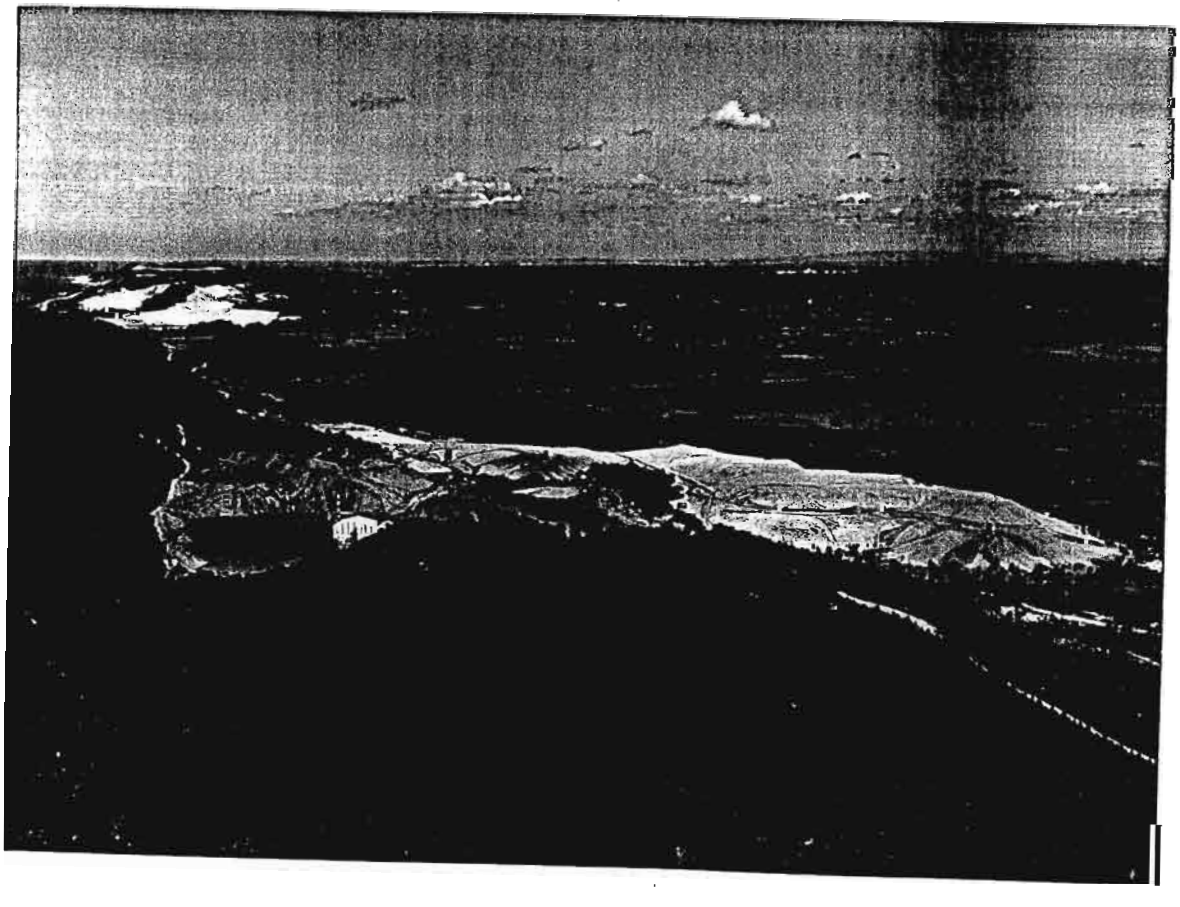

3.3.3 Natal-Transkei

In Natal the coastline consists of irregular rocky headlands and wave-cut platforms separating linear or arcuate beaches. The beaches are narrow and consist predominantly of coarse-grained sands. The beaches are stable and loss of sand during storm periods is replaced by onshore movement of sediment during fair weather periods (Flemming, 1981). A cordon of Pliocene-Pleistocene dunes form a discontinuous ridge up to 120 m high, trending parallel to coast. In places the cordon is adjacent to the beaches and may be partly eroded by shoreline processes, while in other areas the dunes are several kilometres inland, overlying rock at elevations of over 150 m (Maud, 1968). The ridges are heavily dissected by river valleys.

The linear Transkei coast consists mainly of exposed rocky headlands and wavecut platforms dividing small beaches, which consist of coarse sands, shingle and pebbles (Plate 3.2). The Pliocene-Pleistocene dune cordon is not as well preserved as in Natal, but remnants of these dunes are dispersed along the coastline. Modern dunes along the Natal-Transkei coastline are small and active. They are confined mostly to bayheads and river mouths and comprise hummock, blowout and barrier dune types (Tinley, 1985).

The coastal region rises sharply inland and is characterised by steep topography and deeply incised river valleys. Major rivers include the Kei, Mzimvuba, Mtentu and the Mtamvuma Rivers in the Transkei and the Mkomazi, Mgeni and Mvoti Rivers in Natal (Map 1). The Transkei rivers drain catchment areas which consist almost entirely of Karoo sediment, dolerite and basalt. The catchment areas of the northern Transkei rivers also contain outcrops of Natal Group sandstone and basement rocks. In contrast, the Natal rivers drain the entire succession from basement rocks to Karoo basalt (Map 1).

Plate 3.2A View of Xamani Beach, Transkei (Map 1) illustrating the narrow beaches filling embayments between rocky headlands. A small, low dune ridge of recent sands has formed inland of the beach.

Plate 3.2B View of Mgazi River mouth, Transkei (Map 1) showing a remnant of the Pliocene-Pleistocene dune cordon (exposed orange sand on top of ridge) which has been dissected the river.

PLATE 3.2A

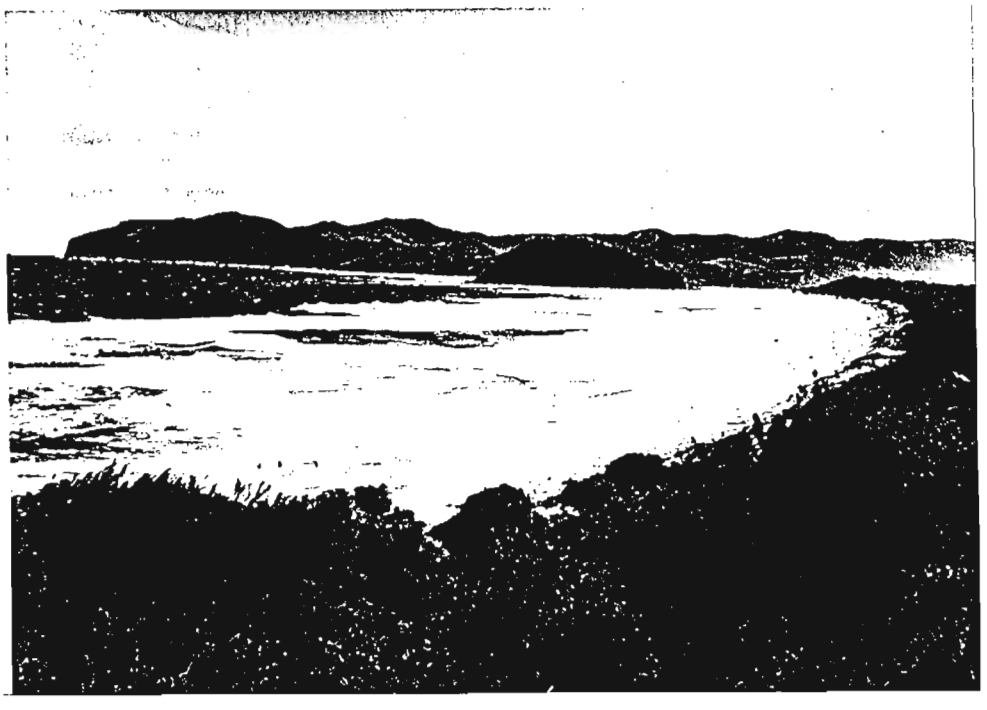

PLATE 3.2B

Plate 3.3A View of the beach immediately south of the Boesmansrivier mouth (Map 1) showing the wide, fine-grained, sandy beaches found along the east Cape coastline. Note the formation of low fore-dunes and the low, vegetated dune cordon in the background.

Plate 3.3B A thick succession of heavy mineral layers found within beach sediment 2 km north of Richards Bay. Layers of heavy minerals in beaches along the east coast of South Africa are typically like those seen at the photograph, but thick concentrates may occur where there is an abundant supply of heavy minerals and the correct energy conditions prevail.

PLATE 3.3A

PLATE 3.3B

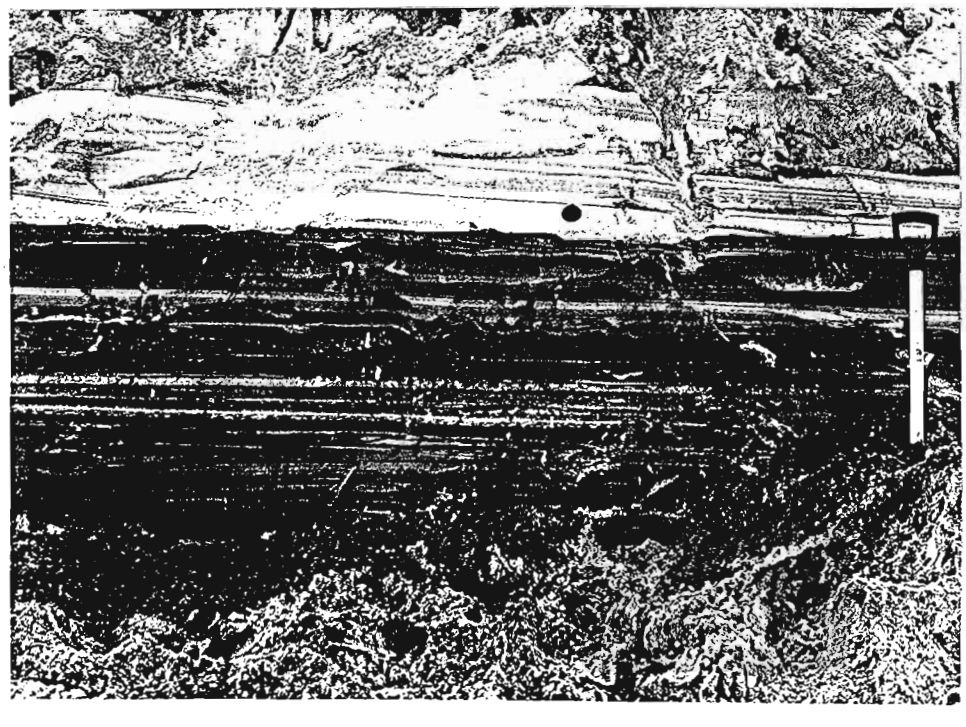

3.3.4 Eastern Cape

From Cape Padrone to East London (Map 1) the coastline consists of large, fine-grained sandy beaches separated by wavecut platforms. North of East London the wavecut platforms become more prominent and the beaches smaller. The entire stretch of coastline contains a vegetated coastal dune field (Plate 3.3A) extending several kilometres inland parallel to the coast. The cordon consists mainly of bidirectional parabolic dunes which reach heights of over 150 m (Tinley, 1985).

The coastal topography is not as steep and rugged as that of Natal and Transkei. The major rivers are the Great Fish and the Great Kei Rivers, which drain catchment areas consisting entirely of Karoo sediment, dolerite and basalt (Map 1).

3.4 GEOLOGICAL SETTING OF THE HEAVY MINERAL DEPOSITS

Heavy minerals are found in most Cainozoic sands and are often concentrated along present-day beaches throughout the area of study (Plate 3.3B). Deposits having demonstrated resources occur in several ages of Cainozoic aeolian sediments, which form individual cordons or dune complexes consisting of dunes of different ages stacked against one another. The aeolian sediments may be broadly sub-divided into older Pliocene-Pleistocene dunes and modern, Late Pleistocene-Holocene dunes that form high coastal dune ridges adjacent to the current coastline. The geological configurations of the deposits depend largely on their region geomorphology and geological settings and they are therefore described by region in the subsequent sections. Demonstrated resources found within the heavy mineral deposits are given in Table 3.1.

Table 3.1 Description of heavy mineral deposits along the east coast of South Africa (see Figure 1.1 and Map 1 for localities).

Region	Deposit	Type	Age	Resources	Economic Minerals	References
Zululand	Tisand ore-body	aeolian	Pleistocene-Holocene	750 Mt	ilmenite, zircon, rutile, monazite, leucoxene	Fockema (1986) Hammerbeck (1976) Hugo (1988) Wipplinger (1985)
	Zulti-North ore-body	aeolian	Pleistocene-Holocene	199 Mt	ilmenite, zircon, rutile, monazite	Fockema (1986) Hammerbeck (1976) Wipplinger (1985)
	Zulti-South ore-body (Port Durnford)	aeolian	Pleistocene-Holocene	395 Mt	ilmenite, zircon, rutile, monazite	Hammerbeck (1976) Wipplinger (1985)
	Cape Vidal	aeolian	Pleistocene-Holocene	104 Mt	ilmenite, rutile, zircon, leucoxene	Hammerbeck (1976) Wipplinger (1985)
	Kingsa-Tojan	aeolian	Pleistocene-Holocene	325 Mt	ilmenite, rutile, zircon, leucoxene	Hammerbeck (1976) Wipplinger (1985)
	Coastal, red dunes, eg. Mtunzini	aeolian	Pleistocene	70 Mt	ilmenite, rutile, zircon	
	Inland, red dunes, eg. Port Durnford and Kwabonambi State forests	aeolian	Pleistocene	unknown	ilmenite, rutile, zircon	
Natal	Umgababa	aeolian (red dunes)	Pleistocene to Holocene	44 Mt	ilmenite, rutile, zircon	Hammerbeck (1976) Wipplinger (1985)
Transkei	Sandy Point	aeolian (reworked beach and red dunes)	Holocene	64 Mt	ilmenite, rutile, zircon	Hammerbeck (1976) Wipplinger (1985)
	Wavecrest	aeolian	Holocene	48 Mt	ilmenite, rutile, zircon	Hammerbeck (1976) Wipplinger (1985)
	Kobongaba	aeolian	Holocene	37 Mt	ilmenite, rutile, zircon	Hammerbeck (1976) Wipplinger (1985)
	Xamani	beach	Holocene	unknown	ilmenite, rutile, zircon	
Eastern Cape	Morgan's Bay	aeolian	Pleistocene to Holocene	64 Mt	ilmenite, rutile, zircon	Hammerbeck (1976) Wipplinger (1985)
	Nickolas	aeolian	Pleistocene to Holocene	64 Mt	ilmenite, rutile, zircon	Wipplinger (1985)

3.4.1 Zululand Coastal dune deposits

3.4.1.1 Port Durnford - Cape St Lucia

The geology of the heavy mineral deposits in the Richards Bay - Port Durnford area (Map 1) is described by Fockema (1986) and Johnson (1986). The mineralised Late Pleistocene-Holocene dunes form a thin, discontinuous cordon extending up to 2 km inland and reach over 90 m in height above sea level (Figure 3.3). The dominant dune type is bidirectional parabolic dunes, although whale-back dunes and reversing buttress dunes are found in some localities. Slightly higher than present sea-levels during the Holocene have resulted in shoreline erosion forming cliffed dunes along the coast.

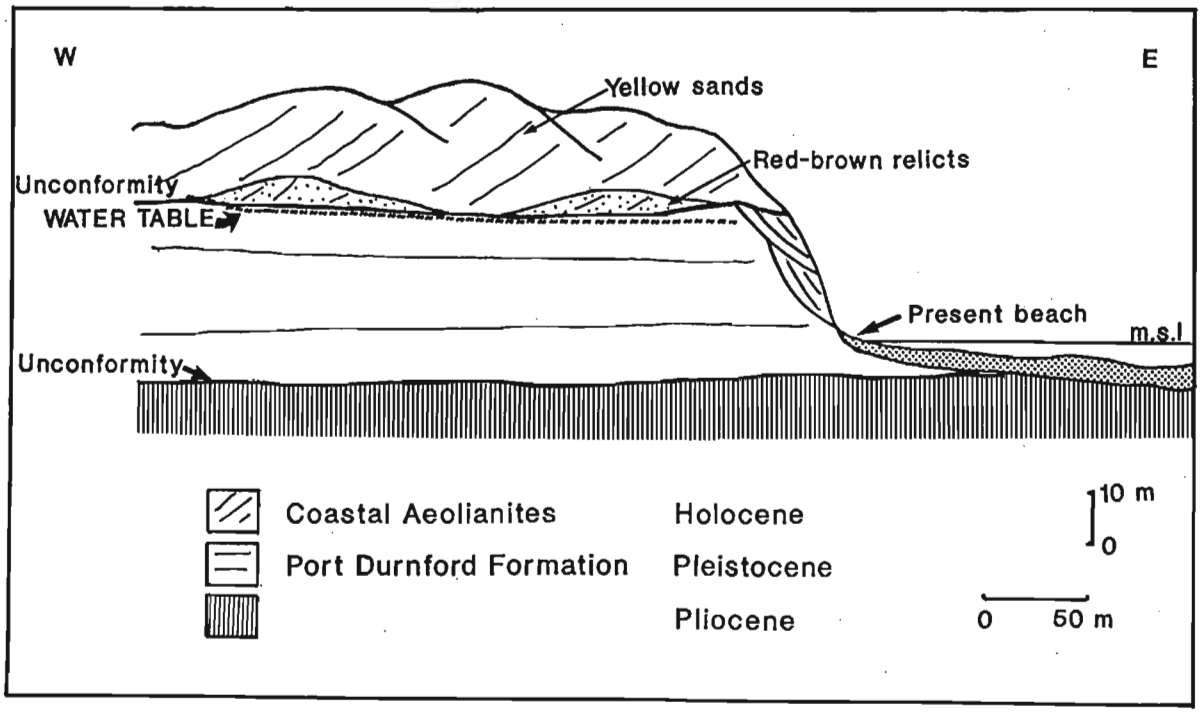

Figure 3.3 Schematic cross-section through the mineralised dunes, Richards Bay. After Johnson (1986) and Hugo and Cornell (1991).

Lithologically the dunes consist predominantly of fine- to medium-grained quartz with variable amounts of heavy minerals and feldspar. Shell fragments and calcareous material are uncommon. The sands tend to be light coloured, unconsolidated and free-flowing, although thin lignite bands may be found in dune troughs. Thin, discontinuous palaeosol horizons are also recognised (Fockema, 1986).

Along the present shoreline, the dunes unconformably overlie the Mid-Pleistocene sediments of the Port Durnford Formation, which represent a barrier-lagoon complex (Hobday and Orme, 1974). Further inland, the dunes rest on the remnants of Pleistocene aeolian sediments and older Holocene lagoon sediments and calcarenites (Johnson, 1986). The base of the dunes lies between 20 and 40 m above sea level and the water table often coincides with this contact (Fockema, 1986). Relicts of an older, reddish-brown dune system are found underlying the abundant yellow-brown dunes (Fockema, 1986). The red dunes have low relief indicating that they have been reworked during the formation of the younger dunes. As the older dunes overlie the Mid-Pleistocene Port Durnford sediments (Fockema, 1986) they are considered to be Late Pleistocene in age. The heavy mineral suites of the older dunes are very similar to those of the younger dunes (Beckering Vinckers, 1986; Fockema, 1986) indicating that they have a similar provenance.

The economic minerals found in the deposits are ilmenite, zircon, rutile and monazite. According to Fockema (1986) the grades of these minerals vary considerably within the deposit, but the ratios between ilmenite, rutile and zircon are fairly constant. Other heavy minerals present include pyroxene, amphibole, garnet, magnetite, hematite and leucoxene, with minor chromite, epidote, apatite, tourmaline, sphene and goethite. The heavy mineral grades range from about 3 per cent to over 15 per cent. Local upgrading by wind erosion also occurs on the landward side of the dunes (Hammerbeck, 1976).

3.4.1.2 Cape St Lucia - Kosi Bay

The mineralised dunes form an almost continuous coastal dune cordon from Cape St Lucia to Mocambique, some 2 km wide and reaching heights of over 170 m above sea level. The topography inland of the dunes is low lying and elevations seldom exceed 20 m above sea level. The dunes consist predominantly of unconsolidated aeolian sands of a Late Pleistocene to Holocene age. The dunes are vegetated and usually covered by younger, Holocene cover sands, but when exposed are composed of bright orange to orange-red, unconsolidated quartz-rich sand (Du Cann, 1976). In some areas thinner, Holocene dune cordons have been superimposed on the older dunes from the east. The morphology of the dunes is similar to those in the Richards Bay area, consisting mainly of bidirectional parabolic dunes. The dunes are partly eroded along the beaches and in some cases form barrier dune systems adjacent to lagoons or lakes such as Lake St Lucia or Lake Sibayi.

The Late Pleistocene sands consist predominantly of quartz, with minor feldspar and shell fragments. Layers of ferruginous sandstone are often found at the base of the dunes as a result of rainwater seepage (Hobday, 1979; Lynn 1989). The heavy mineral suite is similar to that found in the Richards Bay deposits, although Hammerbeck (1976) noted that the proportions of ilmenite decrease from St Lucia to the north.

3.4.2 Older inland dune cordons in Zululand

Along the Zululand coastal plain the older dunes form as many as six north-south trending cordons (Figure 3.4) from the western margin of the plain to the present coastline (Davies, 1976). These dunes have been partially eroded and often redistributed as wind-blown cover sands. The age of the dune cordons is uncertain. McCarthy (1967, 1988b) stated that the older dunes formed during the Pliocene regressions, while others believe that the oldest dunes formed between Pliocene and Pleistocene times (Davies, 1976) and that the other dune cordons are of Mid to Late Pleistocene age (Davies, 1976; Du Preez, 1978; Hobday, 1979). The deep weathered profiles and advanced mineral diagenesis of the older

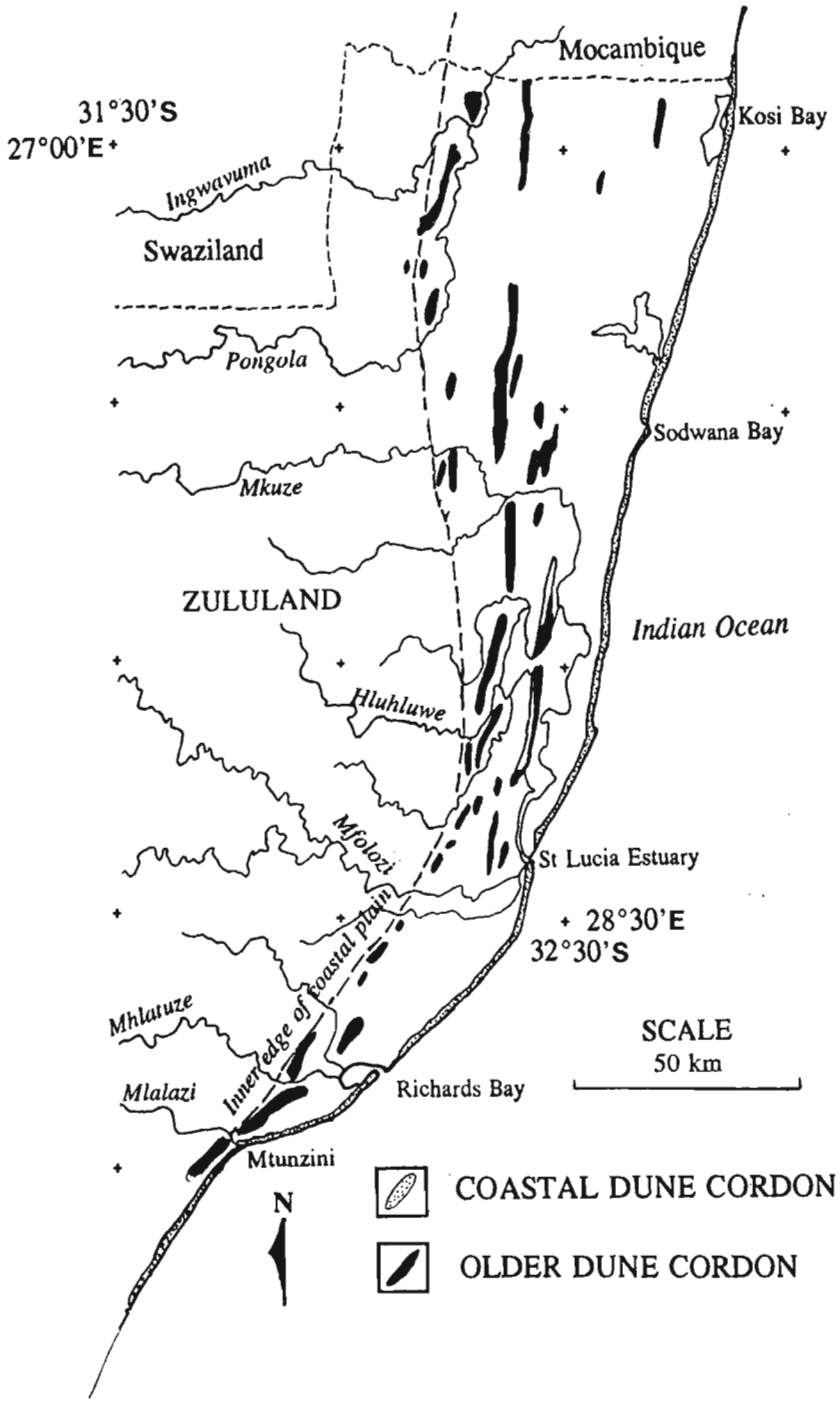

Figure 3.4 Map showing the older dune cordons along the Zululand coastal plain (after Davies, 1976).

dunes (Hobday, 1979) suggests that they were formed at least before the end of the Mid-Pleistocene, when they were subjected to intense tropical weathering during the Eemian interglacial.

The older dunes form broad flat ridges with a maximum height of 30 m and are characterized by their rich red colour, high clay content and deep soil horizons (Hobday, 1979). The younger dunes are steeper and less eroded than the inland dunes and appear to be less weathered. They consist of well-sorted, red-brown to orange-brown sands containing fine-grained, rounded quartz and heavy minerals, with small amounts of kaolin, feldspar and mica and organic material. No published data exists on the heavy mineral content of the different dune cordons.

3.4.3 Natal-Transkei

The heavy mineral deposits along the Natal-Transkei coastline are found within a Pliocene-Pleistocene dune cordon and the smaller Holocene foredune and beach sediments. The aeolian sands often contain a basal layer of conglomerates or gravels up to several metres thick (McCarthy, 1988c) and overlie Pre-Cainozoic rocks of different ages at elevations from 0 m to over 100 m above sea level (Maud, 1968). Like the older dunes along the Zululand coastal plain, the age of the older dunes is uncertain. McCarthy (1967, 1988a, 1988b) maintains that the dunes are Pliocene in age, while other authors (Maud, 1968; Davies, 1976) assign a Pleistocene age to the cordons.

The dunes consist of fine-grained quartz (Maud, 1968) with small amounts of feldspar and shell fragments. They have moderate to high clay contents, which are the result of *in situ* tropical weathering of detrital feldspar and ferromagnesian silicates such as pyroxene and amphibole (pyriboles). The dominant clay mineral is kaolinite (Maud, 1968). The sands are massive, featureless and compact. Their red-brown colour is caused by iron-hydroxide coatings on the surfaces of the quartz grains, which is derived from the alteration of the pyriboles (McCarthy, 1967; Maud, 1968).

The heavy mineral content of the sands ranges from 2 to 25 per cent and averages between 7 to 10 per cent (Hammerbeck, 1976). The heavy mineral suite consists predominantly of ilmenite, with lesser amounts of zircon, rutile and garnet. Minor amounts of pyriboles, magnetite and hematite are also noted. Typical proportions of the heavy mineral suites are given by Hammerbeck (1976) and in Chapter 8 of this study.

The younger Holocene dunes form small blowout and barrier-type dunes which may be superimposed against the older dune cordon. The poor development of these dune systems along much of the Natal-Transkei coast, compared to the Zululand dunes, is a result of the scarcity of fine-grained sand for aeolian transport, combined with an actively eroding shoreline (Tinley, 1985). The aeolian sands have been derived from the reworking of the older dune cordons, together with beach sands and continental shelf sediments exposed during the last glacial maxima (Hammerbeck, 1976; Wipplinger, 1985). The heavy mineral suite of the sands is variable, depending largely on provenance. The common heavy minerals are ilmenite, rutile, zircon, garnet, magnetite and pyriboles.

The more important deposits occur at Umgababa in Natal and Xolobeni, Xamana, Wavecrest, Sandy Point and Kobonqaba in the Transkei (Map 1 and Figure 1.1, page 2). The mineralogy and mineral processing of the Umgababa deposit is described by Nel and Koen (1960) and Langton and Jackson (1961), but details of the geology of these deposits are not found in the literature and only brief descriptions are given by Hammerbeck (1976) and Wipplinger (1985).

3.4.4 Eastern Cape

The grade of heavy minerals in coastal sediments in the eastern Cape is generally much lower than those found further north; only two sub-economic deposits are noted by Wipplinger (1985) and details of these are sketchy.

At Morgan's Bay (Map 1 and Figure 1.1) the heavy mineral deposit is found in young (probably Holocene) aeolian sands resting on an exposed dolerite sill (Wipplinger, 1985).

The unconsolidated sands consist of quartz with small amounts of feldspar. The heavy mineral suite consists of ilmenite, zircon, rutile, with minor magnetite, pyriboles and garnet. The second deposit noted by Wipplinger (1985) occurs near Nickolas, some 40 km south-west of East London, between the Chalumna and Kiwane Rivers (Map 1). Besides the sub-economic resource and grade of the deposit near Nickolas, little is known of its geology.

Generally heavy minerals are found in the Holocene beach and dune sediments along the eastern Cape coast and are most conspicuous near the mouths of major rivers. There is a noticeably decrease in heavy minerals west of the Boesmansrivier mouth (Map 1) and only trace amounts of heavy minerals are found west of Port Elizabeth.

3.5 FORMATION OF HEAVY MINERAL PLACER DEPOSITS

The formation and survival of heavy mineral deposits require the following factors (Baxter, 1977; Lynd and Lefond, 1983; Macpherson and Masters, 1983; Baxter and Devereux, 1986):

1. a provenance for the minerals;
2. transportation (usually fluvial) from the source rocks to an environment where mechanical concentration can occur;
3. mechanical concentration to form the deposit; and
4. preservation from subsequent erosion.

Suitable provenances for heavy minerals usually consist of large areas of exposed basement rocks, particularly granitoids, which have been subjected to intense weathering (Pirkle, 1975; Baxter, 1977). Active erosion of the continent and large perennial river systems ensure that significant volumes of heavy mineral-bearing sediment are transported to the sea. Mechanical sorting along high-energy, micro-tidal coastlines concentrates the heavy minerals as placer deposits in barrier shorelines. These deposits may be reworked several times during sea-level changes until they are eventually deposited by a transgressive-regressive cycle (Hocking *et al.*, 1982; see Figure 1 of Baxter and Devereux, 1986). In

some cases the heavy minerals in barrier systems may be redeposited in coastal dunes by strong onshore winds.

The south-eastern African coastline and particularly the Zululand coastal plain, has all the above critera for the formation of heavy mineral deposits and it is not surprising that large reserves have been found here. Models for the genesis of the deposits and the nature of the heavy mineral concentrate are proposed in Chapter 8.

CHAPTER FOUR

SAMPLING AND ANALYTICAL TECHNIQUES

This chapter describes the sampling and analytical techniques used in the course of the study.

4.1 SAMPLING

4.1.1 Description of samples

The sampling methods attempted to achieve representative samples of the heavy mineral suite and not to determine their quantity in the sediment, as it was not the purpose of this thesis to determine grades within the deposits. The majority of the samples obtained were composite samples, between 5 and 10 kg, consisting of 5 to 15 increments, collected between 0 - 2 m below the surface of the sediments.

The sampling of each environment is described individually, as samples were collected from a range of environments, sometimes for different purposes:

1. *Beaches*: Samples were collected from the swash zones and beach berms of modern day beaches (Appendix A.1).
2. *Dunes*: Because dunes of more than one age are found along the southern African coastline, a distinction was made between the younger Late Pleistocene - Holocene dunes, and the older, red dunes. Both types of dunes were sampled (Appendix A.2) to determine if any differences in the titanium-bearing mineralogy existed, particularly with respect to the degree of alteration of ilmenite. Samples were collected from the slip-faces of dunes. A number of borehole samples were supplied by Richards Bay Minerals.
3. *Rivers*: Samples were collected from major rivers to help determine the general provenance of the titanium-bearing minerals (Appendix A.3). Several tributaries

or streams, exclusively draining one rock-type, were also sampled to determine the nature of the titanium-bearing minerals from that rock-type. Samples were collected from cross-channel and side-channel bars.

4. *Rock samples*: A number of possible source rocks were sampled to study the titanium-bearing minerals within these rocks (Appendix A.4). Usually rock samples of about 5 kg were collected from selected outcrops. Rock samples were also kindly supplied by Deanna Meth, Audrey Pietersen (née Turner), and George Milne (Department of Geology, University of Natal, Durban) and Leslie Turner (Department of Chemical Engineering, University of Natal, Durban).

4.1.2 Sample localities

Sample localities are listed in Appendix A and the distribution of sampling sites within the study area is shown in Map 1. The localities were chosen to conform to one or more of the following criteria:

1. Economic or sub-economic heavy mineral deposit.
2. The existence of heavy mineral-rich layers within the sediment or rock was previously described, or was observed by the author.
3. Heavy mineral-bearing sediments from beach, dunes and rivers occurred in close proximity to each other, so that the influence of depositional environment on heavy minerals from the same provenance area could be studied.
4. The sampling site was accessible.
5. A sample was required to obtain an even geographical distribution of samples.

4.2 SAMPLE PREPARATION

4.2.1 General preparation

A general preparation procedure was used for sand samples for microscopic examination (summarised in Figure 4.1). Samples were split using a rotary splitter and a portion of the original sample was stored. A second portion was wet sieved to remove the $< 63\ \mu m$

fraction. This step is necessary to ensure clean separation during heavy liquid concentration of the heavy minerals, although it is recognised that some silt-sized titanium-bearing minerals are lost in the process. Samples were then dried before undergoing heavy liquid separation using TBE (tetrabromoethane, s.g. = 2.95 $g.cm^{-3}$) to concentrate the heavy minerals. Polished thin-sections were made from the heavy mineral concentrates (HMC's) and studied using reflected light microscopy and scanning electron microscopy, to identify the titanium-bearing minerals and examine their textural relationships. These sections were also used for point-counting to determine mineral proportions in the samples.

4.2.2 Detailed preparation

A more detailed preparation procedure (Figure 4.2) was used for selected samples to obtain grain-size, magnetic susceptibility and chemical data for the titanium-bearing oxides. The initial steps follow the general procedure, although sieving was added to determine the grain-size distributions of various fractions. A Franz Isodynamic Separator, with a forward tilt of 15° and a side tilt of 10°, was used to magnetically separate the heavy minerals. A setting of 10 mA was used to remove magnetite, and a polished thin-section was prepared of this fraction for microscopic and microprobe analysis. Ilmenite was concentrated using a setting of 200 mA. This fraction underwent further density separation using Clerici solution with an s.g. of 4.15 $g.cm^{-3}$. Polished thin-sections, made of the sink fractions, were examined microscopically to determine the impurity minerals present in the ilmenite concentrates. These fractions were also used for grain-size, microprobe and XRF chemical analysis. The latter was performed by Richards Bay Minerals using wavelength dispersive XRF and in-house ilmenite standards and techniques.

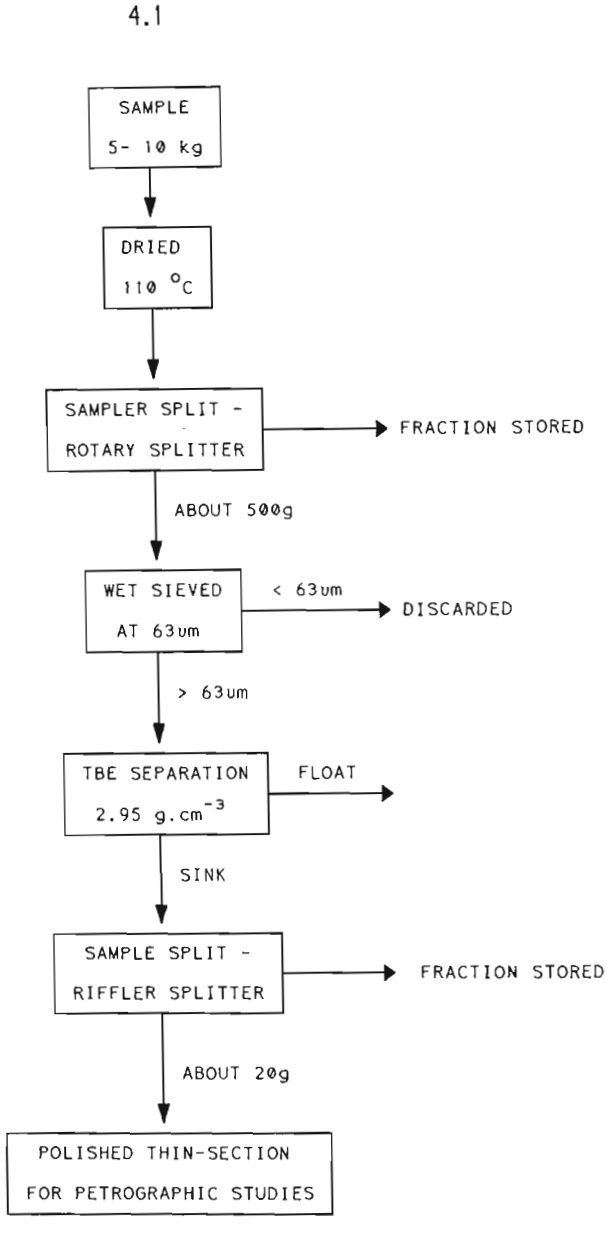

Figure 4.1 Flow-diagram showing the general sample preparation used for petrographic study.

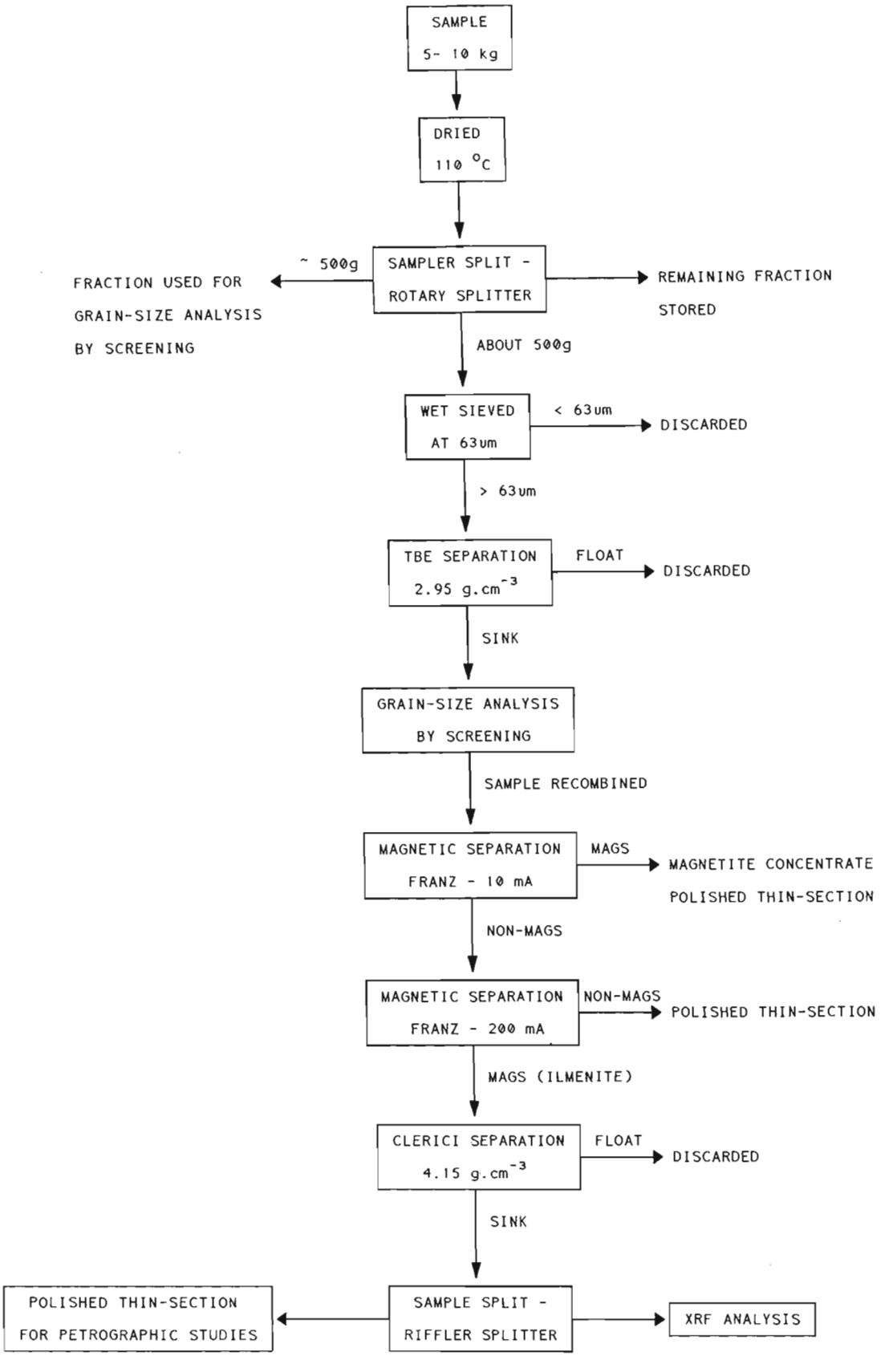

Figure 4.2 Flow-diagram showing the detailed sample preparation used for electron microprobe and XRF analysis of ilmenite concentrates.

4.2.3 Rock samples

Polished thin-sections were made of all the rock samples. In some cases, where the titanium-mineral content was low, the samples were crushed and the heavy minerals extracted by TBE separation. Polished thin-section were made of the heavy mineral concentrates.

4.3 ANALYTICAL METHODS

4.3.1 Microscopy

Prior to mounting in exopy resin on a glass slide, the heavy minerals were mixed thoroughly to minimize mineral segregation effects. The grain mounts were ground using silicon carbide powder to between 50 and 100 μm in thickness and polished, using progressively finer diamond pastes from 30 μm to 1 μm. Such polished thin-sections are good for the examination of mineral grains in both reflected and transmitted light and may also be used in scanning electron microscope (SEM) and electron microprobe analysis.

A Leitz polarising light microscope was used for mineral identification and petrographic descriptions. Both reflected and transmitted light modes were applied, although most of the titanium-bearing minerals are opaque. Oil immersion lenses were used for the reflected light microscopy.

4.3.2 Point counting techniques

Mineral proportions of the heavy mineral concentrates were determined by point-counting in both reflected and transmitted light microscopy. Five hundred grains were counted in reflected light using an oil-immersion lens to determine the modal proportions of opaque grains. The transparent minerals were counted together during this stage. The proportions of the transparent minerals were then determined using transmitted light. Certain phases, such as rutile, which both reflect and transmit light, were only counted in reflected light.

The counts were then converted to volume per cent for each sample. As determined by Hugo (1988), these percentages correspond closely to the mineral mass proportions, the differences often being within the error of point-counting. The reliability of point-count data is dependent not only on how representative the thin-section is, but also on the total number of points counted and the proportions of the minerals present. Van der Plas and Tobi (1965) derived a chart (Figure 4.3) which estimates the reliability of point-counting analysis. From this chart it can be seen that to determine the proportion of a mineral which constitutes 50 volume per cent of a sample to within 2 per cent accuracy, one should count 2500 points. For 500 points the error varies from 1 to 4.5 per cent, hence mineral proportions in this study are rounded to the nearest integer and minerals determined at $<$ 1 per cent are merely reported as "present".

4.3.3 Scanning Electron Microscopy

A Hitachi 520 Scanning Electron Microscope was used for detailed examination of petrographic textures and for photomicrography. Back-scattered electron images are well suited to the study of the iron-titanium oxide textures at magnifications of up to 6000 x, which is well beyond the resolution of the optical microscope. The brightness of a phase in a back-scattered electron image is dependent on the mean atomic number (Z) of its elements. Phases with high Z appear white, whilst those with lower Z are grey. Such images produce strong contrast between different minerals which often have similar optical properties, and are particularly useful for observing textural relationships masked by internal reflections under reflected polarised light.

Semi-quantitative chemical analyses of mineral grains were performed using a JEOL JSM-35 Scanning Electron Microscope, coupled to a KEVEX 7000-77 energy dispersive X-ray analyzer. The QUANTEX Magic V software package was used for data reduction. The general operating conditions of the instrument are as follows: Operating voltage = 20 kV; acquire time = 60 seconds; effective take-off angle = 18°; working distance = 38 mm; lower limit of detection = 0.2 % (approximately).

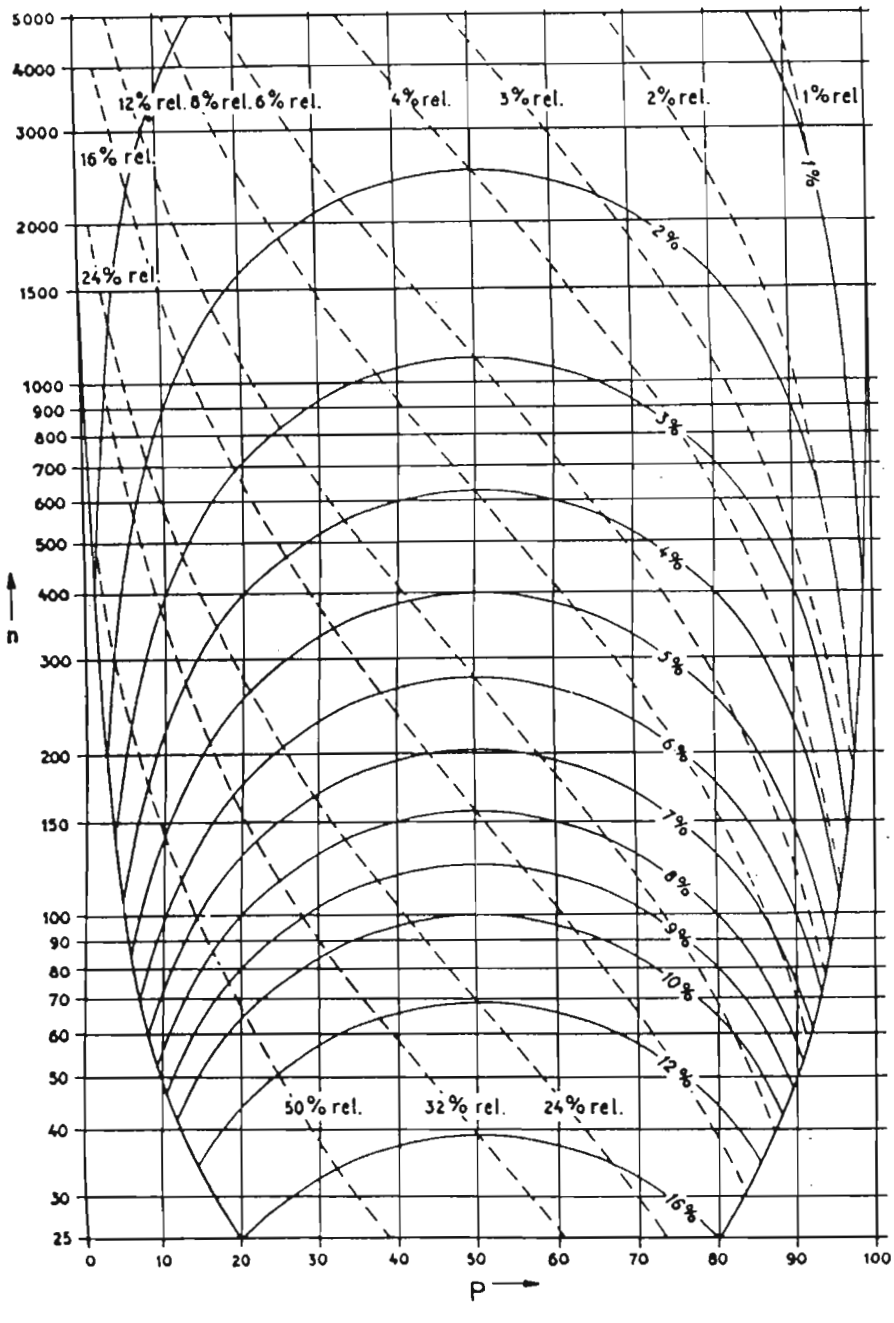

Figure 4.3 Van der Plas and Tobi (1965) chart for estimating the reliability of point-counting results. n = total number of counts; p = the estimated per cent by volume of the mineral; full curves = 2σ values; dashed curves = relative 2σ curves. The 2σ values for mineral percentages determined by point-counting 500 grains are shown in Appendix D.

4.3.4 Electron microprobe analysis

Quantitative chemical analysis was performed using a JEOL Superprobe 733 in the Department of Geology, Rhodes University. The operating conditions were as follows: accelerating voltage = 15 kV; beam current = 0.25 x 10^{-7} (A); beam diameter = 1 μm; peak counting time = 30 seconds; background counting time = 10 seconds. Standards and detection limits are given in Table 4.1. Data correction was based on the method of Duncomb and Reid (1968).

Some electron microprobe data from Hugo (1988) was also used in the study. These analyses were determined using a Cameca Camebax Electron Probe Microanalyzer in the Department of Geochemistry, University of Cape Town, with operating conditions given in Hugo (1988).

Table 4.1 Standards and lower limits of detection used for the JEOL 733 electron microprobe analyses.

Element	Standard	Standard Concentration (%)	Standard Factor	Net Peak Intensity ($c.s^{-1}$)	L.L.D. (%)
Si	Pure	100	0.801	18277	0.03
Ti	Pure	100	0.894	13225	0.02
Al	Spinel	71.66	0.613	12359	0.02
Cr	Chromite	48.95	0.918	8492	0.03
Fe	Ilmenite	33.37	0.866	1557	0.02
Mn	rhodonite	40.77	0.837	1721	0.01
Mg	Spinel	28.34	0.6635	5852	0.02

4.3.5 X-ray diffraction studies

The identity of mineral phases was confirmed by standard X-ray powder diffraction techniques using a Philips 1710 diffractometer and Fe-filtered Co Kα radiation. A Gandolfi camera was used for single grain XRD studies of the alteration phases of titanium-bearing minerals. Selected grains were crushed and mixed with gum acacia, before being rolled into a ball, approximately 0.5 mm in diameter. This method is similar to that described by Nicol (1975). The ball was then mounted in a Gandolfi powder diffraction camera, 114.8 mm in diameter, and exposed to Co Kα radiation for 3 to 12 hours. The phases present were identified from their d-spacings, which were measured on the resulting X-ray photographs.

4.3.6 Transmission Electron Microscopy

Transmission electron microscopy was performed in the Department of Earth Science, Cambridge, England using a JEOL JEM 100CX microscope. The sample preparation and methods used during this study are described in Chapter 6.3.

CHAPTER FIVE

MINERALOGY OF THE IRON-TITANIUM OXIDES

5.1 INTRODUCTION

As outlined in Chapter 1, an understanding of the chemistry and petrography of titanium-bearing minerals found in the area of study is important, because their composition affects both titanium levels and concentrations of impurities or "penalty elements" in potential ores. Petrography is important, as the minerals occur as both monomineralic and composite grains consisting of two or more minerals. Many of the mineral assemblages and textures found in these composite grains have formed in igneous and metamorphic source rocks, either during crystallization or during subsequent events. These textures are preserved during erosion and transportation and are observed in the coastal sediments, providing clues to their provenance. The inclusion of other phases in ore mineral grains changes their physical properties, TiO_2 content and impurity levels, thus affecting their quality and economic potential.

In this chapter the mineralogy of the titanium-bearing minerals is described in terms of the chemical and textural variations formed in the original source rock environment. Variations caused by the alteration of the minerals under conditions of weathering are described in the following chapter.

5.2 NOMENCLATURE OF THE IRON-TITANIUM OXIDES

The literature on iron-titanium minerals and particularly their alteration products, is plagued by the inconsistent terminology of different authors and so it is important to define each term used in this text. Because many of the grains observed consist of two or more minerals, it is necessary to outline the nomenclature used for composite grains.

5.2.1 Mineral Nomenclature

Nearly all the significant titanium-bearing minerals belong to the TiO_2-Fe_2O_3-FeO system. Although most workers adhere to the nomenclature proposed by Buddington *et al.* (1963) (*cf.* Buddington and Lindsley, 1964) for the end-member and intermediate solid solution minerals of this system, the terminology is not universally accepted. The nomenclature used in this thesis is defined below, with reference to Figure 5.1.

1. *Rutile*: A tetragonal phase, consisting of TiO_2 with minor impurities. Rutile may contain both ferrous and ferric iron and is termed ferrian-rutile if the iron content is > 2 per cent. The niobium-rich variety, ilmenorutile, was not found in this study.
2. *Anatase*: A tetragonal phase, essentially pure TiO_2.
3. *Brookite*: An orthorhombic phase, essentially pure TiO_2.
4. *Ilmenite*: A rhombohedral (trigonal) phase consisting of $FeOTiO_2$, with up to 6 per cent Fe_2O_3 in solid solution.
5. *Ferrian-ilmenite*: A rhombohedral phase containing more than 6 per cent Fe_2O_3, after Buddington *et al.*(1963). The abbreviation Ilm_{ss} is used to denote phases with the composition of ferrian-ilmenite (after Haggerty, 1976a).
6. *Hematite* (α-Fe_2O_3): A rhombohedral (trigonal) phase with a stoichiometry approaching Fe_2O_3 (Elsdon, 1975) and with less than 5 per cent TiO_2 (Buddington and Lindsley, 1964).
7. *Titanohematite*: A Fe-Ti phase with a stoichiometry of approximately R_2O_3 (where R is Fe^{3+} or Ti^{4+}) and at least 50 mole per cent hematite (Elsdon, 1975). According to Buddington and Lindsley (1964) titanohematite contains more than 5 per cent TiO_2, usually as $FeOTiO_2$ in solid solution, with a little excess TiO_2. The abbreviation Hem_{ss} is used to denote phases with the composition of titanohematite (after Haggerty, 1976a).
8. *Magnetite*: A spinel phase with a stoichiometry approaching Fe_3O_4 (Elsdon,1975), containing less than 5 per cent TiO_2.

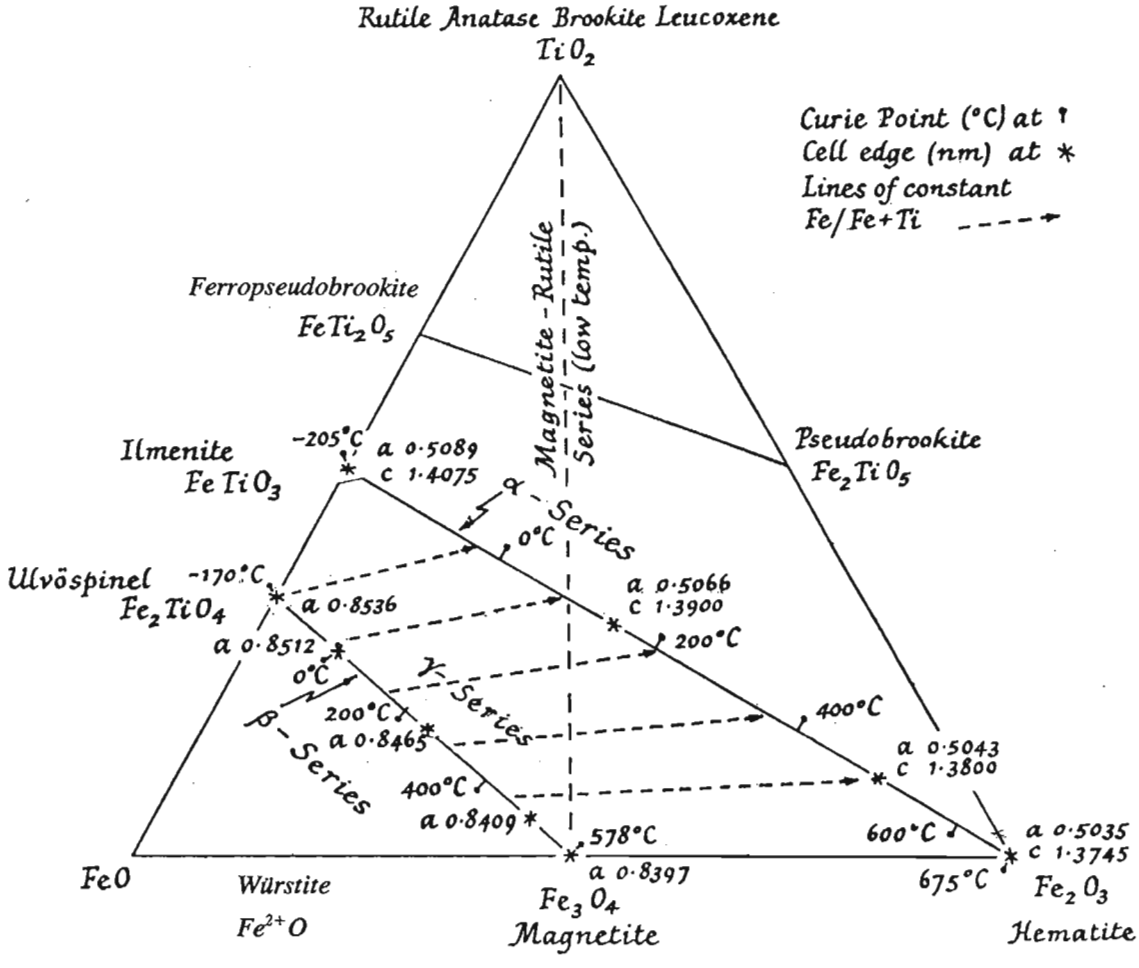

Figure 5.1 The system TiO_2-FeO-Fe_2O_3 from Battey (1981), showing the solid solution series and some of the physical properties of the iron-titanium oxides.

9. *Titanomagnetite*: A phase with an oxide stoichiometry of approximately R_3O_4 (Elsdon, 1975), which can be recalculated in terms of Fe_3O_4, $2FeOTiO_2$ or $FeOTiO_2$, or both, with Fe_3O_4 as the dominant phase (Buddington *et al.*, 1963).
10. *Ulvöspinel*: An optically homogeneous phase with an inverse spinel structure and a stoichiometry approaching Fe_2TiO_4.
11. *Pseudobrookite*: An optically homogeneous, orthorhombic iron-titanium phase with a stoichiometry close to R_3O_5 and having greater than 50 mole per cent Fe_2TiO_5 (Anderson, 1968).
12. *Ferropseudobrookite*: Similar to pseudobrookite, but with less than 50 mole per cent Fe_2TiO_5 (Anderson, 1968).
13. *Maghemite*: The gamma-Fe_2O_3 formed as an oxidation product of magnetite, containing < 2 per cent TiO_2 in solution (Basta, 1959). Maghemite loses Fe ions but retains the spinel structure (Battey, 1981).
14. *Titanite (sphene)*: A monoclinic mineral with the general formula $CaTiSiO_5$.

No standard nomenclature exists for the alteration products of ilmenite and the following nomenclature is used:

1. *Hydrated ilmenite*: Areas of alteration within altered ilmenite grains (defined below) which exhibit TiO_2 contents between 53 and 60 per cent. These areas are distinguished microscopically from ilmenite by their grey-blue colour and weaker anisotropism. The term "hydrated ilmenite" was first used by Dyadchenko and Khatuntseva (1960) and then Frost *et al.* (1983), referring to the small quantity of structurally bound water found within altered ilmenites. Hugo and Cornell (1991) defined hydrated ilmenite and altered ilmenite with between 53 and 60 % TiO_2.
2. *Pseudorutile*: a deformed hexagonal, oxyhydroxide close to $Fe_2Ti_3O_9$ (Temple and Tuefer, 1966; Grey *et al.*, 1983), or $Fe_{1.5}Ti_3O_{7.5}(OH)_{1.5}$ with an extended range of homogeneity (60 to 70 per cent TiO_2) due to hydrogen exchange for iron during hydration (Dyadchenko and Khatuntseva, 1960; Frost *et al.*, 1983). Under reflected light isotropic pseudorutile is blue-grey in colour with a slightly higher reflectance than ilmenite. The mineral is difficult to identify positively as these

optical properties are often indistinct and its major XRD peaks exhibit d-spacings similar to those of ilmenite, rutile and hematite. Historically pseudorutile was called arizonite (Palmer, 1909) or proarizonite (Bykov, 1964).

3. *Leucoxene*: this term is used to describe inhomogeneous, cryptocrystalline, high-TiO_2 (greater than 70 per cent) products of ilmenite alteration, following the terminology of Temple (1966), Grey and Reid (1975), Dimanche and Bartholomé (1976) and Frost *et al.* (1983). Leucoxene is distinguished optically from rutile or anatase by its characteristic sugary, internal reflections, although it may consist almost entirely of crypto- or microcrystalline rutile, anatase or brookite in the final stages of alteration. Golding (1961) quite correctly argues that leucoxene may form from the alteration of any titanium-bearing mineral, such as titanomagnetite or titanite and that these different leucoxenes, with markedly different compositions, should not all be grouped together under one name. From a petrographic point of view, however, it is impractical and at times very difficult, to distinguished the large variety of leucoxene grains encountered and hence the broader use of the word is preferred by the author.

5.2.2 Grain Nomenclature

Titanium-bearing oxides are found in both homogeneous and composite grains and the grain forms the fundamental unit when determining mineral proportions in sediments. The mineral make-up and genesis of these composite grains is varied and it is necessary to classify such grains in a consistent way. The most common mineral in the grain is given first followed by the next most important phase, connected by a hyphen. Minor minerals, which may be absent, are added using the symbol "$\pm$". Examples of the nomenclature of some of the commonly observed composite grains of titanium-bearing minerals are given below:

1. *Ilmenite-hematite (Ilm-Hem)*: These grains usually consist of exsolved lamellae of Hem_{ss} in ilmenite or Ilm_{ss}.
2. *Magnetite-ilmenite (Mt-Ilm)*: These grains usually consist of intergrowths of ilmenite in magnetite formed by oxyexsolution.

3. *Hematite-rutile ± ilmenite ± pseudobrookite (Hem-Rut±Ilm±Psb)*: These grains are usually formed by the high temperature oxidation of ilmenite.
4. *Ilmenite-rutile (Ilm-Rut)*: These grains are usually formed by the hydrothermal or supergene alteration of ilmenite or oxidised ilmenite grains.
5. *Titaniferous magnetite*: A general term for a titanium-bearing magnetite with no implications as to whether the grain consists of homogeneous titanomagnetite or magnetite containing micro-intergrowths (Buddington *et al.*, 1963).
6. *Titaniferous maghemite*: This is a general term for titanium-bearing maghemite without implications as to whether the mineral is homogeneous or contains Ti-rich intergrowths (Reynolds, 1978b).

In parts of the thesis and in particular this chapter, it is important to interpret petrology of the composite grains and then the following abbreviations are used as subscripts to denote the genesis of the grains:

1. ss = solid-solution of two phases, for example, titanohematite may be abbreviated as Hem_{ss} to denote that the hematite contains some ilmenite in solid-solution.
2. ex = true exsolution of one phase in a solid solution series from another, for example, ulvöspinel exsolved from magnetite may be abbreviated Mt_{ss}-Usp_{ex}. In some instances both phases of a solid-solution series may exsolve from each other, in which case both minerals are enclosed in brackets, for example, $(Ilm_{ss}$-$Hem_{ss})_{ex}$.
3. ox = high temperature oxidation as described by Haggerty (1976a), for example, a grain consisting of ilmenite, titanohematite and rutile formed by the oxidation of ilmenite may be abbreviated as Ilm-$(Hem_{ss}$-$Rut)_{ox}$.
4. oe = oxyexsolution (oxidation-exsolution) of one phase from another, for example, ilmenite intergrowths in titanomagnetite, formed by the above process, may be abbreviated as Mt_{ss}-Ilm_{oe}.
5. alt = alteration of one phase to another by either hydrothermal or supergene alteration, for example, the alteration of ferrian-ilmenite to rutile by such a process may be abbreviated as Ilm_{ss}-Rut_{alt}.

The grain nomenclature of ilmenite altered by weathering used in this thesis is of a slightly different nature, although based on the same principles. Two broad types of composite grains are recognised:

1. *Altered ilmenite grains*: grains consisting of mixtures of ± ilmenite ± hydrated ilmenite ± pseudorutile with very little or no microscopic leucoxene present, that is, grains in the composition range Ti/Ti+Fe: 0.5 to 0.7.

2. *Highly altered ilmenite*: grains consisting of mixtures of leucoxene (as defined above) ± ilmenite ± hydrated ilmenite ± pseudorutile ± rutile ± anatase.

5.3 THE IRON-TITANIUM OXIDES

The titanium-bearing minerals are found exclusively in the heavy mineral fraction of the samples studied and it is worthwhile comparing the physical properties of the titanium minerals with other heavy minerals present in deposits within the study area. Table 5.1 lists the iron-titanium oxides and other heavy minerals, together with their physical properties, abundance and economic importance. The optical properties of the minerals observed under reflected and transmitted light are given in Table 5.2. A summary of the structures of the iron-titanium oxides is given in Table 5.3.

Descriptions of the iron-titanium oxides given below are often specific to the area of study and more general information about the mineralogy of the TiO_2-Fe_2O_3-FeO system is reviewed by Elsdon (1975), Rumble (1976), Haggerty (1976a, 1976b, 1991), Reynolds (1978b) and Frost (1991a).

Table 5.1 Physical properties of iron-titanium oxides and other heavy minerals found along the east coast of South Africa.

Mineral	Formula	Density $g.cm^{-3}$	Magnetic Susceptibility	Electrical Conductivity	Percent	Economic value[1]
Oxides						
Ilmenite	$FeTiO_3$	4.7	mod-high	high	c-a	high
Hematite	α-Fe_2O_3	4.9-5.2	mod	mod	r-c	low
Rutile	TiO_2	4.2	non	high	p-c	high
Anatase	TiO_2	4.2	non	high	r-p	high
Brookite	TiO_2	3.8	non	high	r	mod
Magnetite	$Fe^{2+}Fe^{3+}{}_2O_4$	5.2	v. high	-	p-c	low
Ulvöspinel	$Fe^{2+}{}_2Ti^{4+}O_4$	4.8	mod	-	r-p	low
Chromite	$Fe^{2+}Cr_2O_4$	4.1-4.9	mod	mod	r-p	low
Maghemite	γ-Fe_2O_3	4.9-5.2	low-mod	non	r	none
Goethite	FeO.OH	4.3	low-mod	non	r-c	none
Pseudobrookite	$Fe^{3+}{}_2TiO_5$	4.3	low-mod	mod	r	none
Pseudorutile	$Fe^{3+}{}_2Ti_3O_9$	4.2	mod-high	mod	p	mod
Leucoxene	high TiO_2 phase	3.6-4.2	non-mod	mod	p-c	mod
Silicates						
Augite	$(Fe,Mg,Ca)SiO_3$	3.1-3.6	low	non	p-c	poss
Diopside	$Ca(Mg,Fe)Si_2O_6$	3.2	non-low	non	p	poss
Hornblende	Complex hydrated silicate	3.2	mod	mod	p-a	none
Almandine	$Fe^{2+}{}_3Al_2(SiO_4)_3$	4.3	mod	mod	p-c	mod
Grossular	$Ca_3Al_2(SiO_4)_3$	3.6	mod	mod	r-p	low
Zircon	$ZrSiO_4$	4.7	non	non	p-c	high
Epidote	$Ca_2(Al,Fe)_3(SiO_4)_3OH$	3.2-3.5	low-mod	non	r-p	none
Tourmaline	B,Fe,Al complex silicate	3.0-3.2	mod	mod	r	mod
Titanite (sphene)	$CaTiSiO_5$	3.4-3.5	low	non-mod	r-p	low
Kyanite	Al_2SiO_5	3.6	low	non	r	none
Phosphates						
Monazite	$(La,Ce,Th)PO_4$	4.9-5.3	low-mod	non	r-p	high
Apatite	$Ca_5(PO_4)(F,OH,Cl)$	3.2	non-low	mod	r-p	none

(r = trace or <1%; p = 1-10 %; c = 10-20 %; a = > 20 %; mod = moderate; poss = possible value)

[1] Economic value within east coast heavy mineral deposits.

Table 5.2A Optical properties of the opaque minerals found along the east coast of South Africa, as observed in reflected light, under oil. Quantitative data may be found in Craig and Vaughan (1981), Ramdohr (1980) and Uytenbogaardt and Burke (1971).

Mineral	Colour	Reflectance	Bireflectance/ Pleochroism	Anisotropism	Internal Reflections	Notes
Ilmenite	pinkish-brown	moderate > chromite < rutile	moderate-strong	strong blue to green	none	similar in colour to magnetite, but strongly pleo. and anisotr.
Hydrated Ilmenite	light blue-grey	moderate > ilmenite < rutile	moderate - decreases with inc. alteration	moderate-isotropic	none	optical properties change with increasing alteration from ilmenite to psr.
Pseudorutile	blue-grey	moderate > ilmenite = rutile	weak to none	isotropic	none	
Rutile	blue-grey	moderate > magnetite < hematite	slight	moderate-strong	strong - yellow, orange and red	IR often mask anisotropism twinning common
Anatase	blue-grey	moderate = rutile	very faint	obscured by IR	strong - white or blue-grey	
Brookite	grey					
Leucoxene	light-blue grey often masked by strong IR[1]	moderate > rutile	obscured by IR	obscured by IR	very strong - brown, yellow and white	IR oten mask other properties Colour of IR change with TiO_2 content.
Hematite	light-grey to white	moderate highest of oxides	weak	strong, blue and grey	strong, red IR often found	twin laths commonly observed under X-Polars titanohematite is greyer than hematite
Magnetite	light brown	moderate > ilmenite < rutile	none	isotropic	none	martitisation of magnetite common

Figure 5.2A (Cont.) Optical properties of opaque minerals

Mineral	Colour	Reflectance	Bireflectance/ Pleochroism	Anisotropism	Internal Reflections (IR)	Notes
Magnetite	light brown	moderate > ilmenite < rutile	none	isotropic	none	martitisation of magnetite common
Goethite	blue-grey	low-moderate < ilmenite	weak	strong	strong - red	colloform banding may be present grains usually porous and inhomogeneous
Maghemite	blue-grey	low-moderate < ilmenite	weak	weak	none	porous mineral, usually associated with magnetite
Chromite	grey	low < maghemite > silicates	none	isotropic	none	homogenous, dark grey grains
Cr-spinel	green-grey	low < ilmenite > chromite	weak	isotropic	none	commonly show growth zoning - grey core and greenish margins
Pseudobrookite	grey	low < ilmenite > chromite	none	very weak	none	found as small blebs, formed by the oxidation of ilmenite or Ti-magnetite

Table 5.2B Optical properties of transparent minerals found in heavy mineral deposits along the east coast of South Africa. All observations made in transmitted light. See Saggerson (1986) and Heinrich (1965) for more detailed descriptions.

Mineral	Colour	Shape	Cleavage	Relief	Birefringence[1]	Optic Picture	Notes
Quartz	colourless	sub- to rounded	none	low	low-1st order	U (+)	
Zircon	c.less-pale pink, green	eu-to anhedral, clear crystal faces, prismatic grains, often fractured	none	very high	high - colour rings common	U (+)	growth and sector zoning common, metamict grains common
Monazite	c.less to dull yellow	well rounded, small, spherical grains	none	very high, < zircon	high - diffuse colour rings common	B (+)	sometimes difficult to distinguish from zircon
Sphene	yellow to brown, granular appearance	sub- to rounded	none	high, < monazite	high	B (+)	grains are often partly altered
Epidote	c.less to pale yellow, may be slightly pleochroic	rounded, elongated	usually none	medium	medium - anomalous	B (+)	anomalous yellow and blue interference colours common
Garnet	c.less to pink	large, subrounded hexagonal	none	medium to high, > epidote	isotropic	-	may contain numerous inclusions
Pyroxenes	c.less to pale green, may be slightly pleochroic	subrounded, elongated, prismatic to tabular	good, 2 at 90°	medium	2nd to 3rd order	B (±)	may be difficult to positively identify
Amphiboles	pale green to brown and dark green, pleochroic.	subrounded, tabular	good, 2 at 60° and 120°.	medium	2nd to 3rd order	B (±)	may be difficult to distinguish from pyroxene
Apatite	c.less to pale green	well rounded	none	low to medium	bird's eye texture under X Polars	U (-)	mottled interference colours under cross-polars.
Tourmaline	bright green-blue, pleochroic	sub-rounded	none	medium	greens and blue	U (-)	may display zoning

[1] high interference colours are common because the polished thin-sections are usually greater the 30 μm in thickness.

Table 5.3 Summary of iron-titanium oxide structures.

Oxide	System	Unit Cell (nm)	Space Group	Reference
Rutile	Tetragonal (+)	a 0.459 c 0.296	$P4_2/m\ nm$	Deer *et al.* (1962)
Anatase	Tetragonal (-)	a 0.378 c 0.951	$I4/a\ md$	"
Brookite	Orthorhombic	a 0.5446 b 0.9184 c 0.5146	$Pcab$	"
Ilmenite	Trigonal	a_{hex} 0.5089 c_{hex} 1.4163	$R\bar{3}$	"
Hematite	Trigonal	a_{hex} 0.5035 c_{hex} 1.3749	$R\bar{3}c$	"
Pyrophanite	Trigonal	a_{hex} 0.5137 c_{hex} 1.429	$R\bar{3}$	Lindsley (1976)
Geikielite	Trigonal	a_{hex} 0.5054 c_{hex} 1.389	$R\bar{3}$	"
Magnetite	Cubic	a 0.8396	$Fm3m$	"
Ulvospinel	Cubic	a 0.8536	"	"
Chromite	Cubic	a 0.8378	"	"
Maghemite	Cubic or Tetragonal	a 0.833-0.834 c_{tet} $3a$	$P4_332$ $P4_1(P4_3)$	"
Pseudobrookite	Orthorhombic	a 0.9767 b 0.9947 c 0.3717	$Bbmn$	Bowles (1988)
Pseudorutile	Hexagonal	a 1.4375 c 0.4615	$P6_322$	Grey and Reid (1975)

5.4 THE TiO_2 POLYMORPHS: RUTILE, ANATASE and BROOKITE

5.4.1 Structure

As determined by Vegard (1916 and 1926) and Greenwood (1924), the internal structure of rutile consists of Ti ions in six-fold coordination with oxygen ions at the corners of a slightly distorted regular octahedron. Each oxygen atom is surrounded by three Ti ions at the apices of an approximately equilateral triangle. The co-ordination of the titanium and oxygen atoms in anatase is the same as in rutile, but the sequence of co-ordination octahedra differs between the two minerals (Pauling and Sturdivant, 1928). In rutile, the octahedra form chains parallel to (001), (Figure 5.2A). In comparison, the anatase structure contains no distinct chains (Figure 5.2B). The structure of brookite is more complex than that of rutile (Lindsley, 1976), as the Ti ions are displaced from the centres of the deformed co-ordination octahedra, which form zig-zag chains (Figure 5.2C).

Anatase is thermodynamically stable only at low to moderate temperatures and will convert to rutile at approximately 600°C (Dachille *et al.*, 1968), although this is pressure dependent. Rutile is stable over a wide range of temperature and pressure, which accounts for its common occurrence in metamorphic rocks. The mineral is also known to form as an alteration product of ilmenite in the weathering environment (Temple, 1966; Grey and Reid, 1975). Brookite is metastable (Bach, 1962; Elsdon, 1975) and readily transforms to rutile or anatase.

5.4.2 Mineral chemistry

Although rutile consists essentially of TiO_2, the mineral may contain varying amounts of Fe^{2+}, Fe^{3+}, Nb, or Ta and minor amounts of Cr, Al and Si. Isomorphous replacement of Ti^{4+} by Nb^{5+} and Ta^{5+} can occur as they have similar ionic radii. Electrostatic balance is maintained by either lattice vacancies, or by the complementary substitution of Fe^{2+}, Fe^{3+}, or Cr^{3+} ions (Deer *et al.*, 1962). In some cases, however, the iron may occur as fine intergrowths of ilmenite or hematite.

Homogeneous rutile grains were analysed by electron microprobe for Ti, Fe, Cr, Si, Al, Mn and Mg, using the standards and operating conditions outlined in Table 4.1 (page 63). Representative rutile compositions are shown in Table 5.4; the full list of rutile analyses is given in Appendix B.1. The rutiles have TiO_2 contents ranging from 96.5 to 100 per cent. Small amounts of Fe, Cr and Al (Figure 5.3) occur as impurities. Hugo (1988) determined that rutile grains from Richards Bay contain up to 1.5 per cent Nb_2O_5 and it is probably present in small quantities in rutiles from other regions along the east coast of South Africa.

5.4.3 Mineral petrography

In the sediments studied, rutile occurs as small, homogeneous red, amber, black and yellow grains, usually rounded and sub-elongated. In reflected light using oil-immersion lenses, rutile grains are blue-grey in colour, but display strong red, yellow and orange internal reflections (Plate 5.1A). Twin lamellae, at times in several intersecting directions, are common (Plate 5.1B) and rare rutile grains containing ilmenite exsolution lamellae (Ramdohr, 1980) are observed (Plate 5.1C).

Anatase is optically very similar to rutile, although it lacks twinning and has a lower anisotropism (Ramdohr, 1980). Brookite may be distinguished from rutile and anatase in transmitted light by its bi-axial and non-pleochroic properties, however the mineral is very similar to the other two TiO_2 polymorphs in reflected light. For this reason, no distinction was made between homogeneous rutile, anatase and brookite grains in the study. The presence of all three minerals has been determined by powder XRD analysis of density fractions of rutile concentrates from Richards Bay (Figure 5.4). The XRD analyses show that while little anatase and brookite is found in the > 4.0 s.g. fraction, they are common in the 3.6 to 4.0 s.g. fractions. Microscopic study and single grain (Gandolfi) XRD analyses of the density fractions reveal that brookite usually occurs as an alteration product within highly altered ilmenite, leucoxene and titanite grains (see Chapter 6). Rutile and anatase are found as both homogeneous grains and ilmenite alteration products.

5.2A

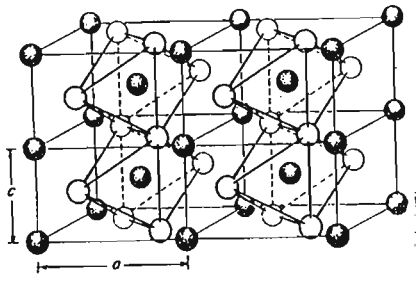

5.2B

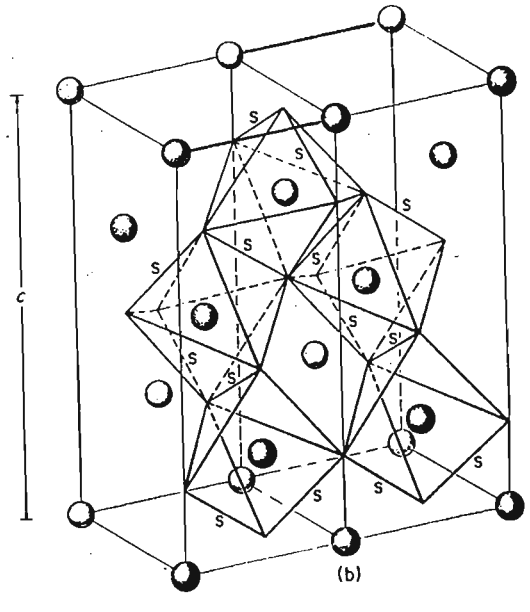

5.3C

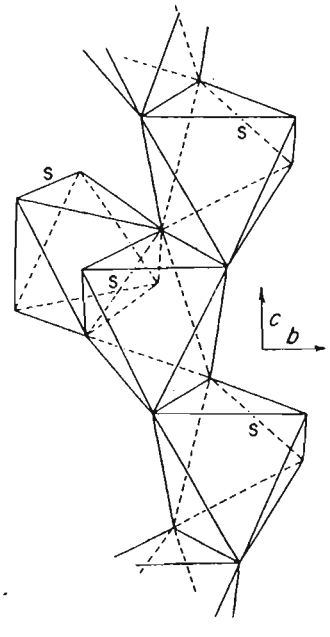

Figure 5.2 The structures of the TiO_2 polymorphs rutile, anatase and brookite (from Lindsley, 1976). **A.** Four unit cells of rutile showing the octahedra of oxygens about the Ti at the centre of each cell. **B.** Two unit cells of anatase showing the distorted octahedra of oxygens about the Ti (the shared edges (s) are shorter than the unshared edges. **C.** The chain of distorted oxygen octahedra about the Ti ions which make up the brookite structure.

Table 5.4 Representative rutile microprobe analyses.

Analysis		SiO2	TiO2	Al2O3	Cr2O3	FeO	MnO	MgO	Total
HZ 13	1	-	98.60	0.02	0.07	0.30	-	-	98.99
HZ 13	2	-	98.59	-	0.21	0.13	-	-	98.94
HZ 13	3	-	99.88	-	0.15	-	-	-	100.04
HZ 13	4	-	99.28	-	0.09	0.10	-	-	99.47
HZ 13	5	-	99.21	0.06	0.09	0.27	-	-	99.63
HZ 13	6	-	99.03	-	-	0.36	-	-	99.39
HZ 13	7	-	99.09	-	0.24	0.16	-	-	99.49
HZ 13	8	-	98.60	0.05	-	0.25	-	-	98.89
HZ 13	9	0.07	98.59	0.13	0.16	0.19	-	-	99.14
HZ 13	10	-	99.04	-	0.07	0.09	-	-	99.20
HN 7	1	-	99.39	-	0.10	0.26	-	-	99.75
HN 7	2	-	98.71	-	0.04	0.12	-	-	98.87
HN 7	3	-	99.41	-	0.08	0.21	-	-	99.70
HN 7	4	-	99.18	-	0.06	0.11	-	-	99.34
HN 7	5	-	98.46	-	0.20	-	-	-	98.67
HN 7	6	-	98.59	-	0.13	-	-	-	98.72
HN 7	7	-	98.75	-	0.17	-	-	-	98.92
HN 7	8	-	98.73	-	0.15	-	-	-	98.88
HN 7	9	-	99.93	-	0.13	-	-	-	100.06
HN 7	10	-	99.56	-	0.10	0.13	-	-	99.79
HT 3	1	-	99.91	0.03	-	0.26	-	-	100.20
HT 3	2	-	99.69	-	-	0.10	-	-	99.79
HT 3	3	0.03	99.95	0.07	-	0.13	-	-	100.18
HT 3	4	-	99.02	0.04	0.07	0.07	-	-	99.19
HT 3	5	-	99.37	0.06	-	0.28	-	-	99.71
HT 3	6	-	99.10	0.06	0.10	0.17	-	-	99.42
HT 3	7	-	99.51	0.03	0.19	0.21	-	-	99.93
HT 3	8	-	99.30	0.03	0.11	0.17	-	-	99.62
HT 3	9	-	99.56	0.02	-	0.51	-	-	100.09
HT 3	10	-	99.81	0.02	0.14	0.19	-	-	100.16
HEC 5	1	-	99.12	0.03	-	0.47	-	-	99.64
HEC 5	2	-	99.40	-	-	0.17	-	-	99.60
HEC 5	3	-	98.95	0.06	-	0.21	-	-	99.23
HEC 5	4	-	98.87	-	-	0.10	-	-	99.00
HEC 5	5	0.03	99.67	0.05	-	0.19	-	-	99.94
HEC 5	6	-	99.11	-	-	0.16	-	-	99.28
HEC 5	7	-	99.55	-	-	0.18	-	-	99.73
HEC 5	8	-	99.33	-	-	0.02	-	-	99.35
HEC 5	9	-	99.31	0.11	-	0.05	-	-	99.47
HEC 5	10	-	98.98	-	-	0.42	-	-	99.44

- = below detection limit

HZ 13 - Sodwana Bay, Zululand
HN 7 - Umdloti, Natal
HT 3 - Port St Johns, Transkei
HEC 5 - Kidd's Beach, Eastern Cape

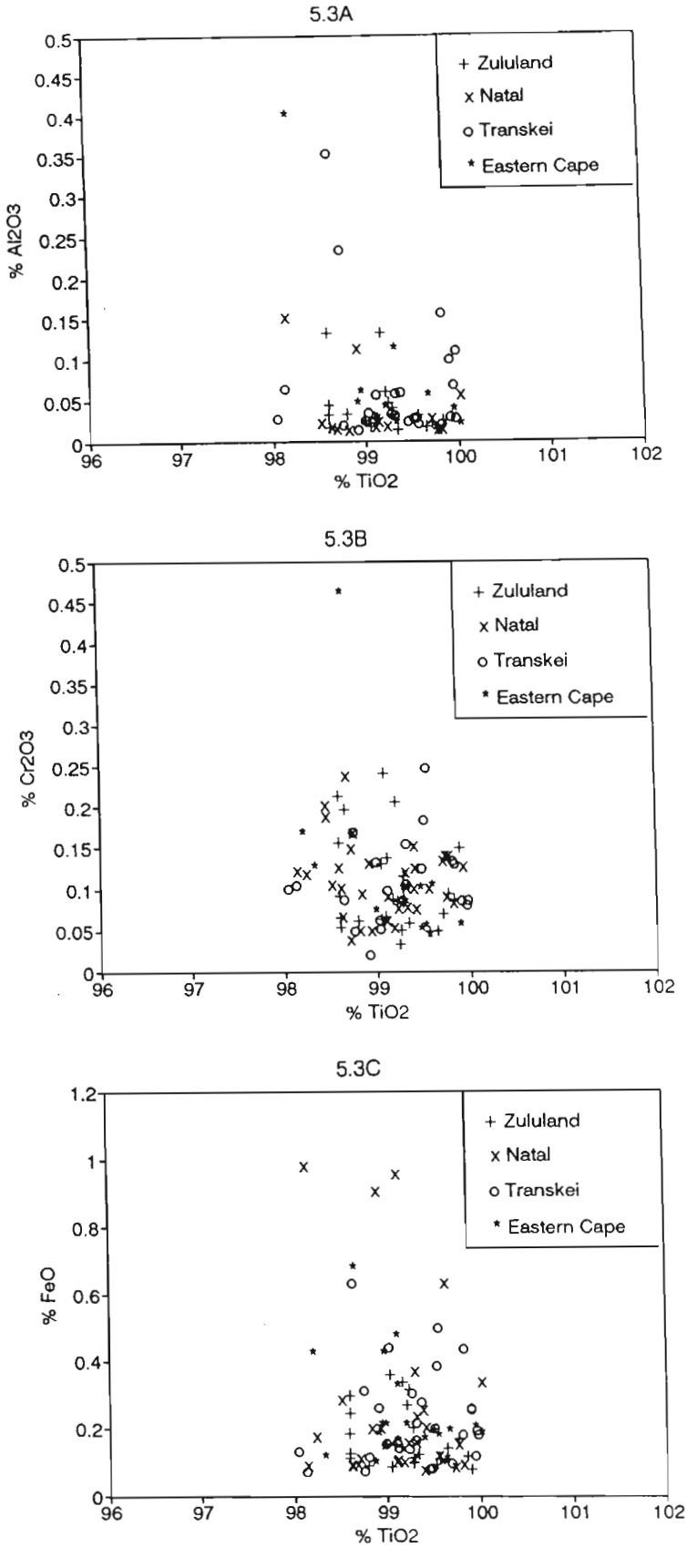

Figure 5.3 Variation of Al_2O_3, Cr_2O_3, and Fe (as FeO) with TiO_2 for selected rutile grains from the east coast of South Africa. The rutile grains contain low impurity levels and no regional variations in the composition of grains is evident.

Plate 5.1 Photomicrographs of rutile grains under plain-polarised reflected light using a 32x oil immersion lens. The single scale bar shown refers to each plate.

A. Homogeneous rutile grain displaying strong internal reflections. Richards Bay, dune (HZ 17). Scale bar 75 μm.

B. Rutile grain displaying intersecting sets of twin lamellae. The dominant set probably formed as a result of strain. Richards Bay, dune (HZ 17). Scale Bar 75 μm.

C. Rare rutile (light grey) grain containing orientated lensoid lamellae of exsolved ilmenite (medium grey). The thin, straight lamellae (medium grey) are rutile twins. Port Durnford, dune (HZ 2). Scale Bar 50 μm.

Plate 5.1

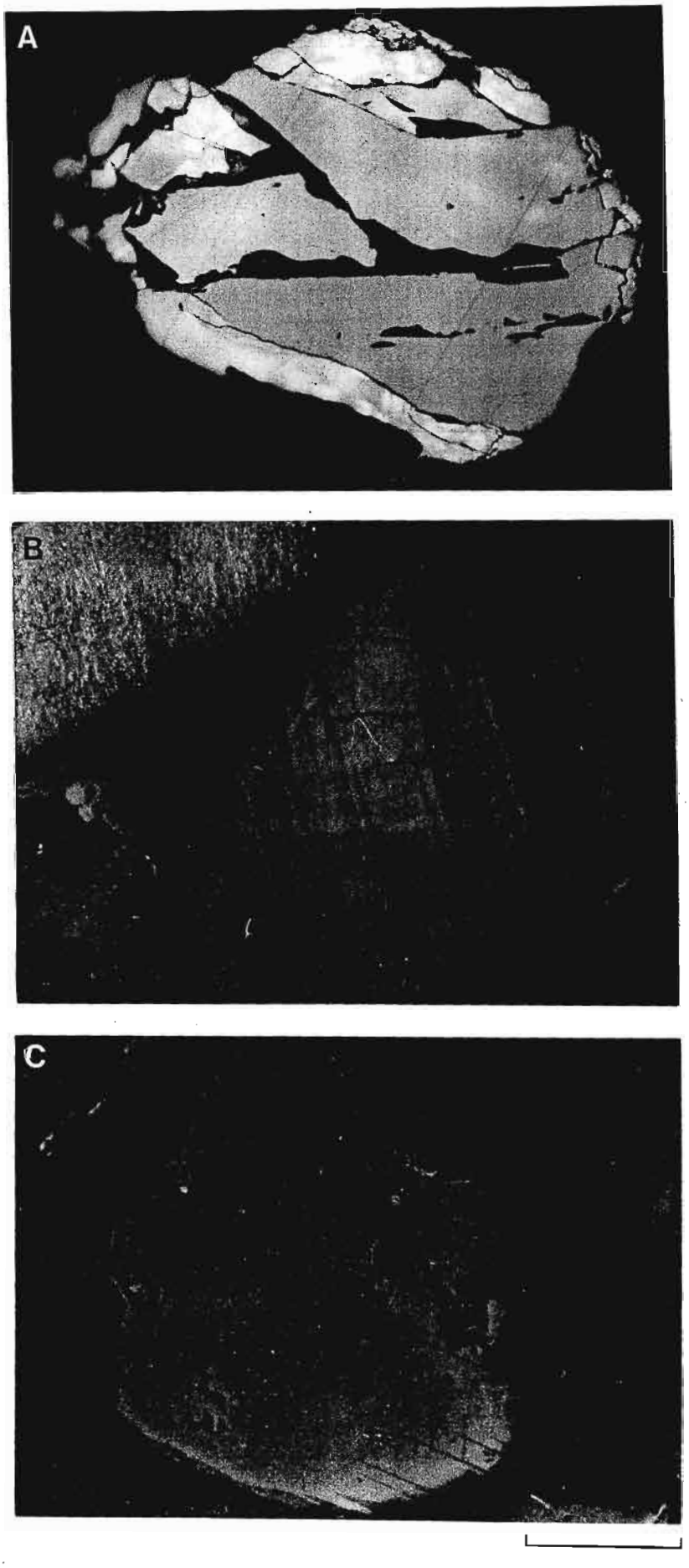

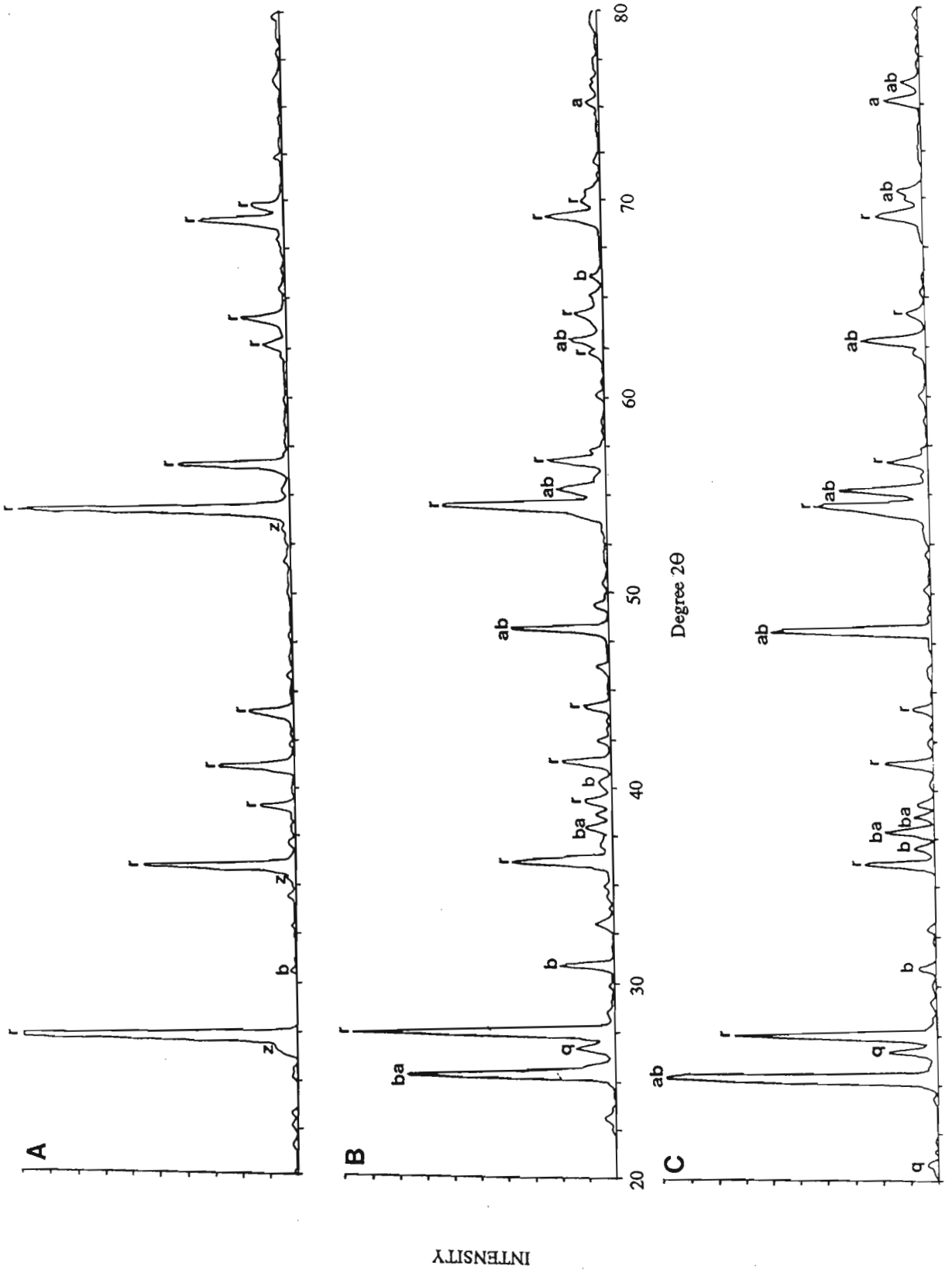

Figure 5.4 Powder XRD traces of TiO_2 polymorphs in rutile and leucoxene concentrates from Richards Bay Minerals. **A.** Rutile concentrate 4.0 $g.cm^{-3}$ sink fraction. **B.** Rutile concentrate 3.8 to 4.0 $g.cm^{-3}$ fraction. **C.** Leucoxene concentrate 3.8 to 4.0 $g.cm^{-3}$ fraction. r = rutile; a = anatase; b = brookite; ab = peak formed by both anatase and brookite; q = quartz; z = zircon.

5.5 ILMENITE-HEMATITE SERIES

5.5.1 Structure

Ilmenite (*R*3) and hematite (*R*3*c*) have very similar rhombohedral structures (Table 5.3). The rhombohedral unit cells are more conveniently treated as hexagonal cells (Lindsley, 1976) and hexagonal ilmenite and hematite indices are used. The two minerals form a continuous solid solution series at high temperatures (greater than *circa* 800°C), but a miscibility gap results in exsolution at lower temperatures (Lindsley, 1976). The minerals form either a disordered ilmenite-hematite or an ordered ilmenite-hematite solid solution series, depending on temperature and mole per cent $FeTiO_3$ (Nord and Lawson, 1989, Figure 1).

The hematite structure consists of sheets of oxygen anions forming a nearly hexagonal, close-packed array lying parallel to (0001). In pure hematite the cations consist of Fe^{3+}, which occupy two-thirds of the potential cation sites (Figure 5.5A) (Lindsley, 1976). In high-temperature, disordered ilmenite-hematite solid solutions, Fe^{3+}, Fe^{2+} and Ti^{4+} are randomly distributed in the cation sites (Nord and Lawson, 1989). In the ordered ilmenite-hematite (*R*3) series, the cations occupy the same positions as in the disordered form, but are segregated into alternating layers along the *c*-axis (Figure 5.5B), so that the sequence of cations along the (0001) axis is Fe-Ti-□-Ti-Fe-□-Fe (Lindsley, 1976), where □ denotes a vacancy.

The rare minerals pyrophanite ($MnTiO_3$) and geikielite ($MgTiO_3$) are isomorphous with ilmenite, although their unit cell dimensions differ slightly (Table 5.3). Although considerable substitution of Mg and Mn for Fe^{2+} in ilmenite can take place, the mineral usually contains only small amounts of these elements (Deer *et al.*, 1962). Magnesium and manganese-rich ilmenites are termed picroilmenites and manganoan ilmenites, respectively.

5.5A

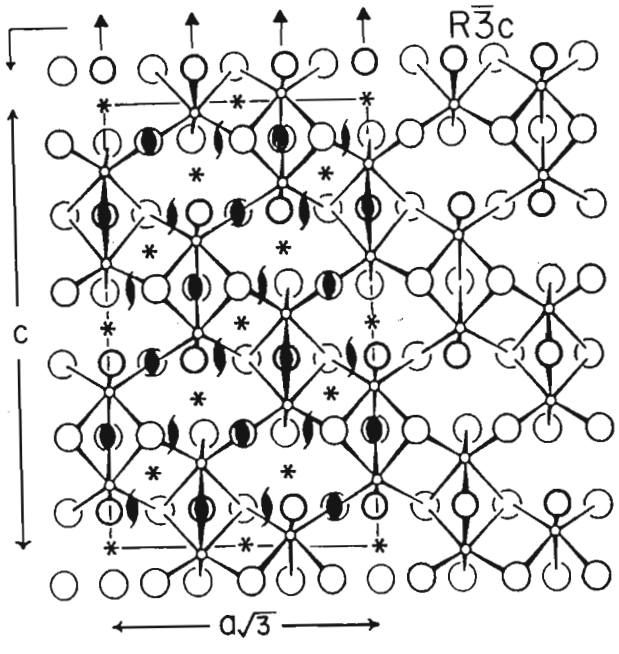

5.5B

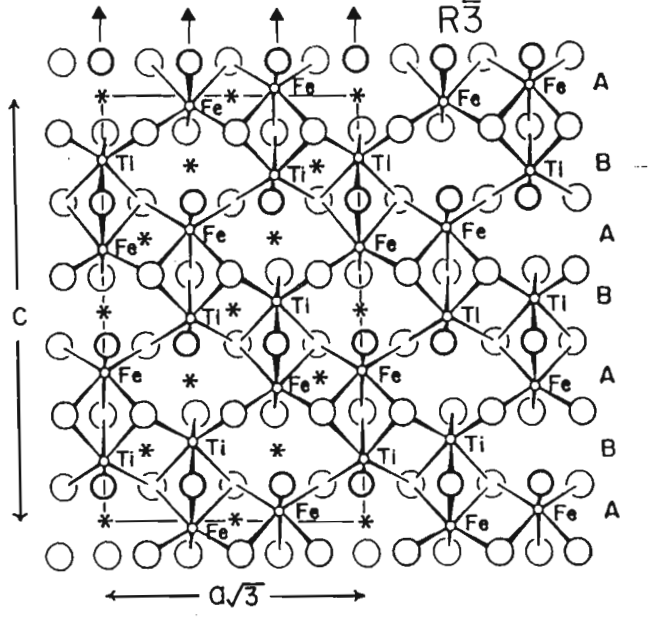

Figure 5.5 The structure of hematite and ilmenite-hematite projected on to the $(11\bar{2}0)$ from Nord and Lawson (1989). **A.** The structure of $R\bar{3}c$ hematite or disordered ilmenite-hematite. **B.** The structure of $R\bar{3}c$ ilmenite-hematite. The small circles represent Fe and Ti cation sites and the large circles represent oxygen atoms.

5.5.2 Ilmenite-hematite chemistry

As outline above, ilmenite may contain significant amounts of Fe^{3+}, Mn and Mg in solid solution and small or trace amounts of V, Cr, Ni, Cu, Zn, Si and Al. Ilmenite grains were analysed for Ti, Fe (as Fe^{2+}), Mn, Mg, Cr, Al and Si by electron microprobe using the standards and operating conditions outlined in Table 4.1 (page 63). Vanadium could not be analysed because of the large overlap between the Ti Kß and V Kα x-ray lines. Step scans across the peak positions of Ni, Cu and Zn revealed that these elements occurred in ilmenite grains in concentrations below the detection limit (generally about 0.02 per cent) of the instrument for the counting time selected (30 seconds for peaks, 10 seconds for backgrounds), so they were not included in the analyses. The Fe_2O_3 content and the mole proportions of $FeTiO_3$, $MnTiO_3$, $MgTiO_3$ and Fe_2O_3 in ilmenite was calculated from stoichiometry on the basis of three oxygen formulae, as outlined by Stormer (1983).

Initially, a number of points were analysed in several ilmenite grains to determine the degree of chemical variation and zonation. These analyses (Table 5.5) show that there is no zonation. Thereafter each grain was analysed once, unless it consisted of two or more phases, or displayed signs of alteration. Between 20 and 70 optically homogeneous ilmenite grains were analysed in each sediment sample. Representative ilmenite analyses are given in Table 5.6; the full results are given in Appendix B.2.

Variations in the chemistry of ilmenite are best illustrated by the quaternary plot of $FeTiO_3$-Fe_2O_3-$MgTiO_3$-$MnTiO_3$ mole proportions, as shown in Figure 5.6. This plot shows that many east coast ilmenites have compositions close to $FeTiO_3$ with less than 20 mole per cent Mn and Mg present. The calculated Fe_2O_3 contents are more variable, but rarely exceed 20 mole per cent.

Tsusue (1973), Neumann (1974) and Haggerty (1976b) noted that MgO and MnO contents of ilmenite may be correlated with the bulk composition of the host rock in which the ilmenites crystallised. Ilmenites formed in ultrabasic and basic rocks have high MgO

values, while those crystallised in felsic, particularly peralkaline, suites have high MnO contents (Neumann, 1974). The increase in $(Mn^{2+}/Fe^{2+})_{ilm}$ with increasing $(Mn^{2+}/Fe^{2+})_{magma}$ is more pronounced for crystallisation at lower temperatures and with increasing Differentiation Index (DI), or SiO_2 content of the host rocks (Buddington and Lindsley, 1964; Lipman 1971; Neumann, 1974). This is caused by the enrichment of Mn in low-temperature magma residues and the similarity between the ionic radii of Fe^{2+} (0.086 nm) and Mn^{2+} (0.091 nm) allowing for substitution in the ilmenite octahedral site.

Oxygen fugacity (fO_2) is a major factor controlling the Fe_2O_3 content of ilmenites. At low fO_2 Fe^{2+} is the dominant iron cation, and phases such as $Fe^{2+}{}_2TiO_4$ and $Fe^{2+}TiO_3$ are formed. As fO_2 increases so does the Fe^{3+}:Fe^{2+} ratio in rocks, which results in the stabilisation of Mt_{ss} and hematite-rich Ilm_{ss} (Haggerty, 1976b).

Table 5.5 Microprobe analyses of single, homogeneous ilmenite grains, which indicate that such grains show no systematic chemical zonation.

Grain	Analysis	SiO_2	TiO_2	Al_2O_3	Cr_2O_3	FeO[1]	MnO	MgO	Total
HN2-GR6	core	0.07	53.22	0.02	-	42.44	3.88	0.17	99.7
		0.07	53.51	-	-	41.50	3.94	0.17	99.1
		-	52.76	-	-	42.80	3.94	0.16	99.6
		-	52.46	-	-	42.80	3.87	0.14	99.3
	margin	-	52.11	0.02	-	43.43	3.51	0.14	99.2
HN2-GR64	core	0.05	52.30	-	-	43.11	2.65	0.13	98.2
		-	53.92	-	-	43.37	3.21	0.12	99.7
		0.03	52.47	-	-	42.83	3.14	0.11	98.6
		-	52.09	-	-	43.09	2.64	0.11	97.9
	margin	-	52.26	-	-	41.78	3.22	0.09	97.4
HN9-GR A	core	0.03	52.98	0.03	0.14	44.01	0.66	0.51	98.3
		-	53.03	0.02	0.15	43.51	0.65	0.51	97.9
		-	53.05	0.02	0.14	43.93	0.66	0.54	98.3
		-	53.48	-	0.16	42.93	0.59	0.51	97.7
	margin	-	52.30	0.02	0.14	44.16	0.57	0.52	97.7
HN9-GR56	core	-	49.28	0.02	0.12	48.19	1.26	0.06	98.9
		0.04	50.45	0.03	0.11	47.76	1.05	0.08	99.5
		0.04	50.04	0.02	0.11	47.72	1.05	0.08	99.0
		0.03	50.03	0.03	0.11	48.03	1.04	0.09	99.3
	margin	0.05	50.27	0.02	0.11	48.11	0.98	0.10	99.6

[1] All iron reported as FeO. HN2 = Umgababa dune; HN9 = Durban beach; - = below detection limit.

Table 5.6 Representative ilmenite microprobe analyses

Analysis		SiO2	TiO2	Al2O3	Cr2O3	MnO	MgO	Recalculated FeO	Recalculated FeO	Recalculated Fe2O3	Total	Calculated mole per cent FeTiO3	Calculated mole per cent MnTiO3	Calculated mole per cent MgTiO3	Calculated mole per cent Fe2O3
HZ 17	1	0.08	48.14		0.09	0.80	0.06	49.43	42.46	7.74	99.37	84.34	1.61	0.21	13.84
HZ 17	2		48.48	0.07		0.37	2.44	46.74	38.88	8.73	98.98	75.54	0.73	8.46	15.27
HZ 17	3		50.04			0.55	0.28	48.25	43.94	4.79	99.61	89.12	1.13	1.01	8.74
HZ 17	4	0.07	52.77			0.68	0.06	46.17	46.17	0.00	99.77	98.29	1.47	0.24	
HZ 17	5	0.04	51.65	0.07		0.45	2.01	45.10	42.46	2.93	99.62	86.42	0.94	7.27	5.37
HZ 17	6	0.04	50.38			0.42	0.73	46.81	43.62	3.55	98.75	89.85	0.88	2.69	6.58
HZ 17	7		51.03			0.67	0.07	47.46	45.11	2.61	99.51	93.48	1.41	0.25	4.86
HZ 17	8	0.04	51.31	0.02		0.69	0.49	46.10	44.61	1.65	98.82	93.58	1.46	1.84	3.12
HZ 17	9		50.33	0.04	0.46	2.15	0.47	44.93	42.27	2.95	98.70	88.17	4.54	1.74	5.54
HZ 17	10	0.05	52.67	0.03		0.94	0.05	45.14	45.14	0.00	98.88	97.75	2.05	0.19	0.00
HZ 17	11		51.89	0.04	0.04	0.45	1.97	44.78	42.71	2.30	99.42	87.59	0.94	7.22	4.25
HZ 17	12		53.82	0.02		0.52	1.07	43.87	43.87	0.00	99.35	94.73	1.15	4.12	
HZ 17	13		50.17	0.03	0.04	0.39	0.82	47.72	43.27	4.94	99.67	87.28	0.79	2.96	8.98
HZ 17	14		49.96			8.75		40.21	36.07	4.61	99.45	73.48	18.04		8.44
HZ 17	15		47.97	0.04	0.08	0.33	1.34	48.42	40.42	8.88	99.08	79.04	0.66	4.67	15.63
HN 9	1	0.06	52.00	0.12		3.66		43.73	43.11	0.70	99.65	90.84	7.82		1.32
HN 9	2	0.10	50.98	0.03		0.48	0.33	47.00	44.88	2.35	99.18	93.35	1.01	1.24	4.40
HN 9	3		52.88			0.57	0.78	44.78	44.78	0.00	99.03	95.80	1.23	2.97	0.00
HN 9	4		51.06			0.79	0.12	46.55	44.91	1.82	98.74	94.43	1.67	0.45	3.44
HN 9	5		50.33	0.04	0.08	0.43	1.18	46.25	42.73	3.91	98.71	87.58	0.90	4.30	7.22
HN 9	6		52.27			1.98	0.08	44.36	44.36	0.00	98.73	95.40	4.31	0.30	
HN 9	7		50.85	0.02		0.61	0.21	46.55	44.76	1.99	98.45	94.16	1.29	0.78	3.77
HN 9	8		50.26	0.05	0.04	1.13	0.22	46.56	43.66	3.22	98.59	90.77	2.38	0.82	6.02
HN 9	9		53.00			1.72		45.01	45.01	0.00	99.75	96.27	3.73		
HN 9	10		50.04	0.04		0.45	0.29	47.61	44.06	3.95	98.85	90.67	0.94	1.06	7.32
HN 9	11	0.04	49.29	0.02	0.04	0.45	0.24	48.52	43.50	5.58	99.16	88.06	0.92	0.85	10.17
HN 9	12		49.20	0.03	0.07	0.42	0.98	48.32	42.09	6.92	99.72	83.37	0.84	3.46	12.33
HN 9	13	0.04	52.42			1.84	0.06	44.71	44.71	0.00	99.08	95.78	3.99	0.23	
HN 9	14		50.43	0.02		0.51	0.19	48.09	44.52	3.97	99.64	90.98	1.05	0.67	7.30
HN 9	15		48.58	0.02		0.35	0.25	48.67	42.91	6.40	98.55	86.73	0.73	0.90	11.64

Table 5.6 (Cont.) Representative ilmenite microprobe analyses

Analysis	SiO2	TiO2	Al2O3	Cr2O3	MnO	MgO	Recalculated FeO	Recalculated FeO	Recalculated Fe2O3	Total	Calculated mole per cent FeTiO3	Calculated mole per cent MnTiO3	Calculated mole per cent MgTiO3	Calculated mole per cent Fe2O3
HT 7 1		49.76	0.10		0.47	1.85	46.51	40.98	6.15	99.32	81.51	0.94	6.54	11.00
HT 7 2		46.86	0.07	0.08	0.58	0.33	50.43	40.96	10.52	99.40	79.37	1.14	1.15	18.34
HT 7 3		50.62	0.05	0.32	0.44	1.72	45.61	42.04	3.97	99.17	85.58	0.91	6.22	7.28
HT 7 4		51.46		0.04	0.51	0.19	46.97	45.42	1.72	99.37	94.96	1.08	0.72	3.23
HT 7 5		51.05	0.02		0.81		47.53	45.07	2.74	99.73	93.17	1.69		5.09
HT 7 6		52.64		0.08	3.13	0.12	44.21	43.97	0.26	100.21	92.41	6.65	0.43	0.50
HT 7 7		49.85	0.03		0.47	0.66	48.06	43.18	5.42	99.64	86.87	0.96	2.36	9.81
HT 7 8		51.38			0.91	0.14	46.74	45.04	1.89	99.40	94.00	1.92	0.54	3.55
HT 7 9		51.50	0.02	0.11	1.60	0.34	45.48	44.09	1.54	99.20	92.45	3.40	1.25	2.90
HT 7 10		51.15	0.03		1.08	0.07	46.18	44.78	1.56	98.66	94.47	2.31	0.26	2.95
HT 7 11		52.86	0.06	0.33	0.34	1.66	43.12	43.12	0.00	98.37	92.89	0.74	6.37	
HT 7 12		49.69	0.08		0.38	1.50	46.55	41.63	5.47	98.79	83.93	0.78	5.37	9.92
HT 7 13		49.28	0.09	0.04	0.35	1.44	45.81	41.39	4.91	97.49	84.94	0.72	5.27	9.07
HT 7 14		51.41	0.09		0.26	0.65	45.93	44.81	1.24	98.44	94.65	0.55	2.44	2.36
HT 7 15		52.01	0.07	0.37	0.45	1.32	45.14	43.96	1.32	99.47	91.67	0.95	4.91	2.47
HEC 3 1	0.05	52.59	0.03	0.22	2.32	0.13	44.80	44.76	0.04	100.13	94.48	4.95	0.49	0.08
HEC 3 2		52.46	0.06		0.47	0.91	45.96	45.09	0.96	99.97	93.85	0.99	3.37	1.79
HEC 3 3		53.03	0.04		0.98	0.29	45.45	45.45	0.00	99.84	96.80	2.11	1.09	
HEC 3 4	0.03	52.48	0.07		0.51	0.96	44.82	44.82	0.00	98.89	95.25	1.10	3.65	
HEC 3 5		52.78	0.06	0.04	0.79	0.60	45.07	45.07	0.00	99.35	96.01	1.71	2.27	
HEC 3 6		50.97	0.08		0.37	1.35	46.12	43.06	3.40	99.24	88.06	0.77	4.92	6.25
HEC 3 7	0.03	51.84			0.90	0.20	46.19	45.39	0.89	99.26	95.67	1.91	0.73	1.68
HEC 3 8		52.25	0.03		1.96	0.09	45.00	44.85	0.16	99.38	95.13	4.22	0.34	0.31
HEC 3 9		51.87	0.06		0.51	0.88	45.86	44.58	1.42	99.35	93.00	1.07	3.27	2.67
HEC 3 10	0.04	50.83	0.02		1.56	0.12	45.97	43.96	2.24	98.78	92.01	3.31	0.46	4.22
HEC 3 11		50.56	0.04		1.42	0.12	46.74	43.82	3.24	99.21	90.57	2.98	0.43	6.03
HEC 3 12		51.13	0.05	0.18	1.28	0.22	46.25	44.29	2.18	99.33	92.39	2.71	0.81	4.09
HEC 3 13	0.04	50.94	0.02	0.05	0.81	0.17	46.29	44.73	1.73	98.49	94.34	1.73	0.64	3.29
HEC 3 14		51.57			1.40	0.06	45.78	44.86	0.96	98.91	94.94	3.00	0.23	1.83
HEC 3 15		52.11	0.05		0.92	0.77	45.66	44.59	1.18	99.64	92.99	1.94	2.85	2.22

HZ 17 - Richards Bay, Zululand
HN 9 - Durban, Natal
HT 7 - Wavecrest, Transkei
HEC 3 - Fish River Mouth, Eastern Cape

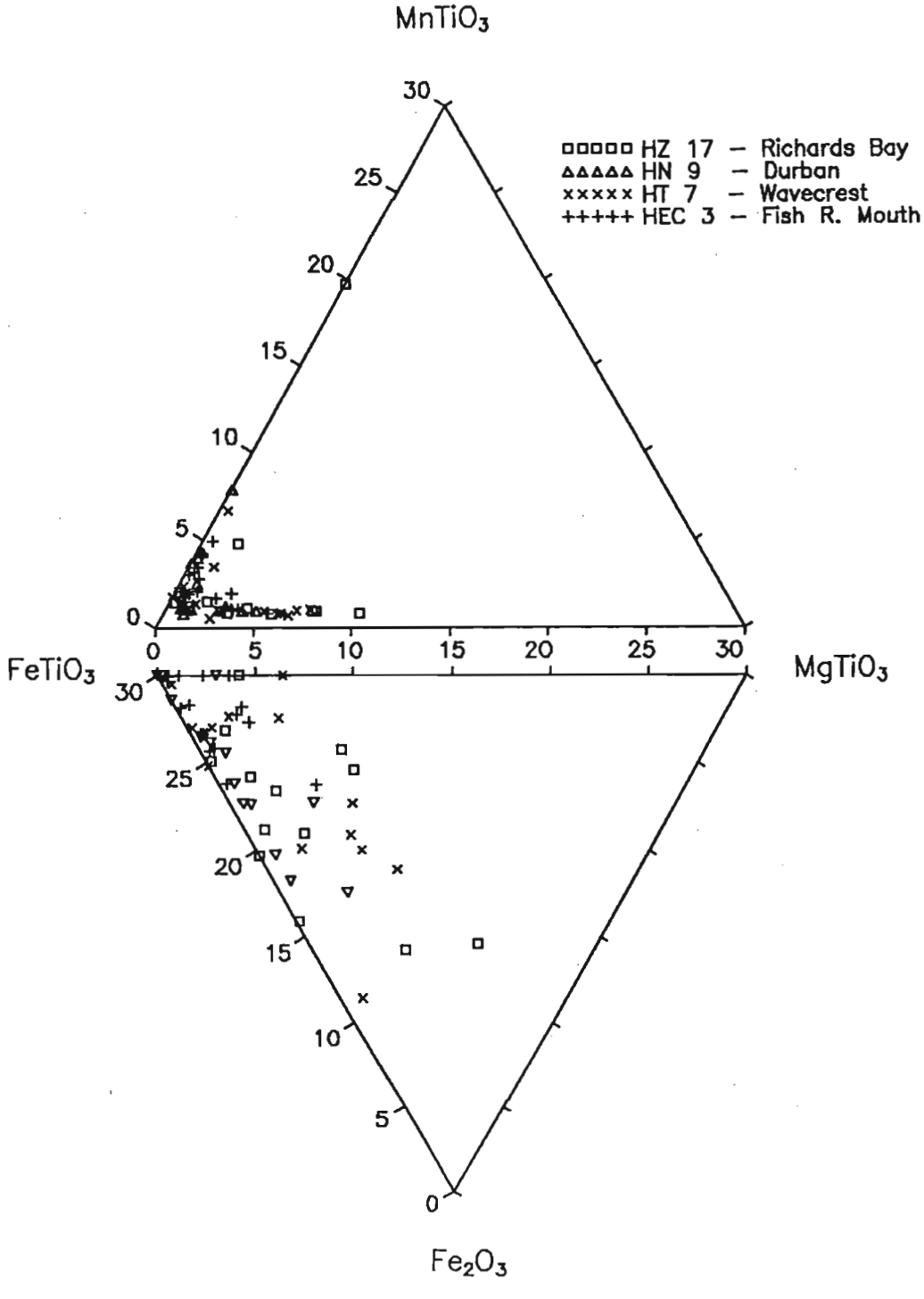

Figure 5.6 Quaternary plot of $FeTiO_3$-Fe_2O_3-$MgTiO_3$-$MnTiO_3$ mole proportions from selected electron microprobe analyses (Table 5.6) of ilmenite grains from the study area.

5.5.3 Petrography of the ilmenite-hematite series

Most ilmenites occur as homogeneous, sub- to well-rounded, slightly elongated grains (Plate 5.2A), which vary in size from 75 μm to 250 μm. Ilmenite is easily recognised in oil-immersion, reflected light by its pinkish-brown colour, moderate pleochroism and bireflectance and strong anisotropism.

Small quantities of skeletal ilmenite crystals are commonly observed in fluvial and coastal sediments. These crystals are almost always surrounded by ferromagnesian silicates, such as augite, (Plates 5.2B and 5.2C) which aids their preservation. Skeletal oxide crystals are formed by the quenching or rapid cooling of magmas. They are derived from volcanic or hypabyssal rocks, more specifically the basalt, rhyolite, or dolerite of the Karoo Igneous Province.

Inclusions of augite, plagioclase, pyrite and other minerals are occasionally found within ilmenite grains. They are either encapsulated in the ilmenite grains (Plate 5.2D) during the growth of ilmenite crystals, or formed by the reaction of ilmenite crystals with the silicate melt (Plate 5.2B). The ferromagnesian silicate inclusions tend to alter readily to clay (Plates 5.2E and 5.2F), or may be leached completely from the ilmenite. The inclusions are important as they contribute to the Si, Ca and Al impurities in ilmenite concentrates. Modal analysis reveals, however, that the inclusions comprise less than 1 per cent in ilmenite concentrates studied (See Chapter 8). A systematic study of the inclusions in ilmenite grains would provide useful information about the provenance of the ilmenite grains.

Under slow cooling conditions in rocks of moderate to high fO_2, hematite (Hem_{ss}) may exsolve from ferrian-ilmenite to form hemo-ilmenite grains $(Ilm_{ss}\text{-}Hem_{ss})_{ex}$ (Plate 5.3A), or ilmenite (ilm_{ss}) may exsolve from titanohematite forming ilmeno-hematite grains $(Hem_{ss}\text{-}Ilm_{ss})_{ex}$ (Plate 5.3B). Typically the exsolutions form lenses parallel to the (0001) direction, or basal plane, of the host. Often two generations of exsolution are observed (Plate 5.3C). Ilmenite-hematite exsolution is most extensive in deep-seated anorthosite suites, but may

also develop in granites (Haggerty, 1976b). Ilmenite-hematite exsolution may also be found in a wide variety of rock types of all metamorphic grades (Rumble, 1976), although Frost (1991a) noted that such textures normally occur in rocks that were oxidised before or during low-temperature metamorphism.

Titanohematite grains in acid igneous suites may contain both ilmenite$_{ss}$ lensoids and rutile lamellae (Plate 5.3D). The latter occur as z-shaped lamellae (Haggerty, 1976b) with strong crystallographic control along the (0111) and (0112) planes of the titanohematite (the "blitz" texture of Ramdohr, 1980). The ilmenite lenses are a result of *sensu stricto* exsolution of ilmenite from the titanohematite host, while the rutile lamellae are formed by oxyexsolution - an exsolution-like process related to oxidation, in the same sense that ilmenite may "exsolve" from magnetite (Haggerty, 1976b). In some instances ilmenite$_{ss}$ lenses may not develop, resulting in assemblages consisting only of hematite$_{ss}$ and rutile (Plate 5.3E).

Ilmenite, in igneous and metamorphic rocks may undergo high-temperature deuteric oxidation. The progress of this oxidation in basalts, as outlined in Table 5.7, has been described in detail by Haggerty (1976a, 1991). Two examples of this oxidation sequence are commonly observed as composite grains in samples from Natal and Zululand:

1. Rutile$\pm$ferrian-rutile+Hem$_{ss}$ as symplectite-like, vermiform or graphic intergrowths within Ilm$_{ss}$, hemo-ilmenite or ilmeno-hematite grains (Plate 5.4). The assemblage is equivalent to the R5 stage of Haggerty (1976a, 1991), but texturally is more like the oxidation of ilmenite from rocks other than basalt (*cf.* Haggerty 1991, Figure 17 and Figure 20 f-j.).

2. Hem$_{ss}$-Rut$\pm$Psb assemblage (Plate 5.5). This assemblage may form by the oxidation of ilmenite or titanomagnetite corresponding to the R5 and C5 stages of oxidation respectively (Haggerty, 1976a). Small amounts of pseudobrookite are occasionally observed, indicating that the R6 and C6 stages of oxidation have been reached. Where ilmenite is the original phase, Hem$_{ss}$ and rutile occur in

approximately equal proportions. Hematite$_{ss}$ dominates the assemblage when titanomagnetite is the original phase.

Microprobe results from Hugo (1988) indicate that ferrian-rutile in these assemblages can contain over 10 per cent FeO, while the TiO_2 content of the hematite$_{ss}$ may be as high as 30 per cent. However, for brevity, the above assemblages are referred to as Ilm-(Rut-Hem$_{ss}$)$_{ox}$, or (Rut-Hem$_{ss}$)$_{ox}$ assemblages in this text.

Ilm-(Rut-Hem) assemblages (excluding pseudobrookite) may also be formed by the hydrothermal or supergene alteration of ilmenite (Ramdohr, 1980; Haggerty, 1976b). Texturally the grains may resemble those formed by deuteric oxidation, although the rutile crystals often form a trigonal network of oriented needles in the basal section of the ilmenite (*cf.* Ramdohr, 1980, Figure 581; see also Grey and Reid, 1975, Figure 4). Anatase-hematite intergrowths may also form from ilmenite as a result of hydrothermal or supergene alteration (*cf.* Haggerty 1976b, Figure 20 h-j; Ramdohr, 1980, Figure 582). Subsequent leaching of hematite results in grains containing a porous network of rutile or anatase microcrystals. Rumble (1976), Ramdohr (1980) and Mücke and Chaudhuri (1991) have noted that rutile or anatase may form directly from ilmenite during hydrothermal or supergene alteration. Grains formed as a result of these processes are described in greater detail in Chapter 6, where they are compared to altered ilmenite grains formed as a result of weathering.

Table 5.7 An outline of the progressive stages of the high temperature oxidation of magnetite (C series) and ilmenite (R series), from Haggerty (1976a).

Stage	Minerals	Notes
C1	magnetite$_{ss}$-ulvöspinel$_{ss}$	optically homogeneous grains
C2	Mt-Usp$_{ss}$-Ilm$_{oc}$	small number of ilmenite lamellae formed along (111) magnetite planes by oxyexsolution
C3	Ti-poor Mt with abundant Ilm$_{oc}$	ilmenite may form trellis, sandwich, or composite types of intergrowths in the magnetite host.
C4	Mt-Ilm$_{oc}$-ferrian-rutile$_{ox}$	mottling within the ilmenite lamellae caused by the formation of ferrian-rutile
C5	Mt-Ilm$_{oc}$-Rut$_{ox}$-Hem$_{ox}$	development of rutile and Hem$_{ss}$ by the oxidation of ilmenite. With more intense oxidation, the rutile and hematite also develop within the magnetite
C6	Rut$_{ox}$-Hem$_{ox}$-Psb$_{ss}$ ± Mt$_{relic}$	incipient pseudobrookite$_{ss}$ forms from rutile and hematite along relic magnetite planes
C7	Psb$_{ss}$-Hem$_{ss}$	most advanced stage of oxidation
R1	Ilmenite	homogeneous grains of ilmenite
R2	ferrian-Ilm + ferrian rutile	wisp-like sigmoidal lenses of ferrian rutile along (0001) and (0111) planes of the ilmenite
R3	ferrian rutile + (ferrian Ilm)	lenses become thicker and more abundant
R4	Ilm + Rut$_{ox}$ + Ti-Hem$_{ox}$	rutile and hematite occur as finely disseminated lamellae in ilmenite host
R5	Rut$_{ox}$ + Hem$_{ss}$	complete replacement of ilmenite by rutile and Hem$_{ss}$
R6	Rut + Ti-Hem ± Psb	this stage is characterised by the incipient development of Psb$_{ss}$
R7	Psb-(Rut + Hem)	Psb$_{ss}$ and hematite become the dominant phases

Plate 5.2 Back-scattered electron images of ilmenite grains.

A. General view of ilmenite concentrate illustrating the homogeneous, sub- to well-rounded nature of the ilmenite grains. Port Durnford, dune (HZ 2). Scale Bar 300 μm.

B. Skeletal ilmenite grain (white), elongated along the *c*-axis, found within a rock matrix of pyroxene (medium grey) with minor plagioclase (dark grey). Note the deep embayment on the right-hand side of the ilmenite, formed by a reaction between the mineral and the surrounding melt. Dolerite, Rooi Rand Dyke Swarm, Pongola River. Scale Bar 60 μm.

C. Skeletal ilmenite grains preserved in a rounded grain of altered pyroxene. Umgababa, dune (HN 2). Scale Bar 60 μm.

D. A subhedral pyroxene inclusion (grey) within an otherwise homogeneous ilmenite grain. Wavecrest, dune (HZ 7). Scale Bar 60 μm.

E. A pyroxene inclusion displaying partial alteration to clay (grey) within a rounded ilmenite grain. Cape Vidal, beach (HZ 10). Scale Bar 60 μm.

F. Clay residue (grey) after the alteration of an inclusion within the ilmenite grain. Port Shepstone, beach (HN 14). Scale Bar 60 μm.

Plate 5.2

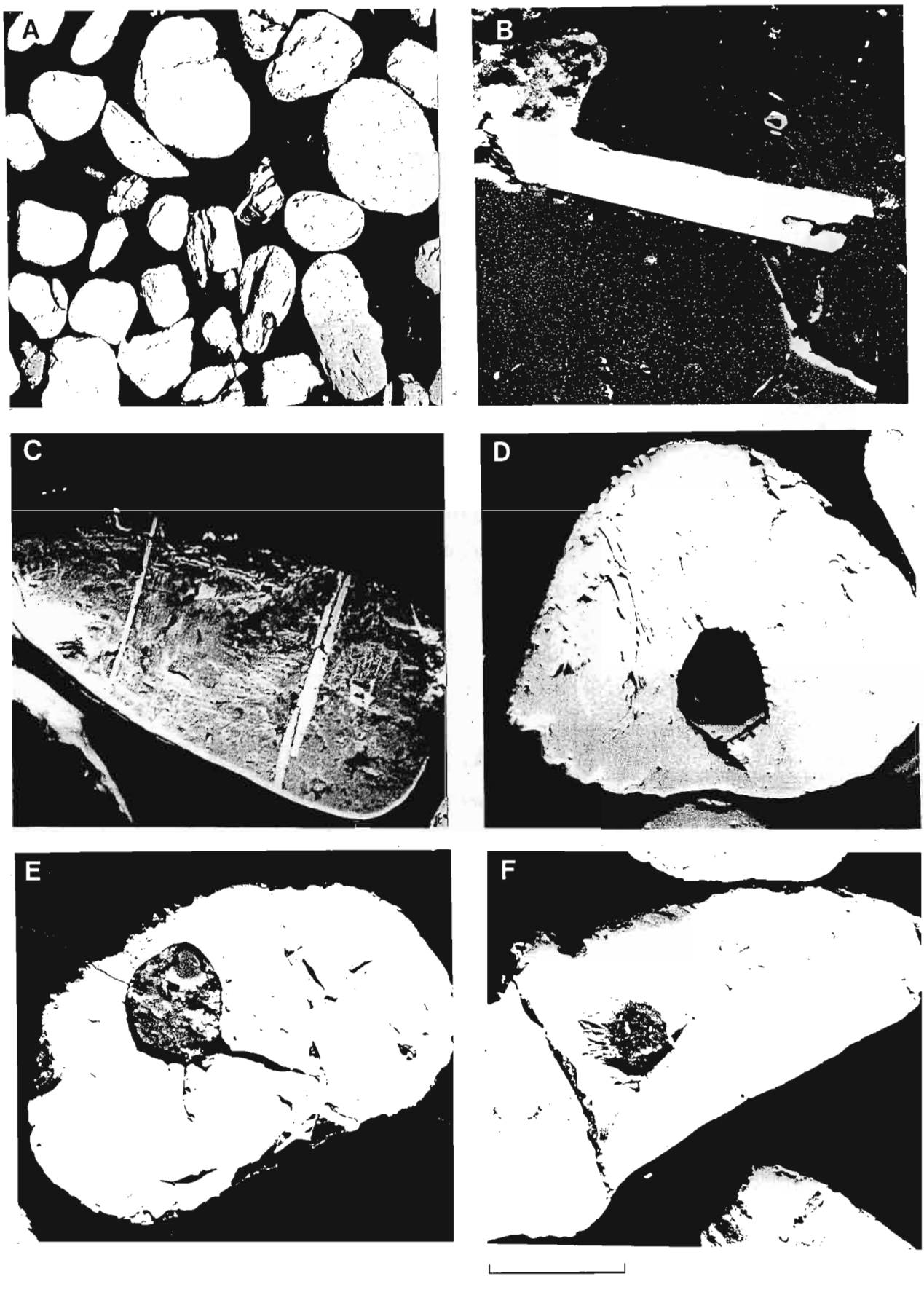

Plate 5.3 Photomicrographs of ilmenite-hematite-rutile grains formed by exsolution and oxyexsolution.

A. Back-scattered electron image of a hemo-ilmenite, $(Ilm_{ss}\text{-}hem_{ss})_{ex}$, grain containing parallel lenses of exsolved Hem_{ss} (white) within the Ilm_{ss} matrix (grey). A much larger $hematite_{ss}$ lamella is observed in the foreground.
Richards Bay, dune (HZ 16). Scale Bar 60 μm.

B. Photomicrograph of an ilmeno-hematite, $(Hem_{ss}\text{-}Ilm_{ss})_{ex}$, grain containing lensoid blebs of exsolved Ilm_{ss} (medium grey) within a Hem_{ss} matrix (white). The large ilmenite lamella at the top of the grain suggests that the grain is a remnant of a much larger grain which contained broad Ilm_{ss} and Hem_{ss} exsolution lamellae. The different size populations of exsolution lamellae (*cf.* Plate 5.3C) suggest that at least two exsolution events occurred. The intimate intergrowth of rutile (dark grey) and hematite (white) within the large ilmenite lamella is formed by oxyexsolution of the ilmenite (*cf.* Plate 5.4). From Hugo (1988). Richards Bay. Reflected light, 32x oil immersion lens. Scale Bar 50 μm.

C. An Ilm-hem_{ss} grain displaying two generations of exsolution. The first exsolution event produced the large lenticular lamellae of Hem_{ss} (white), while the second event formed the small Hem_{ss} and Ilm_{ss} (grey) blebs, within their respective hosts, at lower temperatures. From Hugo (1988). Richards Bay. Reflected light, oil immersion lens. Scale Bar 50 μm.

D. Back-scattered electron image of a $(Hem_{ss}\text{-}Ilm_{ss})\text{-}Rut_{oe}$ grain. The straight rutile lamellae (dark grey), formed by oxyexsolution, cross-cut the lensoid ilmenite exsolution lamellae (light grey). Note how the ilmenite lamellae are partly corroded and no longer homogeneous, in some cases consisting almost entirely of rutile. This suggests that the grain was subjected to further oxidation during cooling, or possibly metamorphism (*cf.* Plate 5.4). Isipingo Beach, beach (HN 4). Scale Bar 43 μm.

E. Back-scattered electron image of a $Hem_{ss}\text{-}Rut_{oe}$ grain. The rutile lamellae (grey), formed by oxyexsolution, create graphic intergrowths within the Hem_{ss} matrix, termed a "blitz" texture by Ramdohr (1980). Durban, beach (HN 9).
Scale Bar 43 μm.

Plate 5.3

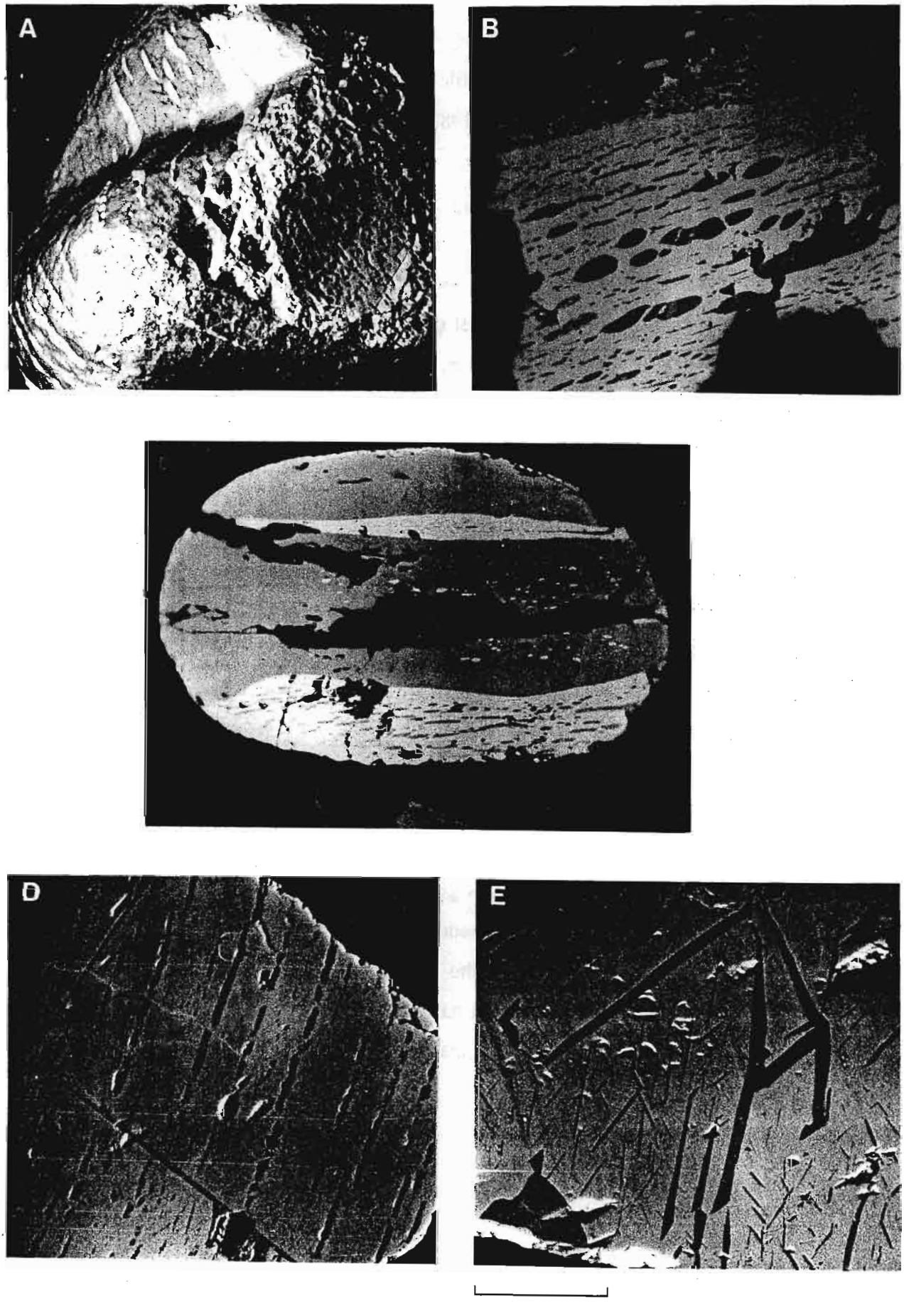

Plate 5.4 Photomicrographs of Rutile + hematite$_{ss}$ + ilmenite$_{ss}$ intergrowths formed by the high-temperature oxidation of ilmenite.

A. Vermiform intergrowth of ferrorutile (grey) and hematite$_{ss}$ (white) formed within an ilmenite grain. From Hugo (1988). Richards Bay. Reflected light, 32x oil immersion lens. Scale Bar 50 μm.

B. A more advanced stage of oxidation, with the ferrorutile (dark grey) - Hem$_{ss}$ (white) intergrowth occupying most of the ilmenite (light grey) grain. Note how the Hem$_{ss}$ has been partially leached from the grain. The complete removal of hematite, probably by acidic groundwater in the weathering environment, results in the formation of ilmenite-rutile grains (see Chapter 6 for details). Port Shepstone, beach (HN 14). Back-scattered electron image. Scale Bar 43 μm.

C. Partial oxidation of ilmenite (medium grey) to rutile (dark grey) + Hem$_{ss}$ (light grey) within an (Ilm$_{ss}$-Hem$_{ss}$)$_{ex}$ grain. Note how the exsolution lamellae of Hem$_{ss}$ have been recrystallised during oxidation. Umdloti, dune (HN 7). Back-scattered electron image. Scale Bar 20 μm.

D. (Hem$_{ss}$-Ilm$_{ss}$)$_{ex}$-Rut$_{oe}$ grain in which the some of the ilmenite lamellae have undergone oxidation to rutile (dark grey) and hematite (light grey). In some cases the rutile-hematite intergrowths pseudomorph the ilmenite lamellae (top, left-hand side), whilst in other instances the lamellae have been partly corroded by the recrystallisation of hematite (right-hand side lamella). Isipingo Beach, beach (HN 4). Back-scattered electron image. Scale bar 30 μm.

Plate 5.4

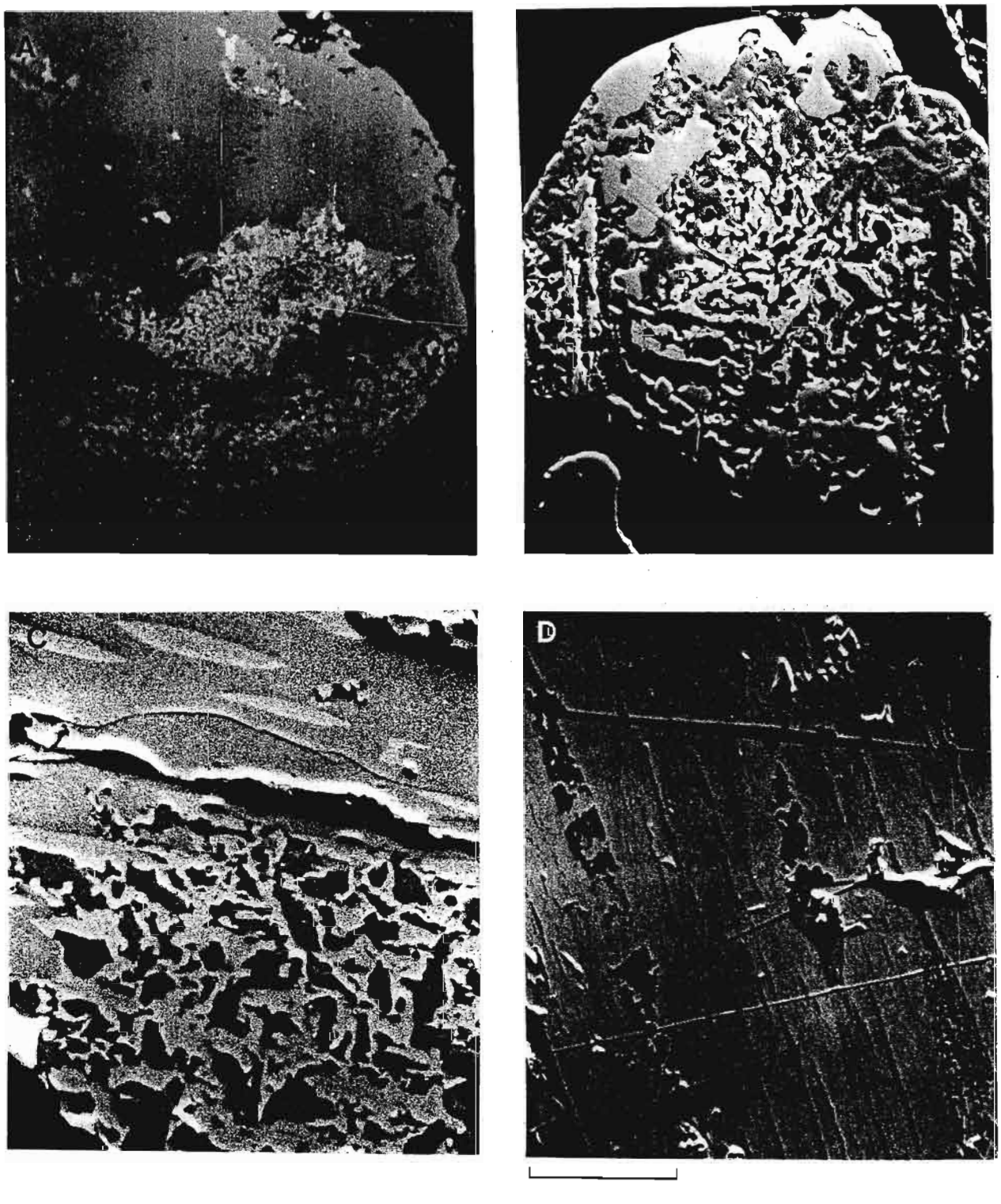

Plate 5.5 Back-scattered electron images of hematite$_{ss}$-rutile$_{ox}$±pseudobrookite grains formed by the high-temperature oxidation of ilmenite.

A. Grain consisting entirely of intergrown Hem$_{ss}$ (white) and Rut$_{ox}$ (grey) corresponding to the R5 stage of Haggerty's oxidation sequence. Tugela River Mouth, beach (HZ 1). Scale bar 50 μm.

B. Complete oxidation of ilmenite in an (Ilm$_{ss}$-Hem$_{ss}$)$_{ex}$ grain to fine-scale rutile (grey) and hematite$_{ss}$ intergrowths. Note how the Hem$_{ss}$ exsolution lamellae have been preserved. Durban, beach (HN 9). Scale bar 43 μm.

C. Sub-graphic intergrowth of ferrorutile (grey) and hematite$_{ss}$ (white) after complete oxidation of an ilmenite$_{ss}$ or (Ilm-Hem)$_{ex}$. Richards Bay, dune (HZ 16). Scale bar 43 μm.

Plate 5.5

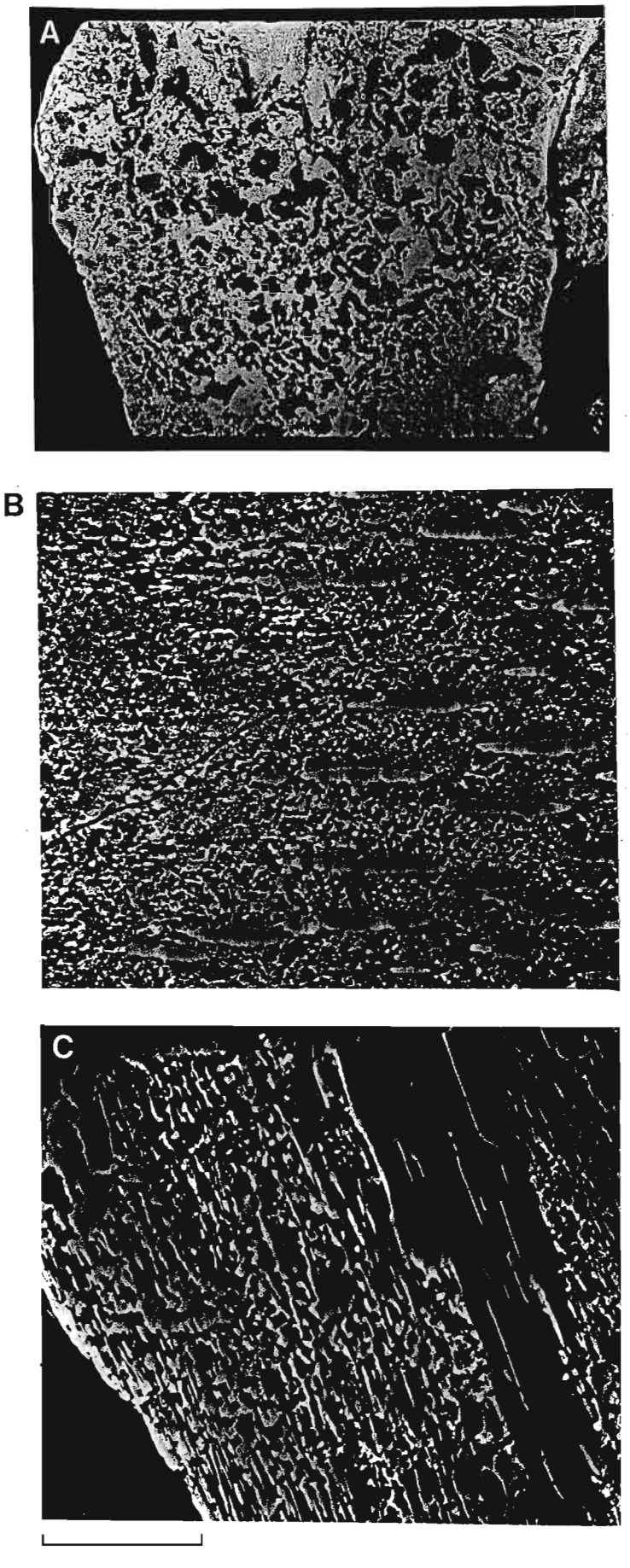

5.6 MAGNETITE-ULVOSPINEL SERIES

5.6.1 Structure

Magnetite ($Fe^{3+}[Fe^{2+}Fe^{3+}]O_4$) has a face-centred, cubic, spinel structure. The unit cell consists of 32 oxygens, which form a nearly cubic-close-packed framework along (111); the divalent and half the trivalent cations occupy octahedral sites, while the remaining trivalent cations occupy tetrahedral interstices between the oxygen layers (Lindsley, 1976).

The spinel structure is able to accept many cations with a wide range of valencies (Lindsley, 1976) and as a result magnetite forms solid-solution series with ulvöspinel ($TiFe_2O_4$), chromian spinels and the pleonaste series ($FeAl_2O_4$-$MgAl_2O_4$). The entire range of composition between magnetite and ulvöspinel is possible, but because of the very low oxygen fugacity required for the formation of stoichiometric ulvöspinel, this mineral is rare. Ulvöspinel usually oxidises to ilmenite to form Mt_{ss}-Ilm_{ss} grains (Elsdon, 1975; Haggerty, 1976b).

5.6.2 Mineral chemistry

In addition to significant amounts of Ti, magnetite may also contain Al, Cr and V substituting for Fe^{3+}, while Mg, Mn, Ca and Co substitute for Fe^{2+} (Elsdon, 1975). Buddington *et al.* (1963) determined that the TiO_2 content of titaniferous magnetites decrease with increasing SiO_2 content of the host rock from basic to felsic. Magnetite from basic rocks of the Karoo Province is thus expected to have higher TiO_2 contents (5 to 30 per cent) than those from granitoids (< 5 per cent TiO_2) in the Natal Metamorphic Province. In addition, the spinel minerals tend to re-equilibrate readily during cooling via inter-grain reactions. As a result magnetites in slow-cooled igneous or metamorphic rocks have compositions close to pure Fe_3O_4, with only small amounts of TiO_2 (< 1 per cent) and trace amounts of other elements (Frost and Lindsley, 1991; Frost, 1991b). Titaniferous magnetite and magnetite are therefore expected to be good indicators of provenance.

Magnetite grains were analysed by electron microprobe for Ti, Fe (reported as FeO), Mn, Mg, Cr, Al and Si as outlined in Table 4.1 (page 63). Homogeneous grains were generally analysed, but some magnetite grains containing ilmenite, ulvöspinel or pleonaste intergrowths were also analysed. The FeO and Fe_2O_3 contents were recalculated from the probe analyses by stoichiometry on the basis of four cations, after Stormer (1983). Representative magnetite analyses are shown in Table 5.8 and the full list of magnetite analyses is given in Appendix B.3.

The chemical variation in magnetite grains found within sediments along the southern African east coast is illustrated in Figure 5.7A-D, which shows the following features:

1. Ti is the major substituent for iron and almost the entire composition range between ulvöspinel and magnetite is present (Figure 5.7A). The wide range in TiO_2 contents suggests that the magnetite grains are derived from a variety of source rocks.

2. The strong negative correlation between the TiO_2 and Fe_2O_3 contents indicates that many of the magnetites have near-stoichiometric compositions and have not been affected by oxidation.

3. Other elements such as Mn, Mg, Al and Cr (Figures 5.7B-D) are present in small, variable amounts, which indicates that there is generally little solid-solution between titanomagnetite and the other spinel series. The variable nature of these elements is probably a function of source rock composition and re-equilibration with ilmenite and silicate grains during cooling.

Table 5.8 Representative magnetite microprobe analyses.

Analysis		SiO2	TiO2	Al2O3	Cr2O3	MnO	MgO	Recalculated FeO	Recalculated FeO	Recalculated Fe2O3	Total
HZ 4	1	0.14	17.59	0.91	0.04	0.79	0.05	76.91	46.80	33.46	99.78
HZ 4	2	0.03	21.31	1.48	0.11	0.46	0.26	72.56	49.89	25.20	98.72
HZ 4	3	0.04	18.86	2.26	0.13	0.55	0.27	75.08	48.12	29.96	100.19
HZ 4	4		0.07	0.05	0.07		0.01	91.26	30.52	67.50	98.25
HZ 4	5	3.92	29.60	2.14		1.68	0.08	62.80	62.46	0.38	100.27
HZ 4	6	0.30	24.86	1.12	0.08	1.04	0.32	69.41	52.88	18.36	98.97
HZ 4	7	0.18	13.02	1.87	0.14	0.50	0.06	79.46	42.89	40.63	99.30
HZ 4	8	0.18	14.44	1.32	0.11	0.48	0.09	78.67	44.05	38.47	99.14
HZ 4	9	1.06	29.40	0.65	0.04	2.65	0.08	57.85	54.65	3.56	92.08
HZ 4	10	0.07	26.69	1.17	0.10	0.12	0.12	64.70	54.03	11.86	94.16
HN 3	1	0.50	12.40	1.93	0.27	0.74	0.18	79.80	42.54	41.40	99.97
HN 3	2	0.07	17.74	1.37	0.17	0.75	0.11	76.59	46.97	32.92	100.08
HN 3	3	0.04	11.75	2.60	0.26	0.20	0.04	80.59	42.15	42.72	99.76
HN 3	4	1.28	12.01	1.89	0.17	0.54	0.65	79.52	42.76	40.86	100.15
HN 3	5	4.44	25.69	1.10	0.11	0.69	0.12	67.87	60.44	8.26	100.84
HN 3	6		0.08	0.06	0.10	0.12		91.99	30.78	68.03	99.18
HN 3	7	1.23	20.71	1.77	0.17	1.23	0.37	71.02	50.08	23.27	98.82
HN 3	8	1.29	22.08	1.54	0.09	0.75	0.22	72.11	52.56	21.73	100.25
HN 3	9			0.06		0.07		90.56	30.16	67.12	97.41
HN 3	10	0.37	23.89	1.01		1.04	0.66	70.93	51.87	21.18	100.02
HT 3	1	0.08	19.99	2.01	0.10	0.80	0.92	71.19	47.17	26.70	97.76
HT 3	2	0.08	33.40	0.63	0.06	1.14	0.04	64.42	61.14	3.64	100.13
HT 3	3	0.21	6.71	0.72	0.13	0.19	0.04	85.57	37.11	53.85	98.95
HT 3	4	0.10	19.35	1.68	0.14	0.34	0.06	75.26	48.97	29.21	99.85
HT 3	5	3.82	10.02	3.63	0.11	0.26	0.14	76.32	44.95	34.86	97.79
HT 3	6	0.31	19.18	1.46	0.15	0.71	0.03	72.51	47.89	27.36	97.08
HT 3	7	0.20	12.05	3.86	0.17	0.29	0.06	76.56	41.89	38.52	97.05
HT 3	8	0.13	23.69	0.83	0.09	0.47	0.15	70.15	51.91	20.27	97.55
HT 3	9	0.13	5.54	1.56	0.13	0.16		87.30	36.62	56.32	100.46
HT 3	10	0.63	2.06	0.62	0.14	0.08	0.09	89.14	33.36	61.98	98.96
HEC 3	1	0.55	11.44	0.80	0.04	0.17	0.26	82.15	41.94	44.69	99.88
HEC 3	2	0.30	29.92	1.33	0.04	0.72	0.10	64.49	57.89	7.34	97.64
HEC 3	3	1.01	12.22	1.42	0.04	0.67	0.25	78.91	42.48	40.48	98.56
HEC 3	4	0.10	14.87	1.37	0.04	0.83	0.09	77.61	43.85	37.52	98.66
HEC 3	5	0.12	17.00	1.44	0.04	0.72	0.05	77.34	46.50	34.27	100.13
HEC 3	6	6.93	1.86	3.79		0.18	0.12	82.56	42.32	44.71	99.94
HEC 3	7	3.13	24.33	1.19		0.72	0.46	67.13	56.08	12.28	98.22
HEC 3	8		8.25	0.51	0.12	0.44	0.07	83.67	37.71	51.08	98.19
HEC 3	9		3.91	1.05	0.16	0.23	0.21	85.96	33.49	58.31	97.36
HEC 3	10		5.42	0.35		0.69	2.58	85.64	31.68	59.96	100.73

HZ 3 - Port Durnford, Zululand

HN 3 - Umgababa, Natal

HT 3 - Port St Johns, Transkei

HEC 3 - Fish River Mouth, Eastern Cape

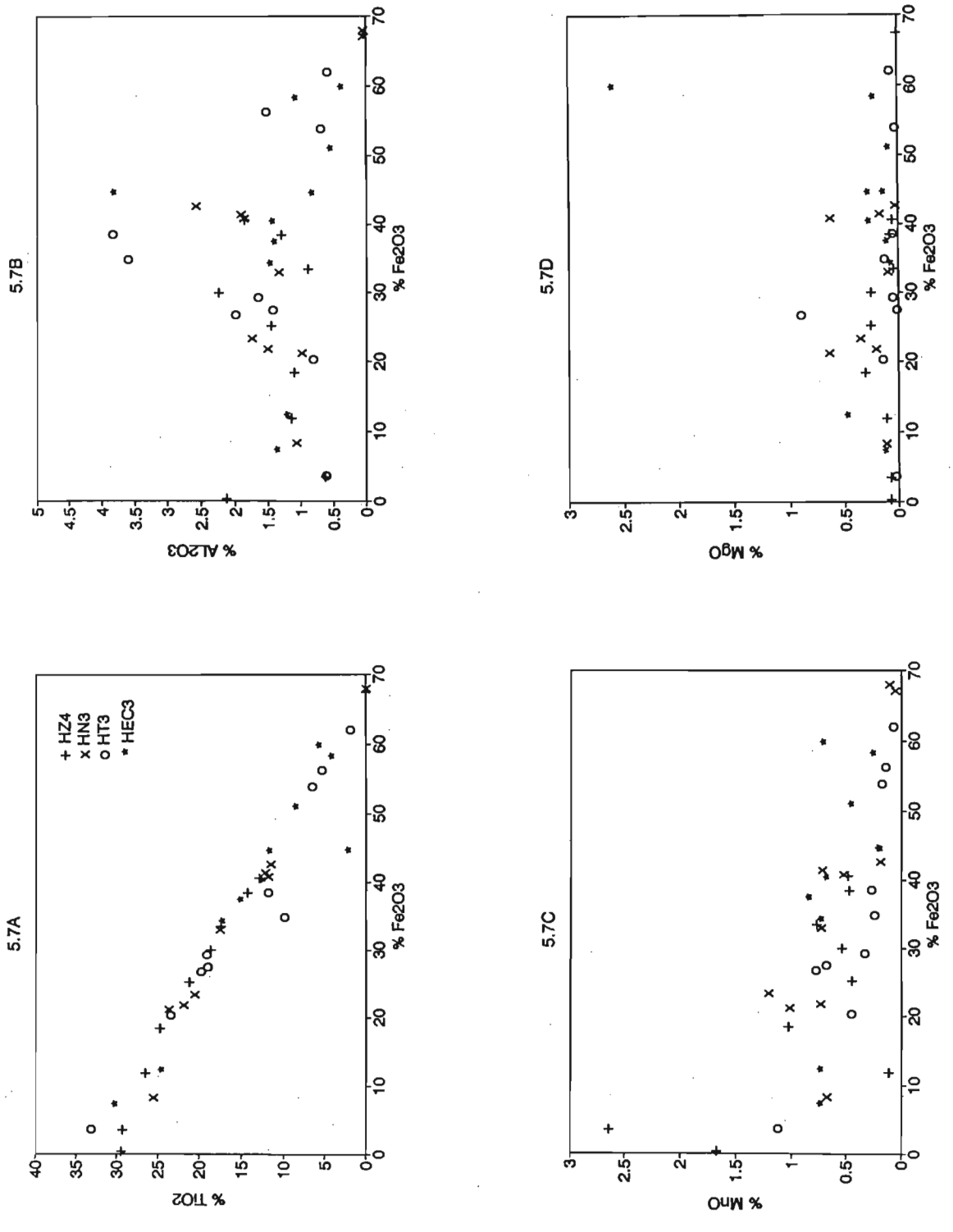

Figure 5.7 Variations in TiO_2 (**A**), Al_2O_3 (**B**), MnO (**C**), and MgO (**D**) versus Fe_2O_3 for magnetites from selected samples along the east coast of South Africa (data from Table 5.8).

A few Cr-rich spinels are found in the coastal sediments. Although these phases contain little titanium, they are of interest as a source of chromium impurities in ilmenite concentrates from the east coast (Logan, 1974; Hugo, 1988). A number of Cr-rich spinels were analysed by electron microprobe, which reveal that two types of Cr-bearing spinel are found in the sediments (Table 5.9 and Figure 5.8): chromian spinel close to chromite in composition, with low Fe^{3+} content and chromian magnetite falling within the $FeCr_2O_4$-$FeAl_2O_4$-Fe_3O_4 quaternary.

The chromites tend to have similar magnetic susceptibilities to ilmenite and are thus found in ilmenite concentrates, while the chromian magnetites are almost as magnetic as magnetite and are therefore easily separated from ilmenite (Logan, 1974; Lee and Poggi, 1978; Hugo, 1988).

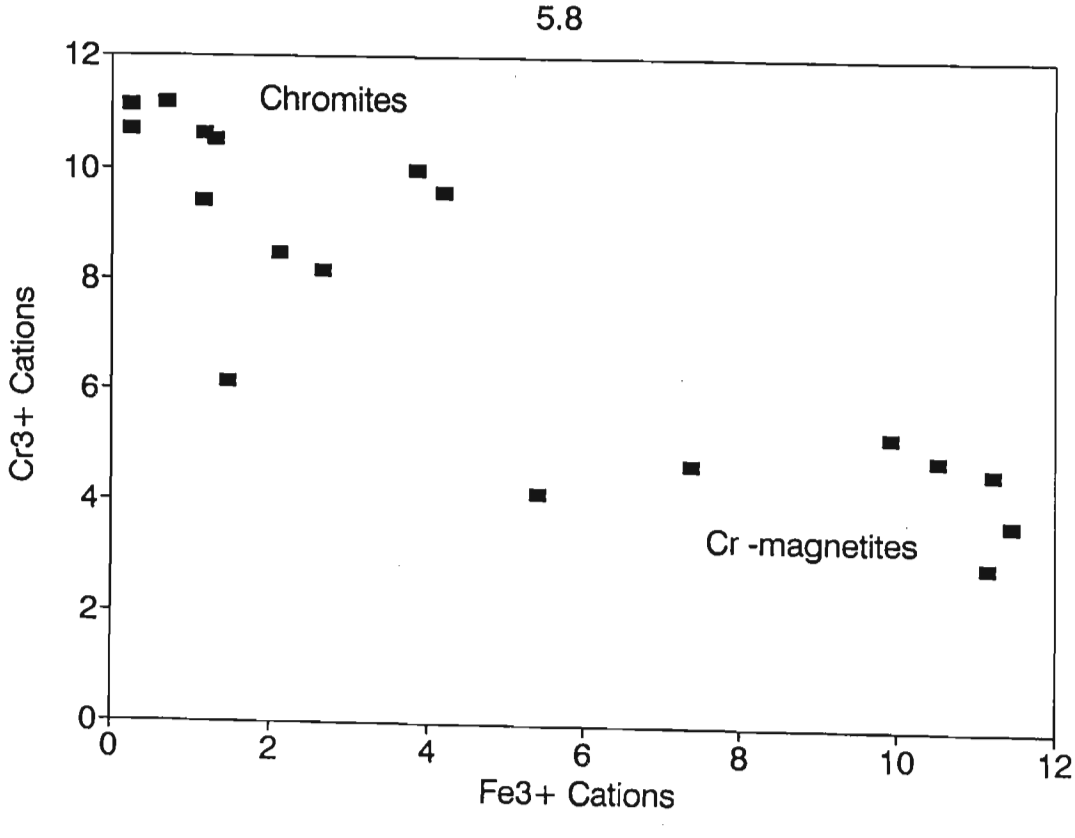

Figure 5.8 Variation diagram showing the difference in composition between chromites and chromian-magnetites found in the east coast sediments (data from Table 5.9).

Table 5.9 Microprobe analyses of Cr-rich spinels.

								Recalculated			Cations per 32 Oxygens							
Sample	SiO2	TiO2	Al2O3	Cr2O3	FeO	MnO	MgO	FeO	Fe2O3	Total	Si4+	Ti4+	Al3+	Cr3+	Mn2+	Mg2+	Fe3+	Fe2+
HZ 17	-	0.72	4.61	12.69	74.59	0.35	1.90	29.40	50.22	99.88	0.00	0.16	1.60	2.95	0.09	0.83	11.13	7.24
HZ 17	-	-	2.42	22.14	62.77	0.55	4.57	23.23	43.94	96.86	0.00	0.00	0.86	5.24	0.14	2.04	9.90	5.82
HZ 17	-	0.10	0.34	18.63	69.46	0.58	1.88	26.67	47.55	95.76	0.00	0.02	0.12	4.62	0.16	0.88	11.21	6.99
HZ 13	-	0.06	1.77	20.20	66.64	0.42	3.43	25.12	46.14	97.15	0.00	0.01	0.63	4.83	0.11	1.55	10.51	6.36
HZ 13	-	5.25	4.99	21.03	60.20	0.35	5.09	29.05	34.61	100.37	0.00	1.12	1.67	4.71	0.08	2.15	7.38	6.89
HZ 18	-	0.99	11.90	49.29	32.03	0.27	4.90	26.98	5.61	99.94	0.00	0.20	3.82	10.62	0.06	1.99	1.15	6.15
HZ 18	-	1.02	11.77	49.00	31.98	0.28	5.38	26.27	6.34	100.07	0.00	0.21	3.77	10.52	0.06	2.18	1.30	5.97
HZ 18	1.21	0.50	12.05	52.61	24.79	0.52	7.56	23.70	1.21	99.36	0.32	0.10	3.79	11.11	0.12	3.01	0.24	5.30
HZ 2	0.49	1.22	10.56	51.67	27.68	0.54	6.43	24.71	3.30	98.92	0.13	0.25	3.40	11.15	0.12	2.62	0.68	5.64
HZ 2	0.58	0.34	14.70	50.58	24.56	0.41	7.21	23.52	1.15	98.50	0.16	0.07	4.63	10.69	0.09	2.87	0.23	5.26
HZ 2	0.25	6.56	5.43	33.15	37.00	0.64	3.31	29.23	8.63	87.20	0.08	1.60	2.07	8.48	0.18	1.60	2.10	7.91
HZ 2	0.19	0.58	1.34	15.65	73.24	0.43	2.65	27.53	50.79	99.17	0.06	0.13	0.47	3.71	0.11	1.18	11.45	6.90
HZ 1	-	10.35	5.56	18.27	59.64	0.52	2.45	37.40	24.72	99.27	0.00	2.26	1.90	4.19	0.13	1.06	5.39	9.07
HZ 1	0.19	2.34	13.51	43.39	26.00	0.19	8.94	21.04	5.51	95.11	0.05	0.48	4.37	9.42	0.04	3.66	1.14	4.83
G121	-	0.13	28.33	31.19	29.85	0.31	8.56	22.86	7.76	99.15	0.00	0.02	8.34	6.16	0.07	3.19	1.46	4.77
G122	-	1.70	4.12	43.71	47.50	0.45	1.44	31.57	17.71	100.69	0.00	0.37	1.41	10.00	0.11	0.62	3.86	7.64
G123	-	0.50	5.83	41.61	46.82	0.25	1.90	29.63	19.10	98.82	0.00	0.11	2.00	9.59	0.06	0.83	4.19	7.22
G124	-	0.60	15.80	38.95	32.56	1.20	8.30	20.60	13.29	98.74	0.00	0.12	4.94	8.17	0.27	3.28	2.65	4.57

Analyses G121-G124 are from Hugo (1988).

HZ 17 - Richards Bay, Zululand
HZ 13 - Sodwana Bay, Zululand
HZ 18 - Umhlatuze, Zululand
HZ 2 - Port Durnford, Zululand
HZ 1 - Tugela River Mouth, Zululand

5.6.3 Petrography of the magnetite-ulvöspinel series

Skeletal grains of magnetite are common in samples from Zululand and are observed in small quantities in samples from other areas. These grains are often idiomorphic, display cruciform or complex morphologies (Plate 5.6) as described by Haggerty (1976a) and are usually partly enclosed in pyroxene grains. The grains are formed by incomplete growth of magnetite crystals, preserved by rapid cooling of the magma (Haggerty, 1976a; *cf.* Eales *et al.*, 1980, Figure 3). Often the magnetites display fine trellis lamellae of ilmenite formed by oxyexsolution of Usp_{ss}.

$Ulvöspinel_{ss}$ may be exsolved as microcrystalline lamellae parallel to (100) in magnetite grains, forming a characteristic cloth or woven texture (Plate 5.7A) (Ramdohr 1953, 1980; Vincent and Phillips, 1954 and many others). This indicates the existence of low fO_2 conditions during cooling of the source rock at temperatures below the magnetite-ulvöspinel solvus (Reynolds, 1983), as ulvöspinel oxidises readily to ilmenite by the reaction (Duchense, 1970; Elsdon, 1975):

$$3\ Fe_2TiO_4 + \tfrac{1}{2}O_2 \rightarrow 3\ FeTiO_3 + Fe_3O_4 \qquad \text{---- (5.1)}$$

If oxidation occurs below the solvus, ulvöspinel will exsolve from magnetite before undergoing an *in situ* transformation to ilmenite (Duchesne, 1970) (Plate 5.7B). This process gives rise to a cloth texture of ilmenite in magnetite. If the oxidation of ulvöspinel occurs above the solvus, ilmenite may "exsolve" directly from magnetite. Grains displaying true cloth texture between ulvöspinel and magnetite are seldom observed.

$Mt\text{-}Ilm_{oe}$ grains consisting of magnetite with ilmenite lamellae are commonly observed. These lamellae may develop parallel to the (111) magnetite planes, resulting in a trellis texture (Plate 5.7C), or only along one set of (111) planes, forming sandwich textures (Plate 5.7D). Ilmenite may also occur as subhedral to anhedral inclusions, or partly enclosed granules within titaniferous magnetite, forming composite grains. The titaniferous magnetite in these composite grains usually contains either trellis (Plate 5.7E) or sandwich (Plate 5.7F) lamellae of ilmenite.

The trellis textures are formed by oxyexsolution of ilmenite from titanomagnetite (Haggerty, 1976a), but the sandwich lamellae may form by either oxyexsolution or simultaneous crystallization of ilmenite and magnetite (Buddington and Lindsley, 1964; Duchesne, 1970; Haggerty, 1976b). Likewise, the composite types may have formed by either process (Haggerty, 1991).

As with ilmenite, Haggerty (1976a, 1991) has classified the stages of high temperature (> 600°C) titanomagnetite oxidation and the trellis and sandwich type grains observed correspond to stages C1 to C3 of Haggerty's oxidation sequence (see Table 5.7, page 94). No grains corresponding to the C4-C6 stages are observed, but graphic or symplectite-like intergrowths of Hem_{ss}-Psb_{ss}-Rut assemblages, resembling the C7 stage of oxidation are often found (Plate 5.8). These assemblages are formed by rapid oxidation of the original titanomagnetite (*cf.* Haggerty, 1991, Figures 11 d-f).

Pleonaste ($FeAl_2O4$-$MgAl_2O_4$) may exsolve from magnetite grains as small orientated blebs, usually post-dating sparse ilmenite oxyexsolution lamellae (Plate 5.9). Such grains are commonly derived from metamorphosed mafic and ultramafic rocks (Grigsby, 1990) and are good indicators of provenance.

Magnetite and ilmeno-magnetite may undergo oxidation to hematite in source rocks at temperatures above 550°C (Lepp, 1957). This results in fairly broad, straight-sided, or anhedral hematite lamellae orientated along the (111) magnetite planes (Plate 5.10A). This replacement is colloquially referred to as martitisation (Haggerty, 1976b). The ilmenite lamellae, if present, are unaffected and extreme oxidation leaves ilmenite lamellae in a matrix of hematite. Martitisation is also known to occur in the sedimentary environment (Haggerty, 1976a; Riezebos, 1979), resulting in thin hematite lamellae, again orientated along (111) magnetite planes. These develop inwards from the grain surfaces (Plate 5.10B to 5.10D). Martitised magnetite grains are commonly observed in the coastal sediments.

At moderate temperatures (200-375°C), in basic igneous rocks magnetite and titaniferous magnetite can undergo oxidation-alteration to the cation-deficient metastable maghemite

or titanomaghemite series (Lepp, 1957; Basta, 1959; Lindsley, 1976). The maghemite develops along cracks within magnetite, or adjacent to ilmenite lamellae (see Plate 5.11A). Ilmenite is unaffected by the alteration and complete maghemitization of Mt-Ilm_{oe} grains results in maghemite-ilmenite assemblages (Plate 5.11B).

Magnetite-ilmenite-titanite assemblages are formed by the late-stage, metasomatic alteration of either ilmenite lamellae or magnetite to titanite in Mt-Ilm_{oe} grains (Haggerty, 1976b; Reynolds, 1986c). Turner (1990) found that the magnetite alters to titanite, while the ilmenite lamellae remain unaltered in Karoo basalt and dolerite (Plate 5.11C and 5.11D). Chlorite, amphibole or quartz may also replace titaniferous magnetite as a result of late-stage metasomatism (Reynolds, 1986c; Richards *et al.*, 1991). The ilmenite lamellae remain unaffected (Plate 5.12A and 5.12B), although in some extreme cases the ilmenite may be recrystallised (Plate 5.12C), or altered to titanite or rutile, as noted by Richards *et al.* (1991). In some cases these replacement minerals are subsequently leached from the grains, leaving an orientated framework of ilmenite lamellae (Plate 5.12D). Grains of this type are rarely observed in coastal sediments.

Vermiform intergrowths of ilmenite and hydrous ferromagnesian silicates are common in Karoo dolerites which have undergone deuteric alteration (*cf.* Reynolds, 1983, Figure 4; Turner, 1990). Reynolds (1983) interpreted these intergrowths as having been formed by the alteration of titaniferous magnetite by late-stage hydrothermal fluids. The rounded nature of the vermiform ilmenite is created by the overgrowth of ilmenite, formed in the reaction, onto existing Ilm_{oe} lamellae. Reynolds (1983) claimed that this explained the optical continuity of the ilmenite bodies in the ilmenite-silicate intergrowths, as the original ilmenite lamellae were orientated along the (111) planes of the original titaniferous magnetite host. In contrast, Plate 5.13 shows that ilmenite in composite ilmenite-magnetite grains may undergo alteration to form the vermiform ilmenite-silicate intergrowths described by Reynolds (1983), while the titaniferous magnetite remains relatively unaltered. It is also clear from Plate 5.13 that the reaction proceeds from the ilmenite-silicate interface and not from titaniferous magnetite as would be expected if the intergrowth were formed by the breakdown of magnetite.

Unfortunately no chemical analyses of the intergrown silicate minerals were obtained and a chemical reaction cannot be proposed to describe the ilmenite alteration. It is worth noting that the vermiform ilmenite-silicate intergrowths are very similar to those formed by the replacement of ilmenite by aenigmatite ($Na_2Fe_5TiSi_6O_{20}$) as described by Haggerty (1976b, Figure Hg-30 g-h). Haggerty (1976b) reasoned that the reaction is caused by Na and Si-rich metasomatic fluids and observed that replacement is common in the pegmatoid zones of thick basalts and that magnetite in ilmeno-magnetite grains is unaffected by this metasomatism. In light of the petrographic evidence it is felt that Haggerty (1976b) provides a better explanation for the formation of vermiform ilmenite grains than Reynolds (1983).

Chromite and chromian magnetite are easily distinguished from magnetite under reflected light by their lower reflectance and grey-brown colour. The chromite grains are homogeneous, but the chromian magnetites often display characteristic growth zoning, or have mantles of titaniferous magnetite (Plate 5.13C). Haggerty (1976b) and Eales *et al.* (1980) note that the cores of these latter spinels are Cr-rich, while the rims are rich in Fe and Ti, due to the reaction of early-formed chromites with Fe-Ti rich liquids.

5.7 OTHER TITANIUM-RICH MINERALS

In addition to the minerals described above, titanium may be present in a number of other phases. A brief description of these minerals, with a discussion of their relevance to the East Coast deposits is given below:

1. *Titanite*: Trace amounts of titanite are found in heavy mineral suites along the east coast. Hugo (1988) noted that unaltered titanites from Richards Bay had near-stoichiometric compositions (ie. $CaTiSiO_5$). However, the titanites display varying degrees of alteration to leucoxene, as described by Golding (1961). The mineral has also been observed by Du Toit (1979) replacing ilmenite in amphibolites which have undergone retrograde metamorphism from high to low grades (Plate 5.13D).

2. *Pseudobrookite*: Homogeneous pseudobrookite is very rare in the deposits and is only occasionally observed in composite grains together with ferrorutile or Hem_{ss} formed by high temperature oxidation of ilmenite or titaniferous magnetite.
3. *Titanium in silicates*: The amount of titanium in the deposits present in silicates such as augite, hornblende and biotite has not been determined, but given the normal provenance of the silicates, the amount of titanium in these phases is expected to be insignificant compared with that of iron-titanium oxide phases.

5.8 DISCUSSION

From a mineral processing viewpoint, the textures within composite grains are of little importance, as it is only the mineral proportions in a grain that determine the grain's behaviour during concentration. The paragenesis of the composite grains does provide useful information regarding the provenance of the titanium-bearing minerals, which in turn controls the distribution of these minerals along the coastline.

Microscopic examination of the iron-titanium oxides clearly demonstrates that the petrography of these phases along the east coast of South Africa is both varied and complex. The textures of composite grains which were formed by processes in the source rocks are often well preserved in the coastal sediments. The composite grains exhibit textures formed by a number of different processes (see Plates 5.4D and 5.12B). As described in the following chapter, alteration of composite grains in the sedimentary environment adds further textural characteristics and at times overprints the source rock textures, making petrographic interpretation difficult. Nevertheless, careful petrographic examination of the composite iron-titanium grains often provides sound evidence for the origin and paragenesis of the mineral assemblage.

Plate 5.6 Back-scattered electron images of skeletal titaniferous magnetite grains.

A. Skeletal titaniferous magnetite crystals preserved within a rounded pyroxene grain. The crystals are of the cruciform and complex types (*cf.* Haggerty, 1976 b, Figure Hg-25). Cape St Lucia, dune (HZ 5). Scale bar 150 μm.

B. Cruciform titaniferous magnetite crystal preserved in a silicate grain (top right). Note how the magnetite appears to have been partially resorbed by the silicate melt before quenching. The magnetite contains small ilmenite lamellae and is partially altered to maghemite (medium grey). Sodwana Bay, beach (HZ 12). Scale Bar 75 μm.

C. Sub-idiomorphic grain of titaniferous magnetite formed by the partial crystallisation of a cruciform-type crystal. The titaniferous nature of the magnetite is displayed by the oxyexsolution of thin ilmenite (light grey) lamellae (see text for explanation). Once again the morphology of the grain has been preserved by its partial enclosure in pyroxene. Cape Vidal, dune (HZ 11). Scale bar 60 μm.

D. Nearly euhedral titaniferous magnetite grain displaying ilmenite (light grey) trellis lamellae (*cf.* Plate 5.7C). Cape St Lucia, dune (HZ 5). Scale Bar 75 μm.

Plate 5.6

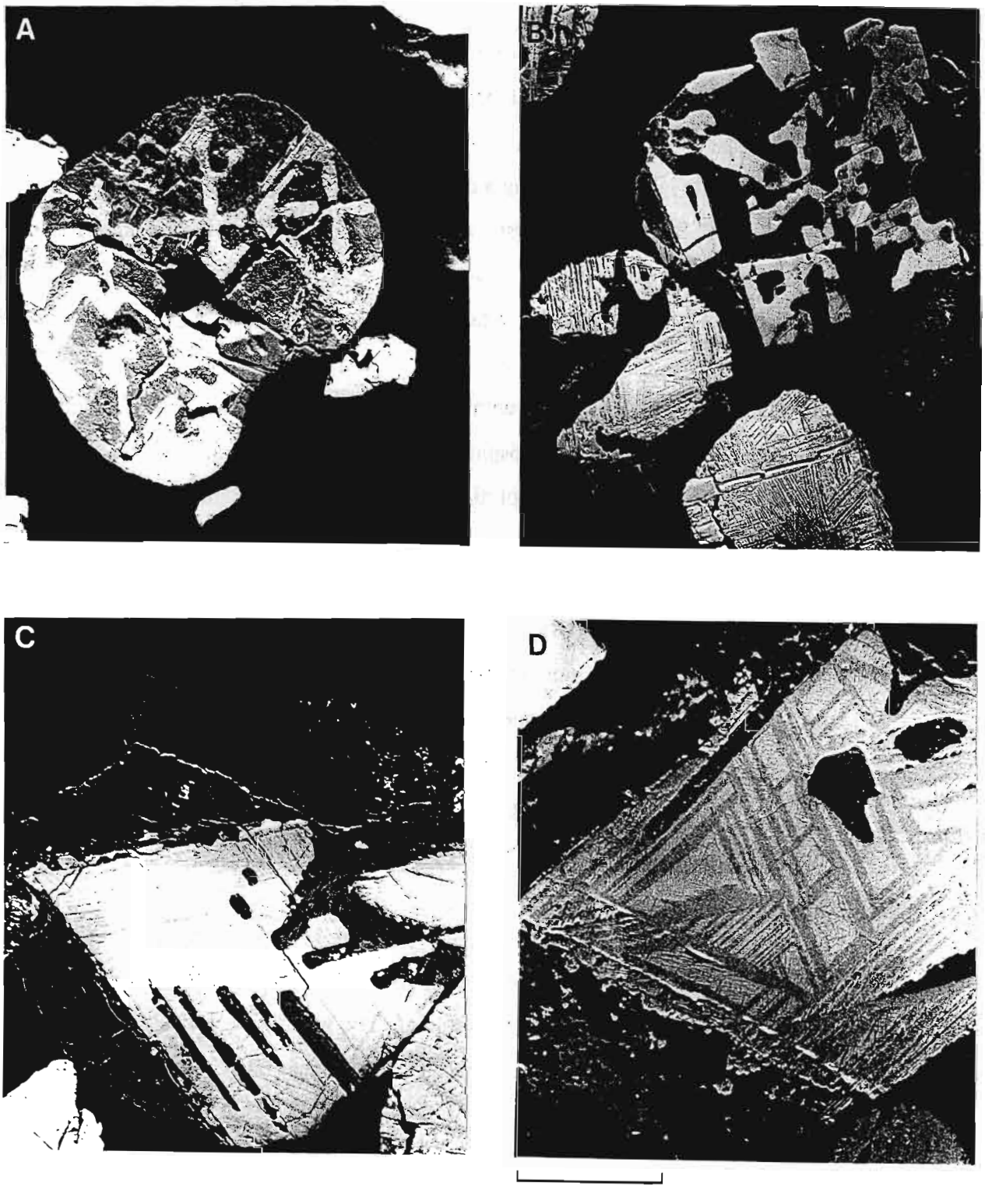

Plate 5.7 Back-scattered electron images of exsolution and oxyexsolution textures within titanomagnetite grains.

A. $Magnetite_{ss}$ (white) containing fine-scale exsolution lamellae of ulvöspinel defining a cloth texture. The homogeneous grey mineral adjacent to the magnetite is ilmenite. Port St Johns, beach (HT 3). Scale Bar 30 μm.

B. Fine-scale ilmenite lamellae defining a cloth or woven texture in a magnetite (light grey) grain. The lamellae were first formed by the exsolution of ulvöspinel from titanomagnetite before undergoing sub-solvus oxidation to ilmenite (see text for details). Hlatimi beach, (HN 11). Scale bar 25 μm.

C. Trellis lamellae of ilmenite (grey) with a magnetite grain. The ilmenite lamellae are formed by the oxidation of ulvöspinel to ilmenite above the solvus resulting in the direct "exsolution", or oxyexsolution of ilmenite from magnetite. Umdloti, dune (HN 7). Scale bar 30 μm.

D. Sandwich lamellae of ilmenite (grey) in magnetite formed by oxyexsolution. The magnetite has subsequently undergone partial alteration to titanite (dark grey). Richards Bay, dune (HZ 17). Scale bar 30 μm.

E. Composite Mt-Ilm grain consisting of homogeneous ilmenite (medium grey) and magnetite (light grey) containing trellis lamellae of Ilm_{oe}. Port St Johns, beach (HT 3). Scale bar 43 μm.

F. Composite Mt-Ilm grain consisting of large homogeneous ilmenite lamellae and magnetite containing Ilm_{oe} sandwich lamellae. The genesis of the composite Mt-Ilm grains is discussed in the text. Morgan's Bay, beach (HEC 7).
Scale Bar 43 μm.

Plate 5.7

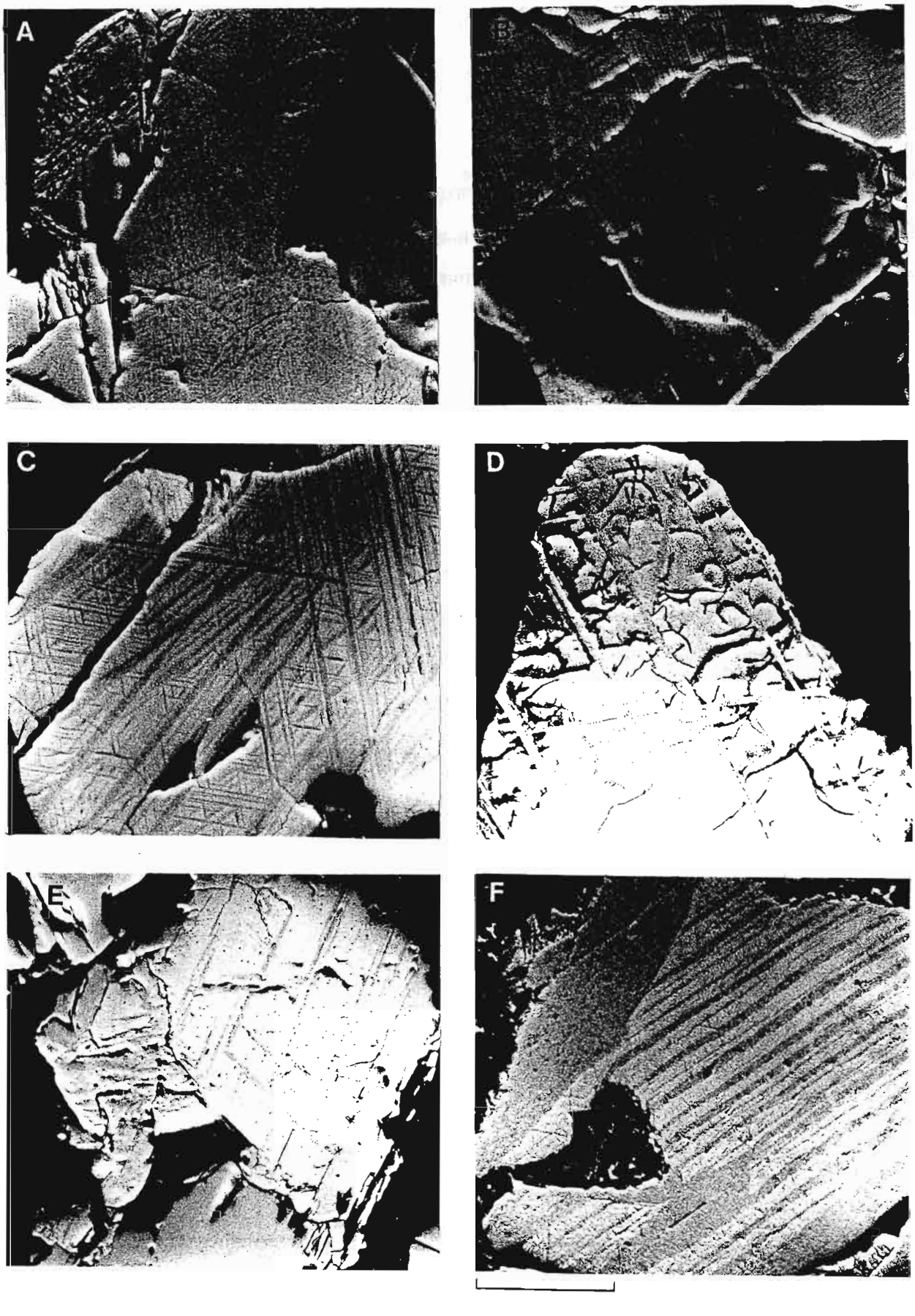

Plate 5.8 Photomicrographs of Hem_{ss}-Psb_{ss}±Rut grains formed by the high-temperature oxidation of titanomagnetite or ilmenite.

A. Coarse intergrowth between Hem_{ss} (white) and Psb_{ss} (dark grey) representing the C7 stage of Haggerty's titaniferous magnetite oxidation series. Richards Bay, dune (HZ 16). Reflected light, 32x oil immersion lens. Scale bar 50 μm.

B. Intimate intergrowth between Hem_{ss} (white) and Psb_{ss} (grey) with remnants of rutile (light grey). The large proportion of homogeneous hematite (top) suggests that the original grain consisted of $(Ilm\text{-}Hem)_{ex}$ and therefore the present assemblage corresponds to the R7 stage of Haggerty's oxidation series. Richards Bay, dune (HZ 17). Reflected light, 32x oil immersion lens. Scale bar 50 μm.

C. A rare grain consisting almost entirely of $pseudobrookite_{ss}$ with little hematite (light grey) and rutile (medium grey). Richards Bay, dune (HZ 17). Reflected light, 32x oil immersion lens. Scale bar 50 μm.

Plate 5.8

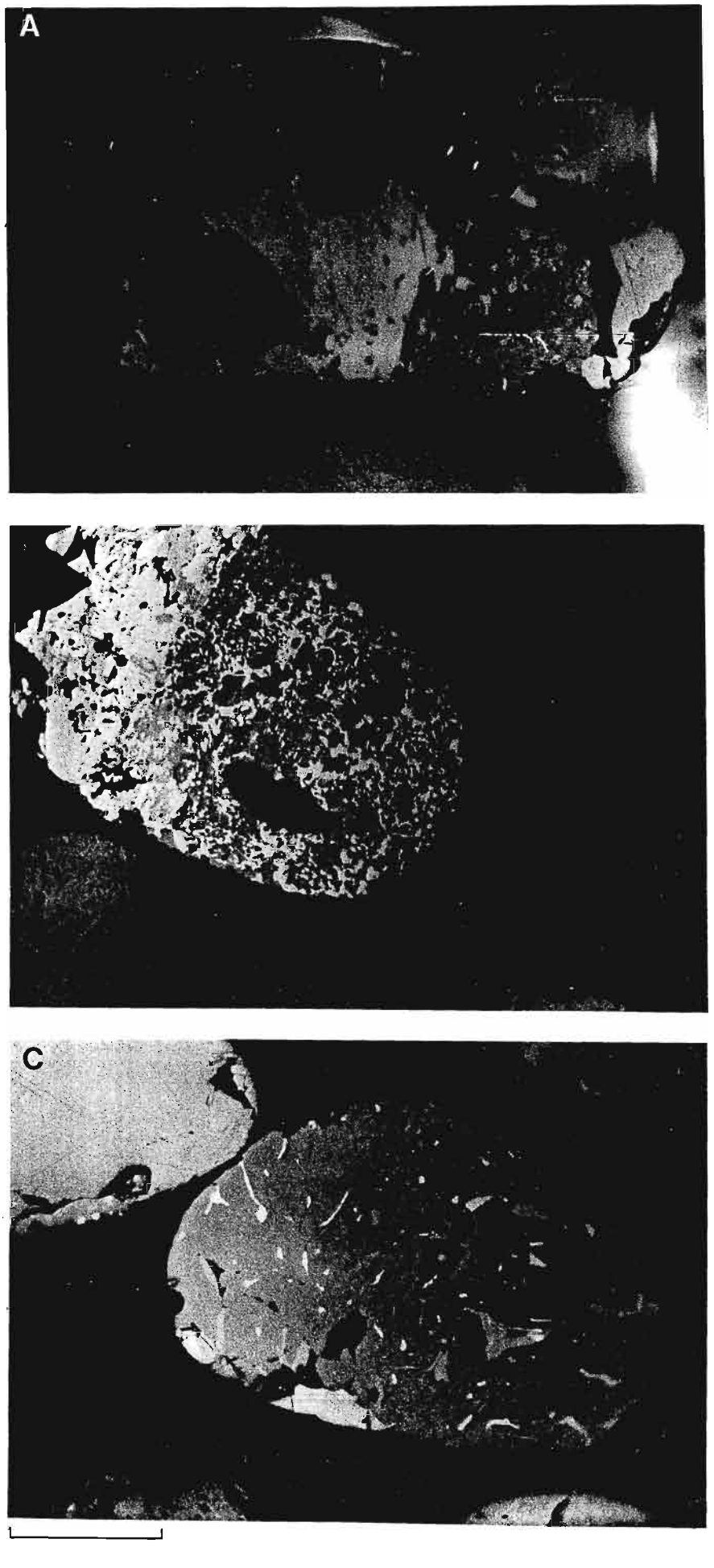

Plate 5.9 Back-scattered electron images of titaniferous magnetites containing exsolved pleonaste.

A. A magnetite grain containing orientated blebs of exsolved pleonaste. Cape St Lucia, dune (HZ 5). Scale Bar 43 μm.

B. Magnetite grain containing a single lamella of ilmenite (medium grey) and orientated blebs of pleonaste. Note how the pleonaste lamellae cross-cut the earlier formed ilmenite. The magnetite grain has been partially altered to titanite (bottom right of grain). Tugela River mouth, beach (HZ 1). Scale bar 43 μm.

C. Magnetite grain containing sparse ilmenite$_{oe}$ lamellae (light grey) and orientated blebs of exsolved pleonaste (dark grey). Again note that the pleonaste exsolution post-dates the ilmenite and in some instances partially replaces the ilmenite. Richards Bay, dune (HZ 17). Scale Bar 43 μm.

Plate 5.9

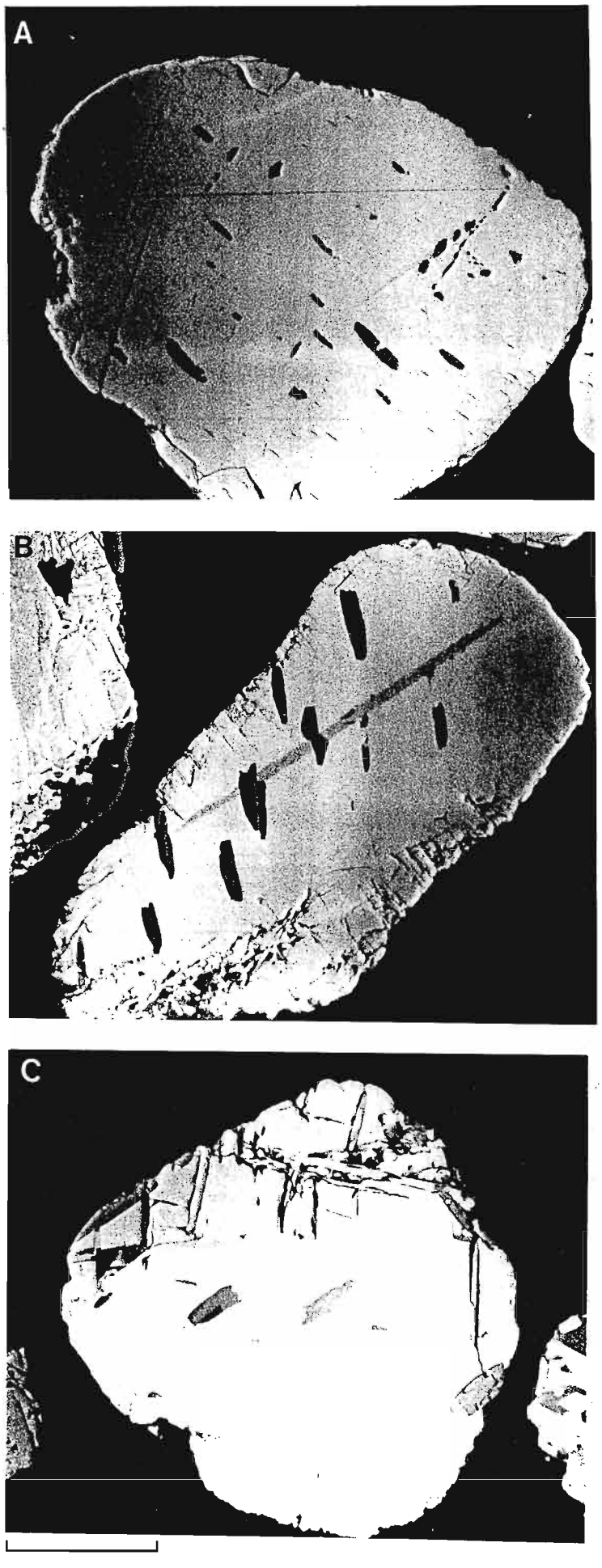

Plate 5.10 Photomicrographs of martitised magnetites.

A. High temperature replacement of magnetite by broad, straight-sided hematite lamellae. The hematite is also anhedral in shape. Richards Bay. Partial cross-polars, reflected light, 32x oil immersion lens. Scale bar 50 μm.

B. Low temperature martitisation of magnetite characterised by the development of thin, orientated hematite lamellae from the surface of the rounded magnetite grain. Richards Bay. Reflected light, 32x oil immersion lens. Scale bar 50 μm.

C-D. More advanced stages of martitisation of magnetite grains in coastal sediments. In some cases hematite may completely replace magnetite. Richards Bay. Partial cross-polars, reflected light, 32x oil immersion lens. Scale bar 50 μm.

Plate 5.10

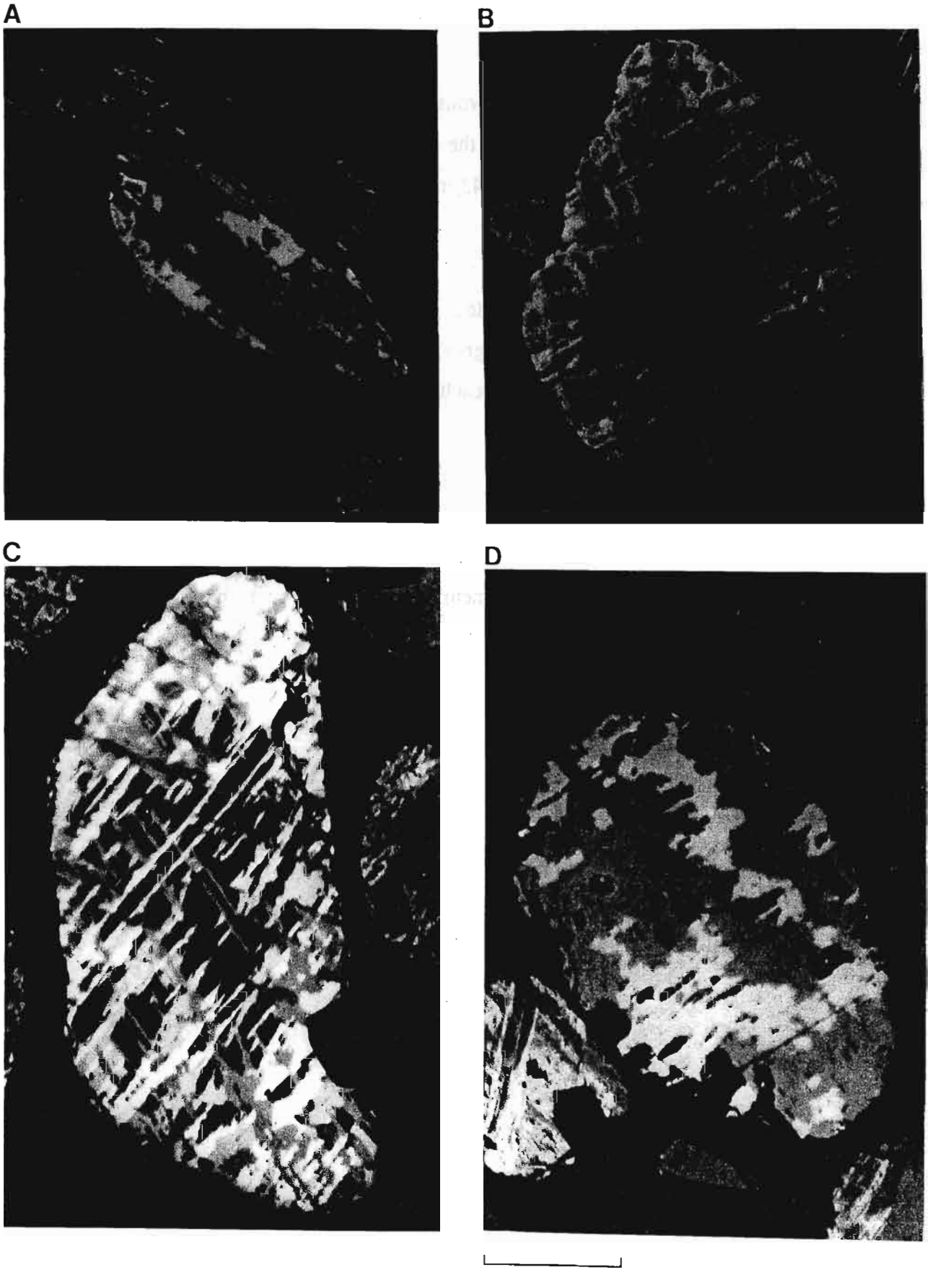

Plate 5.11 Scanning electron images of late-stage alteration reactions of magnetite and titaniferous magnetite.

A. Alteration of magnetite (white) to porous maghemite. Note that, in contrast to hematite, maghemite does not follow the (111) magnetite planes (*cf.* Plate 5.10). Umgababa, dune (HN 1). Scale bar 43μm.

B. Grain consisting of coarse ilmenite$_{oe}$ sandwich lamellae (light grey) and inhomogeneous maghemite (mottled grey) which has almost totally replaced the original magnetite$_{ss}$. Port St Johns, beach (HT 3). Scale bar 60 μm.

C. Replacement of magnetite (mottled white) by titanite (dark grey) as a result of late-stage metasomatism. Note how the ilmenite (light grey) remains unaffected by the alteration. Port Durnford, dune (HZ 2). Scale bar 43 μm.

D. Replacement of magnetite (white) by titanite (dark grey) within a (Mt_{ss}-Usp_{ss})$_{ex}$ grain displaying the characteristic cloth texture.
Umgeni River Mouth, beach (HN 6). Scale bar 43 μm.

Plate 5.11

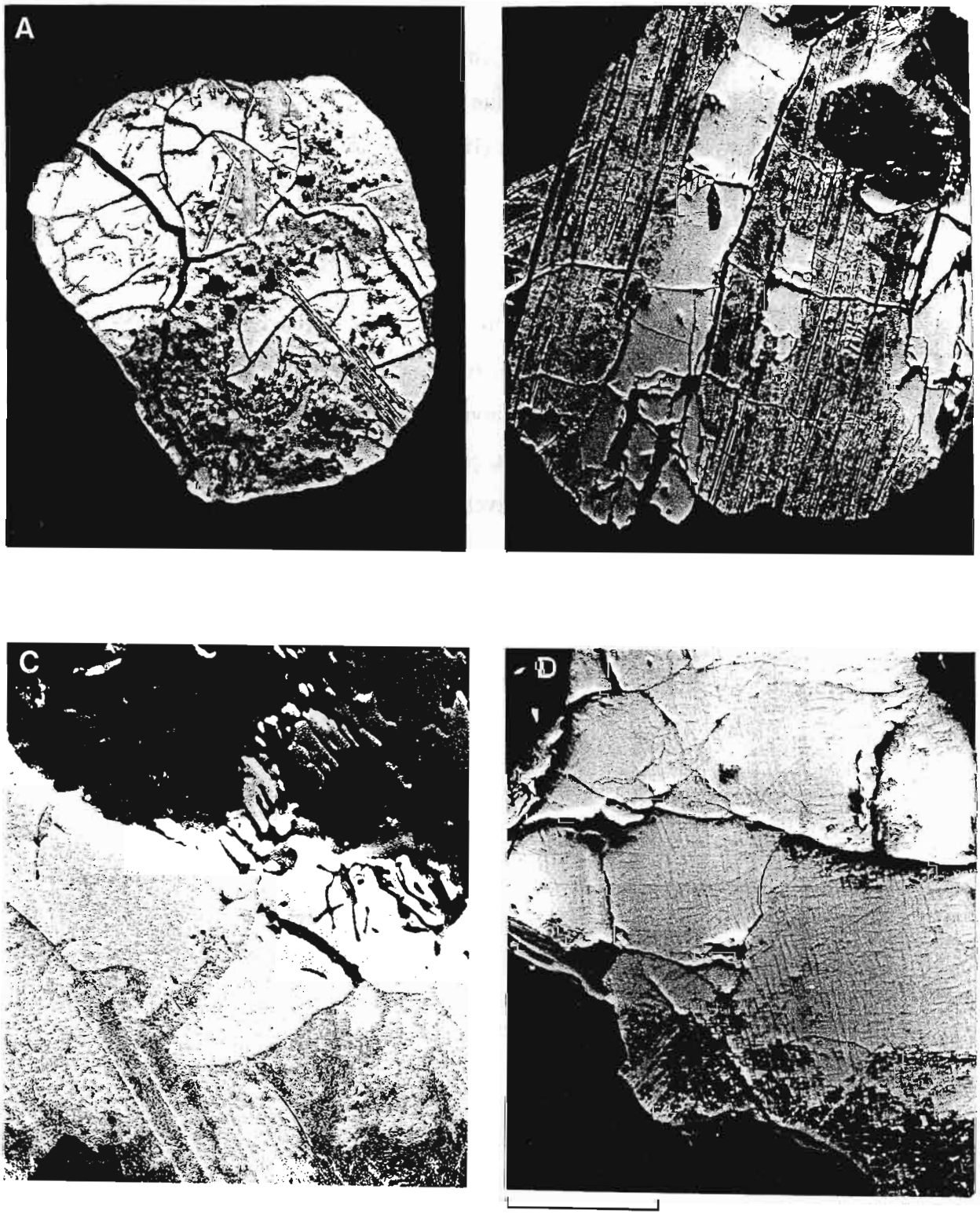

Plate 5.12 Back-scattered electron images illustrating the replacement of magnetite by hydrous ferromagnesian silicates.

A. Replacement of magnetite (white) by chlorite (mottled grey) as a result of late stage metasomatism. Note how the ilmenite lamellae (light grey) remain unaffected by the alteration. Port St Johns, beach (HT 3). Scale bar 75 μm.

B. Complete replacement of magnetite by a hydrous ferromagnesian silicate (medium grey), leaving the ilmenite trellis lamellae unaltered, although some of the ilmenite lamellae show signs of recrystallisation. The bright white blebs within the grain are pyrite, suggesting that the late-stage fluids were reducing in nature. Dolerite, Rooi Rand dyke swarm, Pongola River. Scale Bar 100 μm.

C. Replacement of Mt-Ilm_{oe} grain in which the magnetite has been completely replaced by the silicate phase (dark grey), whilst the ilmenite lamellae have been recrystallised. Umgababa, dune (HN 1). Scale Bar 60 μm.

D. Partial leaching of a silicate phase (dark grey) which has partly replaced the magnetite (light grey) in a Mt-Ilm_{oe} grain, resulting in an orientated framework of ilmenite lamellae. Morgan's Bay, dune (HEC 6). Scale Bar 43 μm.

Plate 5.12

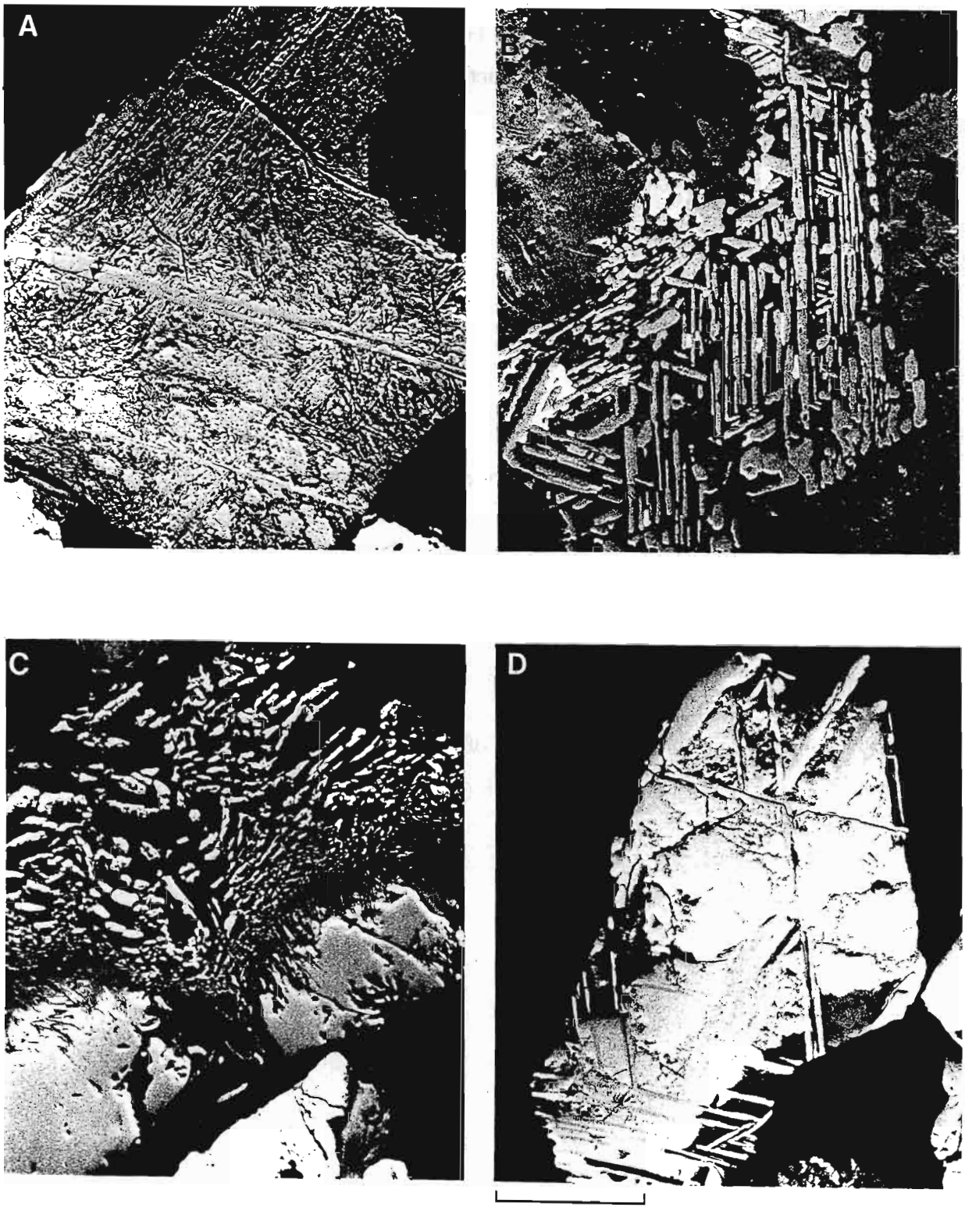

Plate 5.13

A. Replacement of ilmenite (light grey) in a composite ilmeno-magnetite grain by a silicate phase (dark grey) to produce a typical vermiform intergrowth. Note how the magnetite is unaffected by the reaction. Richards Bay, dune (HZ 16). Back-scattered electron image. Scale bar 25 μm.

B. Similar replacement to that described in A. in a large composite ilmeno-magnetite in a dolerite from the Rooi Rand dyke swarm, Pongola River (DM90-25). Back-scattered electron image. Scale bar 60 μm.

C. Back-scattered electron image of a zoned chromian magnetite grain. The core of the grain is chromium-rich, while the rim is chromium-poor and contains titanium. The magnetite has been partially replaced by maghemite. Richards Bay, dune (HZ 17). Scale bar 60 μm.

D. Photomicrograph of the replacement of ilmenite (medium grey) by titanite (dark grey). St. Lucia estuary mouth, beach (HZ 6). Reflected light, 32x oil objective. Scale bar 50 μm.

Plate 5.13

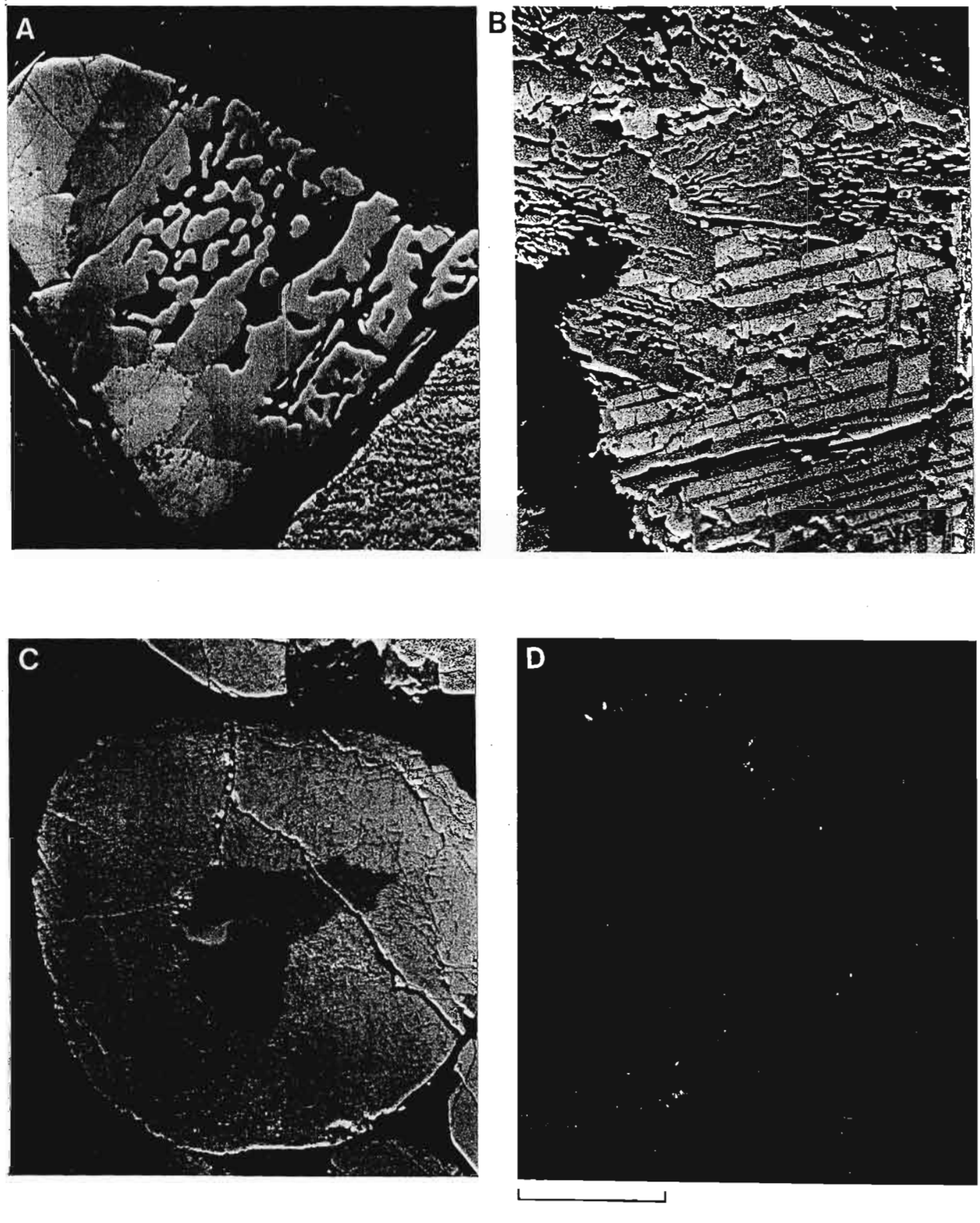

CHAPTER SIX

THE ALTERATION OF ILMENITE

6.1 INTRODUCTION

Ilmenite undergoes alteration in sediments by a process in which iron is removed from the ilmenite structure to finally form rutile or anatase. This alteration process changes the physical and chemical properties of the mineral, which influences its economic value. In the first part of this chapter the literature on ilmenite alteration is briefly reviewed. The central portion is concerned with the findings of a transmission electron microscope study of ilmenite alteration, which was undertaken by the author in the Department of Earth Sciences, Cambridge, England. The last part of the chapter describes the alteration of ilmenite found within the study area. Much of this last section is extracted from Hugo and Cornell (1991), published during the course of this study, which describes the alteration of ilmenite from Zululand, South Africa. The nature of the ilmenite alteration in Zululand is common to the entire study area, and the findings of Hugo and Cornell (1991) hold for all the coastal sediments along the eastern seaboard of South Africa.

6.2 PREVIOUS WORK

6.2.1 The mechanisms of ilmenite alteration

The presence of phases with TiO_2 contents greater than the theoretical 52.7 per cent of ilmenite in sedimentary deposits has been known since the advent of heavy mineral sand mining. The nature of these phases and the process of ilmenite alteration has been the subject of much controversy, as unequivocal optical and chemical identification is often impossible because of the very fine intergrowths formed by alteration products. The poor crystallinity of the alteration phases and the coincidence of their XRD peaks with those of

ilmenite, rutile, anatase and hematite, make their structural identification difficult. These problems are exacerbated by the inconsistent nomenclature used by different workers.

In 1909 Palmer described a monoclinic phase from Arizona with a composition close to the formula $Fe_2O_3.3TiO_2$, which he named arizonite. Subsequent workers used the term arizonite in their description of titaniferous concentrates, although they never positively identified the phase (Gillson, 1949 and 1950; Miller, 1945; Theonen and Warne, 1949). Others challenged the existence of arizonite in these concentrates (Ernst, 1943; Overholt *et al.*, 1950; Lynd *et al.*, 1954) and postulated that the concentrates, consisting of 56 to 63 per cent TiO_2 were formed by the weathering of ilmenite (Cannon, 1949; Overholt *et al.*, 1950; Lynd *et al.*, 1954). From the results of petrographic, chemical, X-ray and magnetic studies, Lynd *et al.* (1954) concluded:

> "Since the composition and structure of [titaniferous] beach sand concentrates corresponds so closely to what would be expected of ilmenites that have altered by oxidation and leaching, there is no reason to postulate the existence of the hypothetical compound, arizonite, to account for the composition of titaniferous beach sand concentrates".

From X-ray analysis of the material studied by Palmer (1909), Lynd *et al.* (1954) stated that arizonite consisted of a mixture of hematite, anatase and rutile, which agreed with the findings of Overholt *et al.* (1950).

Bailey *et al.* (1956) also disputed the existence of arizonite in their study of ilmenite alteration and concluded that ilmenite passed through three successive stages of alteration from ilmenite to leucoxene, which consisted of finely crystalline rutile, or less commonly, brookite. They also proposed that the ilmenite structure broke down during alteration to form an amorphous mixture of titanium and iron oxides prior to the formation of leucoxene: a conclusion reached subsequently by La Roche *et al.* (1962). The presence of leucoxene in titaniferous concentrates and as an alteration product of ilmenite had been recognised before by Cannon (1949) Creitz and McVay (1949) and Spencer (1948).

Although most subsequent workers agreed that iron is oxidised and leached from ilmenite during weathering, resulting in the enrichment of TiO_2, the role of the phase arizonite was still discussed (Karkhanavala, 1959; Karkhanavala and Momin, 1959; Karkhanavala *et al.*, 1959; Flinter, 1959, 1960a and 1960b; Lynd, 1960; Dyadchenko and Khatuntseva, 1960; Bykov, 1964).

Teufer and Temple (1966) identified an iron-titanite of hexagonal structure, with a composition close to $Fe_2Ti_3O_9$, using single crystal XRD analysis. They called this phase pseudorutile. In the same year Temple (1966) published a paper on the alteration of ilmenite in which he stated that the alteration products are completely transitional in composition from ilmenite to the end product of alteration, which has a composition close to rutile. He also determined that the oxidation of FeO to Fe_2O_3 is complete at a composition of about 65-70% TiO_2, which is close to the composition of pseudorutile. Temple (1966) concluded that the alteration of ilmenite proceeded as follows: the initial removal of sufficient iron to allow the oxygen lattice to adjust to the "primitive" hexagonal structure of pseudorutile, with subsequent removal of iron resulting in the conversion of pseudorutile to rutile, and only the phases pseudorutile and rutile were formed in the process.

Pseudorutile was subsequently investigated by Larrett and Spencer (1971), while Grey and Reid (1975) refined the structural data of the mineral and proposed that it was a stable intermediate phase of the weathering of ilmenite in a groundwater environment. They proposed that ilmenite altered by a two-stage mechanism, similar to that suggested by Temple (1966). This mechanism is described in greater detail in Section 6.4.

The alteration of ilmenite to microcrystalline rutile (leucoxene) via the distinct intermediate phase, pseudorutile, has gained acceptance in the recent literature on ilmenite weathering. However, a number of contributions to, and departures from, the findings of Temple (1966) and Grey and Reid (1975) have been made. Grey *et al.* (1983) determined that the phase is an oxyhydroxide with a composition between $Fe_2Ti_3O_9$ and $Fe_2Ti_3O_8(OH)_2$. Frost *et al.* (1983) and Frost *et al.* (1986) determined that ilmenite may alter directly to

leucoxene close to the surface of deposits. Wort and Jones (1980) determined from quantitative XRD that altered ilmenite grains contained significant amounts (12 to 41 per cent) of amorphous material, in addition to ilmenite, pseudorutile, and rutile. Anand and Gilkes (1984 and 1985) determined that anatase, and not rutile is the dominant end-product of ilmenite weathered in laterites. Recently Mücke and Chaudhuri (1991) have proposed that ilmenite does not alter via pseudorutile to rutile (leucoxene), but that "there are continuous phase transitions between ilmenite and its successive products".

6.2.2 Chemical changes accompanying ilmenite weathering

As stated by Temple (1966) there is "a complete range of chemical compositions of [ilmenite] alteration products" from ilmenite to almost pure TiO_2. This range is illustrated by Figure 6.1, which demonstrates that ilmenite and leucoxene concentrates from different localities span the compositions between ilmenite and TiO_2, and that iron is oxidised and lost as weathering proceeds.

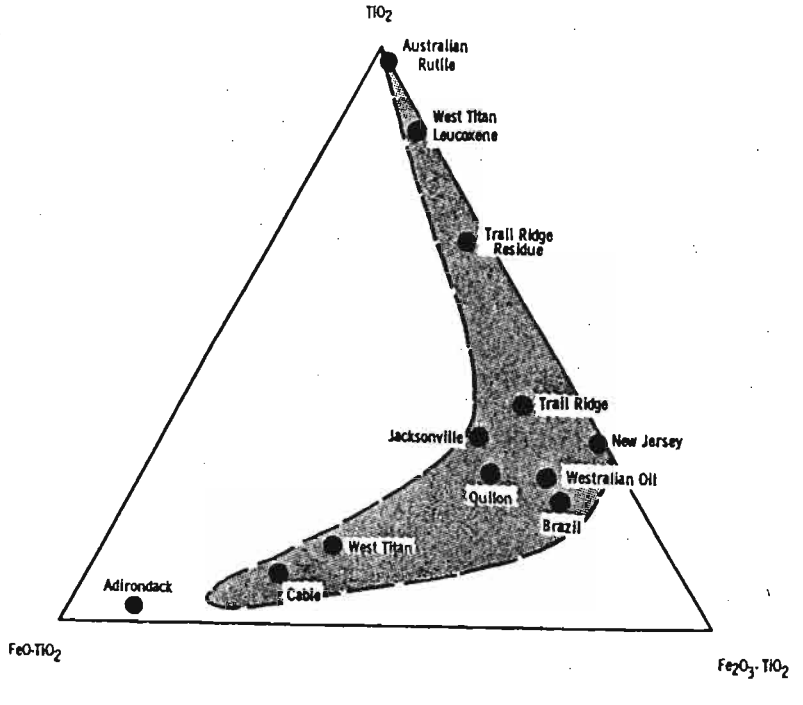

Figure 6.1 The chemical compositions of altered ilmenites (from Temple, 1966).

Frost *et al.* (1983) determined that the SiO_2 and Al_2O_3 levels are low (0.05 and 0.2 per cent, respectively) in hydrated ilmenite, but that these impurities increase (up to 1 per cent SiO_2 and 3 per cent Al_2O_3) during the formation of leucoxene. They concluded that this enrichment is too high for the impurities to be derived from the ilmenite, and that the Si and Al are derived from the "ambient environment and are co-precipitated with, or adsorbed on to, the alteration products". Frost *et al.* (1986) produced similar results for Si and Al enrichment and also determined that MnO is leached together with iron during ilmenite weathering. Anand and Gilkes (1984 and 1985) made similar findings, but determined from transmission electron studies that the Si and Al are present as discrete clay minerals in the weathered ilmenite grains and are not incorporated as impurities in rutile or anatase, as suggested by Frost *et al.* (1983).

The increase in Si and Al, during the formation of leucoxene, has also been noted by Hugo (1988) and Hugo and Cornell (1991) in weathered ilmenites from South Africa, but they found that the SiO_2 and Al_2O_3 in these grains, and particularly leucoxene grains, may be as high as 20 per cent. These results are presented and discussed in greater detail in Section 6.6.

6.2.3 Physical changes accompanying ilmenite weathering

The change in magnetic susceptibility with ilmenite weathering has been studied by Lynd *et al.* (1954), Bailey *et al.* (1956), Wort and Jones (1980 and 1981), Frost *et al.* (1986) and Hugo (1988). These authors have shown that there is a decrease in magnetic susceptibility with increasing ilmenite weathering, as indicated by Table 6.1. Lynd *et al.* (1954) showed that ilmenite concentrates with increasing TiO_2 contents (that is, degree of weathering) were collected at increasing magnetic intensity during magnetic separation. Bailey *et al.* (1956), however, pointed out that the TiO_2, FeO and Fe_2O_3 contents of the weathered ilmenite, in different magnetic fractions, remains relatively constant until the highest magnetic intensities. Similar results were obtained by Wort and Jones (1980 and 1981) and Frost *et al.* (1986), as shown by Figure 6.2 , which illustrates the data of Frost *et al.* (1986).

Table 6.1 Magnetic susceptibilities of ilmenite and its weathered products (data from Wort and Jones, 1981).

Mineral	TiO_2 content (%)	Magnetic Susceptibility. $(X)^*$
ferrian-ilmenite	40 to 50	100 to 361
ilmenite	50	96
pseudorutile	60 to 63	34.5
rutile	100	1

$^* X = \text{x } 10^2 \text{ JT}^{-2}\text{kg}^{-1}$

Wort and Jones (1981) determined that the weathered ilmenite found in the most magnetic fractions have susceptibilities higher than that of pure ilmenite, and concluded that these grains were derived from the alteration of ferrian-ilmenite, which may have magnetic susceptibilities close to that of magnetite. Similar results were obtained by Frost *et al.* (1986).

As with magnetic susceptibility, the density of the weathered products of ilmenite decreases with increasing alteration. The relationship between bulk specific gravity and TiO_2 content of various weathered ilmenite concentrates is shown in Figure 6.3 (from data given in Table 6.2), which indicates that the density decreases linearly with increasing alteration. Furthermore, leucoxenes have lower densities than that of rutile. Hugo (1988) found significant amounts of leucoxenes with densities less than 3.8 $g.cm^{-3}$ in the Richards Bay deposit.

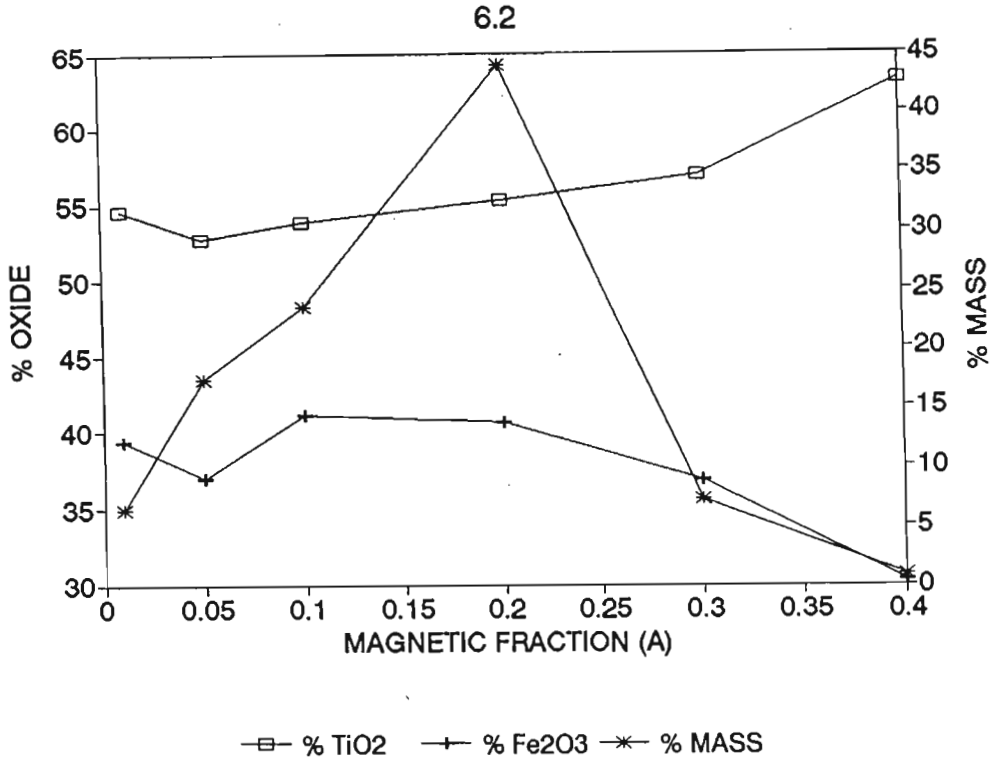

Figure 6.2 Variations in TiO_2 and Fe_2O_3 contents of altered ilmenite in different magnetic fractions (data from Wort and Jones, 1980).

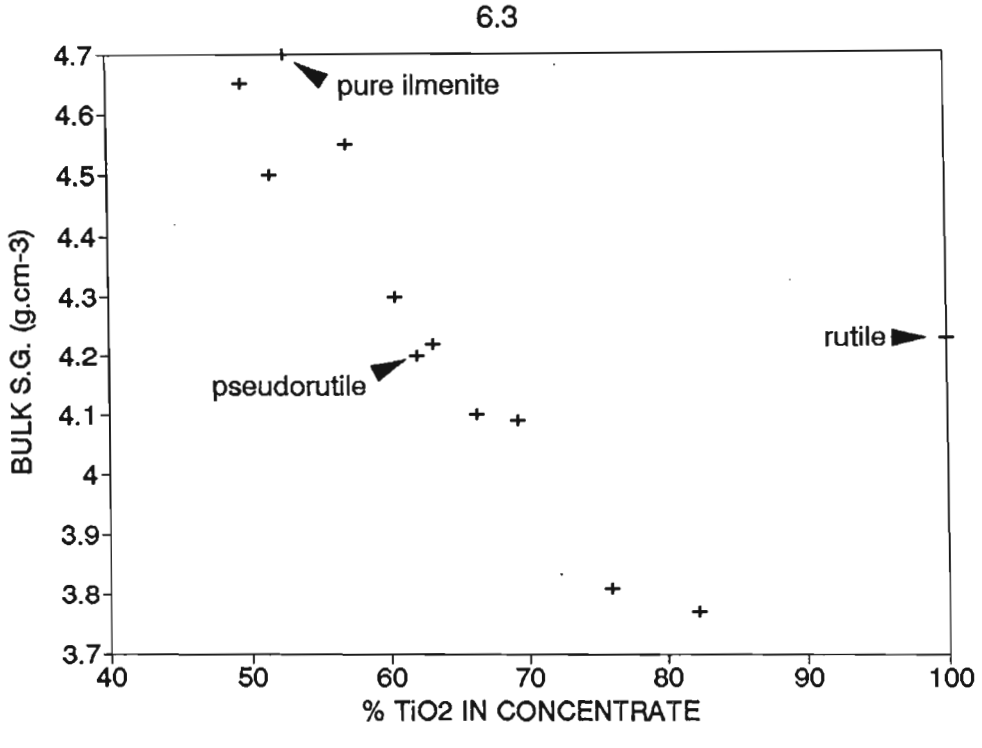

Figure 6.3 The relationship between density and the degree of ilmenite alteration (the TiO_2 content of the altered ilmenite concentrate). From data given in Table 6.2.

Table 6.2 Change in the density of altered ilmenite concentrates with increasing alteration.

Locality	Specific Gravity ($g.cm^{-3}$)	TiO_2 Content (%)	Reference
Pure ilmenite	4.79	52.7	Olhoeft and Johnson (1989)
Richards Bay	4.65	49.6	Milner (1971)
Adirondack	4.50	51.6	Temple (1966)
West Titan deposit	4.55	57.1	"
Brazil	4.30	60.5	"
Quilon	4.22	63.2	"
Jackonsville	4.10	66.3	"
Trail Ridge	4.09	69.3	"
Folkson	3.81	76.1	"
Trail Ridge (leucoxene)	3.77	82.8	"
South Neptune Island, Australia	4.20	62.05	Larrett and Spencer (1971)
Pure rutile	4.25	100.0	Olhoeft and Johnson (1989)

6.3 ELECTRON MICROSCOPY OF ILMENITE WEATHERING

The process of ilmenite alteration has been extensively studied using reflected light microscopy, bulk chemical and single grain (electron microprobe) analysis, and powder and single crystal X-ray diffraction techniques. Recently scanning transmission electron microscopy (STEM) and neutron diffraction studies have been reported by Shoemaker *et al.* (1988). This section describes a further transmission electron microscope study of ilmenite alteration, performed by the author during a six month study visit to the Department of Earth Science, Cambridge, England.

The aim of the visit was to determine the potential of using electron microscopy in the study of ilmenite alteration and then to investigate the alteration of ilmenite using bright and dark field transmission electron microscopy in order to determine by which mechanism ilmenite alters. The following possibilities were envisaged:

1. Direct alteration to pseudorutile, as proposed by Temple (1966), Grey and Reid (1975) and that altered ilmenite grains with compositions between ilmenite and pseudorutile (that is, hydrated ilmenite) consist of mixtures of ilmenite and pseudorutile, as suggested by Frost *et al.* (1983);

2. Alteration to mixtures of other phases such as rutile, hematite and anatase, as suggested by Overholt *et al.* (1950) and Lynd *et al.* (1954);

3. Alteration to an intermediate amorphous material, as suggested by Bailey *et al.* (1956) and Wort and Jones (1980).

A further object of the study was to examine the structural relationships between ilmenite and its weathered products, using transmission electron microscopy.

Information on the theory and practice of electron microscopy may be found in Edington (1975), Wenk (1976), and Putnis and McConnell (1980).

6.3.1 The relationship between pseudorutile and ilmenite

Teufer and Temple (1966) determined that the structure of pseudorutile is hexagonal (a = 0.287 nm, c = 0.461 nm). They proposed that the oxygen anions form a hexagonally closed packed (HCP) structure and that the original ilmenite oxide lattice is little affected by the topotactical transformation of ilmenite to pseudorutile and finally to rutile. These authors considered the metal cations to be randomly distributed amongst the octahedral sites. However, this does not fully explain the diffuse streaks or arcs observed by precession camera patterns, in reciprocal (*hkl*) layers with l odd.

Grey and Reid (1975) refined the structure of pseudorutile and proposed that the extra XRD reflections are due to poor ordering of the metal atoms in the *a-b* plane. They determined that ideally the metal ordering forms a five-fold supercell along *a*, so that $a = 1.437$ nm for pseudorutile. The close agreement between the shape of the diffuse reflections in precession camera patterns of pseudorutile and multiply twinned tivanite (an ordered intergrowth of goethite and rutile-type structures described by Grey and Nickel, 1981) led Grey *et al.* (1983) to propose that "the structure of pseudorutile comprises a statistical distribution of the various twin possible variants of a goethite-rutile intergrowth structure". This argument was substantiated by the close similarities between the structures of pseudorutile and various synthetic rutile-goethite type intergrowth structures.

These authors also determined that the cations are ordered in 4-5 nm microdomains and that the coherency of the anion lattice is maintained over 3-4 twin variants, producing microdomains of about 16 nm. Further, they established that pseudorutile contained approximately 3 per cent structurally bound water, and that the phase should be considered as an oxyhydroxide with a composition between $Fe_2Ti_3O_9$ and $Fe_2Ti_3O_8(OH)_2$. The important role that hydration plays in the alteration of ilmenite in the groundwater environment has been highlighted by other workers (Flinter, 1959; Dyadchenko and Khatuntseva, 1960; Gevorkyan and Tananayev, 1964). Recently Frost *et al.* (1983) stated that pseudorutile may undergo "concomitant hydroxylation" and leaching of iron, as given by the reaction:

$$Fe_2Ti_3O_9 + \tfrac{3}{4}\ H_2O \rightarrow Fe_{1.5}Ti_3O_{7.5}(OH)_{1.5} + \tfrac{1}{2}\ FeO_{1.5} \quad \ldots\ (6.1)$$

A similar reaction has also been proposed by Mücke and Chaudhuri (1991).

Alteration beyond pseudorutile leads to the formation of cryptocrystalline rutile (Teufer and Temple, 1966; Temple, 1966; Grey and Reid, 1975; Frost *et al.*, 1983) or anatase (Anand and Gilkes, 1984). Areas within weathered ilmenite which have (Ti/Ti+Fe) ratios of more than 0.65 to 0.7 usually contain some rutile or anatase together with variable amounts of pseudorutile, ilmenite, hematite, goethite and amorphous material.

6.3.2 Experimental

A sample of altered ilmenite concentrate from the 90 foot strand line, Capel, Western Australia, supplied by Dr Ian Grey of the CSIRO, Australia, was first studied, as this has been well characterised by Frost *et al.* (1983) and Frost *et al.* (1986). Samples from the Port Durnford Formation (HZ 21) and the Late Pleistocene - Holocene dunes near Richards Bay (HZ 17) were also studied. The latter samples yielded similar results to the Western Australian samples, although the ilmenites are less altered.

The concentrates were separated into magnetic fractions using a Cook isodynamic separator in order to concentrate the pseudorutile and to remove minor impurities. The settings given by Frost *et al.* (1986) were used. A gravity separation was then performed on each fraction, using 4.0 $g.cm^{-3}$ Clerici solution, to remove any silicate impurities. The 4.0 $g.cm^{-3}$ sink fractions were analysed using powder X-ray diffraction, reflected light microscopy, SEM back-scatter analysis and electron microscope techniques, to determine the degree and nature of the ilmenite alteration. From these analyses, magnetic fractions which contained the highest proportions of weathered ilmenite, with compositions close to pseudorutile and few impurities, were selected for the study. Grains from these fractions were embedded in resin and then ground and polished to form discs of less than 30 μm thick. These grids were then mounted on titanium grids and ion-beam thinned. Electron microscopy was performed using a JEOL JEM 100CX microscope fitted with a double tilt goniometer stage, allowing for large angles of rotation. The diffraction patterns were indexed with the aid of the *Diffract* software package.

6.3.3 Analytical techniques

All analyses for this study were performed using equipment in the Department of Earth Sciences, Cambridge under the supervision of Dr Andrew Putnis. Reflected light microscopy and a JEOL 6100 scanning electron microscope were used to study the petrography of the weathered ilmenite grains. Microprobe analyses were done on a Cameca Camebax IV microprobe. Powder X-Ray diffraction patterns of magnetic

fractions were obtained using a Philips diffractometer, Co-Kα radiation, with filters, at a scan speed of 1 degree 2Θ per minute.

6.3.4 Petrography and chemistry of the concentrates

The petrography and chemistry of the Capel concentrate has previously been described by Frost *et al.* (1983), and only a summary is provided here. Scanning electron microscopy shows that the weathered areas form patches or stringers, which are usually orientated along the basal plane of the ilmenite grains (Plate 6.1A). Back-scattered electron images (Plate 6.1B and C) indicate that the weathered areas are inhomogeneous and microprobe analyses reveal that the weathered grains have a complete range of compositions from ilmenite to TiO_2, however, most of the analyses from the Capel 0.2 and 0.3 A magnetic fractions fall between the compositions of ilmenite and pseudorutile (Table 6.3). Powder X-ray diffraction patterns of the magnetic fractions (Figure 6.4) show that the 0.3 A fraction contains the highest proportions of pseudorutile. In comparison, the South African samples contain less pseudorutile (Figure 6.5). Optical microscopy and SEM reveal that the magnetic fractions of sample HZ 17, from the Richards Bay Late-Pleistocene - Holocene dunes, contain mostly unaltered ilmenite. Sample HZ 21 from the Mid-Pleistocene Port Durnford Formation consists mostly of altered ilmenite grains, but these show only incipient alteration to pseudorutile.

6.3.5 Transmission electron microscopy

Areas of weathered ilmenite are easily distinguished from ilmenite in bright field mode by their inhomogeneous and mottled appearance (Plate 6.2A) and dark field (Plate 6.2B). It appears that the degree of mottling and inhomogeneity is related to the degree of weathering, but this cannot be substantiated without, at least, semi-quantitative chemical analysis. The weathered areas are preferentially thinned by the ion beam and it is possible that this method of preparation enhances the heterogeneity of the weathered ilmenite.

Plate 6.1 Back-scattered electron images of altered ilmenites in the 0.3 A magnetic fraction from Capel 90 ft Strand Line, Australia.

A. General view of altered ilmenites grains showing the development of weathered areas as patches or stringers, which are commonly orientated along the basal plane of the ilmenite grains. Scale bar 100 μm.

B. A partially altered ilmenite grain illustrating the inhomogeniety of the weathered areas. Scale Bar 10 μm.

C. A magnified view of the above grain, showing the zonations and fine intergrowths which may develop in the weathered areas. Note also the highly porous nature of the weathered zones, which may lead to preferential thinning by the ion-beam during the manufacture of thin-foils. Scale Bar 10 μm.

Plate 6.1

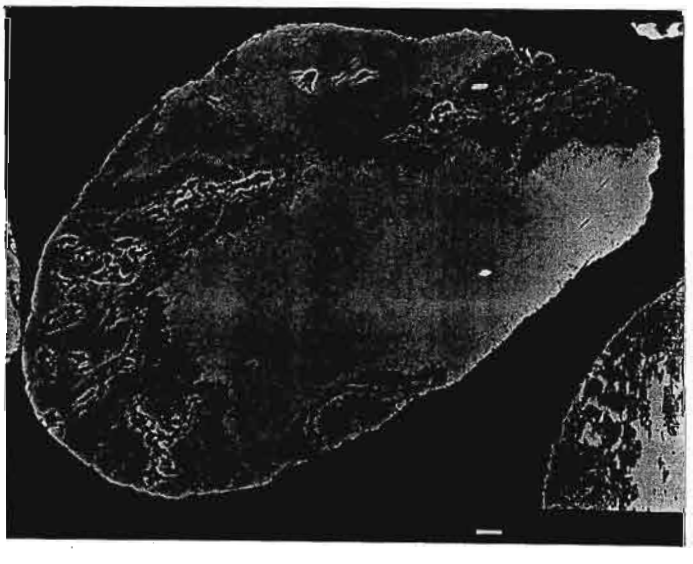

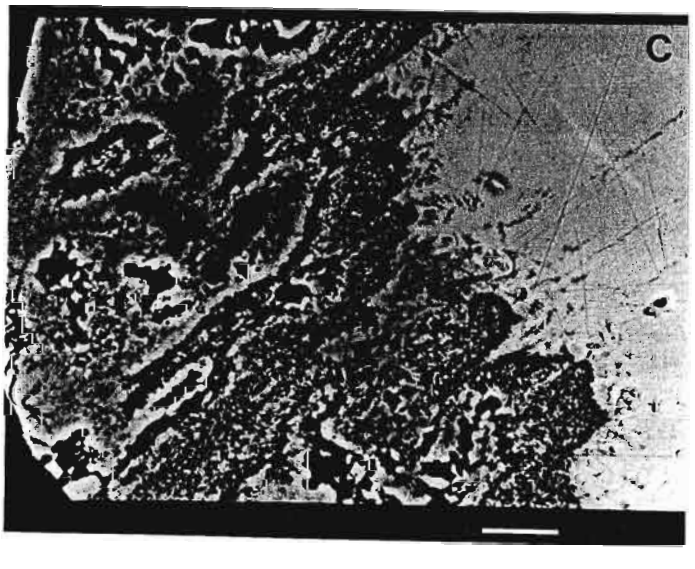

Table 6.3A Representative microprobe analyses of altered ilmenites from Capel 90 Foot Strand line (0.2 A fraction)

Analysis	Phase	TiO2	FeO	Al2O3	SiO2	MgO	MnO	Cr2O3	Total
G2 A1	hyd ilm	54.01	44.35				1.73		100.09
G5 A1	psr ?	64.66	33.10	0.39			1.29		99.44
G6 A1	hyd ilm	57.53	42.30		0.33		0.50		100.66
G9 A1	hyd ilm	56.60	40.63			0.23	0.85		98.31
G9 A2	hyd ilm	60.46	35.42	0.42	0.28	0.16	0.65		97.43
G10 A1	hyd ilm	56.88	40.88				0.82		98.57
G10 A2	hyd ilm	54.37	45.24		0.15		1.15		100.90
G11 A1	ilmenite	50.99	43.08		0.14		1.94		96.15
G11 A2	hyd ilm	59.16	36.49	1.08	0.61		1.75		99.08
G11 A3	leucoxene	68.24	23.36	5.77	1.09		0.78	0.33	99.56
G11 A4	psr ?	63.57	31.52	0.90	0.59		1.78	0.22	98.58
G14 A1	hyd ilm	59.19	37.17	0.30	0.16	0.32	0.57	0.13	97.84
G14 A2	leucoxene	75.89	16.21	0.54		1.62	0.30	0.17	94.73
G16 A1	ilmenite	51.72	46.80		0.13	0.38	0.76		99.79
G16 A2	psr ?	62.23	33.57	0.28	0.38		0.47		96.92
G18 A1	hyd ilm	55.70	44.16				0.97		100.82
G18 A2	leucoxene	74.26	19.80	2.29	1.08		0.29		97.71
G18 A3	hyd ilm	58.26	38.07	0.48	0.39		1.45		98.65

blank = below detection limit
hyd ilm = hydrated ilmenite
psr ? = possibly pseudorutile
G1 A1 = grain 1, analysis 1
all iron is reported as FeO

Table 6.3B Representative microprobe analyses of altered ilmenites from Capel 90 Foot Strand line (0.3 A fraction)

Analysis		TiO2	FeO	Al2O3	SiO2	MgO	MnO	Cr2O3	Total
G1 A1	hyd ilm	56.69	40.44	0.21	0.20		1.08		98.62
G2 A2	hyd ilm	59.55	38.44	0.39	0.23		0.79		99.40
G3 A1	psr ?	63.71	32.78	1.16	0.50		0.77		98.92
G3 A2	hyd ilm	60.08	37.75	0.25	0.20		0.73		99.01
G7 A1	hyd ilm	56.48	42.62			0.25	0.19		99.54
G7 A2	hyd ilm	60.05	38.02	0.19			0.23		98.48
G8 A1	hyd ilm	58.97	36.50	0.36	0.22		1.05		97.10
G10 A1	psr ?	62.44	35.46	0.38	0.18	0.44	0.58		99.48
G10 A2	psr ?	62.45	33.82	0.32	0.15		0.56		97.30
G12 A1	hyd ilm	57.28	40.55		0.23		0.61		98.67
G12 A2	hyd ilm	58.52	40.23				0.59		99.34
G13 A1	hyd ilm	54.82	39.60		0.25	0.39	4.91		99.97
G13 A2	hyd ilm	56.11	38.75	0.17	0.19		3.48		98.71
G15 A1	ilmenite	52.85	42.94	0.21	0.23		0.89		97.11
G15 A2	leucoxene	86.99	7.57	1.09	1.57		0.19		97.42
G16 A1	psr ?	61.57	33.70	0.52	0.79		2.33		98.90
G16 A2	psr ?	62.28	32.23	0.75	1.00		1.70		97.96
G17 A1	psr ?	62.48	33.47	0.53	0.26	0.26	0.97		97.97
G18 A1	hyd ilm	56.17	40.22	0.18	0.22		2.63		99.42
G19 A1	hyd ilm	57.33	39.68	0.20		0.48	0.64		98.55

blank = below detection limit
hyd ilm = hydrated ilmenite
psr ? = possibly pseudorutile
G1 A1 = grain 1, analysis 1
all iron is reported as FeO

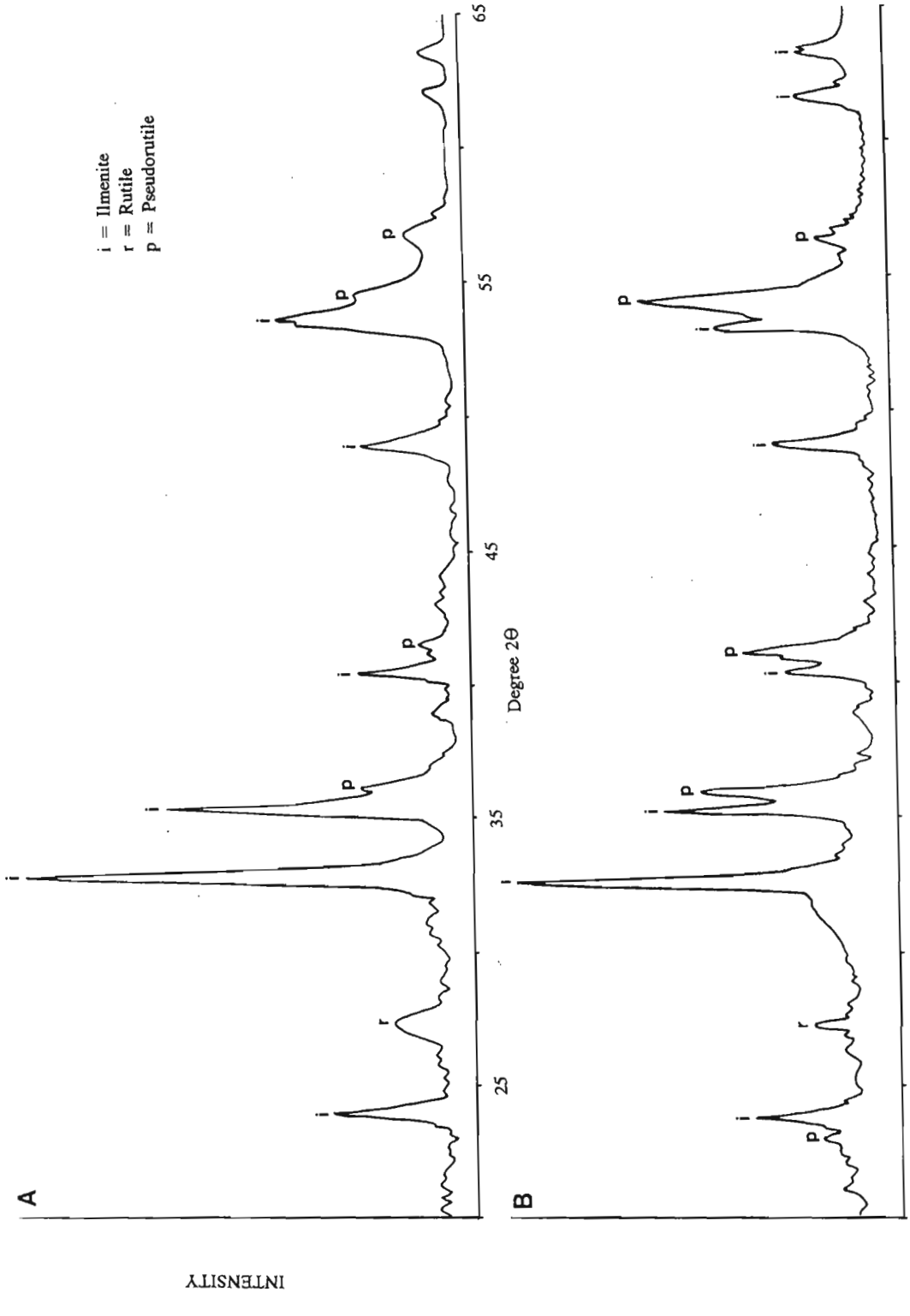

Figure 6.4 Powder XRD patterns of altered ilmenites in magnetic fractions from the Capel 90 ft Strand Line showing the concentration of pseudorutile in the 0.2A (**A**) and 0.3 A (**B**) fractions.

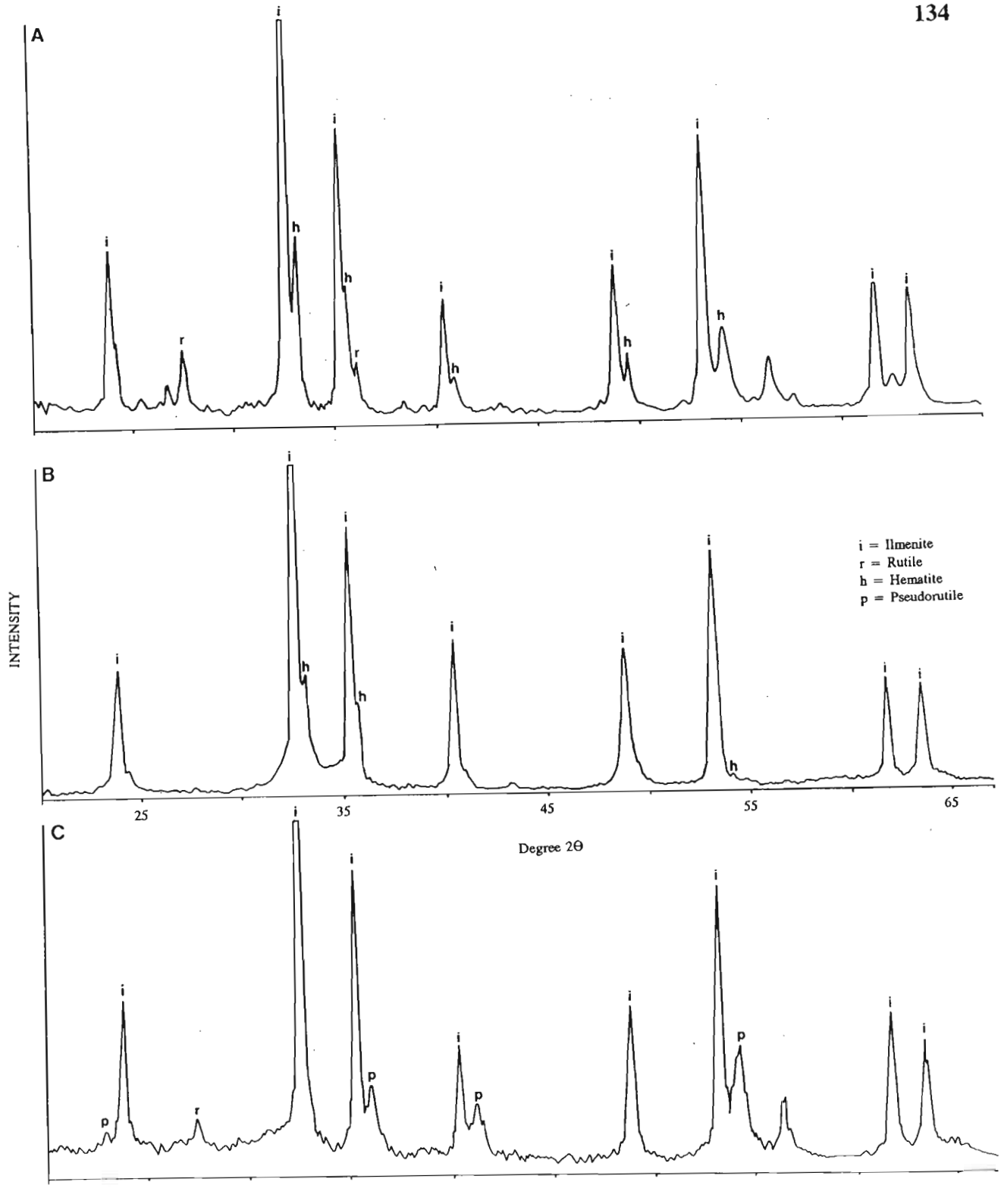

Figure 6.5 Powder XRD patterns of ilmenite magnetic fractions from South African deposits. **A.** Richards Bay (HZ17), 0.1 A. **B.** Richards Bay (HZ17), 0.3 A. **C.** Port Durnford (HZ21). Only the Port Durnford sample shows any evidence of pseudorutile.

Selected area diffraction patterns (SADP) of unaltered ilmenite display only the fundamental reflections of ilmenite, but SADP's of weathered areas show the following features illustrated in Plate 6.3:

1. the fundamental reflections become broadened and may become split or streaked;
2. the intensity of some fundamental reflections of ilmenite decreases and in some cases they become extinct;
3. additional diffuse scattering and streaks appear;
4. extra, superlattice reflections, usually not corresponding to the fundamental reflections, are formed.

Indexed schematic representations are given on the left hand side of the diffraction patterns in Plate 6.3. These show that the fundamental reflections in SADP's of weathered areas may be indexed using the ilmenite lattice. The SADP's indicate clearly that in these samples altered ilmenite between the chemical compositions of ilmenite and pseudorutile does not consist of mixtures of minerals such as rutile and hematite, or goethite. Neither is there any indication of the formation of amorphous material, which would result in SADP's with a circle of diffuse scattering around the transmitted beam and no distinct reflections. No reflections unique to pseudorutile are observed. However, as shown by the schematic diagrams for Plate 6.3, certain reflections indexed using an ilmenite lattice may also be indexed by the fundamental cell of pseudorutile (a = 0.287 nm, c = 0.461 nm) given by Teufer and Temple (1966). It is possible that the ilmenite and pseudorutile reflections are not clearly resolved due to two factors:

1. Spot broadening is caused by the poorly crystalline nature of weathered areas, and the fine domains formed within these areas.
2. The d spacings of ilmenite and the pseudorutile subcell are similar with co-incident axes.

If pseudorutile is formed, then a topotactical relationship clearly exists between ilmenite and this phase, with c_{ilm} parallel to c_{psr} and $(1120)_{ilm}$ parallel to a_{psr} (Figure 6.6), as suggested by Teufer and Temple (1966) and Grey and Reid (1975).

Plate 6.2 Transmission electron microscope images of an altered ilmenite grain from Capel 90 ft Strand Line.

A. Bright field image of weathered ilmenite showing the inhomogeneous nature of the weathered area. The boundary between the unaltered ilmenite (left) and weathered material is fairly sharp and embayed. Scale bar = 1 μm.

B. Dark field image of the above area using an extra pseudorutile reflection along a^*_p. Scale bar = 1 μm.

Plate 6.2

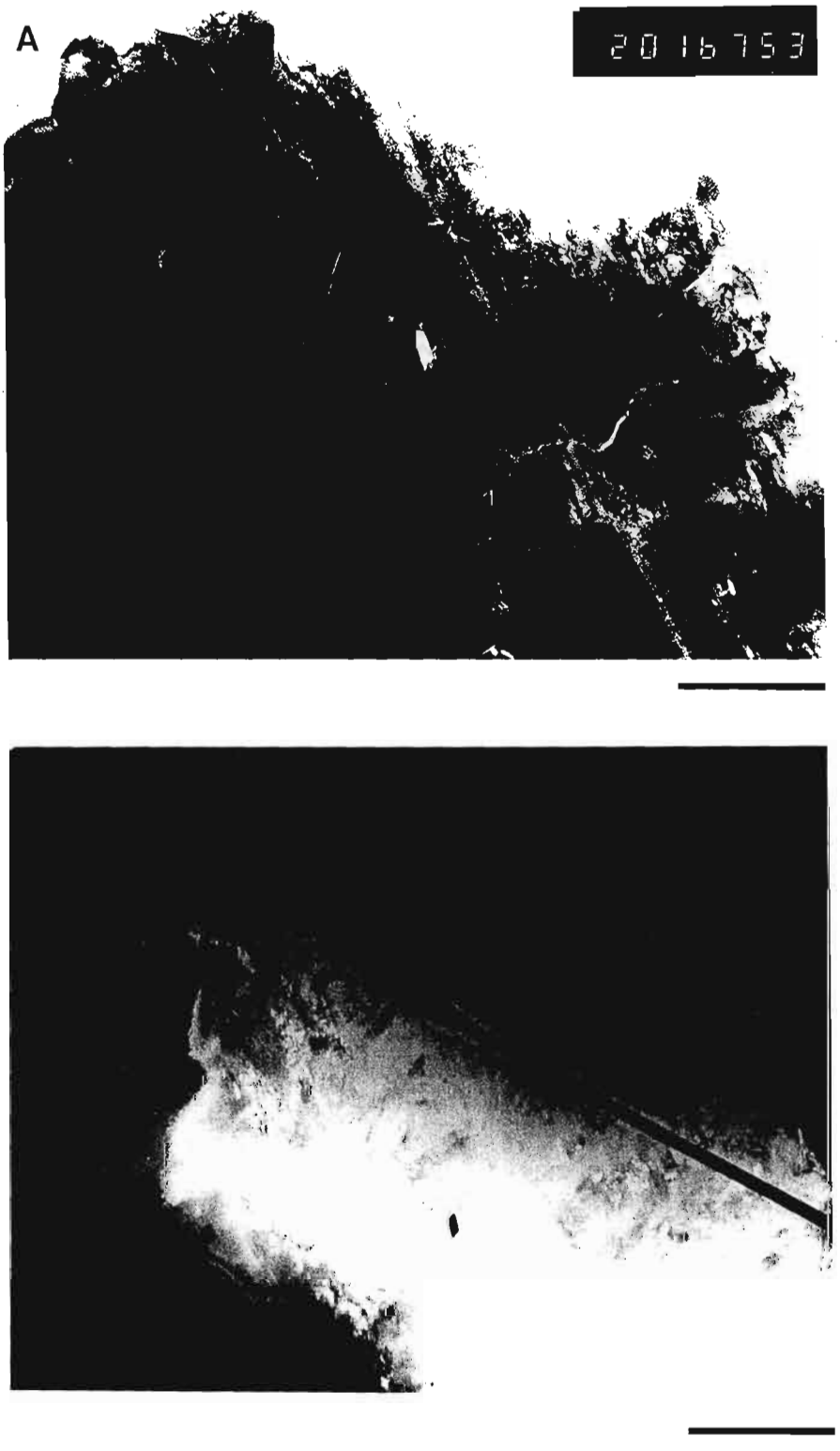

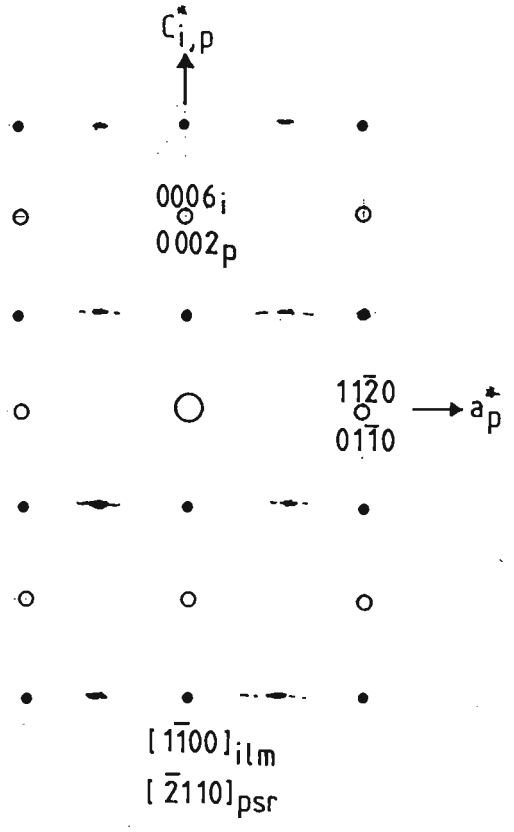
$c^*_{i,p}$
0006_i
0002_p
$11\bar{2}0$
$01\bar{1}0$
a^*_p
$[1\bar{1}00]_{ilm}$
$[\bar{2}110]_{psr}$

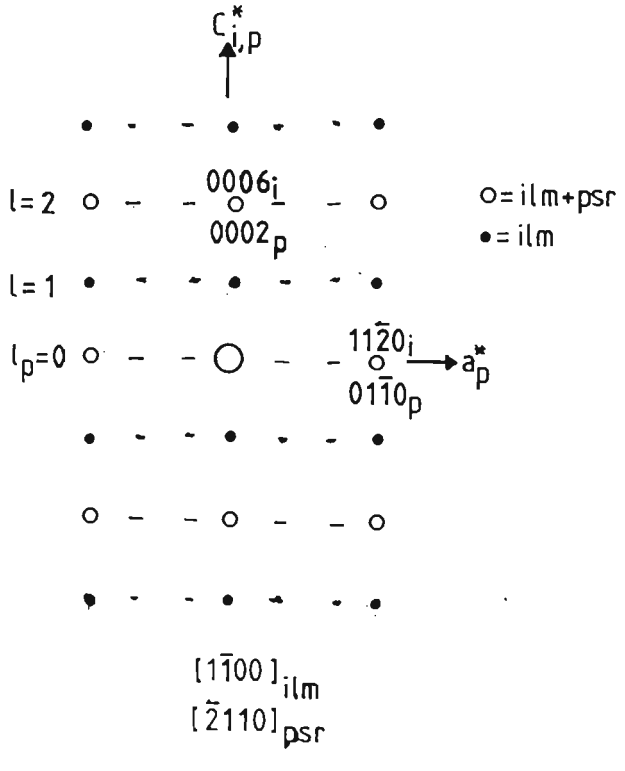
$c^*_{i,p}$
l=2
0006_i
0002_p
o = ilm+psr
• = ilm
l=1
l_p=0
$11\bar{2}0_i$
$01\bar{1}0_p$
a^*_p
$[1\bar{1}00]_{ilm}$
$[\bar{2}110]_{psr}$

Plate 6.3 SADP's of weathered areas orientated along the $[1\bar{1}00]_{ilm}$ zone axis. Sample from Capel, Australia. Note A and B are taken at different camera lengths.

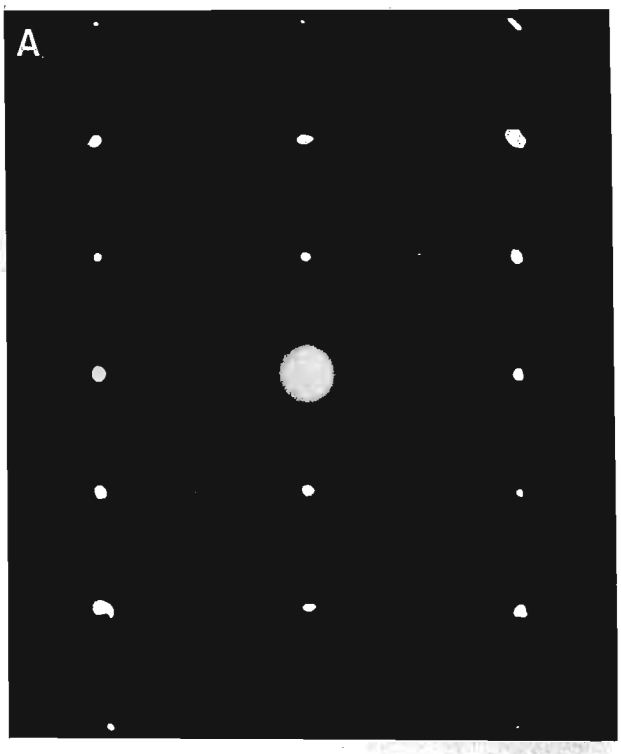

A. Development of streaking and extra reflections parallel to the $(11\bar{2}0)_{ilm}$ direction. The schematic diagrams indicate how the fundamental reflections may be indexed by both ilmenite and the subsell of pseudorutile occurring in a topotactic arrangement.

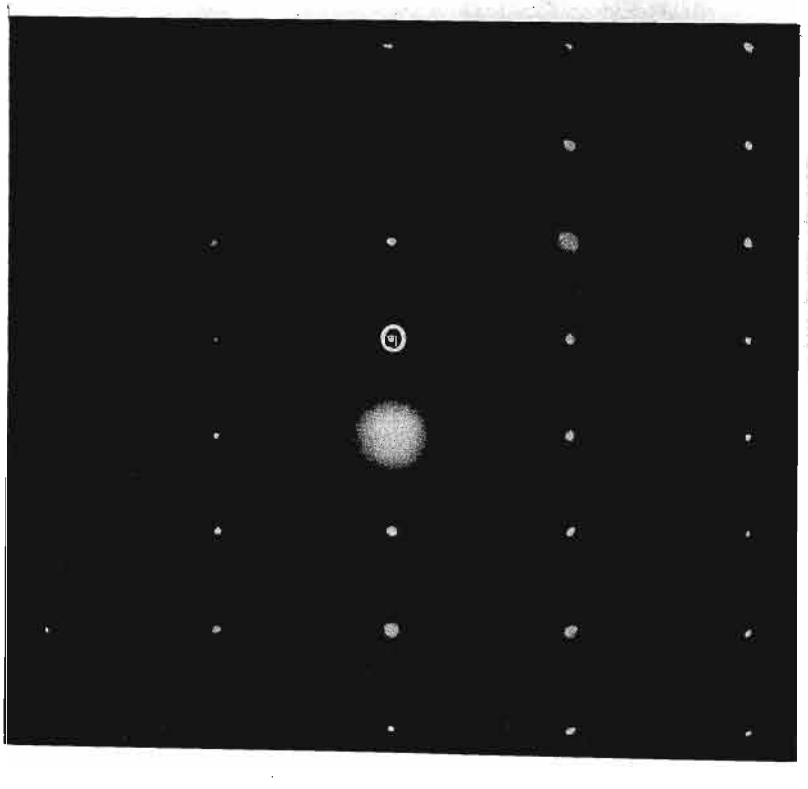

B. Development of superlattice reflection parallel to the $(11\bar{2}0)_{ilm}$ direction. See text for explanation.

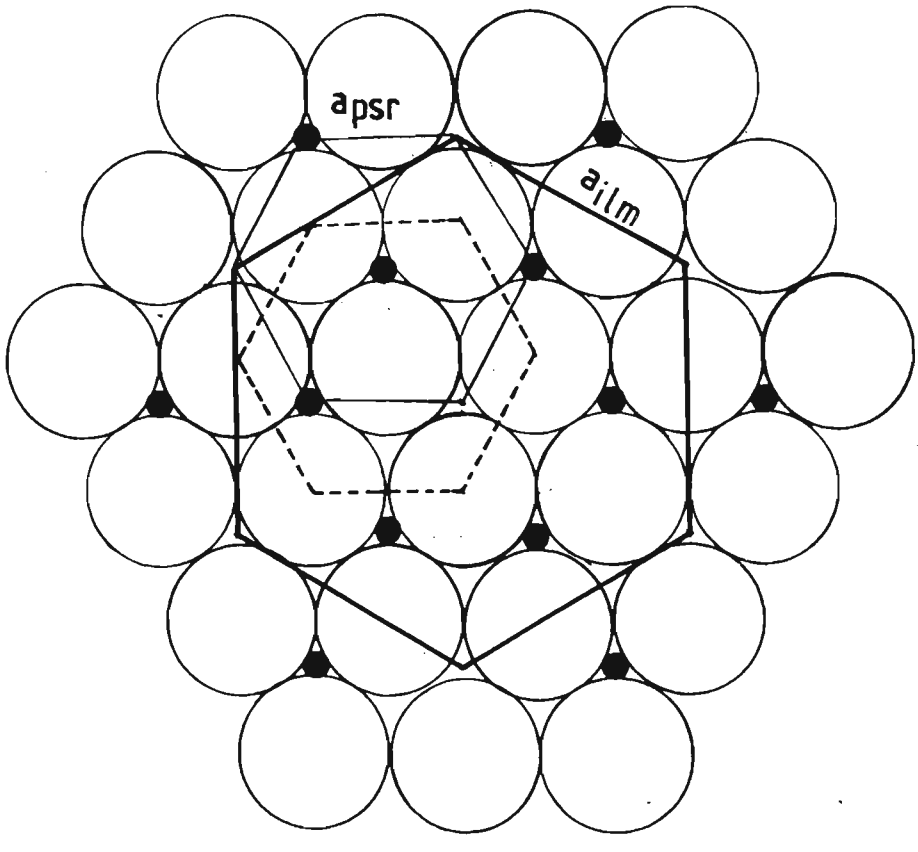

Figure 6.6 Schematic diagram showing the topotactical arrangement of ilmenite and the pseudorutile subcell in real space perpendicular to the *c* axis. Large, open circles represent oxygen anions, while Ti and Fe cations are depicted by the small circles.

As demonstrated by the $[1\bar{1}01]_{ilm}$ and $[2\bar{2}01]_{ilm}$ zone axes in Plate 6.4 A-D, the reflections attributed solely to ilmenite fade as the intensity of the extra reflections increases. Dark field images of these ilmenite reflections show that the heterogeneity of the weathered areas is caused by mixtures of ilmenite and altered material (Plate 6.5A). It is postulated that the proportion of ilmenite in the altered areas decreases with increasing alteration and this causes the ilmenite reflections to fade.

The diffraction pattern of the $[1\bar{1}00]_{ilm}$ (or $[10\bar{1}0]_{psr}$) zone axis in Plate 6.3 clearly shows the presence of extra, superlattice reflections along the $(11\bar{2}0)^*_{ilm}$, or a^*_{psr}, direction. These reflections are not restricted to the $(000l)_{psr}$ (where l is odd) layers, although the intensity of the extra reflections tend to be greater in the l odd layers. Streaking may also occur along the $(11\bar{2}0)^*_{ilm}$, or a^*_{psr}, direction and is found in both the l odd and even layers. These diffuse scattering effects are similar to those noted by Grey and Reid (1975), although it was also noted that in many SADP's of this zone axis, the $(000l)^*_{psr}$ reflections (where l is odd) are not systematically absent as reported by Grey and Reid (1975). This could be caused by relaxation of the Laue conditions due to dynamic scattering effects in electron microscopy or they may be $(000l)^*_{ilm}$ reflections from ilmenite present in the weathered areas (A. Putnis, pers. comm.[1]) The extra reflections are incommensurate, loosely defining 2, 3 or 4-fold multiples of $(11\bar{2}0)^*_{ilm}$, or a^*_{psr}, but no five-fold multiples of a^*_{psr}, as determined by Grey and Reid (1975), are found.

6.7A	**6.7B**	
M-□-M-□-M-□	M-□-M-□-M-□	$c \rightarrow$
M-□-M-□-M-□	□-M-□-M-□-M	

Figure 6.7 Schematic diagram of the metal ordering in the pseudorutile structure (from Grey and Reid, 1975). The chains parallel to the c axis consist of alternately filled (M) and empty octahedral (□) sites and display a high degree of ordering. As indicated by **A.** and **B.** two possibilities exist for ordering between the chains.

[1] Dr A. Putnis, Department of Earth Sciences, University of Cambridge, England.

Grey and Reid (1975) observed that the diffuse scattering peaks indicated a one-dimensional periodic structure parallel to the *c* axis of pseudorutile, and that this chain structure contained a high degree of ordering along the chain, but imperfect ordering between chains. In pseudorutile the highly ordered chains are formed by alternately filled and empty octahedral sites. As stated by these authors, two possibilities exist for the ordering between pairs of chains (Figure 6.7), and

> "if the two types of chains are randomly distributed, the corresponding diffraction [X-ray] patterns will exhibit sheets [streaking] of diffuse intensity perpendicular to the *c* axis",

that is, along $(000l)^*_{psr}$ (Figure 6.7). As this streaking is observed in some SADP's (see Plate 6.3A) it is concluded that in some instances there is little ordering (correlation) between chains in weathered ilmenite. The introduction of correlations between chains will result in the modulation of the diffuse intensity along $(000l)^*_{psr}$ (Grey and Reid, 1975) and hence the formation of extra reflections in this direction (Plate 6.3B). The presence of these extra reflections in some SADP's therefore represent increased ordering (or correlation) between chains in the weathered ilmenite. As these extra reflections may define a number of superstructures (x2, x3 and x4 multiples) of the altered ilmenite lattice, it is postulated that a number of different ordering schemes may develop between the metal-vacancy chains.

The extra, superlattice reflections are observed within $(hkil)_{psr}$, *with* l = odd, layers in SADP's of other zone axes (Plate 6.4), although superlattice reflections are also observed in the $l = 0$ layer of the $[1\bar{1}01]_{ilm}$ zone axis. These reflections are often diffuse and streaked. In SADP's of some zone axes the superlattice reflections are connected by diffuse streaking which has an arced (Plate 6.4B) or sinusoidal form (Plate 6.4D). Complicated streaking effects are also observed in the SADP's of the $[0001]_{ilm}$ zone axis (Plate 6.4E). The SADP's of areas which appear to only be slightly weathered often do not display any superlattice reflections, and only diffuse scattering and streaking are observed (Plates 6.4A and 6.4C).

In dark field mode the diffuse scattering and streaks produce stippled textures as a result of diffraction from small areas within the weathered material. These range in size from 3 to 5 nm, but may coalesce to form larger, inhomogeneous areas of diffraction (Plate 6.5B). Dark field analysis of the extra, superlattice reflections produce images which have a coarser, mottled texture, forming microdomains which range in size from about 5 to 20 nm (Plate 6.5C).

The diffuse scattering and streaking, and their associated dark field images indicate short range order associated with metal-vacancy ordering parallel to the *c axis*, forming microdomains within the weathered areas (Hugo, 1991). The curved shape of the streaks may be caused by diffraction from microdomains having different orientation or twin variants, as suggested by Grey *et al.* (1983). The formation of superlattice nodes with increased weathering, and the larger microdomains contributing to these nodes, suggests that a longer range of ordering is introduced by the correlation between the metal-vacancy chains as weathering proceeds.

Slightly rounded, tabular precipitates are observed in a few weathered grains (Plate 6.6). These vary in size from 25 to 200 nm and are roughly orientated parallel to each other. The precipitates produced extra spots in SADP's which are indexed by a rutile lattice. This indicates that rutile nucleates as discrete precipitates from the weathered matrix.

6.3.6 Conclusions

The TEM study of weathered ilmenites from Australia and South Africa reveals that:

1. The weathered areas within grains are inhomogeneous consisting of mixtures of ilmenite and altered material.

2. The underlying oxide lattice remains intact during the alteration of ilmenite to pseudorutile.

3. Pseudorutile (indexed by the unit cell a = 0.287 nm, c = 0.461 nm) has a topotactic relationship with ilmenite, with $c_{ilm}//c_{psr}$ and $(1\bar{1}20)_{ilm}//a_{psr}$.

4. As the ilmenite is altered by the oxidation and removal of iron, the remaining metal cations form ordered chains with the resulting vacancies parallel to the c axis of the oxide lattice, as determined by Grey and Reid (1975).

5. The ordering (correlation) of different metal-vacancy chains forms a number of superstructures (x2, x3 x4 supercells) in the (000l) plane, suggesting that the x5 supercell of Grey and Reid (1975) is not the only metastable ordering scheme which may exist. The superstructures form microdomains of between 5 and 20 nm within the altered ilmenite.

6. Altered areas between the composition of ilmenite ($FeTiO_3$) and pseudorutile ($Fe_2Ti_3O_9$) do not consist of mixtures of minerals such as rutile or hematite, and no amorphous material is formed.

7. Rutile nucleates as discrete precipitates within the weathered material.

The findings of this study are not conclusive and further research using high resolution electron microscopy is required to examine the causes of short range ordering and superstructuring in greater detail. STEM analysis should be used to correlate the structural changes observed from SADP's with chemical analysis indicating the degree of alteration. Finally, the study was unable to determine the role that hydration plays in the alteration of ilmenite.

The type of ilmenite alteration described above is typical for ilmenite weathered below the water table, in deposits which are slightly reducing and acidic (Grey and Reid, 1975). Ilmenite may alter by different mechanisms when deposited under different physical conditions. These mechanisms are described in the subsequent sections of this chapter

Plate 6.4 SADP's illustrating the effect of increased weathering on the ilmenite structure. Samples from Capel, Australia. Note the SADP's are taken at different camera lengths. Schematic diagrams show the mineral indices.

A. $[1\bar{1}01]_{ilm}$ zone axis showing streaking and diffuse scattering parallel to the $(11\bar{2}0)_{ilm}$ direction.

B. The same zone axis, but note how certain ilmenite reflections fade while the reflections indexed by both ilmenite and the pseudorutile subcell increase in intensity. Note also the development of superlattice reflections and curved or arced, diffuse scattering.

Plate 6.4

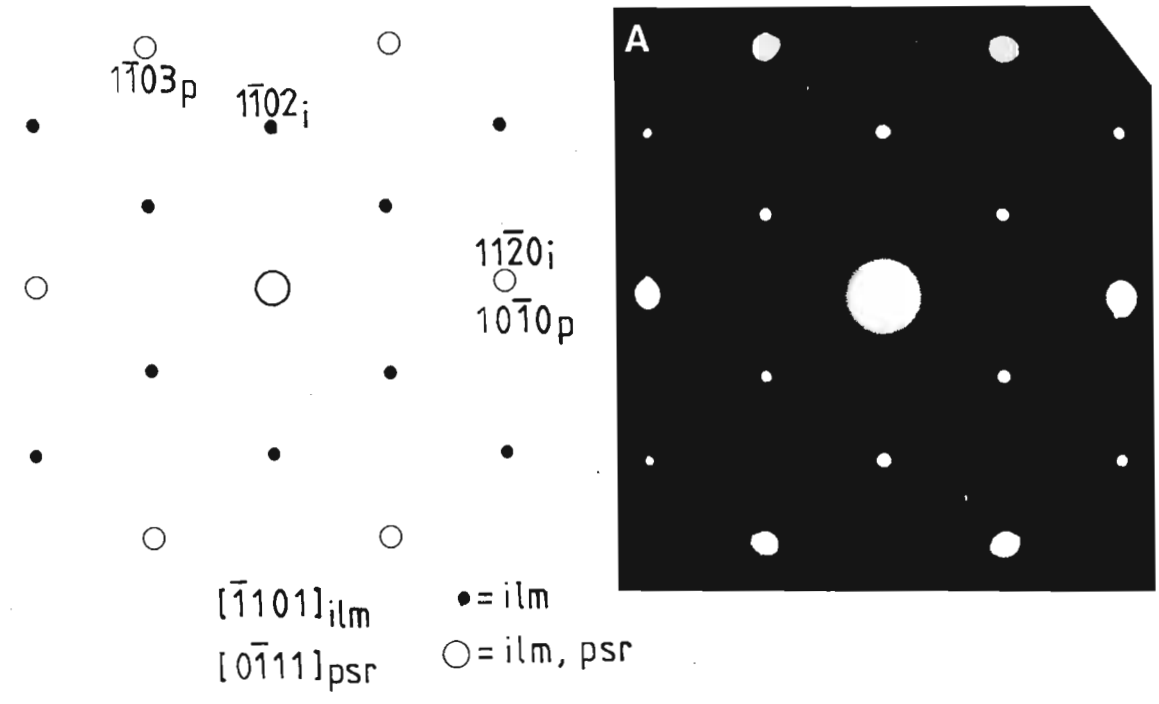
A
$1\bar{1}03_p$
$1\bar{1}02_i$
$11\bar{2}0_i$
$10\bar{1}0_p$
$[\bar{1}101]_{ilm}$
$[0\bar{1}11]_{psr}$
• = ilm
○ = ilm, psr

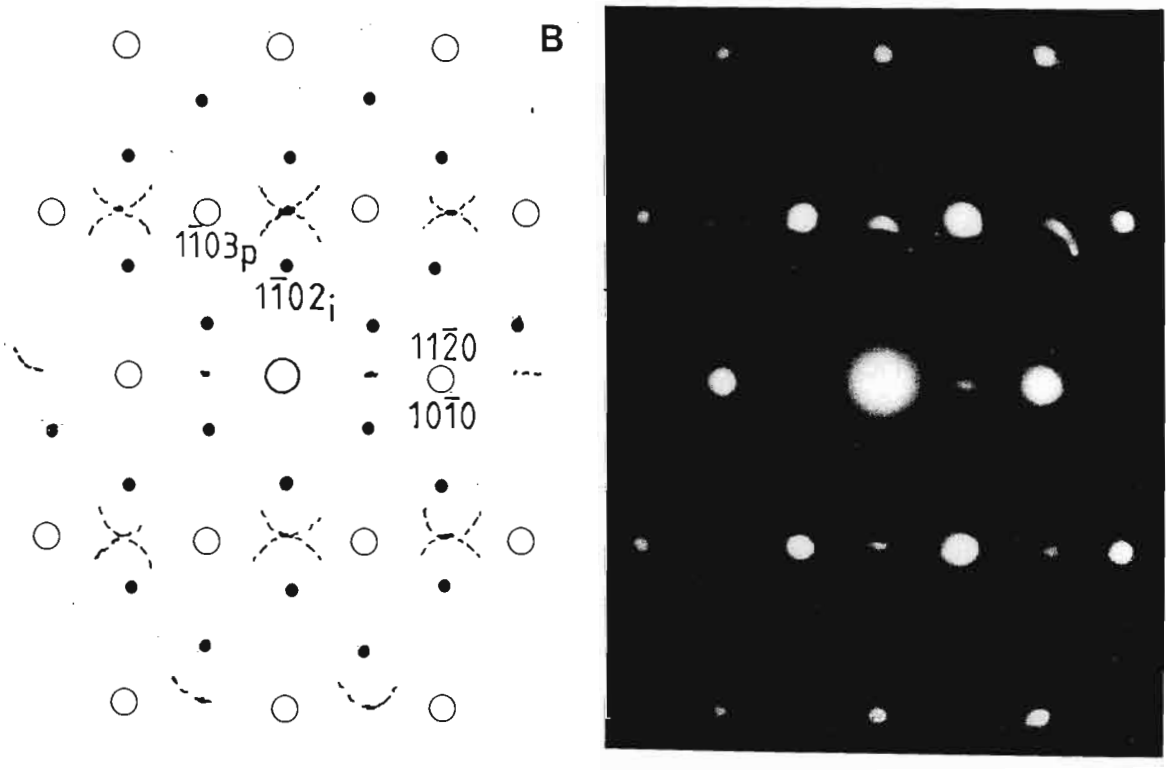
B
$1\bar{1}03_p$
$1\bar{1}02_i$
$11\bar{2}0$
$10\bar{1}0$

Plate 6.4 (cont.)

C. $[2\bar{2}01]_{ilm}$ zone axis showing sharp ilmenite reflections with only faint superlattice reflections and some diffuse streaking parallel to $(11\bar{2}0)_{ilm}$.

D. The same zone axis showing the development of superlattice reflections and curved or sinusoidal diffuse streaking parallel to $(11\bar{2}0)_{ilm}$.

E. $[0001]_{ilm}$ zone axis showing the development of complex diffuse streaking that is formed in the weathered areas.

Plate 6.4 (cont.)

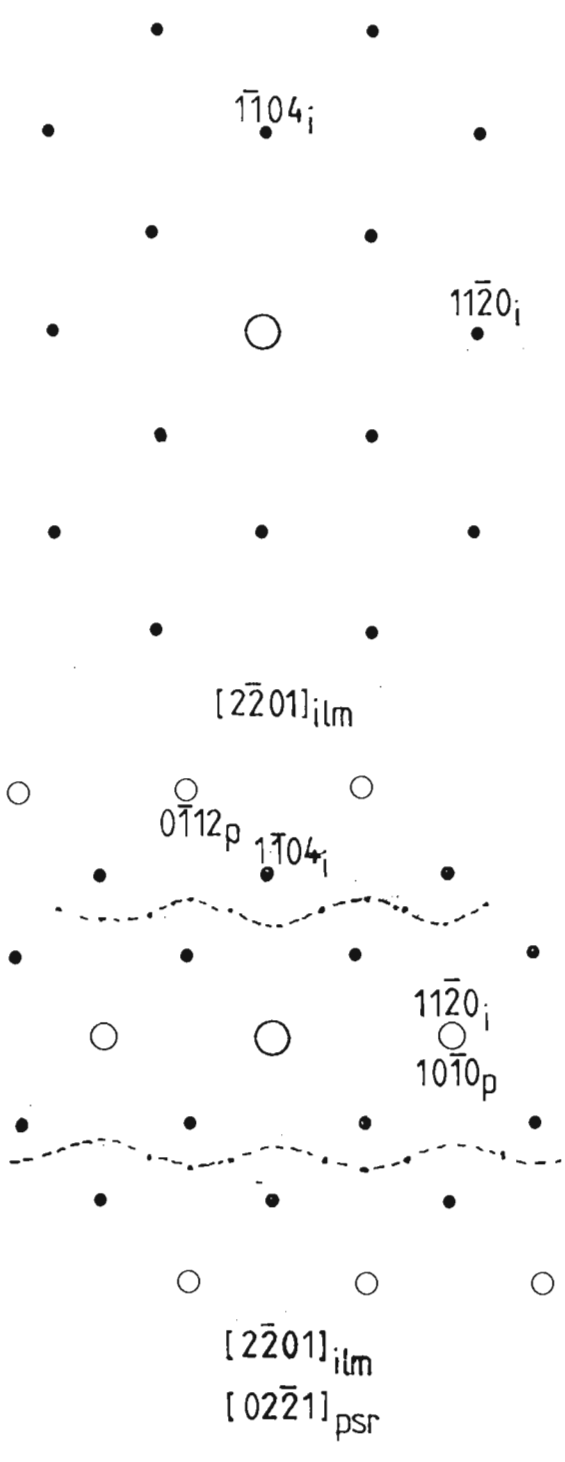

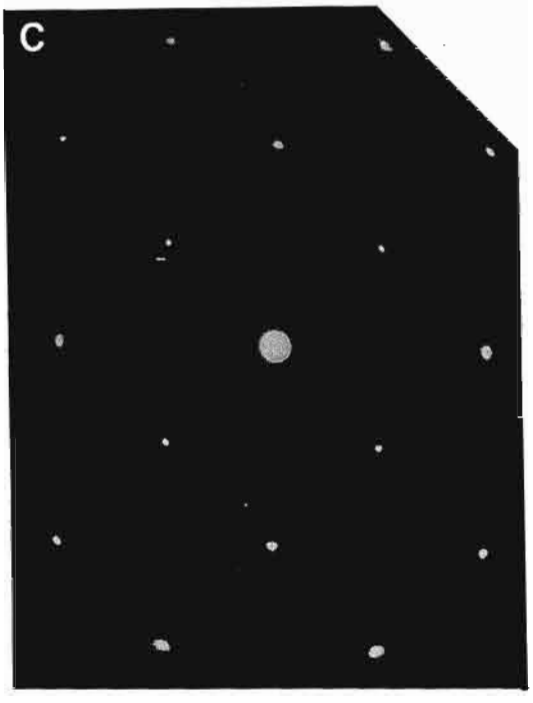

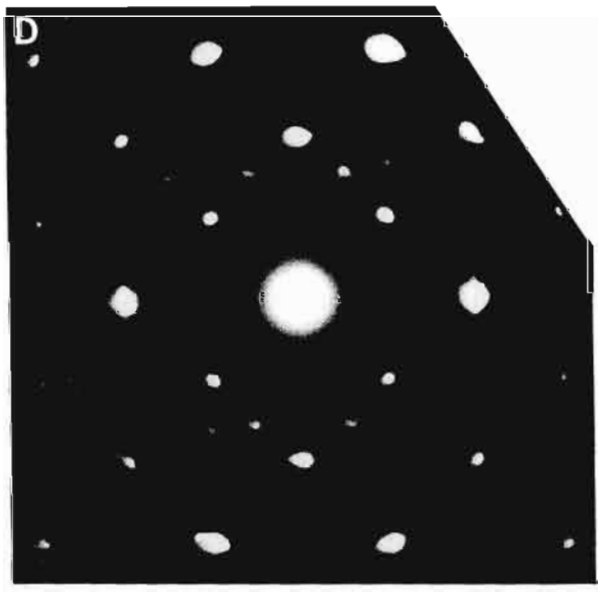

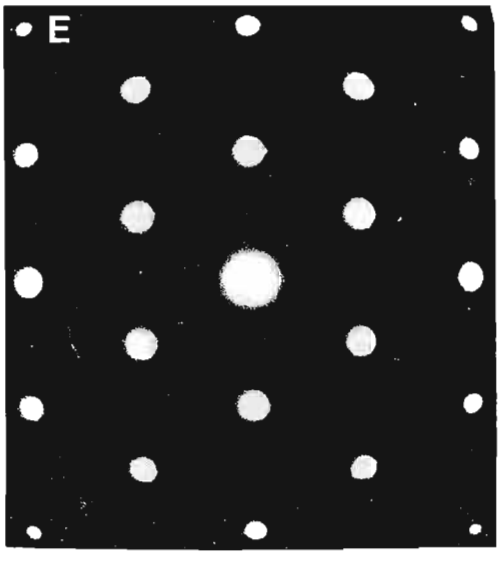

Plate 6.5 Dark field images of weathered ilmenite.

A. Dark field image of weathered area using an ilmenite reflection, as indicated in Plate 6.3B. The image shows clearly the hetrogeneous nature of the weathered area and suggests that these areas consist of mixures of ilmenite and altered material. Sample HZ 21, Port Durnford Formation, South Africa.
Scale Bar = 300 nm.

B. Dark field image of weathered area formed by diffuse scattering, which produces a stippled texture from microdomains of diffraction. Sample from Capel, Australia. Scale bar = 150 nm.

C. Dark field image formed by a superlattice reflection, which produces a mottled texture. Sample HZ 21, Port Durnford Formation, South Africa.
Scale Bar = 150 nm.

Plate 6.5

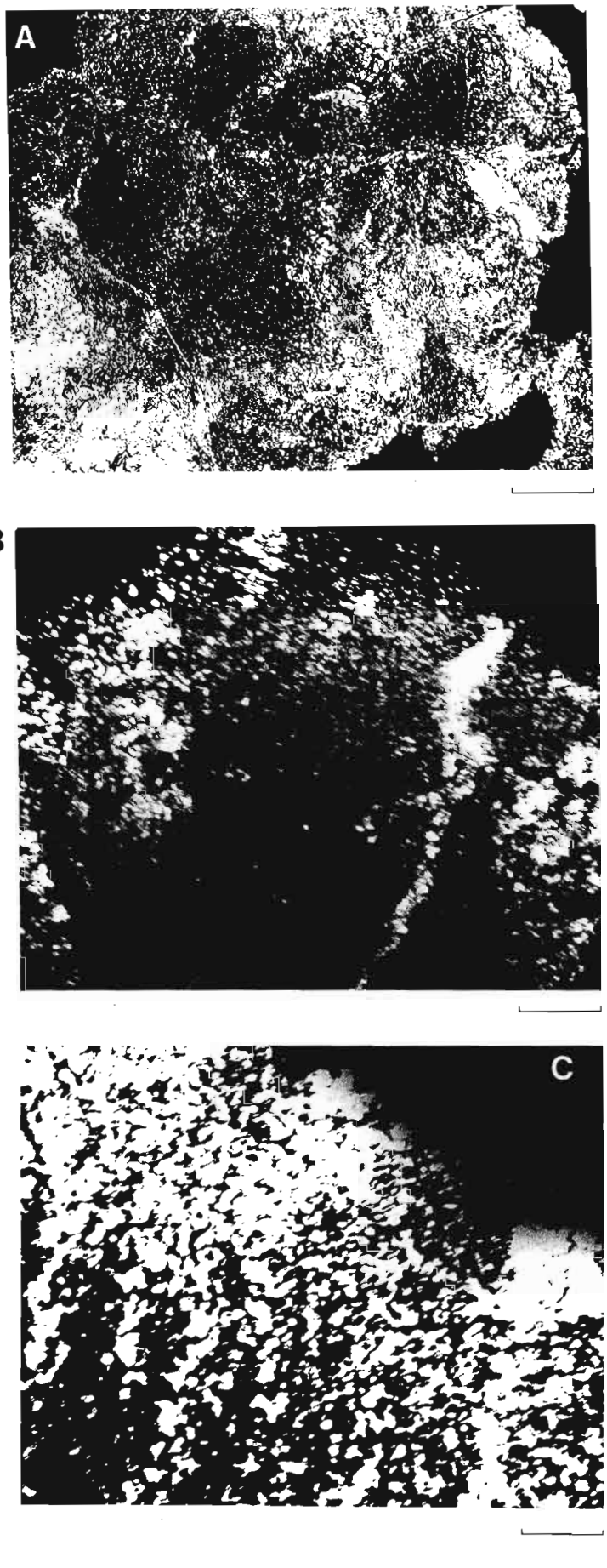

Plate 6.6 Electron microscope images of rutile precipitates in altered ilmenite grains from Capel, Australia.

A. Bright field image of rutile precipitates forming in weathered zone. Scale bar = 77 nm.

B. Dark field of rutile precipitates using rutile reflection. Scale bar = 150 nm.

Plate 6.6

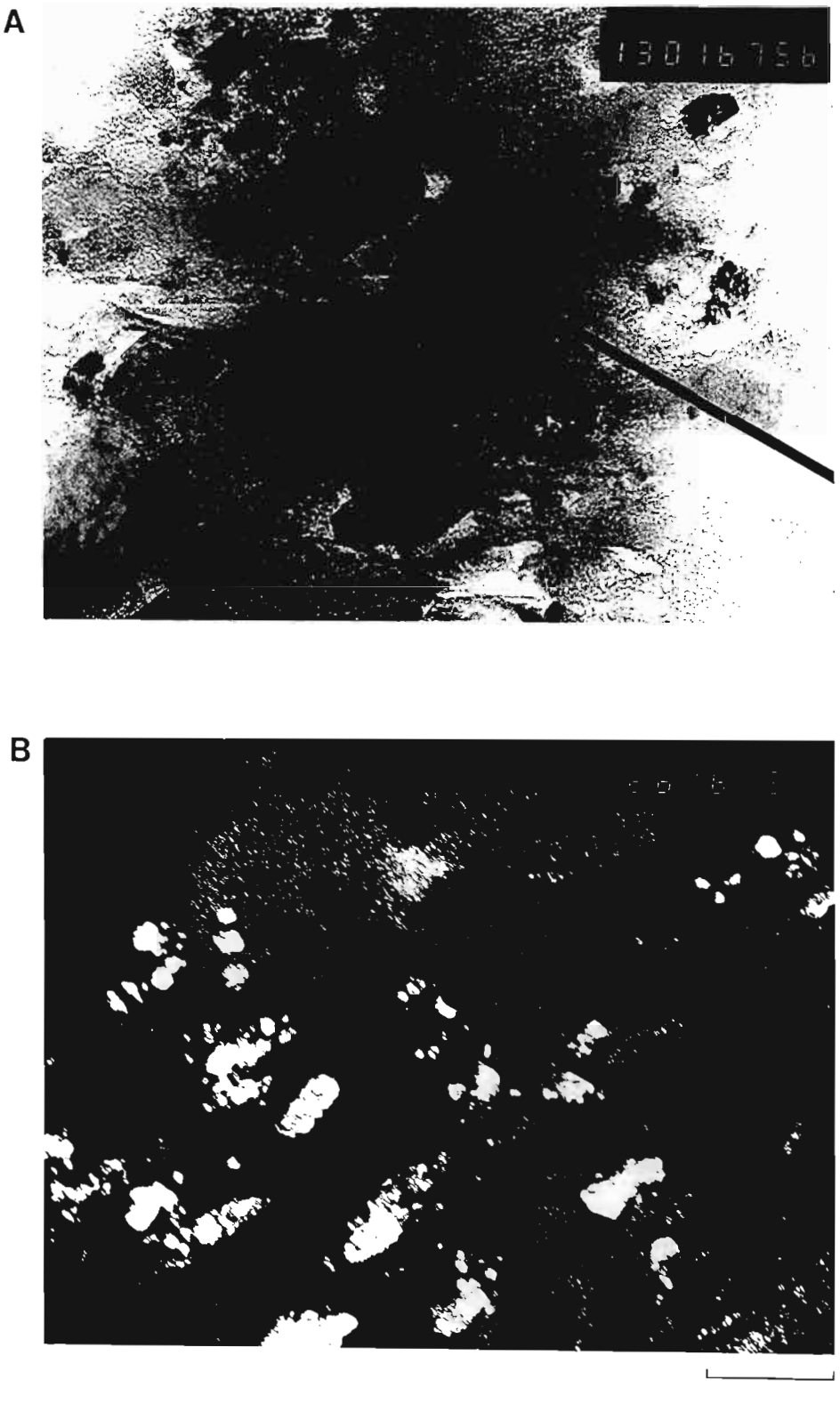

6.4 ALTERATION OF ILMENITE IN THE STUDY AREA

This section describes the petrographic and chemical study of ilmenite weathering from the east coast of South Africa. The nature and types of ilmenite weathering are described and compared to the findings and models of previous authors. The paragenesis of ilmenite weathering is discussed and evidence is presented that some of the alteration prior to final deposition. Much of the data is from Hugo and Cornell (1991), who studied the alteration of ilmenite from deposits in Zululand, however, their findings are true for the entire study area.

6.4.1 Ilmenite mineralogy and alteration

Most of the ilmenite found in the east coast deposits occurs as homogeneous, unaltered grains (see Table 8.1, page 226), however, as described in Chapter 5, ilmenite may be found in composite grains formed by exsolution, oxidation or hydrothermal alteration during cooling of the source rocks. These composite grains containing ilmenite are petrographically distinct from grains formed by alteration processes commonly associated with heavy mineral placer deposits.

Representative microprobe analyses of petrographically homogeneous ilmenite grains (Table 6.4, see also Table 5.6, page 88 and Appendix B.2) show that little or no TiO_2 enrichment has occurred in these grains. In addition, the majority of altered ilmenite grains show only incipient alteration. As a result, ilmenite concentrates produced from the east coast deposits have TiO_2 contents of about 50 per cent (see Table 6.4). In this respect the deposits are distinct from other major heavy mineral placers (such as Eneabba, Western Australia or Trail Ridge, Florida) which tend to contain mostly weathered ilmenite and yield concentrates containing between 54 to 66 per cent TiO_2 (Mackey, 1972a).

Typical relative proportions of ilmenite and its alteration assemblages in the study area are given in Table 6.5 (see also Map 1). This table shows that the entire spectrum from

unaltered and only slightly altered ilmenite grains. Further, the relative proportions of ilmenite and its alteration products show little variation although some samples (for example HZ16 and HZ35) are from sediments below the water table, while others (for example HZ17 and HZ36) are from sediments above the water table. The significance of these observations is discussed further in the Section 6.5.

Table 6.4 Representative microprobe analysis of homogeneous ilmenite grains from the Zululand deposits. Chemical analyses of some ilmenite concentrates are included for comparison (after Hugo and Cornell, 1991).

		Weight % Oxides							
Grain No.	Mineral	TiO_2	FeO[1]	Cr_2O_3	SiO_2	Al_2O_3	MnO	MgO	Total
HZ17-1	homogeneous ilmenite	52.63	45.7	0.04	nd	0.04	0.64	0.26	99.31
HZ2-5	"	51.57	45.78	0.04	nd	0.05	1.32	0.32	99.10
HZ13-6	"	48.60	47.51	nd	nd	1.32	0.47	1.08	97.98
HZ35-10	"	50.21	46.21	0.21	nd	0.21	0.46	2.03	99.33
HZ35-15	"	52.48	43.52	0.10	nd	nd	2.37	0.61	99.08
HZ4-8	"	51.95	46.25	nd	nd	nd	1.08	0.15	99.43
St Lucia	ilmenite concentrate[2]	49.0	45.4	0.38	-	-	-	-	-
Richards Bay	ilmenite concentrate[2]	49.7	46.6	0.19	-	-	-	-	-
Richards Bay	ilmenite concentrate[3]	47.0	45.2	0.3	2.3	0.96	1.3	0.8	97.9

nd = not detected; [1] All iron reported as FeO; [2] Chemical analysis of ilmenite concentrate from Hammerbeck (1976); [3] Chemical analysis of ilmenite concentrate from Lee and Poggi (1978)

Table 6.5 Relative proportions of ilmenite and its alteration assemblages for selected dune samples from the study area (after Hugo and Cornell, 1991).

Assemblage	HZ2	HZ17	HZ16	HZ35	HZ36	HZ13	HN7	HN18	HT5	HT7	HEC6	HEC10
ilmenite	75	70	69	68	71	58	70	71	74	80	79	87
ilmenite-hydrated ilmenite	18	20	20	19	15	23	18	19	10	12	5	7
ilm-hyd ilm-leucoxene	3	3	2	3	3	2	4	5	3	1	4	1
ilmenite-leucoxene	1	1	1	3	1	2	1	tr	1	0	2	tr
ilmenite-TiO_2 pseudomorph[1]	tr	tr	tr	tr	1	-	tr	tr	1	0	2	tr
leucoxene	3	4	8	6	8	15	6	5	11	6	9	4

[1] formed by type III alteration - see text for details; abbreviations: ilm. = ilmenite, hyd ilm = hydrated ilmenite; Sample localities: HZ2 - Port Durnford Dune; HZ17, HZ16, HZ35, HZ36 - Richards Bay; HZ13 - Sodwana Bay; HN7 - Umdloti; HN18 - Mzumbe River Mouth; HT5 - Port St Johns; HT7 - Wavecrest; HEC6 - Morgan's Bay; HEC10 - Kidd's Beach.

Evidence for the following three distinct alteration mechanisms, is observed in the deposits:

Type I: the gradual alteration of ilmenite to leucoxene via hydrated ilmenite and pseudorutile;

Type II: the direct alteration of ilmenite to leucoxene;

Type III: the alteration of ilmenite to hematite plus rutile or anatase in source rocks, followed by the preferred dissolution of the hematite to form ilmenite grains containing a porous network of TiO_2 microcrystals, as described in Chapter 5.

The first two types of ilmenite alteration are described in detail below.

6.4.2 Type I alteration

This style of weathering is identical to that described in the transmission electron microscopy study and has been noted by many other authors (Temple, 1966; Teufer and Temple, 1966; Grey and Reid, 1975; Wort and Jones, 1980; Frost *et al.*, 1983; Mücke and Chaudhuri, 1991). The alteration begins as irregular patches of hydrated ilmenite

along grain boundaries and weaknesses within the grain (Plate 6.7A), or in the form of orientated stringers along the basal plane of the ilmenite (Plate 6.7B).

Microprobe analysis indicates that the altered areas have variable TiO_2 contents ranging between 53 and about 65 percent (Table 6.6). With increasing TiO_2 there is a corresponding decrease in iron content. Slight increases in the Al_2O_3 and SiO_2 contents are noted as the degree of alteration increases, which corresponds to the findings of Frost *et al.* (1983). Back-scattered electron images indicate that the altered areas may be inhomogeneous, consisting of fine intergrowths (< 1 μm) of ilmenite and hydrated ilmenite or pseudorutile (Plate 6.7C). No relationship was noted between the extent (amount of grain altered) and the degree of alteration (percentage TiO_2).

The second stage of alteration is marked by the development of leucoxene, which forms as irregular patches along grain boundaries, or structural weaknesses (Plate 6.7C and D). The development of leucoxene along grain boundaries is less common than expected for the *in situ* alteration of ilmenite. Leucoxene often develops from hydrated ilmenite or pseudorutile but may also replace ilmenite. The boundaries between leucoxene and the other phases may be diffuse, consisting of fine intergrowths of hydrated ilmenite (or pseudorutile) and leucoxene (see Plates 6.7C and D). Such textures indicate that a gradual, continuous alteration has occurred from hydrated ilmenite to leucoxene. In other instances the boundaries between leucoxene, and the phases it is replacing are sharp and embayed (Plate 6.7E). This indicates that the alteration to leucoxene may also be discontinuous, which contrasts with the findings of Mücke and Chaudhuri (1991) who argue that the alteration of ilmenite is a continuous process. In a number of grains the boundaries between leucoxene and the phases it is replacing are truncated by the grain surface, showing that the alteration occurred in a larger grain (Plate 6.7F), which has subsequently been broken during reworking of the sediment.

The alteration of some grains has proceeded until the grain consists entirely of leucoxene. Such grains become more TiO_2-rich with increasing alteration until they consist entirely of crypto- or microcrystalline rutile or occasionally anatase.

Table 6.6 Selected microprobe analyses of altered ilmenite grains (from Hugo and Cornell, 1991).

		Weight % Oxides							
Grain No.	Coexisting phases	TiO_2	FeO[1]	Cr_2O_3	SiO_2	Al_2O_3	MnO	MgO	Total
G15	ilmenite	51.72	46.21	0.07	nd	nd	0.63	1.07	99.70
	hydrated ilmenite	54.17	41.84	0.08	nd	0.04	0.89	0.94	97.96
G12	ilmenite	50.66	48.52	nd	nd	nd	0.70	0.04	99.92
	pseudorutile	66.25	27.95	nd	1.29	0.77	1.14	nd	97.40
G1	ilmenite	50.48	47.41	0.09	nd	0.09	1.54	0.18	99.79
	hydrated ilmenite	55.36	38.52	0.25	0.32	0.27	1.75	0.13	98.85
	pseudorutile	68.82	25.4	0.43	0.57	0.70	2.14	0.18	98.24
G3	ilmenite	51.22	45.59	0.07	0.07	0.10	0.24	2.28	99.57
	pseudorutile	61.26	32.42	0.15	0.73	0.56	0.42	2.12	97.66
	leucoxene	79.72	13.25	0.10	1.10	1.45	0.31	1.82	97.75
G11	ilmenite	49.52	44.56	0.05	nd	nd	5.59	nd	99.72
	hydrated ilmenite	56.80	36.50	nd	0.15	0.26	4.61	nd	98.32
	leucoxene	86.30	7.71	nd	2.21	0.59	1.56	nd	98.37
G37	hydrated ilmenite	57.12	38.42	0.04	0.14	0.08	nd	nd	95.82
	leucoxene	79.14	9.33	nd	5.51	2.21	nd	0.11	96.32
	leucoxene	77.83	16.38	nd	1.85	0.46	0.11	nd	96.55
G30	ilmenite	50.77	46.56	nd	nd	0.06	0.93	1.33	99.66
	leucoxene	83.98	11.3	nd	0.79	0.71	0.65	0.98	98.41
G18	ilmenite	52.18	45.49	0.05	0.06	nd	0.82	nd	98.67
	TiO_2 pseudomorph	97.90	1.52	nd	nd	nd	nd	nd	99.48
G51	ilmenite	52.81	45.02	nd	nd	nd	1.36	0.33	99.58
	TiO_2 pseudomorph	96.92	1.65	nd	0.35	0.04	nd	nd	99.00
G25	leucoxene	77.20	7.09	nd	8.49	4.25	0.15	0.28	97.45
G32	leucoxene	86.09	7.86	nd	0.63	0.65	0.10	0.05	95.39

nd = not detected; [1] All iron is reported as FeO.

Plate 6.7 Back-scattered electron images of ilmenites from Zululand displaying Type I alteration.

A. Patchy alteration of ilmenite (I) to hydrated ilmenite (H). The different shades of grey of hydrated ilmenite in the figure reflect varying degrees of alteration. Richards Bay (HZ 35). Scale bar 75μm.

B. Development of hydrated ilmenite along basal parting of ilmenite. Port Durnford (HZ 2). Scale bar 75μm.

C. A hydrated ilmenite (H) grain altering to leucoxene (L), displaying the inhomogeneous nature of the hydrated ilmenite, and the gradual alteration to leucoxene in the top left hand corner of the grain. Richards Bay (HZ 17). Scale bar 25μm.

D. The gradual replacement of hydrated ilmenite (H) by leucoxene (L) from the grain boundary, and within partings and fractures. Note the zoning of the leucoxene in the grain. Richards Bay (HZ 16). Scale bar 60μm.

E. The replacement of hydrated ilmenite (H) by leucoxene (L). The sharp, embayed boundary between the phases indicates clearly that the alteration of ilmenite to leucoxene via pseudorutile is not always a continuous process (cf. Mücke and Chaudhari, 1991). Note that the grain surface truncates the boundary between the hydrated ilmenite and leucoxene indicating that it has been reworked after alteration. Cape St Lucia (HZ 4). Scale bar 40μm.

F. Rounded ilmenite (I) grain altering to leucoxene (L) via pseudorutile (P) from grain surface. Again note that the grain has been fractured after alteration. Cape Vidal (HZ 11). Scale bar 60μm.

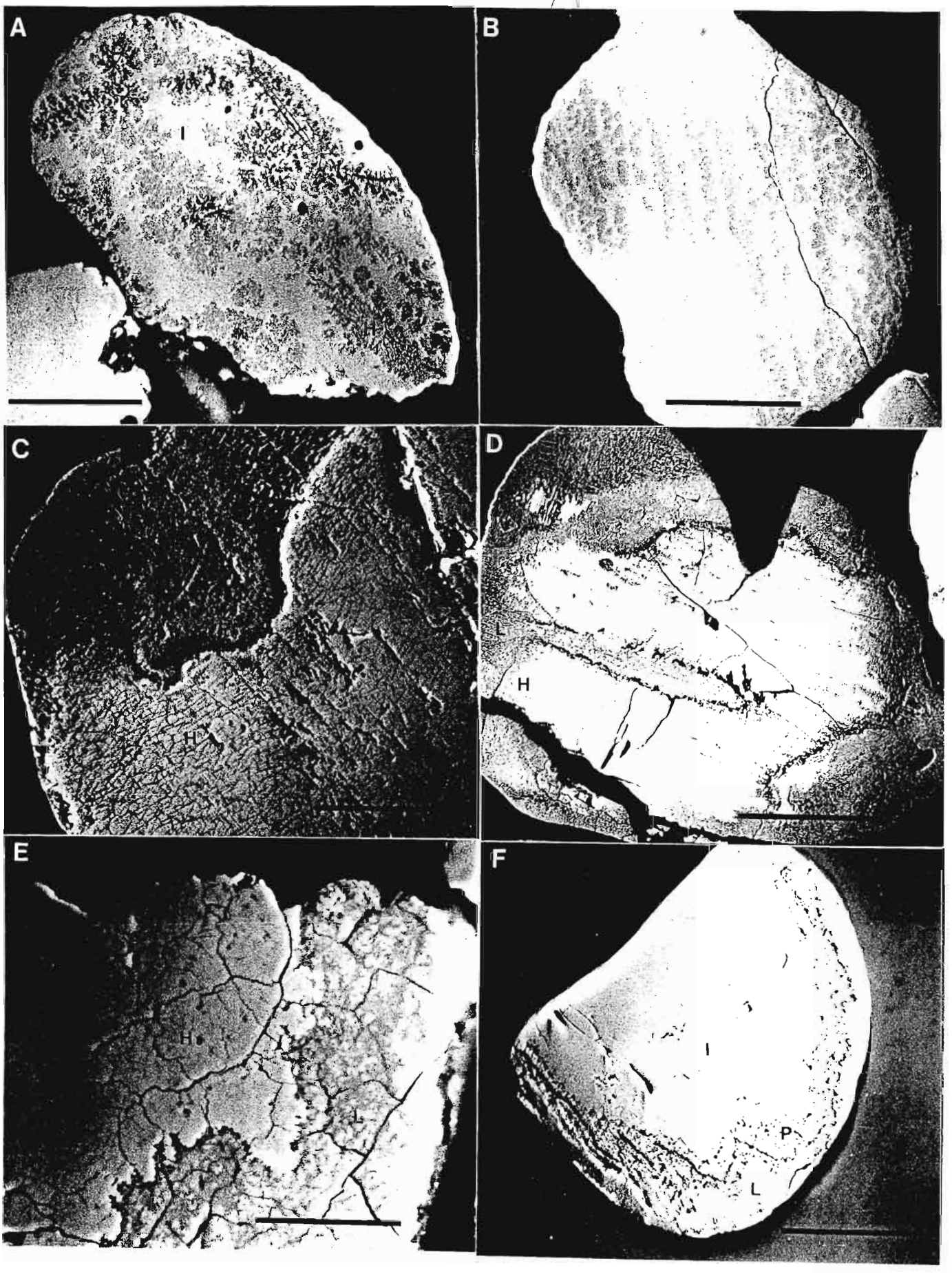
A
I
B
C
H
D
L
H
E
H
L
F
I
P
L

This type of alteration may be explained by the two stage model of Grey and Reid (1975). The first stage of this model involves the oxidation of all the ferrous iron and the leaching of one third of the ferric iron from the ilmenite lattice by electrochemical corrosion. The reaction is:

$$3Fe^{2+}TiO_3 + H^+ + \tfrac{1}{2}O_2 \rightarrow Fe_2^{3+}Ti_3O_9 + Fe^{2+}(OH)^- \quad \text{....(6.2)}$$

Ilmenite Pseudorutile + dissolved iron

This reaction is considered to operate in a mildly acidic groundwater situation (Grey and Reid, 1975; Dimanche and Bartholomé, 1976).

In this model the second stage of alteration beyond pseudorutile occurs via a dissolution-reprecipitation process whereby both iron and titanium are dissolved, but the titanium is redeposited while the iron is leached from the grain. This leads to the formation of rutile in beach sands (Grey and Reid, 1975) and anatase in lateritic soils (Anand and Gilkes, 1984, 1985), described by the reaction:

$$Fe_2Ti_3O_9 + 4H^+ \rightarrow 3TiO_2 + 2Fe^{2+} + \tfrac{1}{2}O_2 + 2H_2O \quad \text{....(6.3)}$$

Pseudorutile rutile (or anatase) + dissolved iron

The second stage of alteration is thought to occur in the near-surface regions of the deposit (Grey and Reid, 1975; Frost *et al.* 1986) in an environment which is rich in organic and inorganic acids derived from the upper soil layer and condensation, creating mildly reducing and acidic solutions (Grey and Reid, 1975; Frost *et al.*, 1983).

Although hydrated ilmenite and pseudorutile develop from ilmenite in the coastal sediments, in accordance with [6.2], these phases appear to be readily replaced by leucoxene in the deposits, and few grains consisting entirely of hydrated ilmenite or pseudorutile are found. This suggests that pseudorutile is unstable in the deposits and alters readily to leucoxene by the dissolution and reprecipitation process of [6.3]. Once

leucoxene forms it may also replace ilmenite by direct leaching and reprecipitation as described below. In this sense the mechanism differs from Grey and Reid's (1975) model.

6.4.3 Type II alteration

In this type of alteration, ilmenite, or slightly altered ilmenite, is observed altering directly to leucoxene. The alteration occurs from grain boundaries (Plate 6.8A), or along weaknesses, such as fractures (Plates 6.8B and 6.8C) within the grains. In some instances leucoxene may grow as replacement fronts across grains (Plate 6.8C) or may mimic the original crystallographic directions of ilmenite grains (Plate 6.8D). The boundary between the ilmenite and leucoxene may consist of a porous area of cellular or microcrystalline leucoxene, indicating that isovolumetric replacement has occurred. SEM analyses indicate that the pores in these areas have silica and aluminum contents well in excess of 10 per cent. Beyond this zone the leucoxene is usually less porous, as shown in Plate 6.8B, however, significant quantities of SiO_2 and Al_2O_3 may still be present (Table 6.6).

This style of alteration is similar to that observed by Hartman (1959), Frost *et al.* (1983), and Frost *et al.* (1986). Hartman (1959), studying iron-titanium oxides during bauxitization, found that ilmenite may alter directly to leucoxene or optically identifiable anatase. Frost *et al.* (1983) noted relatively unaltered ilmenite cores surrounded by leucoxene in a concentrate from the Capel 150 ft strand line, and concluded that these assemblages represent a single step dissolution-reprecipitation process without the formation of pseudorutile. This style of alteration of ilmenite to leucoxene, rutile or anatase may be expressed by the equation:

$$\underset{\text{ilmenite}}{FeTiO_3} + 2\,H^+ \rightarrow \underset{\text{rutile (or anatase)}}{TiO_2} + \underset{\text{dissolved hematite}}{Fe^{2+}} + H_2O \qquad \ldots.(6.4)$$

For the most part the Capel 150 ft strand line lies above the water table and Frost *et al.* (1983) suggest that [6.4] occurs in the near surface regions, or pedogenic zones, of the deposit, where soil acids may directly leach the ilmenite.

The growth of leucoxene from cracks within the grains (Plate 6.8B) illustrates how acidic groundwater may follow these weaknesses to dissolve the ilmenite and leach the iron from the grain, while the titanium is reprecipitated.

6.4.4 Type III alteration

A number of altered ilmenite grains are observed in the deposits, which consist of ilmenite and porous networks of microcrystalline TiO_2 pseudomorphs (see Table 6.5). Two distinct intergrowths are noted. The first type of intergrowth is characterised by the replacement of ilmenite by euhedral to subhedral acicular or prismatic TiO_2 microcrystals (Plate 6.9A). The alteration does not occur along grain boundaries, but rather as patches within grains. Often the microcrystals form a porous trellis-type structure which is filled by siliceous material high in aluminium. In many instances the TiO_2 needles appear orientated (Plate 6.9A). Grains of this nature are interpreted as having formed by hydrothermal or supergene alteration of ilmenite, as similar textures have been described by Rumble (1976), Ramdohr (1980), Haggerty (1976b), Whalen and Chappel (1988) and Mücke and Chaudhuri (1991), for ilmenites which have undergone such alteration in source rocks.

The second type of intergrowth is characterised by the development of anhedral, often vermiform rutile microcrystals in patches within the ilmenite grains (Plate 6.9B). The microcrystals form porous, symplectite-like intergrowths with each other and the ilmenite matrix. In a few instances microcrystals of hematite are found within the rutile intergrowths (Plate 6.9C). Grains containing such intergrowths are considered to have formed by the high temperature breakdown of ilmenite in igneous or metamorphic source rocks to form intergrowths of rutile and hematite as described by Haggerty (1976b) and Haggerty (1991, *cf.* Figure 20 f and g). Subsequent dissolution of hematite has resulted in grains consisting of only ilmenite and microcrystalline rutile. This interpretation is supported by the presence of hematite relicts found within the rutile microcrystals in some grains (see Plate 6.9C). The voids formed by the dissolution are often subsequently filled by siliceous material or clay.

Plate 6.8 Variations of Type II ilmenite alteration observed in Zululand coastal deposits.

A. Back-scattered electron image of leucoxene (L) replacing ilmenite (I) from the surface of the grain. Despite the fairly advanced state of alteration of the grain, the ilmenite relicts are unaltered. Sodwana Bay (HZ 13). Scale bar 40μm.

B. Back-scattered electron image of leucoxene (L) replacing ilmenite (I) from the grain surface and along fractures originating at this surface. Note the partial coating of siliceous material (dark grey) around the grain. Such coatings are uncommon in the dune deposits and indicate that the grain may have been reworked from another sediment. Cape St Lucia (HZ 4). Scale bar 80μm.

C. Magnified view of upper part of grain in **B**, displaying the replacement of ilmenite by leucoxene along a crack within the grain. Scale bar 10μm.

D. Alteration of ilmenite (I) by leucoxene (L). Note the highly porous nature of the leucoxene adjacent to the ilmenite and the truncation of the leucoxene-ilmenite boundary at the grain surface. This latter feature may either be caused by leucoxene advancing as a front across the grain, or by the mechanical weathering of a larger grain altered in a previous environment. From Hugo (1988), Richards Bay. Scale bar 40μm.

E. Photomicrograph of ilmenite (I) altering directly to leucoxene (L) revealing the original crystal planes of the ilmenite. From Hugo (1988), Richards Bay. Scale bar 50μm.

Plate 6.8

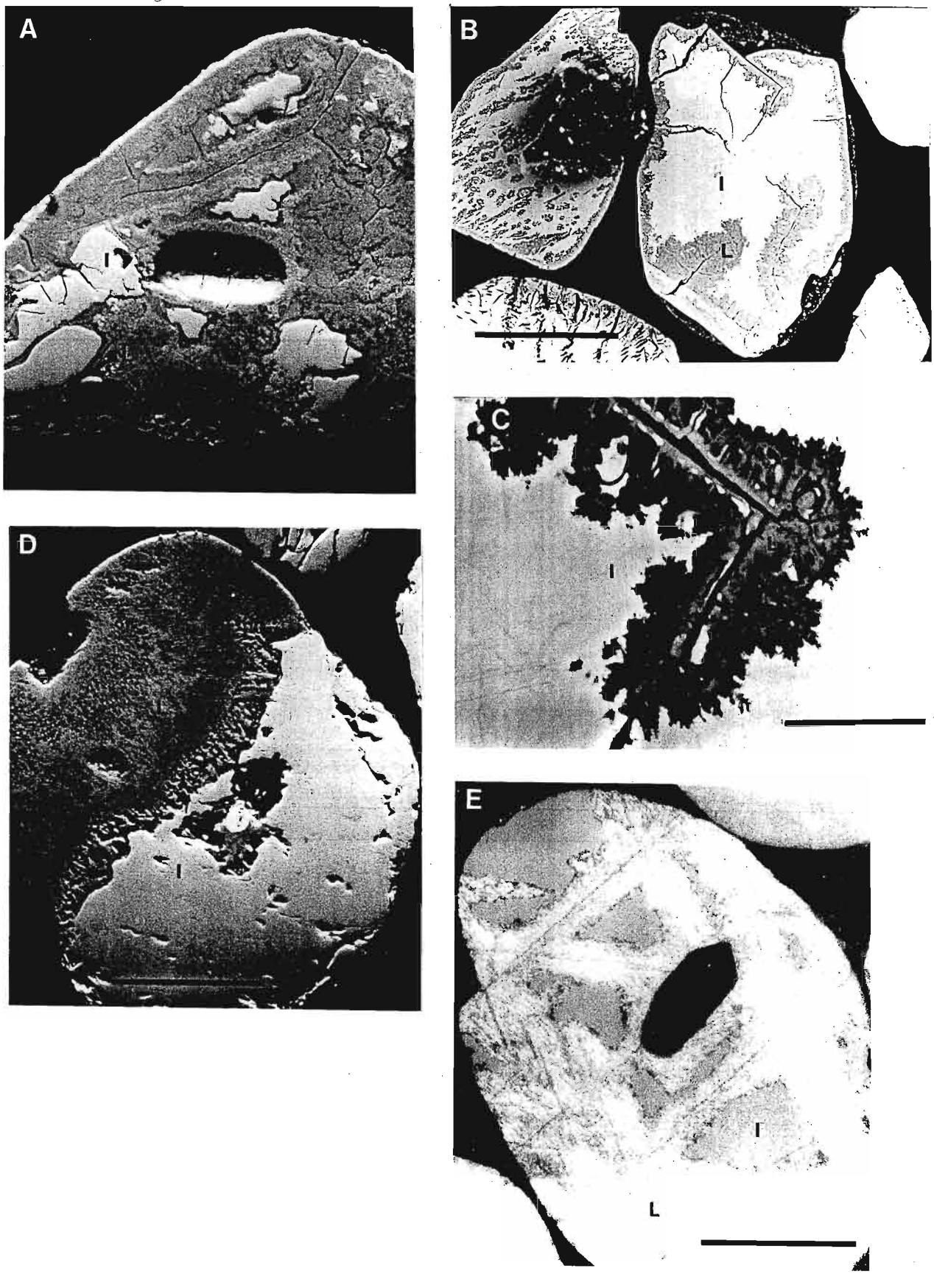

Plate 6.9 Back-scattered electron images displaying variations in type III alteration observed in Zululand deposits.

A. The replacement of ilmenite (I) by acicular TiO_2 (T) microcrystals. Richards Bay (HZ 19). Scale bar 75μm.

B. Patches of vermiform rutile (R) microcrystals forming porous, symplectite-like intergrowths within an ilmenite (I) grain. Port Durnford (HZ 2). Scale bar 75μm.

C. Magnified area of grain shown in B. displaying the symplectite-like intergrowths of rutile microcrystals and the presence of relict hematite microcrystals (h). Note also the the siliceous material (dark grey) filling the spaces between the rutile microcrystals. See text for explanation. Scale bar 20μm.

Plate 6.9

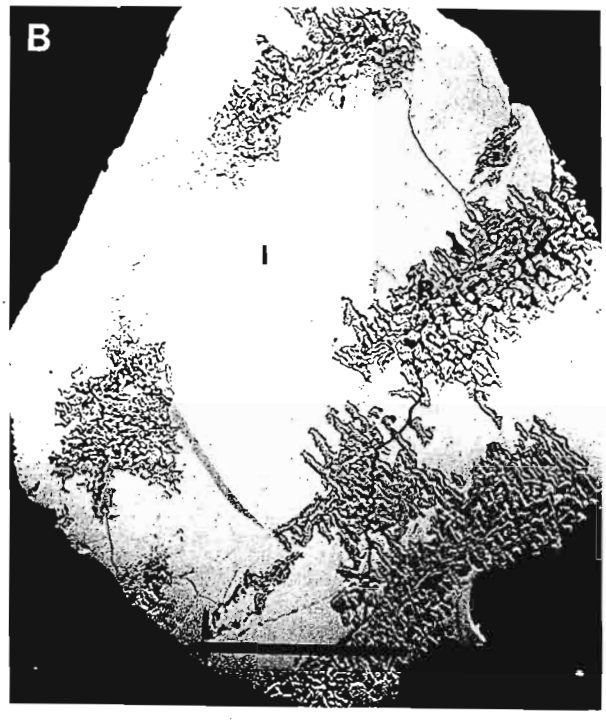

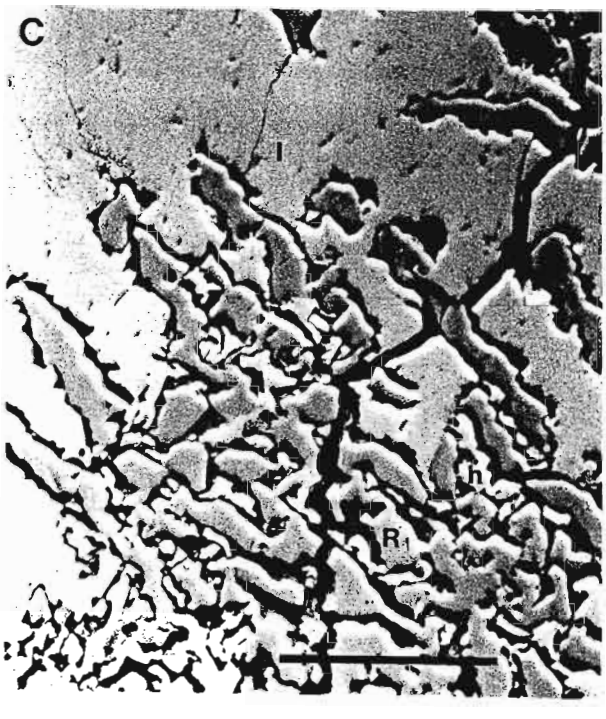

6.5 PARAGENESIS OF ILMENITE ALTERATION

It is important to determine the paragenesis of the ilmenite alteration, because the site of alteration will affect the distribution and proportions of different types of altered grains in the deposits. If the alteration occurred before final deposition then a fairly random distribution of altered grains is expected. However, if alteration occurred after deposition, then the altered grains may be concentrated in areas of the deposit where conditions are most conducive to alteration. Furthermore, according to the models described above, different types of alteration due to weathering are expected to be concentrated above and below the water table if all alteration is post-depositional. As already noted, certain ilmenite alteration products are undesirable and large variations in the distribution of these alteration products due to *in situ* alteration in different environments will affect the local grade and volume of recoverable material.

6.5.1 Evidence for in situ ilmenite alteration in placer deposits

It is widely believed that ilmenite alteration occurs *in situ* in beach and dune deposits for the following reasons:

1. Alteration proceeding from the margins of well-rounded grains is fairly common, suggesting that alteration occurred after rounding of the grains, that is during the late stages of transportation, or after deposition (Bailey *et al.*, 1956).
2. Some beach deposits display a vertical variation in the composition of ilmenite concentrates, particularly about the water table (Temple, 1966; Force, 1991). In these deposits the leucoxene contents of ilmenite concentrates are significantly higher above the water table, or near the surface, suggesting that these areas of higher acidity enhance the alteration of ilmenite. This suggests that the alteration of ilmenite is "due to weathering, and that this for the most part has taken place *in situ* in the sand deposit" (Temple, 1966).
3. Temple (1966) also noted that older deposits generally contain the most altered ilmenite, and cites values from Western Australian raised beaches of different elevations (and consequently different ages) as an example.

4. La Roche *et al.* (1962) noted that the alteration displayed by ilmenite in littoral zones is not observed in the source rocks and is rarely found in alluvial ilmenite grains.

6.5.2 Evidence for multistage alteration of ilmenite

The following observations indicate that alteration of ilmenite in the coastal sediments cannot completely be described by a simple model in which ilmenite grains are eroded, transported, deposited in the dunes, and then altered:

1. Most ilmenite grains are unaltered, or only slightly altered, yet the entire alteration spectrum from ilmenite to leucoxene is found. Further, the amount of alteration end-product leucoxene, which may constitute as much as 15 per cent of the ilmenite alteration assemblage (see Table 6.5, page 149), is high relative to the 60-80 per cent of unaltered ilmenite. This implies that either the ilmenite altered at strikingly different rates, or that some of the ilmenite was altered prior to deposition in the dunes.
2. Two types of ilmenite weathering are observed in *all* the samples studied, regardless of whether they came from above or below the water table (see Table 6.5, page 149). Comparison with existing models indicates that type I alteration develops in a groundwater environment, whereas the type II alteration occurs above the water table in mildly reducing and acidic soils.
3. Ilmenite grains altered by oxidation or hydrothermal processes in the source rocks are observed in the deposits.
4. In some grains the boundaries between ilmenite and phases formed by alteration may be truncated by grain surfaces, which indicates that these grains have been reworked.
5. Ilmeno-hematite or hemo-ilmenite grains present in a single sample may alter in two ways: i) ilmenite alters to hydrated ilmenite or leucoxene while the hematite remains unaltered (Plate 6.10A); ii) ilmenite undergoes alteration and hematite is partially or completely removed from the grain, resulting in pitted grains of altered ilmenite (Plate 6.10B). Dimanche and Bartholomé (1976) used thermodynamic

data to demonstrate that the relative stability of these two phases are related to the pH and Eh conditions of the deposit (see Figure 5 of Dimanche and Bartholomé, 1976). Hematite is less stable than ilmenite under reducing and acidic conditions, but becomes more stable than ilmenite as the Eh increases for constant pH. The two styles of alteration thus probably occur under quite different physical conditions.

6.5.3 Discussion: a multistage model of ilmenite alteration

Hugo and Cornell (1991) proposed that the above observations are best explained by a model in which some of the alteration occurred prior to deposition of the ilmenite in the Holocene sediments, and while reworking of these sediments has blended the *in situ* alteration products.

Table 6.7 Relative proportions of ilmenite and its alteration assemblages from selected beaches, rivers and older heavy mineral-bearing formations (after Hugo and Cornell, 1991).

Assemblage	HZ3	HZ32	HN17	HT3	HEC5	Berea Formation	Port Durnford Formation	Mfolozi River	Mhlatuze River	Tugela River
ilmenite	59	69	76	89	78	70	11	86	89	92
ilmenite-hydrated ilmenite	29	13	12	5	9	21	74	9	7	3
ilm-hyd ilm-leucoxene	2	3	6	3	2	3	4	tr	2	1
ilmenite-leucoxene	2	3	13	1	2	22	1	2	2	2
ilmenite-TiO_2 pseudomorph[1]	1	tr	tr	tr	1	tr	-	1	tr	1
leucoxene	8	13	3	3	8	3	11	2	tr	2

[1] formed by type III alteration - see text for details; abbreviations: ilm. = ilmenite, hyd ilm = hydrated ilmenite; Sample localities: HZ3 - Port Durnford, beach ; HZ32 - Richards Bay, beach; HN17 - Mzumbe River Mouth, beach; HT3 - Port St Johns, beach; HEC5 - Kidd's Beach.

Plate 6.10 Variations in the alteration of ilmeno-hematite or hemo-ilmenite grains.

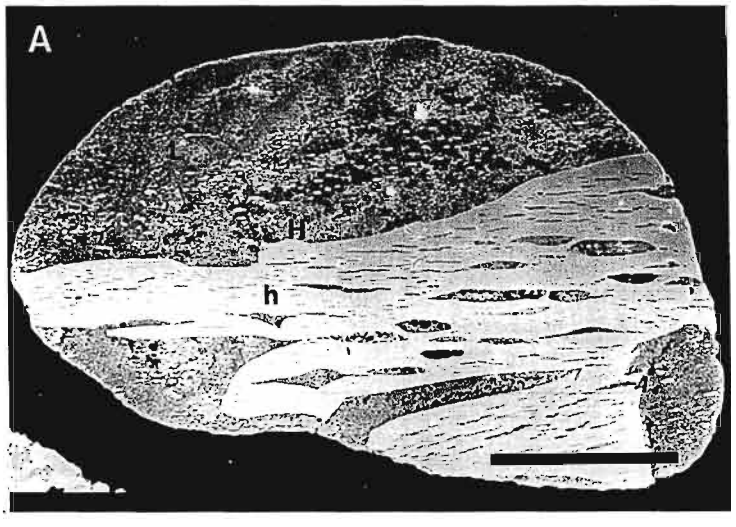

A. Ilmenite exsolution lamellae in the grain have altered to hydrated ilmenite (H) and leucoxene (L) while the hematite (h) remains unaltered. Back-scattered electron image. Richards Bay (HZ 36). Scale bar 50 μm.

B. Secondary electron image of the surface of a hemo-ilmenite grain displaying lenticular voids formed by the leaching of exsolved hematite from the grain. Richards Bay (HZ 36). Scale bar 20μm.

There is clear evidence that some ilmenite has been altered in source areas supplying material to the coastal sediments. Grains containing ilmenite and microcrystalline rutile (type III alteration) indicate that in some instances the alteration of ilmenite began in the igneous or metamorphic source rocks by oxidation and hydrothermal alteration. As mentioned, the sandstones of the Natal Group and the Vryheid Formation are significant intermediate sources of heavy minerals. Behr (1986) has described the alteration of ilmenites in the Vryheid sandstones (see Table 7.1, page 173). Pervasive alteration of ilmenite is found in the sediments of the Port Durnford Formation which underlies the Holocene dunes in many places (Table 6.7).

Ferruginous soils and lateritic soils have developed in the provenance areas of the dune deposits since the Late Pleistocene. As shown by Anand and Gilkes (1984) these soils are conducive to the pedogenic alteration of ilmenite. Fitzpatrick (1978), in his study of soil types along the eastern seaboard of South Africa, noted that ilmenite commonly altered to pseudorutile, anatase or rutile in the freely drained soils in the Mistbelt and Highland Montane regions. Differences in the duration, and other burial conditions, would enhance the variation of the degree of alteration of individual grains eroded from this environment, as suggested by Austin (1960). Furthermore, small quantities of partially altered ilmenite and leucoxene grains are observed in river sediments from Natal and Zululand (Table 6.7).

It is noted in Chapter 8 that there is little difference between the proportions of ilmenite alteration products in beach and dune sediments in the study area (see enclosed map). As the dunes are generally derived from the beach sands (Tinley, 1985; Johnson, 1986), this indicates that the ilmenites were altered prior to deposition in the aeolian environment.

From the above evidence it is concluded that small, but significant quantities of already altered ilmenite grains were deposited in the coastal sediments. Johnson (1986) suggested that the dunes were derived from beach placer deposits, which were exposed during the last glacial maxima. If the beach sands resided under similar conditions to those found in other parts of the world (that is, below the water table, in mildly reducing and acidic conditions), then it is likely that unaltered ilmenite began altering according to [6.2].

Reworking of the beaches to form the dune deposits, which occur above the water table (see Figure 3.3, page 47) would have changed the dominant mechanism of alteration so that further alteration proceeded via the development of leucoxene according to reactions [6.3] and [6.4]. This accounts for the instability of pseudorutile in the dunes and its replacement by leucoxene. Reworking of the Late Pleistocene - Holocene dunes, as indicated by the remnants of the older dune systems, would result in the homogenization of the ilmenite alteration products. Transportation and subsequent reworking of the grains also caused abrasion and fracturing of the altered ilmenite grains. It might explain the truncation by grain surfaces of leucoxene boundaries with ilmenite or pseudorutile.

6.6 THE EFFECT OF ALTERATION ON ILMENITE QUALITY

It has been shown (Temple, 1966; Wort and Jones, 1980 and 1981; Frost *et al.*, 1986) that the magnetic susceptibility of ilmenite decreases with increasing alteration. Hugo (1988) estimated the magnetic behaviour of ilmenite and altered ilmenite in the Richards Bay deposits by determining their mass proportions in different magnetic fractions from a heavy mineral concentrate. These results are reproduced schematically in Figure 6.8, and show the following:

1. Altered ilmenite grains are slightly less magnetic than unaltered ilmenite grains, but most of these grains will behave as ilmenite during magnetic separation.
2. Highly altered ilmenite grains (cf. type I and type II alteration) or TiO_2 pseudomorphs (cf. type III alteration) have a large range of magnetic susceptibility and may report to ilmenite concentrates or magnetic middlings fractions.
3. Leucoxene grains also have a large range of magnetic suseptibility extending from that of ilmenite to that of non-magnetic rutile, and most leucoxene will report to magnetic middlings or rutile concentrate.

It is clear from the results of Hugo (1988) that the degree and type of alteration will affect the recoverability of altered ilmenite grains.

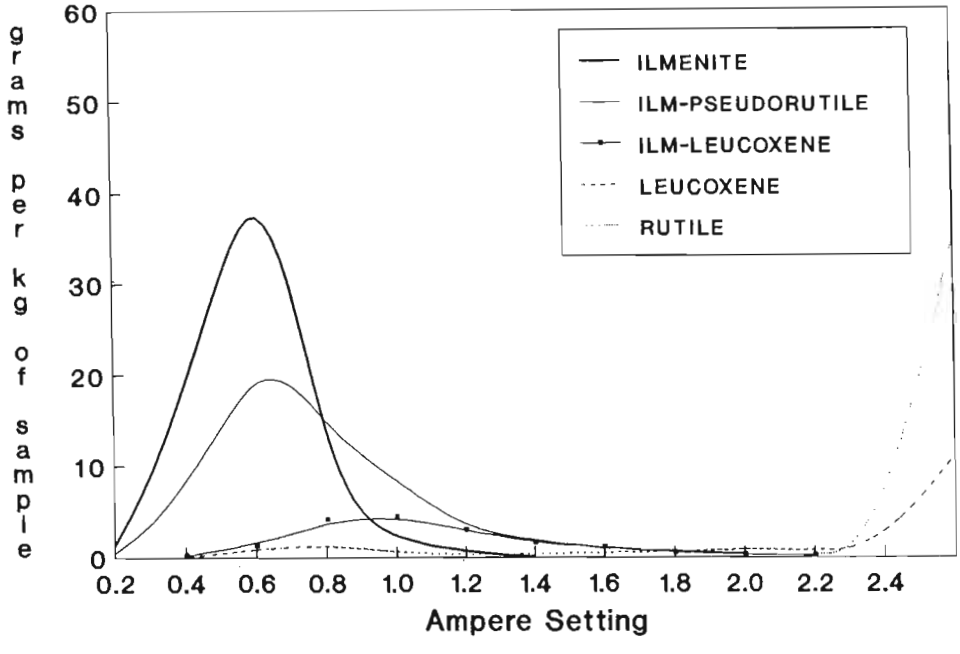

Figure 6.8 Schematic plot of mass proportions (in grams per kg of sample) of ilmenite and altered ilmenite grains in different magnetic fractions of a heavy mineral concentrate, Richards Bay (After Hugo, 1988). The ilmenite mass has been divided by five. (From Hugo and Cornell, 1991).

Frost *et al.* (1983) and Frost *et al.* (1986) have shown that there is a marked increase in the SiO_2 and Al_2O_3 contents of ilmenite alteration phases containing more than 60 percent TiO_2 in Western Australian deposits. The increase in these impurities has been ascribed to their co-precipitation with, or adsorption on to, alteration products (Frost *et al.*, 1983), or to the formation of clay minerals within pore spaces between alteration phases (Anand and Gilkes, 1985). Microprobe analysis of altered ilmenite grains from the Zululand deposits show the same SiO_2 and Al_2O_3 enrichment trends described by Frost *et al.* (1983), but with levels as high as 10 percent (Figures 6.9A and 9B) in contrast to the maxima of 1 and 3 percent respectively, reported by Frost *et al.* (1983). These results indicate that altered ilmenite grains containing leucoxene will contribute to the silica and aluminium impurity levels in ilmenite concentrates. Of greater importance is the large contribution made by leucoxene grains to the levels of these elements in rutile concentrates. In addition, leucoxene may contain up to 20 percent iron (Figure 6.9C) which is another undesirable element in rutile concentrates. It is therefore evident that altered ilmenite grains containing leucoxene, and leucoxene grains themselves, are undesirable as they are either non-recoverable or they contribute to impurity levels in concentrates.

Most of the ilmenite found in the Holocene dune deposits along the Zululand coastline is unaltered or only slightly altered. However, the deposits contain a varied and petrographically complex suite of altered ilmenite grains. These have formed as a result of three different types of ilmenite alteration mechanisms which occur in distinctly different physical environments, yet all samples studied contain grains reflecting all three alteration mechanisms. This, together with other petrographic and mineralogical evidence, indicates clearly that some ilmenite alteration occurred prior to deposition in the Holocene dunes and that reworking of the dunes has blended the alteration products. This has important implications for the mining and recovery of ilmenite from these dunes as it indicates that the distribution of altered ilmenite grains should be fairly constant throughout the dunes and should therefore not affect the quality and grade consistency of the material mined.

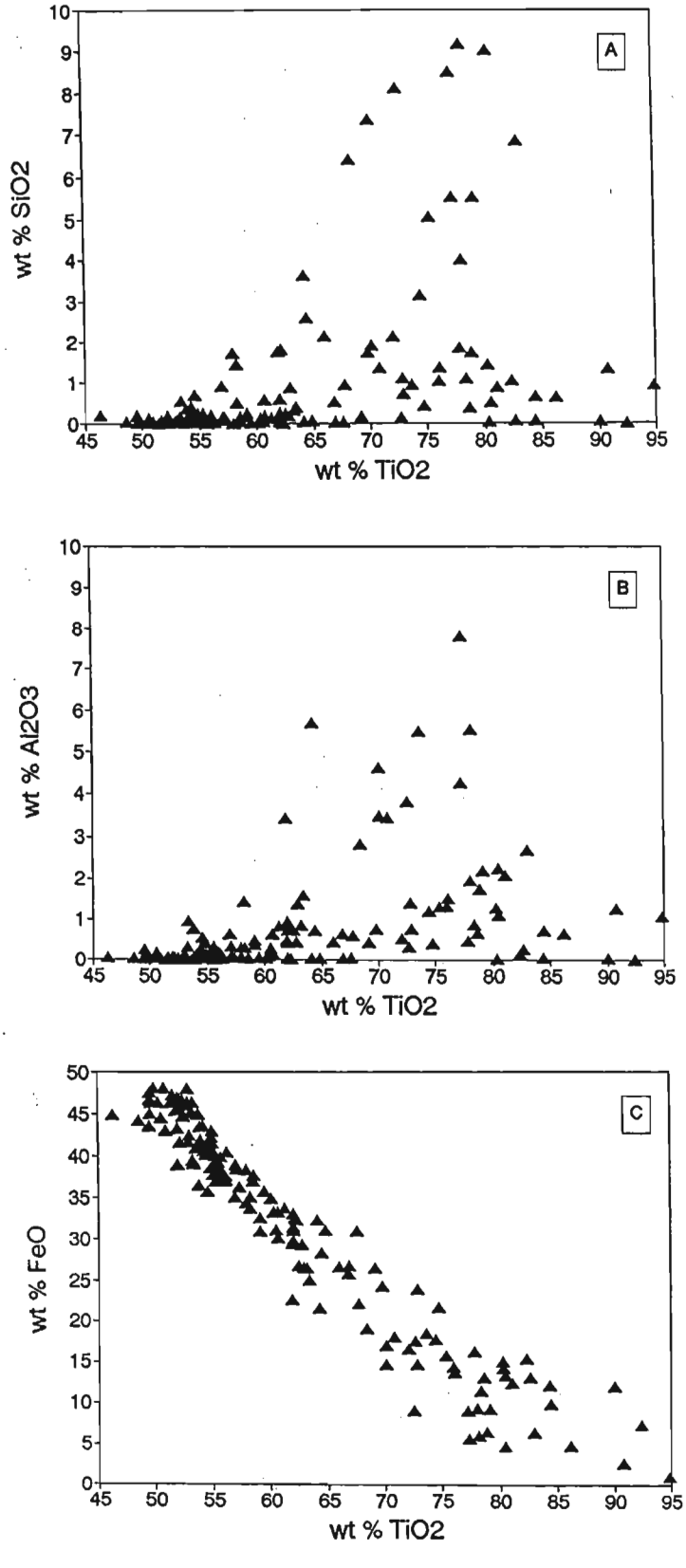

Figure 6.9 Variations in SiO_2, Al_2O_3 and FeO contents with degree of alteration (expressed as TiO_2 percent) in altered ilmenite grains. **A.** SiO_2 weight percent **B.** Al_2O_3 weight percent. **C.** FeO weight percent. (From Hugo and Cornell, 1991).

CHAPTER SEVEN

PROVENANCE OF THE IRON-TITANIUM OXIDES

7.1 INTRODUCTION

Provenance is of primary importance to the interpretation of iron-titanium variations in coastal sediments because it determines the initial distribution of heavy minerals along the coastline. Furthermore, provenance may have subtle influences on the mineralogy of heavy mineral deposits, such as the chemical composition of economic minerals or the textural relationships of composite grains, as described in Chapter 5. This influences the mineral concentrates produced and the mineral processing techniques used.

Hammerbeck (1976) noted that no consensus had been reached about the provenance of the heavy minerals along the eastern coast of South Africa. Fockema (1986) suggested that most of the ilmenite was derived from the basalt and dolerite of the Karoo Igneous Province, while rutile and zircon originate from the basement rocks of the Natal Metamorphic Province. The Kaapvaal Craton forms part of the basement in the north of the provenance area and these Archean rocks are also a source of the iron-titanium oxides. The aim of this chapter is to determine if ilmenite and magnetite from these major provenance areas can be distinguished using their chemical and petrographic criteria.

7.2 Fe-Ti OXIDES AS PROVENANCE INDICATORS - PREVIOUS WORK

The potential of the iron-titanium oxides in provenance studies lies in variations in mineral chemistry and petrographic textures related to source rock paragenesis, as described in Chapter 5. Many iron-titanium oxides occur as intergrown grains in sediments and according to Basu and Molinaroli (1989), these features are considered equal to evidence from rock fragments as fingerprints of their source rocks. In addition, the minerals are relatively durable, easily concentrated, suitable for microscopic examination and are found

in most sands (Pettijohn *et al.*, 1987). As a result, these oxides have been used in a number of provenance studies in recent years.

Ilmenite was first used as a provenance indicator by Darby (1984), who determined the provenance of different sediments in Virginia and Carolina, U.S.A. from the trace element content of the ilmenite. Ilmenite was used as an indicator mineral as it was the most abundant heavy mineral in the sediments, was easy to separate from other minerals and contained a variety of trace elements depending on the paragenesis of the ilmenite. Furthermore, chemical analysis of only one heavy mineral species eliminated factors such as hydraulic sorting and selective weathering, which are inherent problems in provenance interpretation based on heavy mineral suites (Darby and Tsang, 1987).

Darby (1984), and Darby and Tsang (1987) used atomic absorption spectroscopy to determine the Ti, Fe, Mn, Mg, V, Zn, Cr, Cu and Ni contents of ilmenite concentrates from rivers and estuaries to show that ilmenite could be used as a provenance indicator. Although the method provided useful results, its fundamental weakness is that the concentrates are never pure and some of the trace element variation is caused by impurities of other minerals rather than source rock differences. This is particularly so when the concentrates contain large proportions of minerals intergrown with ilmenite.

Basu and Molinaroli (1989, 1991), in a more integrated approach, studied the provenance characteristics of iron-titanium oxides using both the petrographic and chemical variations of ilmenite and magnetite. In their petrographic analysis, they grouped all the major oxide minerals together as "detrital Fe-Ti oxides" (or "DOPQ") and claimed that the most diagnostic features are the presence of exsolution lamellae, minimum lamellae widths and "the number of crystallographic orientation (sic) of the lamellae". The chemical composition of the oxides was determined by electron microprobe analysis for TiO_2, Al_2O_3, Cr_2O_3, Fe (as FeO), MnO, and MgO. Discriminant function analysis, on combined petrographic and chemical data, was used to distinguish oxides from different source rocks.

There are several problems with the method of Basu and Molinaroli (1989). Firstly, they did not distinguish between the different types of iron-titanium oxides, or the intergrowths formed between these minerals. Their rationale was that "almost all intergrowth textures of Fe-Ti oxide minerals (FTM), be they true exsolution or oxidation "exsolution", are products of sub-solidus reactions". This is not strictly true, as certain intergrowths, such as sandwich lamellae of ilmenite in titaniferous magnetites, may have formed by co-precipitation of ilmenite and titanomagnetite (Haggerty, 1976a; Reynolds, 1983). Of greater importance is their interpretation that hematite lamellae within magnetite grains are formed by exsolution (see Basu and Molinaroli, 1989; Figure 3A). This is incorrect as such lamellae are formed by oxidation (martitisation). Furthermore, this oxidation often occurs in the sedimentary environment and may affect magnetite from any rock. It is therefore not characteristic of the source rock.

Another problem with the method of Basu and Molinaroli (1989) is that they used the number of directions of lamellae as a provenance criteria. This is a function of the mineral's crystal structure and not its source. Lamellae in magnetite are usually orientated along the (111) planes, resulting in three intersecting directions of lamellae in section, whereas lamellae in the ilmenite-hematite series are orientated along the (0001) or basal plane and so only one direction of lamellae is observed in section. The reason for Basu and Molinaroli (1989) using this as a criteria for source rocks, instead of variations in ilmenite, hematite and magnetite intergrowths, is unclear.

Recently Grigsby (1989, 1990) studied the use of detrital magnetite as a provenance indicator, using both the petrographic and chemical variations of this mineral. He was able to distinguish magnetites from a wide range of rock-types by integrating the petrographic and chemical data.

The provenance of rutile has been studied by Force (1980), who determined that nearly all rutiles found in coastal sediments are derived from metamorphic rocks. The mineral is most commonly found in pelitic rocks and metabasites (Frost, 1991a). Rutile, in equilibrium with magnetite, is the stable titanium mineral in low grade rocks. The mineral

is found over the whole range of metamorphic temperatures (Frost, 1991a) and is common in a wide variety of granulite and eclogite facies rocks (Force, 1991).

Deer *et al.* (1962) noted that rutile may be widely distributed as minute grains in a variety of igneous rocks. The occurrence of large crystals is restricted to granite pegmatites and quartz veins (Elsdon, 1975). The occurrence of discrete rutile grains in basic igneous rocks is not noted in any major texts on the subject (Haggerty, 1976a; Reynolds, 1978b; Elsdon, 1975), and such grains were not found in samples of these rocks in this study. It is therefore assumed that the rutile in coastal sediments of the study area is derived solely from either the Kaapvaal Craton or the Natal Metamorphic Province.

7.3 METHOD OF STUDY

In this study both the chemical and petrographic characteristics of ilmenite and magnetite are used to study the provenance of the iron-titanium oxides. An inherent weakness in using petrographic features as provenance indicators is that the iron-titanium oxides have different durabilities in the sedimentary environment. Ilmenite is generally more stable than magnetite (Dryden and Dryden, 1946; Pettijohn, 1957; Darby, 1984), which, in turn, is more durable than intergrown oxide grains. Riezebos (1979) and Molinaroli and Basu (1987) found that intergrown grains of ilmenite-hematite survived weathering and transport in rivers better than martite and magnetite-ilmenite grains. This indicates that the proportions of iron-titanium oxides and their intergrowths in coastal sediments will be different from their proportions in source rocks. This difference is expected to increase with age and reworking of the sediment. This has been shown by Arran *et al.* (1992) who found that ilmeno-magnetite grains suffer mechanical breakdown during fluvial transport, resulting in an enrichment of homogeneous grains in river sediments compared to source rocks.

Considering the above, it is best not to group the iron-titanium oxides together (*cf.* Molinaroli and Basu, 1987), and in this work separate discussions of the ilmenite and

magnetite provenances are given. As these minerals are considered to be common to both the major source areas, the consistency of results can be used as a test of their reliability.

Electron microprobe analysis was used to determine the chemical compositions of ilmenite and magnetite. The analyses are rapid and many grains may be analysed, allowing for the creation of a large data base. Approximately 1 μm sized spots in single grains are analysed, so there are no uncertainties related to mineral impurities, or mixing of minerals from different sources, which are problems in methods using bulk analysis. Variations of mineral compositions within individual rock-types and the chemistry of intergrowths within composite grains may also be determined. A disadvantage of the method is that trace elements such as Cu, Zn, and Ni, are difficult to analyse as their concentrations are close to the detection limit of the instrument, while in the case of vandanium there is a large overlap between the VKα and TiKβ lines. However, the studies of Basu and Molinaroli (1989) and Grigsby (1990) have shown that there is enough variation amongst the other elements to distinguish iron-oxide minerals from different source rocks.

The method used to study the provenance of the iron-titanium oxides is outlined as follows:

1. The probable major primary source rocks of the oxides were identified and classified. It was assumed that the iron-titanium oxides are largely derived from source rocks exposed in the present catchment areas. Considering the geological history of the region, as described in Chapter 2, this is a valid assumption.
2. Samples of probable major source rocks were collected along with samples from streams which exclusively drain these rocks. In some cases samples were obtained from colleagues in the Department of Geology and Applied Geology, University of Natal.
3. Polished thin-sections of the rock samples were used to determine the petrography and chemistry of the oxides. Concentrates were made from the fluvial samples by heavy liquid separation (see Chapter 4) and polished thin-sections were made from these concentrates.

4. Discrimination diagrams were used to determine differences in the chemical composition and petrographic features of ilmenite and magnetite from different source rocks. Data from the literature, particularly from Reynolds (1983 and 1986d) were used to compliment the data base generated from this study.
5. Ilmenite and magnetite grains from coastal sediments were then used to test the discrimination diagrams and to determine which source rocks are the major contributors of these minerals.

7.4 SOURCE ROCKS OF IRON-TITANIUM OXIDES IN THE STUDY AREA

The Natal Metamorphic Province and the Karoo Igneous Province (Map 1) are considered to be the two major primary sources of the heavy minerals in the study area (Hammerbeck, 1976; Fockema, 1986; Hugo, 1990). The granite-greenstone terrane of the Kaapvaal Craton crops out within the east coast catchment area and these rocks could also contribute to the iron-titanium oxides in coastal sediments. The Kaapvaal Craton and the Natal Metamorphic Province are grouped together under the term "Natal Basement rocks" because of the similarity of their lithology. Ilmenite and magnetite are common accessory minerals in a wide range of rocks within these provinces. It is therefore important to identify the major source rocks and group these according to their geological association and the similarity of their ilmenite and magnetite mineralogy. The three provinces mentioned above are described in the following section and the major source rocks of iron-titanium oxides within these provinces are identified.

The sandstones of the Vryheid Formation in the Karoo Sequence and the quartzite of the Natal Group are known to contain concentrations of heavy minerals (Hammerbeck, 1976; Behr, 1986). These rocks are considered to be intermediate sources of the heavy minerals in the coastal sediments (Fockema, 1986; Hugo and Cornell, 1991), but are not considered as important provenances of pristine ilmenite and magnetite as it is known that the minerals have undergone alteration in these rocks (Behr, 1986). This is shown by the modal proportions of the heavy mineral suites in some samples of these rocks (Table 7.1).

Table 7.1 Modal proportions of heavy mineral suites from the Natal Group and Vryheid Formation sandstones.

Minerals	Natal Group Sandstones			Vryheid Formation Sandstones			
	Marian-hill	Botha's Hill	Monte-seel	Botha-ville	Botha-ville[1]	Delmas[1]	Carolina[1]
altered ilmenite	3	8	15	55	59.7	56.5	25.1
leucoxene	5	5	2	12	11.4	6.5	22.0
anatase/rutile	11	7	4	4	1.4	tr	2.1
zircon	2	4	1	5	6.8	0.1	1.3
garnet	1	-	-	1	1.7	0.1	16.4
monazite	-	-	-	1	1.0	-	tr
hematite	2	64	70	12	11.4	13.8	17.8
other minerals	6	12	8	10	6.6	23.2	15.4

[1] Average analyses from Behr (1986). tr = trace amounts present; - = not detected

7.4.1 Natal Basement Rocks

7.4.1.1 Kaapvaal Craton

The oldest possible source rocks (*circa* 3000 Ma; Linström, 1987) are the granite gneisses, metabasites and small metamorphosed ultramafic intrusions of the Kaapvaal Craton (see Figure 7.1). The granitoids form the bulk of this Archean basement crop out in the valleys of the Tugela and Buffalo Rivers.

Little information about the iron-titanium oxides is available, but it is assumed that the rocks noted above are sources of iron-titanium oxides as similar rocks, found elsewhere, contain these minerals. Magnetite has been noted in metamorphosed ultramafic intrusions; granoblastites from the Lubana Formation (Empangeni Metamorphic Suite); banded iron formations of the Mozaan Group; and the Post-Pongola Sequence, syenite intrusions. Titaniferous magnetite (Mt-Ilm_{oe}) is found in the ultrabasic intrusions of Usushwana Complex (Reynolds, 1986a) and Hlagothi Suite (Groenewald, 1984). Chromite is also a common minor mineral in these ultrabasic rocks (Groenewald, 1984).

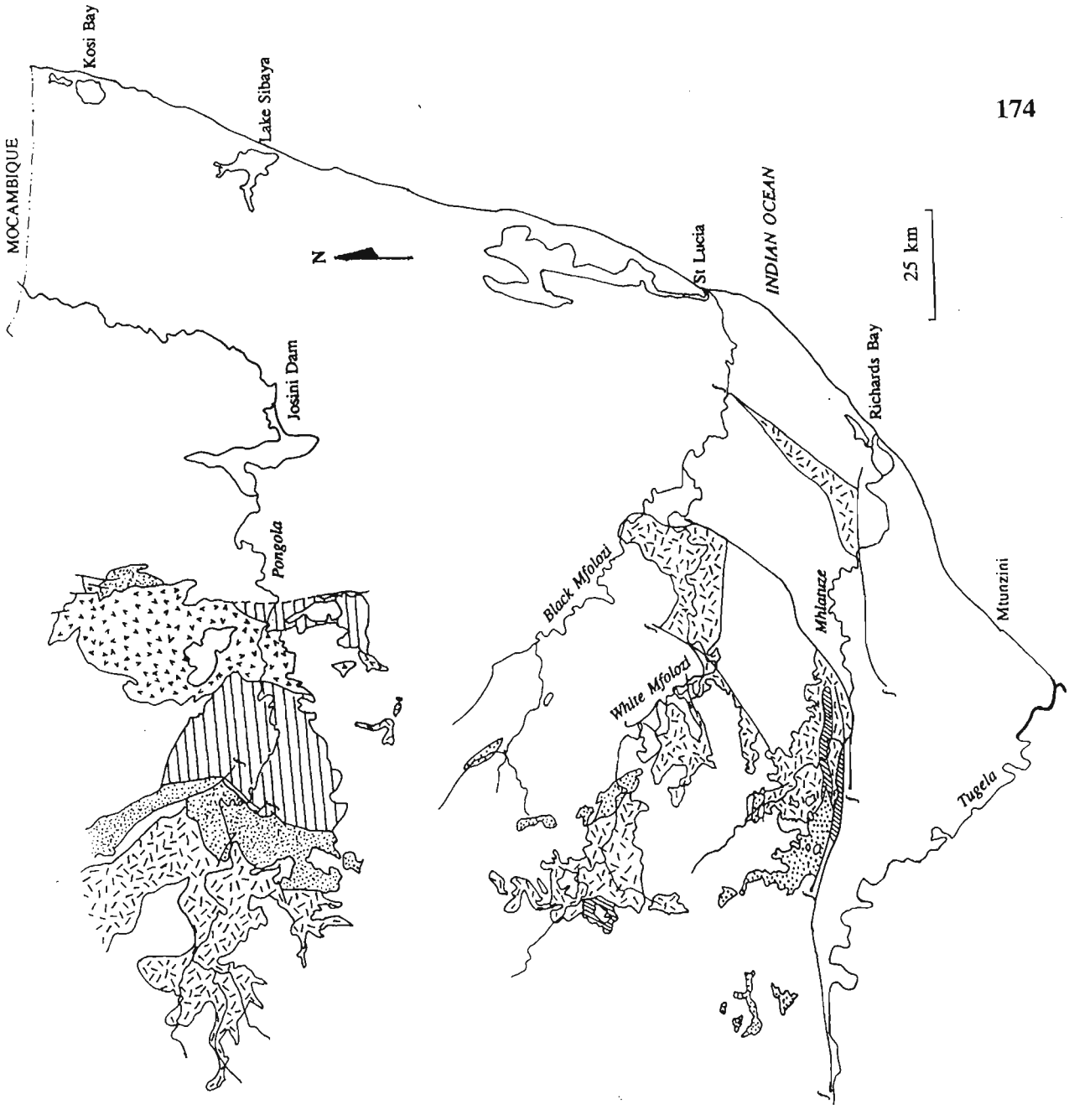

LEGEND

	UNIT	DESCRIPTION
		Younger, cover rocks
		Intrusive granite
	Mozaan Group	Shale, iron formation, quartzite
	Nsuze group	Quartzite with minor other rock types
		Granite and granite gneiss
		Basic lava altered to schists, quartzite, cherts, iron formations

Figure 7.1 Simplified geological Map of the Kaapvaal Craton rocks found within the catchment area of the study area. Map drafted from 1:1000000 geological map of South Africa (South African Geological Survey, 1970).

7.4.1.2 Natal Metamorphic Province

The Proterozoic Natal Metamorphic Province is composed of low to high-grade supracrustal gneisses and granitoids. The rocks are almost continuously exposed as erosional inliers for about 300 km and cover an area of some 10000 km^2 (Thomas *et al.*, 1990). These exposures are subparallel to the coast and crop out from northern Transkei to Empangeni in the north (Figure 7.2). The metamorphic grade increases from greenschist in the north to granulite facies in the south.

The province has historically been subdivided into two major terranes, but this has recently been increased to three terranes by Thomas (1989), based on lithological, structural and tectonic features (Table 7.2). The major rock types in the Natal Metamorphic Province are amphibolites, supracrustal schists and gneisses, and pre- to post-tectonic granitoids.

Table 7.2 Subdivision of the Natal Metamorphic Province, after Thomas (1989) and Thomas *et al.* (1990).

Terrane	Group	Description
Tugela	Ntingwe Group	Greenschist facies shallow-water shelf sediments
	Mfongosi Group	Greenschist facies metabasite and metashale
	Tugela Group	Mainly amphibolite with minor felsic schist
	Intrusive rocks	Mafic/ultramafic complexes, and minor granite
Mzumbe	Mapumulo Group	Upper amphibolite grade pelitic to quartz-feldspar gneiss and migmatite
	Intrusive rocks	Pre-to syntectonic I and S-type granitoid gneiss, rare metabasite. Late to post-tectonic rapakivi granite-charnockite plutons, and K-rich granite plutons
Margate	Mzimkulu Group	Granulite-grade supracrustal gneiss, marble, calc-silicate
	Intrusive rocks (Oribi Gorge Granitoid Suite)	Pre- and syntectonic granitoid gneiss and charnockite, rare metabasite. Late to post-tectonic rapakivi granite-charnockite plutons.

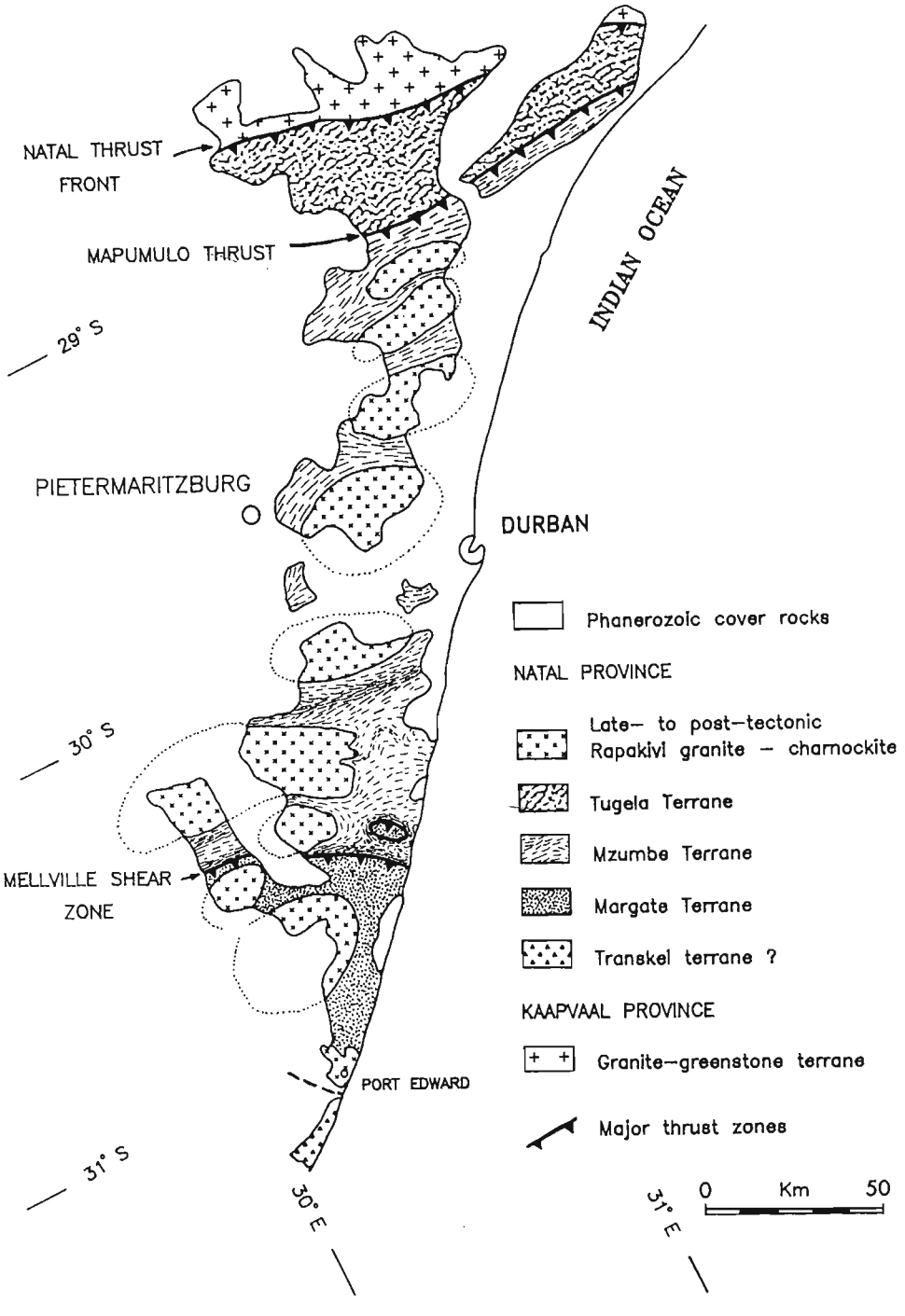

Figure 7.2 The outcrop pattern and major tectnostratigraphic subdivisions of the Natal Metamorphic Province (from Thomas, 1989).

Very little information is found in the literature about the iron-titanium oxides in the Natal Metamorphic Province. Most researchers have not done reflected-light microscopy and group all the opaque minerals together, often under the incorrect term "ore minerals". This makes it difficult to identify possible source rocks of ilmenite and magnetite from this province. Scarce modal analyses, giving proportions of opaque phases, such as those by Scogings (1989) and Du Toit (1979), indicate that all the major rock types contain opaque minerals as accessory phases. This is in accordance with Frost (1991a) who noted that magnetite and ilmenite are the most common iron-titanium oxides in metamorphic rocks and that these minerals can coexist over the range of oxygen fugacities commonly found in metamorphic rocks. Ilmenite is most common in metapelite and metabasite rocks, but is absent in the lowest grade rocks, where rutile or titanite are the stable TiO_2-bearing phases (Frost, 1991a). Magnetite is found in a wide variety of metamorphic rock types, including metaperidotite, metabasite, iron-formations, quartzo-feldspathic gneiss and some metapelites (Frost, 1991a). The following classification was therefore selected for the study:

1. Mafic metamorphic rocks, which consist mainly of mafic schist and gneiss, but include metabasite.
2. Felsic metamorphic rocks, mainly granitoids, but including felsic schist and gneiss, and magnetite-bearing quartzite.
3. Rocks from metamorphosed ultrabasic/basic complexes.

7.4.1.3 Mafic Metamorphic rocks

Mafic schist and gneiss are most common in the central Mzumbe Terrane, where they occur as amphibolite-grade, biotite-garnet and biotite-hornblende gneisses of the supracrustal Mapumulo Group. Metabasite is most commonly found in the Tugela Group of the Tugela Terrane and part of the Mfongosi Group.

Ilmenite and magnetite in these rocks occur as small, homogeneous crystals (usually less than 100 μm), normally occupying less than 1 per cent of the rock. Intergrowth textures between ilmenite and magnetite are seldom observed. Du Toit (1979) noted that the

ilmenite grains are commonly rimmed by titanite in amphibolites which display evidence of retrogression. The oxides are commonly subhedral to anhedral, and are associated with ferromagnesian minerals such as biotite and pyroxene. Magnetite grains commonly have polygonal cross-sections. Often the oxides in these rocks are exclusively either ilmenite or magnetite, depending on the TiO_2 content and fO_2 of the rock.

7.4.1.4 Felsic Metamorphic Rocks

Pre-tectonic granitoid-gneisses and late to post-tectonic granitoids are found as partly exposed, ellipsoidal batholiths in the Mzumbe and Margate Terranes. The litho-stratigraphy of the granitoids is outlined by Thomas (1989). Felsic schists and gneisses are common in the Mapumulo Group of the Mzumbe Terrane), but may be found through-out the Natal Metamorphic Province. Quartzite and quartzitic gneiss are also found within the Mapumulo Group and may be associated with amphibolite in the Tugela Terrane.

Both S- and I-type granite are found in the Natal Metamorphic Province, and so the granitoids may contain ilmenite or magnetite (Thomas, 1989). These minerals usually occur as anhedral grains associated with mafic minerals such as biotite and amphibole. The grains vary in size from less than 100 μm to over 300 μm. The content of the oxides in granitoids may be as high as 10 per cent (Scogings, 1989), but is usually only 1 to 3 per cent. The magnetite grains are usually homogeneous and have polygonal cross-sections. Intergrowths between magnetite and ilmenite are uncommon but composite or granular textures are observed. Ilmenite grains are commonly homogenous, but in some granites may contain extensive hematite exsolution (see Plate 5.3A, page 96). Hematite grains containing exsolved ilmenite (see Plate 5.3B), or oxyexsolution of rutile (see Plates 5.3D and 5.3E) are less common. High temperature oxidation of ilmenite to assemblages of $Ilm_{ss}+Hem_{ox}+Rut_{ox}$ or $Hem_{ss}+Rut_{ox}\pm Psb_{ox}$ (see Plates 5.4 and 5.5, pages 97 and 98) are almost exclusively found in the granitoids. Homogeneous magnetite is the dominant iron-titanium oxide in quartzite and quartzitic gneiss.

7.4.1.5 Ultrabasic and basic complexes

Several metamorphosed ultrabasic and basic complexes are found within the Tugela Terrane. Although not geologically extensive, these complexes locally contain high concentrations and are important sources of iron-titanium oxides. In addition, the rocks are an important source of chromite, which decreases the quality of ilmenite concentrates, as discussed in Chapter 8. The complexes consist of basic and ultrabasic rock types, ranging from gabbro to pyroxenite and serpentinite (Linström, 1987). The two largest intrusions are the Mambula and the Tugela Rand Complexes.

Titaniferous magnetite and chromite are found in the rocks of the Sithilo, Sebenzani, Mambula and Tugela Rand Complexes (Thomas, *et al.*, 1990). At least six vanadiferous-titaniferous magnetite layers, containing V-Ti-magnetite, granular ilmenite, and pleonaste, are found in the Mambula Complex. These layers range in thickness from one to five metres (Reynolds, 1986d).

Reynolds (1979, 1984, and 1986d) has studied the petrography of the V-Ti-bearing ores of the Mambula Complex. The titaniferous magnetite is characterised by a wide variety of ilmenite and pleonaste intergrowths, formed by sub-solidus reactions during amphibolite-grade metamorphism (Reynolds, 1986d). Coarse pleonaste exsolution lamellae in the magnetites are abundant and orientated parallel to (100), whereas the ilmenite lamellae are less common and orientated parallel to (111). Very fine ilmenite granules, formed by the oxidation of ulvöspinel, are also found in some of the magnetites (Reynolds, 1986d). These textures are similar to those shown in Plate 5.9 (page 113).

Chromite is common in the complexes and low-alumina chromite has been mined from podiform chromitite bodies in the Sithilo Complex (Wuth and Archer, 1986).

7.4.2 Karoo Igneous Province

The Karoo Igneous Province is an extensive suite of extrusive and intrusive rocks which are found over a wide area of the southern African subcontinent. Current outcrops cover an area of 140 000 km^2 (Figure 7.3), although Cox (1970) estimated that the lava, and associated dolerite, originally covered an area of 2 000 000 km^2 in southern Africa. The suite consists of basalt and dolerite, with minor rhyolite and gabbro, formed as a result of the fragmenting of Gondwanaland (Eales *et al.*, 1984). Igneous activity began in the late Triassic and continued into the early Cretaceous (Eales *et al.*, 1984), although the majority of the igneous rocks date from the early Jurassic (192 - 171 Ma). The relevant rock-types of this province, together with their iron-titanium mineralogy, are described below.

7.4.2.1 The Stormberg basalts

Basaltic lavas are found in the highlands of Lesotho and the north-eastern Cape. In the Natal Drakensberg these tholeiitic lavas reach thickness of 1400 m. In addition to the Drakensberg lava, basaltic rocks of the Sabie River Basalt Formation are found in Zululand and Swaziland. These rocks are associated with the Lebombo Monocline, and are estimated to range from 3000 to 9000 m in thickness, although this is difficult to determine as the basalts are deeply weathered and poorly exposed (Eales *et al.*, 1984).

Iron-titanium oxides are ubiquitous accessory minerals in the basalt, and have previously been studied by Turner (1990), Arran *et al.* (1992), and Ramluckan (1992). They occur as small (< 150 μm), late-stage titanomagnetite and occasionally as high-Cr spinel. Most of the titanomagnetite has undergone oxyexsolution to form Mt-Ilm$_{oe}$ grains displaying trellis, and sandwich-type textures (Turner 1990). Primary ilmenite crystals are uncommon but acicular laths are found (Ramluckan, 1992). The Mt-Ilm$_{oe}$ grains have commonly undergone deuteric and hydrothermal alteration resulting in the replacement of magnetite by titanite and chlorite as described by Reynolds (1986c), Turner (1990) and Richards *et al.* (1991).

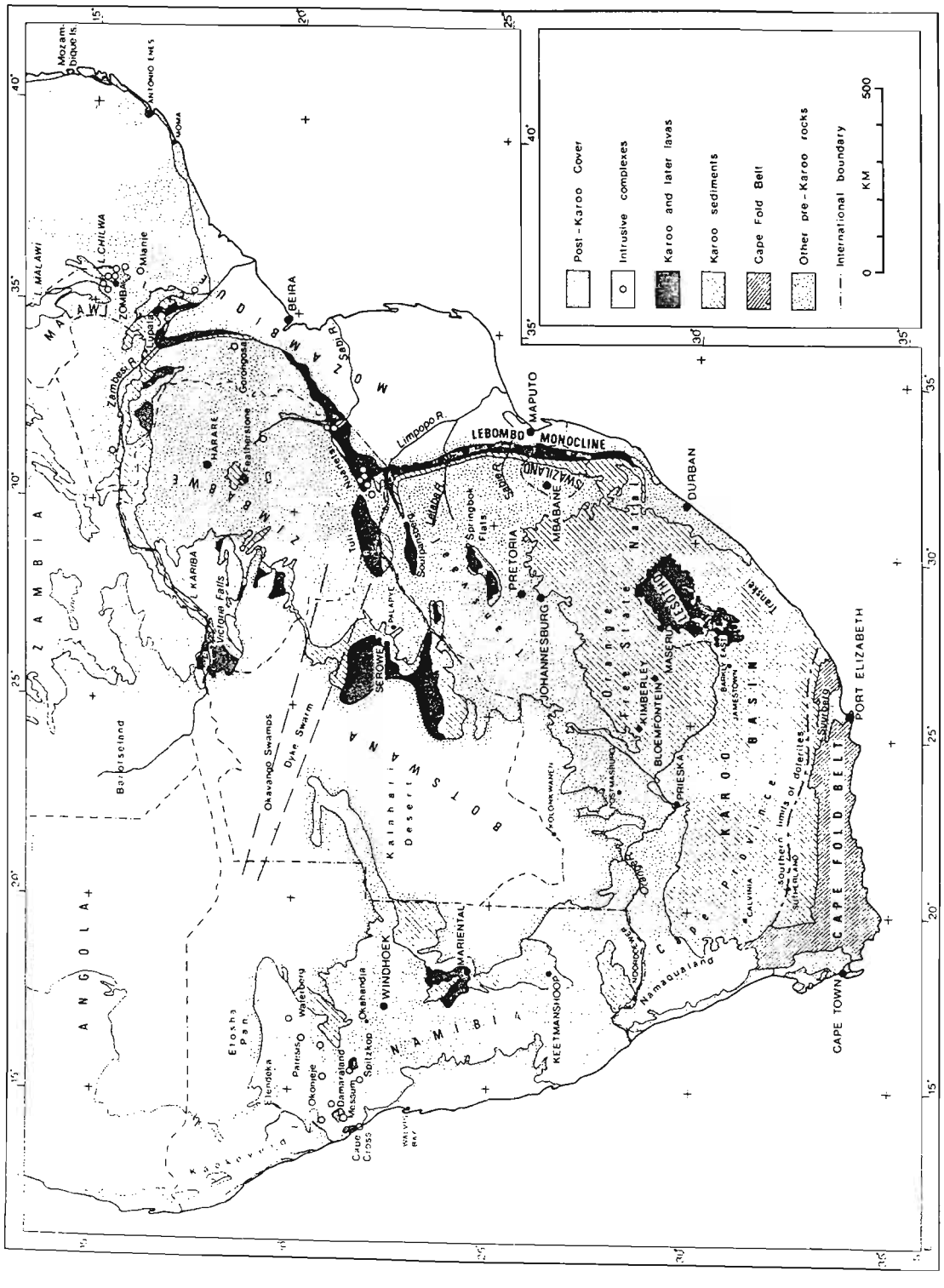

Figure 7.3 Simplified geological Map of southern Africa showing the distribution of Karoo Igneous rocks (from Eales *et al.*, 1984).

7.4.2.2 Dolerite intrusions

The Karoo dolerites have been well described by Walker and Poldervaart (1949). They consist of dykes, sills and bell-jar intrusions which acted as feeder channels to the overlying basalt (Eales *et al.*, 1984). The intrusions are abundant in the sedimentary strata of the Karoo Sequence and extend almost to the outcrop limits of the main Karoo basin (see Figure 7.3). In the central part of the basin the dolerite-sediment ratio may be higher than 0.5 (Winter and Venter, 1970). Few dolerite intrusions are noted in the basement rocks of the Natal Metamorphic Province. The chemical composition of the intrusions is similar to that of the tholeiitic lavas (Eales and Marsh, 1979) although anomalous types do exist (Le Roex and Reid, 1978).

Basic dykes are also found associated with the Lebombo Monocline. These dykes are best developed in the Rooi Rand dyke swarm, which has previously been described by Du Toit (1929), Bristow (1976), Armstrong (1978), Saggerson *et al.* (1983) and Armstrong *et al.* (1984). The swarm crops out for 200 km along the western flank of the Lebombo volcanic belt and consists almost entirely of subalkaline to tholeiitic dykes.

The iron-titanium oxides in Karoo dolerite have been described by Reynolds (1978b and 1983), Turner (1990) and Arran *et al.* (1992). These rocks contain between 0.5 and 4 per cent ilmenite and titanomagnetite, which form as late-stage phases (Reynolds, 1983). Ilmenite is the dominant opaque phase and is found as isolated crystals (generally > 100 μm) or lamellar and granular bodies within titaniferous magnetite grains. Titaniferous magnetite crystallises after ilmenite and usually forms anhedral, composite grains with subhedral ilmenite. These grains commonly contain trellis and sandwich lamellae of ilmenite, formed by oxyexsolution. Turner (1990) and Arran *et al.* (1992) noted that the sandwich and composite-type intergrowths are far more common than trellis lamellae in dolerites, while the latter is more common in Stormberg basalt.

Armstrong *et al.* (1984) noted that opaques phases constitute between 5 and 15 per cent of the Rooi Rand dykes. Titaniferous magnetite is the dominant oxide phase, although homogeneous ilmenite grains are present.

7.4.2.3 Gabbro and picrite

Intrusive sills in the Central Karoo Province may attain thicknesses of several hundred metres and are often internally differentiated by gravity settling or by flow concentration of phenocrysts (Eales *et al.* 1984). Differentiation in the Mount Ayliff intrusions, near Kokstad has resulted in a thick base of ultramafic and mafic cumulates, containing some sulphide mineralisation (Maske, 1966).

Ilmenite in the Mount Ayliff intrusions has been extensively studied by Cawthorn and Groves (1985), Groves *et al.* (1986), and Cawthorn *et al.* (1988) in an attempt to determine the origin of the magnesium-rich rocks found within the differentiated intrusions. Ilmenite in these rocks occurs as discrete, elongated grains, ranging in size from 0.1 to 1 mm in length (Groves *et al.*, 1986). The ilmenite grains are commonly embayed by silicates and sulphides. Cawthorn *et al.* (1988) estimated that ilmenite makes up about 1 per cent of the rock.

The petrography of spinel phases in gabbros, picrites and silicic differentiates of the Central Karoo Province has been studied by Eales *et al.* (1980). These authors noted that true chromites and magnetites are unknown in the tholeiitic rocks of the Central Karoo Province. The spinels constitute less than 2 per cent of the rocks, and range in size from 0.1 mm to 2 mm in size. Chromian-magnetite grains are euhedral to anhedral, depending on how early they crystallised from the magma. These grains often show zonation in the chill margins of intrusions where quenching has prevented homogenization (Eales *et al.*, 1980). The titaniferous magnetites display a variety of habits depending on the paragenesis of the host rock, but generally the grains are intergrown with ilmenite, forming trellis or sandwich lamellae.

7.4.2.4 Rhyolite and other igneous rocks

Rhyolites are exposed for more than 600 km along the Lebombo Monocline, from the Msunduzi River to just south of the Limpopo River in the north and reach a maximum thickness of 5000 m (Cleverly *et al.*, 1984). The rhyolites overlie Karoo basalt and mark the end of the main phase of Karoo volcanism.

Cleverly *et al.* (1984) found titaniferous magnetite to be a ubiquitous phenocryst phase, in addition to being present in the groundmass of the rhyolite. The grains tend to be anhedral, and vary in size from less than 0.1 to rare 2 mm large crystals. In contrast, ilmenite was only identified in one sample. These rocks are therefore an unlikely source of ilmenite.

Iron-titanium oxides have been identified in other rock-types, such as picritic basalts and nephelinites of the Karoo Igneous Province (Cawthorn *et al.*, 1989), but they occur well outside the catchment area of the study area.

7.5 ILMENITE COMPOSITION AS A PROVENANCE INDICATOR

7.5.1 Method

Ilmenite grains from selected rock types, described in Section 7.4, were analysed by electron microprobe, as outlined in Table 4.1 (page 63). Analyses of ilmenite in appropriate source rocks from the literature were also added to the data set. All analyses were recalculated by the method of Stormer (1983) to estimate the Fe_2O_3 and FeO in ilmenite. The full list of analyses used is given in Appendix C.1. Source rocks were grouped together according to their geological association and the similarity of their ilmenite compositions (Table 7.3). The oxides were plotted against each other to determine which oxides best distinguished ilmenites from different source rocks.

Table 7.3 Classification of source rocks for provenance study using ilmenite composition.

Major Division	Rock Group	Description
Karoo Igneous Province	Gabbro	Gabbro in basic differentiates, taken to represent all basic plutonic rocks from this province
	Picrite	Picrite in basic differentiates, taken to represent all ultrabasic plutonic rocks from this province
	Dolerite	Dolerites dykes and sills within Karoo sediments, and the Rooi Rand dyke swarm
	Basalt	Basalt from the Natal Drakensberg
	Granophyre	Granophyre from magmatic differentiates, taken to represent all felsic plutonic rocks in this province
Natal Basement	Granitoid (+Felsics)	Granitoid-gneiss, granite, and charnockite; quartz-feldspar gneiss
	Mafic metamorphic	pelitic and semi-pelitic schist, mafic gneiss and metabasite
	Basic/ultrabasic Complex	metamorphosed basic and ultrabasic rocks in intrusive complexes

7.5.2 Ilmenite compositions in source rocks

The compositions of ilmenites from the source rock groups (Table 7.3) are plotted in Figure 7.4, and described below.

Gabbro:

Analyses of ilmenite from gabbros were obtained from Cawthorn and Groves (1985) and Cawthorn *et al.* (1988). These represent ilmenites from basic plutonic rocks of the Karoo Igneous Province. Ilmenite compositions are variable, but are characterised by Mg substitution for Fe^{2+} in the ilmenite-geikielite solid-solution series (Figure 7.4E). This results in moderately high MgO and TiO_2 contents, intermediate between the picrite and dolerite/basalt fields. The gabbroic ilmenites may also have relatively high Cr_2O_3 levels, ranging between 0.1 and 0.5 per cent (Figure 7.4I).

Picrite:

Analyses of ilmenite from picrites from the Mount Ayliff intrusions were obtained from Cawthorn *et al.* (1988). These rocks were included in the list of source rocks because they may be an important source of ilmenite along the Transkei-southern Natal coastline. Furthermore, they characterise ilmenite from high-MgO basic rocks. The ilmenite compositions are characterised by high TiO_2, MgO, and Cr_2O_3 values, but low FeO contents, compared to other rocks from the Karoo Igneous Province (Figure 7.4). The high MgO content is a function of the high MgO content of the ultrabasic magma (Haggerty, 1976b). The strong negative correlation between MgO and FeO content (Figure 7.4E) reflects the substitution of $MgTiO_3$ for $FeTiO_3$ in the picrite ilmenites. The higher mole per cent of $MgTiO_3$ in the ilmenite accounts for the higher per cent TiO_2, as the atomic weight of Mg (24.305) is considerably less than Fe (55.847).

Dolerite and Basalt:

The dolerite and basalt are characterised by ilmenite with compositions close to the $FeTiO_3$ end-member. Consequently the ilmenite has high FeO contents, and low MgO and MnO levels (Figure 7.4E and 7.4G). There is a strong positive correlation between TiO_2 and FeO (Figure 7.4A), and a corresponding negative Fe_2O_3-FeO correlation, which reflects the dominant ilmenite-hematite solid-solution series in these ilmenites. There is a large overlap between ilmenite from dolerite and basalt. This is expected, given the close geological association of these rock types.

Granophyre:

A small number of ilmenite analyses in granophyre, from Groves *et al.* (1986), are included. These analyses are considered to represent ilmenite compositions in felsic, plutonic rocks from the Karoo Igneous Province. Ilmenite from the granophyres is distinguished from other Karoo igneous rocks by their higher MnO contents, which may reach 7.5 per cent (Figure 7.4G). This represents the substitution of $MnTiO_3$ for $FeTiO_3$, which is common in felsic rocks and increases with the MnO content of the magma, and decreasing temperature of crystallisation (Neumann, 1974).

Granitoid and felsic metamorphic rocks:

Like the granophyres, ilmenites from these rocks are characterised by ilmenite-pyrophanite substitution, resulting in moderate to high MnO levels (Figure 7.4H).

Metabasite and other mafic metamorphic rocks:

Ilmenites from these rocks are similar and are characterised by compositions close to pure $FeTiO_3$. Hematite and pyrophanite substitution may increase the MnO and Fe_2O_3 contents slightly. The "pure" composition of the ilmenite is caused by re-equilibration with surrounding silicates during metamorphism. Cassidy and Groves (1988) noted that the MnO content of ilmenites in metabasite and metapelite decreases markedly with increasing metamorphic grade. The MnO content is also dependent on the proportion of garnet in the rocks, as MnO is strongly partitioned into garnet. (Tracy, 1982).

Ultrabasic and basic complexes:

Analyses of ilmenite from the Mambula Complex are obtained from Reynolds (1986d). These represent ilmenite compositions from metamorphosed basic-ultrabasic complexes (MUBC). These ilmenites have compositions similar to the picrite and gabbro of the Karoo Igneous Province and are the only metamorphic ilmenites enriched in MgO. These ilmenites are prevented from re-equilibration with silicates during metamorphism because they occur in cumulate oxide layers and this preserves their high MgO contents.

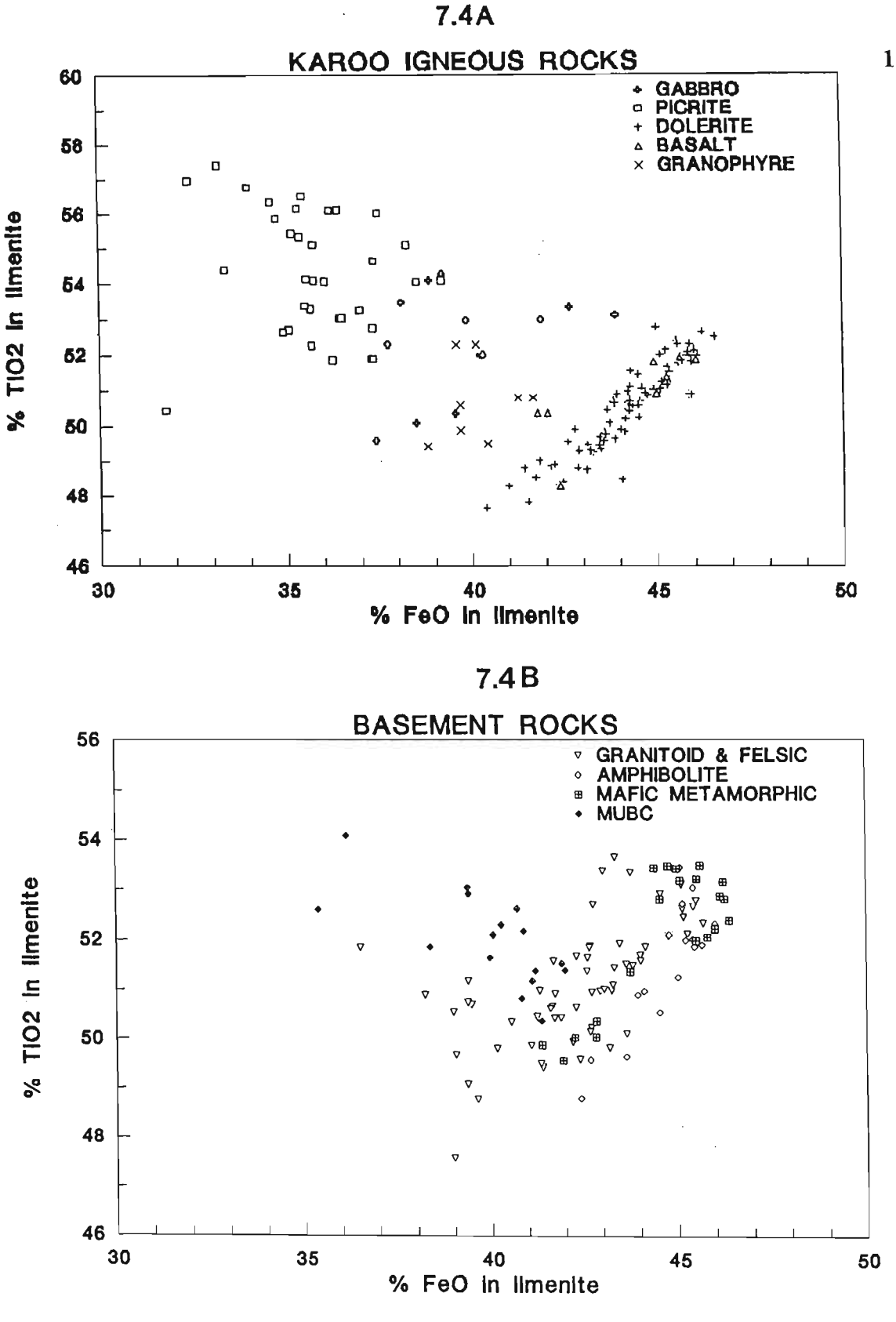

Figure 7.4 Variation diagrams showing the differences in chemical compositions of ilmenite from different source rocks from the Karoo Igneous Province. **A.** TiO_2 versus FeO for Karoo Igneous Rocks. **B.** TiO_2 versus FeO for Natal Basement Rocks.

Note: MUBC = metamorphosed ultrabasic/basic complexes

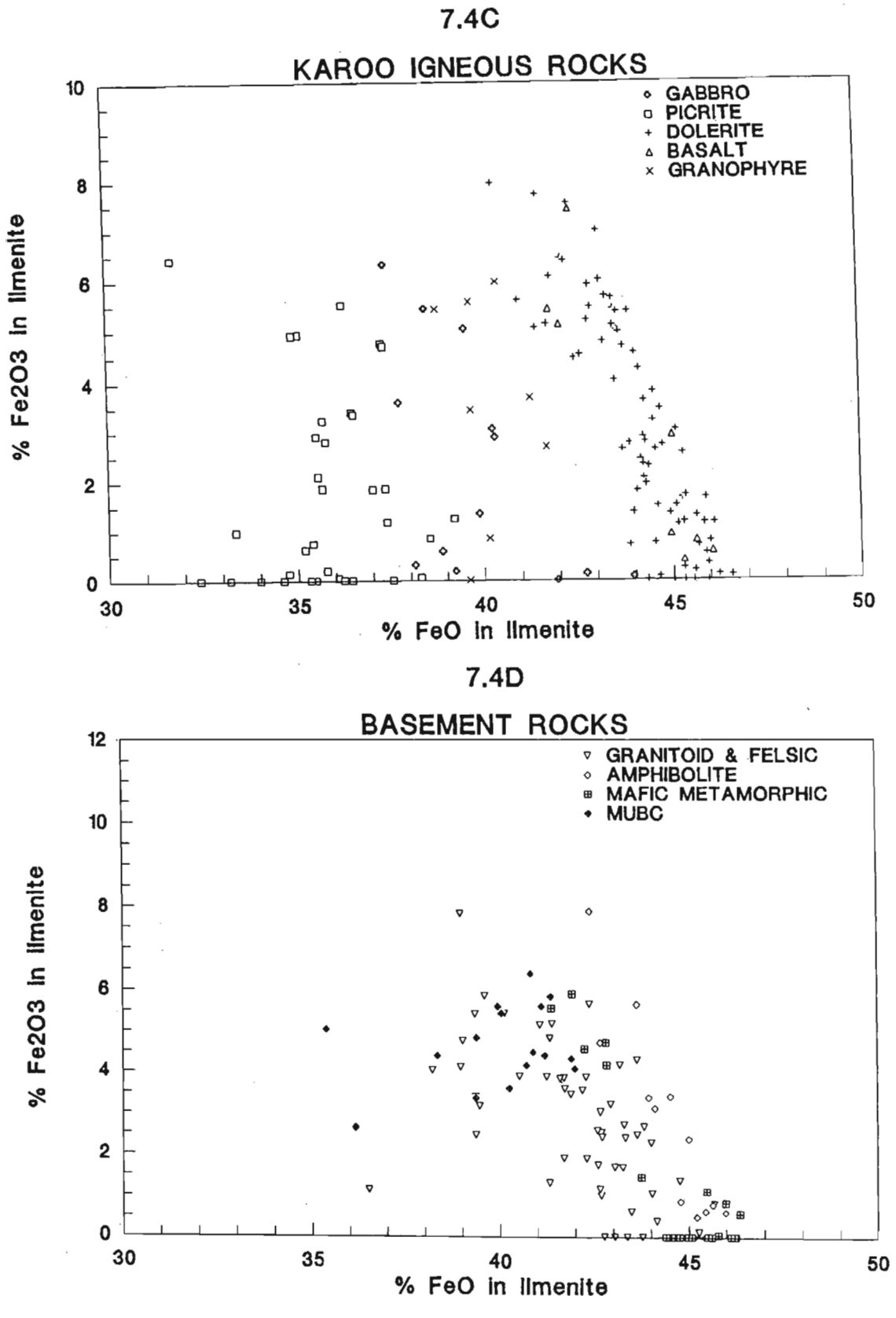

Figure 7.4C. Fe_2O_3 vs FeO in ilmenite from Karoo Igneous Rocks. **D.** Fe_2O_3 vs FeO in ilmenite from Natal Basement rocks.

7.4E

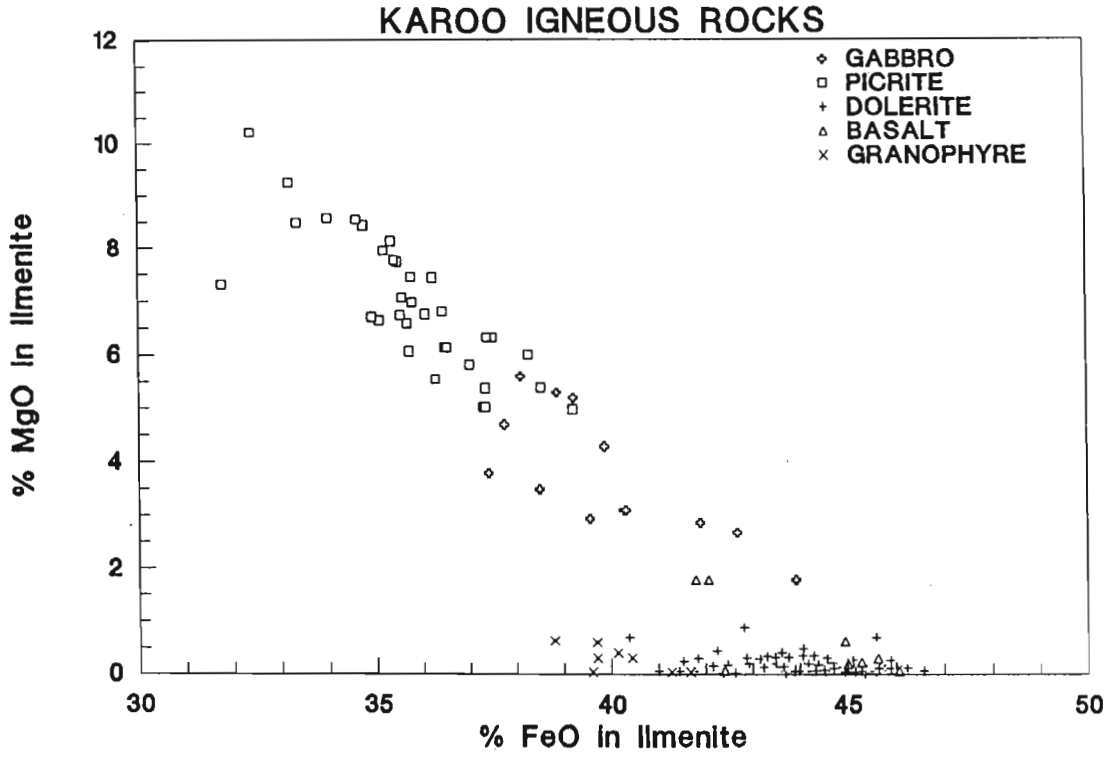

7.4F

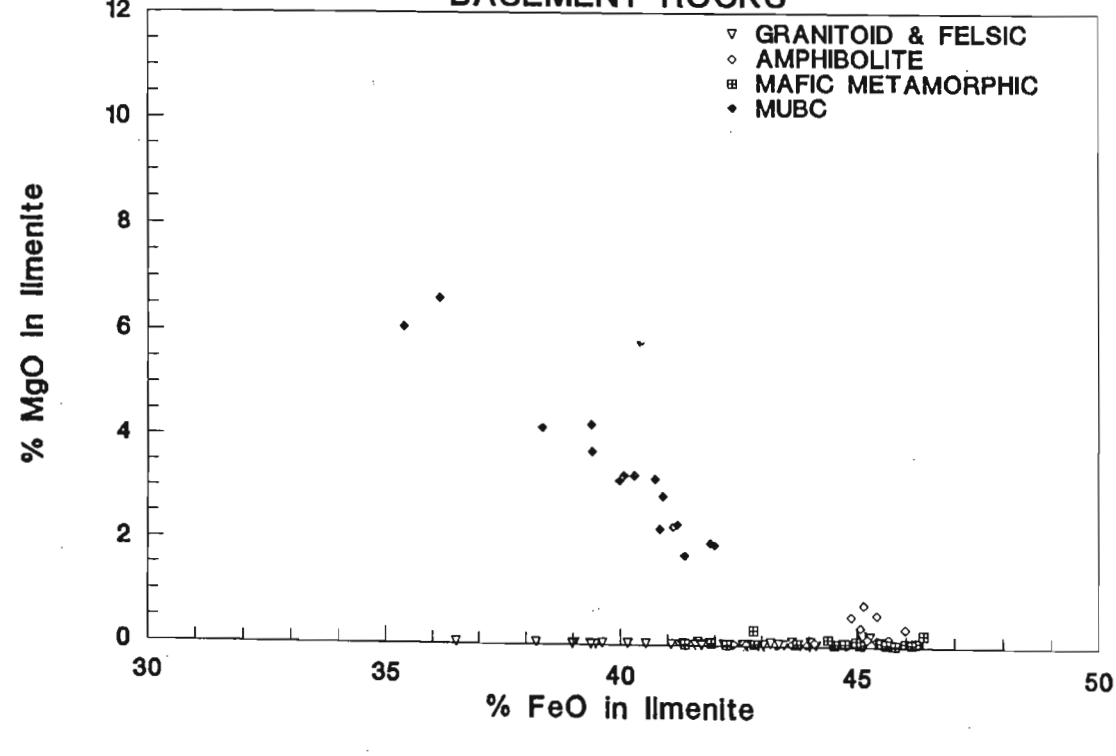

Figure 7.4E. MgO vs FeO in ilmenite from Karoo Igneous Rocks. **F.** MgO vs FeO in ilmenite from Natal Basement rocks.

7.4G

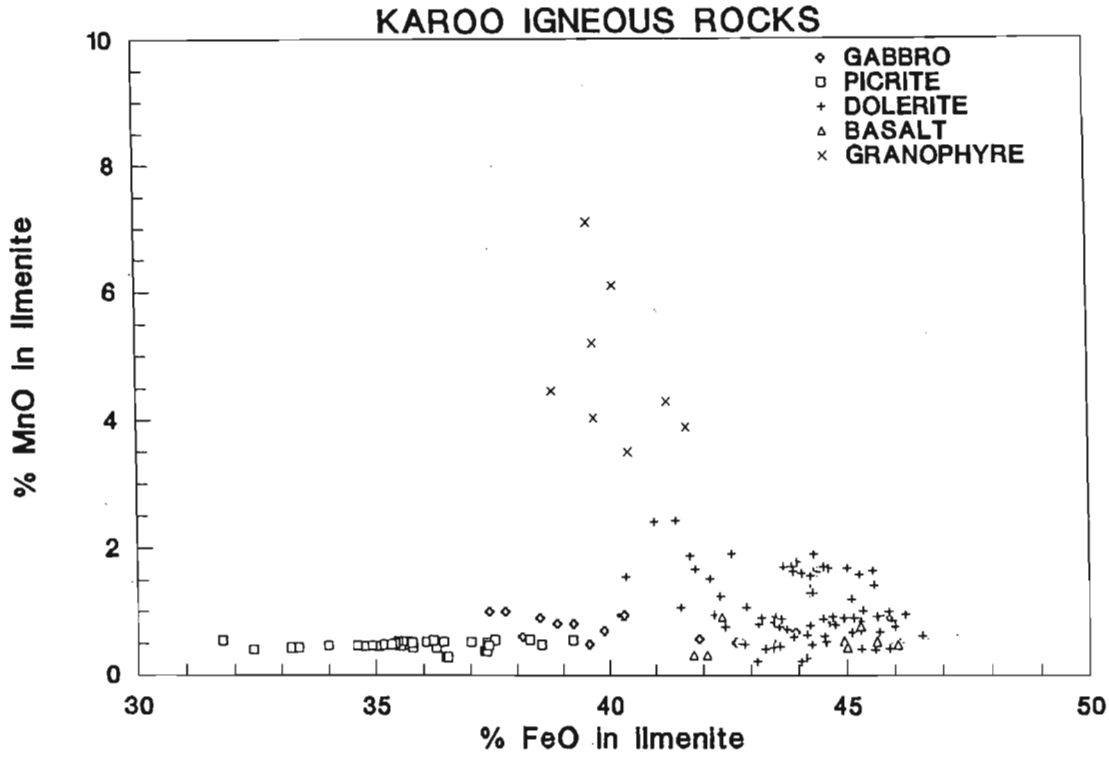

7.4H

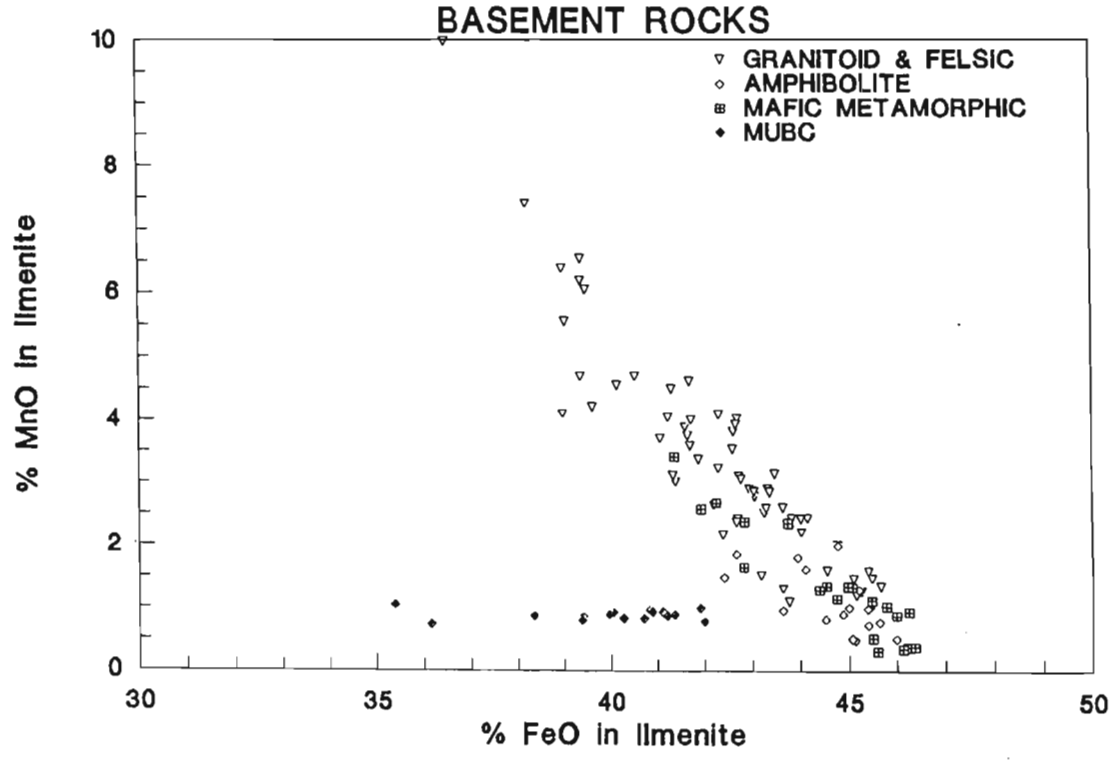

Figure 7.4G. MnO vs FeO in ilmenite from Karoo Igneous Rocks. **H.** MnO vs FeO in ilmenite from Natal Basement rocks.

7.4I

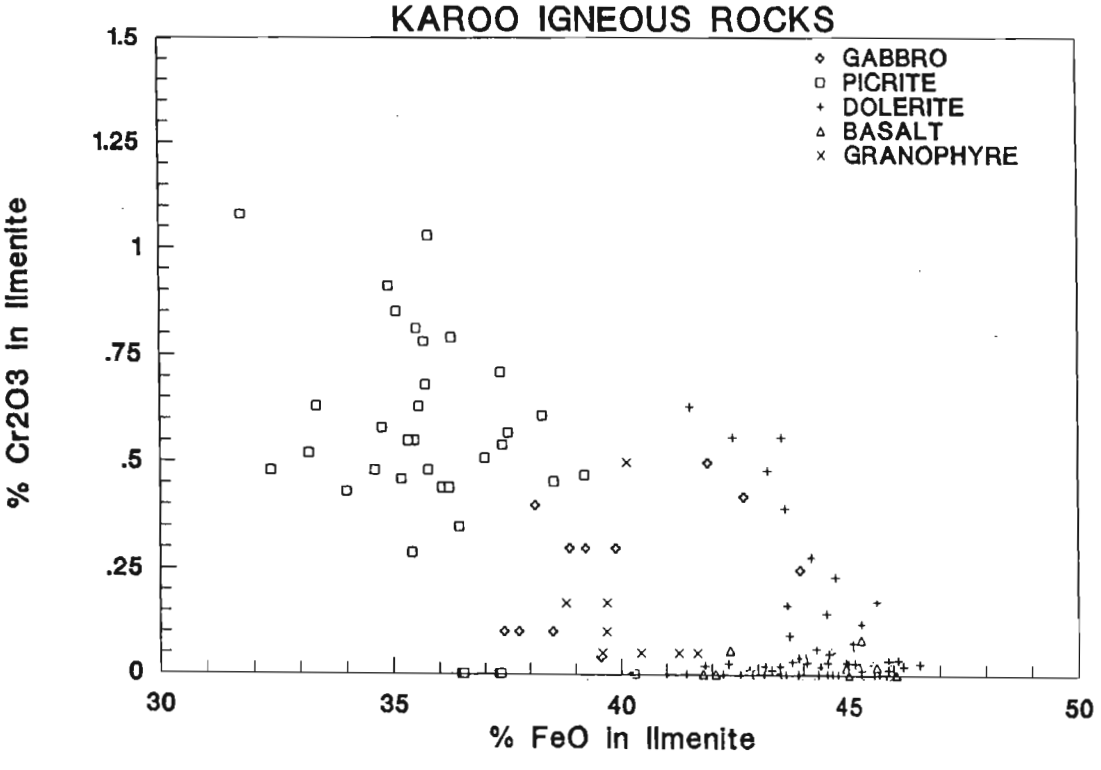

7.4J

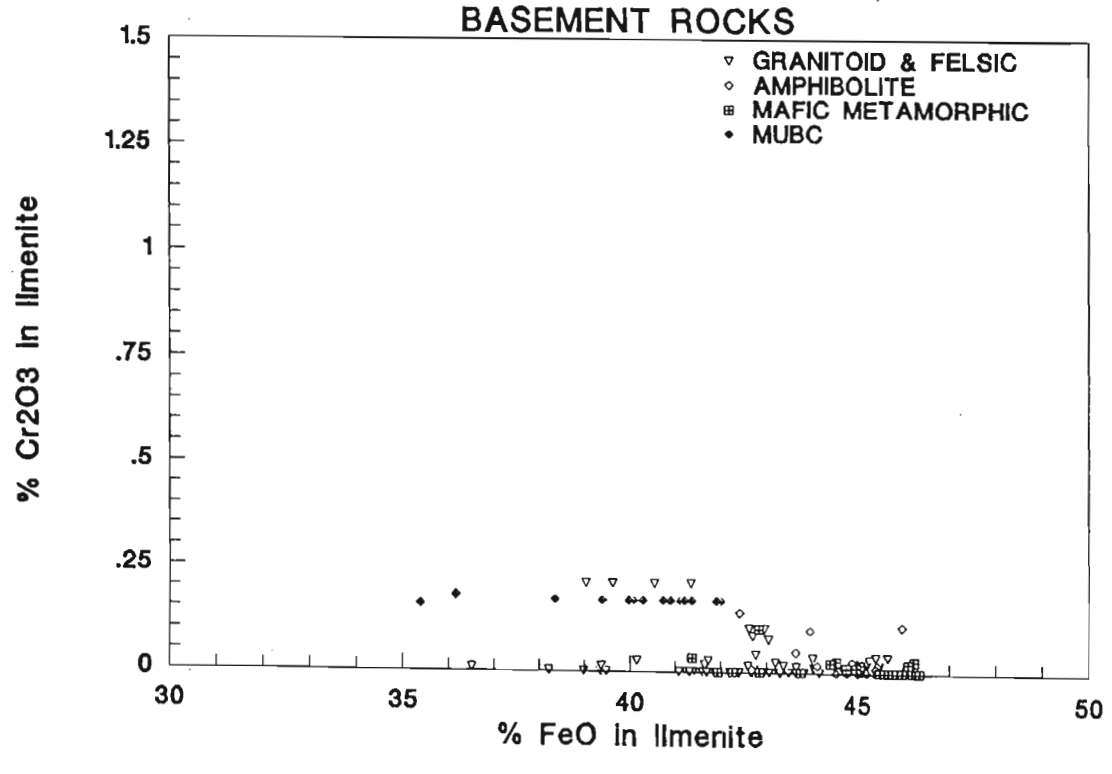

Figure 7.4I. Cr_2O_3 vs FeO in ilmenite from Karoo Igneous Rocks. **J.** Cr_2O_3 vs FeO in ilmenite from Natal Basement rocks.

7.5.3 Distinguishing ilmenite from different source rocks

From Figures 7.4A-J it is evident that there is a large overlap between ilmenites from:

1. dolerite and basalt (Karoo Igneous Province) and metabasite and mafic metamorphic rocks (Natal Basement);
2. granophyre (Karoo Igneous Province) and granitoid and other felsic rocks (Natal Basement);
3. basic and ultrabasic plutonic rocks (Natal Igneous Province) and metamorphosed basic-ultrabasic complexes (Natal Basement).

This suggests that ilmenite chemistry cannot be used to distinguish ilmenite from the two major provenances. However, granophyre (and other felsic rocks) are a minor component of the Karoo Igneous Province, whereas the granitoids and felsic metamorphic are major constituents of the Natal Basement rocks. It is therefore probable that ilmenite containing high MnO contents is from the latter rock types.

Although the ilmenite from basic and ultrabasic rocks is similar in composition, these may be distinguished by geographical locality. The metamorphosed igneous complexes are found in northern Natal and Zululand, while the large basic intrusions of the Karoo Igneous Province occur in southern Natal, Transkei and the eastern Cape.

These observations indicate that chemical composition may be used to distinguish ilmenite from certain rock types. Figure 7.5 plots the compositions of ilmenite from both the Karoo Igneous Province and the Natal Basement together. Certain rock types, containing similar ilmenite compositions are grouped together as follows:

1. *Ultra/basic plutonic*: picrites, gabbros and metamorphosed ultra/basic complexes;
2. *Dolerite and basalt*: dolerites and basalts from the Karoo Igneous Province;
3. *Granitoid and felsics*: granitoids and other felsic rocks from the Natal Basement;
4. *Mafic Metamorphic*: metabasite and other mafic rocks from the Natal Basement.

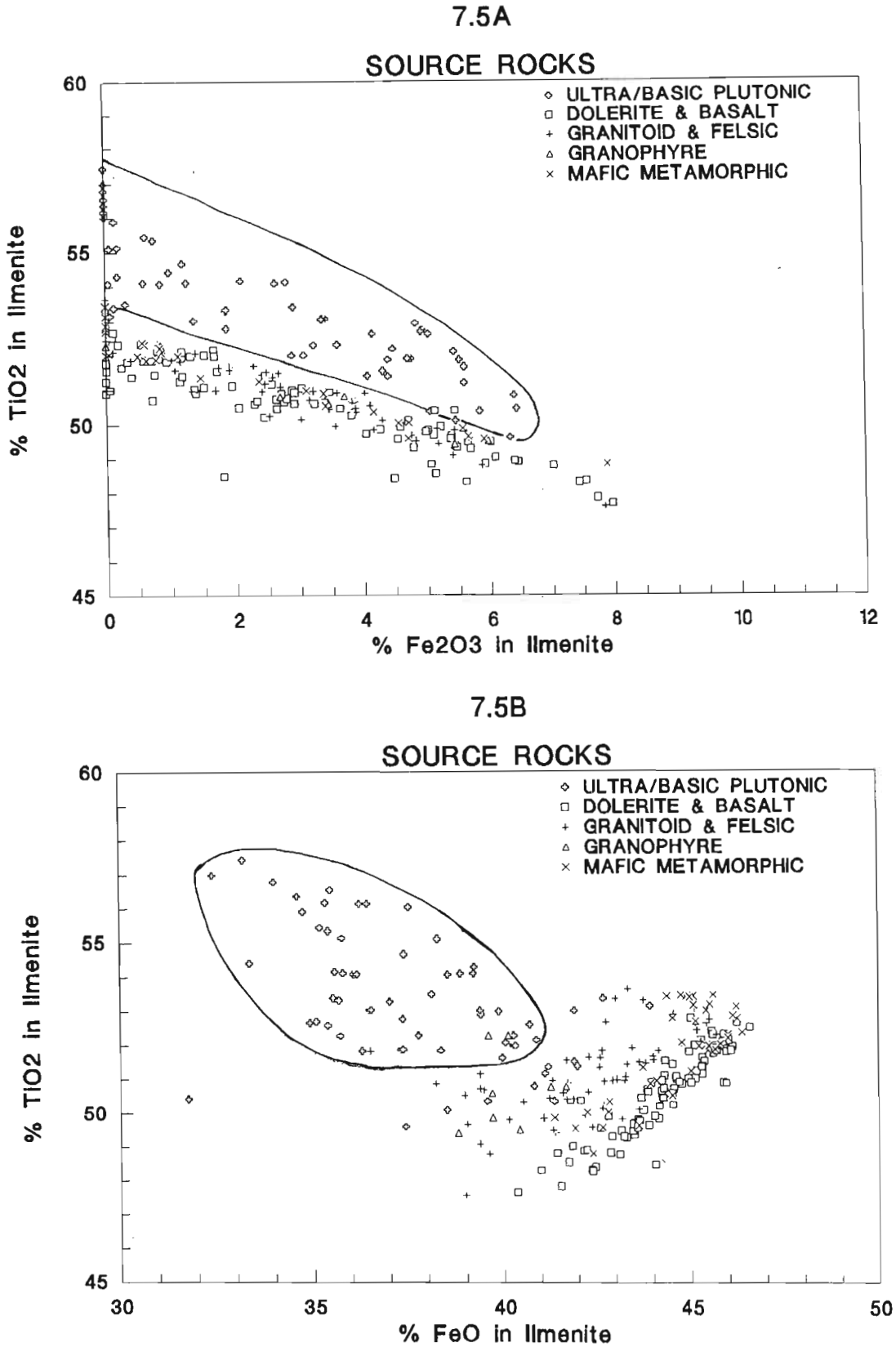

Figure 7.5 Variation diagrams of ilmenite compositions from different source rocks. Fields of composition which are occupied almost exclusively by ilmenites from one rock group are marked on the diagrams. **A.** TiO_2 versus Fe_2O_3. **B.** TiO_2 versus FeO.

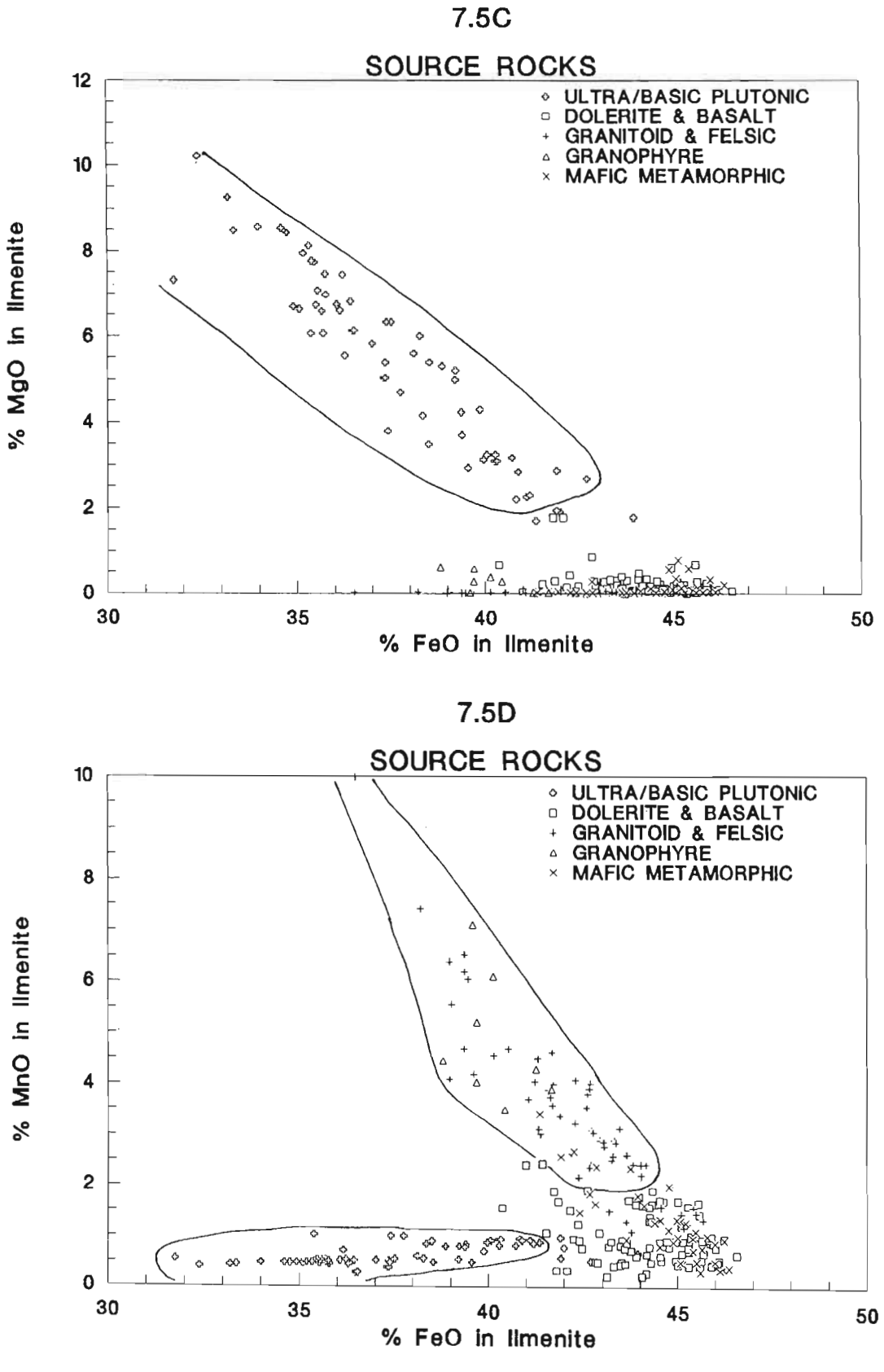

Figure 7.5 Variation diagrams of ilmenite compositions from different source rocks. **C.** MgO versus FeO. **D.** MnO vs FeO.

Fields delineating ilmenite from these different rock groups are shown in Figure 7.5, and indicate that:

1. ilmenite from the ultra/basic plutonic group is most distinct, having high TiO_2, low FeO, and high Cr_2O_3 (see Figure 7.4I and 7.4J);
2. ilmenite from felsic rocks may be distinguished by their high MnO contents;
3. ilmenite from basic igneous rocks (basalts and dolerites) cannot be distinguished from mafic metamorphic rocks, however as a group, all these rocks may be distinguished from other rocks types, as they have high FeO and low MnO contents (Figure 7.5D).
4. MgO and MnO content are the best discriminators of ilmenite source rocks, as the ilmenite compositions tend to fall either along the pyrophanite or geikielite solid-solution series (Figures 7.5C and 7.5D).

Figure 7.6 is a plot of MnO against MgO on a log scale, for ilmenites from the major provenance rock types. Fields for the different source rocks are drawn in and indicate that this diagram is the best discrimination diagram for ilmenite from the different source groups.

7.5.4 Provenance of ilmenite in coastal sediments

The MnO versus MgO contents of all ilmenite analysed in coastal sediments (see Appendix B.2) are plotted in Figure 7.7. The fields demarcated in Figure 7.6 are also shown in these diagrams, indicating the source rocks from which the ilmenite is derived. Each diagram is of ilmenite from one of the major geographical regions along the coast. The samples used range from Port Elizabeth in the south to Sodwana Bay in the north, and the analyses therefore represent ilmenite from the entire study area.

Of the 829 analyses used in Figure 7.7, more than 65 per cent of the ilmenite appear to be derived from basic igneous (dolerite and basalt) or mafic metamorphic rocks. Less than 10 per cent of the ilmenite can be identified as being derived from granitoid, or other felsic rocks, and less than 5 per cent of the ilmenite falls in the basic/ultrabasic field. The

source of the remaining ilmenite cannot be determined. This indicates that the bulk of the ilmenite is derived from the dolerite and basalt of the Karoo Igneous Province and the mafic metamorphic rocks, such as metabasite and mafic schists from the Natal Basement rocks. It is suggested that the proportion of ilmenite derived from the former is far greater, as the Karoo igneous rocks contain more iron-titanium oxides (see Table 7.5, page 212); have a larger area of outcrop than the mafic rocks of the Natal Basement; and the present outcrop area is only a small remnant of the original volume of the basalts and dolerites (Eales, *et al.*, 1984).

Table 7.4 gives a breakdown of the proportions of ilmenites derived from different source rocks for each of the regions, and indicates that there are regional variations in the source rocks of the ilmenite. These variations are discussed in greater detail in Chapter 8.

Table 7.4 Percentage ilmenite in sediments from different regions identified from source rock groups delineated in Figure 7.7.

Source Rock	Zululand	Natal	Transkei	E. Cape
Granitoid & felsic	11	6	3	2
Ultra/mafic plutonic	4	3	2	4
Mafic rocks (basalt, dolerite, mafic meta.)	67	67	76	69
Indistinguishable	18	24	19	24

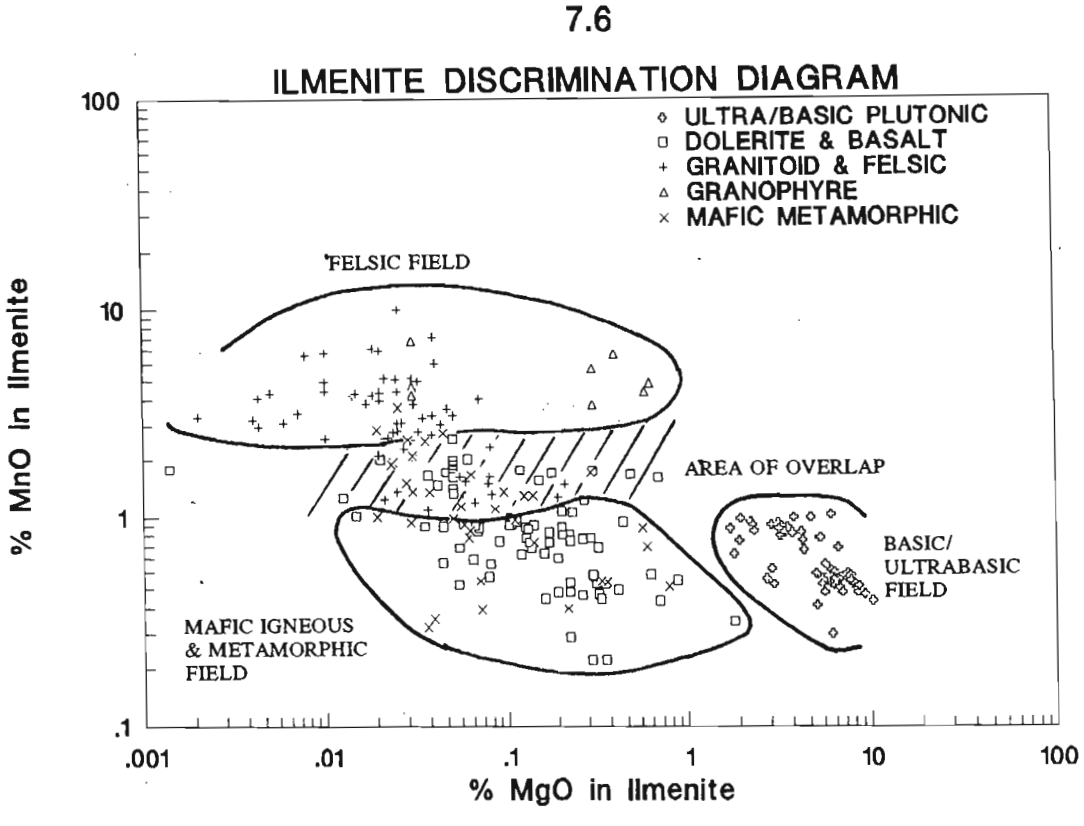

Figure 7.6 Plot of MnO versus MgO using log scale to distinguish ilmenite from different rock groups. The clearly defined fields of most of the different rock groups indicate that this plot is the best discrimination diagram for ilmenite provenance. (Note: the lower limit of detection for MgO in ilmenite, using the operating conditions described Table 4.1 is 0.02).

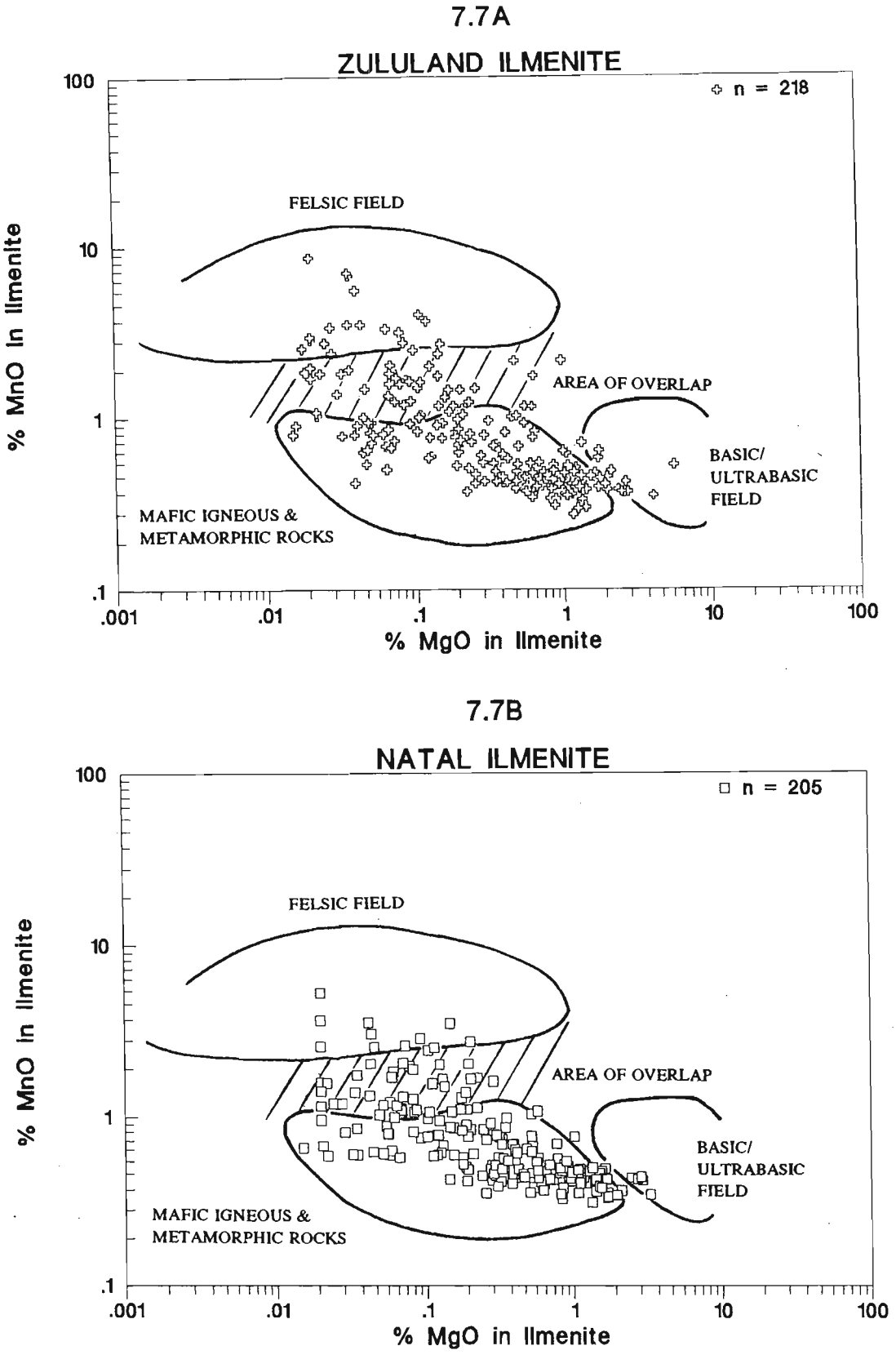

Figure 7.7 MnO versus MgO for ilmenite from coastal sediments in the study area. Data is derived from analyses given in Appendix B.2. The fields shown in the diagrams are from Figure 7.6 and indicate from which source rock the ilmenite is derived. **A.** Ilmenite from Zululand sediments. **B.** Ilmenite from Natal sediments.

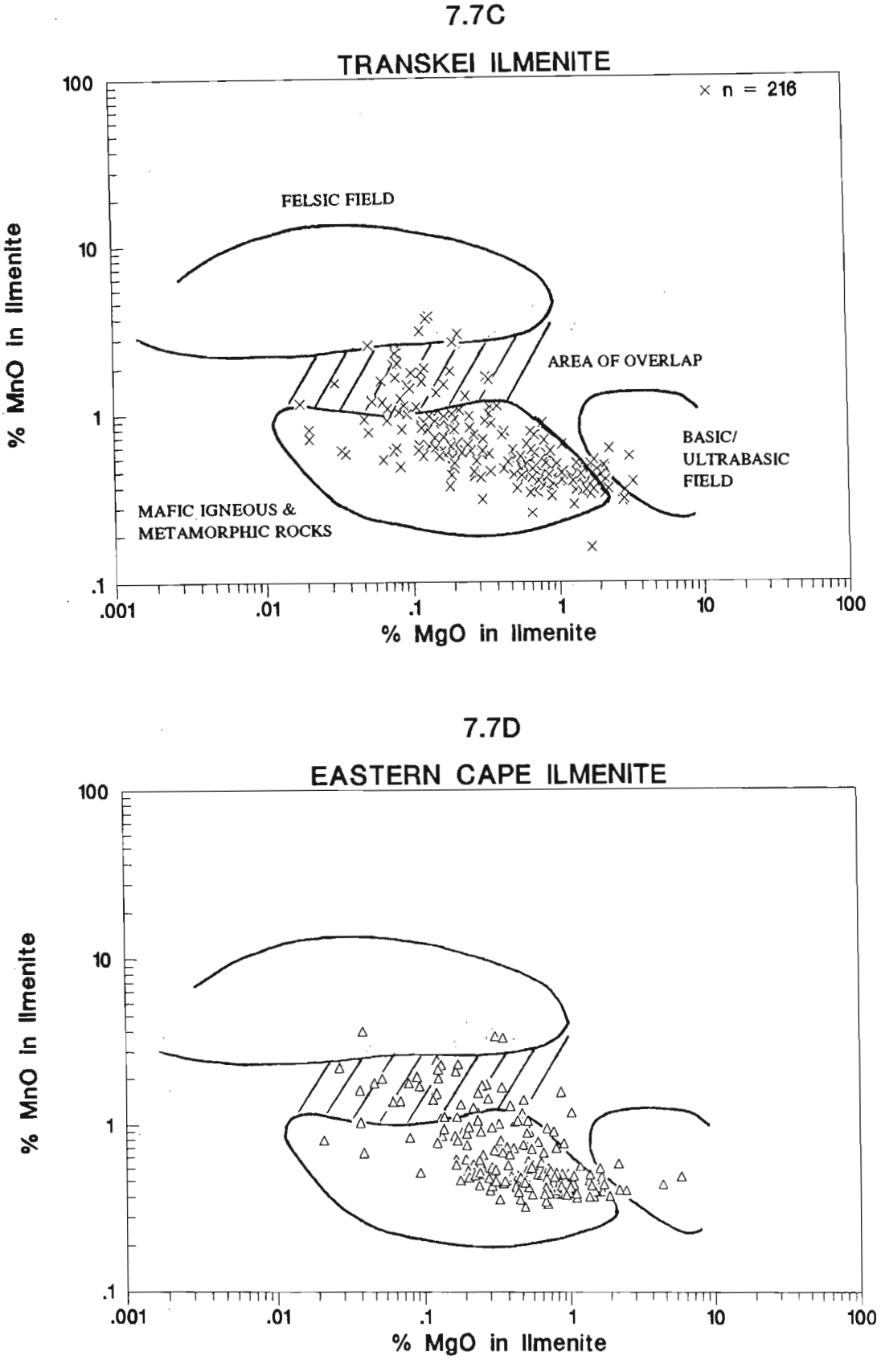

Figure 7.7 MnO versus MgO for ilmenite from coastal sediments in the study area. **C.** Ilmenite from Transkei sediments. **D.** Ilmenite from eastern Cape sediments.

7.6 MAGNETITE CHEMISTRY AS A PROVENANCE INDICATOR

7.6.1 Method

Magnetite from the following rock types and sediments were analysed by electron microprobe, as described in Chapter 4 (see page 63):

1. Karoo dolerite, including the Rooi Rand dyke swarm;
2. Basalt;
3. rivers (Kei and Fish) which exclusively drain the above rock types;
4. granite-gneiss (MS17);
5. mafic gneiss;
6. rivers which exclusively drain the metamorphic terranes (Mgeni River tributaries) consisting mainly of granite-gneiss and porphyroblastic gneiss with mafic enclaves;

Where possible, homogenous magnetite was analysed, but in some rock types, such as dolerite and basalt, most of the magnetite is inhomogeneous, containing ilmenite "oxyexsolution" textures, or exsolution of pleonaste or ulvöspinel. Magnetite analyses were also obtained from the literature to complement the magnetite data base. All analyses were recalculated by the method of Stormer (1983) to estimate the Fe_2O_3 in the grains. The full list of analyses used is given in Appendix C.2.

Source rocks were grouped as follows:

1. Basic Igneous Rocks - mainly dolerite and basalt, with minor gabbro, which are considered to represent rocks from the Karoo Igneous Province.
2. Metamorphic ultrabasic-basic complexes (MUBC) - data from the Usushwana (Reynolds, 1986a) and Mambula Complexes (Reynolds 1986d).
3. Granitoids - granite-gneiss, metagranite, and minor granite.
4. Metamorphic rocks - other metamorphic rocks, including metabasite, mafic schist, ortho- and paragneiss.

Variation diagrams were plotted to determine which oxides best distinguish magnetites from the different source rocks.

7.6.2 Magnetite compositions in source rocks

The major elements in magnetite from the above rock groups were plotted as oxides against Fe_2O_3 (Figure 7.8). From the plots it is evident that the major variation in magnetite chemistry is caused by TiO_2 and Fe_2O_3 content (see Figure 7.8A). The compositions plot along the magnetite-ulvöspinel tie-line, indicating that the variation is caused by ulvöspinel solid-solution within the magnetite. The variation in TiO_2 is a function of the initial TiO_2 content and fO_2 of the magma, the degree of subsequent exsolution of ulvöspinel, or oxyexsolution of ilmenite, from the magma during cooling (Haggerty, 1976b). In some cases the high TiO_2 levels analysed by electron microprobe may be caused by sub-microscopic intergrowths of ulvöspinel in the magnetite. Figures 7.8C and 7.8D indicate that, of the other oxides, Al_2O_3 results in the greatest variation in magnetite composition.

Magnetite from basic igneous rocks (that is, those equated with the Karoo igneous rocks) may be distinguished from those of other rocks, as the former contain higher TiO_2 and Al_2O_3 contents, and correspondingly low Fe_2O_3 levels. The data set is biased towards the volcanic and hypabyssal rocks, which contain magnetites enriched in TiO_2 and rarely have TiO_2 contents of less than 5 per cent. Frost and Lindsley (1991) note that titanomagnetite in MORB and flood basalts contain 50 to 80 per cent ulvöspinel. The TiO_2 content decreases as ulvöspinel or ilmenite is formed from the titanomagnetite. The variability of the TiO_2 content, and to a lesser degree, the other oxides, is an indication of the ease with which spinels tend to undergo cation-exchange with other minerals during slow cooling. Magnetite in volcanic rocks is therefore expected to have higher levels of impurities, as these rocks cool quickly.

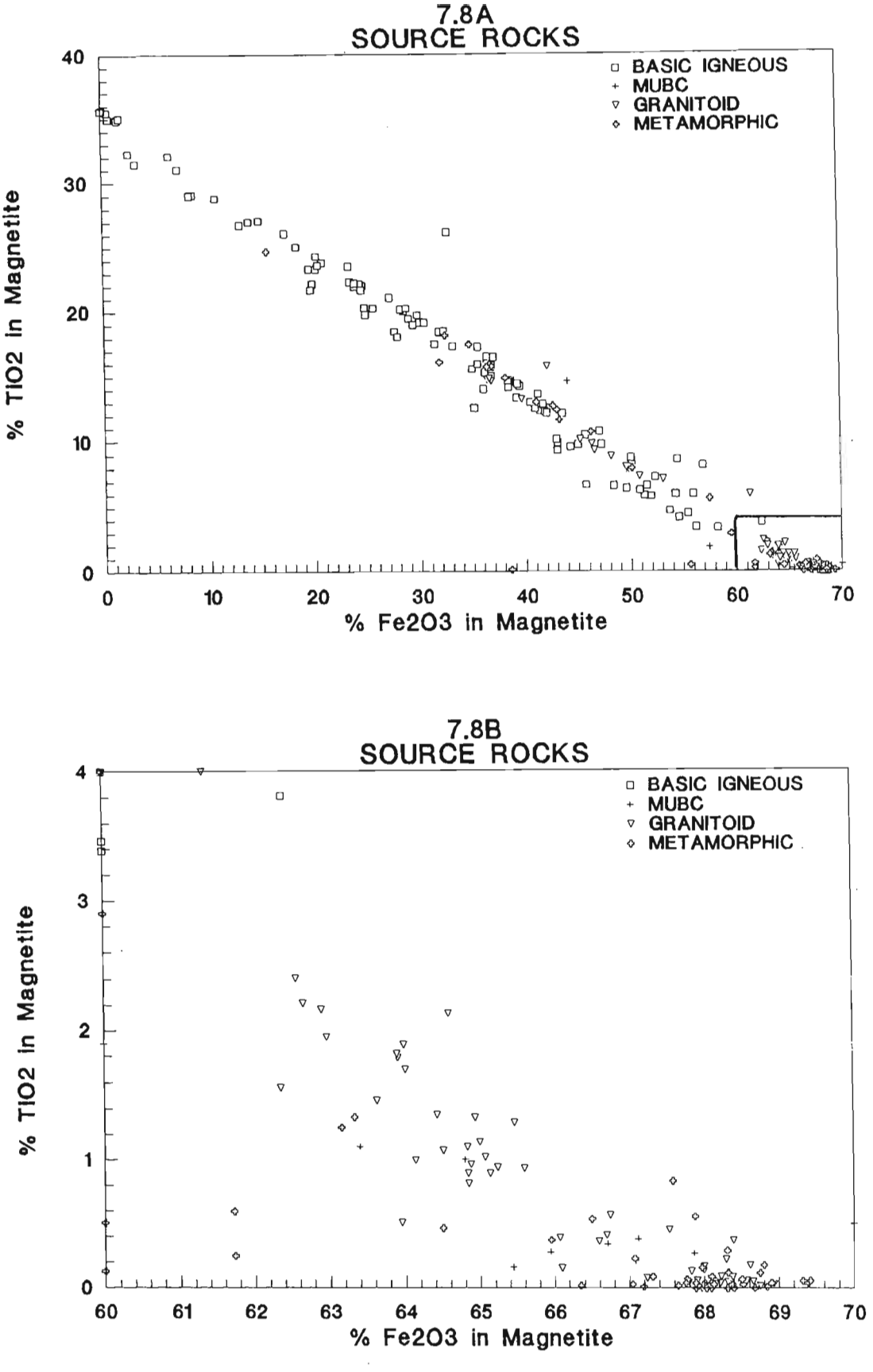

Figure 7.8 Variation diagrams of magnetite compositions from different source rocks as described in the text. **A.** TiO_2 versus Fe_2O_3. **B.** Expanded view of area demarcated in 7.8A.

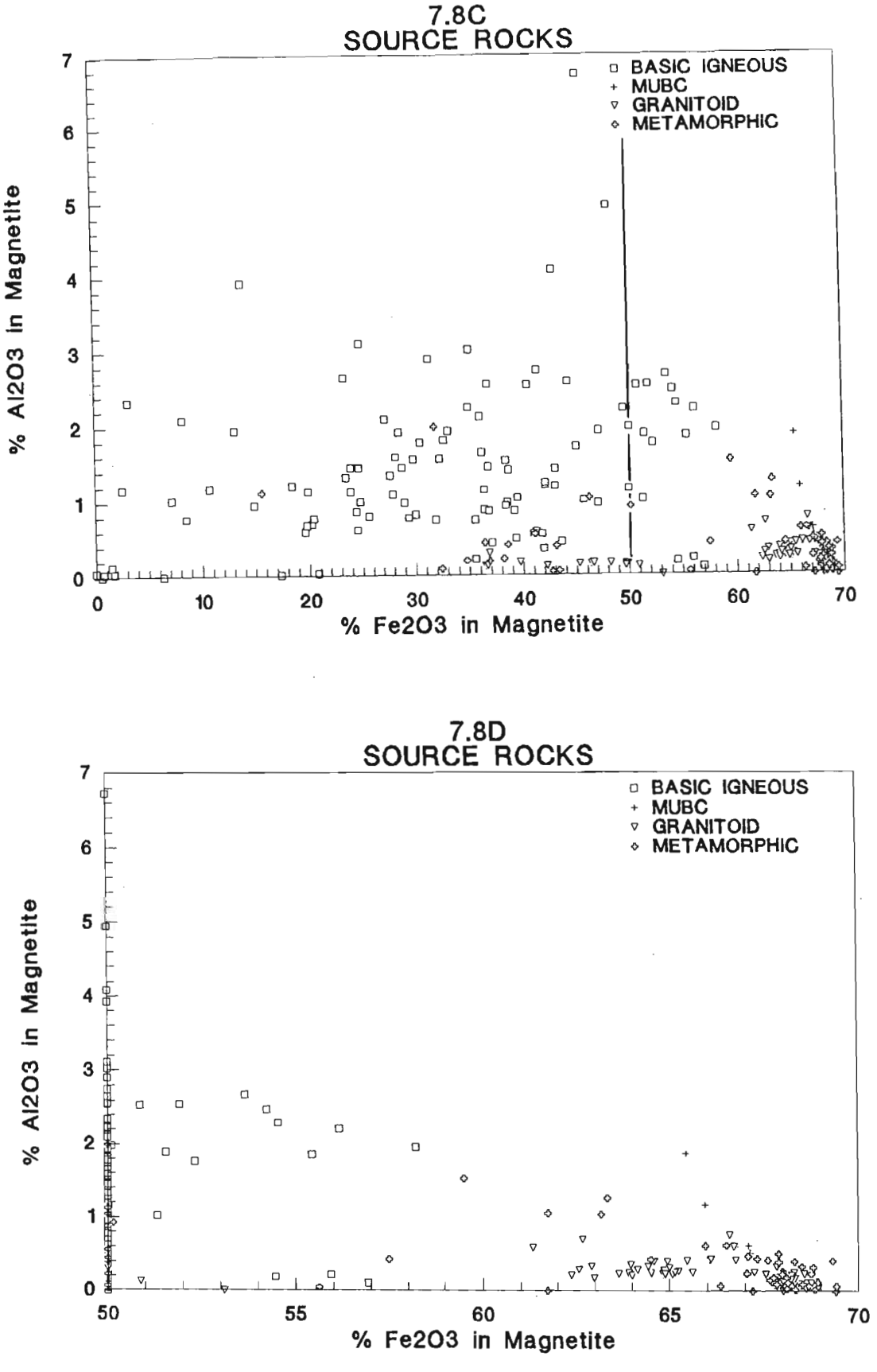

Figure 7.8C. Al_2O_3 versus Fe_2O_3 in magnetite from different source rocks.

D. Expanded view of area demarcated in 7.8C.

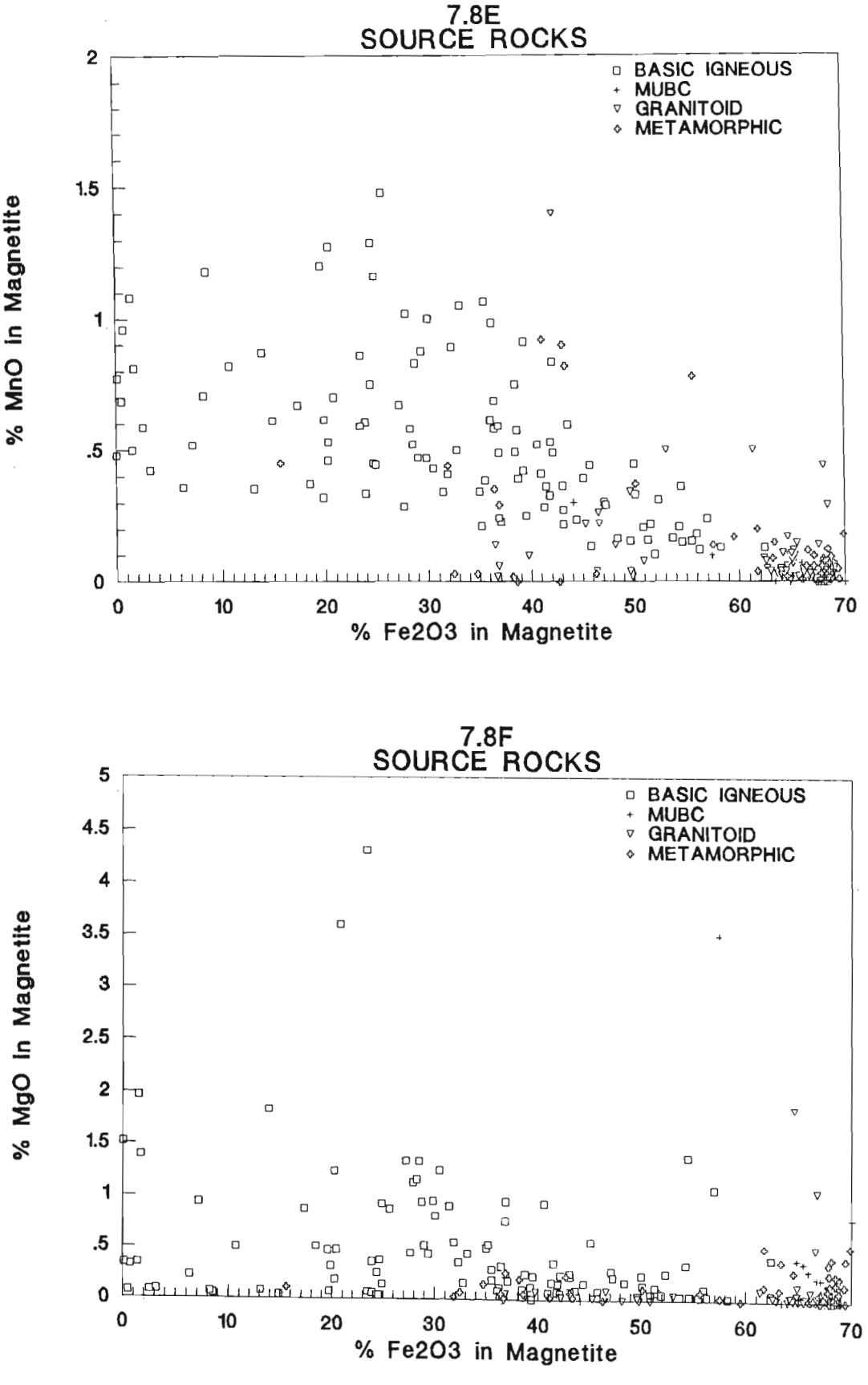

Figure 7.8E MnO versus Fe_2O_3 in magnetite from different source rocks.

F. MgO versus Fe_2O_3.

The magnetite from metamorphic rocks and granitoid rocks (that is, those equated with the Natal Basement rocks) have indistinguishable compositions. Magnetite from granitoid rocks tends to have compositions very close to pure Fe_3O_4, with only minor TiO_2 and Al_2O_3 substitution. This is attributed to extensive sub-solidus re-equilibration of the magnetites with other minerals in these rocks which is enhanced by the presence of aqueous fluids (Frost and Lindsley, 1991).

As with the granitoids, most metamorphic rocks contain pure magnetites, although the solid-solution of ulvöspinel in some magnetites from the data set may be high (up to 24 per cent TiO_2 in the magnetite). Frost (1991b) states that magnetite is nearly pure Fe_3O_4 in most metamorphic rocks and although magnetite in high grade rocks may contain considerable titanium, this is expelled during re-equilibration on cooling.

The variations in Al_2O_3, TiO_2 and Fe_2O_3 contents in the magnetites are combined to form the variation diagram shown in Figure 7.9. Using these field delineators in Figure 7.9, only 2 per cent the basement magnetite, and 2 per cent of the basic igneous magnetite is incorrectly classified. Eight and 10 per cent of the basement and igneous magnetites, respectively, fall within the field of overlap. The plot of Al_2O_3 against $Fe_2O_3/(Fe_2O_3+TiO_2)$ ratio is therefore a good discriminator of magnetite from the two major, primary provenances. This variation diagram is used in Chapter 8 to help interpret variations in the chemistry of magnetites found in the coastal sediments.

Although Al, Ti and Fe^{3+} are effective discriminators, V and Cr are also expected to be useful, as these elements are commonly concentrated in magnetite from basic and ultrabasic plutonic rocks (Haggerty, 1976b; Reynolds, 1986d; Frost and Lindsley, 1991). Grigsby (1990) has shown that V, in particular, is a good discriminator of magnetite source rocks.

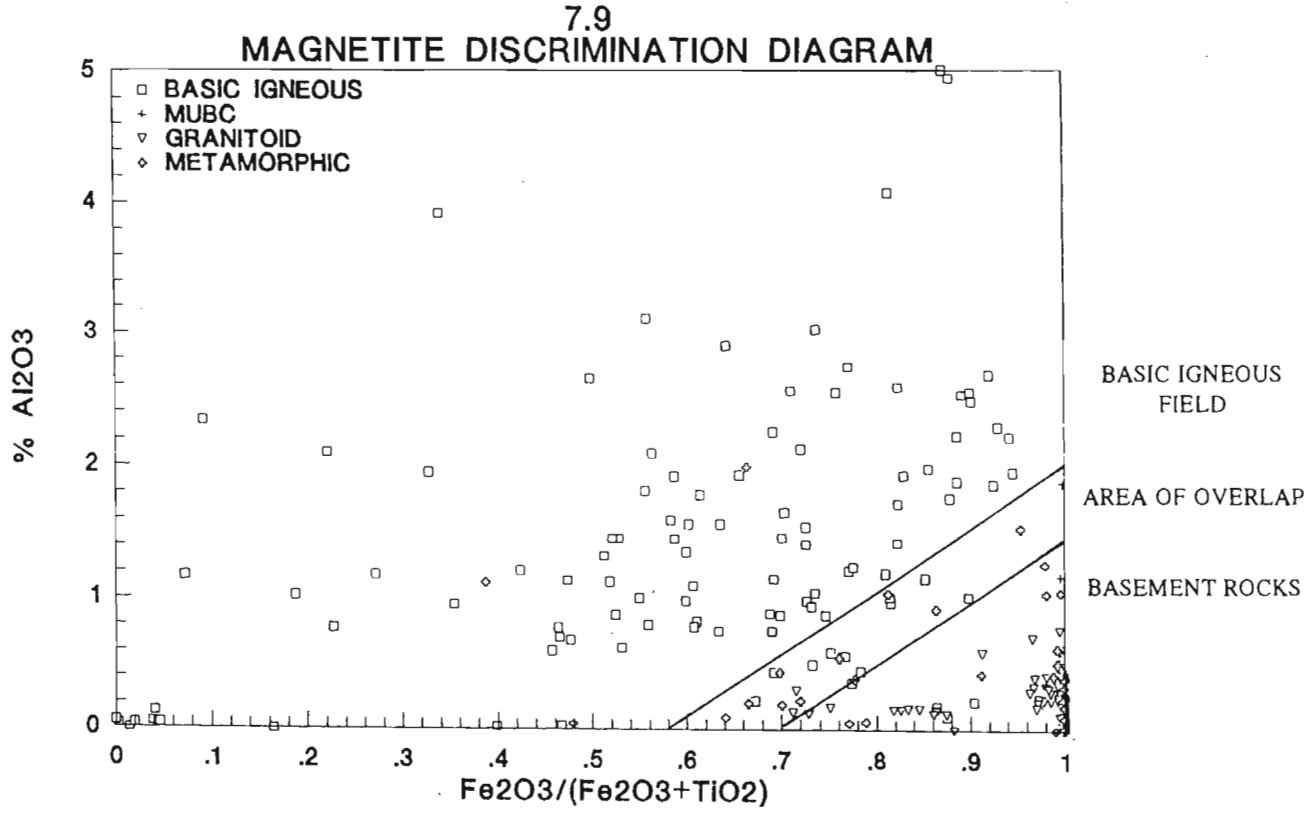

Figure 7.9 A plot of Al_2O_3 versus $Fe_2O_3/(Fe_2O_3+TiO_2)$ in magnetite, which is the best discrimination diagram of magnetite from different source rocks.

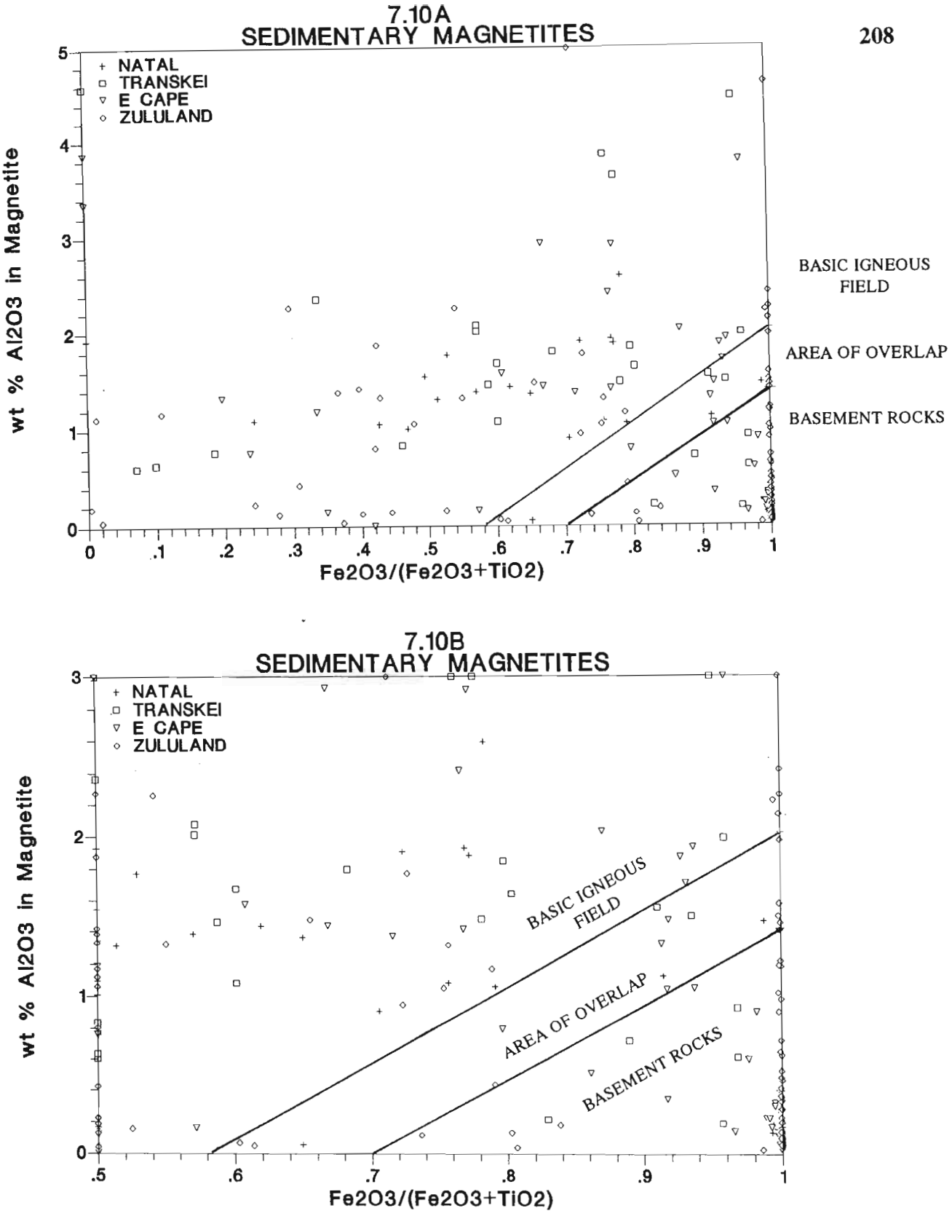

Figure 7.10A Plot of Al_2O_3 vs $Fe_2O_3/(Fe_2O_3+TiO_2)$ in magnetites from coastal sediments within the study area. **B.** Expanded view of area demarcated in 7.10A. The diagrams indicate that magnetite is derived in roughly equal proportions from the Karoo Igneous Province and the Natal Basement rocks.

7.6.3 Provenance of magnetite in coastal sediments

All magnetite analyses, from coastal sediments are plotted on the discrimination diagram described above (Figure 7.10). These analyses (see Appendix B.3) are obtained from samples of the major heavy mineral regions, although there is a bias towards the Zululand sediments, which constitute about 50 per cent of the data base).

Of the 202 analyses plotted in Figure 7.10, about 43 per cent of the magnetites fall in the Karoo Igneous (dolerite and basalt) field, 48 per cent are derived from Natal Basement rocks, and the remaining magnetites (9 per cent) cannot be classified. This clearly shows that magnetite in the coastal sediments is derived from both the major provenances in roughly equal proportions.

7.7 PROPORTIONS OF IRON-TITANIUM OXIDES IN SOURCE ROCKS

7.7.1 Modal proportions in source rocks

The proportions of the iron-titanium oxides in samples of various source rocks were determined by point-counting 100 oxide grains per sample. The proportions of the oxides in the samples were visually estimated. The modal proportions are given in Table 7.5 and indicate that the following intergrowths or textures are exclusive to certain rock groups:

1. Skeletal ilmenite and magnetite grains, Cr-spinels, and magnetite containing trellis and sandwich lamellae of ilmenite, are found almost exclusively in basalt and dolerite of the Karoo Igneous Province and are therefore good provenance indicators of these rocks.
2. $(Ilm\text{-}Hem)_{ex}$, $(Hem\text{-}Ilm)_{ex} \pm Rut_{oe}$, $Ilm\text{-}(Hem+Rut\pm Psb)_{ox}$ and $(Hem\text{-}Rut\pm Psb)_{ox}$ grains are good indicators of granite-gneiss and granitoids from the Natal Metamorphic Province.
3. $Mt\text{-}Pleo_{ex}\pm Ilm_{oe}$ and, to a lesser extent, chromite grains are good indicators of metamorphosed layered intrusions from the Natal Metamorphic Province.

4. The Natal Metamorphic Province is also characterised by rutile, titanite and ilmenite-titanite grains.

The presence of oxides containing these intergrowths or textures in coastal sediments should indicate that the minerals are derived from specific rock groups.

7.7.2 The ilmenite-magnetite discrimination diagram

Homogeneous ilmenite and magnetite grains are found in a wide range of source rocks and are therefore poor petrographic indicators of provenance by themselves. These minerals, together with Mt-$Ilm_{oe} \pm Usp_{ex}$ intergrowths, are the dominant phases in the source rocks examined. When their proportions are plotted on a ternary diagram - the ilmenite-magnetite discrimination diagram (Figure 7.11) - clear differences between the basement and Karoo igneous rocks are noted. The basalts and dolerites contain high proportions of Mt-$Ilm_{oe} \pm Usp_{ex}$ and low amounts of homogeneous magnetite. The basement rocks contain high proportions of homogeneous ilmenite and magnetite and less than 10 per cent intergrown magnetite. An exception is the ultrabasic rocks which plot within the field of the dolerites and basalts, however, most of the magnetite from these rocks contain pleonaste intergrowths and so these rocks can be distinguished from the Karoo igneous rocks.

The differences in the proportions of the iron-titanium oxides from the different source areas are caused by variations in bulk chemistry, fO_2, and cooling rate. As noted by Haggerty (1976a) the low fO_2 of basic rocks results in the crystallisation of ilmenite and the extensive solid-solution of ulvöspinel in magnetite. Slight increases in fO_2 result in the oxyexsolution of ilmenite from magnetite, but the rapid cooling of the basalts and smaller dolerite intrusions ensures that the ilmenite lamellae are intimately intergrown with the magnetite. Coarser intergrowth textures are usually found in the larger dolerite sills, or in the basic plutonic rocks, where slow cooling results in the development of sandwich or composite textures.

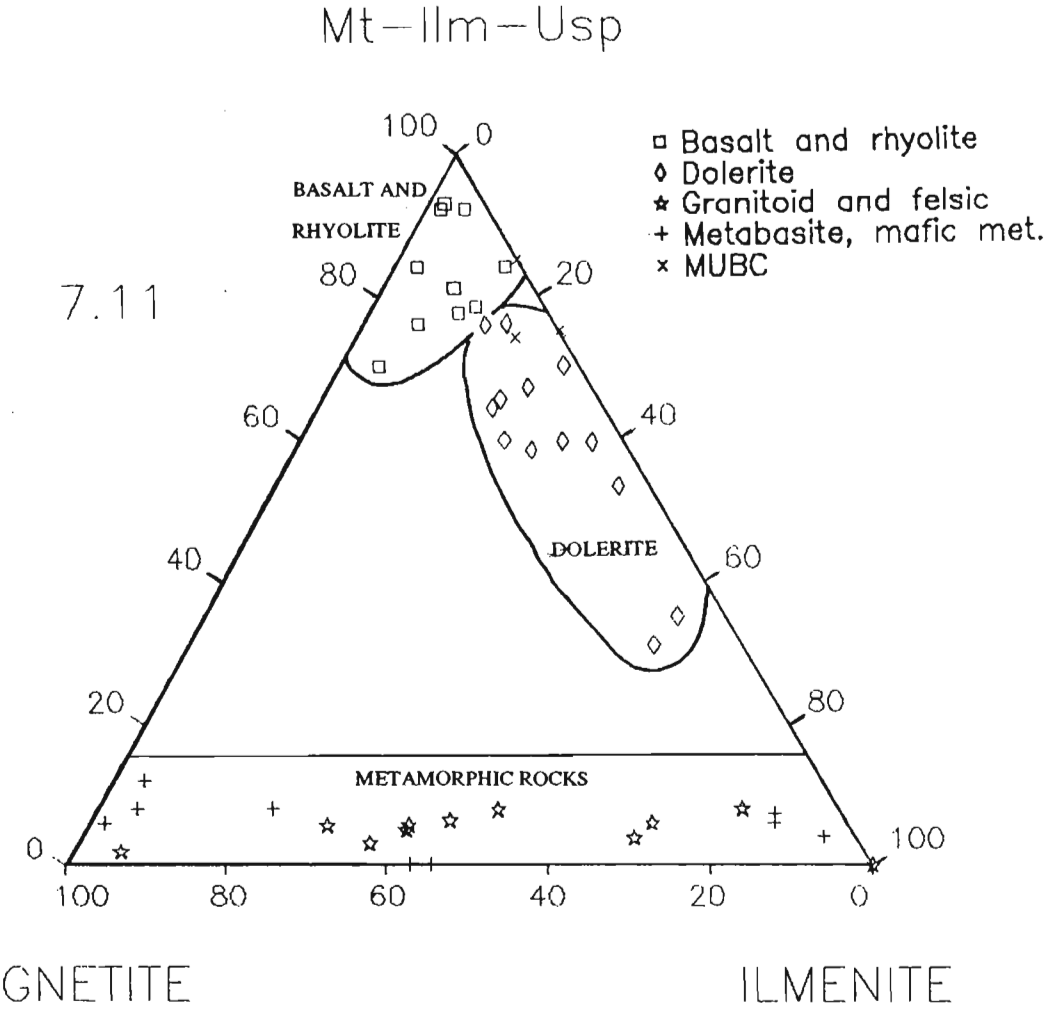

Figure 7.11 The ilmenite-magnetite discrimination diagram, which is a plot of the relative proportions of homogeneous magnetite, ilmenite and Mt-Ilm_{oc}-Usp_{ex}.

Note: MUBC = metamorphosed ultrabasic/basic complexes.

Table 7.5 Modal Proportions of iron-titanium oxide intergrowths in source rocks, determined by point-counting. All values are expressed as a per cent. Sample localities are given in Appendix A.

	BASALTS								RHYOLITES	
Oxide Grain Types	HS1	HS2	HS3	HS4	HS5	HS6	PTA 1	PTA 2	HL1	HL2
Ilmenite	9	5	7	3	15	2	10	12	2	5
vermiform ilmenite	-	-	-	-	-	-	-	-	-	-
skeletal ilmenite	**	**	*	**	**	*	**	**	-	-
Ilm-Hem	-	-	-	-	-	-	-	-	-	-
Hem-Ilm	-	-	-	-	-	-	-	-	-	-
Hem-Ilm-Rut	-	-	-	-	-	-	-	-	-	-
Hem-Rut	-	-	-	-	-	-	-	-	-	-
Ilm-(Hem-Rut-Psb)	-	-	-	-	-	-	-	-	-	-
(Hem+Rut+Psb)	-	-	-	-	-	-	-	-	-	-
(Hem-Psb)	-	-	-	-	-	-	-	-	-	-
Hematite	-	-	-	-	-	-	-	-	-	-
Magnetite	10	25	17	13	19	5	10	8	6	3
skeletal magnetite	**	***	**	**	**	*	**	*	**	*
Mt-Usp	2	6	2	4	r	1	-	-	4	6
Mt-Ilm-Usp	79	64	74	80	66	88	69	72	88	86
trellis	******	*****	******	******	*****	******	****	*****	******	******
sandwich	**	**	**	***	**	***	****	**	**	***
composite		*		*	*	**	**	**		*
Mt-Pleo-Ilm	-	-	-	-	-	1	-	-	-	-
Chromite	-	-	-	-	-	-	-	-	-	-
Cr-Spinel	r	-	r	r	-	3	-	-	-	-
Rutile	-	-	-	-	-	-	-	-	-	-
Sphene	-	-	-	-	-	-	-	-	-	-
Ilm-Sph	-	-	-	-	-	-	-	-	-	-
Altered grains	nd	nd	nd	nd	nd	nd	11	8	nd	nd
Total	100	100	100	100	100	100	100	100	100	100
Per cent of Rock	3.5	2	1	4.5	3	3	nd	nd	1	0.5
Normalised values										
Ilmenite	9.0	5.0	7.0	3.0	15.0	2.1	11.2	13.0	2.0	5.0
Magnetite	10.0	25.0	17.0	13.0	19.0	5.2	11.2	8.7	6.0	3.0
Mag+ilm+ulv+pleo	81.0	70.0	76.0	84.0	66.0	92.8	77.5	78.3	92.0	92.0
Homo magnetite	11.0	26.3	18.3	13.4	22.4	5.3	12.7	10.0	6.1	3.2
Ilmeno-magnetite	86.8	67.4	79.6	82.5	77.6	92.6	87.3	90.0	89.8	90.5
Ulv+Pleonaste Mag	2.2	6.3	2.2	4.1	0.0	2.1	0.0	0.0	4.1	6.3

- = not observed
r = trace amounts
* < 1 %
** 1-10 %
*** 10-25 %
**** 25-50 %
***** > 50 %

Table 7.5 (cont.)

	DOLERITES												
Oxide Grain Types	VD1	VD2	VD3	D6	D8	PTA 3	PTA 4	LHD3	LRRD2	DM90-18	DM90-6	DM90-8	DM90-2
Ilmenite	58	43	59	22	34	19	22	25	22	20	38	28	1
vermiform ilmenite	**	*	-	*	**	-	-	*	*	**	**	-	
skeletal ilmenite	***	**	**	**	***	**	**	**	**	**	**	*	*
Ilm-Hem	-	-	-	-	-	-	-	-	-	-	-	-	
Hem-Ilm	-	-	-	-	-	-	-	-	-	-	-	-	
Hem-Ilm-Rut	-	-	-	-	-	-	-	-	-	-	-	-	
Hem-Rut	-	-	-	-	-	-	-	-	-	-	-	-	
Ilm-(Hem-Rut-Psb)	-	-	-	-	-	-	-	-	-	-	-	-	
(Hem+Rut+Psb)	-	-	-	-	-	-	-	-	-	-	-	-	
(Hem-Psb)	-	-	-	-	-	-	-	-	-	-	-	-	
Hematite	-	-	-	-	-	-	-	-	-	-	-	-	
Magnetite	11	4	6	12	7	11	9	8	14	8	4	2	
skeletal magnetite	**	*	*	**	*	*	*	*	*	*	*	*	
Mt-Usp	4	14	8	3	2	nd	nd	r	3	4	2	3	
Mt-Ilm-Usp	27	39	27	61	56	44	43	67	61	65	56	67	6
trellis	**	**	**	***	***	**	**	***	**	**	**	***	**
sandwich	***	***	**	***	**	****	****	**	****	****	****	***	***
composite	**	***	***	****	****	***	***	****	***	***	****	****	**
Mt-Pleo-Ilm	-	-	-	-	-	-	-	-	-	-	-	-	
Chromite	-	-	-	-	-			-	-	-	-	-	
Cr-Spinel	-	-	-	1	1			-	r	3	-	-	
Rutile	-	-	-	-	-			-	-	-	-	-	
Sphene	-	-	-	-	-			-	-	-	-	-	
Ilm-Sph	-	-	-	-	-			-	-	-	-	-	
Altered grains	nd	nd	nd	nd	nd	26	26	nd	nd	nd	nd	nd	n
Total	100	100	100	99	100	100	100	100	100	100	100	100	10
Per cent of Rock	0.5	0.5	0.5	3	1	nd	nd	2.5	4	4.5	6	8	
Normalised values													
Ilmenite	58.0	43.0	59.0	22.4	34.3	25.7	29.7	25.0	22.0	20.6	38.0	28.0	18.
Magnetite	11.0	4.0	6.0	12.2	7.1	14.9	12.2	8.0	14.0	8.2	4.0	2.0	6.
Mag+ilm+ulv+pleo	31.0	53.0	35.0	65.3	58.6	59.5	58.1	67.0	64.0	71.1	58.0	70.0	76.
Homo magnetite	26.2	7.0	14.6	15.8	10.8	20.0	17.3	10.7	17.9	10.4	6.5	2.8	7.
Ilmeno-magnetite	64.3	68.4	65.9	80.3	86.2	80.0	82.7	89.3	78.2	84.4	90.3	93.1	84.
Ulv+Pleonaste Mag	9.5	24.6	19.5	3.9	3.1	0.0	0.0	0.0	3.8	5.2	3.2	4.2	8.

- = not observed
r = trace amounts
* < 1 %
** 1-10 %
*** 10-25 %
**** 25-50 %

Table 7.5 (cont.)

	GRANITOIDS											
Oxide Grain Types	VG1	VG2	VG3	VG4	VG5	MS17	MS18	UMG	UMG	UMG	UMG	UMG
Ilmenite	35	6	42	80	7	55	80	38	28	53	21	35
vermiform ilmenite	-	-	-	-	-	-	-	-	-	-	-	-
skeletal ilmenite	-	-	-	-	-	-	-	-	-	-	-	-
Ilm-Hem	r	-	r	10	68	r	-	12	8	7	14	21
Hem-Ilm	r	-	-	-	12	-	-	r	4	3	r	6
Hem-Ilm-Rut	-	-	-	-	2	-	-	r	r	-	r	2
Hem-Rut	-	-	-	-	1	-	-	1	3	3	1	1
Ilm-(Hem-Rut-Psb)	4	-	6	8	6	-	-	3	5	4	6	4
(Hem+Rut+Psb)	-	-	-	2	r	-	-	2	1	r	r	r
(Hem-Psb)	-	-	-	-	r	-	-	r	r	-	r	r
Hematite	r	-	-	r	4	-	-	5	6	3	8	12
Magnetite	58	92	46	-	-	40	12	32	38	21	45	12
skeletal magnetite	-	-	-	-	-	-	-	-	-	-	-	-
Mt-Usp	-	-	-	-	-	-	-	-	-	-	-	-
Mt-Ilm-Usp	3	2	6	-	-	5	8	6	4	3	4	3
trellis	-	-	-	-	-	-	-	-	-	-	-	*
sandwich	-	-	*	-	-	*	*	-	-	-	-	-
composite	**	*	**	-	-	*	**	**	**	*	*	*
Mt-Pleo-Ilm	-	-	-	-	-	-	-	-	-	-	-	-
Chromite	-	-	-	-	-	-	-	r	1	-	-	-
Cr-Spinel	-	-	-	-	-	-	-	-	-	-	-	-
Rutile	-	-	-	-	-	-	-	r	2	3	1	3
Sphene	-	-	-	-	-	-	-	1	r	-	-	-
Ilm-Sph	-	-	-	-	-	-	-	r	r	-	-	1
Altered grains	nd	nd	nd	nd	nd	nd	nd	nd	nd	nd	nd	nd
Total	100	100	100	100	100	100	100	100	100	100	100	100
Per cent of Rock	3	1	1.5	0.5	2	0.5	0.5	na	na	na	na	na
Normalised values												
Ilmenite	36.5	6.0	44.7	100.0	100.0	55.0	80.0	50.0	40.0	68.8	30.0	70.0
Magnetite	60.4	92.0	48.9	0.0	0.0	40.0	12.0	42.1	54.3	27.3	64.3	24.0
Mag+ilm+ulv+pleo	3.1	2.0	6.4	0.0	0.0	5.0	8.0	7.9	5.7	3.9	5.7	6.0
Homo magnetite	95.1	97.9	88.5			88.9	60.0	84.2	90.5	87.5	91.8	80.0
Ilmeno-magnetite	4.9	2.1	11.5			11.1	40.0	15.8	9.5	12.5	8.2	20.0
Ulv+Pleonaste Mag	0.0	0.0	0.0			0.0	0.0	0.0	0.0	0.0	0.0	0.0

- = not observed
r = trace amounts
* < 1 %
** 1-10 %
*** 10-25 %

Table 7.5 (cont.)

	AMPHIBOLITES					MAFIC SCHISTS AND GNEISSES				METAMORPHOSED ULTRABASIC		
Oxide Grain Types	NDF 5	VA1	VA2	VA3	VA4	NDF1	VM2	VM3	VM3	VM1	IR1	IR2
Ilmenite	2	5	85	92	22	3	5	81	4	20	15	25
vermiform ilmenite	-	-	-	-	-	-	-	-	-	r	-	-
skeletal ilmenite	-	-	-	-	-	-	-	-	-	-	-	-
Ilm-Hem	-	-	-	-	-	-	-	4	-	-	-	-
Hem-Ilm	-	-	-	-	-	-	-	-	-	-	-	-
Hem-Ilm-Rut	-	-	-	-	-	-	-	-	-	-	-	-
Hem-Rut	-	-	-	-	-	-	-	-	-	-	-	-
Ilm-(Hem-Rut-Psb)	-	-	-	-	-	-	-	r	-	-	-	-
(Hem+Rut+Psb)	-	-	-	-	-	-	-	-	-	-	-	-
(Hem-Psb)	-	-	-	-	-	-	-	-	-	-	-	-
Hematite	-	-	-	-	-	-	-	r	-	-	-	-
Magnetite	92	87	9	4	70	4	6	8	84	6	r	r
skeletal magnetite	-	-	-	-	-	-	-	-	-	-	-	-
Mt-Usp	-	-	-	-	-	-	-	-	-	r	r	r
Mt-Ilm-Usp	6	8	6	4	8	-	-	7	12	2	r	r
trellis	-	-	-	-	-	-	-	-	-	-	-	-
sandwich	-	-	-	-	-	-	-	-	-	*	*	-
composite	**	**	**	**	**	-	-	**	**	*	-	*
Mt-Pleo-Ilm	-	-	-	-	-	-	-	-	-	72	85	75
Chromite	-	-	-	-	-	r	r	-	-	-	-	-
Cr-Spinel	-	-	-	-	-	-	-	-	-	-	-	-
Rutile	-	-	-	-	-	80		-	-	-	-	-
Sphene	-	-	-	-	-	13	1	-	-	-	-	-
Ilm-Sph	-	-	-	-	-	-	88	-	-	-	-	-
Altered grains	nd	nd	nd	nd	nd	nd	nd	nd	nd	nd	nd	nd
Total	100	100	100	100	100	100	100	100	100	100	100	100
Per cent of Rock	2	0.5	0.5	1	1	0.5	1	2	4	80	> 70	> 70
Normalised values												
Ilmenite	2.0	5.0	85.0	92.0	22.0	42.9	45.5	84.4	4.0	20.0	15.0	25.0
Magnetite	92.0	87.0	9.0	4.0	70.0	57.1	54.5	8.3	84.0	6.0	0.0	0.0
Mag+ilm+ulv+pleo	6.0	8.0	6.0	4.0	8.0	0.0	0.0	7.3	12.0	74.0	85.0	75.0
Homo magnetite	93.9	91.6	60.0	50.0	89.7	100.0	100.0	53.3	87.5	7.5	0.0	0.0
Ilmeno-magnetite	6.1	8.4	40.0	50.0	10.3	0.0	0.0	46.7	12.5	2.5	0.0	0.0
Ulv+Pleonaste Mag	0.0	0.0	0.0	0.0	0.0	0.0	0.0	0.0	0.0	90.0	100.0	100.0

- = not observed
r = trace amounts
* < 1 %
** 1-10 %
*** 10-25 %
**** 25-50 %

The higher fO_2 in felsic rocks increases the Fe^{3+}:Fe^{2+} ratio, forming magnetite with compositions close to the Fe_3O_4 end-member. Extensive ilmenite-hematite solid-solutions are also common and the slow cooling of felsic plutonic rocks results in the exsolution of hematite from ilmenite and *vice-versa*. The high proportions of homogeneous ilmenite and magnetite in metamorphic rocks is attributed to the re-crystallisation and re-equilibration of the iron-titanium oxides during metamorphism. Ilmenite is unstable in weakly metamorphosed rocks and breaks down to rutile (Ferry, 1984), or titanite (Cassidy and Groves, 1988), but may re-form from these minerals in the mid-greenschist facies (Cassidy and Groves, 1988). This break down and re-crystallisation of ilmenite results in the destruction of ilmeno-magnetite grains and hence their scarcity in metamorphic rocks, as noted by Rumble (1976) and Frost (1991b). Reported occurrences of magnetite-ilmenite intergrowths are either from sillimanite or higher grade rocks, or from partially re-crystallised igneous rocks (Rumble, 1976).

7.7.3 The application of the ilmenite-magnetite diagram

The large differences in the proportions of the major iron-titanium oxides from various source areas, shown in Figure 7.11, indicate that this discrimination diagram is a good means of determining the provenance of the oxides found in coastal sediments. For example, high proportions of homogeneous magnetite in sediments would indicate that the oxides were derived from basement rocks, notably amphibolites or magnetite-bearing quartzite.

To test the usefulness of the ilmenite-magnetite diagram, the normative proportions of ilmenite, magnetite and Mt-$Ilm_{oe}\pm Usp_{ex}$ from selected coastal sediments, and rivers feeding these sediments (Table 7.6), are plotted on the ilmenite-magnetite diagram in Figure 7.12. Most of the dune and beach samples plot close to the ilmenite apex, within the Natal Basement field. If this were the only data plotted, it would suggest that the Karoo Igneous rocks make little contribution to the ilmenite and magnetite in coastal sediments. However, the distribution of the river samples indicates that the relative proportions of the oxides is not so much a function of provenance, but rather the

differences in durability of ilmenite and magnetite. The composite grains of Mt-$Ilm_{oe}\pm Usp_{ex}$ break down during transportation and sedimentary re-working, as noted by Molinaroli and Basu (1987). This results in a greater number of homogeneous grains, and a shift towards the ilmenite-magnetite axis. In addition, magnetite is less stable than ilmenite in the sedimentary environment (Dryden and Dryden, 1946; Pettijohn, 1957; Darby, 1984) and the oxide assemblages are expected to shift towards the ilmenite apex with increasing sediment maturity and age.

The Tugela River provides a good example of the evolution of the oxide assemblages (Figure 7.13). At the source of the river the oxide assemblage plots close to the Mt-Ilm-Usp apex, as the main source is the basalts of the Natal Drakensburg. Further down the river the oxides plot in a more central position, within the field of the Karoo dolerites as these rocks are the major source. Once the river runs through the Natal Basement rocks, there is a large deviation towards the homogeneous magnetite apex as this is the dominant mineral from these rocks. At the mouth of the river, homogeneous magnetite accounts for almost 70 per cent of the oxide assemblage. The sediment movement is northwards along this stretch of coastline (Flemming, 1981), and the shoreline between the Tugela River mouth and Mtunzini is the only prograding shoreline along the east coast (McCarthy, 1988a). The magnetite content in samples of coastal sediments in this region is soon reduced and the oxide assemblages plot close to the ilmenite apex. This is caused by either the destruction of magnetite along the high energy coastline, or the dissemination of the magnetite into existing heavy mineral suites containing much larger quantities of ilmenite, as discussed in Chapter 8.

The above indicates that the proportions of ilmenite and magnetite in coastal sediments may be very different from that found in their source rocks and that the ilmenite-magnetite discrimination diagram is inappropriate to provenance studies. It also suggests that the method of Basu and Molinaroli (1989, 1991) would give misleading results if applied in the study area.

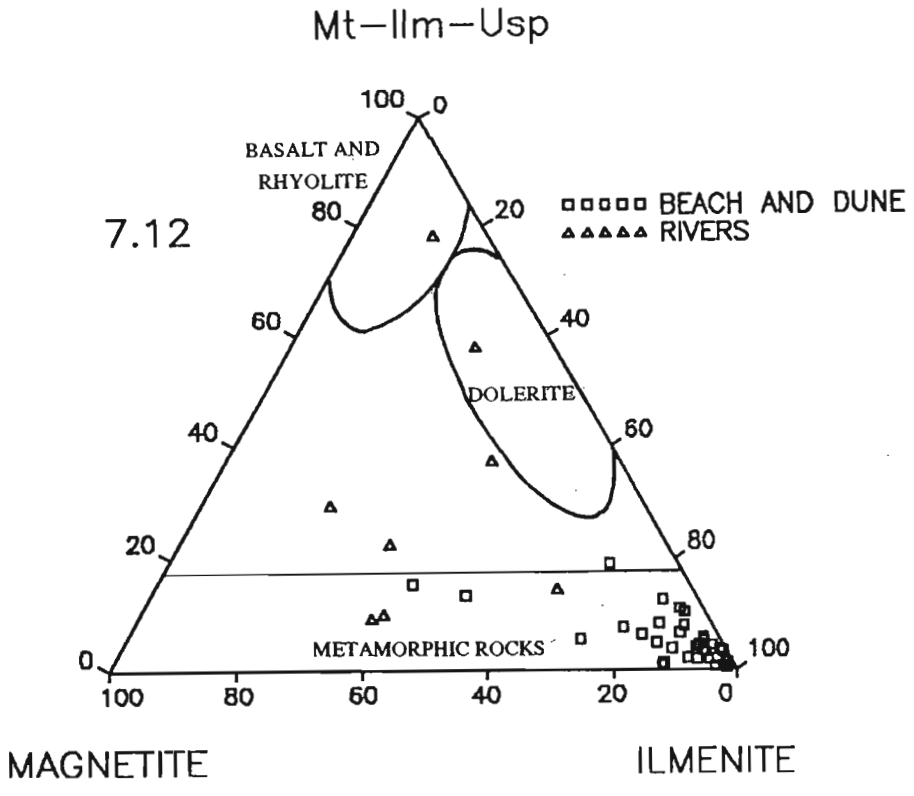

Figure 7.12 The proportions of magnetite, ilmenite and Mt-Ilm_{oe}-Usp_{ex} from selected coastal sediments plotted on the ilmenite-magnetite discrimination diagram. Data is derived from Table 7.6.

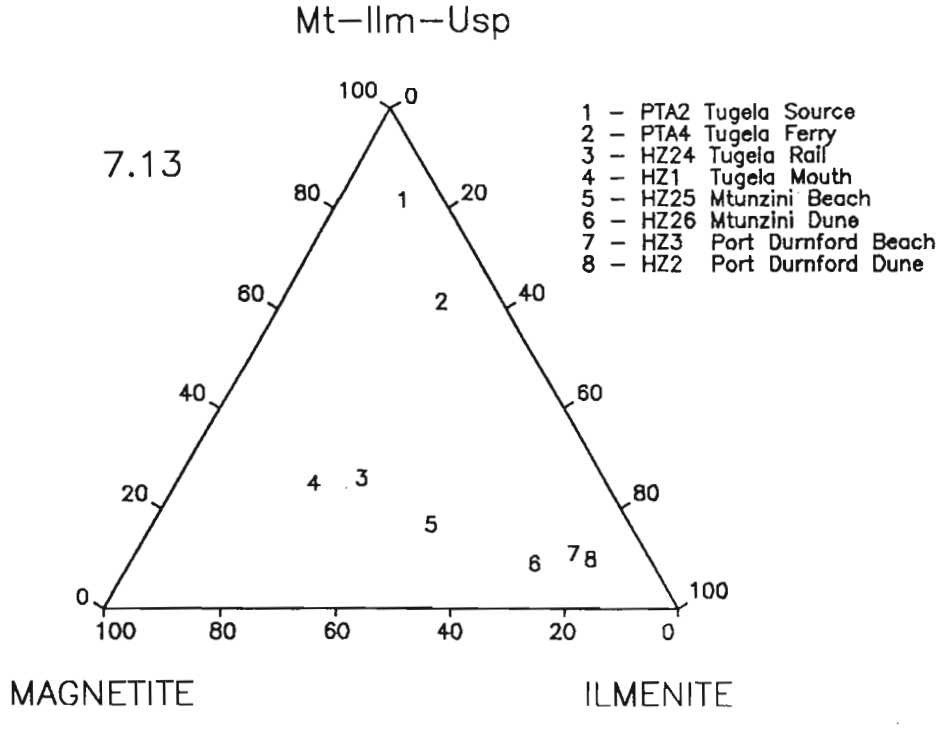

Figure 7.13 Plot of magnetite, ilmenite and Mt-ilm_{oe}-Usp_{ex} from selected sediments related to the Tugela River on the ilmenite-magnetite diagram.

TABLE 7.6 Normative ilmenite and magnetite values of coastal sediments and rivers, shown in Figure 7.12

Sample	Normative Ilmenite	Normative Magnetite	Mt-Ilm-Usp	Mt-Ilm-Us	Normative Homo Magn	Mt-Pleo +Mt-Usp +Chrom
HZ 4	91.3	4.5	4.2	47.2	51.7	1.1
HZ 5	93.5	3.3	3.1	45.3	51.6	3.2
HZ 13	87.5	4.6	7.9	59.8	37.1	3.1
HZ 10	92.6	5.4	2.0	26.5	73.5	0.0
HZ 9	91.7	2.6	5.8	67.0	30.9	2.1
HZ 17	84.8	10.2	4.9	22.1	67.4	10.5
HZ 3	77.8	14.5	7.7	29.6	65.3	5.1
HZ 8	92.9	3.6	3.5	48.4	50.5	1.1
HZ 12	70.0	10.9	19.1	63.8	36.2	0.0
HZ 2	81.4	12.1	6.5	21.1	65.3	13.7
HZ 1	25.3	53.0	21.7	16.5	77.1	6.4
HZ 6	91.7	3.9	4.5	50.5	46.5	3.0
HZ 25	50.0	36.5	13.5	17.0	73.0	10.0
HZ 26	72.0	22.4	5.6	11.0	80.0	9.0
HN 18	96.8	1.4	1.9	54.0	42.0	4.0
HN 4	87.5	8.6	3.9	30.0	69.0	1.0
HN 7	92.2	2.7	5.1	64.0	35.0	1.0
HN 1	93.9	1.7	4.4	72.0	28.0	0.0
HN 5	98.0	0.5	1.4	71.7	26.3	2.0
HN 8	94.6	3.5	1.9	34.7	64.3	1.0
HN 27	98.1	1.4	0.5	26.0	74.0	0.0
HN 30	87.5	11.6	0.9	2.0	92.9	5.1
HN 10	83.3	8.3	8.3	47.9	50.0	2.1
HN 12	95.5	1.0	3.6	73.0	21.0	6.0
HN 34	87.5	11.2	1.3	8.2	89.7	2.1
HN 26	97.6	1.8	0.6	21.6	74.2	4.1
HN 15	90.9	6.9	2.2	19.6	76.3	4.1
HT 3	81.8	5.5	12.6	67.4	30.4	2.2
HT 7	97.0	0.8	2.2	57.3	27.1	15.6
HT 2	87.5	5.8	6.7	52.5	46.5	1.0
HT 11	86.2	3.4	10.4	61.3	24.7	14.0
HT 1				48.9	37.8	13.3
HT 10	93.8	1.9	4.4	63.0	27.0	10.0
HEC 5	96.2	0.5	3.2	84.6	14.3	1.1
HEC 2	96.0	0.6	3.4	83.0	16.0	1.0
HEC 3	85.3	3.7	11.0	74.0	25.0	1.0
HEC 4	97.9	0.8	1.3	60.0	40.0	0.0
HEC 6	98.3	1.0	0.6	38.5	61.5	0.0
River Samples						
HN 34	38.5	51.4	10.1	18.9	76.6	4.5
HZ 14	20.5	50	29.5	35.9	60.9	3.2
HZ 24	33.3	44	22.7	29.4	56.8	13.7
HZ 31	36.9	53.8	9.3	13.8	80.2	6.0
HT 6	63.9	21.3	14.6	52.9	39.7	7.4
HEC 9	42.5	20.8	37.5	59.2	32.9	7.9
PTA 2	13	8.7	78.3	87.3	12.7	0.0
PTA 4	29.7	12.2	58.1	82.7	17.3	0.0

Sample localities are given in Appendix A.

7.7.4 The Magnetite discrimination diagram

The problem caused by the different stabilities of magnetite and ilmenite in rivers and coastlines may be partly overcome by using a single oxide species to determine provenance by petrographic means. Grigsby (1990) used variations in magnetite petrography to distinguish various source rocks. Figure 7.14 is a plot of the magnetite data using ternary diagram of Grigsby (1990). The diagram indicates that clear distinctions may be made between magnetites from:

1. mafic and felsic metamorphic rocks;
2. basalt, dolerite and rhyolite;
3. plutonic basic rocks;
4. metamorphosed ultrabasic-basic rocks.

Figure 7.15 is from Grigsby (1990) and shows that the fields for the different rock types from this study are similar to his fields, although he found more homogeneous magnetite in his mafic volcanic and ultramafic complexes. Grigsby (1990) used sediments derived from the source rocks, and not the rocks themselves, to determine his mineral proportions and this may explain the differences between the two studies. More data is required to define the fields more accurately.

7.7.5 Application of the magnetite discrimination diagram

The usefulness of the magnetite diagram was tested by plotting data (Figure 7.16) from the same sedimentary samples used in the ilmenite-magnetite diagram (Table 7.6). Most of the data plot along the homogeneous magnetite - Mt-Ilm-Usp axis, within the field of mixing. This suggests that the Karoo Igneous Province (basalts and dolerites) and the Natal Basement rocks contribute to the magnetite in coastal sediments. A few samples plot in the field of plutonic igneous rocks and a number of other samples clearly contain magnetites from metamorphosed basic-ultrabasic complexes. This data is far more consistent with the results of the magnetite chemistry than the ilmenite-magnetite discrimination diagram (Figure 7. 11) data. This suggests that the magnetite

discrimination diagram is useful for the interpretation of the effect of provenance on variations in oxide proportions in coastal sediments. The diagram is also applied in Chapter 8.

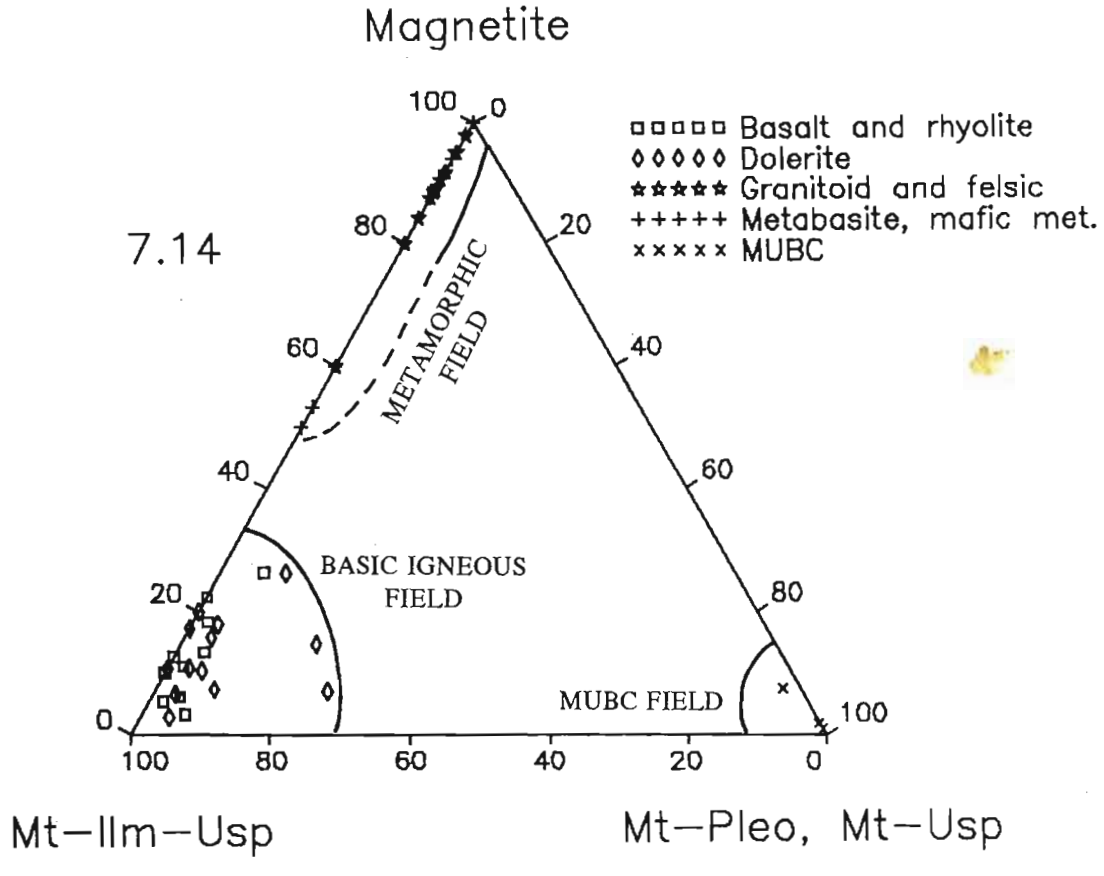

Figure 7.14 The magnetite discrimination diagram, which is a plot of the relative proportions of homogeneous magnetite, Mt-Ilm_{oe}-Usp_{ex} and Mt-$Pleo_{ex}$ + Mt-Usp_{ex}. The plot clearly shows that different source rocks can be distinguished by the proportions of magnetite textures.

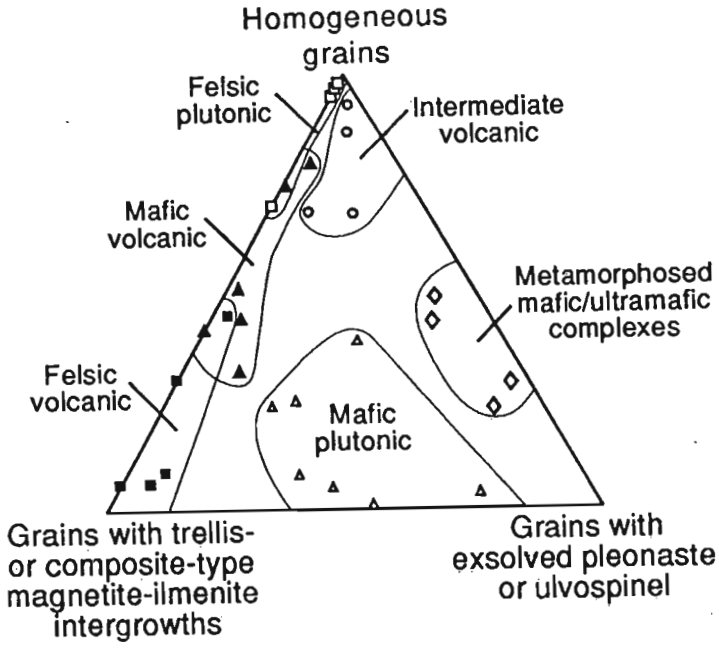

Figure 7.15 Fields for the different rock-types studied by Grigsby (1990).

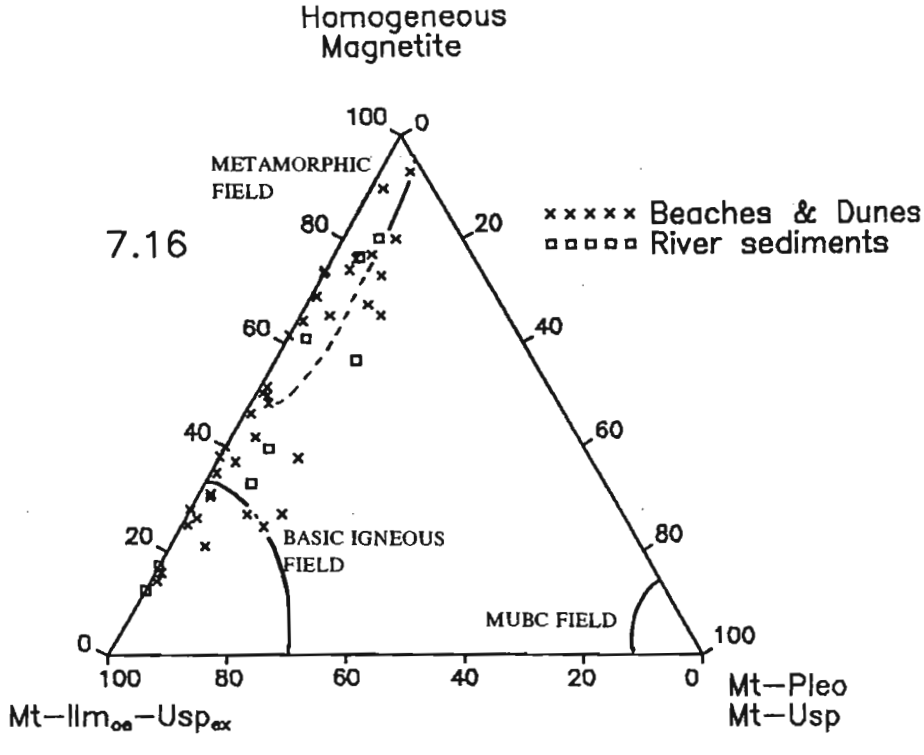

Figure 7.16 Magnetite textural proportions form selected coastal sediments (Table 7.6) plotted on the magnetite discrimination diagram. See text for explanation.

7.8 CONCLUSIONS

The following conclusions are made from the above study of ilmenites and magnetites in probable source rocks:

1. Ilmenite from certain rock groups may be distinguished on the basis of chemical composition, however there are large areas of overlap between ilmenite from basalt and dolerite, and those from a variety of metamorphic rocks. It is possible that trace element chemistry may be able to distinguish ilmenites from these rock types. The only study of trace element chemistry of ilmenite from different rock types was performed by Borisenko and Lyanpunov (1984), and therefore there is little data available to substantiate this.
2. A plot of MnO versus MgO, on a log scale, is the best discriminator of ilmenite provenance, although this diagram effectively only distinguishes ilmenite from granitoids (and other felsic rocks), and ultrabasic/basic plutonic rocks from other rock types.
3. Magnetite from basic igneous rocks is readily distinguished from basement rocks using Al_2O_3, TiO_2, and Fe_2O_3. Magnetite from granitoids and metamorphic rocks cannot be distinguished by minor oxide chemistry.
4. Ilmenite and magnetite from the two major, primary provenances can be identified. In addition, specific source rock types within these areas may be identified using magnetite or ilmenite chemistry.
5. The petrographic textures of the iron-titanium oxides may be used as a provenance indicator as the proportions of the different oxide intergrowths vary markedly between the different major source rocks. In addition, some intergrowths are found almost exclusively in certain source rocks, providing a clear indication of provenance.
6. Although discrimination diagrams based on textural proportions distinguish different source rocks, these diagrams should be used with caution in provenance interpretation, as the oxide proportions change with transport and weathering.
7. The ilmenite-magnetite diagram is inappropriate for provenance studies, but the magnetite discrimination diagram has application.

8. The fields drawn on the discrimination diagrams are not absolute, and the addition of further data will alter the fields.
9. Magnetite in coastal sediments appear to be derived from the basalt and dolerite of the Karoo Igneous Province and the Natal Basement rocks in approximately equal proportions.
10. Ilmenite in coastal sediments is derived mainly from the dolerite and basalt of the Karoo Igneous Province, and the mafic rocks of the Natal Basement. The larger area of outcrop of the former indicates that more ilmenite is derived from these rocks.

The dual provenance of ilmenite and magnetite in coastal sediments along the east coast of South Africa is unique and contradicts authors who state that the provenance of major heavy mineral placer deposits is metamorphic basement rocks (Baxter, 1977; Macpherson and Masters, 1983; Force, 1991).

CHAPTER EIGHT

IRON-TITANIUM OXIDE VARIATIONS IN COASTAL SEDIMENTS

8.1 INTRODUCTION

Variations in the proportion, chemical composition and petrographic texture of iron-titanium oxides, and other minerals, in coastal sediments are caused by differences in provenance; sediment type (eg. beach or dune); age of the deposit; and the physical and chemical environment of the deposit, which affects the weathering of minerals. This chapter describes these variations within the study area and evaluates the influence of the above factors. The effect of regional variations on ilmenite quality is also examined. Finally, a model is proposed to explain the genesis of the mineral assemblages and the formation of the heavy mineral deposits.

8.2 VARIATIONS IN DUNES AND BEACHES

As described in Chapter 3, heavy minerals are found mainly in beach and dune deposits along the south-east African coast. The major economic heavy mineral deposits are found in aeolian sediments, but a number of potential deposits have been located in present-day beaches along the Transkei coast (See Table 3.1, page 46).

8.2.1 The Heavy Mineral Suites

The average mineral proportions, together with minimum and maximum values, for the four major geographical regions are given in Table 8.1 and illustrated in Figure 8.1 (full results are given in Appendix D). The data shows that in nearly all the regions the ilmenite content is higher in dunes, while the pyribole content is higher in beaches. The exception is the eastern Cape, where the proportions of these minerals are similar in both sediment types. Most other heavy minerals are found in the sediments in minor amounts and little difference in their proportions is noted between the beach and dune sediments.

Table 8.1 Average modal proportions of minerals in the heavy mineral suite from beaches and dunes for each of the four major regions in the study area. The range is given in brackets. Full modal analyses are given in Appendix D.

Mineral Grain	HEC B n = 7	HEC D n = 5	HT B n = 5	HT D n = 8	HN B n = 12	HN D n = 8	HZ B n = 7	HZ D n = 10
Ilmenite	38 (15-56)	41 (32-59)	24 (14-36)	41 (23-65)	20 (7-41)	35 (20-52)	15 (5-25)	27 (14-35)
Alt ilmenite	4 (2-7)	4 (2-6)	3 (2-5)	5 (3-10)	4 (2-8)	6 (2-12)	4 (3-7)	8 (4-15)
HAI	1 (1-3)	2 (1-3)	2 (1-3)	1 (0-2)	2 (1-4)	2 (1-4)	1 (1-3)	2 (1-5)
$(Ilm\text{-}Hem)_{ex}$	p	p	1 (1-1)	p	2 (0-5)	1 (0-5)	p (0-1)	1 (1-2)
$(Hem\text{-}Rut)_{ox}$	p	p	p	p	1 (0-3)	1 (1-2)	p (0-1)	1 (0-3)
$Ilm\text{-}(Hem\text{-}Rut)_{ox}$	p	p	p	p	1 (0-2)	1 (0-2)	p	p (0-1)
Leucoxene	6 (2-14)	6 (3-12)	2 (2-3)	3 (1-5)	1 (1-3)	2 (1-4)	3 (1-4)	3 (1-6)
Rutile	5 (3-8)	5 (3-8)	4 (2-4)	3 (2-4)	2 (1-3)	2 (1-4)	2 (1-3)	3 (2-5)
Magnetite	4 (1-9)	4 (1-7)	4 (2-8)	4 (2-7)	3 (1-8)	2 (0-6)	3 (1-5)	4 (2-8)
Chromite	p	p	p	p	p	p	p	p (0-1)
Hematite	1 (0-2)	1 (1-1)	1 (1-2)	1 (1-2)	5 (0-19)	2 (0-7)	1 (0-3)	2 (1-4)
Goethite	p (0-1)	p	p	1 (0-9)	1 (0-2)	2 (0-8)	1 (0-4)	1 (0-4)
Zircon	10 (5-18)	8 (5-12)	5 (3-7)	5 (2-10)	4 (1-6)	4 (2-8)	5 (2-8)	8 (3-12)
Monazite	1 (0-1)	p	p	p	p	p	p (0-1)	1 (0-3)
Pyribole	24 (9-38)	22 (10-31)	51 (43-65)	33 (8-67)	44 (10-67)	34 (2-50)	61 (44-75)	36 (23-64)
Garnet	7 (5-10)	5 (3-8)	5 (3-8)	4 (2-7)	11 (2-17)	7 (1-15)	4 (2-5)	3 (1-5)
Apatite	2 (0-4)	p	p	p	p	p (0-2)	p	p
Tourmaline	1 (0-2)	1 (0-2)	p	p (0-2)	p	p (0-2)	1 (0-2)	p
Epidote	p (0-1)	p	p	p	p	p	p (0-2)	1 (1-2)

HEC B = East Cape beaches; HEC D = East Coast dunes; HT B = Transkei beaches; HT D = Transkei Dunes; HN B = Natal beaches; HN D = Natal dunes; HZ B = Zululand beaches; HZ D = Zululand dunes. HAI = Highly altered ilmenite; Pyribole = pyroxene & amphibole; p = often present, but less than 1 per cent of heavy mineral suite. Sample HZ 1 has been excluded from the average of the Zululand beach samples because it contains very high proportions of magnetite.

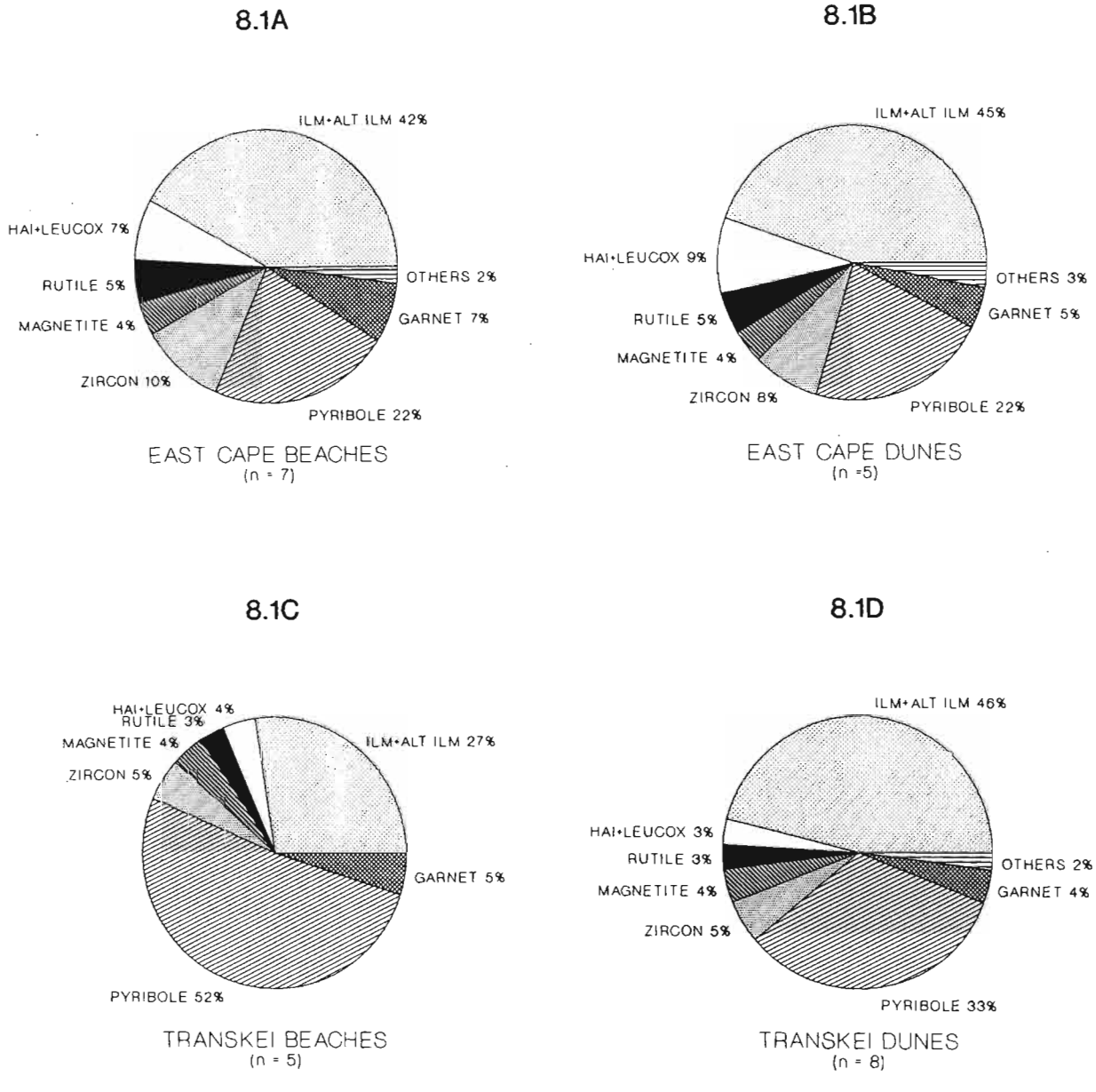

Figure 8.1 Average heavy mineral proportions in beach and dune sediments (Table 8.1) from the different regions in the study area.

8.1E

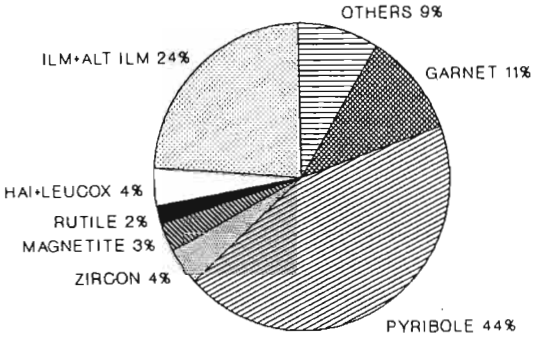

NATAL BEACHES
(n = 12)

8.1F

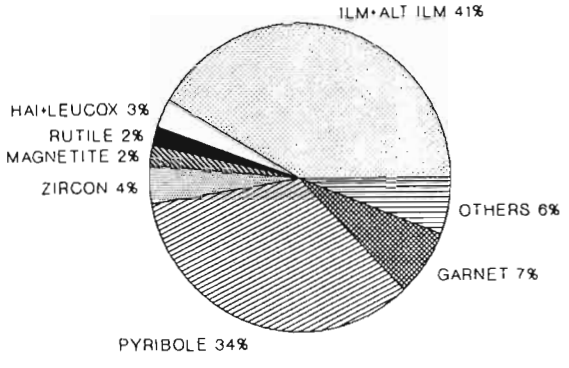

NATAL DUNES
(n = 11)

8.1G

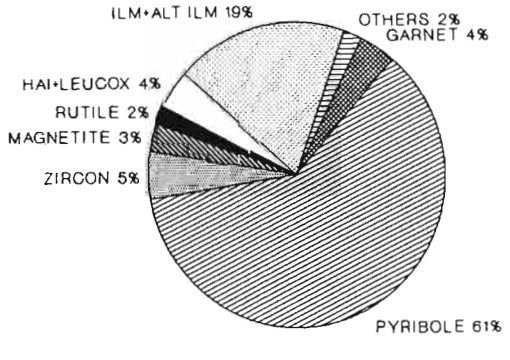

ZULULAND BEACHES
(n = 7)

8.1H

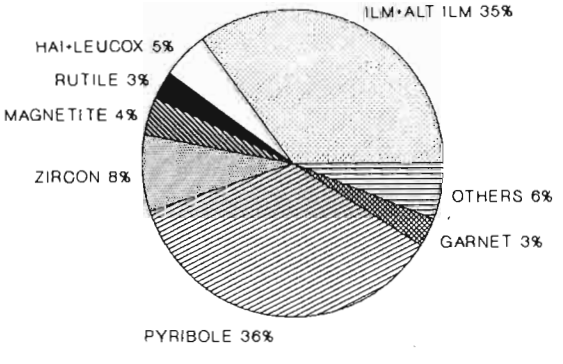

ZULULAND DUNES
(n = 10)

Figure 8.1 (Cont.) Average heavy mineral proportions.

8.2.2 Grain size distribution and mineral proportions

The deposition of sediment in beaches and dunes is caused by very different mechanisms. The energy of wave and current action is far greater than that of wind, thus beaches contain coarser sands than dunes. Prevailing onshore winds winnow the finer sediment from beaches or exposed continental-shelf sediments during periods of marine regression, forming well-sorted aeolian sands. Rubey (1933), in developing the theory of hydraulic equivalence, noted that the proportions of heavy minerals is dependent on the mean grain size of the sediment. Differences in the energy of beach and dune sediments, and hence their grain size distribution, is expected to influence their heavy mineral suites.

The grain size distributions of beaches and dunes were studied to investigate the effect of the energy of deposition on variations in their heavy mineral suites. The grain size distribution of the sediment sample, and its corresponding heavy mineral suite, was determined by screening (Table 8.2). The grain size distributions were plotted on cumulative frequency curves, from which the mode (d_{50}) was read. From Table 8.2 it is noted that the coarsest dune sediment is derived from the coarsest beach and the same applies to the finest beach and dune sediments. This indicates that the grain size of the dunes is related to both the strength of the prevailing on-shore winds and the grain size of the source sediment.

Figure 8.2A shows that the grain size distribution of the heavy mineral suite is related to that of the host sediment. A positive, linear correlation is observed, when d_{50} (the mode) values are compared (Figure 8.2B). This indicates that the grain size distribution of the heavy mineral suite is strongly dependent on the grain size of the sediment containing the heavy minerals.

The grain size distributions of garnet and pyribole were determined by point-counting their proportions in different size fractions of a heavy mineral concentrate from Richards Bay, and their cumulative distributions are given in Table 8.3, together with data from Fockema

KEY TO TABLE 8.2

Sample No.	Locality	Sediment Type
HEC 7	Morgan's Bay	Beach
HEC 6	Morgan's Bay	Dune
HT 8	Sandy Point	Dune
HT 3	Port St Johns	Beach
HN 11	Hlatimi	Beach
HN 14	Port Shepstone	Beach
HN 18	Mzumbe	Dune
HZ 25	Mtunzini	Beach
HZ 26	Mtunzini	Dune
HZ 50	Richards Bay	Dune
HZ 13	Sodwana Bay	Dune

HMS = Heavy Mineral Suite

ILM = Ilmenite concentrate

Table 8.2 Grain-size analysis of selected samples. Recorded as cumulative per cent passing.

Sample	Screen size in μm.									
	710	500	355	250	180	125	90	63	50	d 50
HEC 7	0.0	0.0	0.0	2.7	41.7	87.8	97.2	99.9	100.0	170
HEC 7 HMS	0.0	0.0	0.6	5.7	18.2	54.2	97.9	100.0	100.0	130
HEC 7 ILM	0.0	0.0	0.0	0.8	5.0	28.3	80.0	100.0	100.0	120
HEC 6	0.0	0.0	0.2	1.6	31.1	87.8	97.7	100.0	100.0	165
HEC 6 HMS	0.0	0.0	0.0	0.7	5.3	36.2	86.2	98.9	100.0	120
HEC 6 ILM	0.0	0.0	0.0	0.0	0.5	16.4	90.2	100.0	100.0	120
HT 8	0.0	0.0	0.0	0.5	20.9	62.4	93.8	100.0	100.0	180
HT 8 HMS	0.0	0.0	0.0	0.1	4.7	39.9	91.0	100.0	100.0	118
HT 3	0.0	0.1	2.3	26.2	71.7	93.3	99.4	99.9	100.0	215
HT 3 HMS	0.0	0.0	2.9	21.1	56.2	87.5	98.9	100.0	100.0	190
HN 11	1.1	8.0	29.5	72.5	93.7	98.9	99.9	100.0	100.0	310
HN 11 HMS	0.0	0.0	7.8	42.4	75.5	95.2	99.9	100.0	100.0	200
HN 14	0.4	5.5	35.0	84.9	98.5	99.9	100.0	100.0	100.0	325
HN 14 HMS	0.0	2.2	17.6	66.0	95.3	99.5	99.9	100.0	100.0	280
HN 14 ILM	0.0	0.0	0.0	3.2	35.7	79.2	99.0	100.0	100.0	160
HN 18	0.0	0.1	0.3	8.6	58.8	90.4	99.2	99.8	100.0	190
HN 18 HMS	0.0	0.0	0.0	1.3	15.3	67.4	98.2	100.0	100.0	140
HZ 25	2.0	13.5	41.9	79.1	97.0	99.7	99.9	100.0	100.0	330
HZ 25 HMS	0.0	3.8	29.1	52.5	67.6	84.7	98.2	100.0	100.0	255
HZ 26	0.0	0.8	5.9	31.0	78.7	95.8	99.0	100.0	100.0	225
HZ 26 HMS	0.0	1.3	4.4	16.3	62.0	90.3	95.0	99.0	100	200
HZ 19	0.0	0.3	1.9	19.3	72.1	90.7	98.4	99.5	100.0	210
HZ 19 HMS	0.0	0.0	0.1	0.8	8.0	39.5	92.8	100.0	100.0	135
HZ 50	1.1	3.6	22.6	62.8	89.4	98.4	99.6	100	100	280
HZ 50 HMS	0.5	0.8	2.8	10.5	45.9	77	94.5	100	100	170
HZ 50 ILM	0.0	0.0	0.0	1.4	5.0	42.9	95.9	99.8	100.0	130
HZ 13	0.0	0.5	5.0	28.5	75.2	90.4	96.1	100.0	100.0	220

See Key for sample descriptions.

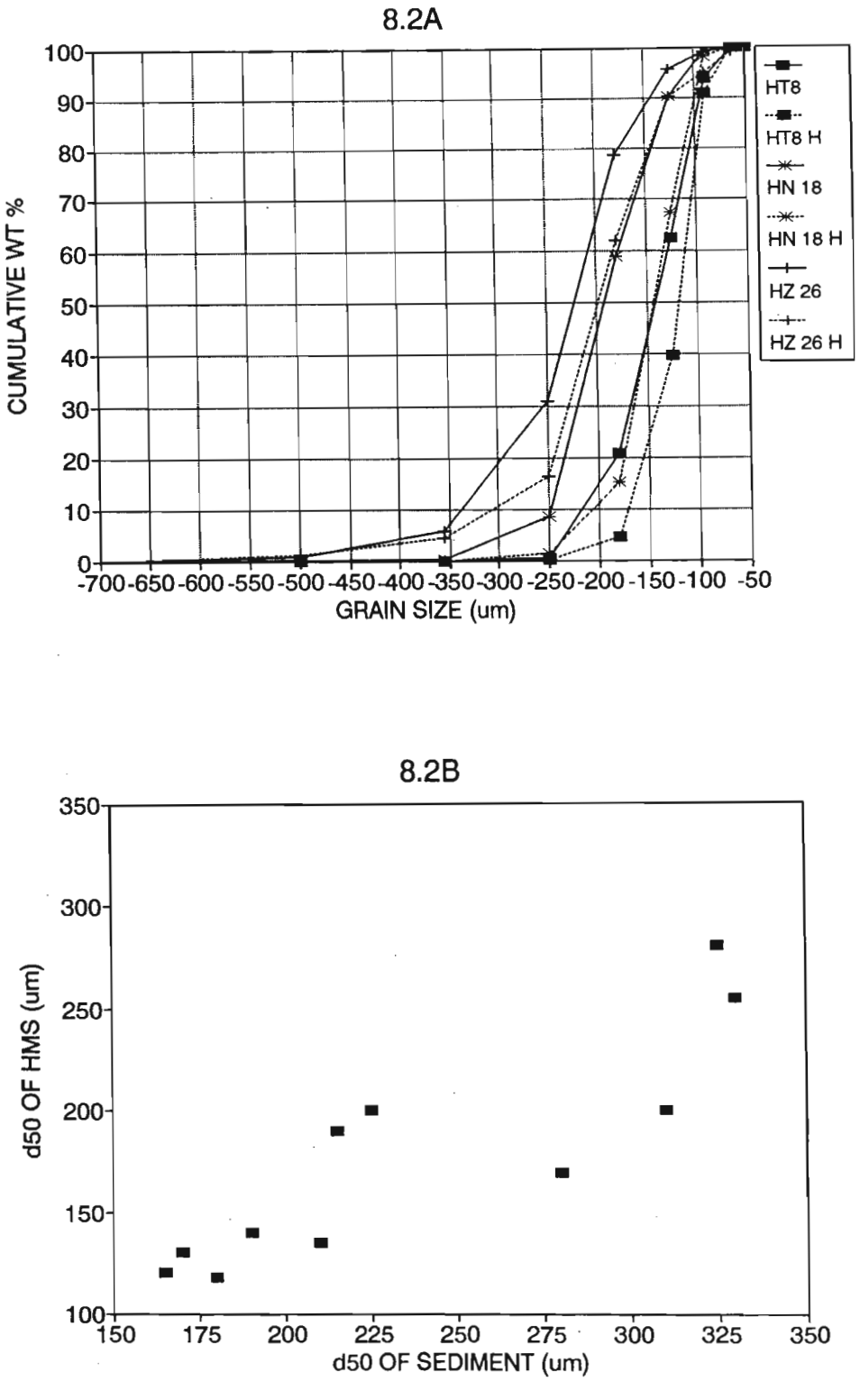

Figure 8.2A. Cumulative frequency distribution curves for sediments and their respective heavy mineral suites (HMS). Sample localities are given in the key to Table 8.2. **B.** A plot of the d_{50} of the HMS versus their host sediment, illustrating the positive correlation between the grain size of the heavy minerals and sediment.

(1986). This table shows that the grain size of garnet and pyribole is distinctly larger than that of ilmenite, rutile and zircon. The amount of ilmenite decreases with increasing grain size of the heavy mineral suite, while there is an antipathetic increase in pyribole content (Figure 8.3). This confirms the findings of Force and Stone (1990), who determined that for a common supply, the proportion of a heavy mineral in the sediment is dependent on the grain size of that mineral in comparison to the grain size of the sediment.

Variations in the relative proportions of heavy minerals from the same provenance, in the beach and dune sediments are caused by selective sorting of these minerals according to the energy of the depositional environment. Ilmenite, zircon and rutile being finer-grained than pyribole, are concentrated in finer sediments. As dunes tend to be finer-grained than beaches, these sediments often contain higher proportions of ilmenite, zircon and rutile.

Table 8.3 Grain size distribution of selected heavy minerals from Richards Bay, expressed as cumulative per cent retained.

Screen Size (μm)	Ilmenite[1]	Rutile[1]	Zircon[1]	Garnet	Pyribole
600				2	0.4
400				12.5	2.4
355				19.8	6.5
250	0.3	0.2	0.9	48.6	22.6
212	1.1	0.6	1.9	64.9	32.6
180	3.6	3.4	7.3	78.8	53.1
150	15.4	20.5	30.2	89.2	67.2
125	34.3	47.2	56.3	97.4	85.7
106	82.4	83.0	86.8	100.0	97.8
90	94.1	93.6	95.8		100.0
75	99.7	98.6	99.3		
-75	100.0	100.0	100.0		

[1] Grain size analysis from Fockema (1986)

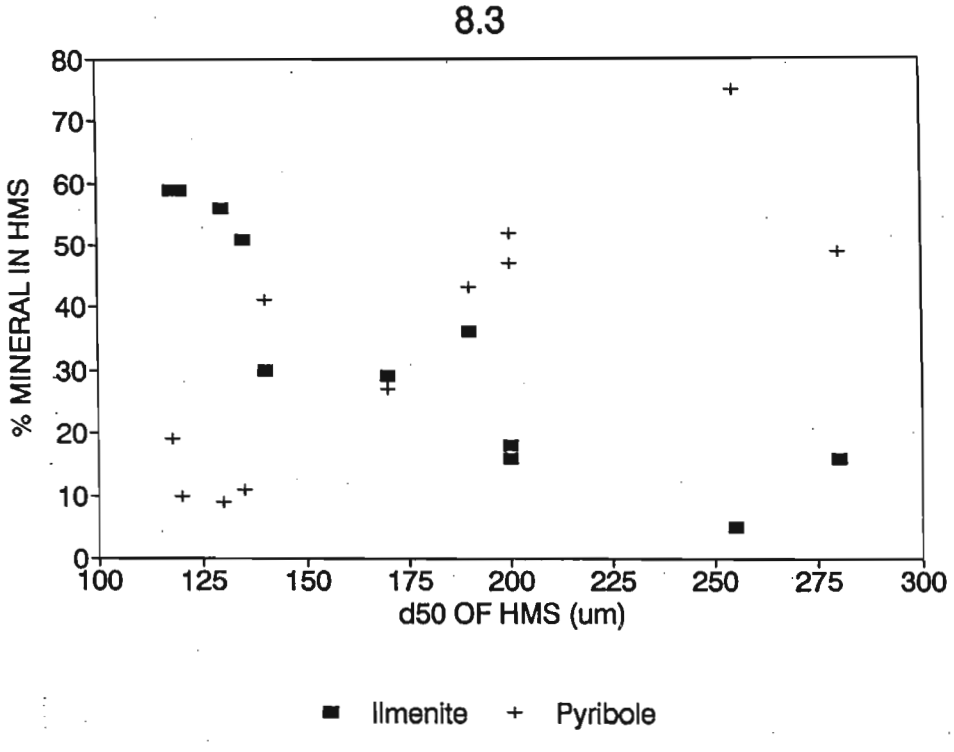

Figure 8.3 Plot of ilmenite and pyribole proportions in the heavy mineral suites given in Table 8.2 versus the d_{50} of the HMS. The plot illustrates the antipathetic behaviour of ilmenite and pyribole with increasing grain size. Modal proportions of the minerals are obtained from Appendix D.

8.2.3 Iron-titanium oxide differences

Figure 8.4 compares the proportions of iron-titanium oxides (calculated from Table 8.1) in the beaches and dunes for each region. Selective sorting of the iron-titanium oxides by wave or wind action is not expected as the minerals have similar densities and grain sizes. Little difference is noted between the sediment types, although the dunes contain more ilmenite and the beaches have more magnetite. The Natal samples (Figures 8.4E and 8.4F) are an exception, as the beach samples contain over 50 per cent more "other oxides" - notably hematite (see Appendix F) - than the dunes.

The proportions of ilmenite and its alteration products in the beach and dune sediment provides further evidence for the multi-stage alteration of ilmenite in the coastal sediments, described in Chapter 6. The beaches contain similar proportions of altered ilmenite grains to the dunes (Figure 8.4). In addition, certain regions, notably the eastern Cape (Figures 8.4A and 8.4B), contain higher proportions of highly altered ilmenites and leucoxenes than altered ilmenite grains, and this is more common in the beach sediments. This may be interpreted in two ways:

1. Assuming the dunes are formed by sand derived from beaches and exposed shelf sediment, then much of the extensively altered ilmenites is not formed *in situ* in the dunes, but is re-worked from other sources.
2. Conversely, the highly altered grains in the beaches may be partly derived from dunes which have been partially eroded during the Flandrian Regression (Johnson, 1986).

Neither interpretation can be proven using the existing data, but both indicate that mixing of unaltered and altered ilmenite has occurred prior to final deposition in the dunes.

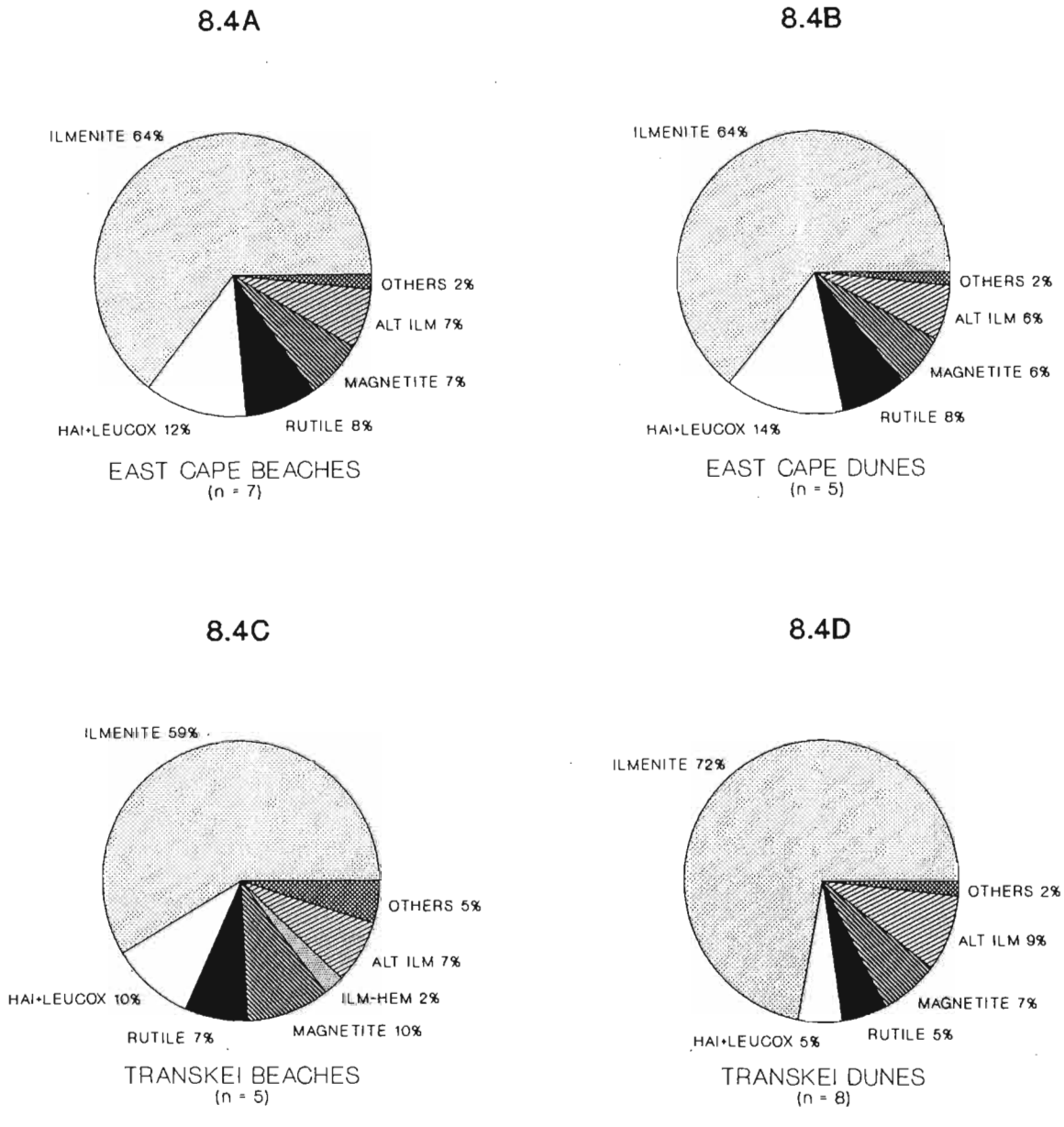

Figure 8.4 Average iron-titanium oxide proportions in beach and dune sediments from the different regions in the study area.

8.4E

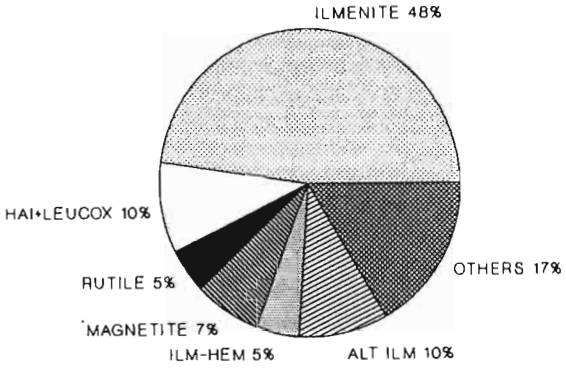

NATAL BEACHES
(n = 12)

8.4F

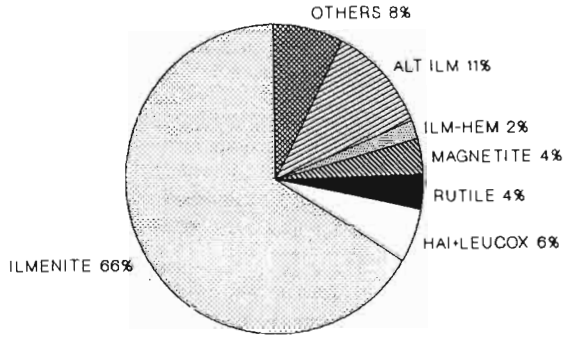

NATAL DUNES
(n = 11)

8.4G

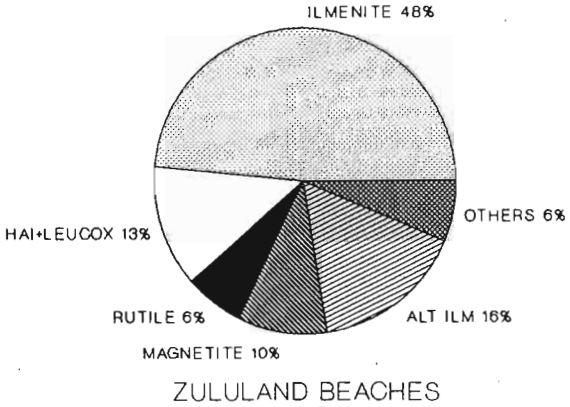

ZULULAND BEACHES
(n = 7)

8.4H

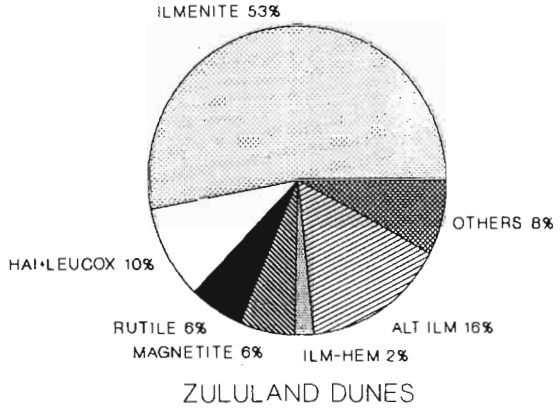

ZULULAND DUNES
(n = 10)

Figure 8.4 (Cont.) Average iron-titanium oxide proportions in beach and dune sediments

8.3 VARIATIONS BETWEEN SEDIMENTS OF DIFFERENT AGES

Heavy minerals in two older aeolian formations were examined to determine the effect of age on the heavy mineral suite. These are the red-brown dune ridges, commonly referred to as the Berea Formation, and the aeolian sequence of the Upper Port Durnford Formation (described in Chapter 3).

8.3.1 Differences in the heavy mineral suites

The proportions of the minerals in the older sediments are given in Table 8.4. The heavy mineral suite of the different sediments are compared in Figure 8.5, which indicates that the red dunes and Port Durnford sands have higher proportions of ilmenite (and altered ilmenite) and zircon, but lower pyribole contents than the Late Pleisocene - Holocene dunes from Zululand and Natal. The Port Durnford samples also contain slightly higher rutile contents (Figure 8.5C). The magnetite content of all three sediment types is similar (Figure 8.5D), although the Port Durnford samples contain little magnetite.

The Port Durnford Formation and red dune sands have slightly finer grain size distributions than the Holocene dunes (Beckering Vinckers, 1986) and the higher proportions of ilmenite, zircon and rutile may be caused by selective sorting of heavy minerals. The highly weathered nature of the older dunes suggests that enrichment of the stable heavy minerals is caused by the removal of ferromagnesian silicates by weathering.

8.3.2 Influence of age and weathering on ilmenite alteration

Many authors have noted that ilmenite alteration increases with the age of the deposit (for example, Temple, 1966; Baxter, 1977; Force, 1991). Given the weathered nature of the older dunes on the Zululand coastal plain, it is expected that the ilmenite in these sediments will be more altered than in the Late Pleistocene-Holocene dunes.

KEY TO SAMPLE LOCALITIES IN TABLE 8.4

Sample	Locality
HT 12	Xamani
HN 13	Htatimi
HN 16	Port Shepstone
HN 19	Mzumbe River mouth
HN 22	Umkomaas
HN 23	Durban North
HN 24	Umhlanga Rocks
HN 25	Ballito Bay
HN 28	Tinley Manor
HN 31	Blythedale Beach
HN 35	Zinkwazi
HZ 27	Mtunzini
HZ 18	Port Durnford
HZ 19	Richards Bay
HZ 40	False Bay, St Lucia
HZ 41	Ridge west of Tshongwe, Zululand coastal plain
HZ 42	Tshongwe
HZ 30	Richards Bay
HZ 43	Lake Sibayi
HZ 44	Lake Sibayi
HZ 45	Sodwana Bay
HZ 46	Charter's Creek, St Lucia
HZ 47	Dukuduku Forest
HZ 9	Mission Rocks
HZ 5	Cape St Lucia
HZ 21	Richards Bay
HZ 22	Richards Bay
HZ 23	Richards Bay
HZ 23	Richards Bay
HZ 51	Richards Bay
HZ 52	Richards Bay

Table 8.4 Proportions of heavy minerals in red dunes and the Port Durnford Formation, determined by point-counting 500 grains per sample (See key for sample localities; sample descriptions are given in Appendix A.2).

Grain Type	Pliocene-Pleistocene Red Dunes																
	HT12	HN13	HN16	HN19	HN22	HN23	HN24	HN25	HN28	HN31	HN35	HZ27	HZ18	HZ19	HZ40	HZ41	HZ42
Ilmenite	52	71	52	64	46	62	55	59	63	66	68	54	50	51	49	37	54
Alt ilmenite	14	3	7	6	7	6	8	10	6	6	5	8	12	9	11	5	8
HAI	2	p	3	1	2	1	2	2	1	2	2	3	1	1	2	1	3
$(Ilm\text{-}Hem)_{ox}$	-	-	-	-		p	p	1	1	2	1	2	3	1	-	1	-
$(Hem\text{-}Rut)_{ox}$	-	-	-	p	1	1	1	p	1	1	1	p	1	-	4	1	1
$Ilm\text{-}(Hem+Rut)_{ox}$	-	-	p	p	1	-	-	-	p	1	p	-	1	-	1	1	1
Leucoxene	4	3	3	2	6	3	8	3	3	2	4	1	1	2	9	3	3
Rutile	9	5	2	2	6	5	6	6	3	2	3	3	5	3	6	4	6
Magnetite[1]	3	4	2	2	5	2	3	1	3	1	1	6	7	3	1	17	7
Chromite	-	p	-	p	-	p	1	-	1	-	p	p	p	p	1	-	-
Hematite	-	2	-	1	1	2	1	2	3	3	3	5	4	2	1	1	1
Goethite	1	1	4	3	5	1	2	1	2	2	p	1	1	1	2	3	-
Zircon	12	9	21	15	10	13	11	10	10	8	8	13	11	13	7	9	11
Monazite	-	-	1	p	-	p	-	p	-	-	-	1	1	1	-	-	-
Pyribole	4	1	2	1	9	1	2	1	2	2	1	2	1	11	5	14	5
Garnet	1	1	2	p	1	p	1	p	1	1	-	1	p	1	1	2	-
Apatite	-	-	-	-	-	-	-	-	-	-	-	-	-	-	-	-	-
Tourmaline	-	-	1	-	2	1	1	1	2	2	2	-	1	-	-	-	-
Epidote	-	-	-	-	-	-	-	-	-	-	-	-	-	1	-	-	-

[1] includes $Mt\text{-}Ilm_{ox}\text{-}Usp_{ex}$, $Mt\text{-}Usp_{ex}$, and $Mt\text{-}Pleo_{ex}\text{-}Ilm_{ox}$ grains; p = less than 1 per cent; - = less than 1 in 500 grains.

Table 8.4 (cont.). Proportions of heavy minerals in beaches and dunes, determined by point-counting 500 grains per sample.

Grain Type	Pliocene-Pleistocene red dunes								Port Durnford Formation				
	HZ30	HZ43	HZ44	HZ45	HZ46	HZ47	HZ9	HZ5	HZ21	HZ22	HZ23	HZ51	HZ52
Ilmenite	40	30	5	28	43	28	33	29	6	14	6	8	12
Alt ilmenite	13	40	49	4	21	8	8	16	55	54	64	43	38
HAI	1	2	2	2	5	2	3	3	3	1	4	8	12
$(Ilm\text{-}Hem)_{ex}$	-	-	-	2	-	-	1	1	1	-	p	p	-
$(Hem\text{-}Rut)_{ox}$	-	-	-	-	-	-	p	p	-	-	-	1	-
$Ilm\text{-}(Hem+Rut)_{ox}$	-	-	-	1	-	-	1	p	-	-	-	-	-
Leucoxene	1	4	11	1	6	5	2	3	11	8	5	8	8
Rutile	2	6	9	2	7	3	3	4	9	7	3	10	8
Magnetite[1]	3	-	-	4	-	-	3	2	1	p	0	2	3
Chromite	-	-	-	-	-	-	p	p	-	-	-	p	-
Hematite	1	-	-	1	1	-	3	1	-	-	-	-	-
Goethite	-	-	-	5	1	45	-	p	-	-	-	-	-
Zircon	8	12	17	7	9	4	5	7	10	11	12	15	13
Monazite	-	-	-	-	-	-	-	p	1	1	1	p	1
Pyribole	28	6	7	40	5	4	32	30	2	4	3	3	1
Garnet	3	-	-	3	2	1	4	3	1	p	p	2	4
Apatite	-	-	-	-	-	-	p	-	-	-	-	-	-
Tourmaline	-	-	-	-	-	-	-	p	1	p	1	-	-
Epidote	-	-	-	-	-	-	1	p	1	p	1	p	-

[1] includes $Mt\text{-}Ilm_{oe}\text{-}Usp_{ex}$, $Mt\text{-}Usp_{ex}$, and $Mt\text{-}Pleo_{ex}\text{-}Ilm_{oe}$ grains; p = less than 1 per cent; - = less than 1 in 500 grains.

The influence of age and weathering on the alteration of ilmenite is examined in Figure 8.6, where the proportions of fresh and altered ilmenite are compared. Ilmenite in the Port Durnford Formation sands is much more altered than in the Late Pleistocene - Holocene sediments. In contrast, most of the red dunes contain no more altered ilmenite grains than the Late Pleistocene-Holocene dunes. The levels of highly altered ilmenite (Figure 8.6B), and leucoxene (Figure 8.6C) are also similar in these older and younger dunes.

The greater proportion of altered ilmenite in the Port Durnford Formation is confirmed by XRF analysis of ilmenite concentrates produced from the different dune types (Table 8.5). Ilmenite from the Holocene and red dunes have similar compositions, whereas the Port Durnford ilmenite has a higher TiO_2 content of about 55 per cent and lower FeO, clearly indicating that alteration has occurred.

Table 8.5 Chemical compositions of ilmenite concentrates from Late Plesitocene-Holocene, Port Durnford Formation and Old Red dunes. Analyses by XRF in RBM laboratories.

Sample Number	Description	TiO_2	FeO[1]	MgO	MnO
HN 5	Holocene dune - Isipingo	48.3	45.8	0.65	1.12
HZ 7	Holocene dune - Mission Rocks	48.3	45.9	0.63	1.22
HZ 17	Holocene dune - Richards Bay	49.1	45.2	0.57	1.3
HZ 18	Red dune - Umhlatuze	49.7	46.2	0.81	0.92
HN 28	Red dune - Tinley Manor	50.5	45.9	0.51	0.88
HZ 30	Red dune - Richards Bay	50.9	45.4	0.62	0.90
HZ 21	Port Durnford Formation - Richards Bay	54.2	40.8	0.61	0.72
HZ 22	Port Durnford Formation - Richards Bay	55.3	39.8	0.45	0.62

[1] All iron reported as FeO

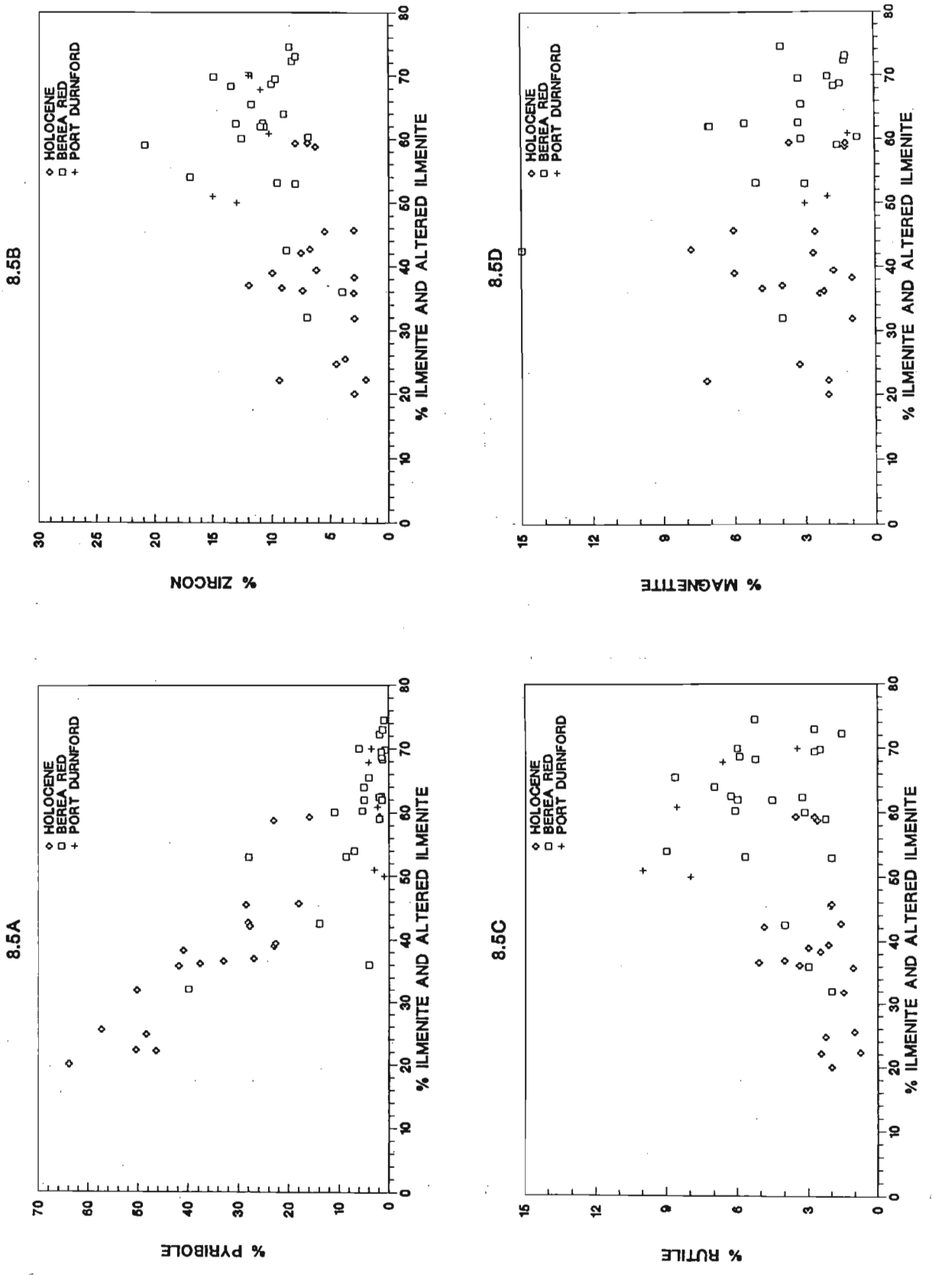

Figure 8.5 Variations in the heavy mineral proportions from sediments of different ages. Late Pleistocene-Holocene dunes are from Natal and Zululand areas.

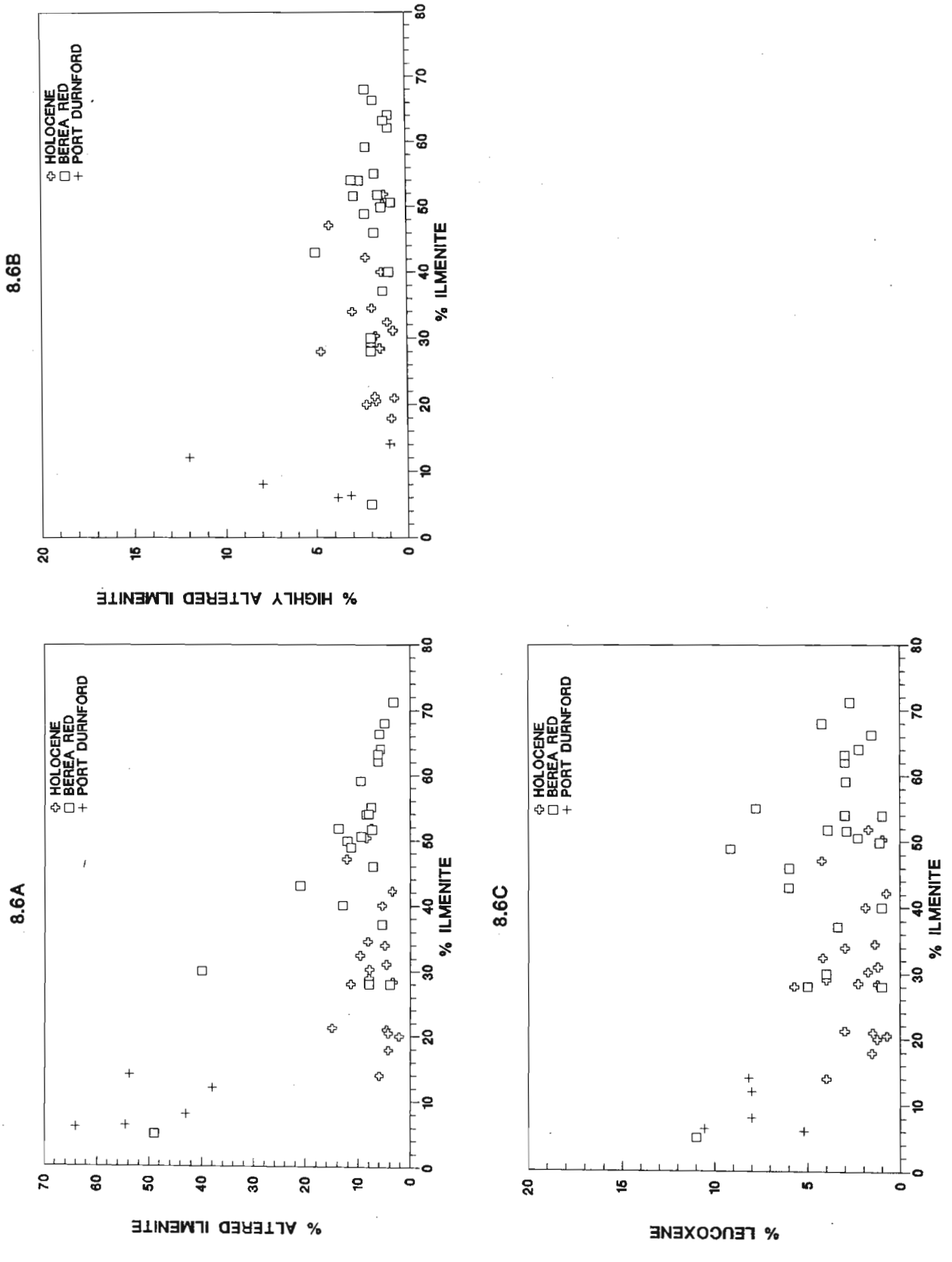

Figure 8.6 Variations in the proportions of fresh and altered ilmenite in sediments of different ages.

8.3.3 Reasons for differences in alteration

Miller and Folk (1955) noted that ilmenite and magnetite are common heavy minerals in redbeds, but are absent in greenish-coloured reduced beds within the redbed sequences. They concluded that ilmenite and magnetite are stable under oxidising conditions, but are dissolved under local reducing conditions after deposition. Dimanche and Bartholomé (1976) noted that the stability of ilmenite, hematite and magnetite is dependent on the pH and Eh of ground water, and showed that hematite and magnetite will dissolve under acidic and reducing conditions, whereas ilmenite will alter under acidic conditions.

The colouration of the red dunes is caused by iron hydroxide coatings on sand grains (Hammerbeck, 1976; Du Preez, 1978; McCarty, 1988b), which were formed by the intense weathering of ferromagnesian silicates during wet, hot climatic conditions (McCarthy, 1988b). The weathering of silicate minerals is also responsible for the high clay contents of these sediments. This re-precipitation of iron-hydroxides indicates that weathering in these sediments proceeded under oxidizing conditions, where ilmenite, hematite and magnetite are stable. In addition, the iron-hydroxides form coatings around the ilmenite grains, which may prevent further alteration (Lissiman and Oxenford, 1973; Baxter, 1986).

The Upper Port Durnford Formation also contains high clay contents from *in situ* alteration of silicates. In the Richards Bay area, the Port Durnford Formation occurs below the water table (Fockema, 1986), and the white, leached appearance of the sediments is due to the removal of iron by acidic, reducing ground waters. These acidic and reducing conditions cause magnetite and hematite to dissolve and ilmenite to alter, as noted by Dimanche and Bartholomé (1976).

The age of the two sediment types is similar and some of the red dunes may be older than the Port Durnford Formation. The unaltered nature of the ilmenite in the red dunes indicates that ilmenite will be preserved in sediments if the Eh and pH are sufficiently

Furthermore, the data indicates that the alteration of ilmenite is more dependent on the physical conditions within the sediment than on the age of the deposit.

8.4 PROVENANCE AND REGIONAL VARIATIONS

Iron-titanium oxides in coastal sediments are ultimately derived from two major source areas - the Karoo Igneous Province and the Natal Basement rocks. The oxides are also re-worked from intermediate sandstones and unconsolidated sands. Source rocks of the Karoo Igneous Province are found throughout the study area, but those of the Natal Basement have a much smaller area of outcrop and are found only in Natal and southern Zululand. Figure 8.4 (page 235) showed that the proportions of iron-titanium oxides in beaches and dunes from the same regions are similar, but that regional variations exist. The extent to which the provenance of the iron-titanium oxides influences these regional variations is investigated here. Both beach and dune samples are studied, but the former are expected to be a closer reflection of the provenance, as these have suffered less mechanical break-down by transportation and sediment re-working.

8.4.1 The influence of provenance on chemical composition

As shown in Chapter 7, ilmenite from different source rocks can be identified using its MnO and MgO contents (see Figure 7.6, page 198). Ilmenite analyses from individual samples within the different regions are plotted in Figure 8.7. All the regions, and most samples studied, contain ilmenite derived from each of the 3 distinguishable source groups. In general, the variation of ilmenite MnO and MgO content is similar for each of the regions. Ilmenite from the eastern Cape (Figure 8.7A) and the Transkei (Figure 8.7B) fall within the basic igneous/metamorphic and the basic plutonic fields and only a small number of grains are derived from granitoid or felsic rocks. Natal (Figure 8.7C) and Zululand (Figure 8.7D) contain more ilmenite derived from granitoids and felsics, suggesting that the influence of these rocks is greater in these areas due to the outcrop of Natal Basement rocks.

Average compositions of ilmenite from the different regions (Table 8.6) are very similar. There is a slight increase in MnO, and corresponding decrease in MgO, from south to north, but otherwise there is little difference in ilmenite compositions along the coastline. This is probably because the majority of ilmenites have low MgO and MnO contents and are close to the ilmenite end-member in composition. There is little regional variation in ilmenite chemistry and provenance has only a minor influence.

It was shown in Chapter 7 that magnetites from different source rocks could be identified by their chemical compositions (Figure 7.9, page 207). The variations in chemistry from different regions are shown in Figure 8.8, which clearly shows that magnetites in the eastern Cape (Figure 8.8A) and Transkei (Figure 8.8B) are derived almost exclusively from the basic igneous rocks of the Karoo Igneous Province. In contrast, over 50 per cent of the magnetites in Natal (Figure 8.8C) and Zululand (Figure 8.8D) are derived from the Natal Basement rocks. This indicates that provenance plays a far greater role in region variations of magnetite compared to that of ilmenite.

Table 8.6 Average compositions of ilmenites from the different regions in the study area, determined by electron microprobe analysis.

Oxide (%)	Zululand	Natal	Transkei	eastern Cape
TiO_2	51.22	50.73	51.01	51.66
Al_2O_3	0.04	0.04	0.04	0.04
Cr_2O_3	0.05	0.04	0.09	0.07
MnO	1.09	0.90	0.80	0.84
MgO	0.58	0.50	0.68	0.69
FeO	43.67	43.76	43.71	44.20
Fe_2O_3[1]	2.56	3.39	2.67	1.90

[1] calculated from stoichiometry

8.7A

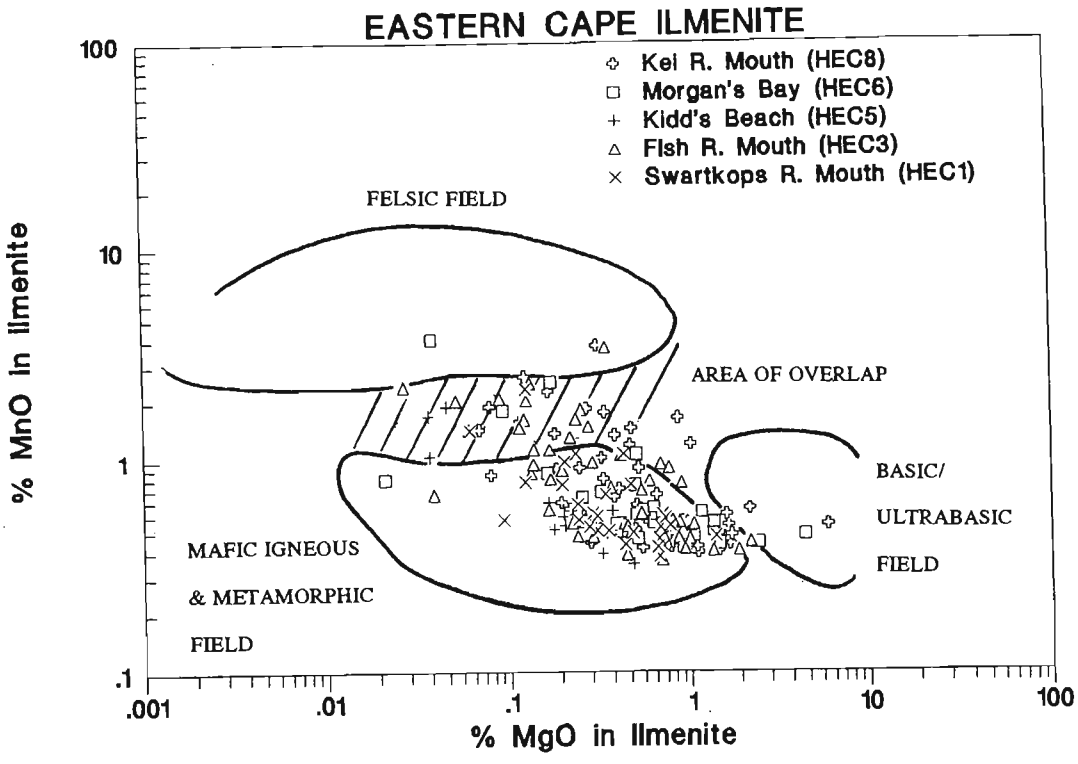

8.7B

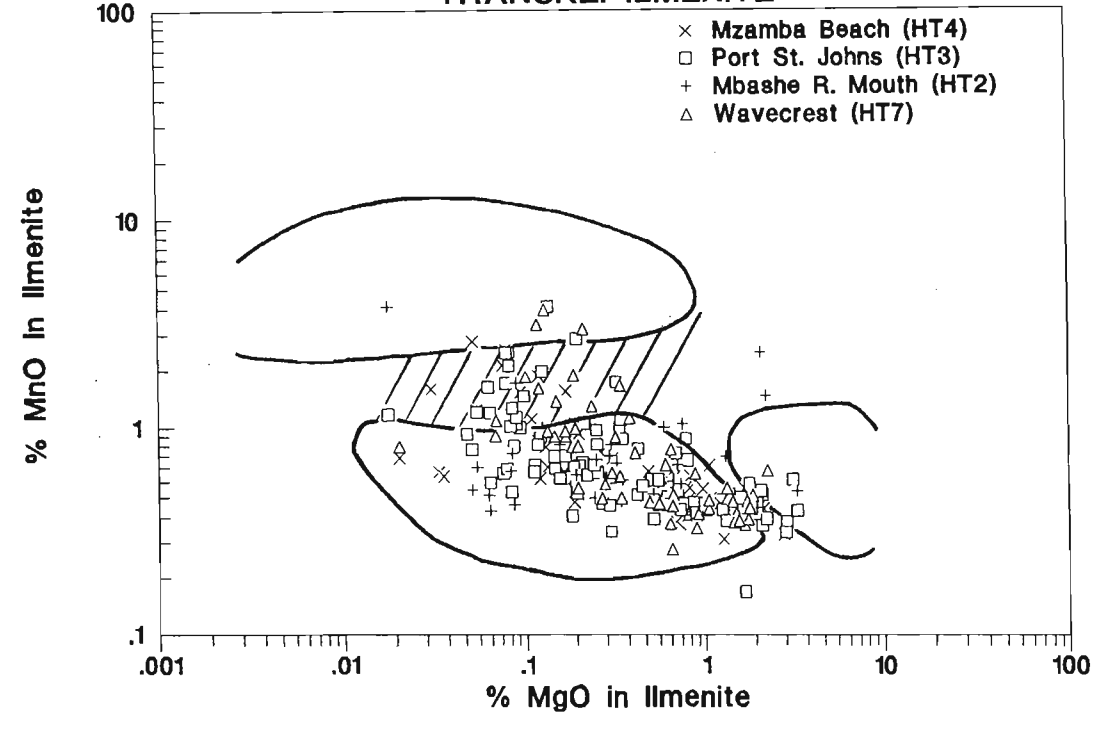

Figure 8.7 Variations in ilmenite MgO and MnO compositions from individual sample localities. The plots indicate from which source rocks the ilmenites are derived and how provenance influences the chemical composition of ilmenite in the different regions. **A.** Eastern Cape samples. **B.** Transkei samples.

8.7C

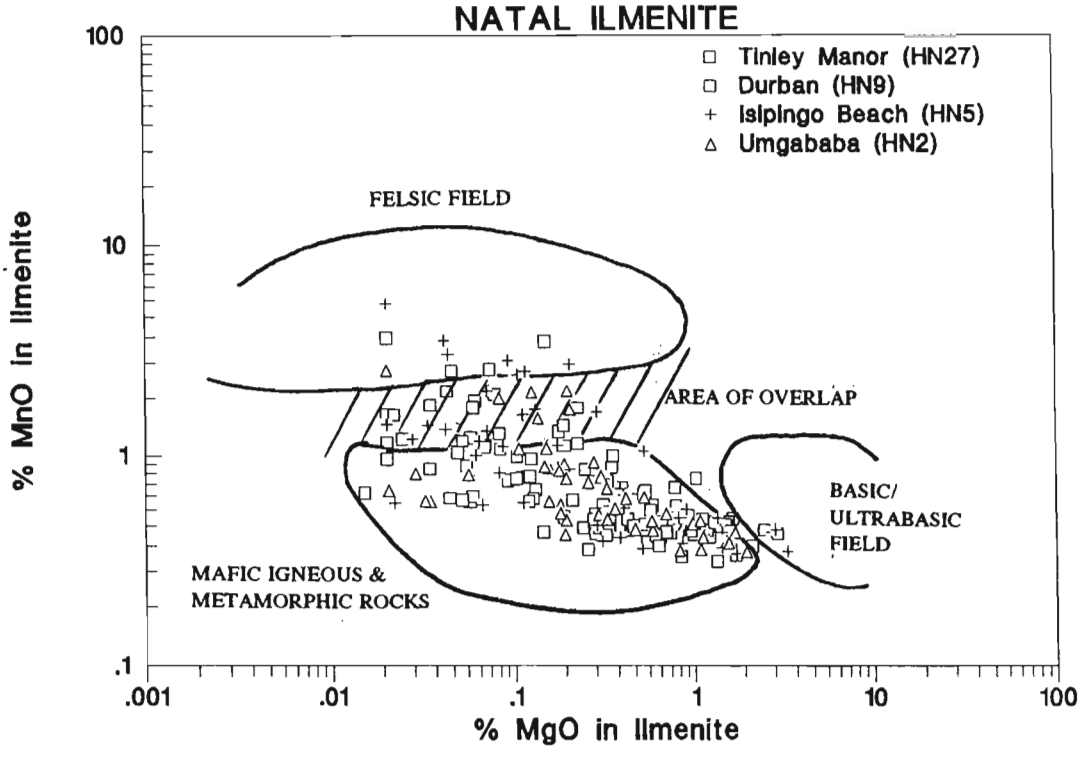

8.7D

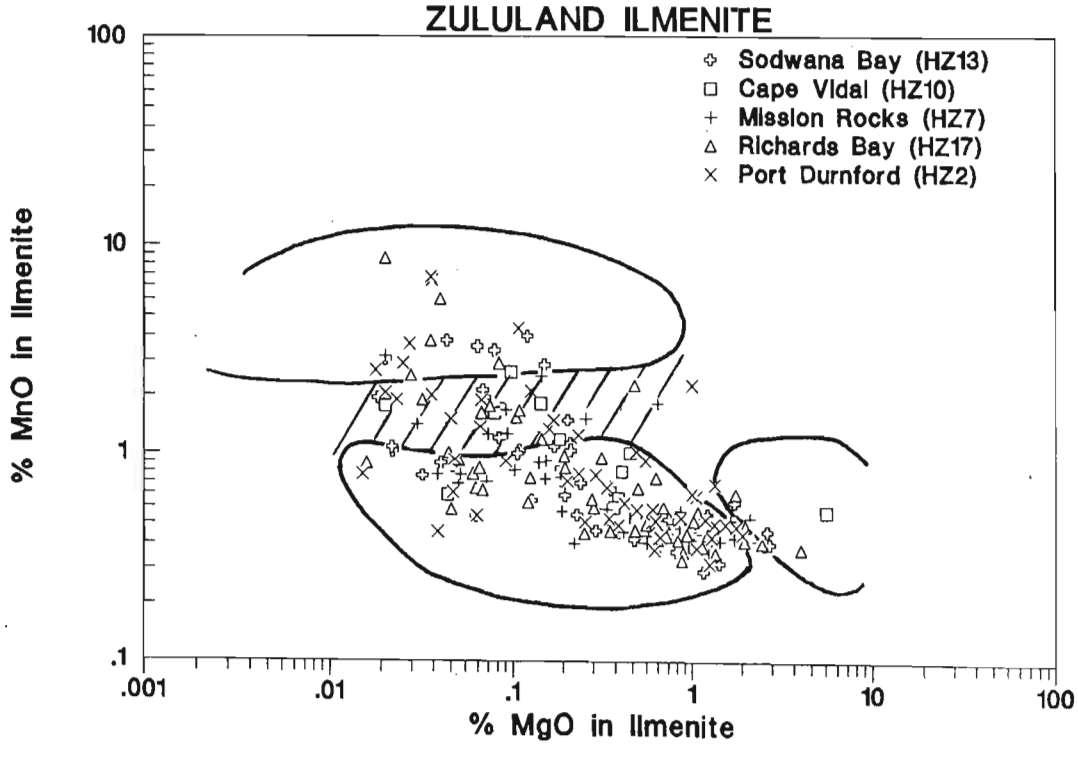

Figure 8.7 (Cont.) Variations in ilmenite MgO and MnO compositions from individual sample localities. **C.** Natal samples. **D.** Zululand samples.

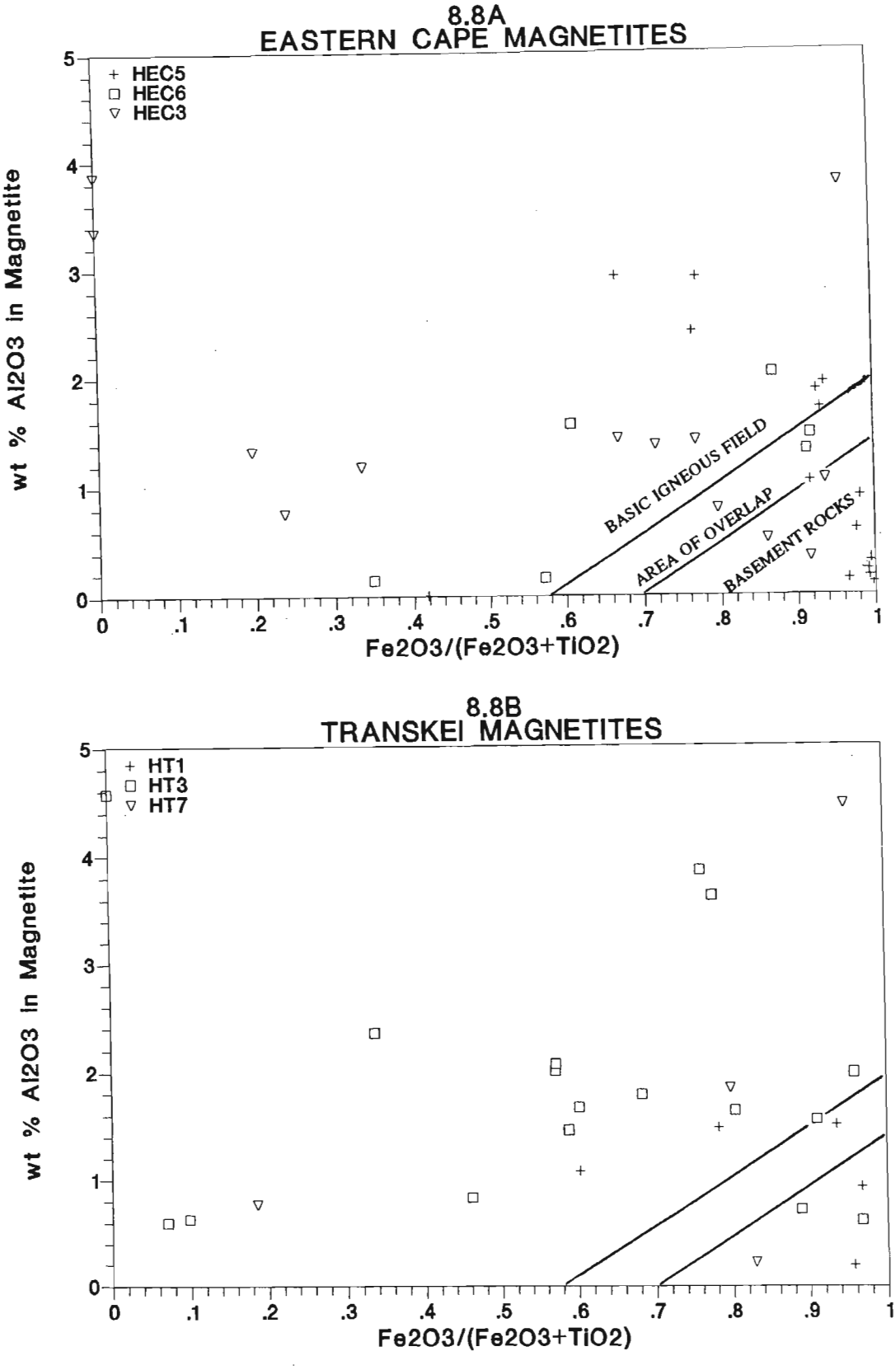

Figure 8.8 Variations in magnetite compositions in individual samples from the different regions. The plots indicate from which source rocks the magnetites are derived and how provenance influences their chemical compositions in the different regions.

A. Eastern Cape samples. **B.** Transkei samples.

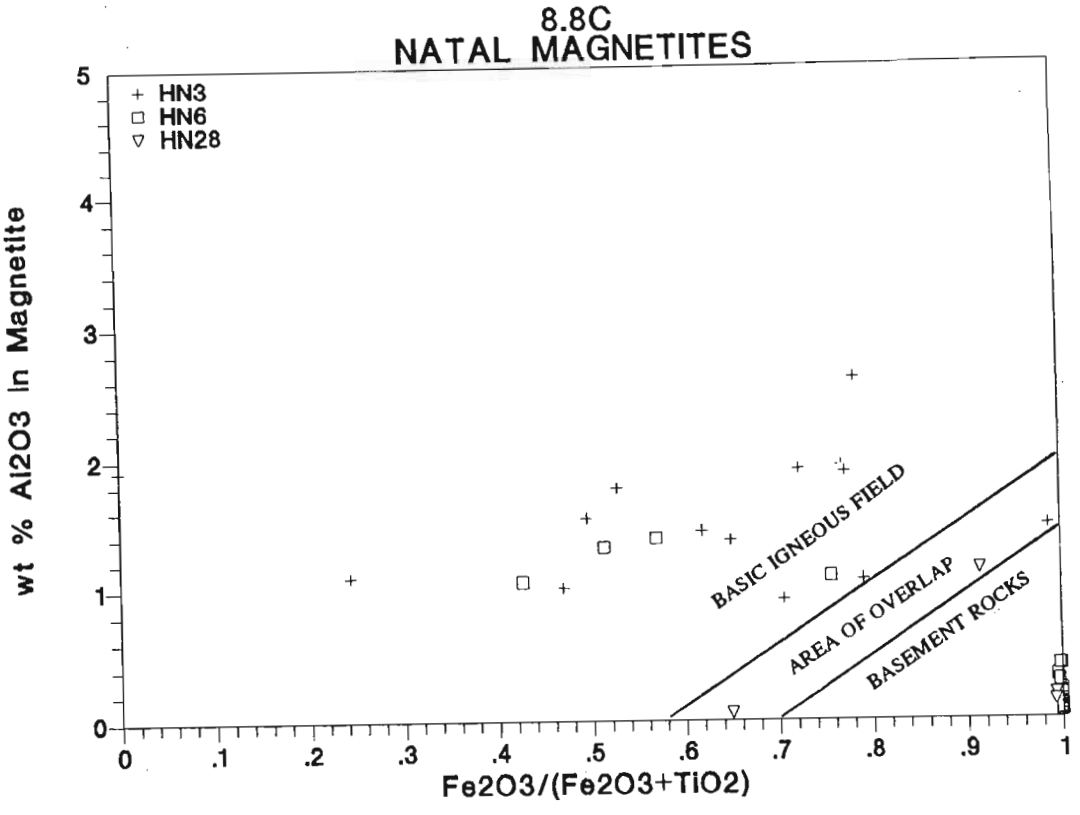

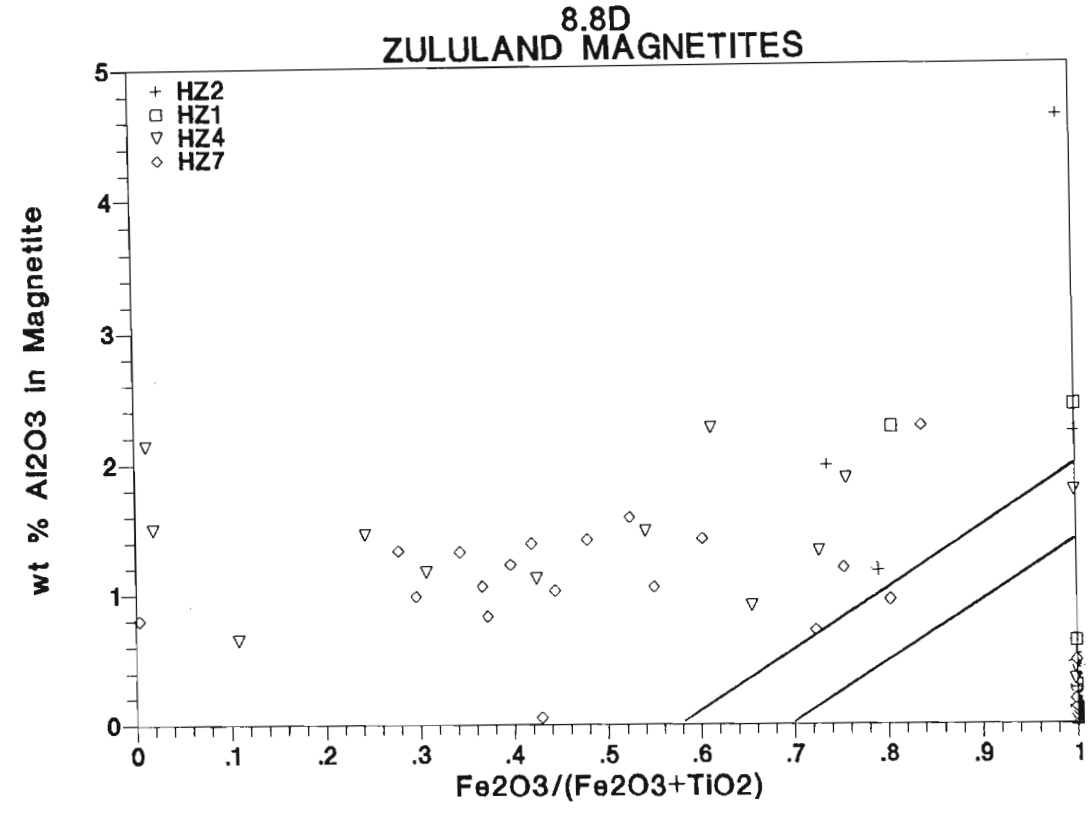

Figure 8.8 (cont.) Variations in magnetite compositions in individual samples from the different regions. **C.** Natal samples. **D.** Zululand samples.

8.4.2 The influence of provenance on petrographic textures

The chemical results given above are confirmed by the petrographic data (see Table 7.6, page 219 and Figure 8.9) which shows that magnetites from the eastern Cape and the Transkei are derived almost exclusively from rocks of the Karoo Igneous Province. Few samples from these regions show signs of provenance mixing. A small number of samples plot outside the basic igeous field, but these samples contain Mt-Usp_{ex} intergrowths and no Mt-$Pleo_{ex}$ is present, indicating that no mixing with metamorphosed ultrabasic/basic rocks has occurred. These samples probably contain magnetite from the large differentiated dolerite intrusions found in the Transkei.

Magnetites in Natal indicate a mixed provenance, although some samples appear to be derived exclusively from the Karoo Igneous Province or the Natal Basement. Samples with a distinct Karoo Igneous signature are found near Hlatimi in southern Natal, and the magnetite is probably from the Mtamvuna River, which erodes little of the Natal Basement. Magnetite from two Natal samples, namely, Zinkwazi (HZ 34) and Blythedale Beach (HZ 30), appear to be derived exclusively from the Natal Basement. These localities are close to the mouth of the Tugela River which has been shown to contain mainly metamorphic magnetite (see Figure 7.13, page 218). The influence of the Tugela River is also evident in the high proportions of metamorphic magnetite found along the southern Zululand coastline (samples HZ 25, HZ 26, HZ 1 and HZ 2). The relatively high proportions of Mt-$Pleo_{ex}$ in southern and central Zululand (Richards Bay) indicate that some input from metamorphosed basic-ultrabasic rocks has occurred. These magnetites were derived from the metamorphosed layered complexes found with the Natal Basement, which are eroded by the Tugela and Mhlatuze Rivers. The remaining magnetites in Zululand have a mixed provenance signature comprising both Karoo Igneous Province and Natal Basement rocks, with little input from the metamorphosed basic-ultrabasic complexes.

The great variability of magnetite intergrowths in different samples indicates that provenance has a far greater influence on the distribution of this mineral than is the case for ilmenite. Conversely, magnetite is a far better indicator of provenance than ilmenite.

It was noted in Chapter 7 that certain iron-titanium oxide intergrowths are characteristic of specific source rocks (see Table 7.5, page 212). The proportions of these intergrowths in the different regions are given in Table 8.1 and Appendix D, and are shown in Map 1. Data from Hugo (1990) is also used. The variations of these characteristic intergrowths are summarised in Table 8.7. Intergrowths diagnostic of the Natal Basement granitoids are most common in Natal and are rare in the eastern Cape and Transkei samples. Intergrowths characteristic of the Karoo Igneous Province are found in all regions.

The chemical and petrographic data presented above clearly indicates that the iron-titanium oxides are derived from both the Karoo Igneous Province and the Natal Basement rocks in the Natal and Zululand, but that the former is far more important as a source of these minerals in the Transkei and eastern Cape. This indicates that the present outcrop distribution of the source rocks has a strong influence on variations of the iron-titanium oxides. This influence is greater on the distribution of magnetite intergrowths and ilmenite-hematite grains than on homogeneous ilmenite.

It is also evident from Map 1 that samples taken close to river mouths have higher proportions of magnetite and intergrown iron-titanium oxides. These samples reflect most clearly the influx of minerals from the source areas. Mechanical breakdown of the intergrown grains by sediment reworking and the dissemination of the recently introduced material into existing, more mature sands, reduces the provenance signature of the samples away from the river mouths. This is demonstrated by the dispersion of magnetite from the Tugela River, as outlined in Section 7.7.3 (page 216).

Table 8.7 Regional variations in iron-titanium intergrowths and minerals, which are characteristic of source rocks (*cf.* Hugo, 1990).

Intergrowth	Source Rock	Zululand	Natal	Transkei	Eastern Cape
$(Ilm\text{-}Hem)_{ex}$	granitoid	*(*)	(*)**	*	
$(Hem\text{-}Ilm)_{ex} \pm Rut_{ox}$	"		*)		
$Ilm\text{-}(Hem+Rut \pm Psb)_{ox}$	"	*	*(**)		
$(Hem+Rut \pm Psb)_{ox}$	"	*	*(**)		
$Hem+Rut_{ox}$ (Blitz texture)	"	*	*		
$Mag\text{-}Ilm_{ox}$ (sandwich lamelle)	basalt/dolerite	(*)**	(*)**	**	**
$Mag\text{-}Ilm_{ox}$ (trellis lamellae)	"	(*)**	(*)**	(*)**	(*)**
Skeletal Magnetite	"	*(**)	*	*(**)	*(**)
Skeletal Ilmenite	"	*	*	*	*
Cr-Spinels	Basic Igneous	*		*	
Chromite	Ultrabasic/ basic complexes	*(**)	*		
$Mt\text{-}Pleo_{ex}\text{-}Ilm_{ox}$	"	*(**)	*		
Rutile	Metamorphic rocks	**	**	**	**
Ilmenite-titanite	Metamorphic rocks	*	*		

* = < 1 per cent; ** = 1-10 per cent; ( ) = occasionally found in these proportions

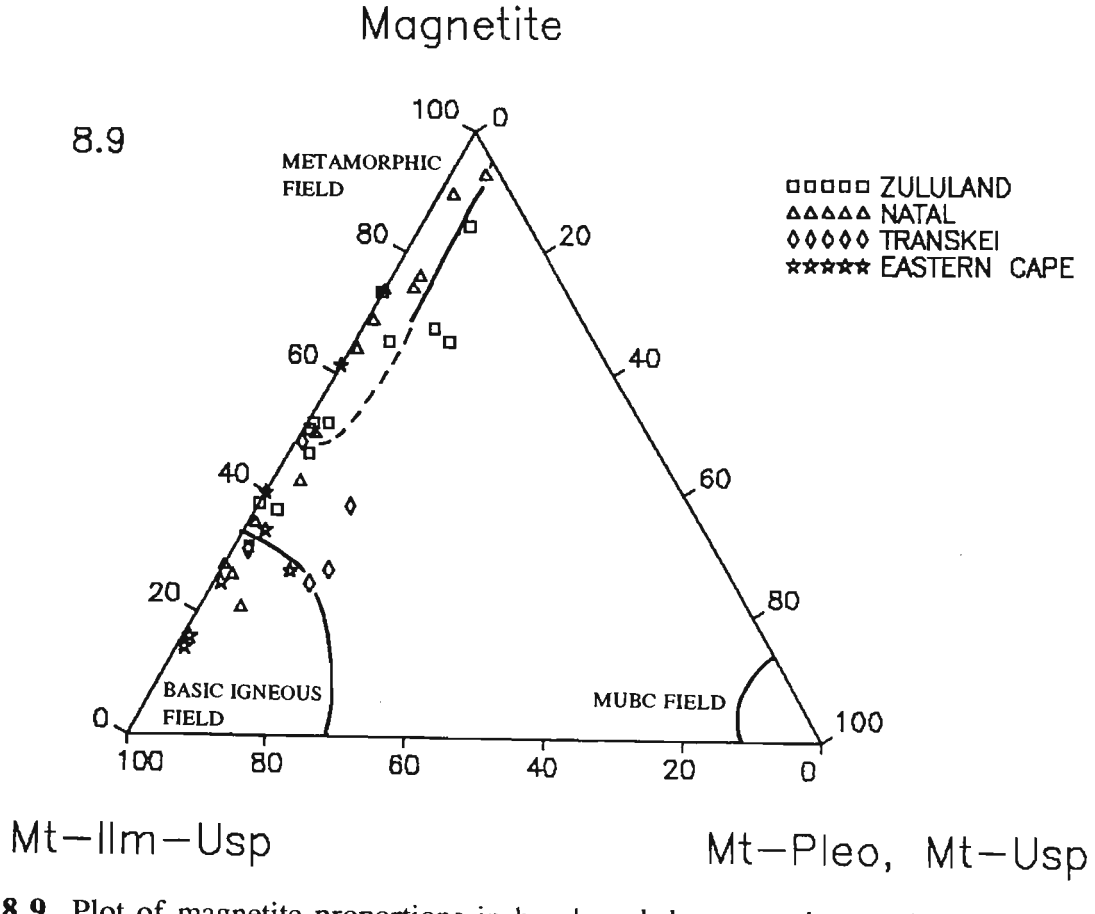

Figure 8.9 Plot of magnetite proportions in beach and dune samples on the magnetite discrimination diagram (Figure 7.14, page 221)

8.4.3 The influence of provenance on the distribution of rutile

Rutile is found in varying amounts in all samples. Microprobe analyses of homogeneous rutile grains, from selected samples are given in Appendix D.1. This data is summarised in Table 8.8 and indicates that there are no distinct differences between regions.

As mentioned in Chapter 7, rutile is thought to be derived exclusively from the Natal Basement rocks, but no work has been done to determine the specific source rocks of this mineral. As rutile is a metamorphic mineral, it is expected that the proportions of this mineral would be higher along the Natal and Zululand coastlines. Examination of Map 1 and Figure 8.4 (page 235) reveals that this is not so, and that the eastern Cape and Transkei have higher relative proportions of rutile than the northern regions. The proportions of zircon and garnet, two other metamorphic minerals, may also be relatively high in these regions (see Figure 8.1, page 227).

As there are no basement source rocks in the eastern Cape and very little basement outcrop in the Transkei, these minerals must be incorporated in the sediments by one of the following processes:

1. The minerals are derived from intermediate sedimentary hosts, which, in turn, were derived from the Natal-Namaqua Mobile Belt or Kaapvaal Craton. Such sediments are probably the Beaufort and Ecca Groups of the Karoo Sequence.
2. The minerals were transported from Natal by the strong southerly Agulhas Current.

The occurrence of heavy minerals in Karoo Sequence rocks from Natal has been described in Chapter 7. Behr (1986) also noted that minor concentrations of heavy minerals, including rutile, zircon and garnet are found in the Beaufort Group in the southern Cape Province. Stavrakis (1980) has described occurrences of these minerals in the Katberg Sandstone (Beaufort Group) in the eastern Cape. Examination of samples from the Fish and Kei Rivers (Table 8.9) reveals that rutile, zircon and garnet are eroded from the source areas of the Transkei and eastern Cape. Some rutile, zircon and garnet is therefore reworked from the Karoo sediments by erosion, and transported to the coastline by rivers.

Table 8.8 Summary statistics of rutile microprobe analyses given in Appendix B.1

Region	% SiO_2	% TiO_2	% Al_2O_3	% Cr_2O_3	% FeO	Total Oxides
Zululand						
Mean	0.05	99.20	0.04	0.10	0.18	99.45
Variance	0.00	0.17	0.00	0.00	0.01	0.14
Minimum	0.00	98.59	0.02	0.04	0.08	98.83
Maximum	0.07	99.90	0.13	0.24	0.36	100.04
n[1]	2	30	19	27	21	30
Natal						
Mean	0.16	99.11	0.04	0.11	0.27	99.45
Variance	0.01	0.26	0.00	0.00	0.07	0.31
Minimum	0.10	98.15	0.02	0.04	0.08	98.37
Maximum	0.30	100.03	0.15	0.24	0.98	100.43
n[1]	3	39	13	34	28	39
Transkei						
Mean	0.12	99.27	0.07	0.11	0.23	99.64
Variance	0.02	0.25	0.01	0.00	0.02	0.32
Minimum	0.03	98.04	0.02	0.02	0.08	98.34
Maximum	0.36	99.98	0.35	0.25	0.64	100.79
n[1]	6	31	24	21	29	31
eastern Cape						
Mean	0.16	99.26	0.08	0.12	0.20	99.52
Variance	0.05	0.16	0.01	0.01	0.02	0.12
Minimum	0.03	98.21	0.02	0.04	0.08	98.60
Maximum	0.71	100.02	0.40	0.46	0.68	100.22
n[1]	7	36	11	12	28	36

[1] n = number of analyses above detection limit.

Table 8.9 Modal proportions of heavy minerals from the Fish and Kei Rivers, determined by point-counting 500 grains per sample.

Grain Type	Kei River (HT6)	Fish River (HEC9)
Ilmenite	16	15
Altered ilmenite	1	1
HAI	tr	-
Rutile	3	2
Hematite	tr	tr
Magnetite	9	7
Mt-$Ilm_{oe} \pm Usp_{ex}$	7	13
Mt-Usp_{ex}	1	1
Zircon	2	4
Garnet	2	1
Pyribole	60	56

tr = trace; - = not observed.

Flemming (1981) studied the dispersal of sediment along the continental shelf of southeast Africa. He noted that the sediment dispersal is controlled by 4 major factors: morphology of the upper continental shelf; wave and wind-driven circulation; the Agulhas Current; and the supply of sediment to the shelf. The continental shelf is narrow and is interrupted by a number of structural offsets, and dissected by a numerous submarine canyons. The near-shore sediments appear to be in equilibrium with the high-energy wave regime and additional sediment entering the system, via rivers, is quickly dispersed onto the central shelf (Flemming, 1981). Here the Agulhas Current dominates the sediment dispersion and the sand is transported south until it spills over the shelf break at one of the structural offsets.

The regional sedimentary dispersal model of Flemming (1981) is reproduced in Figure 8.10. The diagram includes the catchment areas of the major river systems and divides the terrigenous input into 4 sedimentary compartments. The model suggests that sediment introduced to the continental shelf in Natal is either transported northwards by current

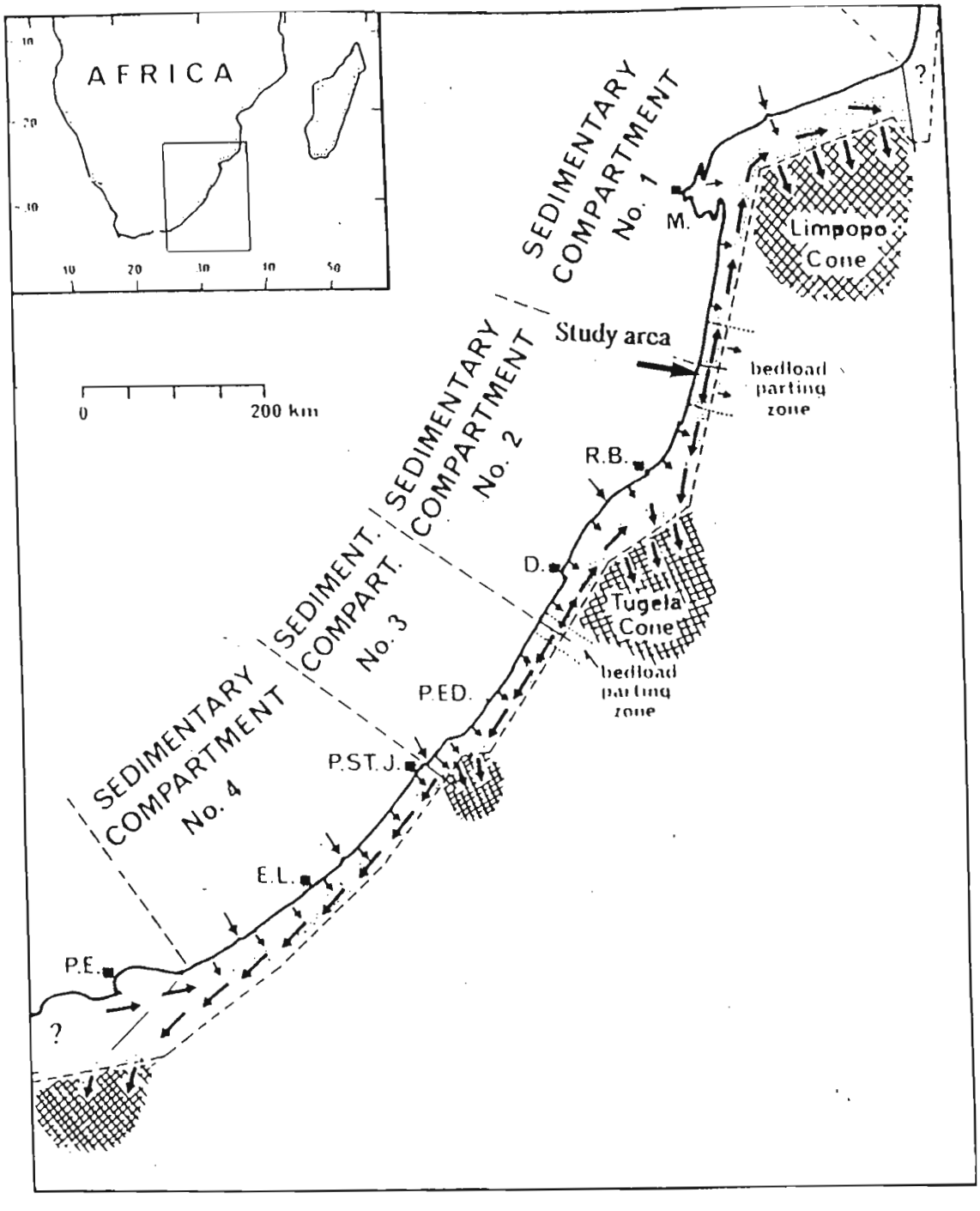

Figure 8.10 Regional sedimentary model summarising the dipsersion of sediments along the east coast of southern Africa. From Flemming (1981).

reversals, or are expelled from the shelf at the shelf break between Port Edward and Port St Johns. Flemming (1981) states that the model applies strictly to interglacial sea-level highs, and that during glacial maxima, "terrigenous sediment would have been supplied directly to the upper continental slope along the entire continental margin". Since the Eemian Interglacial, sea-levels have stood between - 10 and - 130 m. During glacial maxima, much of the terrigenous sediment introduced to the Indian Ocean would have been transported to the continental slope via the river valleys which now form the submarine canyons.

The above model strongly suggests that there is little likelihood of rutile, zircon and garnet being transported from Natal to the Transkei and eastern Cape by the Agulhas current, and that these minerals are derived from the intermediate sedimentary rocks described above.

8.5 THE QUALITY OF ILMENITE CONCENTRATES

It has been shown that regional variations exist in both the heavy mineral suite and the iron-titanium oxides. The effect that these variations have on the quality of ilmenite concentrates is examined here.

8.5.1 Chemical compositions of the concentrates

The quality of titanium mineral products is important as certain impurities reduce the whiteness of TiO_2 pigments. Such impurities include chromium, calcium, manganese, and vanadium, and products should not contain more than a few tenths of a per cent of these elements (Lynd and Lefond, 1983). The ferric to ferrous ratio is also important because, in the sulphate process of TiO_2 pigment manufacture, ferric iron must be reduced to the ferrous state, which increases production costs. TiO_2 products used in the chloride process must be low in calcium, phosphrous and magnesium as these elements form non-volatile chlorides with high boiling points during chlorination (Hamor, 1986). High levels of alumina and silica are also undesirable in feedstocks for the chloride route because of their refractory nature.

Chromium is an important impurity in ilmenite concentrates, as this element imparts a yellow colour to TiO_2 pigments, thereby reducing the quality of the product. The pigment industry requires ilmenite feedstock with less than 0.1 per cent Cr_2O_3. Large reserves of ilmenite along the east coast of Australia are unsaleable because of high Cr_2O_3 levels in the ilmenite concentrates (Lynd and Lefond, 1983). Blaskett and Hudson (1967) noted that this Cr_2O_3 is mainly present in discrete chromite grains, however, the Cr_2O_3 levels cannot be reduced below 0.2 per cent because the chromite has very similar grain size, magnetic susceptibility, and conductivity to the ilmenite. Manganese is an important impurity in ilmenite concentrates if pig iron is a by-product, as is the case at RBM. High MnO contents are detrimental in many end uses of the metal, and low MnO iron (< 1 %) is far more marketable.

Ilmenite concentrates were produced by the method outlined in Section 4.2.2 (page 58). The chemical compositions of the ilmenite concentrates, together with data from previous studies, are given in Table 8.10. The concentrates have similar compositions, but the TiO_2, Cr_2O_3 and MnO levels show some regional variation. The eastern Cape and Transkei concentrates have higher TiO_2 contents than the Natal and Zululand samples (Figure 8.11), and there is a general decrease in TiO_2 from south to north along the coastline. As noted by Hammerbeck (1976) and Fockema (1986) the Cr_2O_3 content of the ilmenite concentrates is low in the eastern Cape and Transkei (generally less than 0.1 per cent), but the levels of this impurity increase northwards and the highest values are found in Zululand. The MnO content is also higher in the Natal and Zululand samples. These analyses agree well with those of previous workers (*cf.* Hammerbeck, 1976; Logan, 1974; Reynolds, 1978b).

The levels of impurities in ilmenite grains may be estimated from electron microprobe analysis and average values, per sample, are given in Table 8.10. Comparison with Table 8.9 indicates that the levels of most of impurity elements are lower in ilmenite grains than the bulk analysis. The Cr_2O_3 content from the bulk and microprobe analyses are compared in Figure 8.12A. This shows that the Cr_2O_3 in ilmenite accounts for the chromium levels in the eastern Cape and Transkei samples, but that other phases must contain the bulk of

Table 8.10 Chemical compositions of ilmenite concentrates.

Sample number	TiO2	FeO	SiO2	Al2O3	CaO	MgO	Cr2O3	MnO
HEC5 Kidd's Beach	50.1	46.2	0.5	0.35	0.08	0.61	0.06	0.55
HEC3 Fish R. Mouth	49.6	47.5	0.6	0.54	0.13	0.63	0.09	0.69
HEC6 Morgan's Bay	49.6	47.6	0.2	0.33	0.04	0.63	0.08	0.43
HT7 Wavecrest	50.3	45.8	0.7	0.43	0.17	0.4	0.11	0.38
HT3 Port St Johns	50.1	46.8	0.4	0.41	0.09	0.74	0.11	0.62
HT5 Mzamba Beach	48.4	47.0	0.9	0.66	0.01	0.65	0.08	0.51
HN2 Umgababa	49.8	45.3	0.9	0.42	0.06	0.66	0.08	1.06
HN5 Isipingo	48.3	45.8	0.4	0.4	0.05	0.65	0.11	1.12
HN27 Tinley Manor	48.9	46.8	0.5	0.53	0.05	0.64	0.12	1.1
HZ2 Port Durnford	47.6	46.8	0.6	0.73	0.12	0.57	0.36	1.76
HZ17 Richards Bay	49.1	45.2	0.4	0.62	0.11	0.57	0.23	1.3
HZ7 Mission Rocks	48.3	45.9	0.7	0.42	0.08	0.63	0.19	1.22
HZ13 Sodwana Bay	48.3	46.2	0.6	0.58	0.12	0.66	0.23	1.3

	Reference	TiO2	FeO	Fe2O3	Al2O3	CaO	MgO	Cr2O3	MnO	V2O5
Morgan Bay	Hammerbeck (1976)	50	38	13.1				0.05		
Sandy Point	"	50.3	36.5	10.9				0.07		
Umgababa	"	49.9	37.2	10.5				0.16		0.33
Isipingo	"	46.6	39.5	9.1				0.1		2.76
Richards Bay	"	49.7	36.6	11.1				0.19		0.29
St Lucia	"	49	32.5	14.3				0.38		
Umgababa	Langton and Jackson (1961)	49	34	13		0.01	0.75	0.18	0.4	1.0
Richards Bay 1	Logan (1974)	48.62	34.56	14.41				0.25		
Richards Bay 2	"	51.6	35.39	10.27				0.05		
Richards Bay 3	"	48.71	34.27	14.11				0.27		
Richards Bay 4	"	50.4	37.89	8.89				0.05		
Jeffery's Bay	Reynolds (1978)b	49.53	35.23	13.88		0.04	0.21	0.08	0.5	
Maitland R.M.	"	50.26	37.51	11.14		0.04	0.37	0.1	0.43	
Swartkops R.M.	"	50.68	38.45	9.7		0.06	0.3	0.06	0.42	
Fish R.M.	"	49.54	40.36	8.36		0.10	0.57	0.04	0.48	
Morgan's Bay	"	49.76	39.27	9.91		0.03	0.36	0.04	0.4	
Nahoon Beach	"	50.47	39.92	7.96		0.05	0.33	0.04	0.39	
Boknes Beach	"	51.08	40.43	7.14		0.06	0.22	0.11	0.42	
Bushman's R.M.	"	51.29	40.3	7.04		0.04	0.33	0.02	0.46	
Kasouga	"	50.97	38.25	9.62		0.04	0.32	0.04	0.4	
Port Alfred	"	49.77	37.71	11.18		0.04	0.23	0.03	0.44	

this impurity in the Natal and Zululand concentrates. Microscopic examination (Table 8.12) reveals that both chromite and less abundant Cr-bearing spinel (probably chromian-magnetite) are present in ilmenite concentrates from these regions. This was also noted by Logan (1974) and Hugo (1988). The regional trend is expected, as chromite is derived from metamorphosed ultrabasic and basic complexes, which are found in Zululand. The level of Cr_2O_3 in ilmenite concentrates is therefore strongly related to provenance.

Zululand concentrates contain Cr_2O_3 levels which are over twice the limit required by the pigment industry. Lee and Poggi (1978) describe how roasting ilmenite at elevated temperatures increases its magnetic susceptibility, thereby enabling the removal of less magnetic chromite. This patented process enables RBM to produce titanium slag with the required chromium specification.

Comparison of MnO content in the concentrates and ilmenite grains (Figure 8.12B) indicates that in many cases ilmenite accounts for all the MnO in the concentrates. The average MnO content of the eastern Cape and Transkei ilmenite is consistently higher than that of the concentrates. This is caused by a small number of grains containing high MnO levels, which elevates the average value of the microprobe analyses. A higher MnO content of Natal and Zululand ilmenite is seen in both the microprobe averages and bulk analyses. As described early, this is due to high-MnO ilmenite from granitoid and felsics of the Natal Basement rocks in these regions.

The level of CaO in ilmenites was found to be below the microprobe detection limit, and this impurity in the concentrates is ascribed to discrete impurity minerals. Hugo (1985) found that garnet and hornblende were the major contributors to CaO in ilmenite concentrates from Richards Bay. Once again the Natal and Zululand concentrates tend to have higher CaO levels than those in the southern regions.

Table 8.11 Average ilmenite microprobe analyses from selected samples in the study area.

Sample	No. Analyses	TiO_2 (%)	FeO[1] (%)	SiO_2 (%)	Al_2O_3 (%)	CaO (%)	MgO (%)	Cr_2O_3 (%)	MnO (%)
HEC 5 Kidd's Beach	15	51.18	46.68	0.07	0.08	nd	0.30	nd	0.71
HEC 3 Fish R. Mouth	57	51.85	45.82	nd	0.03	nd	0.50	0.05	0.90
HEC 6 Morgan's Bay	33	51.42	47.86	nd	0.05	nd	0.18	0.06	0.47
HT 7 Wavecrest	54	50.82	46.40	nd	0.04	nd	0.66	0.10	0.64
HT 3 Port St Johns	73	51.20	46.11	nd	0.05	nd	0.68	0.09	0.74
HT 5 Mzamba Beach	56	51.06	45.96	0.03	0.04	nd	0.69	0.06	0.74
HN 2 Umgababa	45	50.50	47.12	nd	0.05	nd	0.44	nd	0.79
HN 5 Isipingo	56	50.82	46.52	0.03	0.05	nd	0.57	0.06	0.77
HN 27 Tinley Manor	53	51.17	46.75	nd	0.03	nd	0.52	nd	1.24
HZ 2 Port Durnford	53	51.06	45.96	nd	0.04	nd	0.50	0.05	1.16
HZ 17 Richards Bay	55	50.96	46.19	nd	0.02	nd	0.59	nd	0.83
HZ 7 Mission Rocks	47	51.47	45.69	0.04	0.05	nd	0.62	nd	1.17
HZ 13 Sodwana Bay	48	51.42	46.02	nd	0.03	nd	0.54	nd	1.17

[1] all iron reported as FeO; nd = below detection limit.

A study of the mineral impurities in ilmenite concentrates (Table 8.12) reveals that the eastern Cape and Transkei have fewer mineral impurities than the Natal and Zululand samples. The latter concentrates also contain a larger variety of mineral impurities, including more $Ilm\text{-}Hem_{ex}$, and $Hem\text{-}Rut_{ox}$ grains, which may account for their lower TiO_2 contents. A greater number of impurity minerals increases the complexity of mineral processing and makes it harder to achieve grade specifications for the final products.

Economic titanium deposits require large reserves to justify the high capital investment required to develop and exploit the deposits. Generally, new deposits, which cannot be treated in an existing plant, require a minimum reserve of about 1 million tonnes of recoverable TiO_2 in order to be economical (Lynd and Lefond, 1983). In addition to mining, infrastructure and labour considerations, the economic viability of a deposit is influenced by the ability of markets to absorb the titanium concentrates produced, and by

the prevailing prices of the minerals or their upgraded products (Lynd and Lefond, 1983). The eastern Cape and Transkei ilmenites are of better quality than the Natal and Zululand ilmenites, as they contain higher TiO_2 contents, lower Cr_2O_3, CaO and MnO levels, and have fewer mineral impurities. Unfortunately the Cape and Transkei deposits are all sub-economic to marginal due to their small size, and the lack of infrastructure in their vicinity (Hammerbeck, 1976).

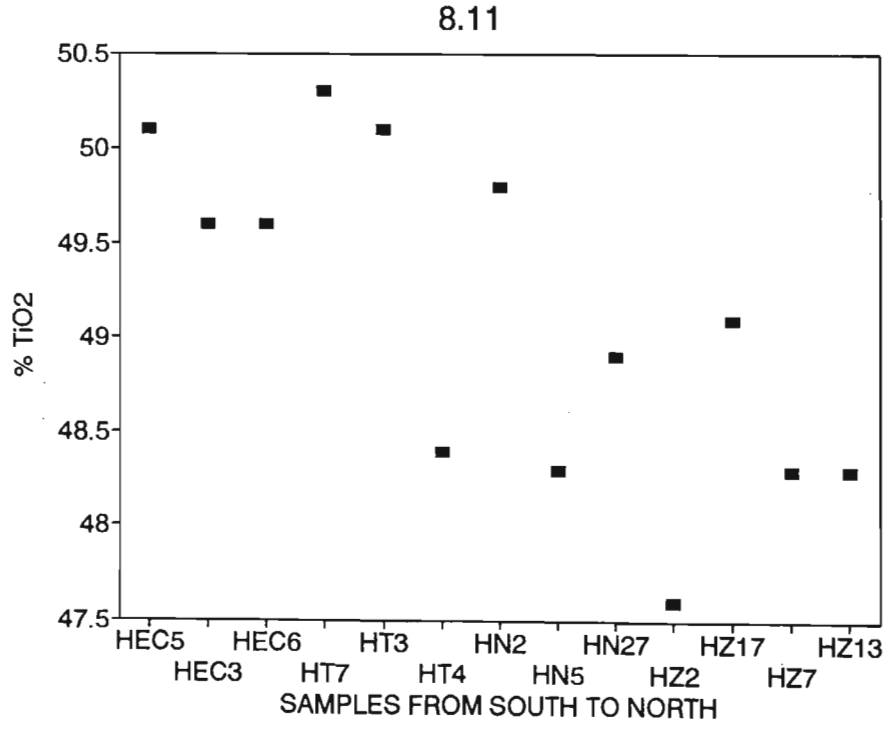

Figure 8.11 Variation in TiO_2 content of ilmenite concentrates from south to north along the coastline. Sample localities are shown in Map 1.

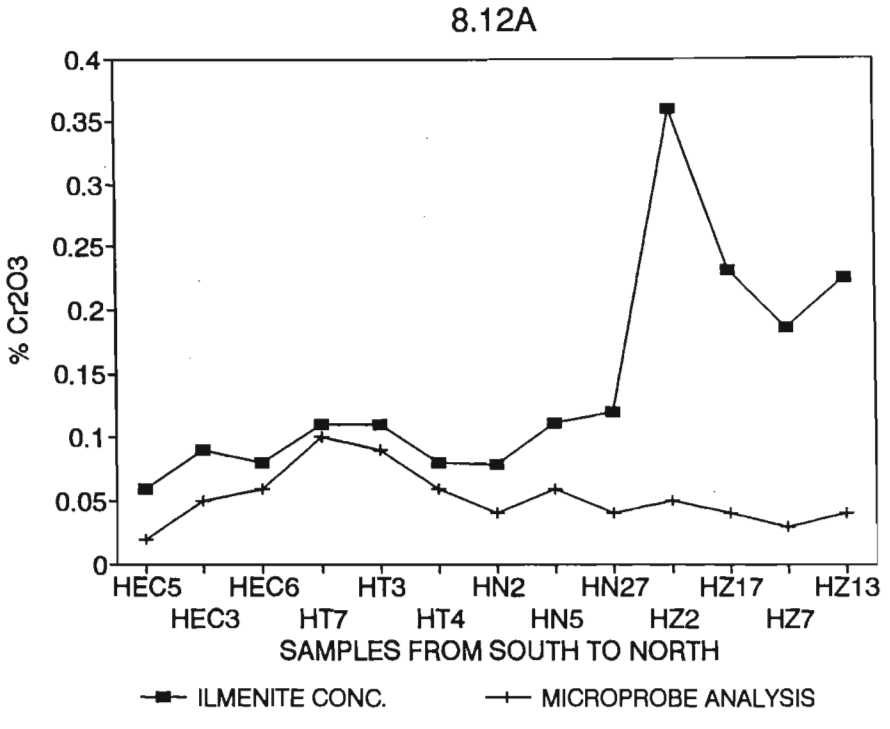

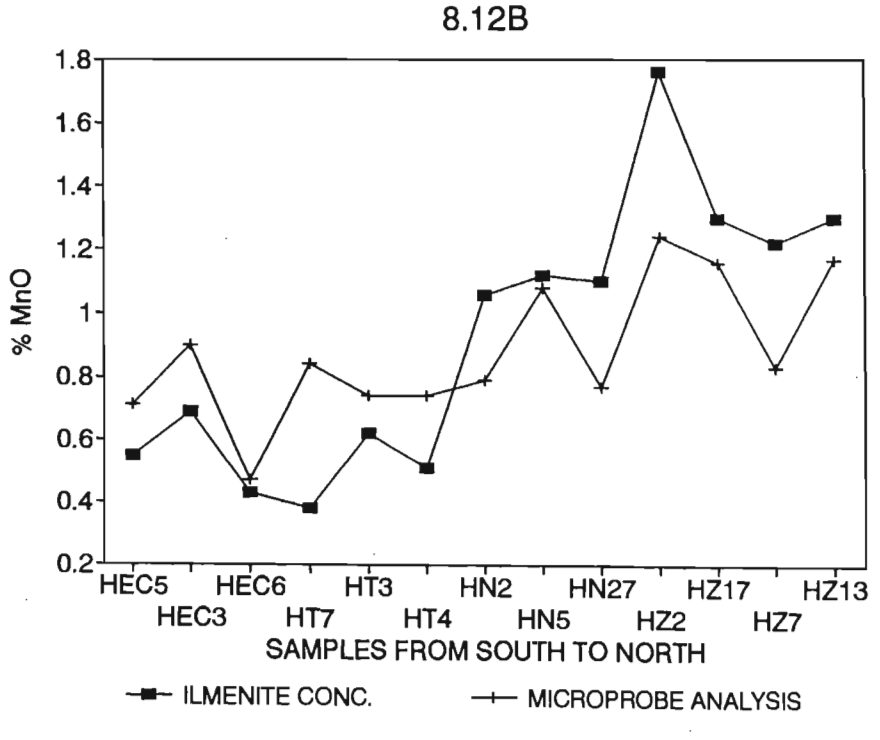

Figure 8.12 Variations in Cr_2O_3 (**A.**) and MnO (**B.**) contents of ilmenite concentrates from south to north along the coastline. Sample localities are shown in Map 1.

Table 8.12 Proportions of impurities in selected ilmenite concentrates. Determined by point-counting 500 grains per sample.

Grain Type	HEC5	HEC3	HEC6	HT7	HT3	HT5	HN2	HN5	HN27	HZ2	HZ17	HZ7	HZ13
Alt ilmenite	****	****	***	***	****	****	****	****	****	****	****	****	****
HAI	***	***	**	**	***	**	***	**	**	**	**	**	***
$(Ilm\text{-}Hem)_{ex}$				*	*	*	**	**	*	*	**	**	*
$(Hem\text{-}Rut)_{ox}$	*		*			*	**	**	**	**	**	**	***
$Ilm\text{-}(Hem+Rut)_{ox}$				*	*	*	**	**	***	***	**	**	**
Leucoxene	*		*				*			*	*	*	*
$Mag\text{-}Ilm_{ox}\text{-}Usp_{ex}$	*		*		*	*		*	*	*	*	*	*
Magnetite				*		*			*	*			
Chromite				*	*	*	*	*	*	**	*	**	**
Cr-spinel							*			*	*		*
Hematite	*		*	*		*	*		**	*	*	*	*
Goethite	*						*					*	
Pyribole	*	*	*	**	**	**	**	**	**	**	**	**	**
Garnet		*	*		*		***	**	*	**	**	**	**
Monazite			*		*	*		*	*	*	*	*	*

* = less than 0.5 %; ** = 0.5 to 1 %; *** = 1 to 5 %; **** = 5 to 10 %

8.5.2 Comparison with other ilmenite deposits

The compositions of some ilmenite concentrates from the South African east coast (Table 8.13) are compared with those from major ilmenite deposits around the world in Figure 8.13A. The plot, first used by Temple (1966), indicates the degree of ilmenite alteration in the concentrates. Data from the other deposits is from Temple (1966) and Baxter (1977). The general trend is due to the initial alteration from ilmenite to pseudorutile, followed by the progressive alteration to TiO_2, via leucoxene. The ilmenite concentrates from the study area are unique as they are practically unaltered, and lie closest to the ilmenite apex of all the deposits (Figure 8.13B). This is reflected in their lower TiO_2 content of 48.5 to 50.5 per cent TiO_2, in comparison to other major ilmenite provinces which produce concentrates containing 53 to 65 per cent TiO_2 (MacKey, 1972a). Two concentrates from the west coast of South Africa are also included in Figure 8.13. These samples contain even lower TiO_2 than the east coast deposits (Table 8.13). Petrographic study of samples from these west coast regions has revealed that many of the ilmenite grains contain extensive hematite exsolution (Hugo, 1990). These grains are incorporated in the ilmenite concentrates, lowering the TiO_2 levels of the ilmenite product.

As outlined by Force (1991) the TiO_2 content of the ilmenite concentrate is economically important, because the greater the TiO_2 content, the more TiO_2 extracted per ton of feedstock. Consequently concentrates with high TiO_2 contents fetch much higher prices, as described in Chapter 2. Generally ilmenite feedstocks with less than 54 per cent TiO_2 are not traded (Force, 1991) and beneficiation of the concentrate is required to sell the material. This indicates that the southern African ilmenite concentrates are of a lower quality than ilmenites from other countries, however, their purity facilitates the production of high-grade titanium slag and pig iron by smelting the ilmenite. The slag contains about 85 per cent TiO_2 and is suitable for both the sulphate and chloride methods of pigment production, making the product very marketable (Lee and Poggi, 1978).

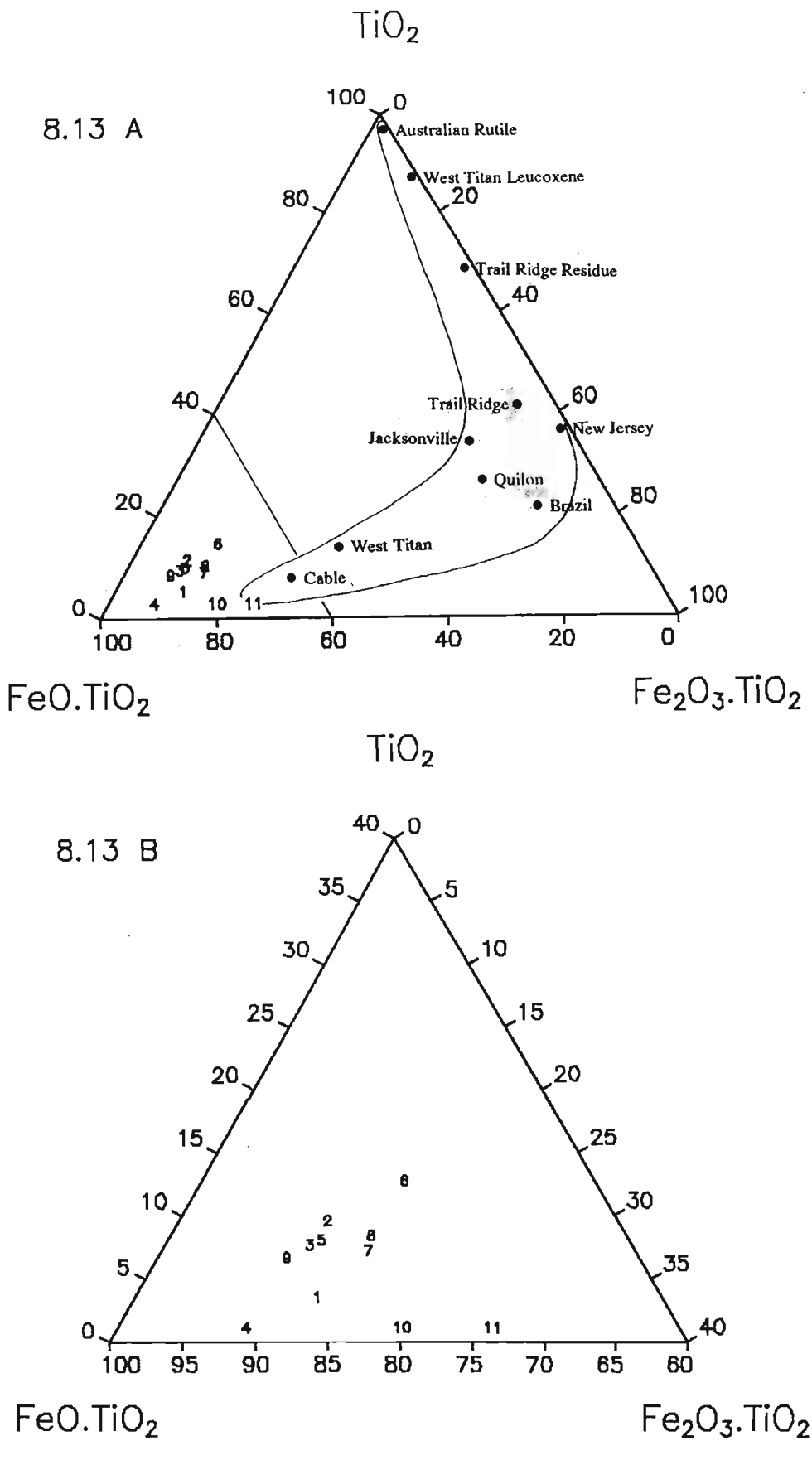

Figure 8.13A Comparison of the TiO_2 and iron contents of southern African ilmenite concentrates (see Table 8.13) with those of other major titanium deposits in the world. Data for the overseas deposits is taken from Temple (1966). **B.** Expanded view of the field in 8.13A, showing the unaltered nature of the southern African ilmenites.

Sample localities: 1 = Morgans Bay; 2 = Sandy Point; 3 = Umgababa; 4 Isipingo; 5 = Richards Bay; 6 = St Lucia; 7 = Richards Bay; 8 = Richards Bay; 9 = eastern Cape; 10 = Vanrhynsdorp; 11 = Soutfontein.

Table 8.13 Ilmenite concentrations from South Africa used in Figure 8.13.

Locality	Reference	Percent			Normalised		
		TiO_2	FeO	Fe_2O_3	$FeO.TiO_2$	$Fe_2O_3.TiO_2$	TiO_2
Morgans Bay	Hammerbeck (1976)	50.0	38.0	13.1	84.51	13.11	2.38
Sandy Point	"	50.3	36.5	10.9	80.69	10.84	8.46
Umgababa	"	49.9	37.2	10.5	82.90	10.53	6.57
Isipingo	"	46.6	39.5	9.1	90.61	9.39	0.00
Richards Bay	"	49.7	36.6	11.1	81.89	11.17	6.93
St Lucia	"	49.0	32.5	14.3	73.76	14.60	11.64
Richards Bay 1	Logan (1974)	48.62	34.56	14.41	79.05	14.83	6.12
Richards Bay 2	"	48.71	34.27	14.11	78.24	14.49	7.27
eastern Cape[1]	Reynolds (1978)	50.3	38.4	9.51	84.90	9.46	5.64
Vanrhynsdorp	Coetzee (1957)	41.6	34.1	19.17	79.81	20.19	0.00
Soutfontein	Herzburg (1970)	41.8	28.45	22.74	73.55	26.45	0.00

[1] Average of 9 analyses from eastern Cape beaches.

8.6 THE GENESIS OF MINERAL ASSEMBLAGES AND ORE-BODIES

8.6.1 A model for magnetite and ilmenite variations

Iron-titanium oxide assemblages in the coastal sediments are dominated by ilmenite and its alteration products. In contrast, magnetite is often the most abundant mineral in the source rocks and rivers from which the oxides are derived. Although magnetite is less durable than ilmenite, it is unlikely that this mineral could be destroyed so quickly after reaching the marine environment, so that its proportions would be so much less than ilmenite in the beach and dune sediments. Some other explanation is required to explain the discrepancy between iron-titanium oxide proportions in river and the modern coastal sediments, and the following model is proposed.

The sea-level curve of Williams *et al.* (1981) shown in Figure 3.1 (page 37) indicates that sea-levels fluctuated between -10 and -130 m between the Eemian high (*circa* 120 000 B.P.) and the last glacial maximum (15 000 - 18 000 B.P.). Seven marine transgression-

regression cycles are identified during this period and terrigenous sediment entering the marine environment would thus have been extensively reworked. During periods of glacial maxima rivers incised deeply into the exposed marine sediments (Fockema, 1986; Van Heerden, 1987) and carried their terrigenous bedload to the outer parts of the continental margin. During the last glacial maxima, when sea-level stood at about -130 m below present m.s.l., the river sediment was transported directly to the continental slope (Flemming, 1981; Sydow, 1988; Ramsey, 1991). This indicates that much of the sediment supplied by rivers during the Late Pleistocene was lost from the continental shelf and the sediment which remained in the shelf system was re-worked. Thus most of the iron-titanium oxide assemblages (and other heavy minerals) found in the Late Pleistocene-Holocene dunes are at least 15 000 years old. This is a realistic period for the breakdown of magnetite (and other, less resistant, heavy minerals), leading to the enrichment of ilmenite in the iron-titanium oxide assemblages of the beaches and dunes.

The Flandrian Transgression has resulted in the deposition of fresh terrigenous sediment on the coastal shelf. Where rivers contain high proportions of magnetite and introduce large volumes of bedload into the shelf system (for example, the Tugela River), the beaches contain correspondingly high amounts of magnetite. The new minerals are, however, soon dispersed by wave and current actions, and disseminated within the much larger "pool" of existing minerals. This obscures the influence of the terrigenous sediments away from the river mouths, and ilmenite remains the dominant iron-titanium oxide.

8.6.2 Formation of the heavy mineral deposits

It is difficult to provide models for the formation of the older (Pliocene-Pleistocene) red dune deposits because of the paucity of geological information concerning these deposits, and the uncertainty of their age. There were, however, periods of marine regression during both the Pliocene and Pleistocene which would have exposed large areas of unconsolidated sands on the continental shelf, providing source material for the dune cordons. Likewise, sea levels remained below present levels during the Late Pleistocene,

exposing sediments on the continental shelf to strong on-shore winds during glacial maxima. It is postulated that the Late Pleistocene dunes, found along the Zululand coast, formed a coastal cordon between *circa* 100 000 - 20 000 B.P. The beach facies of these aeolian sediments may well be the drowned beach rocks described by Ramsey (1991) which form palaeocoastlines. The landward migration of the dunes was probably inhibited by remnants of the Mid-Pleistocene Port Durnford dunes, outcrops of beachrock and aeolianites of a similar age. Subsequent erosion and redistribution of the dune sands flattened and smoothed the relief of the cordons. Subaerial weathering of the deposits produced the red-brown colouration.

The maxima of the Late Pleistocene glaciations occurred between 18 000 and 15 000 B.P., dropping sea level to about 130 m below the present level. This would have moved the shoreline close to the edge of the continental margin, exposing huge volumes of unconsolidated sands. Bathymetric maps of the continental margin (Dingle *et al.*, 1978) show that the greatest volume of sand exposed would have been along the Tugela cone. These would have been driven onshore by strong southerly and northerly winds, blowing sub-parallel to the coast, to form the extensive Late Pleistocene-Holocene dune cordons along the Zululand coast. The dunes overlie the Port Durnford sediments and Late Pleistocene dune remnants, which prevented further landward migration. The Flandrian transgression raised sea-levels up to +1.5 to 2 m. about 5000 B.P. (Yates *et al.*, 1986; Reddering, 1987), and consequently destroyed the dune fields formed on the shelf. Along the Zululand coast the present coastal barrier dune system and underlying rocks were eroded, forming the typical cliff dunes, as the shoreline was shifted approximately 40 m landward (Ramsey, 1991).

The poor development of dune systems along the Natal-Transkei coast is thought to be a result of the scarcity of fine-grained sand supply for aeolian formation, combined with an actively eroding shoreline (Tinley, 1985). The aeolian sands are considered to have been derived from the reworking of the older dune cordons, together with beach sands and continental shelf sediments exposed during the last glacial maxima (Hammerbeck, 1976; Wipplinger, 1985). It is probable that along the Natal and Transkei coastlines the rise in

sea level resulted in the destruction of landward backdunes to form small foredunes during the formation of a new littoral environment. The reworking of the older dunes may explain the high ilmenite contents found in modern dunes from some localities along the Natal and Transkei coastlines. This is particularly evident at places such as Wavecrest and Sandy Point where there is evidence of the re-working of the older red dunes (Hammerbeck, 1976).

As described by Flemming (1981), the continental margin broadens southwards off the East Cape reaching a width of over 40 km. Here again, the Late Pleistocene glacial maxima would have exposed large areas of unconsolidated sands, facilitating the formation of extensive aeolian deposits along the coastline. Towards the south, the eastern Cape does not have the same provenance as the Transkei. As shown in Map 1, the major rivers in this region drain less and less of the Karoo Igneous rocks from East London to Port Elizabeth. Consequently a greater proportion of the heavy minerals is reworked from the Karoo sediments. This results in a more mature heavy mineral assemblage in the coastal sediments, which is reflected by higher proportions of altered ilmenite, leucoxene and rutile.

CHAPTER NINE

SUMMARY AND CONCLUSIONS

9.1 GEOLOGICAL SETTING

The east coast of South Africa contains an estimated 2476 million tonnes of heavy mineral-bearing sands (Wipplinger, 1985). This constitutes the world's largest demonstrated resource of ilmenite in sedimentary deposits (see Table 2.3, page 12). Despite the economic potential, little research has been done on the mineralogy of the economic minerals, notably ilmenite.

The south-eastern African coastline, and particularly the Zululand coastal plain, conforms to all the criteria for the formation of heavy mineral placer deposits. The deposits occur within several ages of Cainozoic aeolian and beach sediments. The most exploitable deposits are found in Late Pleistocene - Holocene dunes, which occur intermittently along the present-day coastline between East London and the Mocambique border. The most economically viable of these deposits are the high coastal dune ridges found between Port Durnford and Cape Vidal, along the Zululand coast. These deposits contain over 1700 Mt (Wipplinger, 1985) of free-flowing, heavy mineral-bearing sand, containing economic grades of ilmenite, zircon, rutile and monazite. The deposits north of Richards Bay are currently dredge-mined by Richards Bay Minerals.

Large resources of heavy minerals are also found in palaeo-dunes of Pliocene - Pleistocene age. These occur as both coastal ridges and inland cordons along much of the coastline. The grade of heavy minerals in these deposits is variable, but the high clay content of the sediment has prevented exploitation.

9.2 IRON-TITANIUM OXIDE MINERALOGY

Little weathering has occurred in the Late Pleistocene - Holocene dunes, or the modern beaches and most of the heavy minerals are still preserved in the deposits. The iron-titanium oxides occur as both monomineralic grains or composite grains, which display a variety of textures formed in the source rocks of the oxides. These include exsolution, oxidation, oxyexsolution, deuteric and hydrothermal alteration textures. Two or more of these textures are often found in single grains. In addition, these primary textures may be overprinted by alteration textures, formed by weathering in the coastal deposits. This makes the petrography of the composite iron-titanium oxide grains both complex and interesting.

The most common composite grains observed in the deposits are Mt-$Ilm_{oe}\pm Usp_{ex}$, Ilm_{ss}-Hem_{oe} and $(Hem\text{-}Rut\pm Psb)_{ox}$ grains. The composite grains are preserved during erosion and transportation, and provide important clues to the provenance of the iron-titanium oxides. These grains play an important role in mineral processing, as they affect the recovery of TiO_2 from the deposits. Titanium-bearing phases in composite grains are difficult to concentrate, because their physical properties are influenced by the other phases present in the grains, and the final concentrate may be of poor chemical quality.

Ilmenite is the most abundant iron-titanium oxide in the coastal deposits. It occurs mainly as homogeneous, subrounded grains, ranging in size from 75 to 250 μm. These grains have chemical compositions close to pure $FeTiO_3$. Limited solid-solution with hematite (Fe_2O_3), pyrophanite ($MnTiO_3$) and geikielite ($MgTiO_3$) occurs in some ilmenite grains (see Figure 5.6, page 90). Ilmenite concentrates from the study area contain between 48 and 52 per cent TiO_2. This TiO_2 content is lower than most ilmenite concentrates from placer deposits and testifies to the unaltered nature of the ilmenites.

Magnetite has a wide range of chemical compositions. Titanium is the major substituent for iron, and extensive solid-solution between ulvospinel and magnetite is found in some grains. These grains usually contain ilmenite lamellae formed by oxyexsolution during

cooling. Other elements, such as Al, Mg, Mn and Cr also substitute for Fe^{2+} and Fe^{3+} in the magnetite grains. Many magnetites have compositions close to Fe_3O_4, which is caused by re-equilibration of the magnetite with other minerals during slow cooling in the source rocks. Most magnetite grains in the coastal sediments display varying stages of martitisation.

Rutile is commonly found as homogeneous grains, with chemical compositions close to pure TiO_2. Minor impurities of Fe, Cr, and Al are found in rutile grains. Niobium is also a common impurity in rutile grains (Hugo, 1988). Rutile, together with anatase, and minor brookite, occurs in leucoxene grains, formed by the alteration of ilmenite.

9.3 ILMENITE ALTERATION

Although most ilmenites in the coastal sediments are unaltered, varying proportions of altered ilmenite grains are found in the different deposits. This alteration is mostly caused by weathering of the ilmenite in the sedimentary environment. Many of these grains display only incipient alteration, but the entire spectrum of alteration products from ilmenite to leucoxene is observed at each locality studied.

Transmission electron microscopy of weathered ilmenites from Australia and South Africa reveals that ilmenite commonly alters to pseudorutile and then to rutile or anatase, as described by Teufer and Temple (1966) and Grey and Reid (1975). The weathered areas within grains are inhomogeneous and consist of mixtures of ilmenite and altered material. No other phases, such as rutile, hematite, or amorphous material, were identified in altered areas with compositions between ilmenite and pseudorutile. The underlying oxide lattice remains intact during the alteration of ilmenite to pseudorutile, which has a topotactic relationship with ilmenite, with $c_{ilm}//c_{psr}$ and $(11\bar{2}0)_{ilm}//a_{psr}$.

As the ilmenite is altered by the oxidation and removal of iron, the remaining metal cations form ordered chains, with the resulting vacancies parallel to the *c* axis of the oxide lattice, as determined by Grey and Reid (1975). The ordering of different metal-vacancy

chains forms a number of superstructures in the (000*l*) plane. The superstructures form microdomains of between 5 and 20 nm within the altered ilmenite. Rutile or anatase nucleate as discrete precipitates within the weathered material.

Two types of ilmenite alteration are observed in the study area:

1. two-stage alteration in which ilmenite alters to leucoxene via pseudorutile, as described in the TEM study;
2. single-stage alteration of ilmenite directly to rutile (or anatase).

These are known to operate under quite different physical conditions in unconsolidated sediments. In addition, ilmenite altered by high temperature oxidation or hydrothermal processes is found in the deposits.

There is clear evidence that some ilmenite was altered in source areas supplying material to the coastal sediments. Grains containing ilmenite and microcrystalline rutile (type III alteration) indicate that some alteration of ilmenite began in the igneous or metamorphic source rocks. Altered ilmenites may also have been derived from intermediate sedimentary hosts, such as the sandstones of the Natal Group, the Vryheid Formation and the Port Durnford Formation, or ferruginous soils common to the eastern seaboard of South Africa. Reworking of both continental shelf sediments and dunes during Pleistocene sea-level fluctuations resulted in the mixing of altered ilmenite grains formed by the different mechanisms. These observations indicate that the alteration of ilmenites found in the coastal sediments is best described by a multistage model, in which some ilmenite grains were altered prior to deposition in the Holocene dunes. *In situ* alteration of ilmenite, followed by subsequent reworking, has mixed the altered ilmenites formed in different environments (Hugo and Cornell, 1991).

9.3.1 Alteration of ilmenite in older sediments

Heavy mineral suites of the older red Pliocene - Pleistocene dunes and the Mid-Pleistocene Port Durnford Formation are markedly different from those of younger beaches and dunes. In particular, the older deposits contain far less ferromagnesian minerals, which have been

weathered in the deposits. Ilmenite in the Port Durnford Formation is partially altered to pseudorutile, but ilmenite in most of the red dunes is unaltered. The re-precipitation of iron in the red dunes indicates that the environment is oxidising, which is conducive to the preservation of ilmenite, magnetite and hematite. As the sediments are of comparable age, this indicates that the alteration of ilmenite is more dependent on the physical conditions within the sediment, than on the age of the deposit.

9.4 PROVENANCE OF THE IRON-TITANIUM OXIDES

Ilmenite and magnetite in the coastal sediments are derived from rocks of both the Karoo Igneous Province and the Natal Basement. Rutile is derived solely from the latter. Ilmenite from certain rock groups may be distinguished by chemical composition, however, there is large overlap between ilmenites from basalt, dolerite, and a variety of metamorphic rocks. Magnetite from basic igneous rocks is readily distinguished from basement rocks using Al_2O_3, TiO_2, and Fe_2O_3 content, but magnetite from granitoid and metamorphic rocks cannot be distinguished. The petrography of the iron-titanium oxides may be used as a provenance indicator, but caution must be used in the interpretation of this data, as the proportions of the oxide intergrowths change with transport and weathering. The dual provenance of ilmenite and magnetite in coastal sediments along the east coast of South Africa is unique, as these minerals are derived solely from metamorphic basement rocks in most major heavy mineral placer deposits.

Provenance has an important influence on the variations of iron-titanium oxides found in the coastal sediments. Ilmenite and magnetite in eastern Cape and Transkei sediments are derived almost exclusively from basalt and dolerite of the Karoo Igneous Province. Those found in Natal and Zululand are derived from both the Karoo Igneous Province and the Natal Basement rocks. In addition, certain minerals, such as chromite, and composite grains, such as $Ilm\text{-}Hem_{ex}$ or $(Hem\text{-}Rut)_{ox}$, are derived exclusively from the Natal Basement rocks. The higher proportions of these phases in the Natal and Zululand sediments produce subtle changes in the chemical compositions of ilmenite concentrates.

Differences between the TiO_2, MnO, and Cr_2O_3 contents of ilmenite concentrates from the different regions are observed.

Rutile, zircon and garnet are found in coastal sediments throughout the region, although their primary source is the Natal Basement rocks. Significant proportions of rutile and zircon are found as far as Port Elizabeth, but it is evident that these minerals have been reworked from the sediments in the Karoo Sequence.

9.5 VARIATIONS IN COASTAL SEDIMENTS

Beaches and dunes contain the same heavy minerals, but the proportions of the minerals in the heavy mineral suites from these sediments are different. Beaches have higher proportions of pyriboles and other less dense heavy minerals compared to dunes. This is caused by selective sorting of these minerals according to the energy of the depositional environment. Ilmenite, zircon and rutile are finer-grained than pyriboles and are concentrated in the finer dune sediment, while the coarser pyriboles and garnet remain in the beach sands.

Clear differences exist between the relative proportions of ilmenite and magnetite in rivers and coastal dunes in the study area. The rivers have higher proportions of magnetite, while ilmenite is the dominant phase in the dunes. This disparity may be explained by the recent geological history of the east coast, which indicates that the iron-titanium oxide assemblages found in the Late Pleistocene-Holocene dunes are at least 15 000 years old and that these minerals have been extensively reworked. This may be a realistic period for the breakdown of magnetite leading to the enrichment of ilmenite in the coastal dunes.

A model for the formation of the deposits proposes that the heavy mineral-bearing dunes were formed during the last glacial maxima (18 000 - 15 000 B.P.), when the drop in sea-level exposed most of the continental margin along the east coast of southern Africa. Prevailing onshore winds reworked the exposed shelf sediments in dune fields which moved inland until their migration was interrupted by a palaeo shoreline.

REFERENCES

Anand, R.R. and Gilkes, R.J. (1984). Weathering of ilmenite in a lateritic pallid zone. *Clays and Clay Minerals*, **32**, 363-374.

---- and Gilkes, R.J. (1985). Some alumina and silica in weathered ilmenite grains is present in clay minerals - a response to Frost *et al.* (1983). *Mineral. Mag.*, **49**, 141-145.

Anderson, A.T. (1968). Oxidation of the LaBlanche Lake titaniferous magnetite deposit, *Quebec. Jour. of Geol.*, **76**, 528-547.

Anon. (1974). Pulmoddai's mineral sands. *Industrial Minerals*, **77**, 27.

Anon. (1978). Titania: the largest producer of titanium minerals in Europe. *Mining Magazine*, **139**, 365-371.

Anon. (1980). Titanio, Anuário Mineral Brasileiro. *Brasilia*, **10**, 358.

Anon. (1981). Sierra Rutile. *Mining Magazine*, **144**, 458-465.

Anon. (1988). Titanium beach sands. *Mining Magazine*, **149**, 397-403.

Anon. (1989). The sands of Cooljarloo. *Mining Magazine*, **150**, 6-7.

Anon. (1991a). W. Australia beach sands: continued growth. *Mining Magazine*, **152**, 288-293.

Anon. (1991b). AAC's mineral sands venture. *Mining Journal*, **317**, 433.

Anon. (1992a). Tough times for titanium. *Mining Journal*, **318**, 12.

Anon. (1992b). Namakwa heavy mineral reserves at 12-million tons a year. *Engineering News, Mining Supplement*,**150**, 13.

Armstrong, R.A. (1978). *A geological and geochemical appraisal of Rooi Rand dyke swarm, Lebombo*. M.Sc. thesis (unpubl.), Univ. Natal, 135 pp.

----, Bristow, J.W. and Cox, K.G. (1984). The Rooi Rand dyke swarm, southern Lebombo. Spec. Publ. geol. Soc. S. Afr., **13**, 77-86.

Arran, P.T., Hugo, V.E., Turner, A, and Cornell, D.H. (1992). The contribution of Fe-Ti oxides in basalts and dolerites to ilmenite in heavy mineral deposits along the Natal-Zululand coastline. *Abstract Geocongress '92, geol. Soc. S. Afr., Bloemfontein*.

Austin, S.R. (1960). Ilmenite, magnetite and feldspar alteration under reducing conditions. *Econ. Geol.*, **55**, 1758-1759.

Baars, F.J. (1990). *Geologic and petrologic evidence for granulite facies partial melting in the Garies-Platbakkies supracrustal gneiss belt, Namaqualand Metamorphic Complex, South Africa.* M.Sc. thesis (unpubl.), Univ. of Cape Town, 128 pp.

Bach, H. (1962). Formation of brookite as thin TiO_2 layers. *Naturwissenschafen*, **51**, 10-11.

Bailey, S.W., Cameron, E.N., Spedden, H.R., and Weege, R.J. (1956). The alteration of ilmenite in beach sands. *Econ. Geol.*, **51**, 263-279.

Barksdale, J. (1966). *Titanium: Its occurrence, chemistry and technology.* Ronald Press Co., New York, 223 pp.

Bartle, W.W. (1988). The Madagascar mineral sands project - its impact on the market. *In*: Clarke G.M. (ed.). Proceedings 8th. Industrial Minerals International Congress, Boston, 82-89.

Basta, E. Z. (1959). Some mineralogical relationships in the system Fe_2O_3-Fe_3O_4 and the composition of titanomagnetite. *Econ. Geol.*, **54**, 689-719.

Basu, A. and Molinaroli, E. (1989). Provenance characteristics of detrital opaque Fe-Ti oxide minerals. *Jour. Sed. Petrol.*, **59**, 922-934.

---- and Molinaroli, E. (1991). Reliability and application of detrital opaque Fe-Ti oxide minerals in provenance determination. *In*: Morton, A.C., Todd, S.P. and Haughton, P.D. (eds). Developments in sedimentary provenance studies. Geol. Soc. Spec. Publ. No. 57., 55-65.

Battey, M.H. (1981). *Mineralogy for students.* 2nd. Ed., Longman, London, 355pp.

Baxter, J.L. (1977). Heavy sand deposits of Western Australia. *Geol. Surv. W. Aust. Mineral Resources bulletin 10*, 137 pp.

---- (1986). Supergene enrichment of ilmenite - is it related to laterization? *The AusIMM Perth Branch, Australia: A world source of ilmenite, rutile, monazite, zircon, Conference September-October 1986.*

---- and Devereux, M. (1986). What gives a shoreline heavy mineral potential on the Swan Coastal Plain? *The AusIMM Perth Branch, Australia: A world source of ilmenite, rutile, monazite, zircon, Conference September-October 1986.*

Beckering Vinckers, J. (1986). *A geological report on the Port Durnford Formation and heavy mineral bearing sands at Richards Bay Minerals.* B.Sc.(Hons) thesis (unpubl.), Univ. Natal, 49 pp.

Behr, S.H. (1965). Heavy-mineral beach deposits in the Karoo System. *Mem. geol. Surv. S. Afr.*, **56**, 110 pp.

--- (1986). Heavy mineral deposits in the Karoo Sequence. *In*: Anhaeusser, C.R. and Maske, S. (eds). Mineral deposits of Southern Africa. Geol. soc. S. Afr., 2105-2118.

Blaskett, K.S. and Hudson, S.B. (1967). Beach sand minerals. *Proc. 8th Commonwealth Mining and Metall. Congress. Aust. I.M.M.*, **3**, 313-340.

Bohlen, S.R. and Essene, E.J. (1977). Feldspar and oxide thermometry of granulites in the Adirondack Highlands. *Contr. Mineral. Petrol.*, **62**, 153-169.

----, Essene, E.J. and Hoffman, K.S. (1980). Update on feldspar and oxide thermometry in Adriondack Mountains, New York. *Geol. Soc. Amer. Bull.*, **91**, 110-113.

Borisenko, L.F. and Lyanpunov, S.M. (1984). Trace elements in ilmenite from various magmatic associations. *Geokhimiya*, **9**, 1308-1317. (reprinted in *Geochem. Int.*, **22**, 137-146).

Bowles, J.F.W. (1988). Definition and range of composition of naturally occuring minerals with the pseudobrookite structure. *Amer. Mineral.*, **73**, 1377-1383.

Brady, E.S. (1981). China's strategic minerals and metals - titanium. *China Business Review*, **8**, 62-65.

Braun, C. and Raith, M. (1985). Fe-Ti oxides in metamorphic basites from the Eastern Alps, Austria: A contribution to the formation of solid solutions of natural Fe-Ti Oxide assemblages. *Contr. Mineral. Petrol.*, **99**, 199-213.

Bristow, J.W. (1976). *The geology and geochemistry of the southern Lebombo.* M.Sc. thesis (unpubl.), Univ. Natal. 331 pp.

Bristow, J.W. (1980). *The geochronology and geochemistry fo Karoo volcanics in the Lebombo and adjacent areas.* PhD. thesis (unpubl.), Univ. of Cape Town.

Brown, A.G. and Nossal, M. (1990). The Congolone heavy mineral sand deposit in Mozambique. *In*: Griffiths, J.B. (ed.). 9th Industrial Minerals International Congress, 228-237.

Buddington, A.F., Fahey, J. and Vlisidis, A. (1955). Thermometric and petrogenetic significance of titaniferous magnetite. *Amer. Jour. Sci.*, **253**, 497-532.

----, Fahey, J., and Vlisidis, A. (1963). Degree of oxidation of the Adirondack iron oxide and iron-titanium oxide minerals in relation to petrography. *Jour. Petrology*, **4**, 138-169.

----, and Lindsley, D.H. (1964). Iron-titanium oxide minerals and their synthetic equivalents. *Jour. Petrology*, **5**, 310-357.

Bugge, J.A.W. (1978). Norway. *In*: Bowie, S.H.U., Kvalheim, A. and Haslam, H.W. eds. Mineral deposits of Europe, Volume 1: Northwest Europe. London: The Inst. Mining and Metall. and the Mineral. Soc., 199-249.

Bykov, A.D. (1964). Proarizonite as a secondary mineral due to supergene alteration of ilmenite. *Dokl. Akad. SSSR*, **156**, 435-438.

Cannon, H.B. (1949). Economic minerals from beach sands of the southeastern United States. *Proc. of the Symp. on Mineral Resources S.E. U.S., Univ. Tennessee Press, Knoxville, Tenn.*, 202-210.

Cassidy, K.F. and Groves, D.I. (1988). Manganoan ilmenite formed during regional metamorphism of Archean mafic and ultramafic rocks from Western Australia. *Canadian Mineral.*, **26**, 999-1012.

Cawthorn, R.G. and Groves, D.I. (1985). Magnesian ilmenite: Clue to high-Mg parental magma of the Insizwa Complex, Transkei. *Canadian Mineral.*, **23**, 609-618.

----, Maske, S., De Wit, M., Groves, D.I., and Cassidy, K.F. (1988). Contrasting magma types in the Mount Ayliff intrusion (Insizwa Complex), Transkei: Evidence from ilmenite compositions. *Canadian Mineral.*, **26**, 145-160.

----, Bristow, J.W. and Groves, D.I. (1989). Magnesian ilmenite in picrite basalts from the Karoo Province, South Africa. *Mineral. Mag.*, **53**, 245-252.

Cleverly, R.W., Betton, P.J. and Bristow, J.W. (1984). Geochemistry and petrogenesis of the Lebombo Rhyolites. *Spec. Publ. geol. Soc. S. Afr.*, **13**, 171-194.

Coetzee, C.B. (1957). Ilmenite-bearing sands along the west coast in the Vanrynsdorp District. *Bull. geol. Surv. S. Afr.*, **25**, 17 pp. In Afrikaans (English summary).

Cox, K.G. (1970). Tectonics and volcanism of the Karoo period and their bearing on the postulated fragmentation of Gondwanaland. *In*: Clifford, T.N. and Gass, I.G. (Eds). African Magmatism and Tectonics. Oliver and Boyd, Edinburgh, 461 pp.

Craig, J.R. and Vaughan, D.J. (1981). *Ore microscopy and ore petrography*. Wiley and Sons, New York, 406 pp.

Creitz, E.E., and McVay, T.N. (1949). A study of opaque minerals in Trail Ridge, Fla. dune sands. *Amer. Inst. Min. Met. Eng. Trans.*, **181**, 417-423.

Dachille, F., Simons, P.Y. and Roy, R. (1968). Pressure-temperature studies of anatase, brookite, rutile and TiO_2-II. *Amer. Mineral.*, **53**, 1929-1939.

Darby, D.A. (1984). Trace elements in ilmenite; a way to discriminate provenance or age in coastal sands. *Geol. Soc. America Bull.*, **95**, 1029-1218.

---- and Tsang Y.W. (1987). Variation in ilmenite element compositions within and among drainage basins: implications for provenance. *Jour. Sed. Petrol.*, **56**, 831-838.

Davies, J.L. (1980). *Geographical variation of coastal development*. (2 ed.), Longman, London, 212pp.

Davies, O. (1976). The older coastal dunes in Natal and Zululand and their relationship to former shorelines. *Ann. S. Afr. Mus.*, **71**, 19-32.

Deer. W.A., Howie, R.A. and Zussman, J. (1962). *The rock forming minerals. Vol. 5: Non-silicates*. Longmans, London. 1st ed. 371pp.

Desmarais, N.R. (1981). Metamorphosed Precambrian ultramafic rocks in the Ruby Range, Montana. *Precamb. Res.*, **16**, 67-101.

Dimanche, F., and Bartholomé, P. (1976). The alteration of ilmenite in sediments. *Minerals Sci. Engng.*, **8**, 187-201.

Dingle, R.V., Goodlad, S.W., Martin, A.K. (1978). Bathymetry and stratigraphy of the northern Natal Valley (SW Indian Ocean). A preliminary report. *Marine Geology*, **28**, 89-106.

Doriaswamy, L.K., Bijawat, H.C. and Kunte, M.V. (1959). Chlorination of ilmenite in a fluidised bed. *Chem. Eng. Prog.*, **55**, 80-88.

Dryden, L. and Dryden, C. (1946). Comparative rates of weathering of some common heavy minerals. *Jour. Sed. Petrol.*, **16**, 91-96.

Du Cann, B.C. (1976). *The Post-Karoo geology of the St. Lucia and Kosibaai sheets.* (unpubl.). geol. Surv. S. Afr.

Duchesne, J.C. (1970). Microtextures of Fe-Ti oxide minerals in the South-Rogaland anorthosite complex (Norway). *Ann. Soc. geol. Belg.*, **93**, 527-544.

Duncomb and Reid (1968). Data reduction method for electron microprobe analysis. *NBS special publication*, **298**, 135pp.

Du Preez, J.W. (1978). *The geology of the area west of Richards Bay.* (unpubl.). Rep. geol. Surv. S. Afr., 155pp.

Du Toit, A.L. (1929). The volcanic belt of the Lebombo: a region of tension. *Trans. R. Soc. S. Afr.*, **18**, 189-218.

Du Toit, P. (1979). *Geology of the Nanda area, Natal.* M.Sc. thesis (unpubl.), Univ. Natal.

Dyadchenko, M.G. and Khatuntseva, A. (1960). Mineralogy and Petrology of the weathering process of ilmenite: *Doklady Akad. Nauk. SSSR Earth Sci. Sect.*, **132**, 435-438.

Dybdahl, I. (1960). Ilmenite deposits of the Egersund anorthosite complex. *XXI International. Geol. Congress, Copenhagen, Guidebook to Excursion No. C-10*, 43-53.

Eales, H.V and Marsh, J.S. (1979). High-Mg rocks and their significance in the Karoo Central Province. *S. Afr. J. Sci.*, **75**, 400-404.

----, Reynolds,I.M. and Gouws, D.A. (1980). The spinel- group minerals of the central Karoo tholeiitic province. *Trans. geol. Soc. S. Afr.*, **83**, 243-253.

----, Marsh, J.S. and Cox, K.G. (1984). The Karoo igneous province: an introduction. *Spec. Publ. geol. Soc. S. Afr.*,**13**, 1-26.

Elgar, G.W. and Stickney, W.A. (1971). Production of high-purity rutile from a domestic ilmenite concentrate. *Bureau of Mines Nonmetallic Minerals Program, TPR-37*, 10 pp.

----, Wright, J.B., Tress, J.E., Bell, H.E., Jordan, R.R. (1986). Producing chlorination-grade feedstock from domestic ilmenite - Laboratory and pilot-plant studies. *U.S. Bureau of Mines, R.I. 9002*, 24 pp.

Ellis, B.A. (1989). Titanium. Mining Annual Review - 1982. *Mining Journal*, C81-C82.

Elsdon, R. (1975). Iron-titanium oxide minerals in igneous and metamorphic rocks. *Minerals Sci. Engng.*, **7**, 48-70.

Edington, J.W. (1975). *Practical electron microscopy in materials science.* Van Nostrand Reinhold, New York, 350 pp.

Ernst, T. (1943). Fusion equilibrium in the system Fe_2O_3-FeO-TiO_2 and notes on the minerals pseudobrookite and arizonite. *Ztsch. Angew. Min.*, **4**, 394-409.

Evrand, P. (1949). Differentiation of titaniferous magmas. *Econ. Geol.*, **44**, 210-232.

Ferry, J.M. (1984). A biotite isogradin south-central Maine, U.S.A.: Mineral reactions, fluid transfer, and heat transfer. *Jour. Petrol.*, **25**, 871-893.

Flemming, B.W. (1981). Factors controlling shelf sediment dispersal along the southeast African continental margin. *Marine Geology*, **42**, 259-277.

Fitzpatrick, R.W. (1978). *Occurrence and properties of iron and titanium oxides in soils along the eastern seaboard of South Africa.* Ph.D. thesis (unpubl.), Univ. Natal.

Flinter, B.H. (1959). The magnetic separation of some alluvial minerals in Malaya. *Amer. Mineral.*, **44**, 738-751.

---- (1960a). The alteration of Malayan ilmenite grains and the question of "arizonite". *Econ. Geol.*, **54**, 720-729.

---- (1960b). Malayan ilmenite vs. arizonite. *Econ. Geol.*, **55**, 1069-1070.

Fockema, P.D. (1986). The heavy mineral deposits north of Richards Bay. *In*: Anhaeusser, C.R. and Maske, S. (eds), Mineral Deposits of South Africa, Geol. Soc. S. Afr., Johannesburg. 2301-2307.

Force, E.R. (1976). Titanium minerals in deposits of other minerals. *In*: Force, E.R. (ed.). Geology and resources of titanium. Professional Paper 959-A to F, US Geological Survey, F1-F5.

Force, E.R. (1980). The provenance of rutile. *Jour. Sed. Petrol.*, **50**, 485-488.

---- and Stone, B.D. (1990). Heavy mineral dispersal and deposition in sandy deltas of glacial Lake Quinebaug, Connecticut. *U.S. Geol. Surv. Bull. 1874*, 21p.

---- (1991). Geology of titanium-mineral deposits. *Geol. Soc. America, Special Paper 259*. 112 pp.

Frost, B.R. and Lindsley, D.H. (1991). Occurrence of iron-titanium oxides in igneous rocks. *Reviews in Mineral.*, **25**, 433-467.

---- (1991a). Stability of oxide minerals in metamorphic rocks. *Reviews in Mineral.*, **25**, 469-487.

---- (1991b). Magmatic petrology: Factors that control the occurrence of magnetite in crustal rocks. *Reviews in Mineral.*, **25**, 489-509.

Frost, M.T., Grey.I.E., Harrowfield, I.R. and Mason, K. (1983). The dependence of alumina and silica contents on the extent of alteration of weathered ilmenites from Western Australia. *Mineral. Mag.*, **47**, 201 - 208.

----, Grey, I.E., Harrowfield, I.R. and Li, C. (1986). Alteration profiles and impurity element distributions in magnetic fractions of weathered ilmenite. *Amer. Mineral.*, **71**, 167-175.

Gadsden. P. (1982). Titanium. Mining Annual Review - 1982. *Mining Journal*, 58-59.

Geis, H.P. (1971). A short description of the iron-titanium provinces of Norway, with special reference to those in production. *Minerals Sci. Engng.*, **3**, 13-24.

Gevorkyan, V.K. and Tananayev, N.V. (1964). Some data on the initial stages of leucoxenization of ilmenite from the sedimentary deposits of the northern Azov area. *Dopov. Adak. Nauk Ukr. RSR*, **10**, 1366-1369.

Gillson, J.L. (1932). Genesis of the ilmenite deposits of St. Urbain, County Charlevoix, Quebec. *Econ. Geol.*, **27**, 554-577.

---- (1949). Titanium. *Industrial minerals and rocks*, 2nd Ed., 1042-1073.

---- (1950). Deposits of heavy minerals on the Brazilian coast. *Trans. A.I.M.E.*, **187**, 685-693.

Gjelsvik, T. (1957). Geochemical and mineralogical investigations of titaniferous iron ores, west coast of Norway. *Econ. Geol.*, **54**, 698-719.

Golding, H.G. (1961). Leucoxene terminology and genesis. *Econ. Geol.*, **56**, 1138-1149.

Grigsby, J.D. (1989). Magnetite and ilmenite as provenance indicators. Ph.D. thesis. (unpubl.), Univ. Cincinnati, 306 pp.

---- (1990). Detrital magnetite as a provenance indicator. *Jour. Sed. Petrol.*, **60**, 940-951.

Greenwood, G. (1924). The crystal structure of cuprite and rutile. *Phil. Mag.*, **48**, 654-663.

Grey, I.E., and Reid, A.F. (1975). The structure of pseudorutile and its role in the natural alteration of ilmenite. *Amer. Mineral.*, **60**, 898-906.

---- and Nickel, E.H. (1981). Tivanite, an new oxyhydroxide mineral from Western Australia, and its structural relationship to rutile and diaspore. *Amer. Mineral.*, **66**, 866-871.

----, Li, C. and Watts, J.A. (1983). Hydrothermal synthesis of goethite-rutile intergrowth structures and their relationship to pseudorutile. *Amer. Mineral.*, **68**, 981-988.

Groenewald, P.B. (1984). *The lithostratigraphy and petrogenesis of the Nsuze Group northeast of Nkandhla, Natal.* M.Sc. thesis (unpubl.), Univ. Natal, 323pp.

Groves, D.I., Marchant, T., Maske, S. and Cawthorn, R.G. (1986). Compositions of ilmenites in Fe-Ni-Cu sulphides and host rocks, Insizwa, Southern Africa: Proof of coexisting immiscible sulphide and silicate liquids. *Econ. Geol.*, **81**, 725-731.

Grutter, H.S. (1986). *The petrography and petrology of polymetamorphic cordierite-quartz gneisses near geselskapbank, northeast of Springbok.* B.Sc.(Hons) thesis (unpubl.), University of Cape Town.

Haggerty, S.E. (1976a). Oxidation of opaque mineral oxides in basalts. *Reviews in Mineral.*, **3**, Hg1-Hg98.

---- (1976b). Opaque mineral oxides in terrestrial igneous rocks. *Reviews in Mineral.*, **3**, Hg101-Hg277.

Haggerty, S.E. (1991). Oxide textures - a mini-atlas. *Reviews in Mineral*, **26**, 128-211.

Hammerbeck, E.C.I. (1976). Titanium. *In*: Coetzee, C.B. (ed). Mineral resources of the Republic of South Africa. Geol. Surv. S. Afr. Handbook. 7, 5th ed. 221-226.

Hammond, P. (1952). Allard Lake ilmenite deposits. *Econ. Geol.*, **47**, 634-649.

Harki, I., *et al.* (1956). The discovery and mining methods at Finland's largest Fe-Ti-V mine. *Mining World*, **18**, 62.

Hamor, L. (1986). Titanium dioxide manufacture. *Australia: a world source of ilmenite, rutile, monazite and zircon. AusIMM, Perth branch Conference Sept-Oct 1986*, 143-146.

Hartman, J.A. (1959). The titanium mineralogy of certain bauxites and their parent materials. *Econ. Geol.*, **54**, 1380-1405.

Hays, J.D. and Pitman, W.C. (1973). Lithospheric plate motion, sea level changes, climatic and ecological consequences. *Nature*, **246**, 18-22.

Heap, A.S. (1990). Titanium. Metals and Minerals Annual Review - 1990. *Mining Journal*, 75-77.

---- (1991). Titanium. Metals and Minerals Annual Review - 1991. *Mining Journal*, 83-84.

Heinrich, E.W. (1965). *Microscope identification of minerals*. McGraw-Hill, New York, 414 pp.

Heister, N.K., Liston, E.M. and Georz, D. (1974). Beneficiation of ilmenite by sulfidization. *Light Metals Proc. 103rd AIME Annu. Meet.*, **2**, 410-424.

Herz, N. (1976a). Titanium deposits in anorthosite massifs. *In*: Force, E.R. (ed.). Geology and resources of titanium. Professional Paper 959-A to F, US Geological Survey, D1-D6.

---- (1976b). Titanium deposits in alkalic igneous rocks. *In*: Force, E.R. (ed.). Geology and resources of titanium. Professional Paper 959-A to F, US Geological Survey, E1-E6.

Herzburg, W. (1970). The deposit of heavy minerals in the dune sand near Soutfontein, in Namaqualand. *S. Afr. Geol. Surv. Report 1970-0050.* Unpublished.

Hocking, R.M., Warren, J.K., and Baxter, J.L (1982). Shoreline geomorphology, *In*: Exploitation of mineral sands: Perth, Western Australia Institute of Technology, 81-92.

Hobday, D.K. and Orme, A.R. (1974). The Port Durnford Formation: a major Pleistocene barrier-lagoon complex along the Zululand coast. *Trans. geol. Soc. S. Afr.*, **77**, 141-149.

---- (1979). Geological evolution and geomorphology of the Zululand coastal plain. *In*: Allanson, B.R. (ed.). Lake SIbaya. Mongraphiae Biologicae, 36, 1-20.

Hugo, V.E. (1985). *Mineralogical study of the Roaster Feed Circuit (Richards Bay Minerals).* Unpubl. Report, Univ. Natal, 44pp.

---- (1988). *A mineralogical and chemical study of titanium losses at Richards Bay Minerals*. M.Sc. thesis (unpubl.), Univ. Natal, 201pp.

---- (1990). The relative abundance and alteration of iron-titanium oxides along the South African coastline. *Abstract Geocongress '90, geol. Soc. S. Afr., Cape Town*, 261-264.

---- (1991). A transmission electron microscope study of the weathering processes of detrital ilmenite. *Electron microscopy of South Africa*, **21**, 275-276.

---- and Cornell, D.H. (1991). Altered ilmenites in Holocene dunes from Zululand, South Africa: petrographic evidence for multistage alteration. *S. Afr. J. Geol.*, **94**, 365-378.

Isokangas, P. (1978). Finland. *In*: Bowie, S.H.U., Kvalheim, A. and Haslam, H.W. (eds). Mineral deposits of Europe, Volume 1: Northwest Europe. London: The Inst. Mining and Metall. and the Mineral. Soc., 39-92.

Johnson C.H. (1986). The geology of the Zululand titanium deposits: *Abstracts Geocongress '86. Geol. Soc. S. Afr, Johannesburg*, 417-420.

Judd, B.P. and Palmer, E.R. (1973). Production of titanium oxide from ilmenite of the west coast South Island, New Zealand. *Proc. Australas, Inst. Min. Metal.*, **247**, 23-33.

Kahn, J.A. (1984). Non-rutile feedstocks for production of titanium. *Jour. Metals*, 33-38.

Karkhanavala, M.D. (1959). The nature of arizonite. *Econ. Geol.*, **54**, 1302-1308.

---- and Momin, A.C. (1959). The alteration of ilmenite. *Econ. Geol.*, **54**, 1095-1102.

----, Momin, A.C. and Rege, S.G. (1959). An X-ray study of leucoxene from Quilon, India. *Econ. Geol.*, **54**, 913-918.

Kennedy, W.J. and Klinger H.C. (1975). Cretaceous faunas from Zululand and Natal, South Africa. Introduction, Stratigraphy. *Bull. Brit. Mus. Nat. Hist.*, **25**, 265-315.

Knittel, D. (1983). Titanium and titanium alloys. *In*: Grayson, M. and Eckroth, D. (eds). Kirk-Othmer encyclopedia of chemical technology. 3rd Ed., Vol. 23: 98-130. Wiley and Sons, New York.

Laird, J. (1980). Phase equilibra in mafic schist from Vermont. *Jour. Petrol.*, **21**, 1-37.

Langton, G. and Jackson, E.J. (1961). Recovery of ilmenite, rutile and zircon at Umgababa. *Trans. 7th Commonw. min metall. Congr.*, **3**, 1075-1091.

Larrett, M.J., and Spencer, W.G. (1971). Contributions to Australasian mineralogy 3 'pseudorutile' from South Neptune Island, South Australia. *Amdel Bull.*, **12**, 74-80.

La Roche, H., de Kern, M., and Bolfa, J. (1962). Contribution à l'é tude de l'altération des ilménites. *Sci. Terre*, **8**, 215-248.

Lee, C.T and Sohn, H.Y. (1989). Recovery of synthetic rutile and iron oxide from ilmenite ore by sulfation with ammonium sulfate. *In. Eng. Chem. Res.*, **28**, 1802-1808.

Lee, H.Y. and Poggi, D. (1978). Mine, mill, and smelting complex at Richards Bay Minerals. *In*: Toguri, J.M. and Weatherly, G.C. (eds). Metall. Soc. of C.I.M. Annual Volume featuring "hydrogen in metals" and "titanium", Montreal, Can. Inst. Min. Metall., 93-96.

Lepp, H. (1957). Stages in the oxidation of magnetite. *Amer. Mineral.*, **42**, 679-681.

Le Roex, J.L. and Reid, D.L. (1979). Geochemistry of Karoo dolerite sills in the Calvina district, western Cape Province, South Africa. *Contr. Miner. Petrol.*, **66**, 351-360.

Lindsley, D.H. (1976). The crystal structure of the oxide minerals as exemplified by the Fe-Ti oxides. *Reviews in Mineral.*, **3**, L1-L60.

Linström, W. (1987). The Geology of the Dundee Area. *Expl. Sheet 2830. geol. Surv. S. Afr.*, 52 pp.

Lipman, P.W. (1971). Iron-titanium oxide phenocrysts in compositionally zoned ash-flow sheets from southern Nevada. *Jour. Geol.*, **79**, 438-456.

Lissiman, J.C. and Oxenford, R.J. (1975). Eneabba rutile-zircon-ilmenite sand deposit, W.A. *In*: Knight, C.L. (ed.). Economic geology of Australia and Papua New Guinea. 1. Metals. AIMM Monograph Series No. 5, 1062-1070.

Lissiman, J.C., and Oxenford, R.J. (1973). The Allied Minerals N.L. heavy mineral sand deposit as Eneabba, Western Australia. *The Aus. I.M.M. Conference, Western Australia, May 1973*, 153-161.

Logan, C. (1974). A mineralogical examination of beach-sand concentrates from a pilot plant at Richards Bay. *NIM Report No. 1632.*

Lynd, L.E., Sigurdson, H., North, C.H., and Anderson, W.W. (1954). Characteristics of titaniferous concentrates. *Mining Engineering*, **6**, 817-824.

---- (1960). Alteration of ilmenite. *Econ. Geol.*, **55**, 1064-1068.

---- and Lefond, S.J. (1983). Titanium minerals. *In*: Lefond S.J. (ed.). Industrial minerals and rocks. American Inst. of Mining and Metall. and petroleum engineers, New York, 1303-1362.

Lynn, B.C. (1989). Landform, geomophology and Geology. *In*: Lubke, R.A., Avis, A.M., and Jackson, P.B. (eds). An environmental appraisal on the effects of dredge mining on the Kingsa/Tojan lease region of the Eastern Shores of Lake St Lucia (Draft), 33-39.

Mackey, T.S. (1972a). Alteration and recovery of ilmenite and rutile. Part 1: World occurence, production, reserves, demand. *Australian Mining, November 1972*, 18-33.

---- (1972b). Alteration and recovery of ilmenite and rutile. Part 2: Alteration of ilmenite in nature. *Australian Mining, November 1972*, 33-44.

Macpherson, M.H., and Masters, B.K. (1983). Exploration for mineral sands. *MMIJ/AusIMM Joint Symposium 1983, Sendai*. 177-192.

Macpherson, R.D. (1982). Mineral processing at Richards Bay Minerals. *In*: Glen, H.W. (ed.). Proc. 12th CMMI Congress, S. Afr. Inst. Min. Metall., Johannesburg., 835-840.

Mann, G. and James, D. (1986). The evaluation and development of the Barrytown ilmenite deposit as a source of titanium dioxide pigment. *Australia: a world source of ilmenite, rutile, monazite and zircon. AusIMM, Perth branch Conference Sept-Oct 1986*, 139-143.

Martini, I.P. (1975). Sedimentology of a lacustrine barrier system at Wasaga Beach, Ontario, Canada. *Sediment. Geol.*, **14**, 169-190.

Maske, S. (1966). The petrography of the Ingeli mountain range. *Ann. Univ. Stellenbosch.*, **41**, 1-109.

Masters, B.K. (1989). Heavy minerals of the Yoganup Formation, W.A. In press - *Aus. I.M.M. Monograph.*

Maud, R.R. (1961). A preliminary review of the structure of coastal Natal. *Trans. geol. Soc. S. Afr.*, **64**, 247-256.

---- (1968). Quaternary geomorphology and soil formation in coastal Natal. *Zeitschrift für Geomorphologie N.F.*, **7**, 155-199.

---- and Orr, W.N. (1975). Aspects of post-Karoo geology in the Richards Bay area. *Trans. Geol. Soc. S. Afr.*, **78**, 101-109.

McCarthy, M.J. (1967). Stratigraphical and sedimentological evidence form the Durban region of major sea-level movements since the Late Tertiary. *Trans. geol. Soc. S. Afr.*, **70**, 135-165.

---- (1988a). Late-Godwana to Recent geology of the Natal north coast. Excursion C guidebook. *Geocongress 88, geol. Soc. S. Afr., Durban.*

---- (1988b). Some observations on the occurrence of "Berea-Type" red sand along the Natal Coast. *Geocongress 88, geol. Soc. S. Afr., Durban*, 403b-403d.

---- (1988c). The geology of Durban. Excursion C guidebook. *Geocongress 88, geol. Soc. S. Afr., Durban.*

McKellar, J.B. (1975). The Eastern Australian rutile province. *In*: Knight, C.L. (ed.). Economic geology of Australia and Papua New Guinea. 1. Metals. Aus. I.M.M. Monograph Series No. 5, 1055-1062.

Meth, D. (1991). *The Rooi-Rand dyke swarm. Classification and intra/interdyke chemical relationships.* B.Sc. (Hons) thesis (unpubl.), Univ. Natal, 30 pp.

Miller, R. (1945). The heavy minerals of the Florida beach sands. *Amer. Mineral.*, **30**, 65-75.

Miller, D.N. and Folk, R.L. (1955). Occurrence of detrital magnetite and ilmenite in red sediments: new approach to significance of redbeds. *Am. Assoc. Petrol. Geol. Bull.*, **39**, 338-345.

Milner, S. (1971). Investigation of beach sands from Bantu Area No. 4, Nhlabane, Zululand. *NIM Report No. 1217.* 3 pp.

Molinaroli, E. and Basu, A. (1987). Studio di minerali opachi in sabbie fluviali oloceniche e nelle corrispondenti rocce madri di zone sottoposte a climi diversi (Montagne Rocciose e Monti Appalachi in U.S.A.). *Rendiconti della Soc. Italiana di Mineral. E. Petrologia.*, **42**, 271-283.

Molyneux T.G. (1970). *A geological investigation of the Bushveld complex in Sekhukhuneland and part of the Steelport valley, eastern Transvaal, with particular reference to the oxide minerals.* D.Sc. Thesis (unpubl.), Univ. Pretoria.

Moore, D.E. (1990). Development of the Cooljarloo mineral sands deposit in Australia. *In*: Griffiths, J.B. (ed.). 9th Industrial Minerals International Congress, 228-237.

Mücke, A. and Chaudhuri, J.N. (1991). The continuous alteration of ilmenite through pseudorutile to leucoxene. *Ore Geology Reviews*, **6**, 25-44.

Nel, H.J and Koen, G.M. (1960). The relative abundance of ilmenite, rutile and zircon in a dune sand at Umgababa, south coast, Natal. *Trans. geol. Soc. S. Afr.*, **63**, 1-7.

Neumann, E-R. (1974). The distribution of Mn^{2+} and Fe^{3+} between ilmenites and magnetites in igneous rocks. *Amer. Jour. Sci.*, **274**, 1074-1088.

Neurgaonkar, V.G., Gorkan, A.N. and Joseph, K. (1986). Beneficiation of ilmenite to rutile by selective chlorination in a fluidised bed. *Jour. Chem. Technol. Biotechnol.*, **36**, 27-30.

Nicol, A.W. (1975). X-ray diffraction. *In*: Nicol, A.W. (ed.). Physiochemical methods of mineral analysis. Plemim Press, London. 508 pp.

Nord, G.L. and Lawson, C.A. (1989). Order-disorder transition-induced twin domains and magnetic properties in ilmenite-hematite. *Amer. Mineral.*, **74**, 160-176.

Nowicki, T.E. (1986). *The petrology of osumilite-bearing and related metapelitic gneisses from the Bitterfontein area, Namaqualand.* B.Sc. (Hons) thesis (unpubl.), Univ. Cape Town.

Olhoeft, G.R. and Johnson, G.R. (1989). Densities of rocks and minerals. *In*: Carmichael, R.S. (ed.). Practical handbook of physical properties of rocks and minerals. CRC Press, Boca Raton, 741 pp.

Oliver, G.H. (1978). Ilmenite-magnetite geothermometry and oxygen barometry in granulite and amphibolite facies gneisses from Doubtful Sound, Fiordland, New Zealand. *Lithos*, **11**, 147-153.

Overholt, J.L, Vaux, G., and Rodda, J.L. (1950). The nature of "arizonite". *Amer. Mineral.*, **35**, 117-119.

Palmer, C. (1909). Arizonite, ferric metatitanite. *Amer. Jour. Sci.* Ser. 4, **28**, 353-356.

Pauling, l. and Sturdivant, J.H. (1928). The crystal structure of brookite. *Z. Kristallogr.*, **68**, 239-256.

Pettijohn, F.J. (1957). *Sedimentary Rocks.* 2nd Ed., Harper and Row, New York, 718 pp.

---- Potter, P.E., and Siever, R. (1987). *Sand and sandstone*, 2 Ed., Springer-Verlag, New York, 533 pp.

Pirkle, E.C. and Yoho, W.H. (1970). The heavy mineral ore body of Trail Ridge, Florida. *Econ. Geol.*, **65**, 17-30.

----, Pirkle, A. and Yoho, W.H. (1974). The Green Cove springs and Boulougne heavy-mineral sand deposits of Florida. *Econ. Geol.*, **69**, 1129-1137.

Pirkle, F.L. (1975). Evaluation of possible source regions of Trail Ridge Sands. *Southeastern Geology.*, **17**, 93-114.

Putnis, A. and McConnell, J. (1980). *The princples of mineral behaviour.* Blackwell Scientific Publications, Oxford, 257 pp.

Ramdohr, P. (1950). *Die Erzmineralien und ihre Verwachsungen*, Akademie Verlag, Berlin, 875pp.

---- (1953). Ulvöspinel and its significance in titaniferous iron ores. *Econ. Geol.*, **48**, 677-687.

---- (1980). *The ore minerals and their intergrowths*. 2nd ed. Pergamon, Oxford. 1174 pp.

Ramluckan, V.R. (1992). *The petrology and geochemistry of the Karoo sequence basaltic rocks in the Natal Drakensberg at Sani Pass*. M.Sc. thesis (unpubl.), Univ. Durban-Westville.

Ramsey, P.J. (1991). *Sedimentology, coral reef zonation, and late Pleistocene coastline models of the Sodwana Bay continental shelf, northern Zululand.* Ph.D. thesis (unpubl.), Univ. Natal, 202 pp.

Reddering, J.S.V. (1987). Evidence for a middle Holocene transgression, Keurbooms Estuary, South Africa. *Palaeoecology of Africa*, **19**, 79-86.

Reynolds, I.M. (1978a). Mineralogical studies of South African titaniferous iron ores: their application to extractive mineralogy. Trans. geol. Soc. S. Afr., 81, 233-240.

---- (1978b). *A mineralogical investigation of co-existing Iron-titanium oxide from various igneous rocks with special reference to some South African titaniferous ores*. Ph.D. thesis (unpubl.), Rhodes Univ., 622 pp.

---- (1979). Vanadium-bearing titaniferous iron ores from the Rooiwater, Usushwana, Mambula, Kaffirskraal, and Trompsburg igneous complexes. *Nat. Inst. Metallurgy, Randburg*, Report 2017, 61 pp.

---- (1983). The iron-titanium oxide mineralogy of Karoo dolerite in the eastern Cape and southern Orange Free State. *Trans. Geol. Soc. S. Afr.*, **86**, 211-220.

---- (1984). Tectonically deformed ilmenite in titaniferous iron ores of the Mambula Complex, Zululand, South Africa. *Canadian Mineral.*, **22**, 411-416.

---- (1986a). The mineralogy and petrography of some titaniferous iron ores from the Usushwana Complex. *In*: Anhaeusser, C.R. and Maske, S. (eds), Mineral Deposits of South Africa, Geol. Soc. S. Afr., Johannesburg. 1267-1286.

Reynolds, I.M. (1986b). Vanadium-bearing titaniferous iron ores of the Rooiwater Complex, North-eastern Transvaal. *In*: Anhaeusser, C.R. and Maske, S. (eds), Mineral Deposits of South Africa, Geol. Soc. S. Afr., Johannesburg. 451-460.

---- (1986c). The mineralogy and ore petrology of the Bushveld titaniferous magnetite-rich layers. *In*: Anhaeusser, C.R. and Maske, S. (eds), Mineral Deposits of South Africa, Geol. Soc. S. Afr., Johannesburg. 1267-1286.

---- (1986d). The mineralogy and petrography of some vanadium-bearing titanferous iron ores of the Mambula Complex, Zululand. *In*: Anhaeusser, C.R. and Maske, S. (eds), Mineral Deposits of South Africa, Geol. Soc. S. Afr., Johannesburg. 1675-1708.

Richards, J.M., Badenhorst, J.C. and Hamilton, C.C. (1991). Some effects of sulphide mineralisation of the titaniferous magnetite of the Bushveld Igneous Complex in the Potgieterus Area, Northern Transvaal. *ICAM '91 Int. Congr. Applied Mineral.* Paper 46.

Riezebos, P.A. (1979). Compositional downstream variation of opaque and translucent heavy residues in some modern Rio Magdalena sands (Colombia). *Sediment. Geol.*, **24**, 197-225.

Rollinson, H.R. (1980). Iron-titanium oxides as an indicator of the role of the fluid phase during cooling of granites metamorphosed to granulite facies. *Mineral. Mag.*, **43**, 623-631.

Rose, E.R. (1969). Geology of titanium and titaniferous deposits of Canada. *Economic Geology Report No. 25, Geol. Surv. Canada*, 177p.

Rubey, W.W. (1933). The size distribution of heavy minerals within a water-laid sandstone. *Jour. Sed. Petrology*, **29**, 153-163.

Rumble, D. III (1976). Oxide minerals in metamorphic rocks. *Reviews in Mineral.*, **3**, R1-R20.

Ryan, P.J. and Whitfield, G.G. (1979). Basinal analysis of the Ecca and lowermost Beaufort beds and associated coal, uranium and heavy mineral beach sand occurrences. Geokongres 77. *Spec. Publ. geol. Soc. S. Afr.*, **6**, 17-21.

Russ-Nabelek, C. (1989). Isochemical contact metamorphism of mafic schist, Laramie Anorthosite Complex, Wyoming: amphibole compositions and reactions. *Amer. Mineral.*, **74**, 530-548.

Saggerson, E.P., Bristow, J.W. and Armstrong, R.A. (1983). The Rooi Rand dyke swarm. *S. Afr. J. Sci.*, **79**, 365-369.

Saggerson, E.P. (1986). *A handbook of minerals under the microscope*. University of Natal press, Pietermaritzburg, 54 pp.

Scogings, A.J. (1989). Peralkaline gneissic granite and alkaline mafic gneisses, northwest of Eshowe, Natal. *S. Afr. J. Geol.*, **92**, 339-351.

Shoemaker, G.L., Shephens, J.D. and Teller, R.G. (1988). Microdiffraction and microanalysis of iron-titanium mineral samples with a VG STEM. *Microbeam Analysis*, **23**, 480-485.

Skidmore, C.A. (1991). Zirconium and Hafnium. Metals and Minerals Annual Review - 1991. *Mining Journal*, 87-89.

Smyth, C.P. (1992). The Namakwa sands project: some mineralogical aspects. *In*: Mineralogy for mineral processing. Course Notes, SAIMM.

Spencer, R.V. (1948). Titanium minerals in Trail Ridge Fla. *U.S. Bureau of Mines R.I. 4208*, 21pp.

Spencer, R.V. and Williams, F.R. (1964). The development of a rutile mining industry in Sierra Leone. *Industrial Minerals*, **67**, 13-26.

South African Committee for Stratigraphy (SACS) (1980). Stratigraphy of South Africa. Part 1 (Comp. L.E. Kent). Lithostratigraphy of the Republic of South Africa, South West Africa/Namibia, and the Republics of Bophuthatswana, Transkei and Venda: *Hanb. geol. Surv. S. Afr.*, **8**, 690 pp.

Stavrakis, N. (1980). Opaque heavy minerals of the Katberg sandstone, South Africa. *Trans. geol. Soc. S.Afr.*, **83**, 17-21.

Stormer, Jr, J.C. (1983). The effects of recalculation on estimates of temperature and oxygen fugacity from analyses of multicomponent iron-titanium oxides. *Amer. Mineral*, **68**, 586-594.

Suttill, K.R. (1987). Mineral sands an on-going success. *Engineering and Mining Journal*, 44-47.

Sydow, C.I. (1988). *Stratigraphic control of slumping and canyon development on the Zululand continental margin, east coast, South Africa*. B.Sc. (Hons) thesis (unpubl.), Univ. Cape Town.

Temple, A.K. (1966). Alteration of ilmenite. *Econ. Geol.*, **61**, 695 - 714.

Teufer, G. and Temple, A.K. (1966). Pseudo-rutile - a new mineral intermediate between ilmenite and rutile in the alteration of ilmenite. *Nature*, **211**, 179-181.

Theonen J.R. and Warne J.D. (1949). Titanium minerals in central and northeastern Florida. *U.S. Bureau of Mines, R.I. 4515.*

Thomas, R.J. (1988). Geology of the Port Shepstone area. *Expl. sheet 3030 (Port Shepstone), geol. Surv. S. Afr.*, 136 pp.

---- (1989). A tale of two tectonic terranes. *S. Afr. J. Geol.*, **92**, 306-321.

---- Bullen, W.D., de Klerk, I, and Scogings, A.J. (1990). The distribution and genesis of precious and base metal mineralisation in the Natal Metamorphic Province. *S. Afr. J. Geol.*, **93**, 683-695.

Thompson J.V. (1977). Appraising large diameter core and percussion drilling for bulk samples. *Engineering and Mining Journal*, **178**, 80-82.

Tinley, K.L. (1985). Coastal dunes of South Africa. *S. Afr. Natl. Sci. Prog. Report No. 109.*

Towner, R.R. (1986). Resources of mineral sands. What of their future? *Australia: a world source of ilmenite, rutile, monazite and zircon. AusIMM, Perth branch Conference Sept-Oct 1986*, 35-50.

---- (1984). Titanium. *Australian Mineral Industry Annual Review for 1984. Canberra: Aust. Govt. Publ. Serv.*, 256-263

---- (1987). Titanium. *Australian Mineral Industry Annual Review for 1985. Canberra: Aust. Govt. Publ. Serv.*, 256-263

---- (1988). Titanium. *Australian Mineral Industry Annual Review for 1986. Canberra: Aust. Govt. Publ. Serv.*, 239-245.

Tracy R.J. (1982). Compositional zoning and inclusions in metamorphic minerals. *Rev. Miner.*, **10**, 355-397.

Truswell, J.F. (1977). *The geological evolution of South Africa*. Purnell, Cape Town, 218 pp.

Tsusue, A. (1973). The distribution of manganese and iron between ilmenite and granitic magma in the Osumi Peninsula, Japan. *Contr. Mineral. Petrol.*, **40**, 305-314.

Turner, A. (1990). *Iron-titanium oxide mineralogy of the Sani Pass Karoo basalts and selected Karoo dolerites in Natal.* B.Sc. (Hons) thesis (unpubl.), Univ. Natal, 26pp.

Uytenbogaardt, W. and Burke, E.A. (1971). *Tables for microscopic identification of ore minerals.* Elsevier Publ. Co., Amsterdam, 429 pp.

Van der Plas, L. and Tobi, A.C. (1965). A chart for judging the reliability of point-counting results. *Amer. Jour. Sci.*, **263**, 87 - 90.

Van Heerden, I.L. (1987). Sedimentation in the greater St. Lucia complex as related to palaeo-sea levels. *Abstract. 6 th National Oceanographic Symposium, Stellenbosch, Paper 157*: B-106.

Vincent, E.A. and Phillips, R. (1954). Iron-titanium oxide minerals in layered gabbros of the Skaergaard intrusion, East Greenland. *Geochim. Cosmo. Acta*, **6**, 1-26.

Vegard, L. (1916). Results of crystal analysis. *Phil. Mag.*, **32**, 65-96.

---- (1926). Results of crystal analysis. *Phil. Mag.*, **ser.7, vol 1**, 1151.

Von Gruenewalt, G. (1977). The mineral resources of the Bushveld complex. *Minerals Sci. Engng.*, **9**, 83-95.

Walker, F. and Poldervaart, A. (1949). Karroo (sic.) dolerites of the Union of South Africa. *Bull. Geol. Soc. S. Afr.*, **60**, 591-706.

Welch, B.K., Sofoulis, J. and Fitzgerald, A.C.F. (1975). Mineral sand deposits of the Capel area W.A. *In*: Knight, C.L. (ed.). Economic geology of Australia and Papua New Guinea. 1. Metals. AIMM Monograph Series No. 5, 1070-1088.

Wenk, H.R. (1976). *Electron microscopy in mineralogy.* Springer-Verlag, Berlin, 564pp.

Whalen, J.B. and Chappell, B.W. (1988). Opaque mineralogy and mafic mineral chemistry of I- and S-type granites of the Lachlan fold belt, south east Australia. *Amer. Mineral.*, **73**, 281-296.

Whitehead, J. (1983). Titanium compounds - inorganic. *In*: Grayson, M. and Eckroth, D. (eds). Kirk-Othmer encyclopedia of chemical technology. 3 rd ed. Vol. 23: 131-176. Wiley and Sons, New York.

Williams, F.R. (1974). William Gregor, 1761-1817. *Educ. Chem.*, **11**, 115.

Williams, D.F., Moore, W.S., and Fillon, R.S. (1981). Role of the glacial Arctic Ocean ice sheets in Pleistocene oxygen isotope and sea-levels records. *Earth Planet. Sci. Lett.*, **56**, 157-166.

Winter, J. de la R., and Venter, J.J. (1970). Lithostratigraphic correlation of recent deep boreholes in the Karoo-Cape sequence. *Proc. Pap. Second Gondwana Symposium, South Africa*, 395-408.

Wipplinger, P.E. (1985). Extract from report: An outline of the economic potential of titanium in South Africa: *S. A. Geol. Surv. Report.*

Wort, M.J., and Jones, M.P. (1980). X-ray diffraction and magnetic studies of altered ilmenite and pseudorutile. *Mineral. Mag.*, **43**, 659-663.

---- and Jones, M.P. (1981). Magnetic properties of ilmenite, detrital altered ilmenite and pseudorutile. *Trans. Inst. Min. Metall.*, **90**, C130-C137.

Wuth, M.G. and Archer, P.D. (1986). Chromite mineralisation at Sithilo, Northern Zululand, 1689-1694. *In*: Anhaeusser, C.R. and Maske, S. (Eds). Mineral Deposits of Southern Africa, II, Geol. Soc. S.Afr., Johannesburg, 2335 pp.

Yamada, S. (1976). Ilmenite beneficiation and its implications for titanium dioxide manufacuture. *Industrial Minerals*, **1**, 33-40.

Yates, R.J., Miller, D.E., Halket, D.J., Manhire, A.H., Parkington, J.E. and Vogel, J.C. (1986). A mid-Holocene high sea level: a preliminary report on the geoarchaeology at Elands Bay, western Cape Province, South Africa, *S. Afr. Jour. Sci.*, **82**, 164-165.

APPENDIX A

List of samples collected in the study area

APPENDIX A.1: LIST OF SAMPLES COLLECTED FROM BEACHES

Sample No.	Region	Locality	Age	Notes
HZ 12	Zululand	Sodwana Bay	Holocene	f-m/g; white; m-h/HM, pyr, opq; 1 km N. of Jesser Point.
HZ 10	"	Cape Vidal	"	f-m/g, beige; m/HM, opq, gt; S. of boat launch area.
HZ 8	"	Mission Rocks	"	m/g, lt.beige; m/HM, opq, pyr, gt; 1 km S. of Mission Rocks.
HZ 6	"	St Lucia Estuary mouth	"	m/g, mottl. brown; l-m/HM; 1.5 km N. of estuary mouth.
HZ 32	"	Richards Bay	"	m-c/g, beige; h/HM, opq, pyr; 2 Mile Beach.
HZ 25	"	Mtunzini	"	c/g, d.beige; h/HM, pyr; beach in nature reserve.
HZ 3	"	Port Durnford	"	m-c/g, d.beige; m/HM, pyr, opq; close to access road.
HZ 1	"	Tugela River Mouth	"	c/g, beige; h/HM, magn, opq, pyr, gt; 500 m N. of r. mouth
HN 33	Natal	Zinkwazi	Holocene	m/g, beige; m/HM, opq, pyr, gt; berm across r. mouth
HN 29	"	Blythedale Beach	"	c/g, lt. beige; l-m/HM, pyr, opq, gt; Main swimming beach.
HN 26	"	Tinley Manor	"	c/g, mottl. beige; l-m/HM, pyr, opq; opposite car park.
HN 8	"	Umhloti	"	m/g, mottl. beige; l-m/HM, pyr, opq, gt, lagoon mouth.
HN 6	"	Umgeni River Mouth	"	m/g, beige; m-h/HM, opq, pyr, gt; south of Blue Lagoon pier.
HN 9	"	South Beach, Durban	"	f-m/g, black; v.h/HM, opq, gt, pyr; after heavy storm.
HN 4	"	Isipingo Beach	"	m/g, lt. beige, m/HM, opq, gt, pyr, near car park.
HN 3	"	Umgababa	"	c/g, mottl. beige, l-m/HM, pyr, opq, gt; 5 km N. of r. mouth.
HN 20	"	Umkomaas	"	c/g, lt. beige, l/HM, pyr, opq, 1 km S. of r. mouth.
HN 17	"	Mzumbe River Mouth	"	m/g, d.beige, m/HM, pyr, gt, opq; 1 km N. of r. mouth
HN 14	"	Port Shepstone	"	c/g, d. beige, m/HM, pyr, opq, gt; 0.5 km north of r. mouth
HN 10	"	Hlatimi		c/g, l. beige, l/HM, pyr, opq; berm across r. mouth
HN 11	"	Hlatimi	"	c/g, l. beige, l-m/HM, pyr, opq; 1 km N. r. mouth

Sample No.	Region	Locality	Age	Notes
HT 4	Transkei	Mzamba Beach	Holocene	m/g, beige; m/HM, opq, pyr; 3 km S. of casino
HT 3	"	Port St Johns	"	m-c/g, grey-brown, h/HM, opq, pyr; 1 km N. of r. mouth
HT 14	"	Mazeppa Bay	"	f-m/g, mottl. beige, m/HM, opq; S. of r. mouth.
HT 9	"	Xamani	"	f-mg/, mottl. grey-beige, h/HM, opq; 3 km N. of river mouth
HT 13	"	Mbashee River Mouth	"	f-m/g, mottl. lt. beige, m/HM, opq, pyr, 1 km N. of r. mouth
HEC 8	eastern Cape	Kei River Mouth	Holocene	f/g, lt.beige; l-m/HM, opq; 0.5 km S. of r. mouth
HEC 7	"	Morgan's Bay	"	f/g, mottl. beige; m/HM, opq; 2 km S. of r. mouth, opposite hotel
HEC 5	"	Kidd's Beach	"	f/g, lt. beige, l-m/HM, opq, pyr; 0.5 km N. of car park.
HEC 4	"	Nahoon Beach	"	f/g, white; l-m/HM, opq; main swimming beach.
HEC 3	"	Fish River Mouth	"	f/g, lt. beige; l-m/HM, opq; 0.5 km S. of r. mouth.
HEC 2	"	Bushmans' River Mouth	"	f/g, mottl. white; l/HM, opq; at r. mouth.
HEC 1	"	Swartkops River Mouth	"	f/g, mottl.white; v.l/HM; near car park.

APPENDIX A.2: LIST OF SAMPLES COLLECTED FROM DUNES

Sample No.	Region	Locality	Age	Notes
HZ 13	Zululand	Sodwana Bay	Late Pleistocene-Holocene	f/g, mottl. white,; collected by Ian Weight, UND.
HZ 45	"	Sodwana Bay	Late Pleistocene	m-f/g, pale orange; Sodwana Bay campsite.
HZ 43	"	Lake Sibayi	"	m/g, orange-red; Sibayi-Sodwana Road.
HZ 44	"	Lake Sibayi	"	f/g, cl., red; Sibayi-Sodwana Road.
HZ 41	"	Ridge west of Tshongwe	Pleistocene	m/g, cl., d. red-brown; Mkuze-Sibayi Road.
HZ 42	"	Tshongwe	"	m/g, cl., d. red; Mkuze-Sibayi Road.
HZ 40	"	False Bay	"	m/g, cl., red-brown; Hluhuwe-False Bay road.
HZ 46	"	Charter's Creek	"	m/g, cl., brown-red; road to Charter's Creek.
HZ 47	"	Dukuduku Forest	"	m-c/g, cl., d. red; lookout tower, Mehlowemamba.
HZ 11	"	Cape Vidal	Late Pleistocene-Holocene	f/g, lt. beige; coastal dunes.
HZ 9	"	Mission Rocks	Late Pleistocene	f/g, orange-red; 2 km N. of Mission Rocks.
HZ 7	"	Mission Rocks	Late Pleistocene-Holocene	f/g, lt. orange; road through coastal dune cordon.
HZ 5	"	Cape St Lucia	Late Pleistocene	f/g, orange-red; coastal dune cordon.
HZ 4	"	Cape St Lucia	Late Pleistocene-Holocene	f/g, lt. beige; coastal dune cordon.
HZ 19	"	Richards Bay	"	m/g, cl. red; overlying Port Durnford Frm., "Scribante Hole" Tisand orebody.
HZ 17	"	Richards Bay	Late Pleistocene-Holocene	borehole sample -36 m, below water table, Tisand orebody.
HZ 16	"	Richards Bay	"	borehole sample -30 m, above water table, Tisand orebody.
HZ 36	"	Richards Bay	"	borehole sample -42 m, below water table, Tisand orebody.
HZ 35	"	Richards Bay	"	borehole sample -20 m, above water table, Tisand orebody.
HZ 30	"	Richards Bay	Pleistocene	f-m/g, cl., red; 1 km S. of Lake Nhlabane.
HZ 18	"	Umhlatuze	Pleistocene	m/g, cl. red; adjacent to Mtunzini toll road.

Sample No.	Region	Locality	Age	Notes
HZ 27	"	Mtunzini	Pleistocene	f-m/g, cl. d.red-brown; Mtunzini town.
HZ 26	"	Mtunzini	Late Pleistocene-Holocene	m/g, lt. beige; coastal foredune, near car park.
HZ 2	"	Port Durnford	"	m/g, lt. beige; coastal foredune.
HN 35	Natal	Zinkwazi	Pliocene-Pleistocene	m-c/g, cl. red; ridge inland of Zinkwazi town.
HN 34	"	Zinkwazi	Late Pleistocene-Holocene	f-m/g, lt. beige; coastal dune cordon, 1 km N. of r. mouth
HN 31	"	Blythedale Beach	Pliocene-Pleistocene	m/g, cl. red; inland dune ridge.
HN 30	"	Blythedale Beach	Late Pleistocene-Holocene	m/g, beige; coastal foredune near car park.
HN 28	"	Tinley Manor	Pliocene-Pleistocene	m/g, cl. d.red; inland dune ridge.
HN 27	"	Tinley Manor	Late Pleistocene-Holocene	f-m/g, beige; coastal dune cordon.
HN 7	"	Umdloti	"	f-m/g, d.beige; coastal foredune, 0.5 km N. of r. mouth.
HN 25	"	Ballito Beach	Pliocene-Pleistocene	m/g, cl. red-orange; dune ridge adj. to N2.
HN 24	"	Umhlanga Rocks	"	m/g, cl. orange; adj. to R106, 5 km N. of Umhlanga Rocks.
HN 23	"	Durban North	"	f/g, cl. d. orange; inland dune ridge, approx. 3 km north of Umgeni River.
HN 5	"	Isipingo Beach	Late Pleistocene-Holocene	f/g, lt. beige; coastal foredune.
HN 1	"	Umgababa	"	m-c/g, beige; old mining site
HN 2	"	Umgababa	Pliocene-Pleistocene	m/g, cl. red; old mining site
HN 22	"	Umkomaas	"	clayey red sand, railway cutting
HN 21	"	Umkomaas	Late Pleistocene-Holocene	f-m/g, white; coastal dune cordon, near beach road.
HN 19	"	Mzumbe River Mouth	Pliocene-Pleistocene	m/g, cl. red; 0.5 km N. of r. mouth, adj. to N2.
HN 18	"	Mzumbe River Mouth	Late Pleistocene-Holocene	m/g, mottl. white, coastal foredune, 1 km N. of r. mouth.
HN 16	"	Port Shepstone	Pliocene-Pleistocene	m/g, cl. red; adj. to N2, 3 km N. of r. mouth.
HN 15	"	Port Shepstone	Late Pleistocene-Holocene	m/g, mottl. beige; coastal foredune; 3 km N. of r. mouth.

Sample No.	Region	Locality	Age	Notes
HN 13	"	Hlatimi	Pliocene-Pleistocene	m/g, cl. red; dune ridge adj. to N2.
HN 12	"	Hlatimi	Late Pleistocene-Holocene	m/g, beige; foredune; 1km N. of river mouth.
HT 5	Transkei	Mzamba Beach	Late Pleistocene-Holocene	f-m/g, lt. beige; coastal foredune, 5 km south of casino.
HT 15	"	Port St Johns	"	f-m/g, mottl. beige; coastal foredune, 3 km N. of r. mouth.
HT 16	"	Mazeppa Bay	"	f/g, lt. beige; coastal foredune, adj. to r. mouth.
HT 11	"	Umgazi River Mouth	"	f-m/g, mottl. beige; coastal foredune, S. of r. mouth.
HT 12	"	Xamani	Pliocene-Pleistocene	m/g, cl. red; high dune ridge; 3 km S. of Umgazi r. mouth.
HT 10	"	Xamani	Late Pleistocene-Holocene	m/g, beige; low coastal foredune, 2 km N. of r. mouth.
HT 2	"	Mbashee River Mouth	"	m/g, beige, coastal foredune.
HT 7	"	Wavecrest	"	m/g, orange; low coastal dune ridge, 1 km S. of hotel
HT 8	"	Sandy Point	"	f/g, lt. beige; coastal foredune, 4 km N. of r. mouth
HEC 6	eastern Cape	Morgan's Bay	Late Pleistocene-Holocene	f/g, lt. beige, coastal dune cordon, 0.5 km N. of r. mouth.
HEC 13	"	Fish River Mouth	"	f/g, white; coastal foredune, 0.5 km S. of river mouth.
HEC 10	"	Kidd's Beach	"	f-m/g, mottl. white, coastal dune cordon, 0.5 km N. of swimming beach.
HEC 11	"	Nahoon Beach	"	f/g, white; coastal dune cordon, 1 km N. of swimming beach.
HEC 12	"	Bushman's River Mouth	"	f/g, mottl. white; low coastal dune cordon, 1 km S. of r. mouth.
HZ 21	Zululand	Port Durnford Formation	Mid-Pleistocene	f-m/g, cl. white; l/HM, opq; "Scribante Hole", Tisand orebody
HZ 22	"	"	"	"
HZ 23	"	"	"	"
HZ 51	"	"	"	m/g, cl. white; l/HM, opq; 2 Mile beach, Richards Bay.
HZ 52	"	"	"	f-m/g, cl. white; l/HM, opq; 5 Mile Beach, Richards Bay.

APPENDIX A.3: LIST OF SAMPLES COLLECTED FROM RIVERS

Sample No.	Region	River	Notes
HZ 24	Zululand	Tugela	side-channel bar, near railway bridge, Mandini
HZ 31	"	Mhlatuze	side-channel bar, N2 bridge
HZ 14	"	Pongola	mid-channel bar, N2 bridge
HZ 34	"	Mfolozi	side-channel bar, N2 bridge
UMG1-UMG5	Natal	Mgeni	tributaries of the Mgeni R. draining rocks of the Natal Struct. and Met. Province; Downstream of Nagal Dam.
HN 32	Natal	Mvoti	mid-channel bar, N2 bridge
HT 6	Transkei	Kei	side-channel bar, N2 bridge
HEC 9	eastern Cape	Fish	mid-channel bar, N2 bridge
HS 6	Natal	Tugela	gravelly, side-channel bar, Royal Natal National Park, sample was pre-concentrated by removing the + 1 mm sized material.
PTA 2	Natal	Tugela	average of 4 river samples, Royal Natal National Park; from Arran *et al.* (1992)
PTA 4	Natal	Tugela	average of 3 river samples, Tugela Ferry area; from Arran *et al.* (1992).

APPENDIX A.4: LIST OF SAMPLES COLLECTED FROM ROCK OUTCROPS

Sample No.	Rock Type	Locality	Notes
HS 1	basalt	Sani Pass	f/g amygdaloidal basalt, adj. to Sani Pass Road.
HS 2	basalt	Sani Pass	f/g basalt, adj. to Sani Pass Road.
HS 3	basalt	Sani Pass	adj. to Sani Pass Road.
HS 4	basalt	Mont-Aux-Sources	f/g basalt, Royal Natal National Park
HS 5	basalt	Mont-Aux-Sources	f/g basalt, Royal Natal National Park
PTA 1	basalt	Mont-Aux-Sources	average of 4 rock basalts, Royal Natal National Park; from Arran *et al.* (1992).
HL 1	rhyolite	Lebombo Mountains	f/g rhyolite, collected adj. to road going to Josini Dam wall.
HL 2	rhyolite	Lebombo Mountains	f/g rhyolite, collected adj. to road going to Josini Dam wall.
VD 1	dolerite	Howick	large dolerite sill, m-c/g, adj. to N3
VD 2	dolerite	Ixopo	m-c/g, large dolerite sill, adj. to main road.
VD 3	dolerite	Kokstad	c/g, dolerite sill, adj. to N2, near South Africa-Transkei border.
D 6	dolerite	Reichenau	dolerite sill, on Underberg road; collected by Turner (1990).
D 8	dolerite	Midmar Dam	dolerite sill, near N3; collected by Turner (1990).
PTA 3	dolerite	Tugela Ferry area	average of 3 dolerite samples; from Arran *et al.* (1992).
LHD 3	dolerite		
LRRD 2	dolerite		
DM90-18	dolerite	Pongola River	dolerite dyke, Rooi Rand dyke swarm, Near N2 bridge across Pongola River
DM90-6	dolerite	Pongola River	"
DM90-8	dolerite	Pongola River	"
DM90-25	dolerite	Pongola River	"

Sample No.	Rock Type	Locality	Notes
VG 1	granite	Kloof End Pluton	unfoliated, m/g granite, Hibberdene
VG 2	granite-gneiss	Ngoye granite-gneiss	magnetite-bearing microgranite, W. of Univ. of Zululand.
VG 3	granite-gneiss	Mgeni Batholith	c/g granite-gneiss, containing feldpar phenocrysts, Mgeni Valley
VG 4	charnockite	Port Edward	coastal outcrop.
VG 5	granite-gneiss	Mzimlilo Suite	m/g, leucocratic; collected near Glenrosa, along Hibberdene-Ixopo road.
MS 17	megacrystic granite-gneiss	Mgeni Batholith	collected by G. Milne, Dept. of Geology, UND
MS 18	"	"	"
NDF 50	amphibolite	Mapumulo Suite	f/g amphibolite, collected by G. Milne, Dept. of Geology, UND.
VA 1	"	Mapumulo Suite	amphibolite, Mgeni River.
VA 2	"	Tugela Group	Silambo Formation, on Eshowe Road.
VA 3	"	"	"
VA 4	"	"	"
NDF 10	biotite schist	Mapumulo Suite	collected by G. Milne, Dept. of Geology, UND.
VM 2	biotite-hbl. gneiss	Mapumulo Suite	Nkandla area.
VM 3	amphibolite-gneiss	Thondo Formation	on Eshowe-Gingingdlovu road.
VM 4	"	"	"
VM 1	Metamorphosed Ultrabasic complex	Mambula Complex	c/g, massive, Fe-Ti oxide layer in ultrabasic host.
IR 1 and 2	"	"	from Reynolds (1986d)

APPENDIX B

Electron microprobe analyses of rutile, ilmenite and magnetite from coastal sediments

APPENDIX B.1 - MICROPROBE ANALYSES OF RUTILE IN COASTAL SEDIMENTS

Analysis		SiO2	TiO2	Al2O3	Cr2O3	FeO	MnO	MgO	Total
HZ 13	1		98.60	0.02	0.07	0.30			98.99
HZ 13	2		98.59		0.21	0.13			98.94
HZ 13	3		99.88		0.15				100.04
HZ 13	4		99.28		0.09	0.10			99.47
HZ 13	5		99.21	0.06	0.09	0.27			99.63
HZ 13	6		99.03			0.36			99.39
HZ 13	7		99.09		0.24	0.16			99.49
HZ 13	8		98.60	0.05	0.06	0.25			98.95
HZ 13	9	0.07	98.59	0.13	0.16	0.19			99.14
HZ 13	10		99.04		0.07	0.09			99.20
HZ 13	11		99.10	0.03	0.14				99.27
HZ 13	12		99.33	0.02	0.06	0.13			99.53
HZ 13	13		99.20		0.21				99.41
HZ 1	1		98.79	0.03	0.06	0.09			98.98
HZ 1	2		98.66		0.20				98.86
HZ 1	3		99.23	0.05	0.04	0.32			99.63
HZ 1	4		99.04	0.02	0.13				99.19
HZ 1	5		99.82	0.03	0.09				99.94
HZ 1	6		99.70	0.02	0.07				99.80
HZ 1	7		99.76	0.02	0.10	0.17			100.04
HZ 1	8		99.16	0.13	0.09	0.34			99.73
HZ 1	9		99.09	0.03	0.07				99.19
HZ 1	10		99.27	0.04	0.12	0.10			99.53
HZ 1	11	0.04	99.55	0.03	0.05	0.11			99.78
HZ 1	12		99.27	0.03	0.09	0.21			99.60
HZ 1	13		99.64	0.02	0.05	0.15			99.86
HZ 1	14		98.59	0.03	0.09	0.12			98.83
HZ 30	1		99.25		0.05				99.30
HZ 30	2		99.85			0.12			99.97
HZ 30	3		99.90			0.08			99.98
HN 28	1		99.75		0.09				99.84
HN 28	2		99.12		0.09	0.11			100.33
HN 28	3		98.82	0.02	0.05				98.89
HN 28	4		99.64			0.64			100.28
HN 28	5		99.82	0.02	0.09	0.10			100.02
HN 28	6	0.10	98.69	0.02	0.24	0.10			99.15

Blank = below detection limit

APPENDIX B.1 - MICROPROBE ANALYSES OF RUTILE IN COASTAL SEDIMENTS

Analysis		SiO2	TiO2	Al2O3	Cr2O3	FeO	MnO	MgO	Total
HN 19	1		99.13	0.03		0.96			100.12
HN 19	2		100.03	0.06		0.34			100.43
HN 19	3	0.30	98.16	0.15		0.98			99.59
HN 19	4	0.10	98.92	0.11	0.13	0.91			100.17
HN 7	1		99.39		0.10	0.26			99.75
HN 7	2		98.71		0.04	0.12			98.87
HN 7	3		99.41		0.08	0.21			99.70
HN 7	4		99.18		0.06	0.11			99.34
HN 7	5		98.46		0.20				98.67
HN 7	6		98.59		0.13				98.72
HN 7	7		98.75		0.17				98.92
HN 7	8		98.73		0.15				98.88
HN 7	9		99.93		0.13				100.06
HN 7	10		99.56		0.10	0.13			99.79
HN 7	11		99.10	0.02	0.06	0.11			99.29
HN 7	12		98.63	0.02	0.07	0.10			98.81
HN 7	13		98.52	0.02	0.11	0.29			98.94
HN 7	14		99.73		0.14	0.09			99.96
HN 2	1		99.40		0.15	0.08			99.64
HN 2	2		99.63						99.63
HN 2	3		98.94		0.05	0.21			99.20
HN 2	4		98.15		0.12	0.10			98.37
HN 2	5		98.24		0.12	0.18			98.54
HN 2	6		98.84		0.10	0.21			99.14
HN 2	7		99.22	0.02	0.08	0.16			99.48
HN 2	8		99.31		0.10	0.17			99.58
HN 2	9		99.77	0.02	0.14	0.16			100.09
HN 2	10		99.32		0.08	0.24			99.64
HN 2	11		98.47		0.19				98.66
HN 2	12		98.62		0.10	0.10			98.82
HN 2	13		99.30		0.12	0.37			99.80
HN 2	14		99.71	0.03	0.14				99.87
HN 2	15		99.41		0.13				99.54
HT 2	1		99.45	0.03		0.09			99.56
HT 3	1		99.91	0.03		0.26			100.20
HT 3	2		99.69			0.10			99.79

Blank = below detection limit

APPENDIX B.1 - MICROPROBE ANALYSES OF RUTILE IN COASTAL SEDIMENTS

Analysis		SiO2	TiO2	Al2O3	Cr2O3	FeO	MnO	MgO	Total
HT 3	3	0.03	99.95	0.07		0.13			100.18
HT 3	4		99.02	0.04	0.07				99.12
HT 3	5		99.37	0.06		0.28			99.71
HT 3	6		99.10	0.06	0.10	0.17			99.42
HT 3	7		99.51	0.03	0.19	0.21			99.93
HT 3	8		99.30	0.03	0.11	0.17			99.62
HT 3	9		99.56	0.02		0.51			100.09
HT 3	10		99.81	0.02	0.14	0.19			100.16
HT 3	11		99.91	0.10	0.09	0.27			100.36
HT 3	12		99.98	0.11	0.09	0.19			100.37
HT 7	1	0.05	98.75	0.24	0.05	0.32			99.41
HT 7	2		99.12			0.15			99.27
HT 7	3		99.08						99.08
HT 7	4		99.23			0.15			99.38
HT 7	5		98.81			0.12			98.93
HT 7	6		98.75	0.02	0.17	0.08			99.02
HT 7	7	0.23	99.83	0.16	0.13	0.44			100.79
HT 7	8	0.03	99.31	0.06	0.16	0.22			99.78
HT 7	9		99.96	0.03	0.08	0.20			100.28
HT 7	10		98.99	0.03	0.14	0.16			99.31
HT 7	11		98.91	0.02	0.02	0.27			99.22
HT 7	12	0.03	98.04	0.03	0.10	0.14			98.34
HT 7	13		99.54	0.03	0.25	0.39			100.21
HT 7	14		99.26	0.04	0.09	0.31			99.69
HT 7	15		98.13	0.07	0.11	0.08			98.38
HT 7	16		99.03		0.05	0.45			99.53
HT 7	17		99.48		0.13	0.09			99.70
HT 7	18	0.36	98.65	0.35	0.09	0.64			100.10
HEC 5	1		99.12	0.03		0.47			99.64
HEC 5	2		99.40			0.17			99.60
HEC 5	3		98.95	0.06		0.21			99.23
HEC 5	4		98.87			0.10			99.00
HEC 5	5	0.03	99.67	0.05		0.19			99.94
HEC 5	6		99.11			0.16			99.28
HEC 5	7		99.55			0.18			99.73
HEC 5	8		99.33						99.35

Blank = below detection limit

APPENDIX B.1 - MICROPROBE ANALYSES OF RUTILE IN COASTAL SEDIMENTS

Analysis		SiO2	TiO2	Al2O3	Cr2O3	FeO	MnO	MgO	Total
HEC 5	9		99.31	0.11					99.47
HEC 5	10		98.98			0.42			99.44
HEC 6	1		99.21	0.04		0.21			99.46
HEC 6	2		99.56			0.11			99.67
HEC 6	3		99.89		0.06				99.95
HEC 6	4		99.52		0.05	0.08			99.66
HEC 6	5		99.56		0.04				99.60
HEC 6	6		99.47		0.05				99.52
HEC 6	7		99.64			0.11			99.75
HEC 6	8		99.22						99.22
HEC 6	9		99.95	0.04		0.20			100.19
HEC 6	10		99.46		0.10				99.56
HEC 1	1		99.50			0.19			99.69
HEC 1	2		99.59		0.10	0.09			99.78
HEC 1	3		99.64			0.10			99.74
HEC 1	4		99.16			0.13			99.29
HEC 1	5		98.81						98.81
HEC 1	6		100.02	0.02		0.18			100.22
HEC 1	7		99.32	0.02	0.10	0.11			99.55
HEC 1	8		98.99	0.02	0.07	0.21			99.29
HEC 1	9	0.71	98.21	0.40	0.17	0.42			99.90
HEC 1	10	0.08	99.12			0.32			99.52
HEC 1	11	0.03	98.33		0.13	0.11			98.60
HEC 1	12	0.04	99.28		0.10	0.10			99.52
HEC 1	13		98.66		0.46	0.68			99.80
HEC 1	14	0.06	98.97			0.14			99.17
HEC 1	15	0.18	98.91	0.04		0.18			99.31
HEC 1	16		98.99			0.14			99.14

Blank = below detection limit

APPENDIX B.2

ZULULAND SAMPLES - ILMENITE MICROPROBE RESULTS

							Recalculated			Molecular proportions			
ANALYSIS	SiO2	TiO2	Al2O3	Cr2O3	MnO	MgO	FeO	Fe2O3	TOTAL	FeTiO3	MnTiO3	MgTiO3	Fe2O3
HZ13-1	0.15	52.28	0.02	0.06	1.65	0.09	44.16	0.00	98.41	96.03	3.64	0.34	0.00
2	-	53.27	0.03	-	3.15	0.08	42.08	0.00	98.66	92.67	7.02	0.31	0.00
3	-	50.63	0.02	-	1.84	0.07	43.57	3.70	99.88	89.13	3.82	0.24	6.81
4	-	49.92	0.02	-	1.88	0.07	42.89	4.57	99.37	87.48	3.88	0.25	8.38
5	-	49.85	0.03	-	1.13	0.21	43.32	5.46	100.01	87.10	2.29	0.74	9.87
6	-	50.87	0.02	-	2.03	0.07	43.59	2.93	99.54	90.06	4.24	0.25	5.45
7	-	49.61	0.02	-	0.45	0.88	42.61	6.09	99.67	85.03	0.91	3.12	10.94
9	-	48.69	0.05	-	0.30	1.41	40.98	8.48	99.97	79.67	0.59	4.90	14.83
10	0.03	52.44	0.03	-	0.59	0.13	45.30	0.00	98.52	98.21	1.30	0.49	0.00
11	0.03	51.74	0.02	-	0.78	0.03	45.72	1.31	99.63	95.75	1.66	0.12	2.47
13	-	52.27	-	-	3.30	0.06	43.57	0.00	99.25	92.66	7.11	0.24	0.00
14	0.05	49.73	0.13	0.10	0.43	2.62	39.68	5.97	98.71	79.11	0.86	9.31	10.71
15	0.03	51.30	0.02	-	0.50	0.06	45.54	2.68	100.13	93.76	1.05	0.23	4.96
16	-	51.67	0.02	0.11	1.04	0.11	45.24	0.37	98.57	96.64	2.24	0.41	0.71
17	0.03	52.99	0.04	-	0.39	0.47	45.61	0.00	99.52	97.37	0.84	1.78	0.00
18	0.03	50.66	0.05	-	0.28	1.15	43.26	4.86	100.32	86.58	0.56	4.11	8.75
19	0.03	52.45	0.04	-	0.43	0.29	46.26	0.27	99.77	97.49	0.92	1.08	0.51
20	-	51.20	0.03	-	0.63	0.19	45.07	2.86	99.99	92.69	1.31	0.70	5.30
21	-	49.66	0.02	0.04	3.50	0.04	41.04	5.43	99.75	82.82	7.16	0.16	9.87
22	-	49.71	-	-	3.66	0.12	40.78	5.43	99.72	82.24	7.48	0.43	9.86
23	-	51.65	-	-	1.03	0.02	45.36	0.81	98.91	96.17	2.21	0.08	1.54
24	-	51.42	-	-	1.86	0.02	44.32	2.37	100.00	91.61	3.90	0.07	4.42
25	-	53.39	-	-	1.46	0.20	44.20	0.00	99.25	96.01	3.22	0.77	0.00
26	-	50.95	0.02	0.20	0.41	1.78	42.23	4.58	100.16	84.57	0.83	6.35	8.25
27	-	52.37	0.02	0.01	0.51	0.22	46.18	0.03	99.33	98.00	1.10	0.85	0.05
28	-	51.31	0.08	-	0.37	2.53	41.26	4.00	99.55	82.96	0.75	9.05	7.24
29	-	51.93	0.02	-	0.38	0.53	45.37	1.61	99.87	94.22	0.80	1.97	3.01
30	0.29	52.81	0.11	0.16	0.90	0.04	44.99	0.00	99.31	97.85	1.99	0.16	0.00
31	0.03	51.04	0.03	-	0.72	0.24	44.78	2.76	99.61	92.49	1.51	0.87	5.13
32	-	53.41	-	-	2.97	-	42.44	0.00	98.84	93.35	6.61	0.04	0.00
34	-	51.39	0.03	-	2.70	0.15	43.24	2.41	99.93	89.33	5.65	0.54	4.48
35	-	51.85	0.04	-	0.39	1.91	42.84	2.43	99.48	87.73	0.80	6.98	4.48
36	-	51.57	-	-	2.87	0.02	43.48	1.96	99.90	90.30	6.05	0.00	3.66
37	-	50.58	0.06	0.38	0.37	2.69	40.32	5.71	100.11	79.64	0.74	9.47	10.14
38	-	50.77	0.07	-	0.59	1.72	42.03	3.89	99.09	85.46	1.21	6.22	7.11
39	0.03	51.11	0.03	-	1.00	0.10	44.80	1.92	98.99	93.88	2.12	0.39	3.61
40	-	52.32	0.02	-	1.05	0.21	45.62	0.03	99.24	96.91	2.25	0.79	0.05
41	0.05	53.22	0.05	0.16	0.51	1.22	43.76	0.00	98.97	94.22	1.12	4.66	0.00
42	-	51.22	0.02	-	0.45	0.36	44.98	2.80	99.87	92.56	0.94	1.31	5.18
43	0.03	50.86	0.02	-	0.48	0.73	43.99	3.72	99.85	89.54	1.00	2.65	6.81
44	0.03	52.96	0.05	-	1.08	0.17	45.27	0.00	99.58	97.01	2.35	0.64	0.00
45	0.03	50.05	0.06	0.04	0.34	0.81	43.26	5.54	100.13	86.46	0.69	2.88	9.97
47	0.03	52.06	0.04	-	0.42	0.38	45.74	0.20	98.90	97.25	0.91	1.45	0.38
48	0.03	52.49	0.02	0.06	1.19	0.08	45.88	0.08	99.83	97.00	2.54	0.31	0.14
49	0.04	51.28	0.03	-	1.08	0.02	45.03	1.32	98.83	95.11	2.31	0.08	2.51

- = below detection limit

APPENDIX B.2

ZULULAND SAMPLES - ILMENITE MICROPROBE RESULTS

							Recalculated			Molecular proportions			
ANALYSIS	SiO2	TiO2	Al2O3	Cr2O3	MnO	MgO	FeO	Fe2O3	TOTAL	FeTiO3	MnTiO3	MgTiO3	Fe2O3
50	0.03	50.56	0.05	-	0.68	0.35	44.19	3.58	99.45	90.72	1.41	1.27	6.61
Average	0.05	51.42	0.04	0.12	1.17	0.55	43.82	2.44					
HZ10													
1	-	51.52	0.02	-	0.63	0.04	45.61	1.01	98.83	96.56	1.36	0.17	1.92
2	-	51.19	0.03	0.04	1.59	0.08	44.29	1.37	98.58	93.70	3.40	0.30	2.61
3	-	52.58	0.03	-	0.83	0.40	45.73	0.18	99.77	96.40	1.76	1.50	0.34
4	-	52.58	-	0.73	0.53	5.55	36.86	3.25	99.48	73.42	1.06	19.70	5.82
5	-	52.86	-	-	1.76	0.14	43.94	0.00	98.71	95.58	3.87	0.55	0.00
6	-	50.72	0.03	0.10	0.40	1.09	43.27	3.17	98.79	89.27	0.84	4.00	5.89
7	-	50.99	0.02	0.04	0.61	0.38	44.55	2.91	99.51	91.91	1.28	1.41	5.40
8	-	50.71	0.03	0.06	0.55	0.36	44.40	2.81	98.93	92.25	1.16	1.35	5.25
9	-	50.22	0.02	-	0.83	0.18	44.00	4.21	99.48	89.88	1.71	0.67	7.74
10	-	51.76	-	0.05	2.48	0.10	43.85	0.04	98.29	94.15	5.40	0.37	0.08
11	-	47.47	0.19	0.30	0.33	1.32	40.00	10.22	99.83	77.10	0.65	4.53	17.72
13	-	49.45	0.04	0.10	0.36	1.02	42.28	5.87	99.13	84.99	0.73	3.66	10.62
14	-	52.49	0.12	0.15	0.43	0.87	44.73	0.00	98.81	95.73	0.94	3.33	0.00
16	-	53.27	0.06	-	0.49	0.48	44.68	0.00	98.98	97.08	1.07	1.85	0.00
17	-	51.06	-	0.05	1.18	0.18	44.40	1.93	98.80	93.18	2.50	0.67	3.64
18	-	51.78	0.06	0.06	1.02	0.44	44.74	0.76	98.86	94.71	2.18	1.67	1.44
19	-	51.16	0.04	0.05	1.71	0.02	44.25	2.53	99.75	91.66	3.59	0.04	4.71
HZ7													
1	0.04	52.11	0.02	-	0.93	0.15	45.69	0.50	99.44	96.49	2.00	0.57	0.95
2	-	50.42	0.03	-	0.42	0.41	44.20	3.71	99.21	90.77	0.88	1.49	6.86
3	-	52.26	0.06	0.08	0.38	2.33	42.46	1.24	98.83	88.24	0.80	8.65	2.32
4	-	50.38	0.03	-	0.71	0.05	44.51	2.76	98.50	93.10	1.51	0.19	5.20
5	0.06	53.12	0.02	-	1.25	0.07	44.48	0.00	99.00	96.97	2.75	0.28	0.00
6	-	48.72	-	-	1.49	0.25	41.86	7.12	99.46	83.34	3.01	0.89	12.76
7	-	51.02	-	-	0.74	0.07	45.03	1.36	98.26	95.55	1.58	0.27	2.60
8	-	50.13	0.03	0.90	0.49	2.09	40.86	3.67	98.18	84.44	1.03	7.70	6.83
9	-	47.79	0.03	-	0.54	0.28	41.94	8.01	98.63	83.54	1.10	1.01	14.36
10	0.04	52.51	0.04	-	1.39	0.03	44.19	0.00	98.23	96.79	3.09	0.12	0.00
11	0.04	52.16	-	-	4.09	-	42.77	0.00	99.08	91.14	8.82	0.04	0.00
12	-	52.33	0.08	-	0.38	1.42	44.16	0.15	98.58	93.51	0.82	5.37	0.30
13	0.03	50.63	0.02	-	0.81	0.05	44.65	3.04	99.22	92.45	1.71	0.18	5.66
14	-	52.60	0.02	-	0.48	1.01	44.68	0.00	98.82	95.11	1.04	3.85	0.00
15	-	51.08	0.03	0.05	0.44	1.39	43.04	3.37	99.42	87.84	0.92	5.04	6.20
16	0.03	51.77	0.02	0.07	0.42	1.09	44.22	1.90	99.52	91.54	0.89	4.02	3.54
17	0.03	51.59	0.05	0.04	0.43	0.87	44.46	1.31	98.77	93.38	0.90	3.25	2.47
18	-	53.50	-	-	1.75	0.63	43.73	0.00	99.63	93.79	3.80	2.41	0.00
19	0.63	51.88	0.45	-	0.70	0.35	44.56	0.00	98.56	97.12	1.54	1.34	0.00
20	0.03	51.71	0.04	-	0.77	0.18	45.43	0.67	98.83	96.37	1.66	0.69	1.28
21	0.07	52.13	0.22	-	0.76	0.15	45.92	0.01	99.25	97.78	1.64	0.57	0.01
22	-	51.09	0.07	-	0.53	0.86	43.91	1.47	97.95	92.84	1.14	3.23	2.80
23	-	52.00	0.06	0.06	0.41	1.18	44.26	0.80	98.78	93.18	0.86	4.44	1.52

- = below detection limit

APPENDIX B.2

ZULULAND SAMPLES - ILMENITE MICROPROBE RESULTS

							Recalculated			Molecular proportions			
ANALYSIS	SiO2	TiO2	Al2O3	Cr2O3	MnO	MgO	FeO	Fe2O3	TOTAL	FeTiO3	MnTiO3	MgTiO3	Fe2O3
24	-	52.10	0.03	-	0.47	1.04	44.56	0.82	99.05	93.57	1.00	3.88	1.55
25	0.03	51.28	0.03	-	0.46	0.77	44.30	2.32	99.24	91.84	0.97	2.86	4.33
26	0.03	51.39	0.03	-	0.49	0.84	44.26	2.20	99.24	91.76	1.03	3.10	4.11
27	-	52.10	0.02	-	0.40	0.56	45.41	0.00	98.52	96.99	0.87	2.14	0.00
28	0.03	52.61	0.02	0.04	2.36	0.14	44.24	0.00	99.45	94.35	5.11	0.54	0.00
29	-	50.56	0.02	-	0.53	0.19	44.62	2.58	98.53	93.33	1.12	0.69	4.86
31	0.03	51.58	-	-	0.79	0.05	45.52	1.10	99.12	96.02	1.69	0.19	2.09
32	-	51.49	0.06	-	0.46	1.64	42.94	2.38	98.98	88.61	0.95	6.03	4.41
33	0.03	50.96	-	-	2.97	0.02	42.85	1.86	98.68	90.16	6.33	0.00	3.51
34	0.07	52.66	0.04	0.07	0.41	1.13	44.78	0.00	99.17	94.83	0.88	4.28	0.00
35	-	48.82	0.08	-	0.39	1.28	41.23	7.01	98.84	82.10	0.78	4.55	12.57
36	-	49.98	0.04	-	0.83	0.10	43.94	3.79	98.70	90.84	1.74	0.37	7.05
37	0.04	50.38	0.05	-	0.91	0.14	44.18	2.70	98.40	92.48	1.92	0.52	5.08
38	0.04	51.91	0.04	-	0.37	0.55	45.38	0.51	98.83	96.15	0.80	2.08	0.98
39	0.03	51.46	0.02	-	0.46	0.84	44.36	1.97	99.16	92.23	0.97	3.11	3.69
40	0.03	53.26	0.04	-	0.70	0.19	44.98	0.00	99.19	97.73	1.53	0.74	0.00
41	0.07	49.86	0.03	-	1.64	0.09	43.10	4.29	99.08	88.36	3.40	0.33	7.91
42	0.04	52.05	0.02	-	0.79	0.04	45.98	0.12	99.03	97.92	1.71	0.15	0.23
44	0.19	53.51	0.31	-	0.48	1.64	42.26	0.00	98.41	92.55	1.06	6.39	0.00
45	0.03	50.67	0.05	-	0.44	0.84	43.66	3.50	99.20	89.55	0.91	3.08	6.46
47	0.04	51.03	0.02	-	0.39	1.71	42.49	3.53	99.22	86.51	0.81	6.20	6.47
48	-	51.76	-	-	1.25	0.09	45.14	0.84	99.11	95.39	2.67	0.35	1.59
49	-	52.80	0.04	-	0.37	0.22	45.14	0.00	98.60	98.34	0.82	0.84	0.00
50	0.03	52.15	0.01	-	0.54	0.33	45.78	0.95	99.79	95.82	1.15	1.24	1.79
Average	0.07	51.47	0.06	0.16	0.83	0.64	44.09	1.78	98.93				
HZ17													
1	0.08	48.14	-	0.09	0.80	0.06	42.46	7.74	99.37	84.34	1.61	0.21	13.84
2	-	48.48	0.07	-	0.37	2.44	38.88	8.73	98.98	75.54	0.73	8.46	15.27
3	-	50.04	-	-	0.55	0.28	43.94	4.79	99.61	89.12	1.13	1.01	8.74
4	0.07	52.77	-	-	0.68	0.06	46.17	0.00	99.77	98.29	1.47	0.24	0.00
5	0.04	51.65	0.07	-	0.45	2.01	42.46	2.93	99.62	86.42	0.94	7.27	5.37
6	0.04	50.38	-	-	0.42	0.73	43.62	3.55	98.75	89.85	0.88	2.69	6.58
7	-	51.03	-	-	0.67	0.07	45.11	2.61	99.51	93.48	1.41	0.25	4.86
8	0.04	51.31	0.02	-	0.69	0.49	44.61	1.65	98.82	93.58	1.46	1.84	3.12
9	-	50.33	0.04	0.46	2.15	0.47	42.27	2.95	98.70	88.17	4.54	1.74	5.54
10	0.05	52.67	0.03	-	0.94	0.05	45.14	0.00	98.88	97.75	2.05	0.19	0.00
11	-	51.89	0.04	0.04	0.45	1.97	42.71	2.30	99.42	87.59	0.94	7.22	4.25
12	-	53.82	0.02	-	0.52	1.07	43.87	0.00	99.35	94.73	1.15	4.12	0.00
13	-	50.17	0.03	0.04	0.39	0.82	43.27	4.94	99.67	87.28	0.79	2.96	8.98
14	-	49.96	-	-	8.75	0.02	36.07	4.61	99.45	73.48	18.04	0.04	8.44
15	-	47.97	0.04	0.08	0.33	1.34	40.42	8.88	99.08	79.04	0.66	4.67	15.63
16	-	49.16	0.06	0.11	0.34	0.88	42.31	6.52	99.40	84.46	0.68	3.14	11.71
17	-	51.01	-	-	0.61	0.27	44.79	3.28	100.01	91.71	1.26	0.99	6.04
19	-	51.41	-	0.05	0.42	0.35	45.20	2.16	99.61	93.81	0.89	1.28	4.03
20	-	50.61	-	0.06	1.50	0.10	43.84	3.35	99.50	90.28	3.13	0.38	6.21

- = below detection limit

APPENDIX B.2

ZULULAND SAMPLES - ILMENITE MICROPROBE RESULTS

							Recalculated			Molecular proportions			
ANALYSIS	SiO2	TiO2	Al2O3	Cr2O3	MnO	MgO	FeO	Fe2O3	TOTAL	FeTiO3	MnTiO3	MgTiO3	Fe2O3
21	-	53.50	-	-	0.96	0.31	44.80	0.00	99.62	96.71	2.11	1.19	0.00
22	-	50.24	-	-	0.54	0.05	44.57	3.86	99.26	91.58	1.12	0.17	7.13
23	-	48.50	0.11	0.39	0.35	4.03	36.08	9.31	98.75	69.40	0.68	13.81	16.11
24	-	50.65	-	-	3.29	-	42.20	3.51	99.68	86.63	6.85	0.03	6.49
25	-	51.12	0.03	-	0.41	1.22	43.38	2.74	98.91	89.56	0.86	4.48	5.09
26	-	50.87	0.03	-	0.39	0.63	44.24	3.72	99.90	90.10	0.80	2.30	6.81
27	-	51.24	0.04	-	0.40	0.71	44.43	2.08	98.91	92.62	0.85	2.63	3.90
28	-	48.34	-	-	1.82	0.03	41.57	7.77	99.56	82.38	3.66	0.11	13.85
29	-	51.32	-	-	0.58	0.12	45.36	2.18	99.60	94.25	1.22	0.45	4.08
30	0.04	53.21	-	-	0.77	0.12	44.97	0.00	99.15	97.83	1.69	0.48	0.00
31	-	50.22	-	-	2.98	-	42.14	4.00	99.40	86.38	6.19	0.05	7.39
32	-	51.23	-	0.04	3.51	0.04	42.46	2.64	99.93	87.61	7.35	0.13	4.91
33	-	51.67	0.06	0.15	0.55	0.68	44.71	1.23	99.07	93.95	1.17	2.55	2.33
34	0.05	53.02	0.05	0.04	0.86	0.07	44.08	0.00	98.16	97.82	1.92	0.26	0.00
35	-	50.47	0.01	0.05	1.59	0.07	43.68	3.57	99.45	89.84	3.31	0.24	6.61
36	0.03	51.96	-	-	0.90	0.02	45.82	0.94	99.70	96.24	1.92	0.06	1.79
37	-	51.99	0.02	0.07	0.41	0.25	45.92	0.30	99.00	97.59	0.89	0.94	0.58
39	-	49.02	-	-	1.71	0.07	42.24	6.42	99.50	84.67	3.47	0.26	11.59
40	0.03	50.71	0.03	-	0.48	1.01	43.35	3.61	99.24	88.67	0.99	3.70	6.64
41	-	49.43	0.02	-	0.77	0.62	42.58	6.51	99.94	84.63	1.55	2.18	11.64
42	-	50.34	0.04	-	0.36	0.61	43.83	3.65	98.89	90.23	0.75	2.25	6.77
43	0.03	52.03	-	-	1.02	0.04	45.71	0.77	99.61	96.21	2.17	0.17	1.45
44	-	48.43	0.06	-	0.31	0.87	41.70	7.60	99.00	82.74	0.63	3.06	13.57
46	-	50.22	-	0.04	1.18	0.14	43.73	3.88	99.22	89.85	2.45	0.52	7.18
47	-	53.03	0.03	-	0.64	1.75	43.72	0.00	99.19	92.08	1.37	6.55	0.00
48	-	50.76	0.03	-	0.43	0.47	44.39	3.58	99.69	90.79	0.89	1.73	6.59
49	-	51.04	0.02	-	0.36	1.14	43.51	3.14	99.22	89.29	0.75	4.17	5.80
50	-	52.82	-	-	0.86	0.19	44.85	0.00	98.74	97.37	1.89	0.75	0.00
51	-	51.54	-	-	2.39	0.03	43.87	1.54	99.38	91.91	5.08	0.10	2.91
52	-	51.35	0.03	-	0.45	0.54	44.75	2.11	99.24	93.08	0.96	2.02	3.94
53	-	51.25	-	-	2.75	0.08	43.17	2.39	99.67	89.47	5.77	0.31	4.46
54	-	52.20	-	0.04	0.98	0.19	45.63	0.30	99.36	96.62	2.10	0.72	0.57
55	-	50.78	-	-	5.57	0.04	39.95	3.22	99.60	82.27	11.62	0.15	5.96
57	-	50.40	0.06	-	0.38	1.95	41.48	4.06	98.37	84.67	0.79	7.09	7.46
58	-	51.69	0.02	0.10	0.41	0.92	44.43	1.30	98.87	93.22	0.87	3.46	2.45
59	-	53.53	-	-	1.63	0.11	44.25	0.00	99.53	96.01	3.57	0.42	0.00
Average	0.05	50.96	0.04	0.11	1.16	0.62	43.36	3.14	99.31	89.69			
HZ2													
1	-	52.02	-	-	6.79	0.04	39.85	0.82	99.54	83.84	14.47	0.13	1.56
2	-	49.66	-	-	1.48	0.05	43.08	4.36	98.63	88.67	3.09	0.17	8.07
3	-	50.41	-	-	0.50	0.06	44.73	3.49	99.22	92.24	1.05	0.23	6.48
4	0.05	49.76	0.07	-	0.30	1.25	42.28	4.87	98.58	85.95	0.61	4.53	8.91
5	-	50.28	0.05	-	0.35	1.05	42.98	3.42	98.14	89.00	0.74	3.89	6.37
6	-	50.71	0.06	-	0.49	0.85	43.61	3.39	99.12	89.62	1.01	3.10	6.27
7	-	51.16	0.06	-	0.46	1.33	43.19	2.93	99.15	88.76	0.96	4.86	5.42

- = below detection limit

APPENDIX B.2

ZULULAND SAMPLES - ILMENITE MICROPROBE RESULTS

							Recalculated			Molecular proportions			
ANALYSIS	SiO2	TiO2	Al2O3	Cr2O3	MnO	MgO	FeO	Fe2O3	TOTAL	FeTiO3	MnTiO3	MgTiO3	Fe2O3
8	-	50.18	0.03	-	0.47	0.59	43.62	4.34	99.24	88.94	0.97	2.13	7.96
9	-	52.44	-	-	1.33	0.16	45.54	0.42	99.90	95.79	2.82	0.59	0.79
10	-	52.90	-	-	1.24	0.23	45.67	0.00	100.06	96.48	2.66	0.86	0.00
11	-	51.31	0.04	-	0.46	0.63	44.58	2.24	99.26	92.54	0.96	2.32	4.18
12	-	51.47	0.04	-	0.45	0.38	45.15	2.04	99.53	93.81	0.95	1.42	3.82
13	0.12	51.98	0.13	-	0.73	0.20	45.67	0.00	98.84	97.65	1.59	0.76	0.00
14	-	51.45	0.04	0.46	0.45	1.76	42.68	2.10	98.95	88.62	0.94	6.51	3.92
15	-	51.63	0.06	-	0.49	0.86	44.41	2.09	99.54	91.91	1.03	3.16	3.90
17	-	52.36	0.02	-	0.79	0.02	45.61	0.00	98.81	98.21	1.73	0.06	0.00
19	-	50.74	0.07	0.11	0.46	1.53	42.44	4.64	100.00	85.20	0.93	5.47	8.39
20	-	50.76	0.02	-	0.69	0.33	44.36	3.89	100.05	90.26	1.42	1.20	7.12
21	0.08	54.89	0.17	0.05	0.94	0.05	40.31	0.00	96.48	97.50	2.30	0.21	0.00
22	-	51.47	0.03	-	1.83	0.02	44.41	1.70	99.50	92.84	3.87	0.09	3.20
23	-	46.71	0.03	0.08	0.54	0.48	40.61	10.96	99.42	78.29	1.05	1.67	19.00
24	-	49.39	-	-	2.74	0.02	41.59	6.53	100.29	82.71	5.52	0.09	11.68
25	-	46.07	0.03	-	0.80	0.23	40.22	12.12	99.51	76.83	1.56	0.78	20.83
26	-	51.47	0.04	0.06	0.54	0.59	44.70	1.33	98.76	94.10	1.16	2.23	2.51
27	0.03	50.50	0.04	0.34	0.40	1.28	42.75	3.90	99.23	87.33	0.82	4.67	7.18
28	0.03	51.56	0.05	-	2.54	0.02	43.80	0.85	98.85	92.86	5.46	0.07	1.62
29	0.03	51.13	0.02	-	0.42	0.04	45.52	2.47	99.65	94.37	0.88	0.14	4.61
30	0.03	49.85	0.02	-	1.92	0.04	42.85	4.54	99.25	87.55	3.98	0.13	8.34
31	-	53.10	-	0.04	0.47	0.25	45.48	0.00	99.36	98.02	1.03	0.96	0.00
32	-	50.84	0.06	-	0.41	1.91	41.90	4.82	99.96	83.71	0.83	6.80	8.66
33	-	47.33	0.05	0.09	0.48	1.18	39.97	9.66	98.76	77.98	0.95	4.11	16.96
35	-	52.05	0.06	-	0.49	0.34	45.73	0.02	98.71	97.61	1.06	1.30	0.04
38	-	50.91	0.03	0.06	0.79	0.29	44.47	2.52	99.08	92.54	1.67	1.06	4.73
39	-	49.35	0.08	0.10	0.72	1.34	41.27	5.50	98.35	83.66	1.47	4.83	10.04
40	-	51.79	-	-	7.07	0.04	39.37	1.52	99.80	82.08	14.93	0.13	2.85
41	-	50.46	0.04	0.06	0.48	0.61	43.80	4.63	100.08	88.41	0.98	2.21	8.40
42	-	51.78	0.06	0.07	0.62	1.05	44.07	1.42	99.07	92.10	1.32	3.91	2.67
43	-	52.38	-	-	0.92	0.09	46.01	1.29	100.73	95.32	1.93	0.34	2.41
44	-	50.22	-	-	3.38	0.03	41.68	4.35	99.70	84.94	6.98	0.10	7.98
45	-	51.32	0.02	-	0.65	0.05	45.41	2.75	100.23	93.38	1.36	0.17	5.09
46	-	49.73	0.09	0.07	0.35	0.61	43.29	5.85	99.98	86.60	0.70	2.17	10.54
47	-	51.99	0.07	-	0.93	0.54	44.85	1.30	99.69	93.58	1.96	2.01	2.45
48	-	52.88	0.03	-	4.01	0.11	42.93	0.00	99.97	90.99	8.61	0.40	0.00
50	-	49.95	0.03	0.25	0.58	0.41	43.60	4.24	99.05	89.46	1.20	1.51	7.83
51	-	53.42	-	-	1.46	0.17	45.57	0.00	100.62	96.25	3.12	0.63	0.00
52	0.03	51.26	0.05	-	2.01	0.12	43.87	1.32	98.66	92.72	4.31	0.47	2.50
53	-	52.89	0.06	-	0.64	0.99	44.34	0.00	98.93	94.82	1.39	3.78	0.00
54	-	51.05	0.04	-	1.03	0.48	44.03	2.01	98.66	92.22	2.19	1.79	3.80
55	-	51.77	0.05	-	1.35	0.07	45.07	0.06	98.37	96.70	2.94	0.25	0.11
56	-	49.24	-	-	1.97	0.02	42.27	4.67	98.17	87.18	4.12	0.03	8.67
57	-	52.30	-	-	1.82	0.07	45.09	0.30	99.61	95.27	3.90	0.25	0.57
58	0.03	53.02	0.18	-	0.40	0.65	44.09	0.00	98.38	96.57	0.88	2.56	0.00

- = below detection limit

APPENDIX B.2

NATAL SAMPLES - ILMENITE MICROPROBE RESULTS

							Recalculated			Recalculated mole fraction			
ANALYSIS	SiO2	TiO2	Al2O3	Cr2O3	MnO	MgO	FeO	Fe2O3	TOTAL	FeTiO3	MnTiO3	MgTiO3	Fe2O3
HN27-1	-	51.35	0.03	0.04	0.44	0.60	44.68	3.02	100.17	91.35	0.92	2.18	5.56
2	-	50.90	0.04	-	0.42	0.28	44.87	2.88	99.44	92.73	0.89	1.02	5.36
3	-	53.34	0.02	0.13	0.66	0.52	44.79	0.00	99.47	96.57	1.44	1.99	0.00
4	-	49.88	0.05	0.05	0.41	0.63	43.34	5.69	100.06	86.69	0.82	2.25	10.24
5	-	52.16	0.02	-	0.66	0.02	46.23	0.31	99.44	97.95	1.41	0.06	0.59
6	-	50.38	0.05	0.15	0.50	1.64	41.89	5.41	100.01	83.49	1.00	5.81	9.70
7	-	49.36	0.09	0.06	0.41	1.21	41.83	6.60	99.55	83.10	0.82	4.28	11.80
8	-	50.77	0.07	0.06	0.44	2.45	40.87	5.37	100.04	80.92	0.88	8.64	9.57
9	-	50.21	0.06	-	0.86	0.34	43.69	4.45	99.64	88.84	1.78	1.24	8.14
10	-	49.96	-	-	1.57	0.02	43.36	4.30	99.22	88.79	3.25	0.03	7.93
12	-	51.49	0.02	-	0.43	0.33	45.28	1.60	99.16	94.82	0.92	1.24	3.02
13	-	52.57	0.03	-	0.48	0.65	45.30	0.00	99.04	96.50	1.03	2.46	0.00
14	0.03	49.76	-	-	0.58	0.30	43.65	5.66	100.00	87.52	1.18	1.09	10.22
15	-	52.09	-	-	2.03	0.04	44.73	0.47	99.37	94.59	4.35	0.16	0.90
16	-	52.18	-	0.05	1.03	0.05	45.81	0.75	99.88	96.22	2.18	0.18	1.42
17	-	51.39	-	0.07	1.21	0.06	44.89	1.68	99.32	94.04	2.58	0.21	3.17
18	-	51.54	0.06	-	0.47	1.27	43.65	2.37	99.37	89.98	0.97	4.65	4.40
19	-	51.02	-	0.07	0.86	0.19	44.69	2.90	99.76	92.13	1.80	0.68	5.39
20	-	51.93	0.02	0.06	1.75	0.03	44.88	0.67	99.35	94.85	3.74	0.13	1.28
21	-	50.54	-	0.05	0.96	0.02	44.49	2.66	98.74	92.95	2.02	0.02	5.01
22	-	48.56	-	0.06	1.30	0.17	42.05	7.97	100.12	82.71	2.58	0.61	14.10
23	-	51.78	0.02	-	0.52	0.28	45.54	1.69	99.86	94.70	1.10	1.03	3.17
24	-	49.85	0.03	0.04	0.55	0.36	43.63	5.34	99.79	87.91	1.13	1.29	9.68
25	-	52.43	0.02	0.06	0.48	0.86	45.13	0.92	99.91	94.06	1.02	3.19	1.73
28	-	51.33	0.04	0.07	0.60	0.06	45.47	1.97	99.55	94.82	1.27	0.21	3.70
29	-	51.79	0.05	-	0.43	0.73	44.86	1.54	99.40	93.52	0.90	2.70	2.89
30	0.03	51.89	0.03	-	1.57	0.02	45.06	0.72	99.31	95.20	3.36	0.08	1.36
31	-	50.50	0.03	0.07	0.42	0.93	43.34	4.30	99.59	87.94	0.86	3.36	7.85
32	-	50.92	0.04	-	0.44	1.05	43.50	4.12	100.12	87.84	0.90	3.77	7.49
33	0.05	52.24	0.06	-	0.38	0.53	45.70	0.00	98.97	97.15	0.82	2.02	0.00
34	-	52.41	0.05	0.02	0.47	0.52	45.62	0.00	99.10	97.02	1.01	1.97	0.00
38	-	51.50	0.02	-	0.85	0.24	45.03	1.64	99.29	94.21	1.80	0.90	3.08
39	-	51.40	0.09	-	0.31	1.34	43.53	2.01	98.70	90.61	0.66	4.96	3.77
40	-	50.05	0.02	-	0.78	0.11	44.05	4.28	99.32	90.10	1.62	0.40	7.88
41	0.03	51.30	0.04	-	0.43	0.69	44.51	2.37	99.39	92.14	0.90	2.54	4.42
43	0.04	52.15	0.03	-	1.17	0.05	45.67	0.08	99.19	97.14	2.52	0.20	0.15
44	0.03	53.40	-	-	1.10	0.19	45.00	0.00	99.74	96.87	2.41	0.72	0.00
45	0.03	49.42	0.04	0.05	0.42	2.91	38.85	7.56	99.29	75.77	0.83	10.13	13.27
46	-	50.19	0.03	-	0.96	0.12	43.97	4.78	100.09	88.90	1.96	0.44	8.70
47	0.03	50.33	0.02	-	0.49	0.27	44.31	3.86	99.35	90.87	1.03	0.99	7.12
48	0.04	50.95	0.02	-	0.68	0.13	44.94	2.33	99.09	93.70	1.44	0.48	4.37
49	-	50.54	0.02	-	0.43	0.14	44.78	3.48	99.43	92.14	0.89	0.52	6.45
50	0.04	50.96	0.04	-	0.63	0.06	45.13	2.88	99.75	93.10	1.33	0.22	5.36
51	-	50.79	0.02	0.04	0.33	1.70	42.31	4.22	99.42	85.51	0.68	6.14	7.67
53	-	51.85	0.05	-	0.41	0.60	45.16	1.72	99.86	93.71	0.87	2.22	3.21

- = below detection limit

APPENDIX B.2

NATAL SAMPLES - ILMENITE MICROPROBE RESULTS

							Recalculated			Recalculated mole fraction			
ANALYSIS	SiO2	TiO2	Al2O3	Cr2O3	MnO	MgO	FeO	Fe2O3	TOTAL	FeTiO3	MnTiO3	MgTiO3	Fe2O3
54	-	51.46	0.03	0.13	1.27	0.08	44.86	2.20	100.05	92.93	2.65	0.30	4.11
55	-	51.26	0.02	0.04	2.60	0.07	43.35	2.85	100.20	89.06	5.40	0.27	5.27
58	-	53.46	0.02	-	0.98	0.10	45.37	0.00	99.97	97.47	2.14	0.39	0.00
59	-	51.61	-	-	0.88	0.05	45.43	2.16	100.15	93.94	1.85	0.20	4.02
60	-	51.56	0.05	-	0.69	0.77	44.30	2.74	100.14	90.72	1.44	2.80	5.04
61	-	52.37	-	-	0.62	0.13	46.14	0.00	99.30	98.19	1.33	0.48	0.00
62	-	51.60	0.02	0.04	0.99	0.35	44.78	1.86	99.64	93.15	2.08	1.29	3.47
63	-	47.30	0.18	0.10	0.50	1.11	40.08	9.61	98.89	78.29	0.98	3.85	16.89
Average	0.03	51.17	0.04	0.07	0.77	0.52	44.23	2.79	99.57	*			
HN9													
1	0.06	52.00	0.12	-	3.66	0.02	43.11	0.70	99.65	90.84	7.82	0.02	1.32
2	0.10	50.98	0.03	-	0.48	0.33	44.88	2.35	99.18	93.35	1.01	1.24	4.40
3	-	52.88	-	-	0.57	0.78	44.78	0.00	99.03	95.80	1.23	2.97	0.00
4	-	51.06	-	-	0.79	0.12	44.91	1.82	98.74	94.43	1.67	0.45	3.44
5	-	50.33	0.04	0.08	0.43	1.18	42.73	3.91	98.71	87.58	0.90	4.30	7.22
6	-	52.27	-	-	1.98	0.08	44.36	0.00	98.73	95.40	4.31	0.30	0.00
7	-	50.85	0.02	-	0.61	0.21	44.76	1.99	98.45	94.16	1.29	0.78	3.77
8	-	50.26	0.05	0.04	1.13	0.22	43.66	3.22	98.59	90.77	2.38	0.82	6.02
9	-	53.00	-	-	1.72	-	45.01	0.00	99.75	96.27	3.73	0.00	0.00
10	0.03	50.04	0.04	-	0.45	0.29	44.06	3.95	98.85	90.67	0.94	1.06	7.32
11	0.04	49.29	0.02	0.04	0.45	0.24	43.50	5.58	99.16	88.06	0.92	0.85	10.17
12	-	49.20	0.03	0.07	0.42	0.98	42.09	6.92	99.72	83.37	0.84	3.46	12.33
13	0.04	52.42	-	-	1.84	0.06	44.71	0.00	99.08	95.78	3.99	0.23	0.00
14	-	50.43	0.02	-	0.51	0.19	44.52	3.97	99.64	90.98	1.05	0.67	7.30
15	-	48.58	0.02	-	0.35	0.25	42.91	6.40	98.55	86.73	0.73	0.90	11.64
16	0.04	51.26	-	-	0.75	0.09	45.22	2.50	99.87	93.44	1.58	0.34	4.64
17	0.03	50.30	0.04	-	0.43	0.95	43.13	4.50	99.42	87.46	0.89	3.45	8.20
18	0.04	48.66	0.04	-	0.33	0.83	41.98	6.66	98.55	84.31	0.67	2.99	12.03
19	0.05	52.73	-	-	0.61	0.05	45.44	0.00	98.89	98.46	1.34	0.20	0.00
20	-	50.84	-	-	1.20	0.02	44.48	2.96	99.53	91.91	2.51	0.09	5.50
21	0.06	48.58	0.04	0.07	0.48	1.29	40.98	7.41	98.90	81.26	0.96	4.56	13.22
22	-	48.32	0.11	0.07	0.37	2.10	39.35	8.74	99.08	76.66	0.72	7.30	15.32
23	-	47.94	0.04	-	0.45	0.33	42.10	8.04	98.95	83.58	0.90	1.17	14.36
24	-	50.03	-	0.04	0.44	0.43	43.79	4.21	98.97	89.73	0.91	1.59	7.77
25	0.03	49.83	0.02	-	0.86	0.03	43.91	3.71	98.41	91.14	1.80	0.13	6.94
26	0.04	48.74	0.05	-	0.37	0.62	42.39	6.30	98.54	85.57	0.75	2.24	11.43
27	-	50.38	0.02	-	0.75	0.32	43.98	4.14	99.63	89.68	1.54	1.18	7.60
28	-	50.39	-	-	1.15	0.02	44.15	3.01	98.77	91.90	2.43	0.03	5.64
29	0.05	51.22	0.08	0.04	1.68	0.22	44.01	1.72	99.03	92.34	3.58	0.84	3.24
30	0.03	48.98	0.02	-	1.70	0.06	42.27	6.59	99.68	84.50	3.43	0.21	11.86
31	0.03	49.31	0.07	0.07	0.48	1.55	41.13	6.59	99.23	81.76	0.97	5.48	11.79
32	-	49.93	0.04	0.15	0.77	1.02	42.34	4.45	98.72	86.52	1.59	3.70	8.18
33	-	51.47	-	-	1.38	0.18	44.58	1.82	99.47	92.98	2.92	0.69	3.41
34	0.04	51.33	0.02	0.08	0.47	1.49	43.08	2.39	98.90	89.08	0.97	5.50	4.45
35	0.04	49.21	0.02	-	0.42	0.32	43.30	5.55	98.85	87.86	0.85	1.15	10.14

- = below detection limit

APPENDIX B.2

NATAL SAMPLES - ILMENITE MICROPROBE RESULTS

							Recalculated			Recalculated mole fraction			
ANALYSIS	SiO2	TiO2	Al2O3	Cr2O3	MnO	MgO	FeO	Fe2O3	TOTAL	FeTiO3	MnTiO3	MgTiO3	Fe2O3
36	0.03	48.53	0.02	-	0.62	0.04	42.97	7.40	99.62	85.36	1.25	0.16	13.23
37	-	49.55	0.04	-	0.57	0.58	42.98	5.27	99.05	87.12	1.18	2.08	9.62
38	-	51.05	-	0.04	1.12	0.07	44.67	1.47	98.45	94.54	2.40	0.26	2.81
39	0.03	48.91	0.02	0.04	0.60	0.12	43.20	6.60	99.53	86.48	1.21	0.42	11.88
41	0.03	50.06	0.04	0.05	0.43	1.61	41.75	5.37	99.34	83.68	0.88	5.75	9.69
42	-	52.80	-	0.04	3.51	0.15	43.58	0.00	100.09	91.95	7.50	0.55	0.00
44	-	51.39	-	0.04	0.77	0.10	45.27	2.38	99.98	93.58	1.61	0.37	4.44
45	-	50.54	0.04	0.05	0.49	0.42	44.22	3.06	98.83	91.71	1.04	1.55	5.71
46	-	49.65	0.04	0.04	0.54	0.56	43.11	4.87	98.84	87.91	1.12	2.04	8.93
47	-	49.63	0.02	0.07	0.67	0.53	43.01	4.71	98.63	88.01	1.39	1.92	8.68
48	-	51.10	0.06	-	0.51	0.92	43.80	2.85	99.26	90.27	1.07	3.37	5.29
49	-	50.39	0.03	0.04	0.70	0.39	43.92	3.74	99.22	90.21	1.45	1.43	6.91
50	-	50.23	0.05	-	0.46	0.45	43.91	5.03	100.15	88.35	0.93	1.62	9.10
53	0.04	50.08	0.02	0.10	1.97	-	43.09	4.48	99.78	87.73	4.06	0.00	8.22
54	0.04	51.64	0.02	0.12	1.10	0.07	45.25	1.20	99.44	95.14	2.34	0.25	2.27
55	0.11	51.19	0.03	0.10	2.55	0.05	43.50	1.70	99.22	91.21	5.41	0.17	3.21
56-60	0.04	50.01	0.03	0.11	1.07	0.08	43.78	4.65	99.77	88.99	2.21	0.30	8.50
HN5													
1	-	50.94	-	0.06	1.40	0.02	44.37	1.85	98.65	93.45	3.00	0.04	3.52
2	-	48.58	0.06	0.72	0.35	3.29	37.47	8.32	98.79	73.23	0.69	11.46	14.62
3	-	51.49	0.02	-	1.33	0.04	44.91	1.21	99.02	94.72	2.83	0.16	2.29
4	-	50.26	0.03	-	1.66	0.13	43.30	3.61	99.03	89.34	3.48	0.48	6.71
5	-	50.78	-	-	1.00	0.06	44.55	2.33	98.74	93.26	2.12	0.23	4.40
6	-	49.33	-	-	0.69	0.38	42.99	5.34	98.76	87.43	1.43	1.38	9.76
7	-	50.43	0.04	-	0.53	0.87	43.27	4.54	99.70	87.54	1.08	3.12	8.26
8	-	48.41	0.03	0.16	0.43	2.69	38.31	8.71	98.74	74.58	0.85	9.32	15.25
9	-	51.78	-	-	0.80	0.06	45.65	1.51	99.79	95.27	1.69	0.21	2.83
10	-	49.59	0.03	0.07	0.36	1.42	41.70	6.39	99.58	82.82	0.73	5.03	11.41
11	-	49.56	0.05	0.07	0.35	1.70	41.20	6.39	99.35	81.85	0.71	6.02	11.42
12	-	53.05	-	0.16	2.87	0.09	44.00	0.00	100.20	93.47	6.18	0.35	0.00
13	-	49.79	0.08	0.07	0.34	1.71	41.41	5.25	98.67	83.61	0.69	6.15	9.55
14	-	51.15	0.02	0.04	0.82	0.08	45.05	2.84	100.03	92.74	1.70	0.30	5.26
15	-	51.09	0.04	-	1.39	0.03	44.49	2.45	99.50	92.38	2.92	0.12	4.58
16	-	50.77	0.02	-	1.19	0.03	44.43	3.61	100.09	90.80	2.46	0.10	6.64
17	-	52.58	0.05	0.04	0.65	0.48	45.67	0.00	99.46	96.80	1.39	1.80	0.00
18	-	49.78	-	-	1.61	0.28	42.63	5.65	99.99	85.52	3.27	1.02	10.19
19	-	50.81	0.05	0.06	1.16	0.06	44.40	2.84	99.38	92.02	2.44	0.23	5.30
21	0.03	49.18	0.41	0.11	0.38	0.85	42.37	6.24	99.58	84.94	0.77	3.03	11.26
24	-	51.24	0.02	-	0.39	0.30	45.17	2.38	99.54	93.63	0.81	1.12	4.43
25	-	51.16	0.02	0.09	0.85	0.20	44.80	2.49	99.61	92.84	1.78	0.74	4.64
26	-	52.03	0.05	0.08	0.47	0.80	45.00	0.15	98.69	95.65	1.00	3.05	0.29
27	-	51.58	-	0.05	2.44	0.10	43.75	1.51	99.47	91.59	5.17	0.39	2.85
28	-	52.79	-	-	0.56	0.40	45.47	0.00	99.25	97.27	1.21	1.52	0.00
29	-	51.88	-	0.09	0.79	0.28	45.37	0.75	99.19	95.82	1.69	1.07	1.42

- = below detection limit

APPENDIX B.2

NATAL SAMPLES - ILMENITE MICROPROBE RESULTS

							Recalculated			Recalculated mole fraction			
ANALYSIS	SiO2	TiO2	Al2O3	Cr2O3	MnO	MgO	FeO	Fe2O3	TOTAL	FeTiO3	MnTiO3	MgTiO3	Fe2O3
30	-	52.75	-	-	3.06	0.04	43.47	0.00	99.34	93.19	6.65	0.17	0.00
33	-	51.39	0.03	-	1.56	0.11	44.46	1.32	98.92	93.76	3.32	0.41	2.50
34	-	50.91	0.08	0.30	0.44	2.84	40.27	5.31	100.16	79.64	0.88	10.03	9.45
35	-	48.70	0.04	0.06	0.48	0.83	41.86	6.96	98.95	83.57	0.97	2.95	12.51
36	0.80	49.05	0.62	-	1.04	0.52	43.09	4.78	99.90	87.30	2.13	1.86	8.71
37	-	51.32	-	-	0.59	0.02	45.54	2.49	100.00	94.05	1.23	0.08	4.63
38	-	51.55	0.02	-	0.64	0.40	45.00	2.43	100.07	92.70	1.34	1.46	4.51
39	-	51.91	0.02	-	1.10	0.09	45.42	0.54	99.09	96.28	2.36	0.32	1.03
40	0.04	51.58	-	-	0.58	0.07	45.73	1.47	99.47	95.75	1.23	0.25	2.77
42	0.03	51.07	0.05	0.04	0.43	1.42	43.00	3.58	99.61	87.43	0.88	5.15	6.55
43	-	52.37	0.03	-	1.11	0.17	45.51	0.00	99.22	96.96	2.40	0.65	0.00
44	-	50.44	0.02	-	5.31	0.02	39.99	4.42	100.24	81.01	10.89	0.04	8.06
45	0.03	51.99	0.03	-	1.31	0.07	45.33	1.09	99.84	94.91	2.78	0.26	2.05
46	-	52.29	-	0.11	2.75	0.20	43.91	1.10	100.38	91.40	5.79	0.74	2.07
47	-	50.60	0.03	-	0.76	0.31	44.20	3.51	99.43	90.80	1.58	1.14	6.48
48	-	52.24	0.03	-	0.57	0.33	45.84	0.49	99.52	96.61	1.22	1.24	0.94
49	-	52.15	0.04	-	0.42	1.13	44.48	1.66	99.92	91.88	0.88	4.16	3.08
50	-	51.07	0.03	-	0.50	0.85	43.94	2.46	98.87	91.23	1.05	3.13	4.59
51	0.03	51.68	0.05	0.05	0.47	1.07	44.13	1.67	99.15	91.90	0.99	3.97	3.13
52	0.04	51.22	-	0.07	2.05	0.07	43.90	1.24	98.60	92.97	4.40	0.26	2.37
53	-	47.86	0.03	0.08	0.50	0.81	41.09	7.80	98.17	82.08	1.01	2.88	14.02
55	-	49.68	0.09	-	0.50	1.35	41.80	6.40	99.87	82.82	1.01	4.76	11.42
56	-	49.55	0.03	-	0.46	0.28	43.59	5.78	99.73	87.59	0.94	1.02	10.45
57	-	49.25	0.02	0.05	0.59	0.11	43.50	6.00	99.53	87.54	1.20	0.40	10.86
58	-	49.57	-	0.17	2.53	0.11	41.83	5.09	99.34	85.06	5.21	0.41	9.32
60	-	50.89	0.03	0.01	0.36	0.50	44.53	3.81	100.15	90.48	0.74	1.83	6.96
61	-	51.32	-	-	3.55	0.04	42.51	2.83	100.27	87.25	7.37	0.15	5.22
62	-	50.40	0.03	0.09	0.55	0.90	43.19	4.43	99.61	87.53	1.13	3.25	8.09
63	-	50.24	0.04	-	0.41	0.38	44.11	4.80	100.02	89.08	0.83	1.37	8.73
Average	0.14	50.82	0.06	0.11	1.08	0.57	43.58	3.27					
HN2													
1	0.06	48.59	-	-	0.87	0.15	42.60	7.27	99.54	84.71	1.75	0.54	13.00
2	-	48.16	0.04	-	0.47	0.97	41.10	8.86	99.59	80.16	0.93	3.37	15.54
3	-	50.66	0.02	-	1.66	0.20	43.53	3.95	100.03	88.62	3.42	0.73	7.23
4	0.04	51.83	0.03	-	0.52	0.29	45.62	1.48	99.81	95.06	1.09	1.08	2.77
5	-	52.19	0.03	-	0.90	0.19	45.70	0.64	99.67	96.17	1.91	0.70	1.22
7	-	50.50	0.05	0.04	0.39	1.51	42.33	5.07	99.88	84.71	0.78	5.37	9.14
8	-	53.00	0.03	-	0.50	0.32	46.02	0.00	99.87	97.71	1.06	1.22	0.00
9	-	50.07	0.04	-	0.44	0.46	43.76	2.52	97.28	92.53	0.94	1.74	4.79
10	-	49.78	-	-	0.80	0.06	43.88	4.46	99.02	89.91	1.67	0.20	8.22
11	-	49.80	0.02	-	0.78	0.30	43.46	4.94	99.33	88.27	1.61	1.08	9.03
12	-	49.02	0.05	-	0.35	1.08	41.81	7.56	99.91	82.13	0.71	3.79	13.37
13	-	48.72	-	-	0.58	0.18	42.93	6.24	98.70	86.82	1.19	0.64	11.36
14	-	49.63	0.02	-	0.62	0.41	43.30	4.93	98.95	88.20	1.27	1.49	9.04
15	-	49.85	0.06	-	1.51	0.13	43.09	2.76	97.42	91.03	3.22	0.50	5.25

- = below detection limit

APPENDIX B.2

NATAL SAMPLES - ILMENITE MICROPROBE RESULTS

							Recalculated			Recalculated mole fraction			
ANALYSIS	SiO2	TiO2	Al2O3	Cr2O3	MnO	MgO	FeO	Fe2O3	TOTAL	FeTiO3	MnTiO3	MgTiO3	Fe2O3
16	0.03	49.38	0.03	-	0.52	0.69	42.69	6.20	99.53	85.34	1.06	2.44	11.16
17	0.03	48.92	0.02	-	0.77	0.19	42.90	5.84	98.67	87.06	1.58	0.69	10.67
20	0.03	44.64	0.13	0.15	0.43	1.68	36.75	15.26	99.07	68.16	0.80	5.56	25.47
21	-	50.64	0.04	0.04	0.44	0.58	44.08	3.48	99.31	90.54	0.91	2.11	6.44
22	-	49.74	0.05	0.12	0.40	1.11	42.34	5.39	99.15	85.39	0.83	4.00	9.79
23	-	51.86	0.05	0.14	0.60	0.03	45.99	0.25	98.93	98.10	1.29	0.13	0.47
24	-	50.24	0.04	0.09	0.88	0.15	44.05	3.84	99.29	90.53	1.83	0.53	7.11
26	-	52.11	-	-	2.03	0.19	44.46	0.07	98.89	94.74	4.38	0.74	0.14
27	-	48.62	0.78	0.05	0.49	0.19	42.90	5.90	98.95	87.46	1.02	0.69	10.83
28	-	52.46	0.02	-	0.60	0.03	46.34	0.00	99.46	98.57	1.30	0.12	0.00
31	0.03	51.85	0.03	-	1.08	0.15	45.30	0.81	99.27	95.60	2.30	0.56	1.54
33	-	51.45	0.04	-	0.55	0.36	45.10	2.54	100.07	92.84	1.15	1.30	4.71
34	-	49.48	0.03	-	0.42	0.19	43.73	6.08	99.95	87.53	0.85	0.67	10.95
35	-	53.26	-	-	1.07	0.10	44.89	0.00	99.37	97.24	2.36	0.41	0.00
36	-	48.38	0.05	0.08	0.73	0.25	42.32	8.08	99.90	83.33	1.46	0.89	14.32
37	0.03	50.43	0.02	0.07	0.83	0.17	44.23	3.98	99.78	90.32	1.73	0.63	7.32
38	-	50.08	0.03	0.05	0.35	0.82	43.25	5.07	99.68	87.15	0.71	2.94	9.20
39	-	48.98	0.09	-	0.34	1.96	40.22	8.47	100.09	77.84	0.67	6.75	14.74
40	-	52.15	0.02	0.08	0.60	0.15	46.03	0.25	99.30	97.66	1.29	0.58	0.47
41	0.03	51.89	0.04	-	1.89	0.08	44.64	1.55	100.15	92.82	3.99	0.30	2.89
42	-	51.16	0.02	0.04	0.69	0.32	44.73	3.67	100.64	90.72	1.42	1.16	6.70
43	-	52.05	-	-	0.81	0.03	45.93	0.08	98.93	97.98	1.76	0.11	0.16
45	-	51.07	-	-	0.53	0.18	45.09	3.00	99.88	92.71	1.10	0.65	5.55
46	-	51.16	0.02	0.04	0.49	0.57	44.52	3.30	100.11	90.86	1.00	2.07	6.07
47	-	51.63	-	-	2.57	0.02	43.83	1.66	99.72	91.43	5.44	0.01	3.12
48	-	53.23	-	0.13	0.48	1.07	44.58	0.00	99.52	94.90	1.04	4.06	0.00
49	-	50.22	0.09	0.06	0.38	1.55	42.03	5.54	99.88	83.79	0.77	5.51	9.93
60	0.04	50.01	0.04	-	2.02	0.12	42.76	4.04	99.05	87.88	4.20	0.45	7.47
63	-	51.36	-	0.15	0.68	0.02	45.48	0.96	98.66	96.64	1.45	0.08	1.83
64	0.03	49.20	0.02	0.15	0.92	0.27	42.86	4.76	98.22	88.26	1.93	1.00	8.81
66-70	-	52.97	0.02	0.15	0.63	0.52	43.71	0.00	98.01	96.56	1.40	2.04	0.00

- = below detection limit

APPENDIX B.2

TRANSKEI SAMPLES - ILMENITE MICROPROBE ANALYSES

							Recalculated			Recalculated mole fractions			
ANALYSIS	SiO2	TiO2	Al2O3	Cr2O3	MnO	MgO	FeO	Fe2O3	TOTAL	FeTiO3	MnTiO3	MgTiO3	Fe2O3
HT4-1	0.04	52.51	0.03	-	0.58	0.68	45.10	0.00	98.95	96.14	1.26	2.60	0.00
2	0.03	52.70	-	-	1.22	0.05	45.36	0.00	99.39	97.16	2.64	0.20	0.00
3	-	50.26	0.02	-	0.45	1.07	42.84	4.26	98.93	87.35	0.94	3.90	7.82
4	-	50.42	0.05	0.13	0.38	1.67	41.99	4.74	99.39	84.62	0.77	6.01	8.59
5	0.03	48.15	0.05	-	0.51	1.66	39.85	9.06	99.41	77.40	1.00	5.76	15.84
6	1.13	51.54	-	-	0.61	0.03	45.62	0.00	98.94	98.53	1.34	0.13	0.00
7	-	50.59	0.03	0.05	2.00	0.07	43.36	1.64	97.77	92.27	4.31	0.28	3.14
8	0.03	50.49	0.03	-	0.52	0.63	43.79	3.04	98.55	90.89	1.09	2.33	5.69
9	0.03	50.25	0.02	0.04	0.34	0.71	43.60	3.69	98.69	89.82	0.71	2.62	6.85
10	0.03	49.57	0.06	-	0.39	0.84	42.73	5.06	98.68	86.90	0.80	3.04	9.26
11	-	51.54	0.05	-	0.50	0.97	44.12	1.63	98.85	92.26	1.07	3.60	3.07
12	-	50.97	0.02	0.05	0.52	0.49	44.45	2.34	98.86	92.67	1.11	1.84	4.39
13	-	51.59	0.06	-	0.45	1.55	43.19	2.35	99.20	89.03	0.93	5.68	4.36
14	-	51.85	0.04	0.10	0.51	0.81	44.68	0.45	98.44	94.97	1.10	3.08	0.86
15	-	51.54	-	-	1.50	0.17	44.54	1.59	99.39	93.21	3.18	0.62	2.99
16	-	51.36	0.04	0.06	0.88	0.14	45.05	2.04	99.58	93.81	1.85	0.53	3.81
17	-	50.04	-	-	0.71	0.02	44.26	3.61	98.66	91.74	1.49	0.04	6.72
18	-	51.12	0.06	-	0.61	0.65	44.21	2.03	98.71	92.48	1.29	2.41	3.83
19	-	52.13	-	-	0.56	0.86	44.77	0.24	98.60	95.06	1.21	3.27	0.46
20	-	50.90	0.02	0.04	0.80	0.13	44.74	1.87	98.51	94.26	1.71	0.48	3.55
21	-	50.19	0.03	-	0.29	1.27	42.60	4.30	98.70	86.90	0.60	4.60	7.90
22	-	51.80	0.03	-	0.58	0.04	45.94	0.95	99.35	96.83	1.24	0.13	1.80
23	-	50.08	0.09	-	0.31	2.77	39.81	5.83	98.92	79.15	0.61	9.81	10.43
24	-	51.44	0.08	0.05	0.41	2.12	42.08	2.21	98.37	87.22	0.85	7.82	4.12
25	-	49.57	0.27	0.05	0.45	1.87	40.79	6.22	99.23	81.29	0.91	6.64	11.16
26	-	51.95	0.02	-	2.59	0.05	44.02	0.60	99.27	93.11	5.55	0.19	1.14
27	-	52.05	0.03	0.07	0.44	1.54	43.63	0.94	98.71	91.53	0.94	5.75	1.78
28	-	50.72	0.02	-	0.64	0.13	44.75	2.67	98.96	93.16	1.35	0.49	5.00
29	-	50.58	-	-	0.57	0.12	44.72	2.64	98.67	93.40	1.20	0.44	4.96
30	-	50.90	0.03	-	0.93	0.20	44.50	2.44	99.01	92.74	1.96	0.73	4.57
31	0.03	52.27	-	0.17	2.37	0.08	44.20	0.00	99.13	94.57	5.14	0.30	0.00
32	-	51.07	0.04	-	1.78	0.12	43.94	1.95	98.95	92.10	3.78	0.44	3.68
34	-	50.90	0.03	-	0.61	0.48	44.32	1.03	97.39	94.86	1.32	1.84	1.98
35	-	51.18	0.02	0.46	0.43	1.21	43.45	1.63	98.40	91.45	0.92	4.55	3.09
36	-	51.14	0.03	-	0.44	1.97	42.05	3.50	99.16	85.54	0.90	7.14	6.42
37	-	50.90	0.03	0.22	0.39	1.45	42.80	3.00	98.82	88.28	0.82	5.34	5.56
38	-	52.60	0.03	-	0.58	0.82	44.33	0.00	98.37	95.60	1.27	3.14	0.00
39	-	50.55	0.04	-	1.10	0.11	44.17	2.35	98.34	92.81	2.34	0.40	4.44
40	0.06	51.40	0.03	-	1.54	0.03	44.68	0.86	98.62	94.92	3.31	0.11	1.65
41	-	51.96	0.04	-	0.48	0.54	45.30	1.78	100.11	93.70	1.00	1.99	3.31
42	-	51.64	0.03	-	0.42	1.00	44.22	1.50	98.82	92.53	0.89	3.74	2.83
44	-	50.67	0.02	0.15	0.48	0.19	44.75	3.49	99.76	91.85	0.99	0.71	6.45
46	-	49.04	0.04	-	0.41	0.74	42.37	5.41	98.03	86.53	0.85	2.68	9.94
47	0.03	51.14	0.04	-	0.71	0.30	44.76	2.87	99.84	92.11	1.47	1.11	5.31
48	-	50.09	0.07	-	0.39	1.60	41.81	4.42	98.41	85.27	0.81	5.81	8.12

- = below detection limit

APPENDIX B.2

TRANSKEI SAMPLES - ILMENITE MICROPROBE ANALYSES

							Recalculated			Recalculated mole fractions			
ANALYSIS	SiO2	TiO2	Al2O3	Cr2O3	MnO	MgO	FeO	Fe2O3	TOTAL	FeTiO3	MnTiO3	MgTiO3	Fe2O3
49	-	52.15	0.02	0.05	0.86	0.12	45.23	0.00	98.43	97.68	1.87	0.45	0.00
50	-	51.86	0.03	0.06	0.44	0.19	45.87	0.14	98.58	98.09	0.94	0.71	0.26
51	-	52.04	0.03	-	0.61	0.16	45.66	0.00	98.52	98.05	1.33	0.62	0.00
52	-	51.11	0.07	0.07	0.39	0.90	43.96	2.39	98.90	91.37	0.83	3.34	4.47
53	-	48.93	0.03	0.33	1.04	0.19	42.61	4.78	97.90	88.23	2.18	0.69	8.90
54	-	51.78	0.05	-	0.35	0.69	45.00	0.90	98.79	94.95	0.75	2.58	1.72
55	-	51.67	0.03	0.04	0.82	0.18	45.31	0.53	98.59	96.51	1.77	0.69	1.02
56	-	48.90	0.06	0.04	0.45	0.79	42.12	5.98	98.33	85.34	0.91	2.85	10.90
57	-	52.76	-	0.25	1.49	0.09	44.18	0.00	98.78	96.34	3.29	0.36	0.00
58	-	52.35	0.02	0.31	0.65	1.05	44.09	0.00	98.49	94.56	1.42	4.02	0.00
60	-	50.65	0.02	0.06	0.75	0.26	44.33	2.71	98.78	92.37	1.58	0.97	5.08
Average	0.14	51.06	0.04	0.13	0.74	0.69	43.87	2.32					
HT3													
1	-	53.28	-	-	2.68	0.19	43.38	0.00	99.56	93.43	5.84	0.74	0.00
2	-	52.20	0.02	0.32	0.56	3.09	40.86	2.14	99.20	83.62	1.16	11.28	3.94
3	0.03	50.65	-	0.05	2.31	0.08	43.10	2.26	98.48	90.51	4.92	0.30	4.27
4	-	53.48	-	-	0.66	0.11	44.76	0.00	99.02	98.11	1.45	0.44	0.00
5	-	50.69	0.03	-	0.89	0.12	44.47	2.34	98.57	93.24	1.90	0.45	4.41
6	-	49.67	0.09	0.57	0.35	2.85	39.24	6.52	99.29	77.64	0.71	10.05	11.61
8	-	49.69	0.05	0.06	0.38	0.81	42.87	4.98	98.86	87.17	0.78	2.93	9.11
9	-	51.55	-	-	1.18	0.06	45.05	0.62	98.47	96.02	2.55	0.24	1.19
10	-	50.80	-	0.04	0.60	0.07	44.94	2.33	98.79	94.05	1.28	0.28	4.39
11	-	52.31	0.06	0.12	0.53	1.76	43.35	0.70	98.84	90.96	1.14	6.60	1.31
12	-	49.76	-	0.06	1.00	0.09	43.59	4.46	98.98	89.35	2.07	0.34	8.23
13	-	51.31	0.04	-	0.67	0.21	45.11	2.26	99.64	93.60	1.41	0.76	4.23
14	-	50.30	0.02	0.19	0.41	0.99	43.05	4.46	99.43	87.40	0.84	3.60	8.15
15	-	50.98	0.03	0.14	0.55	0.53	44.35	2.65	99.24	91.95	1.15	1.96	4.94
16	-	50.99	0.03	0.14	0.50	0.59	44.32	2.52	99.09	92.07	1.05	2.17	4.71
17	-	50.12	0.02	0.10	0.61	0.25	44.00	3.81	98.91	90.74	1.28	0.91	7.07
18	-	51.08	0.04	0.07	1.64	0.08	44.15	2.36	99.43	91.84	3.46	0.29	4.41
19	-	50.66	0.04	0.24	0.65	0.20	44.57	2.12	98.50	93.86	1.39	0.74	4.01
20	-	52.04	0.03	0.22	0.38	1.95	42.94	2.15	99.72	88.10	0.79	7.14	3.96
21	-	51.87	0.05	0.12	0.47	2.08	42.48	1.70	98.81	88.12	0.99	7.70	3.18
22	0.03	51.01	0.04	0.06	0.75	0.68	43.94	2.42	98.92	91.39	1.57	2.51	4.53
24	-	51.23	-	0.10	0.93	0.05	45.06	2.24	99.64	93.67	1.96	0.18	4.19
25	-	51.54	0.02	0.06	1.04	0.09	45.15	1.21	99.12	95.15	2.22	0.33	2.30
26	-	51.07	0.03	0.07	0.64	0.18	44.97	2.37	99.35	93.53	1.35	0.68	4.43
27	-	50.00	0.02	0.43	0.48	1.36	42.07	4.47	98.86	85.85	0.98	4.95	8.21
28	-	51.01	-	0.52	0.45	1.59	42.60	3.24	99.44	87.30	0.94	5.79	5.97
29	-	50.53	0.06	0.08	0.40	1.37	42.62	4.53	99.60	86.03	0.81	4.92	8.24
30	-	51.81	0.02	0.09	0.53	0.50	45.17	1.37	99.51	94.44	1.13	1.86	2.57
31	-	50.27	0.06	0.07	0.42	1.37	42.36	4.58	99.15	85.84	0.87	4.94	8.35
32	0.04	49.28	0.05	-	0.47	0.42	43.15	5.79	99.24	87.02	0.97	1.50	10.51
33	-	52.59	0.02	-	3.83	0.13	42.31	0.00	98.93	91.14	8.35	0.51	0.00
34	0.03	52.29	0.07	0.06	0.44	1.86	43.30	1.19	99.24	89.97	0.93	6.88	2.22

- = below detection limit

APPENDIX B.2

TRANSKEI SAMPLES - ILMENITE MICROPROBE ANALYSES

							Recalculated			Recalculated mole fractions			
ANALYSIS	SiO2	TiO2	Al2O3	Cr2O3	MnO	MgO	FeO	Fe2O3	TOTAL	FeTiO3	MnTiO3	MgTiO3	Fe2O3
35	-	52.11	0.02	0.08	2.30	0.08	44.40	0.99	100.00	92.96	4.89	0.29	1.87
36	-	51.03	0.02	-	0.73	0.16	44.87	2.52	99.38	93.16	1.52	0.61	4.71
37	-	52.45	0.02	-	0.83	0.12	46.03	0.00	99.48	97.78	1.78	0.44	0.00
38	0.03	51.34	0.04	-	0.49	0.68	44.49	2.49	99.58	91.84	1.03	2.51	4.62
39	0.04	51.64	0.05	-	0.56	0.50	45.03	1.96	99.80	93.34	1.17	1.85	3.65
40	-	51.12	0.05	0.16	0.59	0.22	45.00	2.61	99.77	93.09	1.24	0.80	4.87
41	-	51.83	0.02	-	1.00	0.33	45.01	1.50	99.70	93.84	2.11	1.24	2.82
42	-	49.83	0.10	0.08	0.69	0.79	42.71	4.85	99.06	86.84	1.42	2.87	8.87
45	-	52.57	0.03	0.09	0.82	0.25	44.87	0.00	98.63	97.24	1.81	0.95	0.00
46	-	52.38	0.02	0.06	1.42	0.10	44.77	0.00	98.74	96.53	3.10	0.38	0.00
47	-	52.90	-	0.09	0.72	0.14	45.35	0.00	99.22	97.87	1.58	0.55	0.00
48	-	50.10	0.03	0.05	0.56	0.55	43.52	4.72	99.53	88.27	1.15	1.97	8.61
49	-	51.27	-	-	2.01	0.08	43.93	2.14	99.47	91.46	4.23	0.30	4.02
50	-	51.16	0.03	0.11	0.88	0.78	43.73	2.02	98.71	91.44	1.86	2.90	3.80
51	0.05	50.27	0.03	0.08	0.40	1.81	41.64	4.28	98.56	84.78	0.83	6.55	7.84
52	-	49.85	0.14	0.14	0.34	2.08	40.79	5.47	98.80	81.98	0.68	7.45	9.88
53	-	51.74	0.02	0.04	0.42	0.55	45.13	1.29	99.20	94.62	0.90	2.05	2.44
54	0.03	50.43	0.02	0.07	0.61	0.11	44.56	2.60	98.44	93.38	1.30	0.42	4.91
55	-	51.99	0.06	0.06	0.40	0.84	44.85	1.08	99.27	93.97	0.85	3.13	2.04
56	-	52.07	0.15	0.08	0.43	0.92	44.76	0.54	98.96	94.59	0.91	3.48	1.02
57	-	48.28	0.10	0.20	0.31	2.83	38.08	9.05	98.87	73.83	0.61	9.76	15.79
58	-	50.83	0.02	0.14	0.43	0.26	44.81	2.37	98.88	93.65	0.91	0.98	4.46
59	-	50.54	0.03	0.18	0.35	1.61	42.24	3.90	98.86	86.26	0.72	5.86	7.16
60	-	51.23	0.04	-	0.63	0.14	45.20	1.94	99.22	94.49	1.33	0.54	3.64
61	0.06	50.82	0.17	-	0.38	0.18	45.07	1.41	98.09	95.80	0.81	0.68	2.71
62	-	49.30	0.05	-	0.60	0.25	43.28	6.26	99.77	86.62	1.22	0.89	11.27
63	-	51.93	0.02	-	0.63	0.08	45.92	0.11	98.69	98.13	1.36	0.30	0.21
64	-	52.28	0.03	0.05	1.05	0.21	45.58	0.26	99.45	96.47	2.24	0.79	0.49
65	-	52.16	0.02	0.06	0.49	0.08	46.28	0.48	99.58	97.73	1.05	0.31	0.91
66	0.08	49.70	0.05	0.04	0.46	0.61	43.23	4.04	98.22	89.27	0.96	2.26	7.51
67	-	50.84	0.03	0.04	0.36	0.89	43.79	2.64	98.60	91.01	0.77	3.28	4.94
68	-	50.25	0.07	-	0.31	0.30	44.36	3.13	98.47	92.37	0.66	1.10	5.87
69	0.04	52.38	0.05	-	0.42	0.82	45.26	0.41	99.39	95.26	0.89	3.08	0.77
70	0.22	51.02	0.55	-	0.16	1.67	43.00	3.06	99.67	87.96	0.33	6.08	5.63
71	0.04	52.14	0.02	0.05	0.48	0.19	46.11	0.83	99.86	96.70	1.02	0.71	1.56
72	0.02	50.86	0.03	0.06	0.43	0.85	43.80	3.56	99.62	89.46	0.90	3.10	6.54
73	0.04	52.09	0.04	-	0.57	0.19	45.98	(0.00)	98.93	98.07	1.22	0.71	(0.00)
74	-	51.01	0.05	-	0.39	0.88	43.93	2.00	98.32	92.11	0.82	3.30	3.77
75	0.04	51.04	0.06	0.04	0.98	0.14	44.70	2.64	99.64	92.51	2.05	0.53	4.92
76	-	53.81	-	0.08	0.52	0.45	43.86	0.00	98.74	97.08	1.16	1.76	0.00
77	-	50.98	0.05	0.09	0.78	0.42	44.31	2.95	99.59	91.34	1.64	1.55	5.47
Average	0.05	51.20	0.05	0.12	0.74	0.68	43.94	2.41					
HT2-ILM													
1	0.04	50.37	0.03	0.04	1.88	0.12	43.23	2.38	98.10	91.02	4.00	0.46	4.51

- = below detection limit

APPENDIX B.2

TRANSKEI SAMPLES - ILMENITE MICROPROBE ANALYSES

							Recalculated			Recalculated mole fractions			
ANALYSIS	SiO2	TiO2	Al2O3	Cr2O3	MnO	MgO	FeO	Fe2O3	TOTAL	FeTiO3	MnTiO3	MgTiO3	Fe2O3
2	0.03	50.52	0.02	-	1.66	0.32	43.22	3.81	99.59	88.38	3.44	1.16	7.02
3	-	50.55	0.08	0.26	0.43	1.95	41.55	3.68	98.51	85.18	0.89	7.13	6.79
4	-	51.93	0.05	-	0.42	0.66	45.10	1.83	100.01	93.28	0.88	2.43	3.41
5	-	51.38	0.03	-	0.78	0.05	45.34	2.44	100.03	93.66	1.63	0.18	4.53
	-	51.21	-	-	1.02	0.08	44.89	1.52	98.77	94.63	2.18	0.31	2.89
	-	51.27	-	-	1.12	0.09	44.81	2.66	99.98	92.39	2.34	0.32	4.94
	-	51.25	0.08	-	0.49	0.70	44.34	2.67	99.53	91.44	1.03	2.57	4.96
	-	50.09	0.08	0.10	0.40	1.54	41.90	4.67	98.79	85.07	0.82	5.57	8.54
	-	50.33	0.06	0.09	0.36	0.51	43.98	3.75	99.08	90.42	0.75	1.88	6.94
	-	51.58	-	-	1.24	0.08	45.00	1.83	99.79	93.64	2.62	0.31	3.43
	-	51.50	0.02	-	0.57	0.17	45.45	1.46	99.20	95.40	1.21	0.63	2.76
	-	50.85	0.05	-	0.43	0.75	43.97	3.76	99.83	89.52	0.88	2.71	6.89
	-	52.13	0.04	-	1.19	0.05	45.58	0.61	99.63	96.09	2.54	0.20	1.16
	-	51.77	0.05	0.05	0.40	1.25	43.92	2.57	100.01	89.86	0.83	4.57	4.74
	-	52.49	0.02	0.05	0.65	0.24	45.23	0.00	98.70	97.64	1.43	0.92	0.00
	-	51.93	-	-	0.54	0.06	46.06	0.62	99.25	97.42	1.16	0.24	1.19
	-	52.10	0.05	-	0.40	0.72	45.17	0.26	98.72	95.90	0.86	2.74	0.50
	0.21	51.02	0.03	-	0.81	0.09	45.15	1.74	99.07	94.67	1.72	0.32	3.29
	-	52.03	-	-	1.57	0.06	45.09	0.17	98.98	96.04	3.39	0.23	0.33
	-	51.46	0.02	-	1.16	0.02	45.10	1.69	99.47	94.30	2.45	0.06	3.18
	-	51.32	-	-	1.10	0.34	44.44	2.38	99.60	92.01	2.30	1.25	4.44
	-	51.50	0.06	0.23	0.49	2.06	42.14	3.55	100.03	85.14	1.01	7.40	6.45
	-	51.05	0.05	-	0.42	0.29	44.96	3.37	100.16	91.88	0.87	1.06	6.19
	-	51.13	0.04	-	0.57	0.30	44.88	2.55	99.47	92.95	1.20	1.10	4.75
	-	51.08	0.13	0.33	0.40	3.29	39.68	5.51	100.42	77.97	0.79	11.51	9.74
	-	52.92	0.03	-	0.88	0.35	46.10	0.15	100.46	96.57	1.86	1.29	0.27
	0.03	50.82	0.02	-	0.55	0.19	44.84	3.67	100.13	91.44	1.14	0.69	6.73
	0.05	50.14	0.02	-	0.42	0.59	43.67	4.17	99.07	89.30	0.88	2.15	7.68
	0.05	51.96	0.03	-	0.97	0.25	45.36	1.96	100.59	93.44	2.02	0.90	3.64
	0.06	51.58	0.02	-	0.57	0.15	45.60	1.52	99.50	95.36	1.20	0.57	2.87
	0.04	51.49	0.09	0.17	0.36	2.21	42.05	3.55	99.95	84.87	0.74	7.94	6.45
	0.06	52.38	0.06	-	0.35	1.31	44.30	0.00	98.48	94.28	0.76	4.96	0.00
HT7-ILM													
1	-	49.76	0.10	-	0.47	1.85	40.98	6.15	99.32	81.51	0.94	6.54	11.00
3	-	46.86	0.07	0.08	0.58	0.33	40.96	10.52	99.40	79.37	1.14	1.15	18.34
4	-	50.62	0.05	0.32	0.44	1.72	42.04	3.97	99.17	85.58	0.91	6.22	7.28
5	-	51.46	-	0.04	0.51	0.19	45.42	1.72	99.37	94.96	1.08	0.72	3.23
6	-	51.05	0.02	-	0.81	0.02	45.07	2.74	99.73	93.17	1.69	0.05	5.09
7	-	52.64	-	0.08	3.13	0.12	43.97	0.26	100.21	92.41	6.65	0.43	0.50
9	-	49.85	0.03	-	0.47	0.66	43.18	5.42	99.64	86.87	0.96	2.36	9.81
10	-	51.38	-	-	0.91	0.14	45.04	1.89	99.40	94.00	1.92	0.54	3.55
11	-	51.50	0.02	0.11	1.60	0.34	44.09	1.54	99.20	92.45	3.40	1.25	2.90
12	-	51.15	0.03	-	1.08	0.07	44.78	1.56	98.66	94.47	2.31	0.26	2.95
14	-	52.86	0.06	-	0.34	1.66	43.12	0.00	98.37	92.89	0.74	6.37	0.00

- = below detection limit

APPENDIX B.2

TRANSKEI SAMPLES - ILMENITE MICROPROBE ANALYSES

							Recalculated			Recalculated mole fractions			
ANALYSIS	SiO2	TiO2	Al2O3	Cr2O3	MnO	MgO	FeO	Fe2O3	TOTAL	FeTiO3	MnTiO3	MgTiO3	Fe2O3
15	-	49.69	0.08	0.05	0.38	1.50	41.63	5.47	98.79	83.93	0.78	5.37	9.92
16	-	49.28	0.09	0.04	0.35	1.44	41.39	4.91	97.49	84.94	0.72	5.27	9.07
17	-	51.41	0.07	-	0.26	0.65	44.81	1.24	98.44	94.65	0.55	2.44	2.36
18	-	52.01	0.04	0.37	0.45	1.32	43.96	1.32	99.47	91.67	0.95	4.91	2.47
19	-	50.48	0.09	0.17	0.38	0.91	43.38	3.14	98.56	89.97	0.80	3.36	5.87
20	-	51.50	0.03	0.07	0.90	0.31	44.84	1.21	98.85	94.60	1.93	1.18	2.29
21	-	53.53	0.02	0.22	1.11	0.38	43.78	0.00	99.05	96.04	2.47	1.49	0.00
22	-	50.21	0.07	0.38	0.36	1.74	41.68	4.96	99.40	84.00	0.73	6.27	9.00
23	-	50.76	0.06	0.05	0.40	1.01	43.44	3.31	99.03	89.33	0.83	3.71	6.13
24	-	50.32	0.04	-	0.46	0.26	44.33	4.33	99.74	90.18	0.94	0.95	7.92
25	-	51.11	0.06	0.40	0.62	2.25	41.33	2.82	98.59	85.21	1.29	8.25	5.24
26	-	52.40	0.03	0.05	0.53	0.27	46.10	0.40	99.79	97.09	1.13	1.03	0.75
27	-	52.06	-	0.12	1.80	0.18	44.67	1.10	99.93	93.43	3.81	0.69	2.07
28	-	51.73	0.07	-	0.51	1.32	43.65	2.78	100.08	89.04	1.05	4.80	5.10
29	-	51.02	0.07	0.04	0.36	1.55	42.76	3.68	99.47	86.92	0.73	5.61	6.73
30	-	49.75	0.03	0.04	0.75	0.41	43.26	5.19	99.42	87.54	1.53	1.47	9.46
31	-	50.94	0.04	-	0.33	0.89	43.90	2.35	98.47	91.60	0.69	3.31	4.41
32	-	50.58	0.08	0.04	0.40	1.04	43.21	3.80	99.15	88.36	0.84	3.81	7.00
33	-	51.82	-	0.12	3.68	0.13	42.65	0.59	99.00	90.50	7.90	0.48	1.12
34	-	50.94	0.04	0.07	0.99	0.19	44.47	2.58	99.27	92.39	2.08	0.70	4.83
35	-	52.05	-	-	0.80	0.18	45.67	0.74	99.46	96.21	1.72	0.67	1.40
36	-	50.69	0.03	0.04	0.34	0.63	44.12	3.78	99.65	90.04	0.71	2.31	6.95
37	-	51.08	0.05	-	0.66	0.60	44.20	3.12	99.74	90.68	1.37	2.20	5.76
38	-	51.75	0.03	0.04	0.81	0.19	45.37	1.34	99.53	95.04	1.72	0.72	2.52
39	-	49.71	0.04	0.16	0.41	1.77	41.14	5.33	98.55	83.11	0.84	6.37	9.68
40	-	50.62	0.05	0.06	0.60	0.88	43.36	2.72	98.29	90.37	1.26	3.25	5.11
41	-	52.95	0.03	0.05	0.46	0.34	45.11	0.00	98.94	97.69	1.00	1.31	0.00
42	-	50.84	0.04	-	0.90	0.17	44.51	2.38	98.85	93.01	1.91	0.62	4.47
43	0.05	51.37	0.09	-	1.56	0.12	44.47	1.90	99.58	92.70	3.29	0.44	3.57
44	-	49.02	0.02	0.09	0.60	0.30	42.94	6.49	99.46	86.00	1.22	1.07	11.70
45	-	50.75	0.02	0.06	2.98	0.21	42.24	2.60	98.86	88.05	6.30	0.78	4.88
46	-	49.03	0.04	0.10	0.96	0.13	42.88	5.38	98.52	87.64	1.99	0.48	9.89
47	-	50.35	0.06	0.04	0.78	0.64	43.35	4.20	99.43	88.35	1.61	2.33	7.71
48	-	52.62	0.04	-	0.44	0.49	46.01	0.56	100.17	96.21	0.92	1.82	1.05
49	-	49.19	0.02	0.38	0.44	1.05	41.92	6.13	99.14	84.26	0.91	3.74	11.09
50	-	49.50	-	0.04	0.96	0.16	43.25	4.49	98.42	89.06	2.01	0.60	8.33
51	-	50.87	-	-	1.27	0.23	44.04	3.16	99.62	90.64	2.66	0.85	5.85
52	-	52.86	0.03	-	0.43	0.55	45.07	0.00	98.97	96.95	0.94	2.11	0.00
53	-	50.86	0.04	-	1.76	0.10	43.79	3.55	100.13	89.47	3.64	0.36	6.52
55	-	50.04	0.03	0.32	0.42	0.65	43.41	5.05	99.93	87.62	0.86	2.35	9.17
56	-	47.49	0.12	0.19	1.34	0.15	41.09	8.32	98.69	81.86	2.70	0.53	14.92
57	-	49.29	0.06	0.12	0.44	1.43	41.35	6.51	99.20	82.37	0.88	5.07	11.68
58	-	50.75	-	0.04	0.92	0.07	44.59	2.51	98.88	93.10	1.94	0.25	4.71

- = below detection limit

APPENDIX B.2

EASTERN CAPE SAMPLES - ILMENITE MICROPROBE ANALYSES

							Recalculated			Recalculated mole fractions			
Sample	SiO2	TiO2	Al2O3	Cr2O3	MnO	MgO	FeO	Fe2O3	TOTAL	FeTiO3	MnTiO3	MgTiO3	Fe2O3
HEC8-1	-	52.78	0.03	1.66	0.49	5.93	36.39	3.04	100.33	72.50	1.00	21.06	5.45
2	-	51.93	0.04	0.05	0.48	0.44	45.43	0.64	99.02	96.07	1.04	1.67	1.22
3	-	52.43	0.02	0.12	0.42	0.43	45.96	0.26	99.64	97.00	0.90	1.61	0.49
4	-	50.65	0.03	0.60	0.43	1.59	42.28	3.72	99.32	86.46	0.89	5.80	6.85
5	-	51.56	0.06	0.05	0.45	0.82	44.47	2.64	100.07	91.19	0.92	3.01	4.87
6	-	50.81	0.06	0.15	0.40	1.68	42.32	4.17	99.60	85.56	0.81	6.04	7.58
7	-	50.15	0.07	0.14	0.49	1.65	41.66	5.39	99.54	83.42	0.99	5.88	9.71
8	-	51.38	0.02	0.05	0.63	0.19	45.22	2.92	100.42	92.60	1.31	0.71	5.39
9	-	51.39	0.04	0.05	0.54	0.26	45.22	1.80	99.29	94.53	1.13	0.95	3.38
12	-	50.68	0.03	0.04	0.81	0.33	44.17	2.86	98.94	91.72	1.71	1.23	5.34
13	-	51.28	0.04	-	0.47	0.73	44.34	2.58	99.47	91.54	0.98	2.70	4.79
14	-	53.09	0.05	0.12	0.59	2.17	43.28	0.50	99.79	89.81	1.23	8.02	0.94
15	-	51.53	0.03	0.12	1.31	0.39	44.33	0.96	98.68	93.90	2.82	1.46	1.83
16	-	50.81	0.06	0.04	0.36	1.11	43.34	2.92	98.65	89.71	0.76	4.09	5.44
17	-	51.19	0.05	-	0.38	0.54	44.69	2.31	99.19	92.87	0.81	2.01	4.31
18	-	53.48	0.02	0.39	1.69	0.34	43.53	0.00	99.45	94.95	3.73	1.32	0.00
19	-	51.25	0.02	0.04	0.68	0.65	44.25	1.82	98.72	92.69	1.45	2.44	3.42
20	-	50.69	0.04	0.13	0.47	1.36	42.70	3.65	99.06	87.35	0.97	4.96	6.72
21	0.03	51.85	0.03	-	0.40	0.28	45.75	1.55	99.89	95.20	0.85	1.04	2.91
22	-	52.98	0.02	-	0.50	0.29	46.19	0.00	100.01	97.84	1.08	1.08	0.00
23	-	51.34	0.08	0.10	0.37	1.45	43.23	2.82	99.41	88.71	0.77	5.32	5.20
24	-	50.98	0.04	0.11	1.52	0.12	44.11	3.18	100.06	90.54	3.16	0.43	5.88
25	-	49.69	0.04	-	0.39	1.08	42.38	5.71	99.33	85.05	0.79	3.85	10.31
26	0.03	51.66	0.04	-	0.39	1.00	44.32	2.56	100.02	90.82	0.82	3.63	4.73
27	0.03	50.15	0.07	-	0.41	1.50	42.04	5.23	99.45	84.36	0.83	5.38	9.44
28	-	50.87	0.06	-	0.50	0.98	43.51	3.99	99.94	88.17	1.02	3.54	7.27
29	-	51.24	0.05	-	0.39	1.10	43.74	3.42	99.96	88.95	0.80	3.99	6.26
30	0.03	51.65	0.05	-	0.61	0.51	44.96	2.37	100.18	92.49	1.27	1.86	4.38
31	0.10	51.70	0.04	0.13	2.48	0.12	43.88	0.58	99.02	93.10	5.33	0.47	1.10
32	0.04	51.18	0.05	0.04	0.51	0.59	44.50	2.88	99.79	91.44	1.05	2.18	5.33
33	-	50.72	-	0.05	1.79	0.08	43.67	3.52	99.86	89.50	3.72	0.29	6.49
34	-	51.68	0.03	0.13	0.91	0.18	45.25	1.20	99.40	95.11	1.93	0.68	2.27
35	0.04	52.25	0.05	0.14	0.55	1.61	43.61	1.56	99.82	90.04	1.15	5.91	2.90
36	0.03	53.27	0.06	0.10	3.47	0.31	42.10	0.00	99.32	91.20	7.61	1.19	0.00
37	-	51.93	-	-	1.42	0.48	44.44	1.81	100.12	91.91	2.96	1.76	3.37
39	-	52.52	0.07	-	0.45	0.83	45.33	0.62	99.85	94.79	0.94	3.09	1.17
40	-	52.70	0.03	-	0.73	0.41	45.96	0.51	100.36	96.01	1.54	1.51	0.95
41	0.04	51.68	0.03	0.12	2.11	0.17	44.08	1.28	99.51	92.47	4.49	0.62	2.42
42	-	50.64	0.08	0.09	0.44	1.71	42.07	4.08	99.14	85.44	0.91	6.20	7.46
43	0.03	50.94	0.02	0.03	1.40	0.07	44.31	3.55	100.34	90.35	2.88	0.25	6.52
44	0.04	51.36	0.03	-	0.92	0.24	44.86	1.66	99.12	94.02	1.95	0.91	3.12
45	-	49.65	0.04	-	0.43	0.92	42.59	5.00	98.68	86.63	0.89	3.34	9.15
46	0.04	53.87	0.05	0.04	0.67	0.38	44.42	0.00	99.46	97.04	1.47	1.48	0.00
47	-	52.43	-	-	0.92	0.52	45.31	0.47	99.71	95.21	1.95	1.95	0.89
48	0.03	53.62	0.05	-	0.47	0.39	44.44	0.00	99.03	97.44	1.05	1.51	0.00
49	0.03	51.08	0.03	0.24	1.75	0.27	43.71	2.77	99.88	90.20	3.66	0.99	5.15
50	0.18	51.26	0.02	-	1.19	1.02	43.29	2.73	99.71	88.76	2.47	3.72	5.04

- = below detection limit

APPENDIX B.2

EASTERN CAPE SAMPLES - ILMENITE MICROPROBE ANALYSES

							Recalculated			Recalculated mole fractions			
Sample	SiO2	TiO2	Al2O3	Cr2O3	MnO	MgO	FeO	Fe2O3	TOTAL	FeTiO3	MnTiO3	MgTiO3	Fe2O3
51	0.10	50.37	0.03	-	1.58	0.87	42.26	3.28	98.47	87.40	3.31	3.20	6.10
52	0.03	52.09	-	-	0.58	0.22	45.90	1.51	100.34	95.16	1.22	0.80	2.82
53	-	50.85	0.03	0.12	0.39	0.78	43.94	3.92	100.03	89.21	0.80	2.82	7.16
54	-	51.34	0.02	-	0.41	0.79	44.37	3.09	100.06	90.60	0.84	2.88	5.68
55	-	51.89	0.02	-	0.43	0.73	44.96	1.29	99.33	93.97	0.90	2.70	2.43
56	-	53.13	-	-	0.47	0.50	46.06	0.00	100.20	97.13	1.00	1.87	0.00
57	-	52.79	0.03	-	1.03	0.32	45.86	0.05	100.10	96.49	2.19	1.22	0.10
61	-	51.96	-	0.04	1.18	0.47	44.73	1.69	100.09	92.65	2.48	1.72	3.15
67	0.04	52.11	0.03	0.04	0.85	0.08	45.90	0.43	99.47	97.07	1.82	0.30	0.82
68	0.04	52.00	0.04	0.04	1.33	0.18	45.14	0.14	98.92	96.18	2.88	0.68	0.27
HEC6													
1	-	50.17	0.02	-	0.44	1.05	42.81	4.09	98.62	87.72	0.91	3.84	7.53
2	0.05	53.48	0.04	0.52	0.44	4.42	39.83	0.54	99.31	81.90	0.92	16.19	0.99
4	-	52.07	0.02	-	0.76	0.50	45.06	0.00	98.44	96.46	1.64	1.90	0.00
5	-	51.35	0.05	-	0.39	0.91	44.17	2.21	99.09	91.70	0.81	3.37	4.12
6	-	51.94	0.06	-	0.50	0.63	45.09	0.46	98.68	95.67	1.08	2.37	0.88
7	-	50.77	0.04	-	0.50	0.41	44.43	2.61	98.78	92.53	1.05	1.54	4.88
8	0.03	52.26	0.08	-	0.70	0.32	45.75	0.27	99.41	96.78	1.51	1.20	0.51
9	-	52.50	-	-	0.58	0.55	45.02	0.00	98.68	96.63	1.26	2.11	0.00
10	-	50.87	0.05	0.04	0.49	0.39	44.56	2.72	99.14	92.45	1.04	1.44	5.08
11	-	51.42	0.04	-	0.44	0.94	44.12	1.89	98.86	92.03	0.94	3.49	3.55
12	0.04	52.92	0.03	-	0.42	0.68	44.95	0.00	99.05	96.47	0.92	2.60	0.00
13	-	49.62	0.04	0.04	3.73	0.04	40.80	5.13	99.43	82.82	7.66	0.14	9.38
14	-	52.58	0.05	-	0.66	0.25	46.18	0.21	99.95	97.24	1.42	0.94	0.40
15	-	49.66	-	-	0.40	2.44	39.91	6.97	99.42	78.35	0.80	8.54	12.31
16	-	52.29	0.02	0.54	2.35	0.17	44.34	0.57	100.28	93.27	5.00	0.64	1.08
17	-	51.86	0.02	-	0.87	0.16	45.49	0.96	99.41	95.72	1.86	0.61	1.81
18	-	52.07	0.04	-	0.51	0.26	45.86	0.07	98.82	97.79	1.11	0.98	0.13
19	-	49.08	0.06	0.08	0.57	1.17	41.49	6.83	99.28	82.50	1.14	4.14	12.23
20	0.03	51.97	0.04	-	0.46	1.35	43.89	1.62	99.37	91.02	0.98	4.98	3.02
21	0.03	51.39	0.07	-	0.42	0.51	44.91	1.32	98.66	94.67	0.91	1.92	2.50
22	-	53.33	0.02	-	0.47	0.69	45.54	0.00	100.06	96.37	1.01	2.62	0.00
23	-	52.00	0.06	0.07	1.06	0.51	44.80	1.84	100.36	92.49	2.22	1.87	3.42
24	-	53.01	0.04	-	0.41	0.96	45.55	0.22	100.24	95.13	0.86	3.59	0.42
25	-	51.89	0.10	-	0.59	0.63	44.96	2.03	100.24	92.68	1.24	2.31	3.77
26	0.04	49.66	0.05	0.12	0.51	0.86	42.65	5.68	99.57	85.62	1.03	3.08	10.26
27	0.05	49.04	0.09	0.09	0.51	1.37	41.20	6.94	99.29	81.75	1.02	4.85	12.38
28	-	50.27	-	0.04	0.55	0.50	43.76	4.59	99.73	88.69	1.12	1.82	8.37
29	-	51.21	0.02	-	0.41	0.68	44.45	2.92	99.72	91.27	0.85	2.48	5.40
30	-	51.34	0.07	-	0.47	0.43	44.95	1.57	98.85	94.42	0.99	1.62	2.98
31	0.04	51.21	0.09	-	0.42	0.98	43.92	3.17	99.86	89.72	0.86	3.58	5.84
32	0.07	50.36	0.24	-	1.71	0.09	43.47	2.00	97.97	92.16	3.68	0.35	3.81
33	0.03	51.57	0.07	0.05	0.40	1.48	43.36	2.86	99.82	88.54	0.83	5.37	5.26
34	0.03	51.59	0.02	-	0.81	0.02	45.56	0.70	98.73	96.83	1.75	0.08	1.34
Average	0.04	51.42	0.06	0.16	0.73	0.80	44.03	2.21	99.31	91.50	1.53	2.93	4.05

- = below detection limit

APPENDIX B.2

EASTERN CAPE SAMPLES - ILMENITE MICROPROBE ANALYSES

							Recalculated			Recalculated mole fractions			
Sample	SiO2	TiO2	Al2O3	Cr2O3	MnO	MgO	FeO	Fe2O3	TOTAL	FeTiO3	MnTiO3	MgTiO3	Fe2O3
HEC5													
1	0.04	50.37	0.04	0.06	0.47	0.18	44.54	3.49	99.16	91.89	0.98	0.65	6.48
2	0.04	51.74	0.04	-	0.45	0.35	45.50	2.01	100.15	94.05	0.94	1.27	3.73
3	0.03	51.76	0.03	-	0.54	0.20	45.69	1.80	100.08	94.77	1.12	0.74	3.37
4	-	51.45	0.04	-	0.63	0.16	45.36	2.32	100.00	93.75	1.32	0.61	4.32
5	-	51.55	0.04	-	0.57	0.37	45.14	2.35	100.09	93.07	1.20	1.36	4.37
6	-	51.53	0.04	0.06	1.79	0.05	44.47	1.57	99.54	93.07	3.80	0.17	2.96
7	-	50.17	0.04	0.07	1.26	0.23	43.45	2.86	98.08	91.08	2.68	0.84	5.39
8	0.26	50.74	0.14	-	0.32	0.48	44.75	2.24	98.94	93.33	0.68	1.80	4.20
9	-	50.79	0.04	-	0.36	0.32	44.73	3.50	99.75	91.62	0.74	1.19	6.45
12	0.03	49.91	0.01	-	1.04	0.04	43.80	3.96	98.78	90.35	2.17	0.14	7.34
13	-	50.96	-	-	0.49	0.20	45.00	2.82	99.51	92.99	1.02	0.74	5.24
14	-	50.13	0.06	-	0.52	0.65	43.41	4.52	99.30	88.30	1.07	2.35	8.28
15	-	51.94	-	-	0.45	0.42	45.51	0.46	98.82	96.54	0.97	1.60	0.88
16	0.05	52.89	0.02	-	0.43	0.42	45.40	0.00	99.24	97.46	0.93	1.61	0.00
17	0.56	50.55	0.31	-	1.62	0.04	44.42	1.81	99.32	93.00	3.44	0.14	3.42
18	0.05	52.37	0.03	-	0.41	0.71	45.49	1.16	100.23	94.37	0.85	2.61	2.17
Average	0.13	51.18	0.06	0.06	0.71	0.30	44.79	2.31	99.44				
HEC3													
1	0.05	52.59	0.03	0.22	2.32	0.13	44.76	0.04	100.13	94.48	4.95	0.49	0.08
2	-	52.46	0.06	-	0.47	0.91	45.09	0.96	99.97	93.85	0.99	3.37	1.79
3	-	53.03	0.04	-	0.98	0.29	45.45	0.00	99.84	96.80	2.11	1.09	0.00
5	0.03	52.48	0.07	-	0.51	0.96	44.82	0.00	98.89	95.25	1.10	3.65	0.00
6	-	52.78	0.06	0.04	0.79	0.60	45.07	0.00	99.35	96.01	1.71	2.27	0.00
7	-	50.97	0.08	-	0.37	1.35	43.06	3.40	99.24	88.06	0.77	4.92	6.25
8	0.03	51.84	0.02	-	0.90	0.20	45.39	0.89	99.26	95.67	1.91	0.73	1.68
9	-	52.25	0.03	-	1.96	0.09	44.85	0.16	99.38	95.13	4.22	0.34	0.31
10	-	51.87	0.06	-	0.51	0.88	44.58	1.42	99.35	93.00	1.07	3.27	2.67
11	0.04	50.83	0.02	-	1.56	0.12	43.96	2.24	98.78	92.01	3.31	0.46	4.22
13	-	50.56	0.04	-	1.42	0.12	43.82	3.24	99.21	90.57	2.98	0.43	6.03
14	-	51.13	0.05	0.18	1.28	0.22	44.29	2.18	99.33	92.39	2.71	0.81	4.09
15	0.04	50.94	0.02	0.05	0.81	0.17	44.73	1.73	98.49	94.34	1.73	0.64	3.29
16	-	51.57	0.02	-	1.40	0.06	44.86	0.96	98.91	94.94	3.00	0.23	1.83
17	-	52.11	0.05	-	0.92	0.77	44.59	1.18	99.64	92.99	1.94	2.85	2.22
18	-	52.43	-	-	1.13	0.14	45.79	0.87	100.38	95.48	2.38	0.51	1.63
19	-	51.39	0.03	0.14	0.45	0.47	44.93	2.47	99.87	92.75	0.94	1.72	4.59
20	-	50.88	0.05	-	0.52	0.80	43.83	2.99	99.09	90.42	1.08	2.95	5.55
23	0.08	53.27	0.11	0.04	1.74	0.25	43.59	0.00	99.07	95.19	3.84	0.97	0.00
24	0.03	51.89	0.04	-	1.12	0.17	45.27	0.48	99.02	96.05	2.41	0.63	0.91
25	-	51.67	0.04	0.04	0.58	0.17	45.62	1.64	99.76	95.09	1.22	0.61	3.07
26	0.03	51.74	0.04	0.04	0.42	0.72	44.85	0.84	98.68	94.78	0.90	2.73	1.59
27	0.04	52.44	-	0.04	2.23	0.03	43.90	0.00	98.69	95.00	4.90	0.10	0.00
28	0.03	53.52	-	0.05	1.56	0.23	43.38	0.00	98.79	95.59	3.49	0.92	0.00
29	-	53.17	0.05	-	0.50	0.43	44.59	0.00	98.79	97.22	1.10	1.68	0.00
30	0.05	52.63	0.05	0.04	0.49	1.02	44.38	0.00	98.66	95.06	1.05	3.88	0.00
31	0.03	52.38	0.03	-	0.50	0.30	45.37	0.00	98.61	97.75	1.08	1.16	0.00

- = below detection limit

APPENDIX B.2

EASTERN CAPE SAMPLES - ILMENITE MICROPROBE ANALYSES

							Recalculated			Recalculated mole fractions			
Sample	SiO2	TiO2	Al2O3	Cr2O3	MnO	MgO	FeO	Fe2O3	TOTAL	FeTiO3	MnTiO3	MgTiO3	Fe2O3
32	-	50.14	0.04	0.05	0.41	0.90	43.08	4.29	98.94	87.98	0.86	3.27	7.89
33	-	48.19	0.05	0.13	0.38	1.88	39.61	8.63	98.88	77.50	0.74	6.56	15.20
34	-	53.47	0.02	-	0.87	0.13	45.18	0.00	99.70	97.58	1.91	0.51	0.00
35	0.03	52.71	0.05	-	0.42	1.00	45.21	0.47	99.89	94.48	0.90	3.72	0.89
39	-	52.15	0.02	-	0.36	0.45	45.74	0.33	99.02	96.92	0.76	1.69	0.63
41	-	51.30	0.05	-	0.50	1.05	43.75	3.20	99.82	89.28	1.02	3.83	5.87
42	-	51.95	-	-	0.72	0.54	45.03	1.80	100.05	93.16	1.50	1.99	3.35
43	-	50.82	0.02	-	0.34	0.70	44.12	3.46	99.45	90.38	0.70	2.54	6.38
44	-	51.89	0.03	-	0.56	0.54	45.14	2.24	100.38	92.72	1.16	1.97	4.15
45	0.03	53.28	-	-	1.45	0.27	43.89	0.00	98.93	95.74	3.19	1.07	0.00
46	0.04	51.45	-	-	0.43	0.86	44.29	3.13	100.16	90.23	0.89	3.14	5.74
47	-	52.72	0.02	-	1.91	0.05	45.07	0.00	99.78	95.70	4.11	0.20	0.00
48	-	52.25	0.04	-	0.48	0.32	45.94	0.67	99.66	96.52	1.02	1.18	1.28
49	-	51.83	0.02	-	0.51	0.23	45.69	0.99	99.25	96.19	1.09	0.84	1.87
50	-	52.30	0.04	-	1.05	0.42	45.22	0.63	99.61	95.03	2.23	1.56	1.18
51	-	52.63	0.03	0.05	0.77	0.90	44.45	0.00	98.81	94.90	1.67	3.43	0.00
52	0.04	50.89	-	-	0.41	2.19	41.44	4.19	99.16	83.66	0.83	7.89	7.61
53	-	50.43	-	0.07	1.91	0.13	43.19	2.88	98.61	90.09	4.04	0.47	5.41
54	-	51.29	0.02	-	0.74	0.37	44.72	1.34	98.48	94.49	1.58	1.38	2.55
55	-	50.47	-	0.06	0.38	0.94	43.33	3.91	99.10	88.60	0.79	3.42	7.20
56	-	52.12	0.04	0.13	0.50	0.22	45.97	0.67	99.61	96.82	1.07	0.83	1.27
57	-	52.25	0.03	-	0.43	0.29	45.79	0.00	98.78	97.96	0.94	1.10	0.00
58	-	50.46	0.02	0.06	0.95	0.14	44.17	2.70	98.48	92.39	2.02	0.51	5.08
59	-	52.09	-	-	0.48	0.45	45.55	0.91	99.49	95.57	1.03	1.68	1.71
60	-	51.31	0.03	0.97	3.39	0.35	42.08	1.58	99.69	88.49	7.22	1.30	2.99
61	0.03	53.13	0.03	-	0.43	0.24	45.38	0.00	99.25	98.14	0.95	0.91	0.00
62	0.08	51.23	0.25	-	0.96	0.69	43.96	2.89	100.09	90.15	1.99	2.52	5.33
63	0.03	53.06	0.03	-	0.69	0.04	46.48	0.00	100.33	98.38	1.47	0.15	0.00
64	-	51.20	-	-	0.51	0.29	45.03	1.96	99.00	94.16	1.08	1.07	3.70
Average	0.04	51.85	0.04	0.13	0.90	0.50	44.52	1.44	99.31	93.56	1.92	1.86	2.66
HEC1													
2	-	49.29	0.03	0.11	0.56	0.29	43.24	4.51	98.03	89.38	1.17	1.06	8.39
4	-	50.73	0.05	0.04	0.46	0.35	44.53	3.45	99.61	91.38	0.96	1.29	6.37
8	-	51.82	0.04	-	1.07	0.43	44.75	1.46	99.57	93.39	2.26	1.61	2.75
10	-	52.74	0.05	-	0.52	0.24	45.94	0.00	99.50	97.97	1.12	0.91	0.00
11	-	51.46	0.02	-	0.40	0.44	45.10	2.08	99.50	93.66	0.83	1.61	3.89
13	-	53.45	0.05	-	0.35	0.67	45.18	0.00	99.70	96.68	0.76	2.57	0.00
14	-	51.51	0.03	-	0.46	0.31	45.32	1.77	99.40	94.56	0.98	1.14	3.32
15	-	51.20	0.03	-	0.48	0.27	45.07	2.80	99.86	92.81	1.00	1.01	5.18
25	-	52.01	0.03	0.08	0.98	0.20	45.45	1.07	99.84	95.16	2.08	0.75	2.01
26	0.03	52.48	0.02	0.08	0.79	0.12	45.53	0.00	99.05	97.81	1.71	0.47	0.00
27	0.03	52.64	0.08	0.06	0.55	0.70	44.46	0.00	98.53	96.08	1.21	2.71	0.00
29	0.03	51.13	0.03	0.08	1.38	0.06	44.50	0.84	98.05	95.15	2.99	0.24	1.62
30	0.04	51.66	0.07	0.06	0.48	0.68	44.80	0.08	97.87	96.18	1.04	2.61	0.16
36	0.07	51.30	0.05	0.08	0.39	0.71	44.55	0.97	98.13	94.61	0.83	2.70	1.86
37	0.06	52.87	-	0.09	2.16	0.13	44.92	0.00	100.22	94.90	4.63	0.47	0.00

- = below detection limit

APPENDIX B.2

EASTERN CAPE SAMPLES - ILMENITE MICROPROBE ANALYSES

							Recalculated			Recalculated mole fractions			
Sample	SiO2	TiO2	Al2O3	Cr2O3	MnO	MgO	FeO	Fe2O3	TOTAL	FeTiO3	MnTiO3	MgTiO3	Fe2O3
39	0.07	51.54	0.03	0.06	0.45	0.48	45.11	0.35	98.08	96.52	0.98	1.84	0.66
42	0.08	53.27	0.03	-	0.76	0.47	44.56	0.00	99.19	96.50	1.68	1.82	0.00
43	0.03	50.43	0.03	0.07	0.69	0.34	44.08	3.91	99.56	90.14	1.42	1.24	7.19
44	0.04	51.47	0.06	-	0.53	0.73	44.49	2.94	100.24	90.86	1.10	2.65	5.39
48	-	50.69	0.08	0.09	0.44	1.41	42.64	3.97	99.32	86.73	0.90	5.10	7.27
49	0.06	50.46	0.10	0.03	0.42	0.67	43.82	1.44	96.99	93.75	0.92	2.57	2.77
52	0.04	51.45	0.04	-	0.54	0.30	45.22	1.50	99.09	94.87	1.15	1.14	2.84
54	-	52.87	0.03	-	0.52	0.09	45.46	0.00	99.00	98.50	1.14	0.36	0.00
55	-	52.75	0.06	-	0.49	0.77	45.02	0.00	99.11	96.00	1.06	2.94	0.00
56	-	52.54	0.05	-	0.39	0.66	44.73	0.00	98.39	96.62	0.84	2.54	0.00
62	0.03	48.63	-	-	1.07	0.23	42.26	7.51	99.75	83.65	2.15	0.82	13.38
68	-	51.11	-	-	0.76	0.20	44.85	3.12	100.06	91.95	1.58	0.72	5.75
69	0.03	51.42	-	-	0.62	0.24	45.23	1.84	99.39	94.36	1.30	0.88	3.46

- = below detection limit

APPENDIX B.3: MAGNETITE ANALYSES FROM COASTAL SEDIMENTS

Sample	SiO2	TiO2	Al2O3	Cr2O3	FeO	MnO	MgO	Recalculated FeO	Recalculated Fe2O3	Total
HZ2-1	0.03	-	0.13	0.08	92.07	-	-	30.83	68.06	99.18
2	0.37	0.07	0.53	0.12	91.52	0.08	0.08	31.32	66.90	99.45
3	-	0.72	4.61	12.69	74.59	0.35	1.90	29.40	50.22	99.88
4	-	0.05	0.03	-	92.98	-	-	31.06	68.81	100.00
5	-	0.04	0.06	-	93.08	0.21	0.01	30.96	69.04	100.32
6	-	0.07	0.36	0.15	92.06	-	0.07	30.92	67.94	99.54
7	-	-	0.05	0.04	92.60	0.12	-	30.88	68.60	99.73
8	-	-	0.07	0.06	92.43	-	-	30.86	68.42	99.49
9	0.03	0.34	0.46	0.13	91.44	-	0.02	31.12	67.03	99.19
10	-	0.06	2.23	0.13	89.11	-	-	30.81	64.78	98.08
11	-	0.04	0.09	-	92.31	0.11	-	30.79	68.37	99.41
12	-	-	0.23	0.60	90.59	-	0.14	30.35	66.95	98.32
13	-	-	0.08	0.05	93.04	-	-	31.07	68.87	100.09
14	-	-	0.09	0.04	92.70	-	-	30.95	68.61	99.70
15	-	-	0.07	0.05	92.10	-	-	30.75	68.17	99.11
16	-	0.11	0.34	0.18	91.52	-	0.06	30.78	67.50	98.96
17	-	-	0.16	-	92.26	-	-	30.87	68.22	99.30
18	0.13	11.56	1.19	0.09	80.06	0.19	-	41.20	43.19	97.56
19	0.14	11.52	1.17	0.10	80.21	0.25	0.04	41.13	43.43	97.77
20	-	0.06	0.44	0.10	91.69	-	0.07	30.79	67.69	99.15
21	-	0.05	0.33	0.08	91.49	-	0.08	30.62	67.64	98.84
22	-	0.09	0.42	0.10	91.51	-	0.03	30.79	67.49	98.94
23	-	0.06	0.12	0.04	92.63	0.10	-	30.94	68.56	99.81
24	-	0.05	0.37	0.15	91.34	-	0.03	30.66	67.43	98.73
25	0.03	0.05	0.11	0.09	89.95	-	0.03	30.11	66.51	96.95
26	0.86	13.42	1.98	0.05	77.01	0.61	0.35	43.25	37.52	98.04
27	-	-	0.12	-	92.49	0.08	0.02	30.84	68.50	99.60
28	-	0.07	0.20	-	92.13	0.24	-	30.73	68.24	99.48
29	-	0.05	0.29	0.11	92.22	-	0.04	30.91	68.14	99.55
30	-	-	0.06	-	93.58	0.16	-	31.15	69.38	100.82

- = Below detection limit

APPENDIX B.3: MAGNETITE ANALYSES FROM COASTAL SEDIMENTS

Sample	SiO2	TiO2	Al2O3	Cr2O3	FeO	MnO	MgO	Recalculated FeO	Recalculated Fe2O3	Total
HZ1-1	0.08	-	0.03	0.05	92.56	-	-	31.04	68.36	99.63
2	-	-	0.10	0.04	91.47	-	-	30.53	67.72	98.47
3	0.09	10.64	2.26	0.16	80.47	0.19	0.10	40.59	44.32	98.35
4	-	-	0.04	-	92.71	0.07	-	30.93	68.65	99.75
5	0.04	0.04	0.05	-	92.38	0.15	0.02	30.80	68.43	99.54
6	-	-	0.03	0.11	92.45	-	0.08	30.80	68.51	99.58
7	-	-	0.06	0.05	92.24	0.07	-	30.79	68.28	99.29
8	-	-	2.42	22.14	62.77	0.55	4.57	23.24	43.93	96.87
9	0.37	0.04	0.63	0.19	91.17	-	0.10	31.27	66.57	99.15
10	0.05	0.05	0.09	0.19	91.49	-	-	30.70	67.56	98.68
11	0.05	0.13	0.15	0.07	92.41	0.40	-	30.87	68.39	100.05
12	0.07	0.04	0.07	0.09	91.47	0.22	-	30.57	67.68	98.73
13	0.06	-	0.04	0.08	92.04	0.07	-	30.79	68.06	99.13
14	0.05	0.04	0.10	0.16	92.38	0.34	-	30.78	68.46	99.93
15	0.07	0.07	0.12	0.11	92.44	0.39	-	30.83	68.47	100.06
16	0.04	-	0.08	0.06	91.82	0.16	0.02	30.62	68.01	98.99
17	0.05	0.06	0.28	0.10	91.76	_	-	30.87	67.67	99.07
18	0.04	-	0.12	0.15	92.21	0.07	-	30.90	68.13	99.45
HZ7-1	-	0.10	0.34	18.63	69.46	0.58	1.88	26.67	47.55	95.76
2	0.14	17.59	0.91	0.04	76.91	0.79	0.05	46.80	33.46	99.78
3	0.03	21.31	1.48	0.11	72.56	0.46	0.26	49.89	25.20	98.72
4	0.04	18.86	2.26	0.13	75.08	0.55	0.27	48.12	29.96	100.19
5	-	0.07	0.05	0.07	91.26	-	-	30.52	67.50	98.25
6	3.92	29.60	2.14	-	62.80	1.68	0.08	62.46	0.38	100.27
7	0.30	24.86	1.12	0.08	69.41	1.04	0.32	52.88	18.36	98.97
8	0.18	13.02	1.87	0.14	79.46	0.50	0.06	42.89	40.63	99.30
9	0.18	14.44	1.32	0.11	78.67	0.48	0.09	44.05	38.47	99.14
10	-	0.06	1.77	20.20	66.64	0.42	3.43	25.12	46.14	97.15
11	1.06	29.40	0.65	0.04	57.85	2.65	0.08	54.65	3.56	92.08
12	0.07	26.69	1.17	0.10	64.70	0.12	0.12	54.03	11.86	94.16
13	-	0.12	0.43	0.16	91.22	-	0.11	30.67	67.28	98.79
14	11.08	20.92	1.50	-	64.69	0.41	0.35	64.32	0.41	98.99
15	-	0.04	0.05	0.13	91.84	-	0.03	30.67	67.98	98.92
16	-	0.05	0.07	0.05	91.83	-	-	30.69	67.94	98.85
17	1.37	27.95	1.46	0.08	64.57	1.76	0.20	56.49	8.98	98.30
18	-	0.08	0.23	0.58	92.52	-	-	31.23	68.11	100.28
19	-	0.09	0.16	0.04	91.63	-	0.02	30.71	67.70	98.77

- = Below detection limit

APPENDIX B.3: MAGNETITE ANALYSES FROM COASTAL SEDIMENTS

Sample	SiO2	TiO2	Al2O3	Cr2O3	FeO	MnO	MgO	Recalculated FeO	Recalculated Fe2O3	Total
HZ7-1	0.09	26.46	0.83	0.08	68.72	0.44	0.26	54.59	15.71	98.44
2	-	-	0.04	0.04	92.08	-	0.00	30.77	68.13	99.09
3	0.30	25.32	1.22	0.08	67.00	2.38	0.17	51.96	16.72	98.14
4	0.06	18.76	1.42	1.81	72.15	0.19	1.04	46.50	28.51	98.28
5	0.04	0.07	0.07	0.08	92.53	0.08	0.03	30.96	68.42	99.75
6	-	0.04	0.14	0.08	92.30	-	0.01	30.87	68.26	99.49
7	-	-	0.48	0.18	91.37	-	-	30.82	67.30	98.83
8	0.20	14.88	0.72	0.09	79.70	0.35	0.09	44.76	38.83	99.92
9	0.15	11.21	0.95	0.13	81.86	0.57	0.22	40.82	45.60	99.66
10	-	0.09	0.13	0.09	91.65	0.08	-	30.70	67.74	98.83
11	-	22.06	1.58	0.10	72.99	0.30	0.26	51.07	24.36	99.76
12	-	0.07	0.16	0.14	91.89	-	-	30.80	67.88	99.10
13	-	-	0.10	0.16	91.72	-	-	30.68	67.84	98.84
14	0.05	28.40	0.99	0.04	67.37	0.36	0.20	56.59	11.98	98.60
15	-	9.13	2.27	0.18	81.30	0.24	0.22	38.76	47.27	98.09
16	-	0.16	0.18	0.06	92.16	-	-	30.98	67.98	99.43
17	0.39	24.29	1.02	0.09	69.60	1.91	0.02	52.14	19.40	99.26
18	-	0.04	0.14	0.08	91.62	-	-	30.67	67.73	98.68
19	-	25.66	0.06	-	72.22	-	-	54.86	19.29	99.89
20	0.22	28.45	1.33	0.05	64.87	2.51	0.02	55.01	10.96	98.55
21	-	0.07	0.13	0.28	92.10	-	-	30.91	68.00	99.44
22	0.21	23.36	1.41	0.06	71.18	0.63	0.40	51.85	21.48	99.39
23	0.23	26.62	1.06	-	69.37	0.50	0.08	55.48	15.44	99.44
24	0.04	25.10	1.38	0.13	69.97	0.29	0.33	53.58	18.21	99.08
25	0.20	34.93	0.80	0.04	62.81	0.46	0.44	62.69	0.13	99.69
26	-	0.12	0.19	0.05	91.17	0.16	-	30.53	67.39	98.44
27	0.05	13.33	1.19	0.09	79.24	0.32	0.26	42.53	40.79	98.57
28	0.67	20.56	1.05	0.09	71.68	1.45	0.08	49.05	25.15	98.10
29	0.18	27.53	1.32	0.08	68.44	0.64	0.72	55.48	14.40	100.35
HZ30-1	-	25.87	0.14	0.04	69.07	0.64	0.16	53.51	17.29	97.65
2	-	15.43	0.13	-	78.38	0.43	0.48	43.85	38.37	98.73
3	-	5.25	4.99	21.03	60.20	0.35	5.09	29.05	34.61	100.37

- = Below detection limit

APPENDIX B.3: MAGNETITE ANALYSES FROM COASTAL SEDIMENTS

Sample	SiO2	TiO2	Al2O3	Cr2O3	FeO	MnO	MgO	Recalculated FeO	Recalculated Fe2O3	Total
HN3-1	0.50	12.40	1.93	0.27	79.80	0.74	0.18	42.54	41.40	99.97
2	0.07	17.74	1.37	0.17	76.59	0.75	0.11	46.97	32.92	100.08
3	18.10	30.22	1.92	0.15	22.64	0.12	0.11			
4	0.04	11.75	2.60	0.26	80.59	0.20	0.04	42.15	42.72	99.76
5	1.28	12.01	1.89	0.17	79.52	0.54	0.65	42.76	40.86	100.15
6	4.44	25.69	1.10	0.11	67.87	0.69	0.12	60.44	8.26	100.84
7	-	0.08	0.06	0.10	91.99	0.12	-	30.78	68.03	99.18
8	1.23	20.71	1.77	0.17	71.02	1.23	0.37	50.08	23.27	98.82
9	1.29	22.08	1.54	0.09	72.11	0.75	0.22	52.56	21.73	100.25
10	-	-	0.06	-	90.56	0.07	-	30.16	67.12	97.41
11	0.37	23.89	1.01	-	70.93	1.04	0.66	51.87	21.18	100.02
12	0.43	0.37	0.16	-	91.74	-	-	31.75	66.67	99.43
13	-	11.45	1.06	0.10	79.06	0.47	0.16	40.10	43.29	96.64
14	-	15.82	0.91	0.21	78.71	0.18	0.87	44.54	37.97	100.50
15	-	14.60	1.91	0.08	78.74	0.26	0.14	44.34	38.22	99.56
16	-	0.83	1.47	-	91.03	-	0.03	31.97	65.64	99.98
17	-	18.78	1.44	0.05	74.54	0.28	0.73	47.00	30.60	98.87
HN6-1	-	0.05	0.40	-	92.37	0.15	-	30.93	68.27	99.84
2	-	-	0.06	0.23	92.14	0.07	-	30.77	68.20	99.34
3	-	0.04	0.22	0.12	91.96	-	-	30.83	67.94	99.16
4	0.59	21.10	1.39	0.07	72.54	0.57	0.44	47.35	27.99	99.50
5	-	0.05	0.05	-	91.95	0.12	-	30.65	68.12	99.01
6	-	-	0.08	0.06	92.93	0.11	-	30.99	68.83	100.10
7	-	0.05	0.11	0.06	91.77	0.12	-	30.64	67.93	98.90
8	-	0.35	0.33	0.07	91.29	0.09	0.02	30.90	67.12	98.86
9	-	-	0.17	0.06	92.08	0.08	-	30.72	68.19	99.24
10	-	0.21	0.29	-	91.87	0.09	-	30.90	67.76	99.27
11	0.05	-	0.06	0.11	91.36	0.08	0.03	30.25	67.90	98.49
12	-	-	0.13	0.12	91.79	-	-	30.69	67.90	98.92
13	0.07	13.34	1.08	0.05	79.84	0.23	0.30	42.42	41.59	99.06
14	0.03	0.07	0.07	0.05	92.09	-	-	30.69	68.23	99.19
15	0.22	22.28	1.31	0.11	70.90	0.78	0.08	49.70	23.56	98.04
16	0.07	0.17	0.41	0.11	92.32	-	-	30.99	68.15	99.89
17	-	0.04	0.05	0.04	92.48	0.17	-	30.80	68.55	99.65
18	0.80	26.05	1.05	0.10	67.95	1.36	0.40	50.46	19.43	99.66
19	-	0.05	0.19	0.07	91.85	-	-	30.76	67.89	98.96
20	-	-	0.06	0.15	92.05	0.07	-	30.74	68.13	99.15

- = Below detection limit

APPENDIX B.3: MAGNETITE ANALYSES FROM COASTAL SEDIMENTS

Sample	SiO2	TiO2	Al2O3	Cr2O3	FeO	MnO	MgO	Recalculated FeO	Recalculated Fe2O3	Total
HN28-1	-	17.92	0.06	0.04	76.60	0.24	0.10	46.77	33.14	98.28
2	-	5.36	1.13	0.12	83.67	0.21	2.28	32.00	57.42	98.54
3	-	0.45	0.18	-	91.73	0.07	0.03	31.13	67.34	99.22
4	0.03	0.50	0.13	-	91.47	0.26	-	30.86	67.35	99.17
HT3-1	0.06	2.04	0.93	0.10	86.76	0.08	-	31.59	61.30	96.12
2	0.49	19.89	1.08	0.07	73.67	0.79	0.19	46.63	30.05	99.19
3	0.14	12.20	1.48	0.06	78.11	0.42	1.55	38.81	43.67	98.33
4	0.82	2.88	0.19	-	87.81	0.20	0.04	30.03	64.21	98.39
5	0.11	4.72	1.50	0.12	83.74	0.18	0.47	30.94	68.26	99.84
6	0.08	19.99	2.01	0.10	71.19	0.80	0.92	47.17	26.70	97.76
7	-	34.28	0.60	-	64.34	0.21	0.61	62.00	2.60	100.33
8	0.08	33.40	0.63	0.06	64.42	1.14	0.04	61.14	3.64	100.13
9	0.21	6.71	0.72	0.13	85.57	0.19	0.04	37.11	53.85	98.95
10	0.10	19.35	1.68	0.14	75.26	0.34	0.06	48.97	29.21	99.85
11	3.82	10.02	3.63	0.11	76.32	0.26	0.14	44.95	34.86	97.79
12	0.31	19.18	1.46	0.15	72.51	0.71	0.03	47.89	27.36	97.08
13	0.20	12.05	3.86	0.17	76.56	0.29	0.06	41.89	38.52	97.05
14	3.03	24.02	2.36	0.10	67.54	0.41	0.40	56.55	12.22	99.09
15	0.13	23.69	0.83	0.09	70.15	0.47	0.15	51.91	20.27	97.55
16	0.13	5.54	1.56	0.13	87.30	0.16	-	36.62	56.32	100.46
17	0.63	2.06	0.62	0.14	89.14	0.08	0.09	33.36	61.98	98.96
18	0.16	20.28	2.08	0.10	74.60	0.36	-	50.19	27.12	100.29
19	0.05	3.87	2.00	0.17	82.58	0.20	1.18	1.23	90.40	99.09
20	0.11	16.12	1.80	0.23	76.64	0.80	0.02	45.41	34.70	99.19
HT7-1	-	11.30	1.85	-	79.90	0.52	0.74	39.82	44.54	98.77
2	-	10.03	0.22	0.34	83.84	0.17	0.02	40.08	48.63	99.51
3	0.11	31.44	0.77	0.11	66.13	0.88	0.04	59.68	7.17	100.20
4	0.09	3.07	4.46	0.12	83.84	0.30	2.06	31.25	58.44	99.80

- = Below detection limit

APPENDIX B.3: MAGNETITE ANALYSES FROM COASTAL SEDIMENTS

Sample	SiO2	TiO2	Al2O3	Cr2O3	FeO	MnO	MgO	Recalculated FeO	Recalculated Fe2O3	Total
HEC5-1	0.07	4.36	1.71	0.07	85.33	0.42	1.76	32.23	59.01	99.63
2	0.18	0.51	0.33	0.33	87.48	0.19	-	0.46	96.70	98.71
3	1.25	1.51	0.60	0.10	88.34	0.26	0.04	33.34	61.12	98.23
4	0.19	0.24	0.11	0.26	88.23	0.12	-	0.33	97.68	98.94
5	0.45	0.52	0.30	0.08	87.51	0.07	0.07	0.81	96.34	98.64
6	0.24	5.05	1.05	0.06	85.59	0.19	0.02	35.32	55.86	97.79
7	4.50	3.74	1.88	-	82.58	0.16	0.37	39.54	47.83	98.04
8	8.44	11.56	2.93	0.11	70.15	0.46	2.17	49.22	23.26	98.14
9	0.14	3.92	1.94	0.07	85.36	0.50	0.74	33.10	58.07	98.48
10	0.31	0.51	0.17	0.15	90.57	0.10	0.02	31.33	65.83	98.42
11	1.82	1.71	0.90	0.03	86.52	0.11	0.04	3.53	92.22	100.37
12	0.06	12.21	2.92	0.14	79.31	0.24	0.33	42.04	41.42	99.35
13	0.03	25.79	-	-	70.76	0.71	-	54.07	18.55	99.18
14	0.37	1.12	0.23	0.11	87.96	0.13	0.02	1.29	96.31	99.58
15	0.32	3.33	0.14	0.11	87.31	0.20	0.02	3.13	93.54	100.80
16	0.09	12.68	2.42	0.06	78.63	0.37	1.10	41.16	41.64	99.53
17	0.37	0.89	0.23	0.07	87.12	0.15	-	1.07	95.63	98.41
HEC6-1	0.16	5.02	1.48	0.05	85.07	0.28	0.83	34.17	56.56	98.56
2	0.03	27.90	0.15	0.06	70.25	0.32	-	56.78	14.97	100.21
3	0.14	7.52	2.03	0.10	81.74	0.58	0.64	36.32	50.48	97.81
4	0.29	5.28	1.33	0.10	84.65	0.57	0.58	34.58	55.64	98.36
5	0.51	18.79	1.57	-	74.51	0.55	0.24	48.26	29.17	99.13
6	0.32	20.64	0.16	-	74.64	0.27	0.15	49.86	27.54	98.96
HEC3-1	0.55	11.44	0.80	0.04	82.15	0.17	0.26	41.94	44.69	99.88
2	0.30	29.92	1.33	0.04	64.49	0.72	0.10	57.89	7.34	97.64
3	1.01	12.22	1.42	0.05	78.91	0.67	0.25	42.48	40.48	98.56
4	0.10	14.87	1.37	0.04	77.61	0.83	0.09	43.85	37.52	98.66
5	17.65	22.61	3.35	-	41.93	0.69	0.69			
6	0.12	17.00	1.44	0.04	77.34	0.72	0.05	46.50	34.27	100.13
7	6.93	1.86	3.79	-	82.56	0.18	0.12	42.32	44.71	99.94
8	3.13	24.33	1.19	-	67.13	0.72	0.46	56.08	12.28	98.22
9	-	8.25	0.51	0.12	83.67	0.44	0.07	37.71	51.08	98.19
10	-	3.91	1.05	0.16	85.96	0.23	0.21	33.49	58.31	97.36
11	-	5.42	0.35	-	85.64	0.69	2.58	31.68	59.96	100.73
HEC1-1	0.27	29.34	0.76	-	65.23	0.77	0.14	57.02	9.12	97.44

- = Below detection limit

APPENDIX C

Analyses of ilmenite and magnetite from source rocks

APPENDIX C.1

ILMENITE ANALYSIS FROM SOURCE ROCKS

ANALYSIS NO	REFERENCE	ROCK TYPE	LOCALITY	TiO2	Cr2O3	FeO	Fe2O3	MgO	MnO	SiO2	Al2
9	Groves, et al. (1986)	Granophyre	Insizwa	52.30	0.05	39.60	0.00	0.03	7.10		
7	"	"	"	50.80	0.05	41.27	3.70	0.03	4.30		
8	"	"	"	50.80	0.05	41.68	2.69	0.03	3.90		
10	"	"	"	52.30	0.50	40.14	0.85	0.40	6.10		
4	Cawthorn, et al. (1985)	Granophyre	"	50.60	0.10	39.70	3.44	0.30	5.20		
3	"	"	"	49.50	0.05	40.43	5.96	0.30	3.50		
BHPG	Reynolds, 1978	Granophyre	South Africa	49.87	0.17	39.70	5.57	0.59	4.04		0.
IR236	"	"	"	49.42	0.17	38.80	5.43	0.63	4.46		0.
D3+	Reynolds, 1978	Dolerite	eastern Cape	51.79		45.59	0.00	0.70	0.40	0.72	
D7+	"	"	"	50.49		44.25	2.05	0.05	1.38	0.21	
D12 (ilm. conc.)	"	"	"	49.65	0.04	43.90	5.38	0.08	0.60		
D6A+	"	"	"	51.26		45.30	0.00	0.16	0.41	1.08	
D8+	"	"	"	50.91		45.87	0.00	0.20	0.89	1.90	
D13 (ilm. conc.)	"	"	"	49.37		43.51	5.43	0.22	0.49		
D4+	"	"	"	50.90		45.93	0.00	0.22	0.44	1.26	
D5 (ilm conc.)	"	"	"	49.85		44.16	4.26	0.22	0.27	nr	
D6 (ilm conc.)	"	"	"	50.60		44.24	2.91	0.26	0.79	nr	
D9 (ilm conc.)	"	"	"	48.77		43.13	7.01	0.29	0.21		
D10 (ilm conc.)	"	"	"	49.46		43.47	5.64	0.32	0.43		
D11 (ilm conc.)	"	"	"	49.92	0.04	44.05	4.58	0.35	0.21		
724	Reynolds, 1983	Dolerite	eastern Cape	49.92		42.82	5.20	0.88	0.50		0
658	"	"	"	48.88		42.15	6.45	0.15	1.52		0
658	"	"	"	49.32		42.91	5.46	0.20	1.07		0
670	"	"	"	49.47		43.16	6.00	0.29	0.80		0
700	"	"	"	49.02		41.84	6.08	0.30	1.68		0
722	"	"	"	50.10	0.03	43.75	4.70	0.32	0.72		0
662	"	"	"	49.27		43.30	5.68	0.33	0.41		0
691	"	"	"	48.91		42.24	6.39	0.44	0.95		0
DM/13-6	Meth, 1991	Dolerite	Rooi Rand	49.71	0.56	43.52	4.03	0.14	0.92		
DM/13-4	"	"	"	51.66	0.12	45.29	0.24	0.17	0.85		
DM/13-2	"	"	"	48.41	0.56	42.46	4.48	0.17	0.76		
DM/13-5	"	"	"	50.22	0.28	44.17	2.43	0.19	0.64		
DM/13-1	"	"	"	51.01		44.64	0.07	0.22	0.83		
DM/13-3	"	"	"	47.83	0.63	41.53	7.73	0.23	1.06		
D6-1	This work	Dolerite	Underberg	51.08	0.05	44.62	1.50	0.12	1.69	0.17	0
D6-2	"	"	"	50.59		44.38	2.30	0.18	1.64	0.18	0
D6-3	"	"	"	48.48	0.03	44.07	1.81	0.49	1.62	0.71	2
D6-4	"	"	"	52.42		45.55	0.00	0.05	1.66	0.09	0
D6-5	"	"	"	52.15		45.26	1.66	0.04	1.60	0.04	0
DM/4-2	Meth, 1991	Dolerite	Rooi Rand	48.81		41.43	5.05	0.05	2.43		
DM/4-1	"	"	"	48.30		40.99	5.61	0.05	2.41		
DM/4-3	"	"	"	48.54		41.74	5.13	0.05	1.89		
DM/11-4	"	"	"	50.91		43.97	1.38	0.05	1.79		
DM/11-1	"	"	"	51.45		44.52	0.75	0.05	1.72		
DM/11-3	"	"	"	50.71		43.86	0.71	0.05	1.72		

Blank spaces = not reported or below detection limit

APPENDIX C.1

ILMENITE ANALYSIS FROM SOURCE ROCKS

ANALYSIS NO	REFERENCE	ROCK TYPE	LOCALITY	TiO2	Cr2O3	FeO	Fe2O3	MgO	MnO	SiO2	Al2
DM/11-2	"	"	"	52.81		45.01	0.00	0.05	1.70		
DM/5-1	"	"	"	50.65		43.89	2.76	0.05	1.64		
DM/5-5	"	"	"	51.12		44.31	1.95	0.05	1.64		
DM/5-2	"	"	"	50.98		44.24	2.89	0.05	1.58		
DM/5-3	"	"	"	50.67		44.24	2.34	0.05	1.31		
DM/5-4	"	"	"	50.74		44.30	2.80	0.05	1.31		
DM/11-5	"	"	"	51.56		44.32	0.01	0.06	1.91		
DM5 1	This work	Dolerite	"	50.45	0.06	44.29	3.63	0.35	0.48	0.02	0.
DM5 2	"	"	"	49.68		43.49	5.10	0.20	0.82	0.00	0.
DM5 3	"	"	"	49.82		43.61	5.01	0.41	0.45	0.00	0
DM5 4	"	"	"	47.66		40.37	7.96	0.69	1.56	0.28	0
DM5 5	"	"	"	49.56		42.62	4.53	0.02	1.92	0.02	0
DM5 6	"	"	"	48.82		42.87	5.91	0.31	0.49	0.01	0
DM5 7	"	"	"	50.72	0.05	44.57	2.63	0.30	0.52	0.02	0
DM25 1	"	"	"	52.54	0.03	46.57	0.10	0.06	0.63	0.06	0
DM25 2	"	"	"	51.98	0.03	45.89	1.67	0.26	0.43	0.03	0
DM25 3	"	"	"	50.25	0.03	44.54	3.81	0.04	0.61	0.04	0
DM25 4	"	"	"	51.98	0.03	46.10	1.16	0.08	0.52	0.02	0
DM25 5	"	"	"	51.05	0.07	45.11	3.03	0.12	0.67	0.08	0
DM25 6	"	"	"	51.55		45.35	1.71	0.01	1.02	0.04	0
DM25 7	"	"	"	51.17		45.29	2.56	0.05	0.72	0.08	0
DM8 1	"	"	"	51.26	0.03	45.15	1.13	0.04	0.90	0.04	0
DM8 2	"	"	"	51.83		45.94	0.34	0.07	0.86	0.27	0
DM8 6	"	"	"	51.85		45.69	0.71	0.16	0.68	0.02	0
DM8 7	"	"	"	51.41		45.29	1.17	0.13	0.71	0.02	0
DM8 9	"	"	"	51.04	0.03	44.94	1.36	0.03	0.91	0.02	0
DM8 17	"	"	"	52.16		46.01	0.79	0.09	0.76	0.03	0
DM8 20	"	"	"	50.88		44.76	2.72	0.13	0.80	0.04	0
DM6 3	"	"	"	52.01	0.07	45.11	1.51	0.27	1.21	0.03	0
DM6 4	"	"	"	50.46	0.09	43.70	2.64	0.00	1.72	0.05	0
DM6 15	"	"	"	52.10		45.84	1.17	0.06	0.94	0.03	0
DM6 16	"	"	"	52.34		45.88	0.55	0.10	1.00	0.01	0
DM6 20	"	"	"	48.33	0.03	42.36	7.55	0.01	1.25	0.16	0
DM6 22	"	"	"	52.68		46.22	0.12	0.11	0.95	0.01	0
HS1 3	This work	Basalt	Sani Pass	49.31	0.48	43.23	4.78	0.13	0.90	0.02	0
HS1 4	"	"	"	49.57	0.39	43.60	5.37	0.13	0.76	0.02	0
HS1 6	"	"	"	50.60	0.15	44.51	3.23	0.07	0.89	0.03	0
HS1 7	"	"	"	52.32		45.58	0.19	0.04	1.44	0.05	0
HS1 8	"	"	"	51.98	0.17	45.64	1.30	0.11	0.93	0.02	0
HS1 9	"	"	"	50.93	0.23	44.71	3.47	0.10	0.92	0.01	0
HS1 10	"	"	"	49.78	0.17	43.65	4.98	0.13	0.88	0.01	0.
HS4 1	"	"	"	51.82		44.94	0.93	0.63	0.54	0.00	0
HS4 5	"	"	"	48.29	0.06	42.39	7.43	0.07	0.92	0.01	0
HS4 6	"	"	"	51.38	0.08	45.29	0.40	0.22	0.77	0.22	0
HS4 9	"	"	"	51.93		45.63	0.81	0.30	0.53	0.00	0

Blank spaces = not reported or below detection limit

APPENDIX C.1

ILMENITE ANALYSIS FROM SOURCE ROCKS

ANALYSIS NO	REFERENCE	ROCK TYPE	LOCALITY	TiO2	Cr2O3	FeO	Fe2O3	MgO	MnO	SiO2	Al2
HS4 13	"	"	"	51.86		46.06	0.58	0.05	0.48	0.00	0
HS4 14	"	"	"	50.92		45.01	2.92	0.19	0.44	0.00	0
7	Cawthorn et al. (1989)	MgO-poor basalt	Lebombo	50.39		41.80	5.43	1.79	0.32		
29	Bristow (1980)	Low-MgO Basalt	Lebombo	50.39		42.07	5.11	1.79	0.32	0.23	
21/1	Cawthorn et al 1988	Gabbro	Mount Ayliff	53.16	0.25	43.93	0.07	1.79	0.67		
21/14	"	"	"	53.38	0.42	42.69	0.13	2.69	0.51		
21/12	"	"	"	53.03	0.50	41.91	0.00	2.87	0.57		
INS/361	"	"	"	50.36	0.04	39.56	5.05	2.94	0.48		
5	Cawthorn et al. (1985)	Olivine Gabbro	Mount Ayliff	50.10	0.10	38.50	5.45	3.50	0.90	0.50	0
6	"	"	"	49.60	0.10	37.41	6.32	3.80	1.00	0.50	0
1	"	"	"	53.00	0.30	39.88	1.35	4.30	0.70	0.50	0
7	"	"	"	52.30	0.10	37.76	3.60	4.70	1.00	0.10	0
4	"	"	"	54.30	0.30	39.23	0.19	5.20	0.80	0.40	0
3	"	"	"	54.10	0.30	38.87	0.59	5.30	0.80	0.40	0
2	"	"	"	53.50	0.40	38.12	0.31	5.60	0.60	0.50	0
4	"	"	"	52.00		40.27	3.06	3.11	0.94		
7	"	"	"	52.00		40.33	2.89	3.11	0.94	0.05	0
21/10	Cawthorn et al 1988	Picrite	Mount Ayliff	54.10	0.47	39.21	1.25	4.99	0.54		
3	"	"	"	51.89		37.31	4.75	5.03	0.38		
6	"	"	"	51.89		37.36	4.70	5.03	0.38	0.04	0
INS/321	"	"	"	52.78	0.71	37.36	1.86	5.38	0.51		
21/11	"	"	"	54.08	0.45	38.54	0.85	5.39	0.48		
16/1	"	"	"	51.84	0.79	36.28	5.51	5.55	0.44		
INS/185	"	"	"	53.28	0.51	37.01	1.85	5.82	0.52		
16/8	"	"	"	55.11	0.61	38.28	0.07	6.01	0.56		
NGL/56	"	"	"	52.28	0.68	35.71	3.23	6.07	0.48		
2	"	"	"	53.05		36.48	3.40	6.14	0.28		
5	"	"	"	53.05		36.53	3.36	6.14	0.28	0.04	0
16/7	"	"	"	56.04	0.57	37.52	0.00	6.33	0.55		
21/9	"	"	"	54.66	0.54	37.39	1.18	6.33	0.47		
NGL/11	"	"	"	53.33	0.78	35.67	1.86	6.59	0.53		
16/6	"	"	"	52.71	0.85	35.08	4.93	6.65	0.46		
16/5	"	"	"	52.66	0.91	34.92	4.91	6.71	0.47		
16/3	"	"	"	53.40	0.81	35.52	2.91	6.75	0.46		
NGL/9	"	"	"	54.09	0.44	36.06	0.05	6.76	0.52		
16/4	"	"	"	56.14	0.35	36.43	0.00	6.82	0.52		
16/2	"	"	"	54.12	1.03	35.78	2.80	6.98	0.44		
21/8	"	"	"	54.16	0.63	35.56	2.10	7.07	0.53		
NGL/110	"	"	"	50.43	1.08	31.75	6.43	7.32	0.54		
21/5	"	"	"	56.13	0.44	36.22	0.00	7.45	0.54		
21/4	"	"	"	55.13	0.48	35.76	0.20	7.46	0.51		
3/6	"	"	"	56.54	0.55	35.47	0.00	7.75	0.53		
3/8	"	"	"	55.35	0.29	35.40	0.74	7.78	0.50		
21/2	"	"	"	55.44	0.46	35.18	0.62	7.96	0.48		

Blank spaces = not reported or below detection limit

APPENDIX C.1

ILMENITE ANALYSIS FROM SOURCE ROCKS

ANALYSIS NO	REFERENCE	ROCK TYPE	LOCALITY	TiO2	Cr2O3	FeO	Fe2O3	MgO	MnO	SiO2	Al2
3/2	"	"	"	56.17	0.55	35.33	0.00	8.14	0.48		
3/1	"	"	"	55.89	0.58	34.75	0.15	8.44	0.46		
NGL/54	"	"	"	54.41	0.63	33.35	0.98	8.49	0.44		
21/3	"	"	"	56.36	0.48	34.60	0.00	8.55	0.47		
21/6	"	"	"	56.79	0.43	33.99	0.00	8.58	0.47		
3/3	"	"	"	57.43	0.52	33.19	0.00	9.26	0.43		
3/7	"	"	"	56.98	0.48	32.39	0.00	10.22	0.40		
MB6	Reynolds, 1986b	MUBC	Mambula Complex	50.37	0.17	41.36	5.83	1.71	0.88		
MB12	"	"	"	50.82	0.17	40.83	6.39	2.22	0.95		
MB28	"	"	"	51.39	0.17	41.99	4.07	1.92	0.77		
MB33	"	"	"	52.09	0.17	40.06	5.43	3.25	0.91		
MB36	"	"	"	51.18	0.17	41.11	5.59	2.27	0.92		
MB39	"	"	"	52.17	0.17	40.89	4.47	2.85	0.92		
MB42	"	"	"	51.38	0.17	41.20	4.39	2.31	0.86		
MB44	"	"	"	51.53	0.17	41.90	4.31	1.95	0.98		
MB46	"	"	"	52.59	0.16	35.38	5.03	6.07	1.03		
MB49	"	"	"	51.86	0.17	38.35	4.39	4.16	0.85		
MB52	"	"	"	52.90	0.17	39.40	4.83	3.71	0.84		
MB55	"	"	"	52.29	0.17	40.28	3.59	3.25	0.82		
MB60	"	"	"	53.03	0.17	39.38	3.35	4.24	0.78		
MB62	"	"	"	52.61	0.17	40.72	4.15	3.18	0.82		
MB65	"	"	"	51.64	0.17	39.97	5.59	3.14	0.88		
MB70	"	"	"	54.09	0.18	36.15	2.63	6.61	0.72		
VA2 5	This work	Amphibolite	Mgeni River	51.85		45.44	0.62	0.11	1.00	0.02	0
VA2 2	"	"	"	52.01		45.40	0.00	0.11	0.97	0.00	0
VA2 3	"	"	"	51.89		45.64	0.77	0.14	0.76	0.00	0
VA2 4	"	"	"	52.09		44.77	0.85	0.03	1.99	0.00	0
VA2 6	"	"	"	51.99		45.21	0.49	0.14	1.28	0.00	0
VA2 7	"	"	"	49.57		42.66	4.70	0.02	1.85	0.00	0
VA2 8	"	"	"	50.97		44.11	3.10	0.06	1.61	0.01	0
VA2 10	"	"	"	48.81	0.14	42.40	7.88	0.03	1.47	0.04	0
VA2 11	"	"	"	50.89	0.10	43.94	3.37	0.02	1.80	0.04	0
VA2 12	"	"	"	53.03		45.41	0.00	0.60	0.72	0.03	0
VA2 13	"	"	"	52.71		45.13	0.00	0.79	0.47	0.00	0
VA2 14	"	"	"	49.63	0.05	43.63	5.65	0.03	0.94	0.01	0
VA2 15	"	"	"	50.53		44.52	3.40	0.06	0.80	0.00	0
VA2 18	"	"	"	53.42	0.03	44.88	0.00	0.57	0.89	0.00	0
VA2 19	"	"	"	53.44		45.07	0.00	0.36	0.49	0.00	0
VA2 21	"	"	"	52.31	0.11	45.98	0.60	0.33	0.50	0.03	0
NDF50 1	This work	Amphibolite	Natal	51.25		45.01	2.37	0.05	0.99	0.01	0
NDF50 2	"	"	"	50.03	0.10	42.82	4.71	0.29	1.64	0.01	0
NDF50 3	"	"	"	49.88	0.03	41.37	5.56	0.03	3.40	0.01	0
VM3 1	"	Amphibolite-gneiss	Eshowe	50.36		42.84	4.16	0.03	2.38	0.01	0
VM3 2	"	"	"	51.36		43.74	1.45	0.04	2.35	0.00	0

Blank spaces = not reported or below detection limit

APPENDIX C.1

ILMENITE ANALYSIS FROM SOURCE ROCKS

ANALYSIS NO	REFERENCE	ROCK TYPE	LOCALITY	TiO2	Cr2O3	FeO	Fe2O3	MgO	MnO	SiO2	Al2
VM3 3	"	"	"	50.03		42.25	4.55	0.02	2.67	0.00	0.
VM3 5	"	"	"	49.56		41.92	5.90	0.04	2.57	0.03	0.
VM3 6	"	"	"	51.98		45.48	1.10	0.09	1.10	0.00	0.
VM3 7	"	"	"	53.17		45.07	0.00	0.04	1.32	0.01	0.
VM3 9	"	"	"	53.20		45.50	0.00	0.07	0.50	0.00	0.
VM3 11	"	"	"	52.21		45.99	0.83	0.06	0.86	0.02	0.
VA4 1	"	Amphibolite	Eshowe	53.46		44.75	0.00	0.06	1.13	0.02	0.
VA4 2	"	"	"	53.47		45.60	0.00	0.04	0.30	0.03	0.
VA4 4	"	"	"	52.05		45.78	0.05	0.02	1.01	0.03	0.
VA4 5	"	"	"	52.79	0.03	46.24	0.00	0.06	0.93	0.00	0.
VA4 6	"	"	"	53.41		44.98	0.00	0.10	1.33	0.01	0.
VA4 8	"	"	"	53.14		46.20	0.00	0.07	0.36	0.02	0.
VA4 10	"	"	"	52.79	0.03	44.53	0.00	0.03	1.33	0.03	0.
NDF10 1	"	Biotite schist	Mapumulo Suite	52.86		46.12	0.00	0.04	0.33	0.02	0.
NDF10 3	"	"	"	53.43		44.39	0.00	0.12	1.27	0.02	0.
NDF10 4	"	"	"	52.38		46.36	0.57	0.21	0.37	0.01	0.
MS17-1	This work	Granite-gneiss	Mgeni Valley	50.99		43.25	1.69	0.04	2.52	0.02	0.
MS17-2	"	"	"	49.94		42.19	3.55	0.03	2.64	0.00	0.
MS17-3	"	"	"	51.92		43.47	0.61	0.04	3.13	0.01	0.
MS17-4	"	"	"	50.24		42.70	2.52	0.03	2.41	0.01	0.
MS17-5	"	"	"	50.15		42.66	3.02	0.03	2.37	0.01	0.
MS17-6	"	"	"	51.86		44.15	0.38	0.02	2.43	0.01	0.
MS17-7	"	"	"	51.44		43.32	2.41	0.03	2.89	0.03	0.
MS17-8	"	"	"	51.49		43.81	2.67	0.02	2.43	0.01	0.
MS17-9	"	"	"	51.38		42.58	2.58	0.03	3.53	0.01	0.
MS17-10	"	"	"	51.52		43.64	2.48	0.03	2.61	0.01	0
MS17-11	"	"	"	49.58		42.38	5.65	0.03	2.16	0.02	0
UMG5 1	"	Granite-gneiss	Mgeni River	49.50	0.21	41.33	4.82	0.05	3.11	0.05	0
UMG5 2	"	"	"	49.67	0.24	39.03	4.75	0.04	5.55	0.05	0
UMG5 3	"	"	"	50.35	0.21	40.53	3.89	0.03	4.69	0.05	0
UMG5 4	"	"	"	48.78	0.12	39.62	5.86	0.03	4.20	0.05	0
UMG5 5	"	"	"	50.45		41.24	3.88	0.02	4.04	0.00	0
UMG5 8	"	"	"	52.09		44.77	0.85	0.03	1.99	0.00	0
UMG5 10	"	"	"	49.87		41.07	5.15	0.02	3.69	0.00	0
UMG5 12	"	"	"	50.54		38.98	4.10	0.02	6.38	0.02	0
UMG5 15	"	"	"	51.67		42.30	1.90	0.03	4.08	0.01	0
UMG5 16	"	"	"	51.57		41.69	1.90	0.02	4.62	0.03	0
UMG5 17	"	"	"	50.43		41.88	3.45	0.05	3.36	0.01	0
UMG5 19	"	"	"	52.69	0.04	42.76	0.00	0.03	3.05	0.00	0
UMG3 1	"	"	"	50.65		42.29	3.87	0.01	3.22	0.02	0
2	"	"	"	50.95		42.71	2.42	0.00	3.10	0.03	0
3	"	"	"	50.97	0.10	42.94	3.21	0.01	2.89	0.03	0
4	"	"	"	51.65	0.10	42.61	1.74	0.00	3.81	0.02	0
5	"	"	"	51.88	0.09	42.68	1.01	0.01	4.01	0.09	0
6	"	"	"	52.07		44.76	1.37	0.02	2.01	0.01	0

Blank spaces = not reported or below detection limit

APPENDIX C.1

ILMENITE ANALYSIS FROM SOURCE ROCKS

ANALYSIS NO	REFERENCE	ROCK TYPE	LOCALITY	TiO2	Cr2O3	FeO	Fe2O3	MgO	MnO	SiO2	Al2
7	"	"	"	51.69	0.03	44.01	2.28	0.01	2.42	0.00	0
9	"	"	"	50.66		41.64	3.82	0.07	3.74	0.00	0
VG1 1	"	Granite	Kloof End Pluton	51.85		42.65	1.16	0.02	3.92	0.03	0
2	"	"	"	50.42		41.70	3.85	0.02	3.58	0.01	0
3	"	"	"	51.17		39.38	2.46	0.02	6.52	0.00	0
4	"	"	"	53.09		45.10	0.00	0.21	1.45	0.06	0
5	"	"	"	51.10		43.29	2.70	0.02	2.59	0.00	0
6	"	"	"	50.62		41.59	3.83	0.01	3.88	0.02	0
7	"	"	"	49.83		43.19	4.16	0.06	1.50	0.00	0
8	"	"	"	49.42		41.39	5.17	0.00	3.01	0.00	0
9	"	"	"	51.00		43.05	1.69	0.00	2.78	0.00	0
10	"	"	"	49.87		41.07	5.15	0.02	3.69	0.00	0
12	"	"	"	50.54		38.98	4.10	0.02	6.38	0.02	0
13	"	"	"	52.11	0.03	45.27	0.11	0.19	1.25	0.01	0
15	"	"	"	51.67		42.30	1.90	0.03	4.08	0.01	0
16	"	"	"	51.57		41.69	1.90	0.02	4.62	0.03	0
17	"	"	"	50.43		41.88	3.45	0.05	3.36	0.01	0
18	"	"	"	53.36	0.08	43.03	0.00	0.02	2.85	0.03	0
19	"	"	"	52.69	0.04	42.76	0.00	0.03	3.05	0.00	0
VG4 1	"	Charnockite	Port Edward	52.91		44.55	0.00	0.05	1.58	0.02	0
2	"	"	"	49.08		39.36	5.40	0.02	4.69	0.02	0
3	"	"	"	50.70		39.47	3.15	0.01	6.04	0.01	0
4	"	"	"	53.33		43.77	0.00	0.04	1.09	0.16	0
5	"	"	"	52.60		45.13	0.00	0.02	1.22	0.03	0
6	"	"	"	47.57		38.98	7.84	0.01	4.10	0.30	0
7	"	"	"	50.98		41.31	1.31	0.01	4.50	0.02	0
8	"	"	"	50.11		43.64	4.30	0.08	1.29	0.02	0
9	"	"	"	52.32	0.04	45.67	0.80	0.02	1.33	0.01	0
11	"	"	"	50.74		39.37	3.39	0.01	6.19	0.02	0
12	"	"	"	50.89		38.21	4.03	0.04	7.41	0.02	0
14	"	"	"	49.81	0.03	40.15	5.42	0.03	4.55	0.02	0
15	"	"	"	51.84		36.51	1.13	0.03	9.98	0.03	0
16	"	"	"	51.58		44.02	1.06	0.08	2.20	0.01	0
18	"	"	"	52.44		45.16	0.00	0.07	1.18	0.03	0
20	"	"	"	53.64		43.36	0.00	0.04	2.84	0.01	0
21	"	"	"	52.65	0.04	45.41	0.00	0.08	1.57	0.01	0
22	"	"	"	52.77		45.49	0.00	0.08	1.46	0.00	0
23	"	"	"	50.90	0.03	41.72	3.58	0.01	4.00	0.02	0

Blank spaces = not reported or below detection limit

APPENDIX C.2

MAGNETITE COMPOSITIONS FROM SOURCE ROCKS

								RECALCULATED	
Reference/Sample	Rock Type	SiO2	TiO2	Al2O3	Cr2O3	MnO	MgO	FeO	Fe2O3
Reynolds (1983)	dolerite	nd	25.01	1.21	0.06	0.37	0.51	53.82	18.41
Reynolds (1983)	dolerite	nd	21.99	1.45	0.07	0.45	0.38	50.47	24.62
Reynolds (1983)	dolerite	nd	16.18	1.15	0.01	0.58	0.32	45.09	36.40
Reynolds (1983)	dolerite	nd	15.70	1.46	0.10	0.59	0.76	43.98	36.79
Reynolds (1983)	dolerite	nd	14.64	1.41	0.17	0.39	0.25	43.90	38.70
Reynolds (1983)	dolerite	nd	12.32	2.74	0.18	0.36	0.36	41.76	41.45
Reynolds (1983)	dolerite	nd	10.71	0.97	0.13	0.30	0.28	40.36	47.08
Reynolds (1983)	dolerite	nd	9.74	1.93	0.27	0.29	0.22	39.55	47.25
Reynolds (1983)	dolerite	nd	8.46	1.98	0.18	0.33	0.14	38.62	50.11
Reynolds (1983)	dolerite	nd	5.99	2.48	0.17	0.21	0.34	36.18	54.25
Eales et al. (1980)	ferrotholeiite	nd	26.13	1.81	0.00	0.50	0.16	38.71	32.72
Eales et al. (1980)	ferrotholeiite	nd	7.27	1.76	0.56	0.31	0.26	37.28	52.33
Armstrong et al. (1984)	dolerite	0.39	12.54	1.21	nd	0.49	0.24	42.00	42.12
Armstrong et al. (1984)	dolerite	0.34	22.10	0.87	nd	0.75	0.26	50.03	24.38
Haggerty (1976b)	basalt	0.14	26.10	0.02	nd	0.67	0.87	53.20	17.30
Haggerty (1976b)	basalt	nd	23.80	0.03	nd	0.70	3.60	47.60	20.80
Haggerty (1976b)	basalt	0.22	23.30	0.70	nd	0.46	1.24	51.00	20.20
Haggerty (1976b)	basalt	nd	24.29	nd	nd	0.53	0.19	51.80	20.27
Haggerty (1976b)	gabbro	0.10	3.81	nd	nd	0.13	0.40	30.46	62.39
Haggerty (1976b)	gabbro	nd	8.57	0.18	nd	0.36	1.38	32.18	54.48
Haggerty (1976b)	gabbro	nd	8.16	0.10	nd	0.24	1.07	31.21	56.93
Sample D 8	dolerite	-	32.07	-	-	0.36	0.23	59.74	6.31
Sample D 8	dolerite	0.23	16.49	0.89	-	0.69	0.32	45.93	36.38
Sample D 8	dolerite	-	15.55	2.25	0.32	0.34	0.50	44.25	34.98
Sample D 8	dolerite	0.06	8.71	1.16	0.08	0.45	0.24	38.30	50.03
Sample D 8	dolerite	0.11	15.94	0.75	0.33	1.06	0.19	44.20	35.52
Sample D 8	dolerite	1.60	9.71	1.72	0.23	0.39	0.56	41.49	45.08
Sample D 8	dolerite	-	18.46	1.35	0.19	0.29	0.45	45.59	27.64
Sample D 8	dolerite	-	35.52	-	-	0.69	0.07	63.30	0.52
Sample D 8	dolerite	0.10	34.98	0.05	0.16	1.08	0.34	62.19	1.40
Sample D 8	dolerite	0.09	34.92	0.13	0.21	0.50	1.97	59.87	1.49
Sample D 8	dolerite	0.04	35.05	0.04	0.18	0.81	1.39	60.71	1.69
Sample D 8	dolerite	0.05	35.02	0.04	0.17	0.96	0.33	61.96	0.69
Sample D 8	dolerite	0.04	35.65	0.03	0.14	0.77	0.34	62.95	0.10
Sample D 8	dolerite	0.14	15.26	1.65	0.17	0.98	0.11	44.09	36.19
Sample D 8	dolerite	-	35.62	0.06	0.22	0.48	1.52	61.05	(0.00)
Sample D 8	dolerite	0.07	22.12	1.14	0.26	0.61	0.32	48.61	19.87
Sample D 8	dolerite	0.11	13.98	2.12	0.38	0.61	0.09	42.52	36.06
Sample HEC 9	dol. and basalt	0.05	31.06	1.02	0.07	0.52	0.94	57.77	7.16
Sample HEC 9	dol. and basalt	0.10	13.63	0.59	0.15	0.28	0.17	43.21	41.25

- = Below detection limit; nd = not reported

APPENDIX C.2

MAGNETITE COMPOSITIONS FROM SOURCE ROCKS

								RECALCULATED	
Reference/Sample	Rock Type	SiO2	TiO2	Al2O3	Cr2O3	MnO	MgO	FeO	Fe2O3
Sample HEC 9	dol. and basalt	0.65	14.55	0.98	0.15	0.57	0.06	45.15	38.57
Sample HEC 9	dol. and basalt	0.10	18.43	0.75	0.06	0.41	0.55	46.89	31.87
Sample HEC 9	dol. and basalt	0.55	10.45	1.01	0.23	0.44	0.03	41.00	45.70
Sample HEC 9	dol. and basalt	1.00	12.29	0.36	0.20	0.53	0.16	42.88	41.91
Sample HEC 9	dol. and basalt	0.30	12.11	0.45	0.11	0.60	0.10	41.69	43.58
Sample HEC 9	dol. and basalt	0.21	19.15	0.82	0.12	1.00	0.81	46.64	30.01
Sample HEC 9	dol. and basalt	0.50	14.25	1.05	0.11	0.25	0.23	44.71	39.49
Sample HEC 9	dol. and basalt	0.11	17.27	0.22	0.12	0.38	0.29	46.61	35.51
Sample HEC 9	dol. and basalt	0.06	12.86	0.56	0.16	0.33	0.08	42.06	41.77
Sample HEC 9	dol. and basalt	0.09	16.48	0.44	0.10	0.23	0.18	46.32	37.04
Sample HEC 9	dol. and basalt	0.44	15.85	0.87	0.14	0.24	0.25	46.12	36.84
Sample HEC 9	dol. and basalt	0.22	21.91	1.45	0.15	0.33	0.36	50.78	23.86
Sample HEC 9	dol. and basalt	0.08	22.30	1.32	0.12	0.86	0.07	50.83	23.44
Sample HEC 9	dol. and basalt	0.07	19.42	0.98	0.14	0.47	0.52	47.50	28.97
Sample HEC 9	dol. and basalt	0.03	14.55	1.54	0.21	0.49	0.10	44.03	38.43
Sample HEC 9	dol. and basalt	0.44	5.96	0.22	0.12	0.18	0.11	36.77	55.94
Sample HEC 9	dol. and basalt	0.23	13.33	0.87	-	0.42	0.12	42.15	39.23
Sample HEC 9	dol. and basalt	0.53	12.50	0.56	-	0.41	0.07	42.06	40.97
Sample HEC 9	dol. and basalt	0.70	12.18	1.24	0.19	0.83	0.07	42.52	42.09
Sample HEC 9	dol. and basalt	1.01	14.12	0.94	0.22	0.75	0.04	45.03	38.42
Sample HEC 9	dol. and basalt	0.22	14.41	0.50	0.15	0.91	-	43.61	39.31
Sample HEC 9	dol. and basalt	0.65	18.96	0.78	0.20	0.87	0.44	47.84	29.36
Sample HEC 9	dol. and basalt	0.44	18.50	1.56	0.19	0.89	0.36	48.50	32.29
Sample DM90-5	dolerite	0.66	20.22	0.80	-	1.48	0.87	46.99	25.62
Sample DM90-5	dolerite	0.69	20.29	1.00	-	1.16	0.92	47.18	24.80
Sample DM90-5	dolerite	0.38	23.31	0.60	0.04	1.20	0.47	50.02	19.58
Sample DM90-5	dolerite	0.14	29.07	0.77	0.04	1.18	0.06	55.72	8.52
Sample DM90-5	dolerite	0.84	18.06	1.10	-	1.02	1.13	44.77	27.90
Sample DM90-5	dolerite	1.88	21.69	0.68	0.06	0.32	0.08	52.44	19.73
Sample DM90-5	dolerite	0.45	23.61	0.78	0.09	1.27	0.48	51.14	20.40
Sample DM90-25	dolerite	0.59	6.63	1.89	0.16	0.22	0.08	37.58	51.56
Sample DM90-25	dolerite	0.36	22.18	1.13	0.12	0.60	0.06	51.62	23.89
Sample DM90-25	dolerite	0.30	28.98	2.09	0.13	0.71	0.07	57.25	8.24
Sample DM90-25	dolerite	1.09	5.88	1.02	0.19	0.16	0.12	36.69	51.32
Sample DM90-25	dolerite	0.15	6.69	6.73	0.21	0.13	0.09	37.53	45.73
Sample DM90-25	dolerite	1.58	12.57	3.02	0.14	0.21	0.53	43.24	35.15
Sample DM90-25	dolerite	1.54	9.29	1.42	0.23	0.27	0.23	40.20	43.07
Sample DM90-25	dolerite	0.12	31.45	2.34	0.04	0.42	0.09	59.36	3.17
Sample DM90-25	dolerite	0.67	9.53	2.59	0.23	0.23	0.16	40.11	44.35
Sample DM90-25	dolerite	0.12	5.81	2.55	0.18	0.10	0.06	35.78	51.93

- = Below detection limit; nd = not reported

APPENDIX C.2

MAGNETITE COMPOSITIONS FROM SOURCE ROCKS

Reference/Sample	Rock Type	SiO2	TiO2	Al2O3	Cr2O3	MnO	MgO	RECALCULATED FeO	RECALCULATED Fe2O3
Sample DM90-25	dolerite	0.19	26.77	1.94	0.11	0.35	0.08	55.40	13.06
Sample DM90-25	dolerite	0.14	32.27	1.17	0.08	0.59	0.08	59.63	2.52
Sample DM90-25	dolerite	0.16	9.86	4.08	0.15	0.22	0.08	40.11	43.10
Sample DM90-25	dolerite	0.15	6.62	4.94	0.25	0.17	0.17	37.17	48.37
Sample DM90-25	dolerite	1.50	10.13	1.19	0.15	0.36	0.26	41.24	43.01
Sample DM90-8	dolerite	0.15	4.51	1.86	0.18	0.16	0.03	34.61	55.45
Sample DM90-8	dolerite	0.25	27.06	0.96	0.10	0.61	0.04	55.97	14.85
Sample DM90-8	dolerite	0.56	4.70	2.68	0.25	0.17	0.04	35.69	53.67
Sample DM90-8	dolerite	0.17	4.17	2.29	0.28	0.15	0.04	33.96	54.55
Sample DM90-8	dolerite	0.19	19.73	3.11	0.16	0.44	0.15	48.67	24.88
Sample DM90-8	dolerite	0.50	6.40	2.22	0.11	0.16	0.04	36.41	49.59
Sample DM90-8	dolerite	0.12	3.39	1.95	0.15	0.13	0.02	33.85	58.22
Sample DM90-8	dolerite	0.56	6.27	2.53	0.17	0.21	0.06	37.06	50.86
Sample DM90-8	dolerite	0.17	3.47	2.21	0.24	0.12	0.04	33.39	56.18
Haggerty (1976b)	basalt	nd	20.01	1.92	0.06	0.52	1.34	47.55	28.49
Haggerty (1976b)	basalt	nd	12.96	2.54	0.07	0.52	0.93	41.34	40.55
Haggerty (1976b)	basalt	nd	19.70	1.56	0.05	0.47	0.95	47.80	29.83
Haggerty (1976b)	basalt	nd	17.34	1.93	0.15	1.05	0.44	45.68	33.13
Haggerty (1976b)	basalt	nd	15.01	2.56	0.13	0.49	0.95	43.23	36.84
Haggerty (1976b)	basalt	nd	21.07	2.09	-	0.67	1.34	48.53	27.19
Haggerty (1976b)	basalt	nd	20.15	1.59	0.05	0.58	1.16	47.40	28.21
Haggerty (1976b)	basalt	nd	19.12	1.78	0.04	0.43	1.25	46.68	30.47
Haggerty (1976b)	basalt	nd	20.22	1.45	0.06	0.83	0.94	47.30	28.74
Haggerty (1976b)	trachybasalt	nd	21.65	0.62	0.01	1.29	0.04	49.30	24.50
Haggerty (1976b)	trachybasalt	nd	23.52	2.65	-	0.59	4.31	46.39	23.35
Haggerty (1976b)	tholeiite	nd	17.50	2.90	-	0.34	0.90	46.00	31.40
Haggerty (1976b)	tholeiite	nd	28.80	1.18	-	0.82	0.50	56.10	10.70
Haggerty (1976b)	tholeiite	nd	26.98	3.92	0.04	0.87	1.83	53.40	13.88
Reynolds (1986d)	MUBC	nd	0.38	0.52	0.10	-	0.10	31.13	67.12
Reynolds (1986d)	MUBC	nd	0.34	0.61	0.10	-	0.22	30.67	66.71
Reynolds (1986d)	MUBC	nd	0.21	0.62	0.14	-	0.21	30.66	67.08
Reynolds (1986d)	MUBC	nd	0.28	1.17	0.11	0.07	0.29	30.46	65.94
Reynolds (1986d)	MUBC	nd	0.16	1.87	0.14	-	0.37	30.43	65.44
Reynolds (1984)	MUBC	nd	0.27	0.40	0.13	-	0.10	30.99	67.87
Gjelsvik (1957)	MUBC	0.90	1.10	nd	nd	nd	0.00	31.30	63.40
Gjelsvik (1957)	MUBC	0.10	0.50	nd	nd	nd	0.80	26.10	71.80
Gjelsvik (1957)	MUBC	3.60	1.90	nd	nd	0.10	3.50	31.40	57.40
Gjelsvik (1957)	MUBC	0.20	1.00	nd	nd	nd	0.40	32.00	64.80
Gjelsvik (1957)	MUBC	nd	14.60	nd	nd	0.30	0.00	41.50	44.10
Haggerty (1976b)	granite	nd	5.92	0.59	nd	0.50	0.10	29.55	61.33

- = Below detection limit; nd = not reported

APPENDIX C.2

MAGNETITE COMPOSITIONS FROM SOURCE ROCKS

								RECALCULATED	
Reference/Sample	Rock Type	SiO2	TiO2	Al2O3	Cr2O3	MnO	MgO	FeO	Fe2O3
Haggerty (1976b)	granite	nd	0.17	nd	nd	0.44	0.00	30.60	68.00
Haggerty (1976b)	granite	nd	7.10	nd	nd	0.50	0.05	36.20	53.10
Haggerty (1976b)	granodiorite	nd	2.13	0.40	0.03	0.17	1.85	29.89	64.59
Haggerty (1976b)	granodiorite	nd	0.37	0.10	nd	0.29	0.03	30.70	68.40
Rollinson (1980)	metagranite	0.15	14.73	0.13	0.08	0.14	nd	43.21	36.45
Rollinson (1980)	metagranite	0.14	14.63	0.30	0.10	0.06	0.06	43.28	36.81
Rollinson (1980)	metagranite	nd	15.77	0.12	0.07	1.40	0.03	33.85	42.21
Rollinson (1980)	metagranite	0.11	14.81	0.13	0.11	0.02	nd	43.51	36.65
Rollinson (1980)	metagranite	0.16	13.20	0.17	0.10	0.10	0.08	41.91	39.71
Rollinson (1980)	metagranite	0.12	9.28	0.16	0.05	0.26	nd	37.75	46.52
Rollinson (1980)	metagranite	0.16	9.80	0.15	0.11	0.04	nd	38.98	46.35
Rollinson (1980)	metagranite	nd	9.30	0.16	0.09	0.22	0.09	37.46	46.58
Rollinson (1980)	metagranite	nd	10.07	0.15	0.07	0.22	0.02	38.34	45.24
Rollinson (1980)	metagranite	nd	7.84	0.15	0.09	0.34	0.01	36.21	49.61
Rollinson (1980)	metagranite	0.17	7.31	0.12	0.04	0.08	nd	36.44	50.88
Rollinson (1980)	metagranite	0.17	8.82	0.16	0.09	0.14	nd	37.93	48.17
Rollinson (1980)	metagranite	0.16	7.88	0.14	0.07	0.02	nd	37.06	49.81
Rollinson (1980)	metagranite	0.14	8.02	0.12	0.11	0.04	0.02	37.12	49.61
Rollinson (1980)	metagranite	nd	1.02	0.23	0.07	0.07	0.02	31.20	65.07
Rollinson (1980)	metagranite	nd	0.94	0.27	0.04	0.10	0.03	31.10	65.24
Rollinson (1980)	metagranite	nd	1.07	0.24	0.07	0.06	0.01	31.07	64.51
Rollinson (1980)	metagranite	nd	0.89	0.25	0.06	0.12	0.02	30.69	65.14
Rollinson (1980)	metagranite	nd	0.89	0.24	0.06	0.10	0.06	30.76	64.84
Rollinson (1980)	metagranite	nd	1.79	0.22	0.13	0.05	nd	32.14	63.91
Rollinson (1980)	metagranite	nd	1.56	0.21	0.11	0.09	0.06	31.71	62.35
Rollinson (1980)	metagranite	nd	0.81	0.28	0.13	0.01	0.14	30.63	64.85
Rollinson (1980)	metagranite	nd	0.93	0.25	0.12	0.02	0.03	31.34	65.60
Rollinson (1980)	metagranite	nd	0.56	0.42	0.12	0.03	1.05	29.49	66.74
Rollinson (1980)	metagranite	nd	0.36	0.76	0.12	0.02	0.50	30.29	66.59
Rollinson (1980)	metagranite	nd	2.21	0.70	0.09	0.05	nd	32.65	62.66
Rollinson (1980)	metagranite	nd	1.10	0.23	0.11	0.02	nd	31.34	64.83
Rollinson (1980)	metagranite	nd	0.96	0.23	0.12	0.01	nd	31.13	64.88
Rollinson (1980)	metagranite	nd	1.70	0.22	0.07	0.02	nd	32.02	64.01
Rollinson (1980)	metagranite	nd	1.46	0.23	0.12	0.03	nd	31.44	63.63
Rollinson (1980)	metagranite	nd	1.82	0.24	0.10	0.04	nd	32.20	63.90
Rollinson (1980)	metagranite	nd	2.21	0.70	0.09	0.05	nd	32.65	62.66
Rollinson (1980)	metagranite	nd	2.16	0.33	0.11	0.04	0.02	32.39	62.90
Rollinson (1980)	metagranite	nd	1.89	0.21	0.09	0.04	0.01	32.13	63.99
Rollinson (1980)	metagranite	nd	2.40	0.29	0.09	0.08	0.04	32.56	62.56
Rollinson (1980)	metagranite	nd	1.95	0.17	0.07	0.04	nd	31.95	62.97

- = Below detection limit; nd = not reported

APPENDIX C.2

MAGNETITE COMPOSITIONS FROM SOURCE ROCKS

								RECALCULATED	
Reference/Sample	Rock Type	SiO2	TiO2	Al2O3	Cr2O3	MnO	MgO	FeO	Fe2O3
Rollinson (1980)	metagranite	nd	1.35	0.33	0.08	0.04	0.02	31.61	64.43
Sample UMG1	granitoid	-	0.22	0.26	-	-	0.02	31.34	68.29
Sample UMG1	granitoid	-	0.04	0.08	-	-	-	30.60	67.83
Sample UMG1	granitoid	-	0.02	0.07	-	-	0.03	30.93	68.69
Sample UMG1	granitoid	-	0.05	0.18	-	-	-	30.89	68.32
Sample UMG1	granitoid	-	0.17	0.04	-	-	0.03	31.20	68.61
Sample UMG1	granitoid	-	0.06	0.24	-	-	-	31.12	68.56
Sample UMG1	granitoid	-	0.05	0.11	0.04	0.06	-	30.98	68.65
Sample UMG1	granitoid	-	0.09	0.02	-	-	0.02	30.89	68.38
Sample UMG3	granitoid	-	0.14	0.10	-	-	-	30.91	68.00
Sample UMG3	granitoid	-	0.05	0.07	-	-	0.02	30.77	68.19
Sample UMG3	granitoid	-	0.45	0.23	-	0.14	-	31.22	67.54
Sample UMG3	granitoid	-	0.06	0.19	0.05	-	-	30.78	67.91
Sample UMG3	granitoid	-	0.04	0.05	0.04	-	-	31.10	68.93
Sample UMG3	granitoid	-	0.08	0.04	-	0.06	-	30.76	68.09
Sample UMG3	granitoid	-	0.13	0.33	0.04	-	-	30.96	67.83
Sample UMG3	granitoid	-	0.02	0.13	0.04	-	-	30.63	67.86
Sample UMG3	granitoid	-	0.09	0.22	0.04	0.02	-	31.02	68.23
Sample UMG3	granitoid	-	0.02	0.11	0.04	0.01	-	31.04	68.75
Sample UMG3	granitoid	-	0.04	0.16	0.04	0.03	-	30.87	68.21
Sample UMG3	granitoid	-	0.40	0.61	0.52	0.03	-	31.38	66.70
Sample UMG4	granitoid	0.06	0.50	0.35	0.08	0.03	-	30.06	63.95
Sample UMG4	granitoid	0.11	1.00	0.29	0.10	0.11	0.04	30.97	64.14
Sample UMG4	granitoid	0.03	0.08	0.26	0.10	-	0.03	30.59	67.23
Sample UMG4	granitoid	0.03	1.14	0.32	0.11	0.08	0.02	31.54	65.00
Sample UMG4	granitoid	0.04	0.39	0.42	0.14	-	-	30.84	66.07
Sample UMG4	granitoid	0.03	1.33	0.40	0.13	0.11	-	31.89	64.94
Sample UMG4	granitoid	0.15	0.15	0.43	0.16	-	0.09	30.55	66.10
Sample UMG4	granitoid	0.04	1.29	0.41	0.04	0.15	-	32.03	65.47
Sample UMG4	granitoid	0.09	0.20	0.22	0.25	0.12	-	31.10	67.54
Sample UMG5	granitoid	0.05	0.16	0.09	0.25	0.21	0.04	30.67	67.52
Sample UMG5	granitoid	0.04	0.30	0.27	0.26	0.19	0.02	30.94	67.16
Sample UMG5	granitoid	0.05	0.14	0.14	0.33	0.13	0.03	31.08	68.08
Sample UMG5	granitoid	0.05	0.15	0.16	0.27	0.12	0.03	30.68	67.18
Sample UMG5	granitoid	0.05	0.17	0.05	0.26	0.22	0.03	30.94	68.09
Sample UMG5	granitoid	0.03	0.21	0.21	0.24	0.15	0.03	30.89	67.53
Sample UMG5	granitoid	0.05	0.20	0.10	0.23	0.19	0.03	30.85	67.69
Sample MS 17	granitoid-gneiss	-	0.02	0.16	0.08	0.14	-	29.74	65.92
Sample MS 17	granitoid-gneiss	-	0.04	0.05	0.09	0.13	-	30.43	67.56
Sample MS 17	granitoid-gneiss	-	0.07	0.11	0.07	0.13	-	30.97	68.60

- = Below detection limit; nd = not reported

APPENDIX C.2

MAGNETITE COMPOSITIONS FROM SOURCE ROCKS

								RECALCULATED	
Reference/Sample	Rock Type	SiO2	TiO2	Al2O3	Cr2O3	MnO	MgO	FeO	Fe2O3
Sample MS 17	granitoid-gneiss	-	0.05	0.15	0.09	0.09	0.03	30.86	68.35
Sample MS 17	granitoid-gneiss	0.03	0.04	0.03	0.23	0.10	-	30.82	68.11
Sample MS 17	granitoid-gneiss	0.09	0.38	0.37	0.11	0.15	-	30.93	66.41
Sample MS 17	granitoid-gneiss	0.03	0.01	0.02	0.08	0.16	-	30.57	68.02
Sample MS 17	granitoid-gneiss	0.03	0.03	0.06	0.15	0.06	0.02	30.66	67.84
Sample MS 17	granitoid-gneiss	-	0.06	0.14	0.11	0.09	-	30.52	67.47
Sample MS 17	granitoid-gneiss	-	0.03	0.13	0.10	0.11	0.02	30.81	68.27
Sample NDF 10	gneiss	0.04	0.01	0.12	0.11	0.07	-	30.70	67.85
Sample NDF 10	gneiss	0.05	0.04	0.10	0.11	0.09	-	30.81	68.01
Sample NDF 10	gneiss	0.04	0.04	0.13	0.08	0.07	-	31.21	68.90
Sample NDF 10	gneiss	0.03	0.02	0.12	0.07	0.07	-	30.80	68.12
Sample NDF 10	gneiss	0.03	0.00	0.08	0.12	0.12	-	30.82	68.39
Sample NDF 10	gneiss	0.05	0.03	0.06	0.05	0.08	-	30.89	68.37
Sample NDF 10	gneiss	0.04	0.00	0.25	0.14	0.09	-	30.82	67.97
Sample NDF 10	gneiss	0.07	0.00	0.18	0.18	0.08	-	30.90	68.09
Sample NDF 10	gneiss	0.05	0.00	0.07	0.17	0.10	-	31.04	68.67
Sample NDF 10	gneiss	0.04	0.01	0.09	0.12	0.08	-	30.77	68.05
Nowicki (1986)	metapelitic gneiss	nd	0.00	0.40	0.37	-	-	31.07	67.89
Nowicki (1986)	metapelitic gneiss	nd	0.00	0.12	0.34	-	-	30.89	68.03
Nowicki (1986)	metapelitic gneiss	0.46	1.33	1.26	0.27	0.15	0.38	32.17	63.33
Nowicki (1986)	metapelitic gneiss	nd	0.00	0.04	0.25	0.00	0.00	31.22	68.31
Grutter (1986)	cord-qtz-gneiss	nd	nd	0.12	0.06	nd	nd	31.25	68.92
Grutter (1986)	bio-opx-gneiss	nd	0.05	nd	nd	nd	nd	31.98	68.11
Grutter (1986)	bio-opx-gneiss	nd	nd	nd	nd	nd	nd	31.98	68.01
Russ Nabelek (1989)	mafic schist	0.48	16.10	1.99	nd	0.44	0.03	45.34	31.85
Russ Nabelek (1989)	mafic schist	0.48	2.90	1.53	nd	0.17	nd	34.04	59.51
Russ Nabelek (1989)	mafic schist	0.96	24.70	1.12	nd	0.45	0.11	53.87	15.59
Oliver (1978)	hbl-gt-gneiss	0.05	18.16	0.09	nd	0.03	0.07	47.27	32.43
Oliver (1978)	feld-hbl-gneiss	0.00	17.46	0.20	nd	0.03	0.15	46.71	34.71
Oliver (1978)	hornblendite	0.00	15.75	0.19	nd	0.29	0.26	44.07	36.84
Oliver (1978)	anorthosite	0.03	14.87	0.22	nd	0.02	0.20	43.74	38.16
Oliver (1978)	hbl-eclogite	0.11	12.70	0.05	nd	nd	0.23	41.59	42.70
Oliver (1978)	hbl-eclogite	0.06	11.62	0.06	nd	nd	0.03	40.40	43.33
Oliver (1978)	feld-hbl-gneiss	0.05	0.09	0.03	nd	nd	0.13	30.90	68.10
Oliver (1978)	gt-hyp-gneiss	0.07	0.29	0.40	nd	nd	0.08	31.40	68.31
Oliver (1978)	gt-hyp-gneiss	0.05	0.13	0.41	nd	nd	0.06	31.21	38.56
Oliver (1978)	hbl-harzburgite	0.03	0.46	0.43	1.24	0.02	0.28	30.26	64.50
Oliver (1978)	hbl-harzburgite	0.04	0.25	1.05	2.62	0.04	0.51	30.19	61.73
Oliver (1978)	peridotite	0.16	0.59	0.00	2.67	0.20	0.14	33.49	61.72
Oliver (1978)	peridotite	0.11	0.12	0.02	1.10	0.07	0.10	31.50	68.32

- = Below detection limit; nd = not reported

APPENDIX C.2

MAGNETITE COMPOSITIONS FROM SOURCE ROCKS

Reference/Sample	Rock Type	SiO2	TiO2	Al2O3	Cr2O3	MnO	MgO	RECALCULATED FeO	RECALCULATED Fe2O3
Bohlen (1980)	ortho + paragneiss	0.10	0.09	0.44	nd	nd	0.07	30.89	67.31
Bohlen (1980)	ortho + paragneiss	0.09	60.50	0.04	nd	0.78	0.08	35.51	55.63
Bohlen (1980)	ortho + paragneiss	0.20	0.37	0.61	nd	0.01	0.02	31.23	65.95
Bohlen (1980)	ortho + paragneiss	0.16	12.96	0.55	nd	0.92	0.03	41.62	41.11
Bohlen (1980)	ortho + paragneiss	0.13	1.25	1.04	nd	0.09	0.11	31.45	63.16
Bohlen (1980)	ortho + paragneiss	0.12	7.94	0.92	nd	0.37	0.11	37.23	50.15
Bohlen (1980)	ortho + paragneiss	0.07	0.23	0.47	nd	0.10	0.08	30.88	67.07
Bohlen (1980)	ortho + paragneiss	0.06	12.39	0.39	nd	0.90	0.07	41.08	43.09
Bohlen (1980)	ortho + paragneiss	0.13	0.53	0.62	nd	0.12	0.04	31.44	66.50
Bohlen (1980)	ortho + paragneiss	0.10	15.72	0.44	nd	0.35	0.06	45.14	36.39
Bohlen & Essene (1977)	ortho + paragneiss	nd	10.70	1.04	nd	0.03	nd	41.27	46.26
Bohlen & Essene (1977)	ortho + paragneiss	nd	0.83	0.42	nd	0.00	0.03	31.13	67.59
Bohlen & Essene (1977)	ortho + paragneiss	nd	5.60	0.43	nd	0.14	0.03	35.96	57.49
Desmarais (1981)	meta ultramafic	nd	nd	nd	nd	0.18	0.52	30.24	69.89
Laird (1980)	mafic schist	0.25	0.01	nd	nd	0.01	0.01	30.26	67.19
Laird (1980)	mafic schist	0.03	0.04	nd	nd	0.01	nd	31.32	69.39
Braun & Raith (1985)	metabasite	nd	0.03	0.18	0.05	0.03	0.16	30.39	67.80
Braun & Raith (1985)	metabasite	nd	0.01	0.02	0.02	0.04	0.23	30.56	68.84
Braun & Raith (1985)	metabasite	nd	0.03	0.27	0.06	0.04	0.15	30.55	67.98
Braun & Raith (1985)	metabasite	nd	0.02	0.07	0.01	0.06	0.02	29.85	66.35
Braun & Raith (1985)	metabasite	nd	0.03	0.24	0.06	0.06	nd	30.35	67.04
Braun & Raith (1985)	metabasite	nd	0.02	0.10	0.01	0.06	nd	30.61	67.92
Braun & Raith (1985)	metabasite	nd	0.06	0.07	0.00	0.01	0.40	30.67	69.41
Braun & Raith (1985)	metabasite	nd	0.06	0.08	0.08	0.02	0.01	30.98	68.50
Braun & Raith (1985)	metabasite	nd	0.12	0.24	0.03	0.05	0.14	31.03	68.74
Braun & Raith (1985)	metabasite	nd	0.16	0.23	0.01	0.01	0.16	30.74	67.97
Braun & Raith (1985)	metabasite	nd	0.06	0.41	0.02	0.05	0.15	31.28	69.32
Braun & Raith (1985)	metabasite	nd	0.18	0.32	0.01	0.04	0.09	31.31	68.80
Braun & Raith (1985)	metabasite	nd	0.55	0.51	0.02	0.06	0.11	31.64	67.88
Braun & Raith (1985)	metabasite	nd	0.07	0.09	0.03	0.03	0.06	30.56	67.77
Braun & Raith (1985)	metabasite	nd	0.03	0.09	0.08	0.06	0.36	29.97	67.83
Braun & Raith (1985)	metabasite	nd	0.04	0.39	0.03	0.02	0.26	30.42	67.89
Braun & Raith (1985)	metabasite	nd	0.03	0.11	0.03	0.00	0.41	30.07	68.12
Braun & Raith (1985)	metabasite	nd	0.02	0.15	0.06	0.01	0.07	30.47	67.65
Braun & Raith (1985)	metabasite	nd	0.04	0.18	0.01	0.03	0.11	30.46	67.75
Braun & Raith (1985)	metabasite	nd	0.03	0.09	0.04	0.04	0.17	30.62	68.52
Braun & Raith (1985)	metabasite	nd	0.07	0.33	0.05	0.07	0.25	30.69	68.50

- = Below detection limit; nd = not reported

APPENDIX D

Modal proportions of heavy minerals in beaches and dunes

APPENDIX D: STANDARD DEVIATION ASSOCIATED WITH POINT-COUNTING 500 GRAINS

p	Sigma	p	Sigma
0.5	0.32	51	2.24
1	0.44	52	2.23
2	0.63	53	2.23
3	0.76	54	2.23
4	0.88	55	2.22
5	0.97	56	2.22
6	1.06	57	2.21
7	1.14	58	2.21
8	1.21	59	2.20
9	1.28	60	2.19
10	1.34	61	2.18
11	1.40	62	2.17
12	1.45	63	2.16
13	1.50	64	2.15
14	1.55	65	2.13
15	1.60	66	2.12
16	1.64	67	2.10
17	1.68	68	2.09
18	1.72	69	2.07
19	1.75	70	2.05
20	1.79	71	2.03
21	1.82	72	2.01
22	1.85	73	1.99
23	1.88	74	1.96
24	1.91	75	1.94
25	1.94	76	1.91
26	1.96	77	1.88
27	1.99	78	1.85
28	2.01	79	1.82
29	2.03	80	1.79
30	2.05	81	1.75
31	2.07	82	1.72
32	2.09	83	1.68
33	2.10	84	1.64
34	2.12	85	1.60
35	2.13	86	1.55
36	2.15	87	1.50
37	2.16	88	1.45
38	2.17	89	1.40
39	2.18	90	1.34
40	2.19	91	1.28
41	2.20	92	1.21
42	2.21	93	1.14
43	2.21	94	1.06
44	2.22	95	0.97
45	2.22	96	0.88
46	2.23	97	0.76
47	2.23	98	0.63
48	2.23	99	0.44
49	2.24		
50	2.24		

Sigma is the the standard deviation = sqr((p*(100-p)/n)

p = mineral content in volume per cent
n = total number of points counted

(see van der Plas and Tobi (1965) for details)

Appendix D: Proportions of heavy minerals in beaches and dunes, determined by point-counting 500 grains per sample (See Appendix A for sample localities and descriptions).

Grain Type	HEC1	HEC2	HEC3	HEC5	HEC4	HEC7	HEC8	HT4	HT3	HT9	HT14	HT13	HN10	HN11	HN14	HN17	HN20	HN3
Ilmenite	15	24	29	51	47	56	40	14	36	23	27	19	10	16	16	25	7	16
Alt ilmenite	4	3	2	6	7	4	2	2	2	3	5	5	3	3	5	4	4	3
HAI	3	p	1	1	1	1	2	1	p	1	2	3	3	2	2	3	3	2
$(Ilm\text{-}Hem)_{ex}$	-	-	-	p	-	-	-	1	p	-	p	1	-	p	p	p	1	1
$(Hem\text{-}Rut)_{ox}$	-	-	-	p	-	-	-	p	-	-	-	p	p	-	-	p	-	p
$Ilm\text{-}(Hem+Rut)_{ox}$	-	-	-	-	-	-	-	-	-	-	-	p	p	p	1	2	p	p
Leucoxene	14	7	5	6	5	2	2	2	p	2	2	3	1	3	1	1	1	1
Rutile	8	5	3	3	5	6	3	2	2	3	4	2	3	2	2	p	1	1
Magnetite[1]	1	1	9	2	1	1	6	4	8	2	4	4	2	1	1	1	1	3
Chromite	-	-	-	-	-	-	-	-	p	p	p	p	p	-	-	-	-	-
Hematite	-	p	p	1	1	2	1	p	p	p	1	2	-	-	p	1	1	4
Goethite	p	-	p	1	p	-	-	-	-	-	p	-	-	-	1	2	1	1
Zircon	18	9	5	11	7	12	6	3	4	7	6	4	2	6	3	5	2	1
Monazite	p	1	p	p	-	p	-	p	p	-	-	-	-	-	-	-	-	-
Pyrobole	22	38	36	9	20	9	33	65	43	54	46	49	59	52	49	55	67	55
Garnet	10	9	7	7	5	7	5	5	6	4	3	8	15	15	17	2	11	12
Apatite	4	2	1	1	1	-	-	-	p	-	-	-	p	1	1	-	p	p
Tourmaline	2	2	p	1	-	p	-	-	-	-	-	p	p	-	1	p	p	-
Epidote	1	p	p	-	1	-	-	-	-	-	-	p	-	-	-	-	-	-

[1] includes $Mt\text{-}Ilm_{ox}\text{-}Usp_{ex}$, $Mt\text{-}Usp_{ex}$, and $Mt\text{-}Pleo_{ex}\text{-}Ilm_{ox}$ grains; p = less than 1 per cent; - = less than 1 in 500 grains.

Appendix D (cont.). Proportions of heavy minerals in beaches and dunes, determined by point-counting 500 grains per sample.

Grain Type	HN4	HN6	HN8	HN9	HN26	HN29	HN33	HZ1	HZ3	HZ25	HZ6	HZ8	HZ10	HZ32	HZ12
Ilmenite	21	17	35	21	41	24		11	14	5	22	13	25	22	7
Alt ilmenite	8	5	6	5	6	2		2	7	p	5	4	3	4	3
HAI	3	2	1	2	4	3		1	1	p	1	3	1	2	1
$(Ilm\text{-}Hem)_{ox}$	5	1	1	4	3	2		1	1	p	1	p	p	1	-
$(Hem\text{-}Rut)_{ox}$	3	1	1	2	2	3		1	1	p	-	-	1	1	-
$Ilm\text{-}(Hem+Rut)_{ox}$	1	p	1	2	2	1		p	p	p	p	-	-	p	p
Leucoxene	1	1	2	3	1	3		1	2	1	1	3	3	4	4
Rutile	3	1	2	4	3	1		1	2	p	1	2	2	3	p
Magnetite[1]	3	2	2	6	1	8		41	4	5	2	1	2	5	3
Chromite	-	p	p	p	p	-		p	-	-	p	p	p	p	p
Hematite	19	2	4	6	9	5		3	1	1	p	3	p	2	1
Goethite	-	p	p	p	1	2		1	-	4	-	1	-	p	-
Zircon	5	4	5	7	4	6		3	4	4	6	3	5	8	2
Monazite	p	-	p	-	-	p		p	p	-	1	-	-	p	-
Pyrobole	21	53	35	32	10	43		28	58	75	56	65	55	44	73
Garnet	8	11	4	6	17	8		5	4	2	4	3	3	4	5
Apatite	p	p	p	p	-	-		-	-	-	-	-	-	p	p
Kryptonite	-	-	-	-	-	-	-	-	-	-	-	-	-	-	-
Tourmaline	p	-	p	-	-	-		p	p	2	-	-	-	p	p
Epidote	p	p	-	-	-	-		p	-	2	p	p	-	p	p

[1] includes $Mt\text{-}Ilm_{oe}\text{-}Usp_{ex}$, $Mt\text{-}Usp_{ex}$, and $Mt\text{-}Pleo_{ex}\text{-}Ilm_{oe}$ grains; p = less than 1 per cent; - = less than 1 in 500 grains.

Appendix D (cont.). Proportions of heavy minerals in beaches and dunes, determined by point-counting 500 grains per sample.

Grain Type	HEC12	HEC11	HEC10	HEC6	HEC13	HT2	HT5	HT7	HT8	HT10	HT15	HT16	HT11	HN12	HN15
Ilmenite	32	33	45	59	38	49	23	65	59	30	35	42	25	21	20
Alt ilmenite	6	4	3	5	2	7	3	10	5	4	4	6	3	21	20
HAI	2	3	3	1	3	p	p	p	-	-	1	2	-	1	2
$(Ilm\text{-}Hem)_{ex}$	-	-	-	-	-	-	-	-	-	-	-	-	-	p	p
$(Hem\text{-}Rut)_{ox}$	-	-	-	-	-	p	-	-	-	-	-	-	-	p	p
$Ilm\text{-}(Hem+Rut)_{ox}$	-	-	-	-	-	-	-	-	-	-	-	-	-	p	1
Leucoxene	12	7	6	3	4	2	4	5	3	2	3	2	1	2	1
Rutile	8	4	7	5	3	3	2	4	2	2	3	2	2	1	1
Magnetite[1]	2	5	4	1	7	7	2	2	4	2	3	5	4	p	2
Chromite	-	-	-	-	-	-	-	-	-	-	-	p	-	p	p
Hematite	p	p	p	1	p	1	1	1	p	1	2	p	1	-	p
Goethite	-	p	-	-	-	-	9	p	-	-	p	-	-	p	3
Zircon	12	5	7	8	6	10	8	3	5	5	6	2	5	4	2
Monazite	p	p	-	p	-	p	p	-	-	-	-	-	-	-	-
Pyrobole	16	31	22	10	31	15	43	8	19	48	40	35	54	57	51
Garnet	5	8	3	4	6	7	3	2	3	6	3	4	5	8	15
Apatite	2	-	-	p	-	p	-	-	-	-	-	-	-	p	p
Tourmaline	2	p	-	1	-	-	2	-	-	-	-	-	-	2	-
Epidote	p	p	-	-	-	p	p	-	-	-	-	-	-	-	-

[1] includes $Mt\text{-}Ilm_{oe}\text{-}Usp_{ex}$, $Mt\text{-}Usp_{ex}$, and $Mt\text{-}Pleo_{ex}\text{-}Ilm_{oe}$ grains; p = less than 1 per cent; - = less than 1 in 500 grains.

Appendix D (cont.). Proportions of heavy minerals in beaches and dunes, determined by point-counting 500 grains per sample.

Grain Type	HN18	HN21	HN1	HN2	HN5	HN7	HN27	HN30	HN34	HZ2	HZ26	HZ16	HZ17	HZ35	HZ36	HZ4	HZ7	HZ13
Ilmenite	30	28	31	40	50	47	52	21	42	35	18	32	28	34	29	21	28	14
Alt ilmenite	8	3	5	5	8	12	7	4	4	8	4	10	8	5	8	15	11	6
HAI	2	1	1	1	1	4	1	2	2	2	1	1	2	3	2	2	5	1
$(Ilm\text{-}Hem)_{ex}$	p	1	1	1	1	2	1	2	5	1	1	p	1	1	2	p	1	p
$(Hem\text{-}Rut)_{ox}$	p	p	p	p	1	1	1	2	2	p	p	1	-	1	p	1	3	p
$Ilm\text{-}(Hem+Rut)_{ox}$	p	p	-	-	-	1	-	1	2	p	p	p	-	1	p	p	-	-
Leucoxene	2	1	1	2	1	4	2	1	1	1	2	4	2	3	4	3	6	4
Rutile	2	1	1	2	3	4	3	2	2	2	2	5	5	3	4	3	2	2
Magnetite[1]	1	1	2	3	1	4	1	3	6	8	7	3	5	6	4	2	2	2
Chromite	-	-	-	1	-	p	-	-	-	p	p	p	p	p	p	p	p	p
Hematite	-	p	2	1	1	3	1	4	7	3	2	3	2	4	2	1	4	p
Goethite	-	p	-	p	-	8	p	1	p	p	2	p	-	p	1	p	4	p
Zircon	3	3	3	6	6	7	8	5	3	7	9	8	9	10	12	7	6	3
Monazite	-	-	p	p	p	p	-	1	p	p	p	p	p	p	3	p	1	-
Pyrobole	41	50	42	29	23	2	16	49	18	28	47	28	33	23	27	38	23	64
Garnet	7	6	12	10	4	1	5	6	6	4	4	2	3	5	4	3	1	4
Apatite	2	p	p	p	-	-	p	-	-	-	-	-	-	p	p	-	p	-
Tourmaline	p	p	p	-	-	-	p	-	-	p	-	-	-	p	-	p	p	p
Epidote	-	-	p	-	p	-	-	-	-	p	p	2	1	1	1	p	p	p

[1] includes $Mt\text{-}Ilm_{oo}\text{-}Usp_{ex}$, $Mt\text{-}Usp_{ex}$, and $Mt\text{-}Pleo_{ex}\text{-}Ilm_{oo}$ grains; p = less than 1 per cent; - = less than 1 in 500 grains.